

**Hemilabile, Non-innocent (Poly)arylene Donors for
Accessing Novel Reactivity at Transition Metal Centers**

Thesis by
Choon Heng Low (Marcus)

In Partial Fulfillment of the Requirements
for the Degree of Doctor of Philosophy

Caltech

CALIFORNIA INSTITUTE OF TECHNOLOGY
Pasadena, California

2019
(Defended on May 7th, 2019)

© 2019
Choon Heng Low
ORCID: 0000-0002-9219-3377
All Rights Reserved

*To Mom and Dad,
and my elder brother Choon Meng*

*“The only real stumbling block is fear of failure.
In cooking, you've got to have a what-the-hell attitude.”*

– Julia Child

ACKNOWLEDGMENTS

Although graduate school can often feel particularly isolating, especially for someone who's traveled almost 9000 miles away from home, the connections I have made in the past 5 years or so have truly been transformative for me both as a scientist and as an individual. This I owe to the people around me, mentors, coworkers, friends, and family who have inspired me, challenged me, supported me, and guided me through good times and bad times. I would like to take this opportunity to acknowledge these special individuals.

First, I must thank my advisor, Prof. Theodor Agapie. I want to sincerely thank you for accepting me into the group. I hadn't initially applied to Caltech with joining the group in mind, but having met you first at visit weekend, and later again after I've come to Caltech, the intensity and fervor you exhibited really drew me in. I want to thank you for always pushing me to try harder. Under your supervision, I've learned an incredible amount in the field of synthetic inorganic chemistry. Even though I wasn't trained in the lab by you, I've had the luck and pleasure of learning from those who did, which has made me a better, a more independent, and most importantly, a more rigorous synthetic chemist both mentally and physically. Your seemingly endless suggestions when I run into obstacles in science have both help guide me out of the depths, and shaped and enriched my own thinking. Thank you for being there, and being supportive and understanding during my recovery after the small lab mishap. I wish you and the group the best, and I can't wait to see what new and exciting avenues the group moves into and flourish in the future.

I would also like to thank the rest of my committee, Prof. Jonas Peters, Prof. Brian Stoltz, and Prof. Robert Grubbs, for all the insightful criticism, comments, and ideas into

my research and proposals. You guys have always pushed me to think about the bigger picture, which can easily be overlooked while caught up in the minutia of day to day lab experiments and is something I keep in the back of my head as I move on in my scientific research career. You've all shown me in what it takes to be a good mentor, each in your own different way.

I, and others in my year, had the privilege of briefly overlapping with Theo's first crop of students and boy was it an eye-opener as a first-year graduate student. Maddy, Emily, Sibó, Paul, Sandy, Jacob, and Davide were the amongst the brightest, most caring (though sometimes more on the side of tough love), and motivated people I have ever met. Along with Kyle, Guy, Justin, Josh, and Po Heng, these folks made me feel so welcomed in the group and have helped me adjust to graduate school life. Emily, I'll always remember your odd late night work hours, and the times when you would invite me to breakfast at IHOP or DuPars after I had pulled an all-nighter day before subgroup (even though I must have seemed like an annoying "trying too hard" first-year to you, come to think of it). To Sibó, thanks for showing me the ropes with regards to glovebox use. It's been a pleasure sharing a box with you, albeit briefly. Thanks for bearing with my initial slowness and clumsiness. To Sandy, and by extension Kyle too, thanks for being almost as obsessed with good food as I am, so I didn't feel like a crazy person. You guys showed me all the good places to get food at around the San Gabriel Valley and the greater LA area, and I've managed to keep that going, transferring knowledge to the youngins. To Paul, thanks for being the positive light, with a dash of salt, in the lab. Your weird but often spot-on observations and jokes never fail to crack me up. To Guy, you've been an incredibly patient mentor and I thank you for helping get me planted in the group.

Mentorship aside, your impressions (“I AM MAAAARCUUUUSS!!!” and others) will always be dearly missed.

To Josh, my coworker, bay mate, box mate, and very dear friend, I’ve had the incredible privilege of working with you and skimming off the wisdom and expertise that you exude. Your enthusiasm for and care you take in the science you do is something I continue to look up to. Thanks for putting up with me both in bay 4 and box 4, I know I’ve definitely tried your patience more than a few time (hoping that has made you a more tolerant person too). Thanks for always being there when I have questions about science (even like in the past few weeks while I’m writing my thesis) and always giving insightful advice and suggestions. Also thanks for always being there to eat everything I bake — I can’t eat it all myself.

During the time spent in the group, I’ve also have had the pleasure of overlapping with some incredible folks who have joined the group since. To Naoki, it’s been a pleasure getting to know you. I hope I’ve helped you developed not only as a synthetic chemist but also as a home cook. I’ll also never forget our epic 36-hour trip to the Grand Canyon, the day before you had to legally leave the US (thanks for insisting on driving both ways). To Siti, my fellow Singaporean, thanks for all the advice in and out of the lab, and also with regards to my career choices; I’ll see you back home soon. HB, thanks for always being available to talk science. We haven’t always seen eye to eye with regard to lab techniques but your passion and breadth of knowledge have always impressed me. I wish you the best at your post-doc position with JR. To Nate, thanks for helping keep up the rigorous standards in lab. Your presence has been missed in both the office and lab in the past few months, but it’s always nice suddenly seeing you show up to use the high-vacuum line ever so often. To Ryan, I’m so glad you made it back to the group, it has

been a real pleasure and I hope your remaining time in graduate school goes swimmingly. The group is definitely better with you around. To Charlie, you're going to be the only senior lab member left in a few months, keep the junior students on their toes and uphold the standards in the group. To Meaghan (I hope I spelled it right) and by extension Zuri, it was a great experience being able to mentor you. The anthracene project lives on with you. Keep on keeping on! Also, take good care of Zuri. You'll both be missed. To Angela, thanks for all the (very timely) GoT trivia, you bring a great positivity to the lab (and honestly remind me a lot of Sandy too). Sam, I'll remember you for all your quirky one-liners and shuffling (I guess it's safer than running?). To Anna, keep up the good work. Those clusters are going to be a beast to tame, but I have faith in you. I wish all the first and second years all the best in your projects! The road is long, just keep putting one foot in front of the other. Eventually, you'll get there (like I am right now). I've also had the pleasure of getting to know the Canadians, Gwen and Manar, who whole-heartedly embodied the Canadian stereotype of being the nicest, most respectful people around. We've all grown to be close friends in an incredibly short period of time and I will miss you guys dearly when I leave. Keep the other folks in lab in check, and spread your positivity and niceness to the other lab member (there are days I can think of when we were sure in need of some).

Caltech, as a top-notch research institute, has amazing personal running excellent facilities. I thank Dave, and Mona and Naseem for upkeeping the NMR and Mass Spec facility, respectively, which have been invaluable in all my projects. I would especially like to thank Larry Henling and Mike Takase for the work they put into not only running the X-ray crystallography facility but the time and effort they spend fishing around my usually cruddy, mostly amorphous samples, trying their hardest to pick the best (and hopefully

single) crystal to put on, without which I would have been unable to carry any of my projects forwards.

I would also like to thank my past mentor, Prof. Andrew Ashley at Imperial College, who gave me my first real taste of inorganic synthesis and what it's like to be in graduate school. Many of my first synthetic experiences, such as learning how to use a Schlenk line and a solvent system, or interpret NMR data, he taught me. Additionally, coworkers I've had during my time at ICES before graduate school have had a tremendous impact on me. Martin van Meurs, Ludger Stubbs, James Nobbs, and Xinyi See, I thank you for your guidance and support.

Outside of the group, I've also made some exceptional friends. To my two roommates of five years, Annet Blom and Matt Smarte at The Devon, thanks for being the most wonderful roommates anyone could ask for. Annet, you're one of the first friends I made when I first started at Caltech. It has been a pleasure and honor being part of your life and attending your wedding with Asher in the Netherlands. Matt, thanks for putting up with me as a roommate and always being down to go to some new restaurant (and driving too) when I'm in the mood. Being an avid board game lover, I've been lucky to find some likeminded friends who indulge my gaming needs. Tim Miles, Josh Kretchmer, Danielle Ownbey, Noah Duffy, Shruti Kopar, Chris Marotta, Lisa Mauger, Ethan van Arrnam, and Meaghan Foster, I thank you.

Throughout the long rough road of grad school, the one person who was always there to provide care and support, though physically separated by 345 mi, is my boyfriend, Matthew Rienzo. I could not have imagined taking the arduous journey without you. You're always there when I needed someone to talk to, and always made me feel better, even if things were falling apart in the lab. You're such a beautiful and sensitive soul and

care so much for everyone around you, and learning from you has helped me become a better person. I love all the time we spend together, whether at home cooking up a storm, or out looking for an adventure, and I'm sure we have many more meals and adventures ahead of us. Additionally, I would like to thank the Rienzos, Joe, Claudia, and Mia, who have essentially become my second family away from home and showered me with much care and support.

Lastly, I would like to thank my family. 妈妈 and 爸爸, thank you for everything. You have given me everything that I have needed to thrive and grow, the care and support are felt even with all the time and distance I spent away from home. I know I've not been the most communicative son to you during the time I've spent abroad, it's simply not one of my strong suits, but I very much look forward to being home again. Thanks for equipping me with, from a young age, the necessary skills of independence which have no doubt aided my survival during my many years away from home. Choon Meng, or "Gor Gor" to me, thanks for always being supportive of the things I do. Thanks for helping take care of Mom and Dad all these years when I wasn't around. All this is only possible because of you all. Thanks for always pushing me to follow my dreams.

ABSTRACT

Understanding the effects that ligands have on the coordination environment and reactivity of metal complexes is an endeavor that drives much of the field of inorganic chemistry. The use of ligands capable of flexible binding modes and redox states further enriches the chemistry of these complexes. This dissertation describes studies on metal complexes bearing pendant (poly)arylene donors that demonstrate hemilability and redox non-innocence. Within this context, conditions that result in coordination mode change and the multi-electron bond transformation that is made possible by the hemilability and/or non-innocence of the ligand are discussed.

Chapter 2 investigates the *meta*-terphenyl diphosphine framework bearing a central phenolate donor as an anionic POP pincer on a variety of first-row transition metals. The circumstances under which coordination mode change from the phenolate donor to the arene face are investigated. Reduction of the cobalt and nickel complexes induced a coordination mode change from phenolate oxygen to metal-arene binding, while Lewis acid additives induced a coordination mode change in some iron POP complexes. Additionally, it was found that iron chloride POP complex initially not amendable to two-electron reduction was cleanly reduced in the presence of Lewis acids, suggesting a role the Lewis acid plays in quenching the negatively charged phenolate and stabilizing the overall transformation.

Chapter 3 discusses reactivity on 1,4-naphthalenediyl diphosphine molybdenum complexes in the context of carbon monoxide (CO) coupling. Similar to the previously studied phenylene system, the reductive coupling of CO can be carried out. However, the naphthalene system showed a distinct and exclusive selectivity for the two-electron reductive CO coupling to a *bis*(siloxo)acetylene motif, without C–O bond cleavage. This

difference in selectivity is proposed to be a result of accessible η^4 -arene binding modes previously not observed in the phenylene variant. Additionally, the *bis*(siloxy)acetylene complex also displays η^4 -binding to the central arene. Further CO catenation can be effected from this species, providing a metallacyclobutenone complex that bears a C_3 fragment derived completely from CO.

In Chapter 4, the reactivity of 9,10-anthracenediyl *bis*(phenoxide) zirconium complexes is presented. The more expanded polyaromatic system with a milder reduction potential allowed the anthracene motif to function as a non-innocent ligand. This enabled facile reductive elimination of ancillary benzyl ligands on the metal center without the use of harsh reductants. This reduced complex was then able to oxidatively couple alkynes, and alkynes with nitriles. Furthermore, further insertion of an additional nitrile followed by reductive elimination, likely facilitated by the non-innocent anthracene motif, allowed for the catalytic synthesis of pyridines and pyrimidines with high yields and selectivities. This reactivity was further leveraged in the final Chapter of this dissertation. Chapter 5 presents the development of a new methodology towards the synthesis of pyridine or pyrimidine-containing polycyclic aromatic hydrocarbons (PAHs) using polyaromatic alkyne and nitrile building blocks. Because conventional methods of oxidative cyclodehydrogenation towards N-doped nanographenes proved ineffective with these PAHs, a new reductive cyclization route was developed offering a complementary method towards the challenging synthesis of these N-doped nanographenes.

Appendix A briefly explores additional reactivity on the 1,4-naphthalenediyl diphosphine complexes with regard to nitrile activation. Appendix B explores the synthesis of iron complexes supported by a benzene *tris*(thiophenolate) ligand towards potential model compounds for the iron molybdenum cofactor in nitrogenase. Appendix

C presents preliminary studies on the 9,10-anthracenediyl *bis*(phenoxide) zirconium complex towards oxidative coupling of alkynes with CO₂.

PUBLISHED CONTENT AND CONTRIBUTIONS

Parts of this thesis have been adapted both from published articles and those that are currently in preparation that the author has co-written:

The following articles will be reproduced, in part, with permission from the American Chemical Society:

Choon Heng Low, Jeffrey N. Rosenberg, Marco A. Lopez, and Theodor Agapie “Oxidative Coupling with Zr(IV) Supported by a Noninnocent Anthracene-Based Ligand: Application to the Catalytic Cotrimerization of Alkynes and Nitriles to Pyrimidines” *J. Am. Chem. Soc.*, **2018**, *140*, 11906-11910. DOI: 10.1021/jacs.8b07418

I developed the ligand synthesis, carried out the mechanistic studies and performed all the optimization and substrate screening.

Parts of the work described in this dissertation are the result of scientific collaborations, without which the reported studies would not have been possible.

In Chapter 3, the initial synthesis and structural characterization of diene complexes **8**, **9**, and **10** were reported by Dr. Joshua Buss.

In Chapter 4, the initial ligand synthesis was developed in collaboration with Jeffrey Rosenberg and was further improved on in collaboration with Marco Lopez. Initial metalation and alkyne reactivity studies were also carried out in collaboration with Jeffrey Rosenberg while the labeling studies for the crossover experiments were done in collaboration with Marco Lopez.

In Chapter 5, initial optimization studies for the generation of pyridine **4aa** were carried out in collaboration with visiting scholar Miku Oi.

TABLE OF CONTENTS

Dedication	iii
Acknowledgments	iv
Abstract	x
Published Content and Contributions	xiii
Table of Contents	xiv
List of Figures	xvii
List of Schemes	xxi
List of Tables	xxiv
Chapter 1	1
General Introduction	
Chapter 2	9
First-Row Transition Metal Complexes Supported by a Hemilabile <i>meta</i> -Terphenyl-based Anionic POP Ligand	
Abstract	10
Introduction	11
Results and Discussion	14
Conclusions	33
Experimental Section	34
References	54
Chapter 3	58
1,4-Naphthalenediyl-linked Diphosphine Molybdenum Complexes Towards Catenation of Carbon Monoxide to a C ₃ Product at a Single Metal Site	
Abstract	59
Introduction	60
Results and Discussion	62
Conclusions	70
Experimental Section	71
References	82
Chapter 4	85
Oxidative Coupling with Zr(IV) Supported by a Non-Innocent Anthracene-Based Ligand: Application to the Catalytic Cocoupling of Alkynes and Nitriles to N-Heteroaromatics	
Abstract	86
Introduction	87
Results and Discussion	88
Conclusions	102
Experimental Section	103
References	125

Chapter 5	130
Synthesis of N-doped Nanographenes through Zirconium Catalysis and Reductive Cyclization	
Abstract	131
Introduction	132
Results and Discussion	134
Conclusions	152
Experimental Section	153
References	173
Appendix A	177
Synthesis of Carbonyl-free Molybdenum Arylene Diphosphine Complexes: Observations of Nitrile Activation and Coupling	
Abstract	178
Introduction	179
Results and Discussion	180
Conclusions	187
Experimental Section	188
References	190
Appendix B	191
Design and Synthesis of <i>Tris</i> (thiophenolate)benzene Iron Complexes As Potential Nitrogenase FeMoco Models	
Abstract	192
Introduction	193
Results and Discussion	194
Conclusions	201
Experimental Section	202
References	206
Appendix C	207
Metal Complexes Supported by 1,9-Anthracenediyl-Linked [O,O]-Pincers Towards the Coupling of Unsaturated Organic Fragments with CO ₂	
Abstract	208
Introduction	209
Results and Discussion	210
Conclusions	211
Experimental Section	221
References	229
Appendix D	232
NMR Spectra	
Chapter 2	233

Chapter 3	247
Chapter 4	254
Chapter 5	266
Appendix A	279
Appendix B	281
Appendix C	283

LIST OF FIGURES

Note: Figures listed below correspond to those included in the main text of each chapter. Remaining figures can be found in the respective Experimental Sections.

Chapter 1

- Figure 1.1.** 3
 β -H transfer facilitated by hemilabile pendant arene.
- Figure 1.2.** 4
 Arene to phenolate coordination mode change in arene-linked diphosphine complexes.

Chapter 2

- Figure 2.1.** 12
 Reported complexes featuring anionic POP ligands.
- Figure 2.2.** 17
 Solid-state structure of **2**.
- Figure 2.3.** 18
 Solid-state structure of **3-6**.
- Figure 2.4.** 21
 Solid-state structure of **7**.
- Figure 2.5.** 22
 Solid-state structure of **8**.
- Figure 2.6.** 23
 Solid-state structure of **9**.
- Figure 2.7.** 24
 Solid-state structures and central arene bond metrics of **10**.
- Figure 2.8.** 26
 Solid-state structures and central arene bond metrics of **11** and **12**.
- Figure 2.9.** 28
 Solid-state structure and central arene bond metrics of **13**.
- Figure 2.10.** 30
 Solid-state structures and central arene bond metrics of **14**.
- Figure 2.11.** 31
 Solid-state structures and central arene bond metrics of **15**.
- Figure 2.12.** 32
 Solid-state structures and central arene bond metrics of **17**.

Chapter 3

- Figure 3.1.** 61
 Sequential CO catenation of a C₃-containing complex to a C₄-containing complex.
- Figure 3.2.** 61

Reversible oxidative addition of H ₂ to anthracene-supported Mo complex facilitated by anthracene ring-slippage.	
Figure 3.3. Solid-state structures of 2 and 3 .	63
Figure 3.4. Naphthalene and naphthalenediyl linker bond metrics of complexes 2 and 3 .	63
Figure 3.5. Solid-state structures of 5 and 6 .	65
Figure 3.6. Naphthalenediyl linker bond metrics of complexes 5 and 6 .	66
Figure 3.7. Experimental and simulated partial ¹³ C{ ¹ H} (126 MHz, 25 °C, C ₆ D ₆) and ³¹ P{ ¹ H} (202 MHz, 25 °C, C ₆ D ₆) NMR spectra of 11- ¹³ C	68
Figure 3.8. Truncated preliminary solid-state structure of 10 .	68
Chapter 4	
Figure 4.1. Non-innocent anthracene moiety facilitating reductive elimination.	87
Figure 4.2. Solid-state structure and central ring bond metrics of 1 .	90
Figure 4.3. Solid-state structure and central ring bond metrics of 2 .	91
Figure 4.4. GC-MS trace of bibenzyl products observed from reductive elimination of a 1:1 mixture of 1 and 1-d ₁₄ .	92
Figure 4.5. Solid-state structure of 3a .	93
Figure 4.6. Solid-state structure of 5 .	97
Figure 4.7. NMR spectra of stoichiometric reactions of 3a and 5 with phenylacetylene or benzonitrile.	99
Figure 4.8. GC-MS chromatograph from the reaction of 5 with benzonitrile (5 equiv.) after 1 h heating at 90 °C	120
Figure 4.9. GC-MS chromatograph from the reaction of 3b with benzonitrile (5 equiv.) after 1 h heating at 90 °C	120
Chapter 5	
Figure 5.1. Biphenyldiynes 2c and 2d containing solubilizing groups.	137
Figure 5.2.	139

NMR spectra of 4ca and 5ca .	
Figure 5.3.	140
Solid-state structure of 5ca .	
Figure 5.4.	141
Solid-state structure of 5da .	
Figure 5.5.	147
Preliminary solid-state structure of $[4gf-(H)_2]^{2+}$.	
Figure 5.6.	150
1H NMR spectra of 4hh , 5hh , and 4gh .	
Figure 5.3.	141
Preliminary solid-state structure of 5hh .	
Appendix A	
Figure A.1.	181
Solid-state structure, and central arene bond metrics for 3 .	
Figure A.2.	182
Solid-state structure, and central arene bond metrics for 4 .	
Figure A.3.	183
Solid State Structure of 6	
Figure A.4.	186
Solid-state structure of 8 showing linear nitrile and bent nitrile.	
Appendix B	
Figure B.1.	196
Solid-state structure of 1 .	
Figure B.2.	197
1H NMR spectra of 2 in C_6D_6 and CD_3CN .	
Figure B.3.	198
Solid-state structure of 2 .	
Figure B.4.	199
Solid-state structure of 3 .	
Appendix C	
Figure C.1.	213
Solid-state Structure of 4	
Figure C.2.	215
IR spectra of 6	
Figure C.3.	217
Solid-state structure of 8	
Figure C.4.	218
Solid-state structure of 9	
Figure C.5.	220
Solid-state structure of 11	
Appendix D	

Note: Appendix D contains the characterization NMR spectra for the complexes reported in this dissertation (Figures D.1. – D.151), a complete list of which is impractical.

LIST OF SCHEMES

Chapter 2	
Scheme 2.1.	14
Synthesis of diphosphine aminophenol 1-H	
Scheme 2.2.	15
Synthesis of complexes 2-6	
Scheme 2.3.	21
Reduction of complexes 3, 5, and 7	
Scheme 2.4.	25
Reaction of 10 with trialkylaluminiums	
Scheme 2.3.	29
Stepwise reduction of 13	
Chapter 3	
Scheme 3.1.	62
Synthesis and reactivity of naphthalenediyl-linked diphosphine molybdenum complexes	
Scheme 3.2.	66
Synthesis and reactivity of cyclohexadienediyl-diphosphine Mo complexes	
Chapter 4	
Scheme 4.1.	88
Synthesis <i>bis</i> (phenol) proligand LH₂	
Scheme 4.2.	89
Synthesis and reactivity of <i>bis</i> (phenoxide) zirconium complexes with pendant anthracene	
Scheme 4.3.	91
Potential pathways for formation for photolysis of 1	
Scheme 4.4.	98
Stoichiometric reactions involving catalytically relevant species	
Scheme 4.5.	100
Stoichiometric reactions with tethered diynes and benzonitrile	
Chapter 5	
Scheme 5.1.	132
Catalytic synthesis of N-heteroaromatics by complex 1	
Scheme 5.2.	134
Proposed synthesis of pyridine-containing nanographenes	
Scheme 5.3.	136
Synthesis of asymmetric biphenyldiyne 2b and subsequent coupling with 3a	
Scheme 5.4.	138
Synthesis pyridine-containing N-doped nanographenes	

Scheme 5.3.	142
Proposed synthesis of dipyridine-containing nanographenes	
Scheme 5.3.	145
Proposed synthesis of dipyrimidine-containing nanographenes	
Scheme 5.3.	146
Formation of 4'df under standard catalytic conditions	
Scheme 5.3.	147
Reaction of 2e with 3f or 3g under standard catalytic conditions	
Scheme 5.3.	148
Catalytic synthesis of 4hh	
Scheme 5.3.	149
Reductive cyclization of 4hh	
Appendix A	
Scheme A.1	181
Photolytic decarbonylation of 1	
Scheme A.2	183
Reduction of 3	
Scheme A.3	184
One-electron reduction of 3	
Scheme A.4	185
Synthesis and reduction of PrCN adduct	
Appendix B	
Scheme B.1	194
Synthesis of LH₃	
Scheme B.2	195
Metalation of LH₃ to afford 1	
Scheme B.3	197
Metalation of LH₃ to afford 2	
Appendix C	
Scheme C.1	211
Proposed Zr-catalyzed coupling of alkynes with CO ₂	
Scheme C.2	212
Stepwise reaction of 1 with diphenylacetylene	
Scheme C.3	213
Reactivity of 2 with CO ₂	
Scheme C.4	215
Reactivity of 5 with CO ₂	
Scheme C.5	216
Reactivity of 1 with AdN ₃	
Scheme C.6	218
Synthesis of vanadium <i>bis</i> (phenoxide) complexes	
Scheme C.7	219

Synthesis of monoanionic monophenoxide ligand
Scheme C.8
Synthesis of **11**

LIST OF TABLES

Chapter 2	
Table 2.1.	19
Selected structural metrics for complexes 4-7	
Table 2.2.	52
Crystal data and structure refinement for 2, 3, 4, and 5	
Table 2.3.	52
Crystal data and structure refinement for 6, 7, 8, and 9	
Chapter 3	
Table 3.1.	81
Crystal data and structure refinement for 2, 3, 5, and 6	
Chapter 4	
Table 4.1.	95
Cycloaddition of phenylacetylene with benzonitrile under various conditions	
Table 4.2.	96
Substrate scope of cycloaddition of alkynes with nitriles to pyrimidines	
Table 4.3.	96
Cycloaddition of 1,6-heptadiyne with benzonitrile under various conditions	
Table 4.4.	121
Additional substrates screened under optimized catalytic conditions	
Table 4.5.	124
Crystal data and structure refinement for 1, 2, 3a, and 5	
Chapter 5	
Table 5.1	135
Optimization of 1 -catalyzed coupling of 2a with 3a	
Table 5.2	143
Optimization of catalytic conditions for 2c with 2,2'-dicyanobiphenyl	
Table 5.3	172
Crystal data and structure refinement for 5ca and 5da	

CHAPTER 1

General Introduction

This dissertation focuses on the study of a series of transition metal complexes supported by (poly)arylene-linked ligands. Although a variety of donor sets were explored (phosphines, phenoxides, thiolates), they are all designed to bind rigidly to metal centers in order to encourage metal-arene interactions at the linker. The arylene linkers studied include *meta*-phenylene, 1,4-naphthalenediyl, and 9,10-anthracenediyl linkers with different aspects of the arene ligands leveraged in each case to engender novel reactivity and/or metal coordination environments. The range of complexes studied demonstrate the ability of these arylene motifs to function 1) as hemilabile donors, alleviating the varying electronic demands upon changes in the metal coordination sphere and/or redox state, and 2) as redox non-innocent ligands, allowing multiple electrons to be stored within the arene framework upon reductive processes and delivering them upon oxidation. The latter alleviates the need for the metal center to take on large and/or unfavorable redox state changes, mediating novel chemistries that would not be feasible in the absence of said ligands. The work discussed herein seeks to address the use of these functions, separately or in combination, with respect to exploring new coordination modes, and engendering challenging bond breaking and forming transformations. While as detailed background with the appropriate references is incorporated in the introduction of each chapter, this chapter aims to provide a more general overview of the main concepts that are tackled and provide a narrative for this research.

The first metal-arene complex was isolated by Hein in 1919,¹ but it was not until the 1950s that definitive composition and structural assignment of these complexes were obtained.²⁻⁵ Since then, the chemistry of metal-arene complexes has burgeoned, and complexes on a wide variety of metals featuring the full range of possible hapticities (η^0 to η^6) have been reported.⁶⁻⁸ A central function of ligands is to serve as a source of electrons, filling vacant bonding molecular orbitals present, and thus overall stabilizing the metal complex.

When electron count at the metal increases, anti-bonding orbitals may become filled, often resulting in the dissociation of the ligand. In that regard, hemilabile ligands that can bind reversibly or change their coordination modes to modulate the number of electrons they donate into the metal center can help in mediating redox and coordination sphere changes at the metal.⁹⁻¹² The change in coordination environment can also be leveraged as a switch to turn on and off reactivity at a metal site.¹³⁻¹⁶ Arenes being able to change their hapticity modes from η^0 to η^6 (donating 0 to 6 electrons) allows them to function as potential hemilabile ligands. Hessen and coworkers reported a Ti complex supported by a cyclopentadienyl ligand featuring a pendant arene that is capable of carrying out ethylene trimerization to 1-hexene (Figure 1.1).¹⁷⁻¹⁸ It is proposed that the β -H transfer is mediated by an η^1 to η^6 -binding mode change in the pendant arene stabilizing the Ti(II) intermediate. In contrast, in the absence of the pendant arene, ethylene polymerization is observed instead.

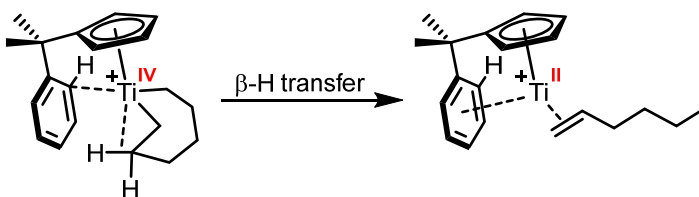


Figure 1.1. β -H transfer facilitated by hemilabile pendant arene.

In our group, the use of hemilabile arene diphosphine ligands has been interrogated extensively on a variety of transition metals complexes.¹⁹⁻²⁵ The flexibility of the central arene donor allows the support of not only monometallic complexes in a wide range of oxidation states but also that of multimetallic complexes. In extending the nature of hemilability of these phenylene-linked diphosphine ligands, the introduction of a phenolate linker capable of coordinating as two distinct types of donors was studied with first-row transition metals (Chapter 2). Based on prior observations made by Dr. Paul Kelley and Dr. Guy Edouard on complexes supported by a similar POP binding motif,²⁶⁻²⁷ we had evidence that a *meta*-phenyl

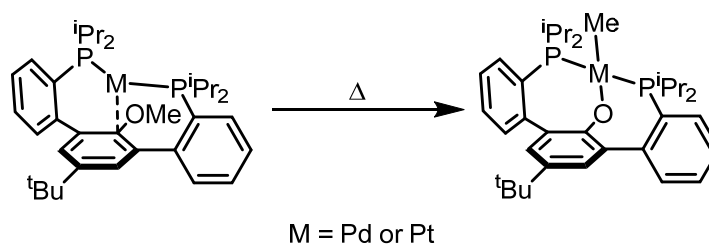


Figure 1.2. Arene to phenolate coordination mode change in arene-linked diphosphine complexes.

framework could support metals both on the arene face and on the phenolate oxygen upon C–O bond cleavage (Figure 1.2). Conditions that engendered a coordination mode change from phenolate O-donor to the phenolate arene donor and enable further reactivity at the metal center were investigated.

The extension of arene into polyarenes, such as naphthalene, can modify the preferred metal-arene binding modes by stabilizing the η^4 -arene interaction and result in great lability of the arene.²⁸⁻³⁰ This effect was investigated with 1,4-naphthalenediyl-linked diphosphine molybdenum complexes in the context of both carbon monoxide (CO) coupling (Chapter 3) and nitrile activation (Appendix A). It was found that access to an η^4 -arene interaction, which had not been observed in the phenylene-link variant,³¹⁻³² can result in both a complete switch in selectivity in reductive CO coupling and subsequently allowed for a rare example of further CO catenation to a C₃ fragment completely derived from CO.

In the past few decades, the use of redox non-innocent ligands has flourished due to their ability to facilitate novel and challenging multi-electron bond transformations and to support catalysis.³³⁻³⁵ This is enabled by the ability of the ligand to function as an electron reservoir, due to the availability of low-lying vacant ligand-based orbitals that are more readily reduced than those on the metal. In the activation of many small molecules (N₂, CO, O₂) at a single metal site, this feature allows multi-electron transformations to occur simultaneously rather than stepwise by drawing reducing equivalents from both the ligand and the metal

center. This avoids potentially high energy intermediates that would otherwise be inaccessible or lead to detrimental side reactivity. It was previously shown that under sufficiently reducing potentials, phenylene linkers can be reduced,^{32, 36} storing up to two electron equivalents and adopting a cyclohexyldienediyl-type motif.³⁷⁻³⁸ This has been used to great effect by Dr. Josh Buss in the group in his study of *para*-terphenyl diphosphine molybdenum complexes, both in showing the range of formal oxidation states that can be accessed (+VI to -III), and the ability for four-electron deoxygenative reductive coupling of CO to a C₂O₁ product. The same redox non-innocence was leveraged with a 1,4-naphthalenediyl-linked diphosphine system (Chapter 3) as mentioned earlier towards CO coupling. It was also found that due to the more extended π -system, the central arene was also more amenable to reduction, allowing milder reductants to be used.

The aspects discussed above, when used in combination, led us to the study of 9,10-anthracenediyl *bis*(phenoxide) in its use as hemilabile, non-innocent ligands in zirconium complexes (Chapter 4). In most cases of non-innocent ligands, upon redox changes at the ligand, a rearrangement of ligand-based π bonds occurs without any change in the coordination mode to the metal center.^{35, 39-41} The use of non-innocent ligands that involve both a change in the redox state of the ligand and simultaneous change in coordination framework at the metal is rare. These two characteristics of the anthracene-based ligand allowed for the synthesis of formally two-electron reduced zirconium(IV) complexes, effectively masking a “Zr(II)” species and for the oxidative coupling of alkynes, cocoupling of alkynes with nitriles, and cocoupling of alkynes with CO₂ (Appendix C). Moreover, the more accessible reduction potential of the anthracene motif facilitated the turnover of this system, catalyzing the cotrimerization of alkynes with nitriles to either pyrimidines or pyridines. This methodology was then further developed in Chapter 5 towards the synthesis

of nitrogen-containing polycyclic aromatic hydrocarbons (PAHs). In addition, a new strategy towards the planarization of these PAHs to provide N-doped nanographenes via a reductive cyclization followed by oxidative dehydrogenation was developed. This represents a new route towards the synthesis of atomically-precise N-doped nanographenes, which are of great interest in the fields of electronic and optical materials.⁴²

Overall, this work aims to establish the multifaceted nature of arylene donors as hemilabile, non-innocent motifs. Specifically, it seeks to demonstrate that while they are powerful tools separately, when used in a complementary nature, they allow for the challenging multi-electron bond transformations to be mediated or even catalyzed to yield valuable products such as $C_{n>2}$ species from CO, N-heterocycles, and N-doped nanographenes.

REFERENCES

- (1) Hein, F., *Berichte der deutschen chemischen Gesellschaft (A and B Series)* **1919**, *52*, 195-196.
- (2) Zeiss, H. H.; Tsutsui, M., *J. Am. Chem. Soc.* **1957**, *79*, 3062-3066.
- (3) Fischer, E., *Z. Anorg. Allg. Chem* **1956**, *286*, 146-158.
- (4) Fischer, E.; Hafner, W., *Z. Anorg. Allg. Chem.* **1956**, *286*, 146-148.
- (5) Fischer, E. O.; Seus, D., *Chem. Ber.* **1956**, *89*, 1809-1815.
- (6) Muetterties, E. L.; Bleeke, J. R.; Wucherer, E. J.; Albright, T., *Chem. Rev.* **1982**, *82*, 499-525.
- (7) Pampaloni, G., *Coord. Chem. Rev.* **2010**, *254*, 402-419.
- (8) Calderazzo, F.; Pampaloni, G., *J. Organomet. Chem.* **1995**, *500*, 47-60.
- (9) Barrett, B. J.; Iluc, V. M., *Inorg. Chem.* **2014**, *53*, 7248-7259.
- (10) Gunanathan, C.; Ben-David, Y.; Milstein, D., *Science* **2007**, *317*, 790-792.
- (11) Drover, M. W.; Love, J. A.; Schafer, L. L., *Chem. Soc. Rev.* **2017**, *46*, 2913-2940.
- (12) Slone, C. S.; Weinberger, D. A.; Mirkin, C. A., *Prog. Inorg. Chem.* **1999**, 233-350.
- (13) Kita, M. R.; Miller, A. J. M., *J. Am. Chem. Soc.* **2014**, *136*, 14519-14529.
- (14) Gregor, L. C.; Grajeda, J.; Kita, M. R.; White, P. S.; Vetter, A. J.; Miller, A. J. M., *Organometallics* **2016**, *35*, 3074-3086.
- (15) Grajeda, J.; Kita, M. R.; Gregor, L. C.; White, P. S.; Miller, A. J. M., *Organometallics* **2016**, *35*, 306-316.
- (16) Kita, M. R.; Miller, A. J. M., *Angew. Chem. Int. Ed.* **2017**, *56*, 5498-5502.
- (17) Deckers, P. J. W.; Hessen, B.; Teuben, J. H., *Angew. Chem. Int. Ed.* **2001**, *40*, 2516-2519.
- (18) Otten, E.; Batinas, A. A.; Meetsma, A.; Hessen, B., *J. Am. Chem. Soc.* **2009**, *131*, 5298-5312.
- (19) Buss, J. A.; Edouard, G. A.; Cheng, C.; Shi, J.; Agapie, T., *J. Am. Chem. Soc.* **2014**, *136*, 11272-11275.
- (20) Buss, J. A.; VanderVelde, D. G.; Agapie, T., *J. Am. Chem. Soc.* **2018**, *140*, 10121-10125.
- (21) Horak, K. T.; Lin, S.; Rittle, J.; Agapie, T., *Organometallics* **2015**, *34*, 4429-4432.
- (22) Suseno, S.; Horak, K. T.; Day, M. W.; Agapie, T., *Organometallics* **2013**, *32*, 6883-6886.
- (23) Velian, A.; Lin, S.; Miller, A. J. M.; Day, M. W.; Agapie, T., *J. Am. Chem. Soc.* **2010**, *132*, 6296-6297.
- (24) Chao, S. T.; Lara, N. C.; Lin, S.; Day, M. W.; Agapie, T., *Angew. Chem. Int. Ed.* **2011**, *50*, 7529-7532.

- (25) Lin, S.; Day, M. W.; Agapie, T., *J. Am. Chem. Soc.* **2011**, *133*, 3828-3831.
- (26) Edouard, G. A.; Kelley, P.; Herbert, D. E.; Agapie, T., *Organometallics* **2015**, *34*, 5254-5277.
- (27) Kelley, P.; Lin, S.; Edouard, G.; Day, M. W.; Agapie, T., *J. Am. Chem. Soc.* **2012**, *134*, 5480-5483.
- (28) Zhu, G.; Janak, K. E.; Figueroa, J. S.; Parkin, G., *J. Am. Chem. Soc.* **2006**, *128*, 5452-5461.
- (29) Bennett, M. A.; Lu, Z.; Wang, X.; Bown, M.; Hockless, D. C. R., *J. Am. Chem. Soc.* **1998**, *120*, 10409-10415.
- (30) Kündig, E.; Perret, C.; Spichiger, S.; Bernardinelli, G., *J. Organomet. Chem.* **1985**, *286*, 183-200.
- (31) Buss, J. A.; Agapie, T., *J. Am. Chem. Soc.* **2016**, *138*, 16466-16477.
- (32) Buss, J. A.; Agapie, T., *Nature* **2016**, *529*, 72-75.
- (33) Lyaskovskyy, V.; de Bruin, B., *ACS Catal.* **2012**, *2*, 270-279.
- (34) Luca, O. R.; Crabtree, R. H., *Chem. Soc. Rev.* **2013**, *42*, 1440-1459.
- (35) Chirik, P. J.; Wieghardt, K., *Science* **2010**, *327*, 794-795.
- (36) Kurogi, T.; Ishida, Y.; Kawaguchi, H., *Chem. Commun.* **2013**, *49*, 11755-11757.
- (37) Sattler, A.; Parkin, G., *J. Am. Chem. Soc.* **2012**, *134*, 2355-2366.
- (38) Cassani, M. C.; Gun'ko, Y. K.; Hitchcock, P. B.; Lappert, M. F.; Laschi, F., *Organometallics* **1999**, *18*, 5539-5547.
- (39) Bart, S. C.; Chlopek, K.; Bill, E.; Bouwkamp, M. W.; Lobkovsky, E.; Neese, F.; Wieghardt, K.; Chirik, P. J., *J. Am. Chem. Soc.* **2006**, *128*, 13901-13912.
- (40) Bouwkamp, M. W.; Bowman, A. C.; Lobkovsky, E.; Chirik, P. J., *J. Am. Chem. Soc.* **2006**, *128*, 13340-13341.
- (41) Blackmore, K. J.; Ziller, J. W.; Heyduk, A. F., *Inorg. Chem.* **2005**, *44*, 5559-5561.
- (42) Muhammad, S.; Chaudhry, A. R.; Irfan, A.; Al-Sehemi, A. G., *RSC Adv.* **2017**, *7*, 36632-36643.

CHAPTER 2

First-Row Transition Metal Complexes Supported
by a Hemilabile *meta*-Terphenyl-based Anionic POP Ligand

ABSTRACT

The synthesis of a novel anionic *meta*-terphenyl diphosphine ligand bearing a central aminophenolate and its subsequent metalation with a series of first-row transition metals halide (Cr, Mn, Fe, Co, Ni) were carried out. In all cases except Mn(II), monometallic complexes with the metals binding through the phenoxide and both phosphines arms were observed. With MnBr₂, a 3:2 metal:ligand complex was obtained with a “MnBr₂” moiety bridging two diphosphine phenoxide bound Mn units through the phenoxide oxygen. Reductions of the monometallic complexes **3-6** were investigated. With cobalt and nickel POP complexes **5** and **6**, reduction led to a binding mode change from the hard phenoxide to the softer central arene, binding in a η^1 and η^6 fashion, respectively. Additionally, the effects of Lewis acids and redox changes have been probed on a series of iron POP complexes starting from **4** and triflate analog **10**. The presence of Lewis acids was vital for stabilizing the intermediates involved in the two-electron reduction of iron(II) chloride complex **4** to either AlEt₃-bound complex **14** or Lewis acid-free **17** when BEt₃ is used. While high spin complexes Fe were observed in the POP binding mode, the P-arene-P binding mode tended to support low-spin Fe complexes. The ability to support a variety of metal oxidation and coordination environments demonstrates the coordinative flexibility of this POP pincer ligand.

INTRODUCTION

Since the early work by Shaw and coworkers on PCP pincers in the late 1970s,¹⁻⁷ pincer ligands have garnered much interest and have been employed widely in catalysis and organic synthesis.⁸ They are characterized by their tridentate nature with three contiguous donors along the ligand backbone. This chelating nature often provides increased stability to their complexes, minimizing undesirable ligand exchange reactions. The rigid, typically meridional, coordination geometry the ligand enforces around the metal center also allows for better control of the vacant binding site, allowing for selective small molecule binding and activation. Another advantage pincer ligands offer is their tunability; by changing the electronics and sterics of the sidearm and central donors, and sidearm flexibility, the reactivity at the metal center can be rationally modified.⁹

Recently, the use of non-innocent and hemilabile pincer ligands in catalysis and small molecule activation has also become more prevalent via the inclusion of moieties that function as pendant bases,¹⁰⁻¹¹ or pendant acids.¹²⁻¹⁴ Milstein and coworkers have also shown such acid or base cooperativity can be engendered by aromatization/dearomatization of the arene system of the central donor upon proton transfer.¹⁵⁻¹⁷ Redox non-innocence of pincer ligands has also been leveraged towards novel and challenging redox transformations. One example is redox-active pyridyl diimine ligands (PDI) employed by Chirik and coworkers wherein the reduction of an Fe(II) PDI complex resulted in ligand-based rather than metal-based redox change.¹⁸⁻²⁰

The capability of a ligand to provide flexible coordination modes to stabilize varying metal oxidation states and coordination environments has been demonstrated to imbue novel reactivity in transition metal complexes.²¹⁻²⁵ In some cases, hemilabile pendant groups can also function as a switch, turning on and off a catalyst by the addition or sequestration of an

additive, such as an extraneous alkali metal cation.²⁶⁻²⁹

In our group, terphenyl pincer ligand frameworks featuring both functionalized and non-functionalized central arene moieties have been employed in supporting a wide variety of mono- and multimetallic complexes.³⁰⁻³⁹ Depending on the oxidation state of the metal centers and/or the ancillary ligands present, the central arene moiety is capable of providing a range of coordination modes and, in certain instances, even acts a redox-active moiety by functioning as an electron sink.³⁸ Additionally, the phosphine arms are also hemilabile, coming off and back on depending on the electronic requirements of the bound metal center.³⁹

Owing to the divalent nature of oxygen, they commonly feature as the central donor in a variety of diphosphine pincer ligands as ethereal donors such as that in Xantphos.⁴⁰⁻⁴¹ However, because of that, an anionic central oxygen donor that is bound contiguously to two adjacent ligand-based atoms is an impractical motif. Instead, a pincer-like POP ligand bearing an alkoxide or a phenoxide central O donor bound to a carbon atom that is adjacent to the phosphine donor arms could be envisioned. To the best of our knowledge, there have only been three examples of such POP pincer-like ligands in the literature, and their complexes limited to Mn, Ni, Rh, Ir, Pd and Pt (Figure 2.1).⁴²⁻⁴⁵ Additionally, the anionic POP motif of the anthrone-based Pt complex (Figure 2.1, left) was generated post metalation *via* ligand-based oxidation. More recently, Lacy and coworkers reported a POP supported Mn complex capable of catalyzing a Tishchenko reaction.⁴⁵

We envisaged that the introduction of an anionic phenolate donor in place of the

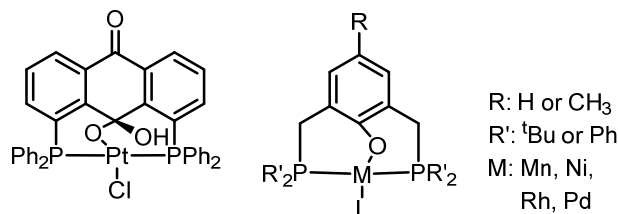


Figure 2.1. Reported complexes featuring anionic POP ligands.

central phenylene in a terphenyl diphosphine ligand framework could allow for novel coordination geometries for metal complexes and would add to the small library of anionic POP motifs in the literature. Targeting a *meta*-terphenyl framework would allow the metal center to be able to access the phenolate to bind as an anionic donor, while still allowing a potential change in binding mode to the central arene as a P-arene-P pincer.⁴⁶⁻⁴⁸ The addition of electron-rich amino group at the *para* position of the central arene further favors potential arene binding and may allow for potential redox non-innocence by acting as a source of electrons, a feature that has been observed in other aminophenolate-supported complexes.⁴⁹

Herein, we report the synthesis of the targeted *m*-terphenyl diphosphine ligand bearing a central aminophenolate moiety. Metalation was explored with first-row transition metal halides ranging from manganese to nickel, and their solid-state structures characterized. Subsequent chemical reductions were explored for a number of the synthesized complexes with a change in binding mode from phenoxide to arene observed in the cobalt and nickel examples. Investigation in the effect of Lewis acid coordination to the phenolate oxygen affecting binding modes was also investigated, and it was observed that for the Fe complex, the presence of Lewis acid interaction allowed for facile reduction that would have otherwise resulted in decomposition.

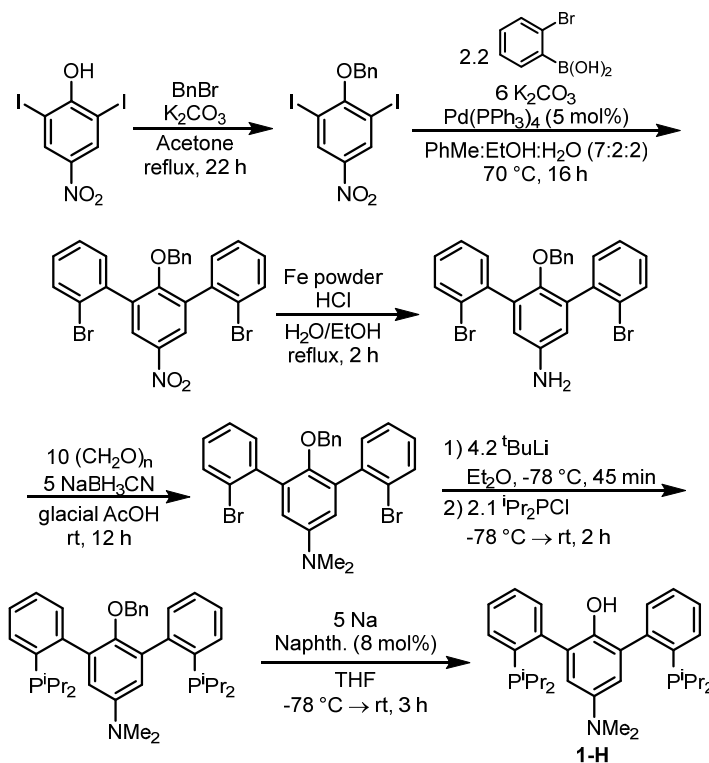
RESULTS AND DISCUSSION

Ligand Synthesis

Our group has previously reported the synthesis of the structurally related anisoyl *m*-terphenyl diphosphine ligand, which was used in the context of metal-mediated aryl-ether bond cleavage chemistry.⁴⁷⁻⁴⁸ However, in targeting the free phenol **1-H**, we found the use of a benzyl protecting group instead of a methyl group to be more amenable due to the greater compatibility of the subsequent deprotection conditions employed in the presence of the phosphine groups.

The synthesis of diphosphine phenol **1-H** is shown in Scheme 2.1. 2,6-diiodo-4-nitrophenol, synthesized from the iodination of commercially available 4-nitrophenol, was first protected by benzylation. Suzuki coupling with 2-bromoboronic acid, followed by a Bechamp reduction of the nitro group, and reductive amination with formaldehyde provided

Scheme 2.1. Synthesis of diphosphine aminophenol **1-H**

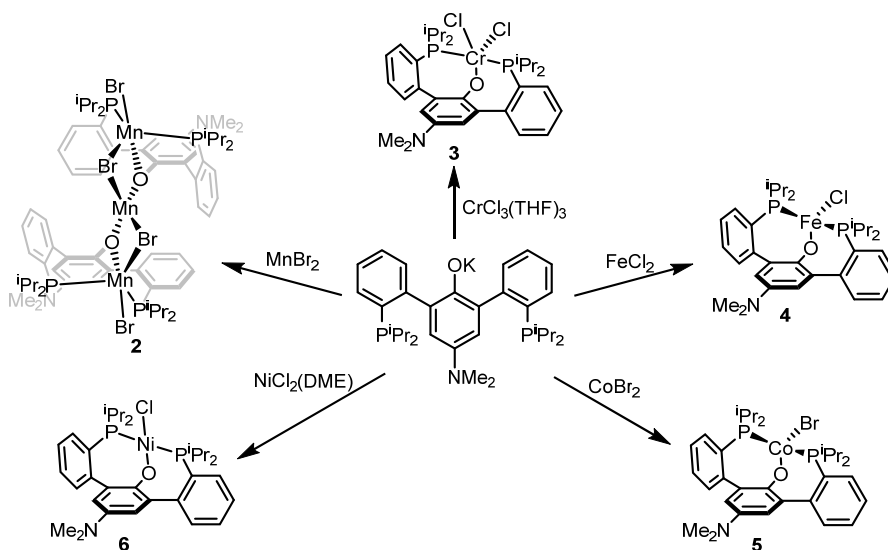


the benzyl-protected terphenyl dibromide. This dibromide was then phosphinated via a lithium-halogen exchange and quenching with chlorodiisopropylphosphine to provide the benzyl-protected diphosphine. Initial efforts towards benzyl group deprotection proved to be particularly challenging, with conventional methods such as hydrogenation with 10 wt% Pd/C or Pearlman's catalyst ($\text{Pd}(\text{OH})_2/\text{C}$) being ineffective in engendering benzyl cleavage. Only under the more forcing reducing conditions of catalytic sodium naphthalenide was deprotection successfully effected to provide **1-H**. Under those conditions, care also needs to be taken to limit the reaction time as prolonged stirring also led to detrimental reductive P–C bond cleavage and formation of phosphine side products. P–C bond cleavage has been reported under similar conditions with alkali metals, including Na, in THF.⁵⁰

Synthesis of first-row transition metal complexes

Metal complexes of Cr(III), Mn(II), Fe(II), Co(II), and Ni(II) were prepared by the reaction of their corresponding metal halides with the terphenyl diphosphine phenoxide proligand (henceforth abbreviated as POP), formed via initial deprotonation of **1-H** by benzyl potassium. The metalations were all carried out in THF except **3** wherein dichloromethane

Scheme 2.2. Synthesis of complexes **2-6**



was used. Reprecipitation of the residue from benzene/pentane yielded the desired metallated complexes as powders.

With Mn(II) bromide, using a 1:1 stoichiometry of ligand to metal halide did not lead to complete consumption of ligand even after stirring for 12 hours. Instead of a monometallic complex, a trimetallic complex **2** wherein a MnBr_2 moiety bridges two $\text{MnBr}(\text{POP})$ units through the phenolate oxygen was formed (Scheme 2.2). This may stem from the slow rate of metalation, which in turns provide a longer window for the $\text{Mn}(\text{POP})$ complex to react with MnBr_2 still present to form the bridged trimetallic species. This complex does not go on to react with the excess ligand to yield the targeted monometallic complexes even with extended stirring times. Rationally using a 3:2 ratio of MnBr_2 to **1-K** led to the formation of **2** in good yields. In the ^1H NMR spectrum, predominantly broad paramagnetically shifted peaks were observed for **2**. This bridging moiety also suggests that the metallated phenoxide is still able to act as a competent Lewis base, which could be leveraged as a means to tune the electronic nature of the phenoxide donor, and by extension reactivity of the complex, by the addition of extraneous Lewis acids.

With Cr(III), Fe(II), Co(II), and Ni(II), monometallic complexes with the ligand binding through the phenolate oxygen and both phosphine arms were obtained from the respective metalations (Scheme 2.2). From the ^1H NMR spectra, broad paramagnetically-shifted peaks were observed with $\text{CrCl}_2(\text{POP})$ (**3**), while slightly sharper paramagnetically-shifted peaks were observed for $\text{FeCl}(\text{POP})$ (**4**) and $\text{CoBr}(\text{POP})$ (**5**). The ^1H NMR spectra of $\text{NiCl}(\text{POP})$ (**6**) showed the presence of a diamagnet, and a single resonance was observed in the ^{31}P NMR at 13.57 ppm. The diamagnetic nature of this species supports a square planar ligand coordination environment around a Ni(II) center.

Solid-state characterization

Single crystals suitable to X-ray diffraction (XRD) of complex **2** was obtained by slow vapor diffusion of pentane into a saturated THF solution of **2** while those of complexes **3-6** were obtained by slow vapor diffusion of pentane into saturated benzene solutions of the complexes. The solid-state structure of Mn(II) complex **2** is shown in Figure 2.2. A MnBr₂ moiety (Mn3, Br2, Br4) bridges two moieties of diphosphine phenoxide-bound manganese bromide through Mn1/Mn2 and O1/O2. The geometry around Mn1 and Mn2 are both trigonal bipyramidal, with the oxygen and non-bridging bromide atoms occupying the axial positions. The geometry around the bridging manganese (Mn3) is a highly distorted square planar ($\tau^2_4 = 0.402$),⁵¹ with Br2 and Br4 *cis* to each other. This represents a rare example of a

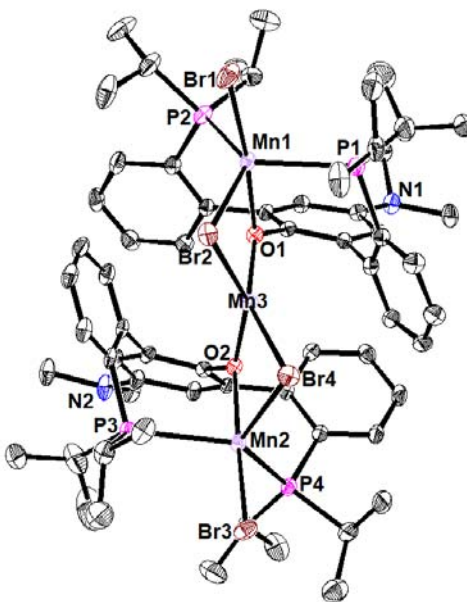


Figure 2.2. Solid-state structure of **2**. Thermal ellipsoids shown at 50% probability. Solvent molecules and hydrogen atoms omitted for clarity. Relevant bond distances (Å) and angles(°): (2) Mn1–O1 2.148(3), Mn1–P1 2.6825(12), Mn1–P2 2.6928(13), Mn1–Br1 2.5370(8), Mn1–Br2 2.6490(8), Mn2–O2 2.141(3), Mn2–P3 2.7138(12), Mn2–P4 2.6485(13), Mn2–Br3 2.5362(8), Mn2–Br4 2.6562(8), Mn3–O1 2.0473(3), Mn3–O2 2.025(3), Mn3–Br2 2.5674(8), Mn3–Br4 2.5837(8), \angle P1–Mn1–P2 123.54(4), \angle P3–Mn2–P4 126.21(4), \angle Br1–Mn1–O1 173.81(8), \angle Br3–Mn2–O2 176.96(8).

square planar manganese(II) motif not ligated by a rigid ligand such as a pincer or macrocycle. The distortion from planarity is likely due to sterics imposed by the POP ligands, forcing the square planar coordination environment to twist in order to minimize the steric clash between phenylene arms of opposing ligands.

The solid-state structures of **3-6** are shown in Figure 2.3 and their relevant structural metrics in Table 2.1. The solid-state structure of **3** revealed a five-coordinate Cr center bound to both phosphine arms, the phenoxide and two chloride ligands. In contrast to five-coordinate Mn centers in complex **2**, the geometry of about the chromium center in **3** is that

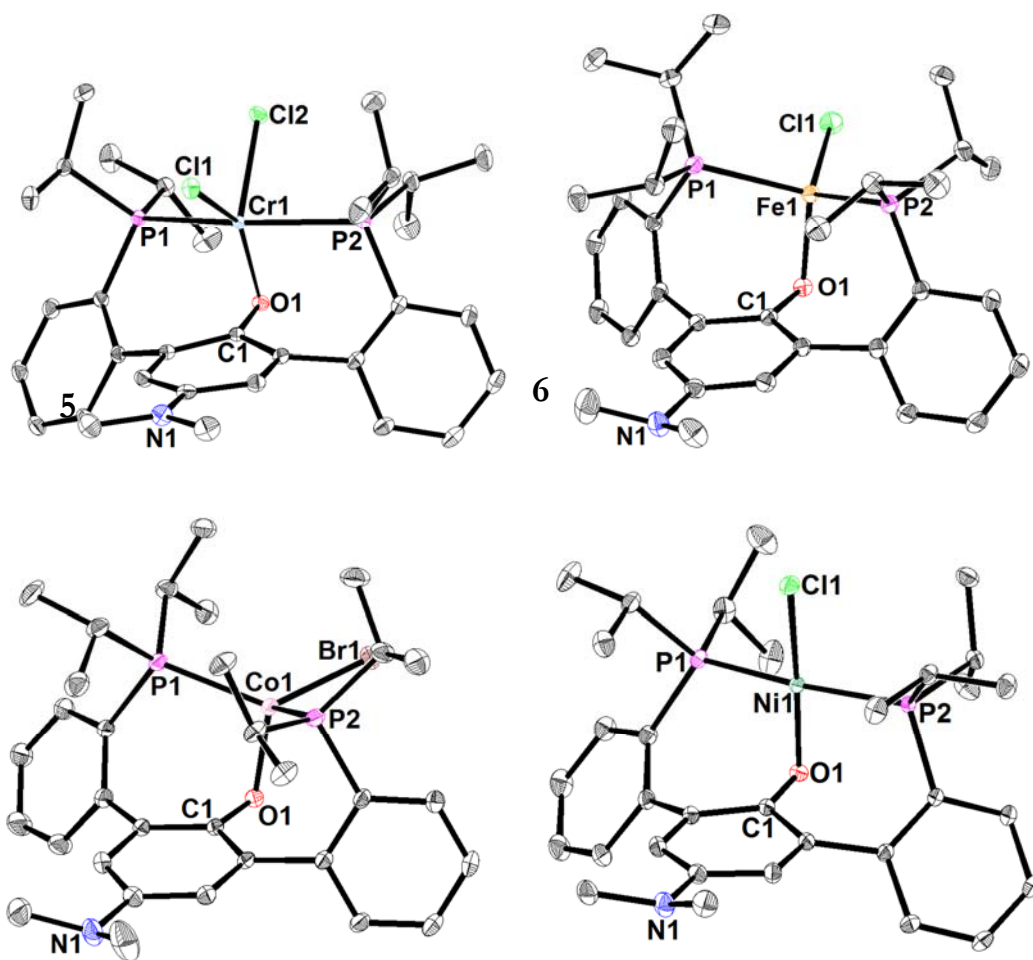


Figure 2.3. Solid-state structures of **3-6**. Thermal ellipsoids shown at 50% probability. Solvent molecules and hydrogen atoms omitted for clarity.

of a distorted square pyramidal ($\tau_5 = 0.24$),⁵² with Cl1 occupying the axial position. O1 and Cl2 lie below the basal plane with deviations of 0.648 Å and 0.332 Å, while P1 and P2 lie above the plane with deviations of 0.479 Å and 0.502 Å, respectively. This geometry also results in a rather acute C1–O1–Cr1 angle (82.25(6)°) and a relatively short Cr1–C1 distance (2.2245(12) Å). This suggests that there may be some amount of delocalization of the negative charge of the phenoxide into the central ring with the Cr binding to the C–O moiety through a π -bond. However, lack of significant bond localization within the central ring, < 0.05 Å difference in C–C bonds lengths *vs.* 0.11 Å difference in a reported Rh cyclohexadienone complex,⁴³ indicates that this resonance contribution is minimal and that the short Cr1–C1, is more likely due to a geometrical constraint.

The solid-state structures of **4** and **5** both showed distorted tetrahedral geometries about the iron and cobalt centers with τ_4' values of 0.830 and 0.844, respectively, bound to both phosphines, the phenoxide oxygen, and a halide ligand. Due to the geometrical constraint imposed by the POP ligand, the P1/P2–M1–O1 angles are contracted significantly from ideal in complex **4**, slightly less so in complex **5**. Compared with **4**, the metal center in **5** also sits further out from the POP ligand “pocket”, as evidenced by the smaller P1–Fe1–P2 and larger

Table 2.1. Selected structural metrics for complexes **4-7**

Distance (Å)/angle (°)	4 CrCl ₂ (POP)	5 FeCl(POP)	6 CoBr(POP)	7 NiCl(POP)
^a M1–X1	2.3006(3)	2.2502(5)	2.3832(3)	2.1778(2)
M1–Cl2	2.3143(4)	-	-	-
M1–O1	1.9587(9)	1.8938(13)	1.8971(13)	1.8813(6)
M1–P1	2.4932(4)	2.4350(6)	2.3743(5)	2.2244(3)
M1–P2	2.5324(4)	2.4426(5)	2.3480(6)	2.2300(2)
P1–M1–P2	156.51(1)	117.39(2)	123.90(2)	167.58(1)
P1–M1–O1	83.74(3)	100.72(4)	97.82(4)	88.05(2)
P2–M1–O1	85.37(3)	94.06(4)	105.05(4)	89.71(2)
C1–O1–M1	85.25(6)	111.3(1)	104.5(1)	93.53(5)

^aX = Cl1 (**4**, **5**, **7**), Br1 (**6**).

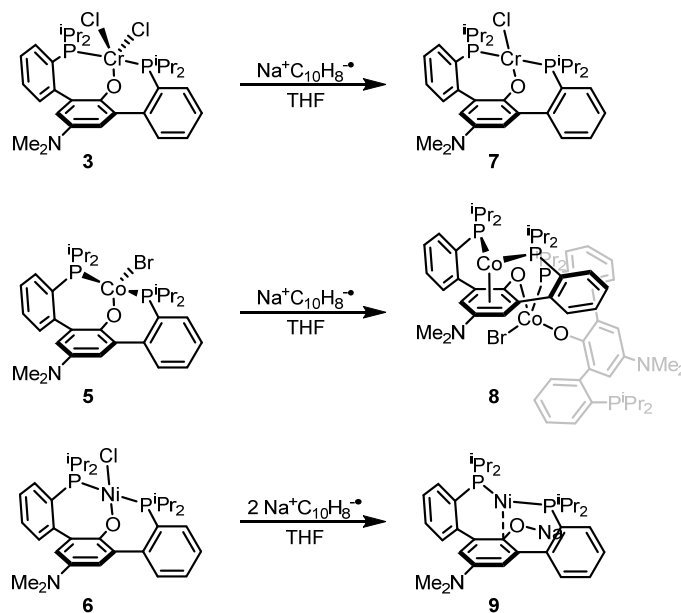
C1–O1–Co1 angles, probably due to the larger steric profile of bromine compared to chlorine.

In the solid-state structure of Ni(II) complex **6**, the metal center is ligated to both phosphine arms, the phenoxide oxygen, and a chloride. The geometry around the Ni center is square planar ($\tau_4' = 0.098$), consistent with the diamagnetic species observed by NMR spectroscopy. Due to the constraint the square planar geometry imposes on the Ni center, a short Ni1–C1 distance (2.3798(8) Å) and acute Ni1–O1–C1 angle (93.53(5)°) were observed in the structure, similar to that in complex **3**.

Reduction of complexes 3-6

We were interested to explore reductions of monometallic complexes **3-6** in order to probe the ability of the POP ligand to support variations in metal oxidation states (Scheme 2.3). Reduction of chromium complex **3** in THF with one equiv. of sodium naphthalenide resulted in the formation of a green-brown material that was NMR silent. Further addition of a second equiv. of reductant did not result in significant changes in the NMR spectrum. Green crystals suitable for single-crystal XRD were grown by vapor diffusion of pentane into a

Scheme 2.3. Reduction of complexes **3**, **5**, and **7**



saturated benzene solution. The solid-state structure revealed the product of reduction to be a monometallic Cr(II) complex (**7**) (Figure 2.4) generated from a one-electron reduction of **3**. The geometry around Cr1 is square planar ($\tau_4' = 0.082$), similar to that in Ni(II) complex **6**. As with **6**, a short Cr1–C1 distance (2.3161(3) Å) and an acute Cr1–O1–C1 angle were present. When CoCp₂ was used instead as a reductant, free ligand was observed to form via ³¹P and ¹H NMR spectroscopy, suggesting some decomposition.

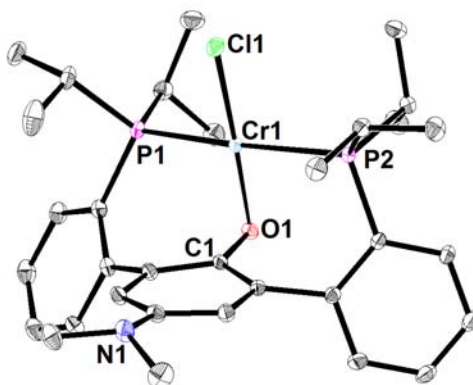


Figure 2.4. Solid-state structure of **7**. Thermal ellipsoids shown at 50% probability. Solvent molecules and hydrogen atoms omitted for clarity. Relevant bond distances (Å) and angles (°): Cr1–O1 1.9897(7), Cr1–P1 2.4548(3), Cr1–P2 2.4644(3), Cr1–Cl1 2.3673(9), \angle Cr1–O1–C1 88.27(5).

Reductions were attempted with Fe complex **4** using a variety of reductants (cobaltocene, sodium naphthalenide, sodium-mercury amalgam, and potassium graphite). Under these conditions, intractable mixtures showing no significant paramagnetic peaks, accompanied by significant amounts of free ligand, were obtained. These observations indicate that the reduced iron species were likely unstable and that decomposition *via* demetalation upon reduction was taking place.

Reduction of Co complex **5** with one equiv. of sodium naphthalenide in a thawing THF solution resulted in an immediate purple to red color change and the observation of a new paramagnetic species in the ¹H NMR spectrum. Single crystals suitable for XRD were

grown from vapor diffusion of pentane into a saturated benzene solution. In the solid-state structure of complex **8**, an asymmetric dicobalt species is observed wherein one of the cobalt centers (Co1) has lost a bromide ligand and has shifted to bind to the central arene in an η^6 -fashion while the second cobalt center (Co2) is now bound to only one phosphine (P3), two phenoxides (O1, O2), and a bromide (Figure 2.5). Overall, this represents a one-electron reduction per two molecules of **5**. However, repeating the reaction and allowing for extended stirring with the remaining reductant did not lead to further reaction, suggesting that, once formed, the formally Co(II) center in **8** (Co2) is stable to excess naphthalenide. The geometry around Co2 is tetrahedral ($\tau_4' = 0.877$), while Co1 takes on a two-legged piano stool geometry. The central arene bound to Co1 is slightly puckered with C1 and C4 further away (2.258(4) - 2.294(4) Å) and C2, C3, C5, and C6 closer to the metal center (2.058(4) – 2.098(4) Å), which could indicate ligand non-innocence behavior. However, the absence of C–C bond

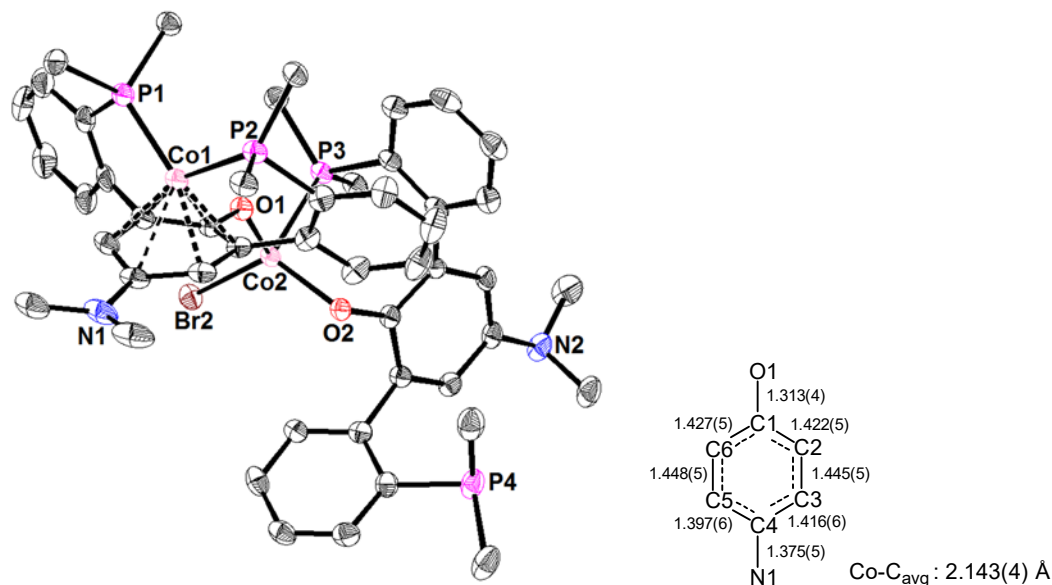


Figure 2.5. Solid-state structure of **8**. Thermal ellipsoids shown at 50% probability. Solvent molecules, *iso*-propyl methyls, and hydrogen atoms omitted for clarity. Relevant bond distances (Å) and angles (°): Co1–P1 2.1934(11), Co1–P2 2.2257(12), \angle P1–Co1–P2 110.31(4). Central arene bond lengths shown in Å.

localization within the central arene and the lack of shortening of C1–O1 and/or C4–N1 would suggest that no significant redox changes are occurring at the ligand.

Reduction of nickel complex **6** with two equiv. of sodium naphthalenide resulted in a rapid color change from deep green to brown. A new diamagnetic species was observed by NMR spectroscopy with a ^{31}P resonance at 38.5 ppm. The product was revealed by single crystal XRD to be a nickel(0) diphosphine complex **9** (Figure 2.6). Upon reduction, the nickel center shifts from the phenoxide oxygen to bind to the adjacent of the central arene (C1). Two POP units are present in the unit cell (space group $P\bar{1}$) related by an inversion center. The two phenoxides are bridged by two sodium ions generating a diamond core.

Lewis acid effects on ligand coordination mode

The binding mode changes in both complexes **8** and **9** from the hard phenoxide donor to the softer central arene donor upon reduction of the bound metal center demonstrates the coordinative flexibility of the POP ligand to accommodate a variety of electronic states. Additionally, in both examples, the binding mode changes are accompanied by the association

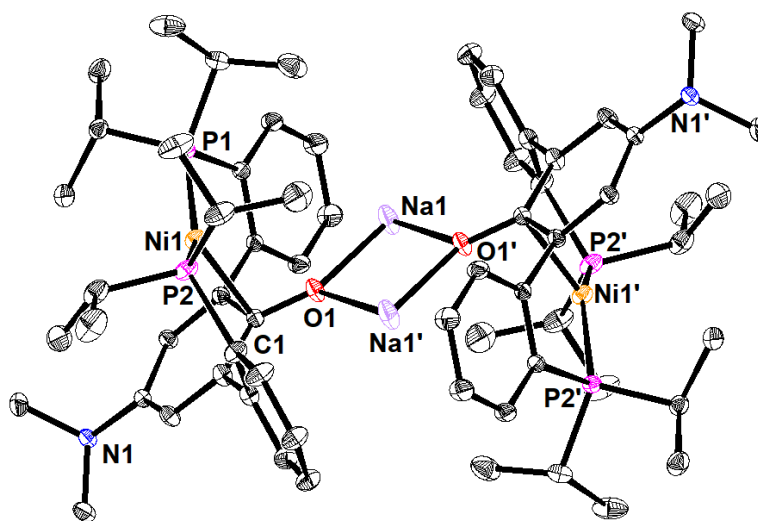


Figure 2.6. Solid-state structure of **9** (grown). Thermal ellipsoids shown at 50% probability. Solvent molecules and hydrogen atoms omitted for clarity. Relevant bond distances (Å) and angles (°): Ni1–P1 2.1300(3), Ni1–P2 2.1469(3), Ni1–C1 2.0636(11), $\angle\text{P1–Ni1–P2}$ 141.92(1).

of a Lewis acid moiety at the phenoxide oxygen (either a Co(II) center or a sodium ion). In order to further probe the effects of redox changes and presence of Lewis acid motifs on the coordination mode of this ligand framework, iron chloride complex **4** and its triflate analog **10** were further studied in greater detail.

Synthesis of triflate complex **10** was accomplished in a similar manner to complex **4** by the reaction of **L-K** with 1.1 equiv. $\text{Fe}(\text{OTf})_2(\text{MeCN})_2$ in THF, yielding an orange microcrystalline solid. Paramagnetically-shifted peaks were observed in the ^1H NMR spectra along with a broad signal in the ^{19}F NMR spectrum (13.2 ppm), suggesting the presence of an interaction of the triflate counterion with the metal center. To probe the solution-state magnetic moments, measurements were determined by the Evans method⁵³⁻⁵⁵ to be $4.5 \mu_{\text{B}}$ and $4.6 \mu_{\text{B}}$ for **4** and **10**, respectively, indicative of a tetrahedral d^6 high-spin electronic configurations ($S = 2$) in both complexes. Structural characterization by single-crystal XRD

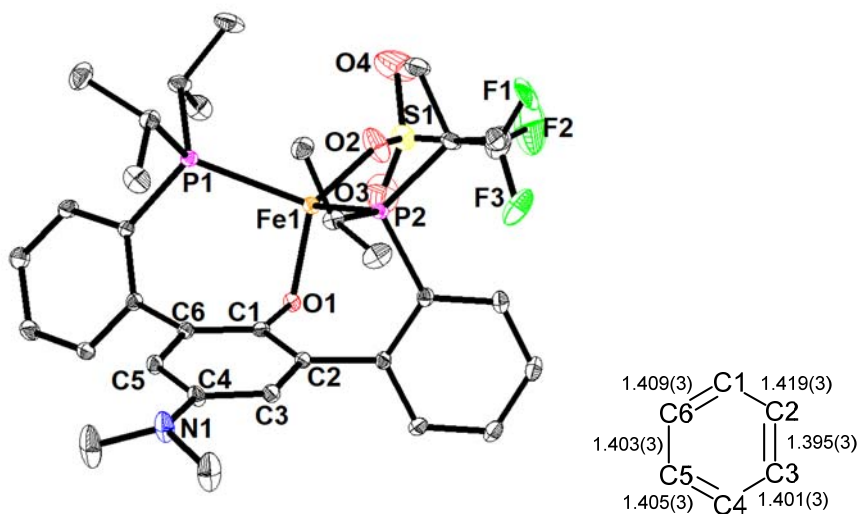
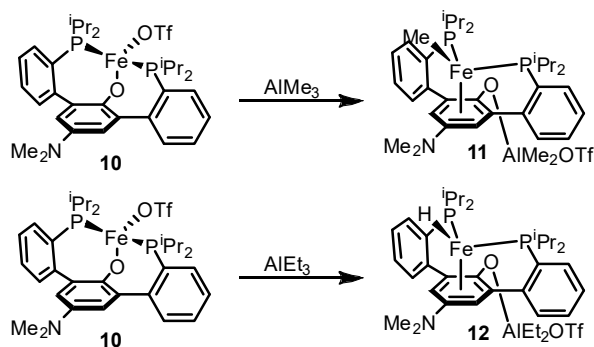


Figure 2.7. Solid-state structures (left), and central arene bond metrics (right) of **10**. Thermal ellipsoids shown at 50% probability. Solvent molecules and hydrogen atoms omitted for clarity. Relevant bond lengths (\AA) and angles ($^\circ$): Fe1-O2 1.985(2), Fe1-P1 2.4451(6), Fe1-P2 2.4451(8), Fe1-O1 1.875(1), C1-O1 1.357(2), C4-N1 1.412(3), $\angle\text{Fe1-O1-C1}$ 108.8(1).

was obtained for **10** (Figure 2.7), revealing a distorted tetrahedral geometry around the iron center, with binding to the phenolate, both phosphines, and the triflate, the latter being consistent with the broad signal observed in the ^{19}F spectrum. the P1/2-Fe-O1 angles ($\sim 100^\circ$) are contracted from ideal, likely a result of the geometrical constraints of the POP pincer.

The reactivities of **4** and **10** towards exogenous Lewis acids that might coordinate to the phenolate oxygen was investigated. We anticipate that such reactivity would weaken the Fe–O bond and facilitate a coordination mode change, allowing the metal center to slip to bind to the central arene. The reaction of **10** with trimethylaluminum (Scheme 2.4) resulted in the formation of a new diamagnetic species by ^1H NMR and $^{31}\text{P}\{^1\text{H}\}$ spectroscopy. A peak corresponding to a methyl resonance was observed at -0.5 ppm in the ^1H NMR spectrum while a singlet at 65.09 ppm. Solid-state characterization showed the formation of iron methyl complex **11** that resulted from a ligand exchange between iron and aluminium (Figure 2.8). The phenoxide oxygen is bound to an AlMe_2OTf group while the iron center slips to bind to the central arene in an η^6 -fashion. The central arene retains aromaticity with relatively uniform C–C bond distances. Slight puckering of the central arene is present, with shorter longer Fe–C1/C4 distances compared with the other carbons in the ring. The reaction of **10** with triethylaluminium did not yield an analogous iron ethyl complex (Scheme 2.4). Instead, ^1H NMR spectroscopy revealed a new species **12** showing a triplet signal with a chemical shift of

Scheme 2.4. Reaction of **10** with trialkylaluminiums



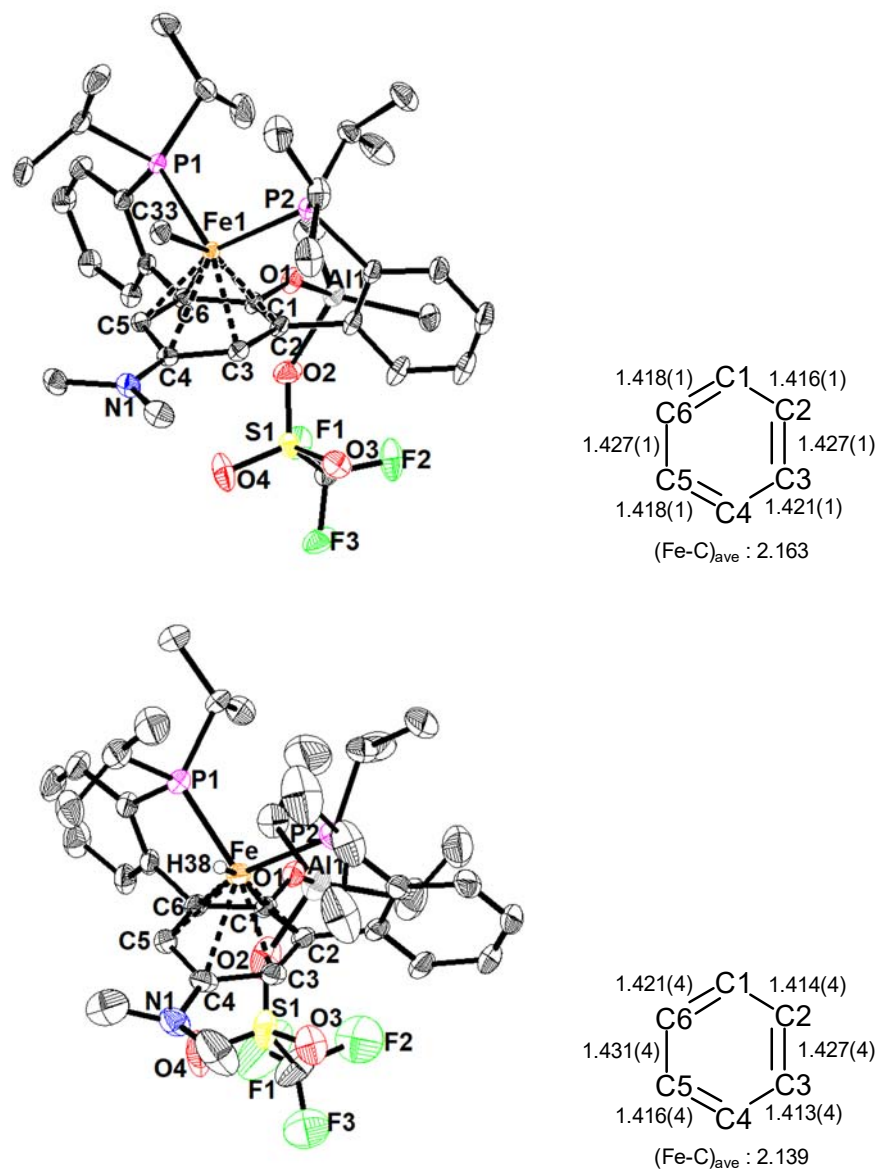


Figure 2.8. Solid-state structures (left), and central arene bond metrics (right) of **11** and **12**. Thermal ellipsoids shown at 50% probability. Solvent molecules and hydrogen atoms omitted for clarity. Relevant bond lengths (Å) and angles (°): **11** Fe1–P1 2.3132(3), Fe1–P2 2.3193(3), Fe1–C33 2.0529(9), C1–O1 1.319(1), C4–N1 1.350(1), \angle P1–Fe1–P2 107.14(3); **12** Fe1–P1 Fe1–H38 1.20(6), C1–O1 1.327(4), C4–N1 1.381(4), \angle P1–Fe1–P1 104.10(6) 2.251(2).

–10.25 ppm that integrated to one proton and is consistent with other reported iron hydrides in the literature.⁵⁶ The triplet multiplicity arises from coupling with the two phosphine arms and displays a $^2J_{\text{PH}}$ value of 83.2 Hz typical of similar reported diphosphine iron hydride

complexes.⁵⁷ In the $^{31}\text{P}\{^1\text{H}\}$ NMR spectrum, a broad singlet was observed at 91.40 ppm, and upon selectively coupling the hydridic proton signal, this resonance then appears as a broad doublet with $^2J_{\text{PH}}$ of 74.2 Hz, similar to that for the corresponding hydride in the ^1H NMR spectrum.

Crystals suitable for single crystal XRD revealed the identity of **12** as iron hydride complex (Figure 2.8). The iron center that binds through the central arene moiety in an η^6 -fashion, with relatively uniform C–C bond distances in the arene ring and average C–Fe distances of (2.139 Å). As with **11**, slight puckering of the central arene is present, with C1/4–Fe1 bonds being the longest (2.19–2.25 Å) and C2/6–Fe1 being the shortest (2.08 Å), likely due to the constraint placed upon it by the phosphine arms. From the residual electron density in the Fourier transform map, a hydride bound to iron could also be located. The Fe–H distance of 1.20(6) Å is relatively short compared to other iron hydrides in the literature but isn't unique.⁵⁸

The presence of the hydride, alongside an AlEt_2OTf group bound to the phenolate oxygen suggests that initial alkylation at the iron center, as with **11**, is followed by a β -hydride elimination that generates complex **12**. This was further supported by the presence of ethylene gas that is formed via elimination of the ethyl ligand, detected by ^1H NMR both in the reaction mixture and upon vacuum transfer of the volatile reaction products into a J-Young tube. It has been proposed that the availability of empty d-orbitals facilitate β -hydride elimination in Fe(II) low spin complexes.^{59–60} This observation along with their solid-state structures agrees well with the diamagnetic nature and electronic configuration of complexes **11** and **12** (pseudo-octahedral d^6 low spin). Additionally, shortening of the C4–N1 bond distance was observed upon slippage of the iron center from the phenolate oxygen to the arene (from 1.415(2) Å in **10** to 1.350(1) Å **11** and 1.381(4) Å **12**), suggesting contribution of the N-lone pair into the more

electron deficient central arene.

The reaction of iron chloride complex **4** with AlEt₃ did not afford the analogous hydride complex. Instead, a paramagnetic species was observed by ¹H NMR spectroscopy. Solid-state characterization by single crystal XRD showed the formation of adduct **13**, wherein AlEt₃ binds through the phenolate oxygen (Figure 2.9). The lack of exchange with the chloride moiety could be attributed to the stronger coordination of the chloride group to the iron center compared with the triflate group in **10**. Coordination of the Al Lewis acid to the phenolate did not result in a change in ligand binding mode like in **11/12**, suggesting that the identity of the ancillary ligand (H/alkyl vs. Cl) affects the preferred coordination mode. However, Al coordination at the phenolate does result in the weakening and lengthening of the Fe–O1 bond (from 1.8932(9) Å in **4** to 1.960(1) Å in **13**), suggesting that both factors are significant in determining the preferred ligand binding mode. The solution-state magnetic moment of **4** was determined to be 4.7 μ_B, consistent with a d⁶ high spin complex (S=2),

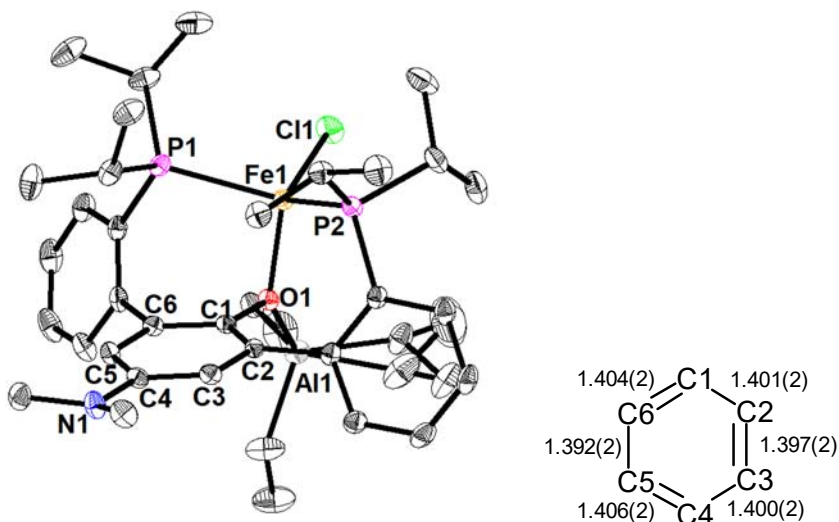


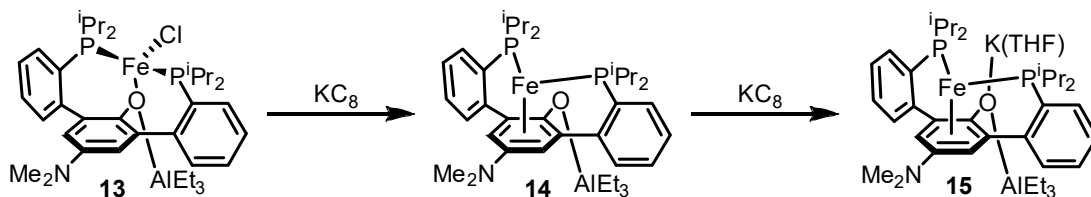
Figure 2.9. Solid-state structure (left), and central arene bond metrics (right) of **13**. Thermal ellipsoids shown at 50% probability. Solvent molecules and hydrogen atoms omitted for clarity. Relevant bond lengths (Å) and angles (°): Fe1–P1 2.4586(4), Fe1–P2 2.4688(4), Fe1–O1 1.960(1), Fe1–Cl1 2.2279(4), C1–O1 1.386(1), C4–N1 1.383(2), ∠Fe1–O1–C1 108.20(7).

consistent with the solid-state structure.

Next, investigation of the effect of metal oxidation state on ligand coordination mode of these Lewis acid adducts was carried out. Reduction of the iron center would be expected to render it a softer ion, potentially engendering a binding mode change from the hard phenoxide donor to the softer arene donor. As described in the previous section, reduction of iron chloride complex **4** under a variety of conditions led to either decomposition to free ligand or NMR-silent species which have eluded further characterization. We hypothesized that the presence of a Lewis acidic moiety could facilitate binding mode change by coordination to the anionic phenolate oxygen, quenching the negative charge resulting from a one-electron reduction and stabilizing the consequential slippage of the iron center to the central arene. This observation is consistent with the two examples of reduction induced coordination mode changes (on Co complex **8** and Ni complex **9**).

Reduction of AlEt₃ adduct **13** with one equiv. of KC₈ led to the formation of a dark yellow paramagnetic product (Scheme 2.5). Slow diffusion of pentane into a saturated THF solution provided dichroic yellow-brown rod-shaped crystals suitable for single crystal XRD. The solid-state characterization revealed the solid to be Fe(I) complex **14** (Figure 2.10). In the structure, the iron center is bound to both phosphines, and to the central arene in an η⁶-fashion. The central arene shows relatively uniform arene C–C bond lengths. Puckering of the central arene and contraction of the C4–N1 distance similar to that in **11** and **12** were also observed. The coordination geometry around iron can be described as a two-legged piano

Scheme 2.5. Stepwise reduction of **13**



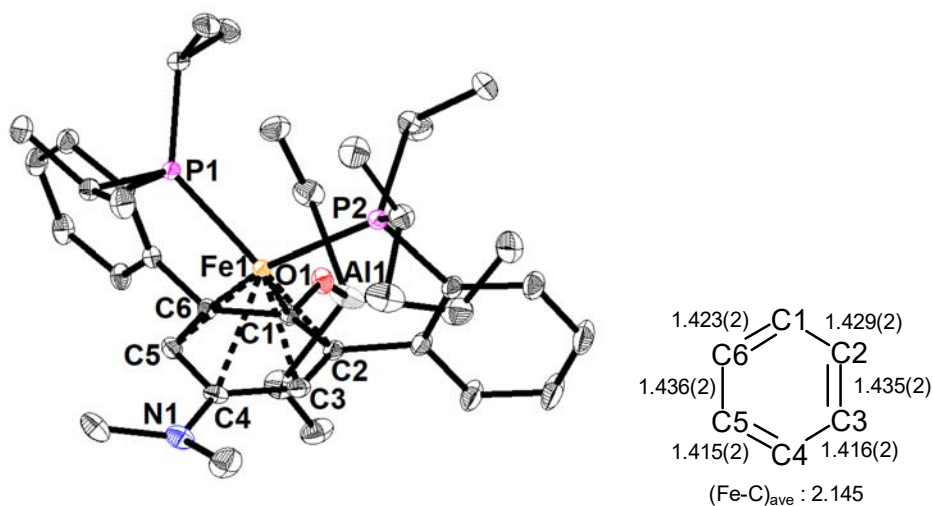


Figure 2.10. Solid-state structures (left), and central arene bond metrics (right) of **14**. Bond distances in Å and angles in °. Thermal ellipsoids shown at 50% probability. Solvent molecules and hydrogen atoms omitted for clarity. Relevant bond lengths (Å) and angles (°): Fe1–P1 2.2716(5), Fe1–P2 2.2495(4), C1–O1 1.311(2), C4–N1 1.375(2), \angle P1–Fe1–P1: 110.10(2)

stool. There have only been two previously reported examples of iron bound to a diphosphine and an untethered arene in a similar geometry,⁶¹⁻⁶² but this is the first example in which both the arene and phosphine moieties are part of the same chelate. Solution-state magnetic susceptibility determined by the Evans method provided a value of $2.8 \mu_B$, or $S = 1$, an unusual value for a Fe(I) complex. Variable temperature (VT) Evans method⁶³ measurement from -80 °C to 70 °C show no significant change in its magnetic moment, suggesting that a spin-crossover transition is not occurring between those temperatures.

The reaction of **14** with an additional equiv. of KC_8 resulted in a new diamagnetic species **15** observed by 1H and ^{31}P NMR spectroscopy (Scheme 2.5). Both spectra featured broad, poorly resolved peaks reminiscent of the potassium phenolate salt **L-K**. The solid-state identity of the complex was confirmed by single crystal XRD, showing the formation of Fe(0) complex **15** (Figure 2.11). The iron center is observed to retain η^6 -binding to the central arene while the additional K ion coordinates to the phenoxide oxygen. The crystal structure also

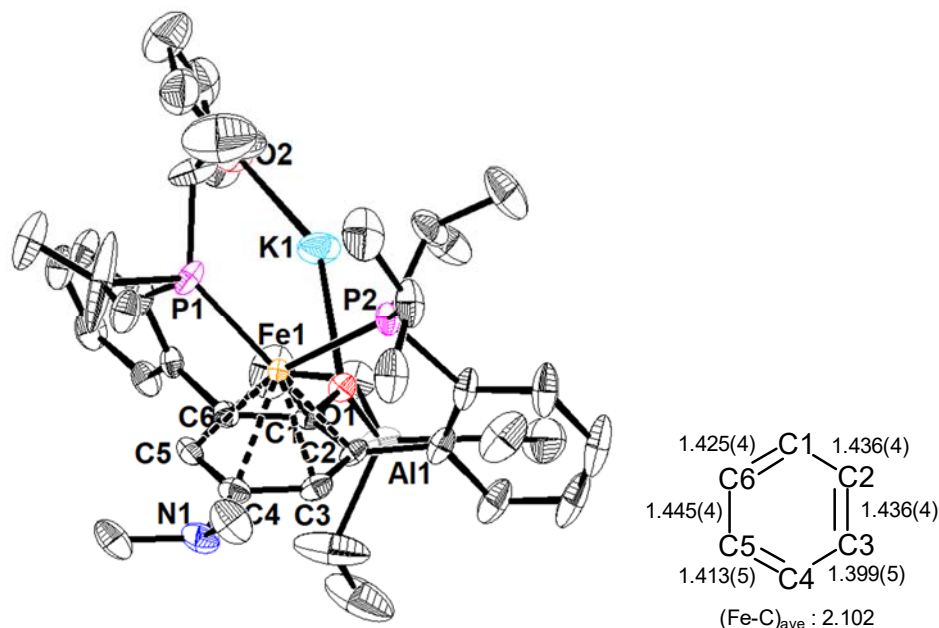


Figure 2.11. Solid-state structures (left), and central arene bond metrics (right) of **15**. Bond distances in Å and angles in °. Thermal ellipsoids shown at 50% probability. Solvent molecules and hydrogen atoms omitted for clarity. Relevant bond lengths (Å) and angles (°): Fe1–P1 2.2005(9), Fe1–P2 2.2086(9), C1–O1 1.352(4), C4–N1 1.434(4), \angle P1–Fe1–P1: 107.32(4) reveals the formation of a coordination polymer, where the amine moiety coordinates to the potassium ion of an adjacent molecule, which if similar oligomeric structures persist in solution may account for the peak broadening observed in the NMR spectra.

Exploring if similar reactivity can be achieved with other Lewis acids. The reaction of triflate complex **10** with NaHBET_3 resulted in the formation of a Fe hydride complex **16** that shows very similar features to **12** with a hydride triplet at -11.12 ppm ($J = 80.8$ Hz). Seeing that boron-based Lewis acids appear capable of engendering similar reactivity, a boron analog of **15** was targeted. Addition of BEt_3 to iron chloride complex **4** followed by reaction with two equiv. KC_8 resulted in the formation of an NMR silent paramagnetic green species. Solid-state analysis by single crystal XRD showed the formation of Fe(0) complex **17** (Figure 2.12). Only a potassium ion was observed to be bound at the phenolate, in contrast to that in **15**

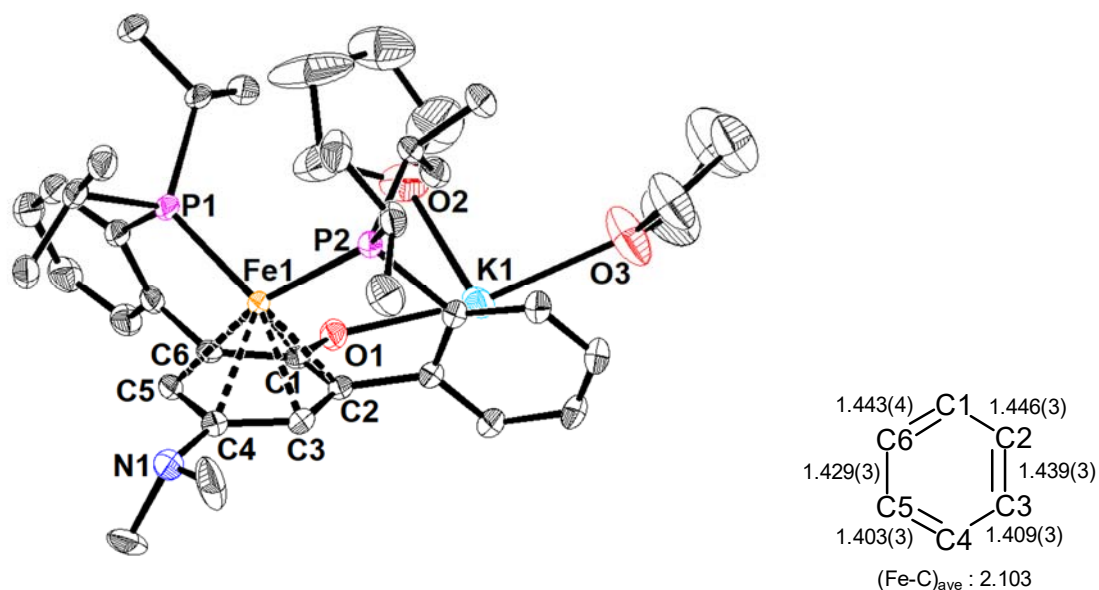


Figure 2.12. Solid-state structures (left), and central arene bond metrics (right) of **17**. Bond distances in Å and angles in °. Thermal ellipsoids shown at 50% probability. Solvent molecules and hydrogen atoms omitted for clarity. Relevant bond lengths (Å) and angles (°): Fe1–P1 2.1800(6), Fe1–P2 2.1917(6), C1–O1 1.292(3), C4–N1 1.439(3), ∠P1–Fe1–P1: 106.29(2)

where the initially coordinated Lewis acid stays bound. Although the BEt_3 does not stay bound, it appears to be crucial in stabilizing the intermediate on route to the Fe(0) complex, since in its absence, significant decomposition was observed (*vide supra*). Notably, C1 is canted downwards away from the Fe center, with a significantly longer Fe–C1 (2.232(2) Å) bond compared to the other ring carbons. Additionally, looking at the central ring bond metrics, slight disruption of the aromaticity is observed, with significantly longer C1–C2 and C1–C6 distances. Along with a shorter C1–O1, it suggests some delocalization of O-lone pair into the ring, with the negative charge spread out between C2 to C6. The subtle electronic difference in the iron coordination environment also results in a high-spin complex, distinct from **15**. Further reactivity studies with boron-based Lewis acid are ongoing.

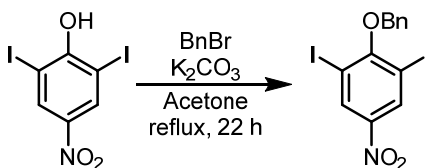
CONCLUSION

The synthesis of a novel *meta*-terphenyl diphosphine pincer-like proligand bearing a central aminophenol and subsequent metalations with first-row transition metal halides ranging from Cr to Ni have been demonstrated. This ligand is observed to bind to the metal centers via both phosphine arms and the phenoxide. The phenoxide moiety is slightly Lewis basic, and in the case with MnBr_2 , metalation resulted in the formation of a trimanganese complex with a MnBr_2 moiety bridging through phenoxide oxygen atoms of two $\text{MnBr}(\text{POP})$ units. Reductions of monometallic complexes **3-6** were carried out. With Cr(III) complex **3**, a one-electron reduction provided monochloride Cr(II) complex **7**. Reductions of cobalt complex **5** and nickel complex **6** resulted in binding mode changes from the phenoxide to the central arene in η^6 and η^1 fashions, respectively. Further studies on POP-supported iron complexes demonstrate that aluminium-based Lewis acid coordination to the phenolate can effect coordination mode changes. Lewis acid coordination to the phenolate was also found to stabilize reduction on the iron center allowing Al-bound adducts of Fe(I) and Fe(0) complexes to be isolated and characterized. With triethylborane coordination, reduction to Fe(0) provided borane-free Fe(0) complex, suggesting that even if the Lewis acid does not ultimately stay bound, its transient coordination is still crucial for stabilizing the reduction and/or binding mode changes, potentially at the Fe(I) state. The coordination environment was found to depend on the oxidation state of the iron center, and/or the identity of other ancillary ligands bound to iron, demonstrating the flexibility of this ligand framework. While the POP binding mode supports high spin Fe(II) complexes, the P-arene-P binding mode tends to favor the formation of low spin Fe complexes (with some exceptions) and is capable of supporting a variety of iron oxidation states.

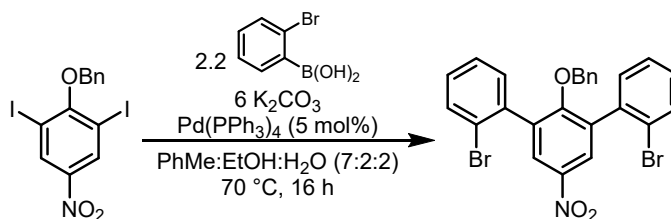
EXPERIMENTAL SECTION

General Considerations

Unless otherwise specified, all operations involving air- or water-sensitive reagents were carried out in an MBraun drybox under a nitrogen atmosphere or using standard Schlenk and vacuum line techniques. Solvents for air- and moisture-sensitive reactions were dried by the method of Grubbs.⁶⁴ Deuterated solvents were purchased from Cambridge Isotope Laboratories and vacuum transferred from sodium benzophenone ketyl (C_6D_6) or calcium hydride ($CDCl_3$) before use. All solvents, once dried and degassed, were stored under an inert atmosphere over 4 Å molecular sieves. 2,6-diiodonitrophenol,⁴⁸ benzyl potassium,⁶⁵ potassium graphite,⁶⁶ were prepared according to literature procedures. Sodium naphthalenide solution was prepared by stirring a THF solution of naphthalene in the presence of a sodium mirror for 30 min, filtered through a glass-fiber filter plug and used immediately. All other reagents were used as received. Pre-reduced Teflon-coated stir bars (prepared via stirring a $Na[C_{10}H_8]$ solution overnight followed by rinsing three times with THF) were utilized in any stirred reaction in which KC_8 or naphthalenide is employed. 1H , $^{13}C\{^1H\}$, ^{19}F NMR, and $^{31}P\{^1H\}$ NMR spectra were recorded on Varian Mercury 300 MHz or Varian 400 MHz spectrometers at ambient temperatures unless otherwise denoted. 1H and $^{13}C\{^1H\}$ NMR spectra are reported referenced internally to residual solvent peaks reported relative to tetramethylsilane. ^{19}F NMR chemical shifts are referenced to an external standard of C_6F_6 (-164.9 ppm). ^{31}P NMR chemical shifts are referenced to an external standard of 85% H_3PO_4 (0.0 ppm). Fast atom bombardment-mass spectrometry (FAB-MS) analyses were performed with a JEOL JMS-600H high-resolution mass spectrometer.



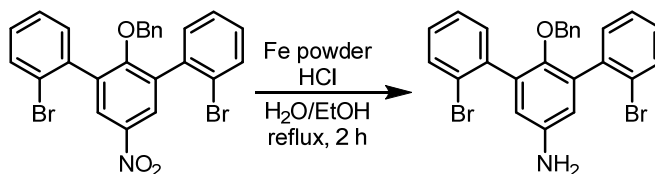
2-(benzyloxy)-1,3-diiodo-5-nitrobenzene. Modified from a previously reported procedure.⁶⁷ To a stirred solution of 2,6-diiodo-4-nitrophenol (10.00 g, 25.6 mmol) in acetone (20 mL) was added anhydrous potassium carbonate (6.7 g, 48.6 mmol) then benzyl bromide (2.90 mL, 24.3 mmol) and the reaction refluxed until complete consumption of benzyl bromide (ca. 22 h, as monitored *via* ¹H NMR). After cooling to room temperature, the volatiles were removed in vacuo. The residue was partitioned in water (100 mL) and ethyl acetate (100 mL) and the organic layer separated. The aqueous layer was extracted with ethyl acetate (2 × 100 mL) and the combined organic extracts were washed with 3 M NaOH (3 × 100 mL) to remove excess phenol, then dried over magnesium sulfate, filtered, and concentrated in vacuo to yield a bright orange solid. Recrystallization from ethyl acetate provided the product as pale yellow needles in two crops (9.71 g, 83.1%). ¹H NMR (300 MHz, CDCl₃): δ 8.68 (s, 2H, central *ArH*), 7.65 (dd, *J* = 7.9, 1.7 Hz, 2H, *ArH*), 7.48 – 7.38 (m, 3H, *ArH*), 5.09 (s, 2H, CH₂); ¹³C {¹H} NMR (75 MHz, CDCl₃): δ 163.02 (CNO₂), 144.95 (aryl-C), 135.29 (aryl-C), 135.24 (aryl-C), 129.02 (aryl-C), 128.77 (aryl-C), 90.54 (aryl-C), 75.1 (CH₂); HRMS (FAB+) *m/z* Calcd. for C₁₃H₈I₂NO₃ [M + H]⁺ 479.8594, found 479.8609.



2-(benzyloxy)-1,3-bis(2'-bromophenyl)-5-nitrobenzene. Modified from a previously reported procedure.⁶⁸ A mixture of 2-(benzyloxy)-1,3-diiodo-5-nitrobenzene (15.00 g, 31.2 mmol), 2-bromophenyl boronic acid (13.78 g, 68.6 mmol), and anhydrous potassium

carbonate (25.90 g, 187 mmol) was suspended in a mixture of toluene (525 mL), ethanol (150 mL), and water (150 mL) in a Schlenk tube fitted with a screw-in Teflon stopper. The suspension was degassed by three freeze-pump-thaw cycles after which tetrakis(triphenylphosphine) palladium(0) (1.80 g, 1.56 mmol) was added under a counter flow of nitrogen. The reaction flask was then sealed and warmed to 70 °C for 16 h. After cooling to room temperature, water (200 mL) was added and the organic layer was separated. The aqueous layer was extracted with dichloromethane (3 × 150 mL). The combined organic extracts were dried over magnesium sulfate, filtered, and then concentrated in vacuo to the crude product (17.9 g) as a yellow solid, which was used in the next step without further purification.

The crude product can be purified by silica gel column chromatography (1:9 ethyl acetate:hexanes) providing 2-(benzyloxy)-1,3-bis(2'-bromophenyl)-5-nitrobenzene as a white solid (93.6%). ¹H NMR (300 MHz, CDCl₃): δ 8.22 (s, 2H, central ArH), 7.71 (d, *J* = 7.7 Hz, 2H), 7.46 – 7.21 (m, 6H, ArH), 7.19 – 6.96 (m, 3H, ArH), 6.57 (s, br, 2H, ArH), 4.34 (s, 2H, CH₂); ¹³C {¹H} NMR (75 MHz, CDCl₃): δ 159.28 (CNO₂), 142.96 (aryl-C), 137.63 (aryl-C), 136.21 (aryl-C), 135.78 (aryl-C), 133.01 (aryl-C), 131.73 (aryl-C), 130.00 (aryl-C), 128.20 (aryl-C), 128.05 (aryl-C), 127.89 (aryl-C), 127.48 (aryl-C), 126.91 (aryl-C), 123.70 (aryl-C), 75.33 (CH₂); HRMS (FAB+) *m/z* Calcd. for C₂₅H₁₇Br₂NO₃ [M + H]⁺ 539.9633, found 539.9622.

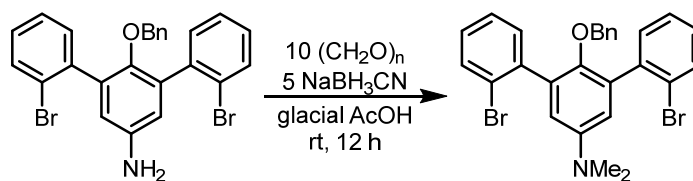


4-(benzyloxy)-3,5-bis(2'-bromophenyl)aniline. To a round bottom flask containing crude 2-(benzyloxy)-1,3-bis(2'-bromophenyl)-5-nitrobenzene (17.9 g) suspended in ethanol (120 mL) and water (10 mL), was added excess concentrated hydrochloric acid (7.5 mL) slowly,

followed by excess iron powder (7.5 g) slowly (caution: effervescence). The flask was then fitted with a reflux condenser and heated to reflux for 2 h. After cooling to room temperature, the black suspension was filtered over diatomaceous earth, and the black residue washed with dichloromethane (200 mL). The filtrate was then diluted with water (200 mL), the organic layer was separated, and the aqueous layer extracted with dichloromethane (2×150 mL). The combined organic extracts were dried over magnesium sulfate, filtered, and concentrated in vacuo to yield the crude product as a tacky tan solid (18.3 g), which was used in the next step without further purification.

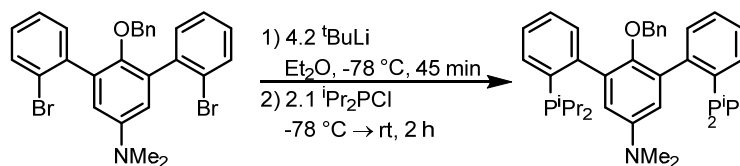
Crude product can be purified by silica gel column chromatography (1:4 ethyl acetate:hexanes) to yield 4-(benzyloxy)-3,5-bis(2'-bromophenyl)aniline as a pale tan solid (82.4% over 2 steps).

^1H NMR (300 MHz, CDCl_3): δ 7.70 (dd, $J = 8.0, 1.3$ Hz, 2H, ArH), 7.41 (dd, $J = 7.6, 1.9$ Hz, 2H, ArH), 7.33 (td, $J = 7.5, 1.3$ Hz, 2H, ArH), 7.23 (td, $J = 7.5, 1.8$ Hz, 2H ArH), 7.15 – 6.99 (m, 3H, ArH), 6.65 (s, 2H, central ArH), 6.55 (s, br, 2H, ArH), 4.22 (s, 2H, CH_2), 3.65 (s, br, 2H, NH_2); $^{13}\text{C}\{^1\text{H}\}$ NMR (75 MHz, CDCl_3): δ 146.11 (aryl-C), 141.63 (aryl-C), 139.70 (aryl-C), 137.06 (aryl-C), 136.14 (aryl-C), 132.60 (aryl-C), 131.98 (aryl-C), 128.87 (aryl-C), 128.08 (aryl-C), 127.96 (aryl-C), 127.49, 126.99, 123.91, 117.69, 75.30 (CH_2); HRMS (FAB+) m/z Calcd. for $\text{C}_{25}\text{H}_{19}\text{Br}_2\text{NO}$ $[\text{M} + \text{H}]^+$ 509.9891, found 509.9915.



4-(benzyloxy)-3,5-bis(2'-bromophenyl)-*N,N*-dimethylaniline. Modified from a previously reported procedure.⁶⁹ To round bottom flask charged with a solution of crude 4-(benzyloxy)-3,5-bis(2'-bromophenyl)aniline (18.3 g) in glacial acetic acid (75 mL) was added paraformaldehyde (9.65 g, ca. 10 equiv.) and sodium cyanoborohydride (9.79 g, ca. 5 equiv.)

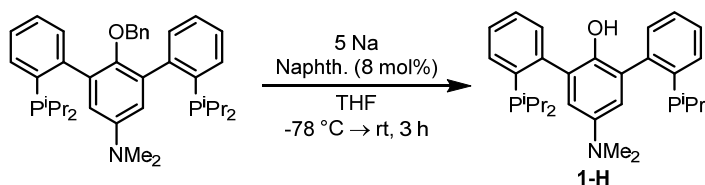
(caution: effervescence). The reaction was allowed to stir at room temperature for 12 h under a nitrogen atmosphere. The mixture was poured onto an ice (200 mL) and sodium hydroxide (40 g) mixture, stirring to ensure neutralization of the acid. The mixture was then filtered, and the residue washed with dichloromethane. The organic layer in the filtrate was separated and the aqueous layer was extracted with dichloromethane (2×100 mL). The combined organic layers were dried over magnesium sulfate, filtered, and concentrated in vacuo to yield a black solid. Purification by silica gel column chromatography (1:9 ethyl acetate:hexanes) yields 4-(benzyloxy)-3,5-bis(2'-bromophenyl)-*N,N*-dimethylaniline as a white solid (12.1 g, 72.3% over 3 steps). ^1H NMR (300 MHz, CDCl_3): δ 7.75 (dd, $J = 7.9, 1.3$ Hz, 2H, ArH), 7.50 (dd, $J = 7.7, 1.8$ Hz, 2H, ArH), 7.38 (td, $J = 7.5, 1.3$ Hz, 2H, ArH), 7.27 (td, $J = 7.6, 1.8$ Hz, 2H, ArH), 7.17 – 7.06 (m, 3H, ArH), 6.75 (s, 2H, central ArH), 6.61 (d, br, $J = 7.0$ Hz, 2H, ArH), 4.28 (s, 2H, CH_2), 3.03 (s, 6H, $\text{N}(\text{CH}_3)_2$); $^{13}\text{C}\{^1\text{H}\}$ NMR (75 MHz, CDCl_3): δ 146.22 (aryl-C), 144.73 (aryl-C), 140.33 (aryl-C), 137.21 (aryl-C), 135.82 (aryl-C), 132.64 (aryl-C), 132.13 (aryl-C), 128.80 (aryl-C), 128.23 (aryl-C), 128.08 (aryl-C), 127.96 (aryl-C), 127.45 (aryl-C), 126.97 (aryl-C), 124.09 (aryl-C), 115.16 (aryl-C), 75.33 (CH_2), 41.08 ($\text{N}(\text{CH}_3)_2$); HRMS (FAB+) m/z Calcd. for $\text{C}_{27}\text{H}_{23}\text{Br}_2\text{NO}$ [$\text{M} + \text{H} - \text{H}_2$] $^+$ 536.0048, found 536.0033.



4-(benzyloxy)-3,5-bis(2'-diisopropylphosphinophenyl)-*N,N*-dimethylaniline. Modified from a previously reported procedure.⁶⁸ To a stirred solution of 4-(benzyloxy)-3,5-bis(2'-bromophenyl)-*N,N*-dimethylaniline (12.0 g, 22.3 mmol) in diethyl ether (250 mL) at -78 °C was added dropwise a pentane solution of tert-butyl lithium (55.2 mL, 1.7 M, 93.8 mmol) forming a pale yellow milky suspension. After stirring at -78 °C for an additional 45 minutes,

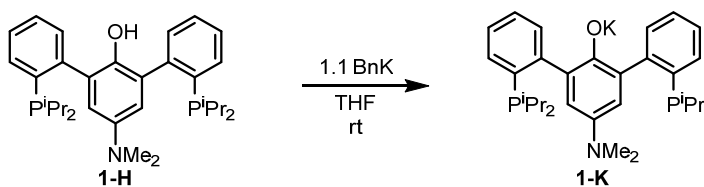
chlorodiisopropylphosphine (7.5 mL, 46.9 mmol) was added dropwise and the reaction was then allowed to warm to room temperature forming a pale yellow-orange suspension. After stirring 2 h at room temperature, the volatiles were removed *in vacuo*, and the workup was carried out in a nitrogen-purged wet box using degassed solvents. The residue was partitioned between dichloromethane (150 mL) and water (150 mL). The organic layer was separated and the aqueous layer extracted with dichloromethane (2×150 mL). The combined organic extracts were concentrated under vacuum yielding an oily solid that was triturated with methanol (30 mL), sonicating briefly to induce precipitation, filtered, washed with MeOH (2×10 mL) and dried *in vacuo* at 60 °C overnight to provide 4-(benzyloxy)-3,5-bis(2'-diisopropylphosphinophenyl)-*N,N*-dimethylaniline as a white solid (11.7 g, 85.6%). Atropisomers observed from NMR spectra (*ca.* 3:1 anti:syn based on ^1H and ^{31}P NMR integration). ^1H NMR (300 MHz, C_6D_6) anti isomer: δ 7.67 (q, $J = 3.9$ Hz, 2H, ArH), 7.55 – 7.44 (m, 2H, ArH), 7.28 – 7.17 (m, 3H, ArH), 6.97 – 6.89 (m, 2H, ArH), 6.76 (s, 2H, central ArH), 6.66 – 6.57 (m, 2H, ArH), 4.59 (d, $J = 10.6$ Hz, 1H, CH_2), 4.37 (d, $J = 10.6$ Hz, 1H, CH_2) 2.67 (s, 6H, $\text{N}(\text{CH}_3)_2$), 1.96 (dhept, $^2J_{\text{P,H}} = 38.1$ Hz, $^3J_{\text{H,H}} = 7.0$ Hz, 4H, $\text{CH}(\text{CH}_3)_2$), 1.14 – 0.96 (m, 24H, $\text{CH}(\text{CH}_3)_2$); syn isomer: 4.45 (s, 2H, CH_2), 2.07 – 1.76 (m, 4H, $\text{CH}(\text{CH}_3)_2$), 0.88– 0.88 (dd, $^3J_{\text{P,H}} = 13.1$, $^3J_{\text{H,H}} = 7.0$ Hz, 24H, $\text{CH}(\text{CH}_3)_2$); $^{13}\text{C}\{^1\text{H}\}$ NMR (75 MHz, C_6D_6): δ 148.22 (d, $^1J_{\text{P,C}} = 31.4$ Hz, aryl-C), 145.93 (d, $^2J_{\text{P,C}} = 18.2$ Hz, aryl-C), 138.38 (aryl-C), 137.25 (d, $^2J_{\text{P,C}} = 17.3$ Hz, aryl-C), 137.05 (d, $J_{\text{P,C}} = 2.5$ Hz, aryl-C), 132.44 (aryl-C), 132.39 (aryl-C), 131.88 (d, $J_{\text{P,C}} = 5.8$ Hz, aryl-C), 131.30 (aryl-C), 128.20 (aryl-C), 127.92 (aryl-C), 127.32 (aryl-C), 126.74 (aryl-C), 117.12 (d, $J_{\text{P,C}} = 3.5$ Hz, aryl-C), 75.26 (syn CH_2) 74.98 (anti CH_2), 41.17 ($\text{N}(\text{CH}_3)_2$), 26.74 (d, $J_{\text{P,C}} = 16.7$ Hz, $\text{PCH}(\text{CH}_3)_2$), 24.51 (d, $J_{\text{P,C}} = 15.1$ Hz, $\text{PCH}(\text{CH}_3)_2$), 21.07 (d, $J_{\text{P,C}} = 15.5$ Hz, syn $\text{PCH}(\text{CH}_3)_2$), 20.63 (d, $^1J_{\text{P,C}} = 18.3$ Hz, $\text{PCH}(\text{CH}_3)_2$), 20.56 (d, $J_{\text{P,C}} = 15.6$

Hz, PCH(CH₃)₂); ³¹P{¹H} NMR (75 Hz, C₆D₆): δ -2.15 (s, anti isomer), -3.67 (s, syn isomer); HRMS (FAB+) m/z Calcd. for C₃₉H₅₂NOP₂ [M + H]⁺ 612.3524, found 612.3553.



2,6-bis(2'-diisopropylphosphinophenyl)-4-dimethylaminophenol (1-H). Modified from a previously reported procedure.⁷⁰ To a solution of 4-(benzyloxy)-3,5-bis(2'-diisopropylphosphinophenyl)-*N,N*-dimethylaniline (19.64 g, 32.1 mmol) in tetrahydrofuran (750 mL) stirring over a sodium mirror (3.70 g, 160 mmol) (made by warming sodium lumps in a Schlenk tube under vacuum) was added slowly a solution of naphthalene (329 mg, 2.54 mmol) in tetrahydrofuran (50 mL). The reaction was stirred at room temperature and reaction progress check *via* ³¹P NMR. After complete conversion, about 3 h, the reaction was worked up in a nitrogen-purged wet box using degassed solvents. The solution was decanted and the flask washed with tetrahydrofuran (50 mL). The washings were combined with the initial decanted solution and water (10 mL) added slowly leading to rapid loss of the deep yellow-brown color to give a yellow solution. The solvent was reduced in volume *in vacuo* to about 50 mL. Water (150 mL) was added, and the mixture extracted with dichloromethane (3 × 200 mL). The combined organic extracts were dried over MgSO₄, filtered, and concentrated *in vacuo* to yield a yellow viscous oil. After further drying the solid at 60 °C overnight, methanol (*ca.* 40 mL) added and stirred vigorously to induce precipitation of the product. The precipitate was collected by filtration and washed with a minimal methanol (2 × 30 mL). Drying the residue *in vacuo* provided **1-H** as an off-white solid. (10.99 g, 65.7%). Broad peaks due to atropisomers observed in ¹H NMR at room temperature. ¹H NMR (300 MHz, C₆D₆, 70 °C): δ 7.48 – 7.41 (m, 4H, *ArH*), 7.19 – 7.11 (m, 4H, *ArH*), 6.74 (s, 2H, central *ArH*), 4.97 (s, br,

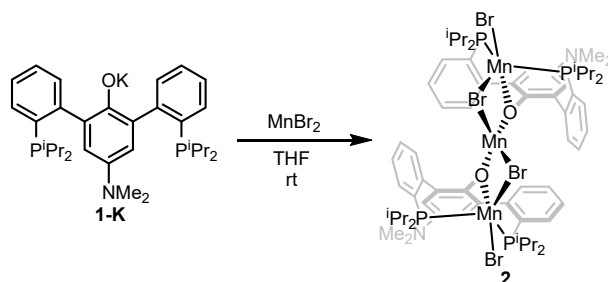
1H, OH), 2.67 (s, 6H, N(CH₃)₂), 1.97 (hept, *J* = 6.8 Hz, 4H, CH(CH₃)₂), 1.05 (dd, ³*J*_{PH} = 13.8, ³*J*_{H,H} = 7.0 Hz, 12H, CH(CH₃)₂), 0.96 (dd, ³*J*_{PH} = 11.6, ³*J*_{H,H} = 7.0 Hz, 12H, CH(CH₃)₂); ¹³C {¹H} NMR (75 MHz, C₆D₆, 70 °C): δ 148.34 (aryl-C), 147.93 (aryl-C), 144.95 (aryl-C), 142.03 (aryl-C), 136.84 (d, ¹*J*_{PC} = 21.1 Hz, aryl-C), 132.53 (aryl-C), 131.87 (aryl-C), 128.88 (aryl-C), 126.99 (aryl-C), 118.55 (aryl-C), 41.74 (N(CH₃)₂), 25.10 (br, PCH(CH₃)₂), 20.62 (d, ²*J*_{PC} = 20.4 Hz, PCH(CH₃)₂), 20.47 (d, ²*J*_{PC} = 22.9 Hz, PCH(CH₃)₂), 20.24 (s, br, PCH(CH₃)₂); ³¹P {¹H} NMR (75 Hz, C₆D₆): δ -0.90 (s); ³¹P {¹H} NMR (75 Hz, C₆D₆, 70 °C): δ 1.13 (s); HRMS (FAB+) *m/z* Calcd. for C₃₂H₄₆NOP₂ [M + H]⁺ 522.3055, found 522.3035.



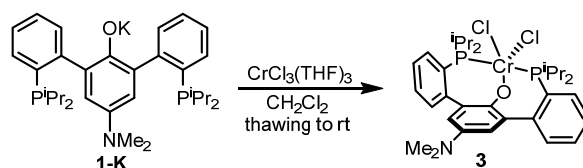
Synthesis of 1-K. To a solution of 2,6-bis(2'-diisopropylphosphinophenyl)-4-dimethylaminophenol (200 mg, 0.387 mmol) in tetrahydrofuran (10 mL) was added dropwise a solution of benzyl potassium (52.9 mg, 0.407 mmol) in tetrahydrofuran (5 mL) at room temperature forming a bright yellow solution upon addition. After stirring for 10 minutes at room temperature, the volatiles were removed in vacuo and the residue triturated with hexanes. The residue was extracted benzene (3 × 10 mL), filtered through diatomaceous earth, and lyophilized to afford **1** as a bright yellow solid (215 mg, quantitative). ¹H NMR (300 MHz, C₆D₆, 70 °C): δ 7.35 (dt, *J* = 6.5, 2.0 Hz, 2H, ArH), 7.28 (dt, *J* = 6.5, 3.1 Hz, 2H, ArH), 7.05 – 6.97 (m, 4H, ArH), 6.86 (s, 2H, central ArH), 2.78 (s, 6H, N(CH₃)₂), 2.00 (heptd, *J* = 7.0, 1.9 Hz, 4H, CH(CH₃)₂), 1.08 (dd, ³*J*_{PH} = 12.4 Hz, ³*J*_{H,H} = 7.0 Hz, 12H, CH(CH₃)₂), 0.95 (dd, br, ³*J*_{PH} = 11.7 Hz, ³*J*_{H,H} = 7.0 Hz, 12H, CH(CH₃)₂); ¹³C {¹H} NMR (75 MHz, C₆D₆, 70 °C): δ 161.87 (aryl-C), 154.56 (d, *J* = 29.0 Hz, aryl-C), 139.93 (d, ¹*J*_{PC} = 25.0 Hz, aryl-C), 137.02 (aryl-C), 132.44 (aryl-C), 132.38 (aryl-C), 130.26 (aryl-C), 127.74 (aryl-C), 125.62 (aryl-C), 121.87

(aryl-C), 44.69 (N(CH₃)₂), 24.58 (br, PCH(CH₃)₂) 21.32 (d, ²J_{PC} = 16.4 Hz, PCH(CH₃)₂), 20.32 (d, ²J_{PC} = 18.5 Hz, PCH(CH₃)₂); ³¹P{¹H} NMR (121 MHz, C₆D₆, 70 °C) δ 2.53 (br, s).

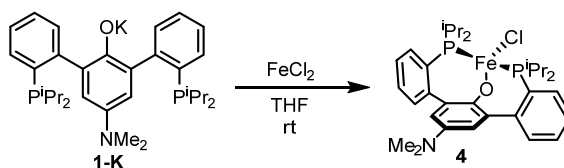
General work-up procedure for metalations. After stirring for the required time, the reaction was concentrated under vacuum. If tetrahydrofuran was used as a solvent, the resulting residue was further triturated with hexanes and the volatiles removed *in vacuo*. The solid was extracted with benzene and filtered through diatomaceous earth. The filtrate was reduced in volume under vacuum and pentane was then added to induce precipitation. The precipitate was then collected by filtration and dried under reduced pressure to provide the complexes as powders.



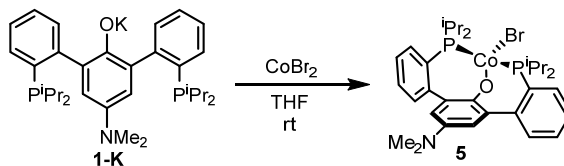
Synthesis of [MnBr(POP)]₂MnBr₂ (2). To a stirred suspension of Mn(II) bromide (55.5 mg, 0.258 mmol) in tetrahydrofuran (4 mL) was added a solution of **1-K** (100 mg, 0.167 mmol) in tetrahydrofuran (3 mL) at room temperature. The reaction was allowed to stir at room temperature for 12 h turning from bright yellow to pale yellow before being worked up. **2** was obtained as a pale yellow powder (104 mg, 76.3%). ¹H NMR (300 MHz, C₆D₆): δ 12.10 (br, s), 10.83 (br, s), 5.21 (br, s), 3.35 (s), 2.11 (s), 1.23 (s), 1.15 (s), 0.88 (s); Anal. Calcd. C₆₄H₈₈Br₄Mn₃N₂O₂P₄•2C₆H₆ (%): C, 53.93; H, 6.37; N, 1.86. Found: C, 54.27; H, 5.99; N, 1.67.



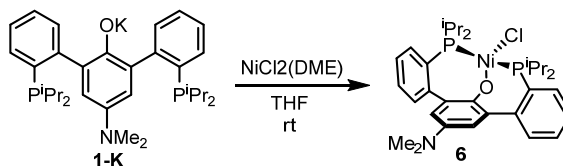
Synthesis of CrCl₂(POP) (3). To a thawing solution of chromium(III) chloride *tris*(tetrahydrofuran) complex (35.9 mg, 0.089 mmol) in dichloromethane (5 mL) was added a thawing solution of **1-K** (50 mg, 0.089 mmol) in dichloromethane (2 mL) with stirring. The solution turned deep purple upon addition and was allowed to warm to room temperature and stirred an additional 2 h before being worked up to provide **3** as a green-black powder (43.6 mg 76.2%). X-ray quality crystals were grown by slow diffusion of pentane into a benzene solution of **3**. ¹H NMR (300 MHz, C₆D₆): δ 13.50 (br, s), 5.18 (br, s), 3.84 (br, s), 2.11 (s), 1.21 (s), -1.16 (br, s), -45.63 (br, s); Anal. Calcd. C₃₂H₄₄Cl₂CrNOP₂•0.5C₆H₆ (%): C, 61.58; H, 6.94; N, 2.05. Found: C, 61.21; H, 6.96; N, 2.18.



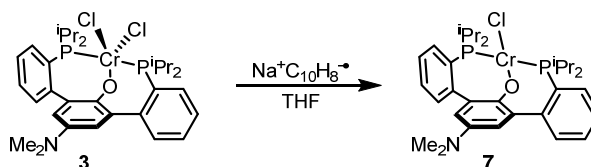
Synthesis of FeCl(POP) (4). To a suspension of iron(II) chloride (70.4 mg, 0.555 mmol) in tetrahydrofuran (6 mL) was added **1-K** (296 mg, 0.529 mmol) as a solution in tetrahydrofuran (4 mL) at room temperature with stirring. The reaction turned from bright yellow to orange-red over about 1 h. After stirring an additional hour, the reaction was worked up to provide **4** as an orange powder (315 mg 97.3%). X-ray quality crystals were grown by slow diffusion of pentane into a benzene solution of **4**. ¹H NMR (300 MHz, C₆D₆): δ 36.72 (br, s), 18.72 (s), 12.13 (br, s), 9.42 (br, s), 7.37 (s), 7.34 (s), 7.23 (s), 3.28–1.07 (m), -1.76 (br, s); Anal. Calcd. C₃₂H₄₄ClFeNOP₂ (%): C, 62.81; H, 7.25; N, 2.29. Found: C, 63.07; H, 7.42; N, 2.19.



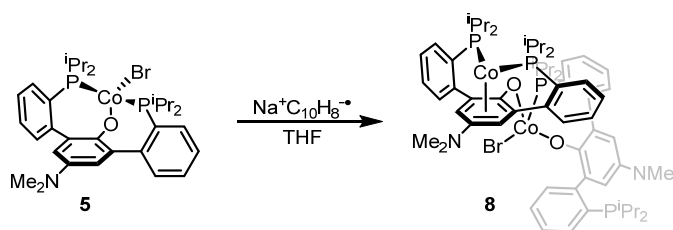
Synthesis of CoBr(POP) (5). Prepared in a similar manner as to **4** starting with cobalt (II) bromide affording a deep purple solid (195 mg, 82.8%). X-ray quality crystals were grown by slow diffusion of pentane into a benzene solution of **6**. ^1H NMR (300 MHz, C_6D_6): δ 43.09 (br, s), 34.66 (br, s), 18.48 (br, s), 11.73 (s); Anal. Calcd. $\text{C}_{32}\text{H}_{44}\text{BrCoNOP}_2$ (%): C, 58.28; H, 6.73; N, 2.12. Found: C, 57.94; H, 6.35; N, 1.89.



Synthesis of NiCl(POP) (6). Prepared in a similar manner as to **4** starting with nickel(II) chloride ethylene glycol dimethyl ether complex affording a dark green powder (78.1 mg, 76.2%). X-ray quality crystals were grown by slow diffusion of pentane into a benzene solution of **7**. ^1H NMR (300 MHz, C_6D_6): δ 7.25 – 7.10 (m, 6H, *ArH*), 7.00 (s, 2H, central *ArH*), 6.98 (td, $J = 7.4$ Hz, 2H, 1.4 Hz, *ArH*), 2.78 (s, 6H, $\text{N}(\text{CH}_3)_2$), 2.67 – 2.58 (m, 2H, $\text{CH}(\text{CH}_3)_2$), 2.20 – 2.05 (m, 2H, $\text{CH}(\text{CH}_3)_2$), 1.85 (app q, $^3J_{\text{H,H}} = 7.5$ Hz 12H, $\text{CH}(\text{CH}_3)_2$), 1.25 (dt, $^3J_{\text{H,H}} = 8.5$, 7.4 Hz, 6H, $\text{CH}(\text{CH}_3)_2$), 0.66 (dt, $J = 7.1$, 5.5 Hz, 6H, $\text{CH}(\text{CH}_3)_2$); $^{13}\text{C}\{^1\text{H}\}$ NMR (101 MHz, C_6D_6): δ 148.11 (app t, $J_{\text{PC}} = 6.9$ Hz, aryl-C), 146.12 (aryl-C), 134.90 (app t, $J_{\text{PC}} = 1.6$ Hz, aryl-C), 133.21 (app t, $J_{\text{PC}} = 4.1$ Hz, aryl-C), 131.17 (aryl-C), 130.40 (aryl-C), 128.59 (aryl-C) 125.00 (app t, $J_{\text{PC}} = 2.8$ Hz, aryl-C), 123.19 (t, $J_{\text{PC}} = 19.5$ Hz, aryl-C), 118.68 (aryl-C), 41.76 ($\text{N}(\text{CH}_3)_2$), 23.27 (app t, $J_{\text{PC}} = 9.0$ Hz, $\text{CH}(\text{CH}_3)_2$), 21.18 (app t, $J_{\text{PC}} = 10.7$ Hz, $\text{CH}(\text{CH}_3)_2$), 19.59 (app dt, $J = 8.8$, 3.2 Hz, $\text{CH}(\text{CH}_3)_2$), 19.04 (app t, $J_{\text{PC}} = 2.3$ Hz, $\text{CH}(\text{CH}_3)_2$), 15.30 (app t, $J_{\text{PC}} = 2.5$ Hz, $\text{CH}(\text{CH}_3)_2$); $^{31}\text{P}\{^1\text{H}\}$ NMR (121 MHz, C_6D_6): δ 13.57 (s); Anal. calcd. for $\text{C}_{32}\text{H}_{44}\text{ClNiNOP}_2$ (%): C, 62.52; H, 7.21; N, 2.28. Found: C, 62.38; H, 6.99; N, 2.28.

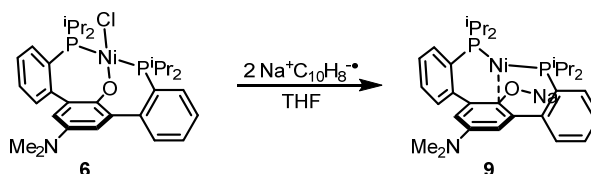


Synthesis of CrCl(POP) (7). To a vial charged with a reduced Teflon-coated stir bar and a solution of **3** (50 mg, 0.078 mmol) in THF (5 mL) was added dropwise a THF solution of sodium naphthalenide (1.1 equiv.) with stirring at room temperature forming a brown-green solution. After stirring an additional 2 h, the volatiles were removed *in vacuo*. The residue was triturated with hexanes and concentrated under vacuum. The resulting solid dissolved in a minimal amount of benzene and reprecipitated by addition of pentane. The suspension was filtered, and the solid was recrystallized in slow vapor diffusion of pentane into a benzene solution providing **7** as a microcrystalline green solid after washing with pentane and drying *in vacuo* (29.5 mg, 62.5 %). Crystals suitable for single crystal XRD were obtained under similar crystallization conditions. Anal. calcd. for $C_{32}H_{44}CrClNOP_2$ (%): C, 63.21; H, 7.29; N, 2.30. Found: C, 63.46; H, 7.01; N, 2.46.



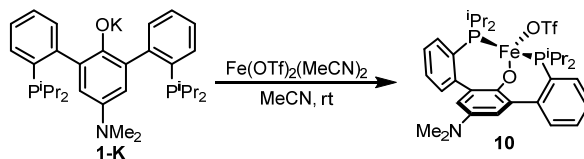
Synthesis of Co(POP)CoBr(POP) (8). To a vial charged with a reduced Teflon-coated stir bar and a THF solution of **5** (100 mg, 0.152 mmol) was added dropwise a THF solution of sodium naphthalenide (1.1 equiv.) with stirring at room temperature resulting in the formation of a deep red solution. After stirring an additional 2 h, the volatiles were removed under reduced pressure. The solid was triturated with hexanes and dried again *in vacuo*. The solid was extracted with benzene and concentrated under vacuum. The resultant red solid was

recrystallized from slow vapor diffusion of pentane into a saturated benzene solution providing **8** as deep red crystals after washing with pentane and drying under vacuum (44.3 mg, 47.2 %). Crystals suitable for single crystal XRD were obtained under similar crystallization conditions. ^1H NMR (300 MHz, C_6D_6): δ 43.09 (br, s), 34.66 (br, s), 18.48 (br, s), 11.73 (s); Anal. Calcd. $\text{C}_{64}\text{H}_{88}\text{BrCo}_2\text{N}_2\text{O}_2\text{P}_4$ (%): C, 62.04; H, 7.16; N, 2.26. Found: C, 61.72; H, 6.98; N, 2.10.

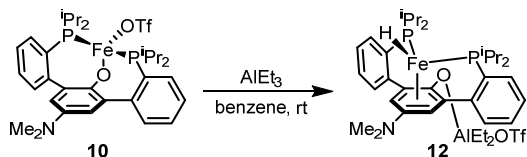


Synthesis of Na[Ni(POP)] (9). To a vial charged with a reduced Teflon-coated stir bar and a solution of **6** (100 mg, 0.163 mmol) in THF (5 mL) was added dropwise a solution of sodium naphthalenide (2.1 equiv.) with stirring at room temperature. The reaction turned from deep green to brown upon mixing. The reaction was allowed to stir an additional 2 h before the volatiles were removed *in vacuo*. The residue was triturated with hexanes and concentrated under vacuum. The solid was extracted with benzene, dried under vacuum, and recrystallized from slow diffusion of pentane into a THF solution to provide **9** as a brown crystalline solid after washing with pentane and drying *in vacuo* (62.3 mg, 63.6%). X-ray quality crystals were grown by slow diffusion of pentane into a benzene solution of **9**. ^1H NMR (400 MHz, C_6D_6): δ 7.37 (d, $^3J_{\text{H,H}} = 7.4$ Hz, 2H, ArH), 7.07 – 6.92 (m, 6H, ArH) 6.08 (t, $J_{\text{R,H}} = 2.4$ Hz, 2H, central ArH), 2.69 (s, 6H, $\text{N}(\text{CH}_3)_2$), 2.22 – 2.11 (m, 2H, $\text{CH}(\text{CH}_3)_2$), 1.90 (sept, $^3J_{\text{H,H}} = 7.2$ Hz 2H, $\text{CH}(\text{CH}_3)_2$), 1.27 (app q, $^3J_{\text{H,H}} = 7.0$ Hz 6H, $\text{CH}(\text{CH}_3)_2$), 1.06 (app p, $^3J_{\text{H,H}} = 6.8$ Hz, 12H, $\text{CH}(\text{CH}_3)_2$), 0.72 (app q, $^3J_{\text{H,H}} = 7.1$ Hz, 6H, $\text{CH}(\text{CH}_3)_2$); $^{13}\text{C}\{^1\text{H}\}$ NMR (101 MHz, C_6D_6): δ 152.11 (aryl-C), 142.09 (app t, $J_{\text{R,C}} = 14.6$ Hz, aryl-C), 139.64 (aryl-C), 130.32 (app t, $J_{\text{R,C}} = 7.3$ Hz, aryl-C), 129.74 (br, aryl-C), 128.54 (br, aryl-C), 127.33 (br, aryl-C), 124.36 (app t, $J_{\text{R,C}} = 3.0$

Hz, aryl-C), 117.96 (br, aryl-C), 110.20(aryl-C), 43.93 (N(CH₃)₂), 27.88 (app t, $J_{\text{PC}} = 7.0$ Hz, CH(CH₃)₂), 20.54 (app t, $J_{\text{PC}} = 5.6$ Hz, CH(CH₃)₂), 20.10 (br, CH(CH₃)₂), 20.02 (app dt, $J_{\text{PC}} = 46.4, 2.3$ Hz, CH(CH₃)₂), 19.22 (app t, $J_{\text{PC}} = 6.2$ Hz, CH(CH₃)₂); ³¹P {¹H} NMR (162 MHz, C₆D₆): δ 38.50 (s). Anal. calcd. for C₃₂H₄₄NNaNiOP₂ (%):C, 63.81; H, 7.36; N, 2.33. Found: C, 63.37; H, 7.02; N, 2.02.

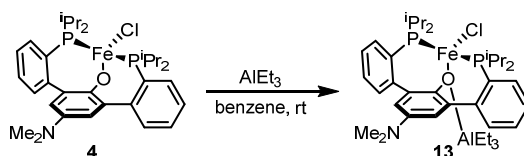


Synthesis of 10. A solution of **1** (200 mg, 0.357 mmol) in THF (5 mL) was added to a suspension of Fe(OTf)₂(MeCN)₂ (156 mg, 0.357 mmol) in THF (5 mL) at room temperature and stirred for 12 h resulting in the formation of an orange-red solution. The volatiles were removed *in vacuo*, and the residue triturated with hexanes (10 mL) and dried under vacuum. The residue was extracted with benzene (20 mL) and filtered over diatomaceous earth. The filtrate was lyophilized to provide **10** as an orange-red powder (235.2 mg 91%). X-ray quality crystals were grown by slow diffusion of pentane into a saturated benzene solution. ¹H NMR (300 MHz, C₆D₆): δ 35.70, 18.71, 11.88, 9.46, 2.58, 1.86, 0.93, -2.93; ¹⁹F NMR (296 MHz, C₆D₆): δ 13.23 (br); μ_{eff} (Evans' NMR method) = 4.8 μ_{B} .

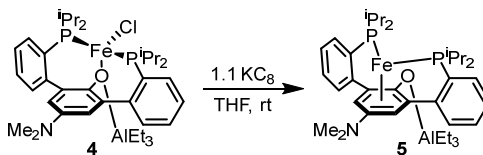


Synthesis of 12. To a solution of triethylaluminium (4.1 μL , 0.028 mmol) in benzene (3 mL) was added a solution of **10** (20.0 mg, 0.028 mmol) at room temperature with stirring. The solution was allowed to stir for 1 h, turning from orange-red to pale yellow-brown. The reaction was filtered through diatomaceous earth. The filtrate was concentrated *in vacuo*. The

solid was washed with pentane, extracted with diethyl ether, and dried under vacuum to provide **12** as a yellow-brown powder (14.1 mg 62%). X-ray quality crystals were grown by slow diffusion of pentane into a saturated diethyl ether solution. ^1H NMR (300 MHz, C_6D_6): δ 8.51 (s, 2H, ArH), 7.41 (s, 2H, ArH), 7.09 (s, 2H, ArH), 7.00 (s, 2H, ArH), 3.39 (s, 2H, central ArH), 2.09 (s, 2H, $\text{CH}(\text{CH}_3)_2$), 1.87 (s, 6H, $\text{N}(\text{CH}_3)_2$), 1.62 (s, 2H, $\text{CH}(\text{CH}_3)_2$), 1.37 (s, 6H, CH_2CH_3), 0.89 (s, 12H, $\text{CH}(\text{CH}_3)_2$), 0.62 (s, 12H, $\text{CH}(\text{CH}_3)_2$), 0.29 (s, 4H, CH_2CH_3), -10.25 (t, $J = 83.2$ Hz, 1H, FeH); $^{31}\text{P}\{^1\text{H}\}$ NMR (121 MHz, C_6D_6) δ 91.41 (s).



Synthesis of 13. To a solution of triethylaluminium (4.8 μL , 0.033 mmol) in benzene (3 mL) was added a solution of **4** (20.0 mg, 0.033 mmol) at room temperature with stirring. The solution turned from orange-red to pale orange over about 10 min and was allowed to stir for 1 h. The solvent volume was reduced in vacuo and pentane was added to induce precipitation. The precipitate was then collected via filtration and dried under vacuum to provide **4** as an orange powder (22.7 mg 95.6%). X-ray quality crystals were grown by slow evaporation of a saturated benzene solution or from slow diffusion of pentane into a saturated THF solution. ^1H NMR (300 MHz, C_6D_6): δ 25.43, 24.07, 23.32, 16.03, 12.03, 3.57, 3.04, 1.39, 0.89, -4.24; μ_{eff} (Evans' NMR method) = 4.9 μB ; Anal. Calcd. $\text{C}_{38}\text{H}_{59}\text{AlClFeNOP}_2$ (%): C, 62.86; H, 8.19; N, 1.93. Found: C, 63.03; H, 8.51; N, 1.57.



Synthesis of 14. To a solution of **13** (20 mg, 0.028 mmol) in THF (3 mL) charged with a pre-reduced Teflon stir bar, was added KC_8 (4.1 mg, 0.030 mmol) at room temperature. The

solution turned from orange to deep yellow immediately and was allowed to stir for 10 min. The volatiles were then removed in vacuo. The residue was triturated with hexanes, extracted with benzene, and filtered through diatomaceous earth. The filtrate was reduced in volume in vacuo to provide **14** as a dark yellow powder (17.2 mg 88.4%). X-ray quality crystals were grown by slow diffusion of pentane into a saturated THF solution.

CRYSTALLOGRAPHIC INFORMATION

CCDC deposition numbers 1868525, 1868526, 1868527, 1868528, 1868529, 1868530, 1868531, and 1868532 contain the supplementary crystallographic data for this paper.⁷¹

These data can be obtained free of charge from The Cambridge Crystallographic Data Centre via www.ccdc.cam.ac.uk/data_request/cif.

Refinement Details

In each case, crystals were mounted on a glass fiber or MiTeGen loop using Paratone oil, then placed on the diffractometer under a nitrogen stream. Low temperature (100 K) X-ray data were obtained on a Bruker D8 VENTURE Kappa Duo PHOTON 100 CMOS based diffractometer (Mo I μ S HB micro-focus sealed X-ray tube, $K\alpha = 0.71073 \text{ \AA}$ OR Cu I μ S HB micro-focused X-ray tube, $K\alpha = 1.54178$). All diffractometer manipulations, including data collection, integration, and scaling, were carried out using the Bruker APEXII software.⁷² Absorption corrections were applied using SADABS.⁷³ Space groups were determined on the basis of systematic absences and intensity statistics and the structures were solved in the Olex 2 software interface⁷⁴ by intrinsic phasing using XT (incorporated into SHELXTL)⁷⁵ and refined by full-matrix least squares on F2. All non-hydrogen atoms were refined using anisotropic displacement parameters, except in some cases with heavily distorted solvent. Hydrogen atoms were placed in the idealized positions and refined using a riding model. The structure was refined (weighted least-squares refinement on F2) to convergence. Graphical representations of structures with 50% probability thermal ellipsoids were generated using Diamond 3 visualization software.⁷⁶

Special Refinement Details for 2. **2** crystallizes in a $P2_1/c$ space group with one molecule in the asymmetric cell along with 1 cocrystallized molecule of tetrahydrofuran. There is additional solvent disorder which could not be satisfactorily modeled and was masked in Olex2. The volume of the solvent accessible void space was found to be 203.5 \AA^3 in which $47.3 e^-$ were located.

Special Refinement Details for 4. **4** crystallizes in a $P2_1/c$ space group with one molecule in the asymmetric cell along with 0.5 cocrystallized molecules of pentane. The pentane molecule is disordered and lies along a symmetry element. It was assigned an occupancy of 0.5 and placed in part -1.

Special Refinement Details for 5. **5** crystallizes in a $P2_1/c$ space group with one molecule in the asymmetric cell. There is additional solvent disorder which could not be satisfactorily modeled and was masked in Olex2. The volume of the solvent accessible void space was found to be 274.6 \AA^3 in which $39.9 e^-$ were located.

Special Refinement Details for 6. **6** crystallizes in a $P-1$ space group with one molecule in the asymmetric cell along with a cocrystallized molecule of benzene. The benzene molecule is disordered over two positions (59% and 41%).

Special Refinement Details for 8. **8** crystallizes in a $C2/c$ space group with one molecule in the asymmetric cell and a cocrystallized molecule of benzene. There is additional solvent disorder which could not be satisfactorily modeled and was masked in Olex2. The volume of the solvent accessible void space was found to be 726.7 \AA^3 in which $123.8 e^-$ were located.

Special Refinement Details for 9. **9** crystallizes in a $P2_1/n$ space group with one molecule in the asymmetric cell. There is additional solvent disorder which could not be

satisfactorily modeled and was masked in Olex2. The volume of the solvent accessible void space was found to be 249.9 Å³ in which 100.4 e⁻ were located

Table 2.2. Crystal data and structure refinement for 2, 3, 4, and 5

	2	3	4	5
CCDC Number ⁷¹	1868525	1868526	186857	1868528
Empirical formula	C ₆₈ H ₉₆ Br ₄ Mn ₃ N ₂ O ₃ P ₄	C ₃₂ H ₄₄ Cl ₂ CrNOP ₂	C _{34.5} H _{47.5} ClFeNO P ₂	C ₃₂ H ₄₄ BrCoNOP ₂
Formula weight	1597.80	643.52	645.47	659.46
Temperature/K	100.0	100.15	100.0	100.15
Crystal system	monoclinic	monoclinic	monoclinic	monoclinic
Space group	P2 ₁ /c	P2 ₁ /c	P2 ₁ /c	P2 ₁ /c
a/Å	12.7338(4)	12.7224(6)	20.653(2)	20.7193(14)
b/Å	18.6052(5)	12.0619(6)	14.0103(13)	13.9728(10)
c/Å	30.8375(8)	21.4128(11)	12.0635(9)	12.1197(9)
α/°	90	90	90	90
β/°	92.2200(10)	102.756(2)	95.005(3)	94.999(4)
γ/°	90	90	90	90
Volume/Å ³	7300.4(4)	3204.8(3)	3477.3(5)	3495.4(4)
Z	4	4	4	4
ρ _{calc} /cm ³	1.454	1.334	1.233	1.253
μ/mm ⁻¹	7.887	0.649	0.629	1.748
Crystal size/mm ³	0.2 × 0.11 × 0.020.23 × 0.17 × 0.140.4 × 0.3 × 0.2			0.4 × 0.3 × 0.1
Radiation	CuKα (λ = 1.54178)	MoKα (λ = 0.71073)	MoKα (λ = 0.71073)	MoKα (λ = 0.71073)
2θ range/°	5.548 to 159.352	4.71 to 66.336	3.518 to 66.344	3.52 to 72.634
GOF	1.037	1.042	1.055	1.019
R ₁ , ^a wR ₂ ^b [I > 2σ(I)]	0.0505, 0.1031	0.0354, 0.0786	0.0442, 0.1132	0.0419, 0.0913

$$^a R_1 = \frac{\sum ||F_0| - |F_c||}{\sum |F_0|}, \quad ^b wR_2 = \frac{[\sum [w(F_0^2 - F_c^2)^2]]}{\sum [w(F_0^2)^2]}^{1/2}$$

Table 2.3. Crystal data and structure refinement for 6, 7, 8, and 9

	6	7	8	9
CCDC Number ⁷¹	1868529	1868530	1868531	1868532
Empirical formula	C ₃₈ H ₅₀ ClNNiOP ₂	C ₃₂ H ₄₄ ClCrNOP ₂	C ₇₄ H ₁₀₀ BrCo ₂ N ₂ O ₂ P ₄	C ₃₂ H ₄₄ NNaNiOP ₂
Formula weight	692.89	608.07	1371.20	602.32
Temperature/K	100.15	99.99	100.02	99.98
Crystal system	triclinic	monoclinic	monoclinic	monoclinic
Space group	P-1	P2 ₁ /c	C2/c	P2 ₁ /n
a/Å	8.8347(5)	19.2768(10)	32.8193(12)	10.9895(11)
b/Å	10.6981(6)	11.2697(5)	21.4610(8)	23.516(2)
c/Å	19.9640(12)	14.7713(7)	24.2762(9)	13.3967(13)
α/°	87.183(2)	90	90	90
β/°	87.712(2)	105.519(2)	117.7800(10)	107.834(4)
γ/°	69.332(2)	90	90	90
Volume/Å ³	1762.80(18)	3092.0(3)	15127.9(10)	3295.8(6)
Z	2	4	8	4
ρ _{calc} /cm ³	1.305	1.306	1.204	1.214
μ/mm ⁻¹	0.747	0.585	1.093	0.723
Crystal size/mm ³	0.44 × 0.3 × 0.2	0.3 × 0.2 × 0.1	0.21 × 0.17 × 0.14	0.23 × 0.23 × 0.15
Radiation	MoKα (λ = 0.71073)	MoKα (λ = 0.71073)	MoKα (λ = 0.71073)	MoKα (λ = 0.71073)
2θ range/°	4.93 to 80.5	4.766 to 79.972	4.616 to 61.028	5.212 to 74.798
GOF	1.031	1.038	1.036	1.062
R ₁ , ^a wR ₂ ^b [I > 2σ(I)]	0.0364, 0.0758	0.0447, 0.0873	0.0610, 0.1361	0.0411, 0.0975

$${}^a R_1 = \sum ||F_o| - |F_c|| / \sum |F_o|. \quad {}^b wR_2 = [\sum [w(F_o^2 - F_c^2)^2] / \sum [w(F_o^2)^2]]^{1/2}$$

REFERENCES

- (1) Briggs, J. R.; Constable, A. G.; McDonald, W. S.; Shaw, B. L., *J. Chem. Soc., Dalton Trans.* **1982**, 1225-1230.
- (2) Crocker, C.; Empsall, H. D.; Errington, R. J.; Hyde, E. M.; McDonald, W. S.; Markham, R.; Norton, M. C.; Shaw, B. L.; Weeks, B., *J. Chem. Soc., Dalton Trans.* **1982**, 1217-1224.
- (3) Crocker, C.; Errington, R. J.; Markham, R.; Moulton, C. J.; Odell, K. J.; Shaw, B. L., *J. Am. Chem. Soc.* **1980**, *102*, 4373-4379.
- (4) Crocker, C.; Errington, R. J.; Markham, R.; Moulton, C. J.; Shaw, B. L., *J. Chem. Soc., Dalton Trans.* **1982**, 387-395.
- (5) Empsall, H. D.; Hyde, E. M.; Markham, R.; McDonald, W. S.; Norton, M. C.; Shaw, B. L.; Weeks, B., *J. Chem. Soc., Chem. Commun.* **1977**, 589-590.
- (6) Errington, R. J.; McDonald, W. S.; Shaw, B. L., *J. Chem. Soc., Dalton Trans.* **1982**, 1829-1835.
- (7) Moulton, C. J.; Shaw, B. L., *J. Chem. Soc., Dalton Trans.* **1976**, 1020-1024.
- (8) Szabó, K. J.; Wendt, O. F., *Pincer and pincer-type complexes: applications in organic synthesis and catalysis*. John Wiley & Sons: 2014.
- (9) Albrecht, M.; van Koten, G., *Angew. Chem. Int. Ed.* **2001**, *40*, 3750-3781.
- (10) Chakraborty, S.; Lagaditis, P. O.; Förster, M.; Bielinski, E. A.; Hazari, N.; Holthausen, M. C.; Jones, W. D.; Schneider, S., *ACS Catal.* **2014**, *4*, 3994-4003.
- (11) Bielinski, E. A.; Förster, M.; Zhang, Y.; Bernskoetter, W. H.; Hazari, N.; Holthausen, M. C., *ACS Catal.* **2015**, *5*, 2404-2415.
- (12) Lin, T.-P.; Peters, J. C., *J. Am. Chem. Soc.* **2013**, *135*, 15310-15313.
- (13) Tseng, K.-N. T.; Kampf, J. W.; Szymczak, N. K., *J. Am. Chem. Soc.* **2016**, *138*, 10378-10381.
- (14) Lindley, B. M.; Bruch, Q. J.; White, P. S.; Hasanayn, F.; Miller, A. J. M., *J. Am. Chem. Soc.* **2017**, *139*, 5305-5308.
- (15) Zell, T.; Milstein, D., *Acc. Chem. Res.* **2015**, *48*, 1979-1994.
- (16) Gunanathan, C.; Milstein, D., *Acc. Chem. Res.* **2011**, *44*, 588-602.
- (17) Zhang, J.; Leitius, G.; Ben-David, Y.; Milstein, D., *J. Am. Chem. Soc.* **2005**, *127*, 10840-10841.

- (18) Bouwkamp, M. W.; Bowman, A. C.; Lobkovsky, E.; Chirik, P. J., *J. Am. Chem. Soc.* **2006**, *128*, 13340-13341.
- (19) Bart, S. C.; Chlopek, K.; Bill, E.; Bouwkamp, M. W.; Lobkovsky, E.; Neese, F.; Wieghardt, K.; Chirik, P. J., *J. Am. Chem. Soc.* **2006**, *128*, 13901-13912.
- (20) Chirik, P. J.; Wieghardt, K., *Science* **2010**, *327*, 794-795.
- (21) Barrett, B. J.; Iluc, V. M., *Inorg. Chem.* **2014**, *53*, 7248-7259.
- (22) Mancano, G.; Page, M. J.; Bhadbhade, M.; Messerle, B. A., *Inorg. Chem.* **2014**, *53*, 10159-10170.
- (23) Gunanathan, C.; Ben-David, Y.; Milstein, D., *Science* **2007**, *317*, 790-792.
- (24) Deckers, P. J. W.; Hessen, B.; Teuben, J. H., *Angew. Chem. Int. Ed.* **2001**, *40*, 2516-2519.
- (25) Otten, E.; Batinas, A. A.; Meetsma, A.; Hessen, B., *J. Am. Chem. Soc.* **2009**, *131*, 5298-5312.
- (26) Kita, M. R.; Miller, A. J. M., *J. Am. Chem. Soc.* **2014**, *136*, 14519-14529.
- (27) Gregor, L. C.; Grajeda, J.; Kita, M. R.; White, P. S.; Vetter, A. J.; Miller, A. J. M., *Organometallics* **2016**, *35*, 3074-3086.
- (28) Grajeda, J.; Kita, M. R.; Gregor, L. C.; White, P. S.; Miller, A. J. M., *Organometallics* **2016**, *35*, 306-316.
- (29) Kita, M. R.; Miller, A. J. M., *Angew. Chem. Int. Ed.* **2017**, *56*, 5498-5502.
- (30) Buss, J. A.; Edouard, G. A.; Cheng, C.; Shi, J.; Agapie, T., *J. Am. Chem. Soc.* **2014**, *136*, 11272-11275.
- (31) Henthorn, J. T.; Agapie, T., *Inorg. Chem.* **2016**, *55*, 5337-5342.
- (32) Henthorn, J. T.; Lin, S.; Agapie, T., *J. Am. Chem. Soc.* **2015**, *137*, 1458-1464.
- (33) Horak, K. T.; Lin, S.; Rittle, J.; Agapie, T., *Organometallics* **2015**, *34*, 4429-4432.
- (34) Horak, K. T.; Velian, A.; Day, M. W.; Agapie, T., *Chem. Commun.* **2014**, *50*, 4427-4429.
- (35) Lin, S.; Day, M. W.; Agapie, T., *J. Am. Chem. Soc.* **2011**, *133*, 3828-3831.
- (36) Tsui, E. Y.; Agapie, T., *Proc. Natl. Acad. Sci. USA* **2013**, *110*, 10084-10088.
- (37) Velian, A.; Lin, S.; Miller, A. J. M.; Day, M. W.; Agapie, T., *J. Am. Chem. Soc.* **2010**, *132*, 6296-6297.
- (38) Buss, J. A.; Agapie, T., *Nature* **2016**, *529*, 72-75.
- (39) Buss, J. A.; Agapie, T., *J. Am. Chem. Soc.* **2016**, *138*, 16466-16477.
- (40) van Leeuwen, P. W. N. M.; Kamer, P. C. J.; Reek, J. N. H.; Dierkes, P., *Chem. Rev.* **2000**, *100*, 2741-2770.

- (41) Birkholz, M.-N.; Freixa, Z.; van Leeuwen, P. W. N. M., *Chem. Soc. Rev.* **2009**, *38*, 1099-1118.
- (42) van der Boom, M. E.; Liou, S.-Y.; Ben-David, Y.; Shimon, L. J. W.; Milstein, D., *J. Am. Chem. Soc.* **1998**, *120*, 6531-6541.
- (43) van der Boom, M. E.; Zubkov, T.; Shukla, A. D.; Rybtchinski, B.; Shimon, L. J. W.; Rozenberg, H.; Ben-David, Y.; Milstein, D., *Angew. Chem. Int. Ed.* **2004**, *43*, 5961-5963.
- (44) Hu, J.; Xu, H.; Nguyen, M.-H.; Yip, J. H. K., *Inorg. Chem.* **2009**, *48*, 9684-9692.
- (45) Kadassery, K. J.; MacMillan, S. N.; Lacy, D. C., *Dalton Trans.* **2018**, *47*, 12652-12655.
- (46) Chao, S. T.; Lara, N. C.; Lin, S.; Day, M. W.; Agapie, T., *Angew. Chem. Int. Ed.* **2011**, *50*, 7529-7532.
- (47) Edouard, G. A.; Kelley, P.; Herbert, D. E.; Agapie, T., *Organometallics* **2015**, *34*, 5254-5277.
- (48) Kelley, P.; Lin, S.; Edouard, G.; Day, M. W.; Agapie, T., *J. Am. Chem. Soc.* **2012**, *134*, 5480-5483.
- (49) Lionetti, D.; Medvecz, A. J.; Ugrinova, V.; Quiroz-Guzman, M.; Noll, B. C.; Brown, S. N., *Inorg. Chem.* **2010**, *49*, 4687-4697.
- (50) Dogan, J.; Schulte, J. B.; Swiegers, G. F.; Wild, S. B., *J. Org. Chem.* **2000**, *65*, 951-957.
- (51) Okuniewski, A.; Rosiak, D.; Chojnacki, J.; Becker, B., *Polyhedron* **2015**, *90*, 47-57.
- (52) Addison, A. W.; Rao, T. N.; Reedijk, J.; van Rijn, J.; Verschoor, G. C., *J. Chem. Soc., Dalton Trans.* **1984**, 1349-1356.
- (53) Evans, D. F., *J. Chem. Soc.* **1959**, 2003-2005.
- (54) Crawford, T. H.; Swanson, J., *J. Chem. Educ.* **1971**, *48*, 382.
- (55) Britovsek, G. J. P.; Gibson, V. C.; Spitzmesser, S. K.; Tellmann, K. P.; White, A. J. P.; Williams, D. J., *J. Chem. Soc., Dalton Trans.* **2002**, 1159-1171.
- (56) Zlatogorsky, S.; Ingleson, M. J., *Dalton Trans.* **2012**, *41*, 2685-2693.
- (57) Patel, D.; Wooles, A.; Cornish, A. D.; Steven, L.; Davies, E. S.; Evans, D. J.; McMaster, J.; Lewis, W.; Blake, A. J.; Liddle, S. T., *Dalton Trans.* **2015**, *44*, 14159-14177.
- (58) Bhattacharya, P.; Krause, J. A.; Guan, H., *J. Am. Chem. Soc.* **2014**, *136*, 11153-11161.
- (59) Bellows, S. M.; Cundari, T. R.; Holland, P. L., *Organometallics* **2013**, *32*, 4741-4751.
- (60) Vela, J.; Vaddadi, S.; Cundari, T. R.; Smith, J. M.; Gregory, E. A.; Lachicotte, R. J.; Flaschenriem, C. J.; Holland, P. L., *Organometallics* **2004**, *23*, 5226-5239.
- (61) Kubo, H.; Hirano, M.; Komiya, S., *J. Organomet. Chem.* **1998**, *556*, 89-95.

- (62) Daifuku, S. L.; Kneebone, J. L.; Snyder, B. E. R.; Neidig, M. L., *J. Am. Chem. Soc.* **2015**, *137*, 11432-11444.
- (63) Weber, B.; Walker, F. A., *Inorg. Chem.* **2007**, *46*, 6794-6803.
- (64) Pangborn, A. B.; Giardello, M. A.; Grubbs, R. H.; Rosen, R. K.; Timmers, F. J., *Organometallics* **1996**, *15*, 1518-1520.
- (65) Maaranen, J.; Hoikka, J.; Rautio, S. Process. US2007/37939 A1, 2007.
- (66) Weitz, I. S.; Rabinovitz, M., *J. Chem. Soc., Perkin Trans. 1* **1993**, 117-120.
- (67) Malik, Q. M.; Ijaz, S.; Craig, D. C.; Try, A. C., *Tetrahedron* **2011**, *67*, 5798-5805.
- (68) Feng, X.; Pisula, W.; Müllen, K., *J. Am. Chem. Soc.* **2007**, *129*, 14116-14117.
- (69) Hodges, J. A.; Raines, R. T., *Org. Lett.* **2006**, *8*, 4695-4697.
- (70) Alonso, E.; Ramón, D. J.; Yus, M., *Tetrahedron* **1997**, *53*, 14355-14368.
- (71) Crystallographic data have been deposited at the CCDC, 12 Union Road, Cambridge CB2 1EZ, UK and copies can be obtained on request, free of charge, by quoting the publication citation and the respective deposition numbers.
- (72) APEX2, Version 2 User Manual, M86-E01078, Bruker Analytical X-ray Systems, Madison, WI, June 2006.
- (73) Sheldrick, G. M., "*SADABS (version 2008/1): Program for Absorption Correction for Data from Area Detector Frames*". University of Göttingen: 2008.
- (74) Dolomanov, O. V.; Bourhis, L. J.; Gildea, R. J.; Howard, J. A. K.; Puschmann, H., *J. Appl. Crystallogr.* **2009**, *42*, 339-341.
- (75) Sheldrick, G., *Acta Crystallographica Section A* **2008**, *64*, 112-122.
- (76) Brandenburg, K. (1999). DIAMOND. Crystal Impact GbR, Bonn, Germany.

CHAPTER 3

1,4-Naphthalenediyl-Linked Diphosphine Molybdenum Complexes: Catenation of Carbon Monoxide to a C₃ Product at a Single Metal Site

ABSTRACT

The synthesis and characterization of a series of naphthalenediyl-diphosphine molybdenum complexes are reported. Dicarbonyl complex **3** can be reduced and quenched with Me₃SiCl to yield symmetric *bis*(siloxy)acetylene complex **5** displaying η⁴-arene binding demonstrating exclusive C–C coupling, distinct from the phenylene-linked analog. This selectivity is proposed to be a result of the greater propensity for η⁴-arene interaction with the naphthalenediyl-linker. Additionally, further CO catenation can be engendered from **5** under mild conditions, providing metallacyclobutenone complex **6**, with a C₃ organic fragment entirely derived from CO.

INTRODUCTION

With the increasing levels of anthropogenic carbon dioxide (CO₂) coupled with the dwindling global reserves of fossil fuels, significant efforts have been focused on seeking out CO₂-neutral means of energy production.¹⁻³ Synthesis gas, a mixture of carbon monoxide (CO) and hydrogen (H₂), is readily derived from natural gas, coal, or biomass and poses an attractive alternative.⁴ It is utilized in the Fisher–Tropsch (F–T) process, which generates a Schultz-Flory distribution of hydrocarbons.⁵ Increasing the selectivity of the process is of much interest, and although many homogenous organometallic systems have been reported for the selective generation of C₂ products,⁶⁻¹¹ the generation of higher homologs is still more desirable as their properties better resemble fuels employed in the current energy infrastructure.¹² Moreover, besides the F–T process,^{4-5, 13} CO electroreduction on Cu electrodes¹⁴ and CO reduction by nitrogenases¹⁵⁻¹⁶ all result in a distribution of products that include C_{>2} products.

Insight into the nature of species capable of enchainment of more than two carbons is of interest for future catalyst design.¹⁷⁻²⁷ Despite that, there has only been one reported example of sequential catenation of CO to a C₂ product and then to C₃ and C₄ products employing cooperative reactivity of W(CO)₆ and an Al(I) reductant (Figure 3.1).²⁸ Previous work in our group has demonstrated that single-site Mo complexes supported by a *para*-terphenyl diphosphine ligand are capable of reductive coupling of CO via two distinct pathways, either with or without C–O bond cleavage preceding C–C bond formation, depending on temperature.²⁹⁻³⁰ However, further sequential catenation of the C₂ products at these complexes has not been observed. We postulated that modification of the central arene donor may allow new pathways of CO catenation to be uncovered.

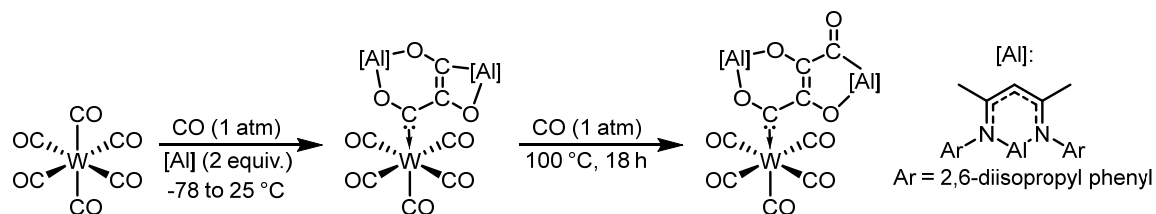


Figure 3.1. Sequential CO catenation of a C₃-containing complex to a C₄-containing complex.

It has been reported that extension of arene ligands (benzene to naphthalene or anthracene) on metal-arene complexes can significantly increase the lability of the arene and alter the reactivity at the metal center.³¹⁻³³ Chromium *bis*(naphthalene) has been shown to display much higher substitutional lability compared to its benzene analog.³⁴⁻³⁵ In a series of (η^6 -arene)Mo(PMe₃)₃ complexes (arene = benzene, naphthalene or anthracene), only with anthracene was oxidative addition of H₂ at the metal center observed, accompanied by a η^6 -to- η^4 ring slip (Figure 3.2).³⁶ Additional computational studies in that report proposed that this increased propensity for ring slippage stems from the increasingly favorable η^4 - vs. η^6 -arene interaction with lengthening of the aromatic system. In order to seek out novel CO catenation pathways and/or products that similar Mo diphosphine complexes may engender as a result hapticity changes at the basal arene, we set out to target a diphosphine with a naphthalene-based arene donor.

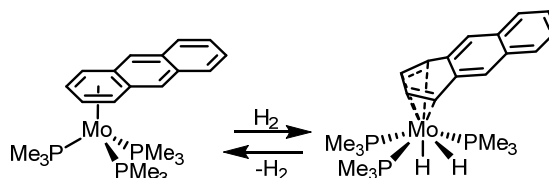
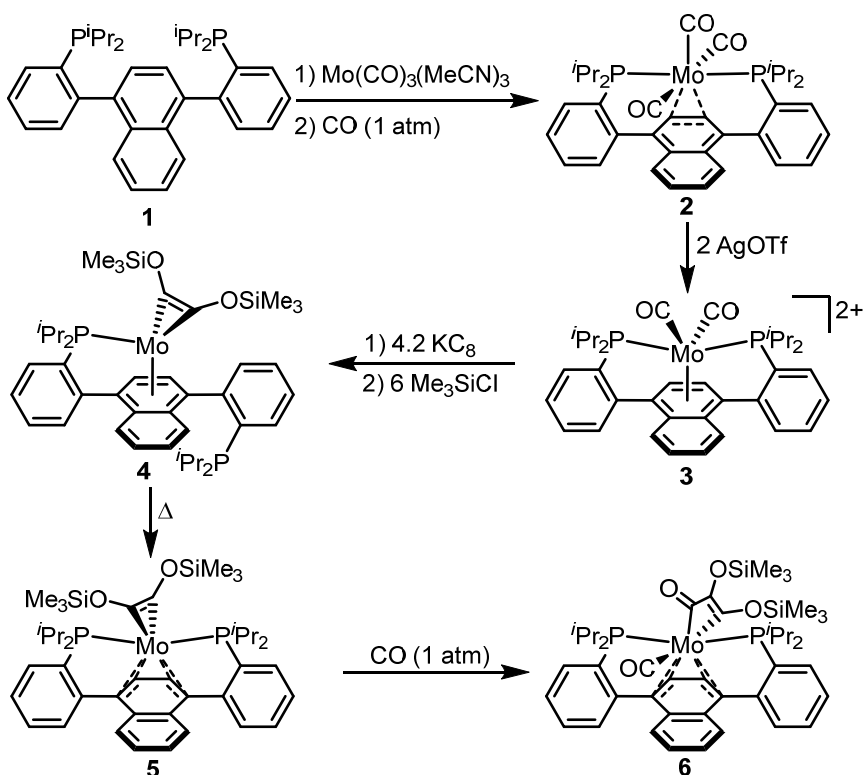


Figure 3.2. Reversible oxidative addition of H₂ to anthracene-supported Mo complex facilitated by anthracene ring-slippage.

RESULTS AND DISCUSSION

Naphthalenediyl-linked diphosphine **1** can be synthesized in an analogous manner to previously reported phenylene-linked variant starting from 1,4-diiodonaphthalene.³⁷ Metalation of **1** with $\text{Mo}(\text{CO})_3(\text{MeCN})_3$ provided tricarbonyl complex **2** along a minor amount (~5%) of a monocarbonyl species which cleanly converts to **2** when stirred under one atmosphere of CO (Scheme 3.1). Neither the formation of the monocarbonyl complex nor its conversion back to the tricarbonyl complex was observed in the phenylene-linked system. This conversion may be attributed to the more accessible η^4 -binding mode facilitating η^2 -to- η^6 ring slippage and concomitant loss of two CO ligands. Single crystal X-ray diffraction (XRD) analysis of **2** confirmed η^2 -binding to the edge carbons of the naphthalenediyl linker (Figure 3.3). Mild disruption of the central arene aromaticity is observed, with shortening of the C2–

Scheme 3.1. Synthesis and reactivity of naphthalenediyl-linked diphosphine molybdenum complexes



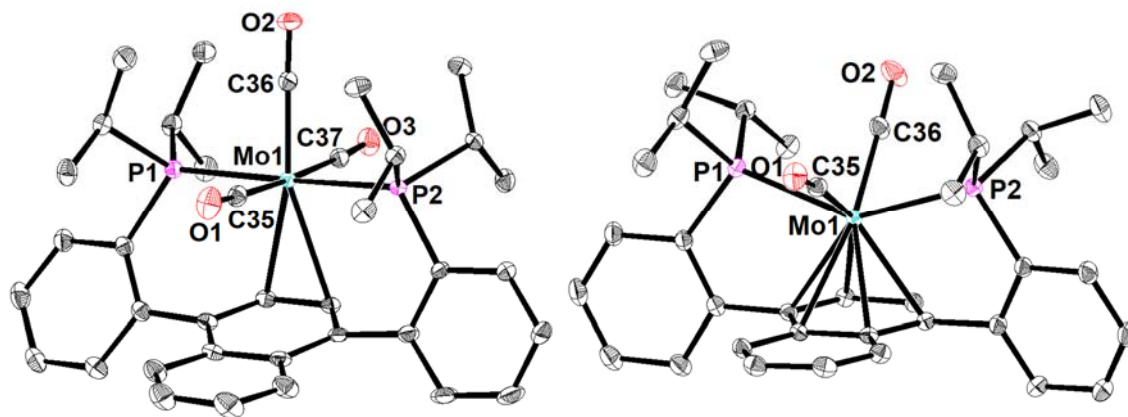


Figure 3.3. Solid-state structures of **2** and **3**. Thermal ellipsoids shown at 50% probability. Solvent molecules, counterions, and hydrogen atoms omitted for clarity.

C3 bond and lengthening of the C1–C2 and C3–C4 bonds compared to those in free naphthalene (Figure 3.4).³⁸

Oxidative decarbonylation by the reaction of **2** with two equiv. silver trifluoromethanesulfonate yielded dicationic dicarbonyl complex **3** as orange microcrystals. The solid-state structure of **3** displays η^6 -binding to the central arene, maintaining an 18-electron count at the metal center (Figure 3.3). Significant changes in the C–C bond lengths of the outer ring of the naphthalene, such as localized double bond character in C6–C7 and C8–C9, suggest disruption of aromaticity (Figure 3.4). In contrast, aromaticity is mostly maintained in the core Mo-bound ring.

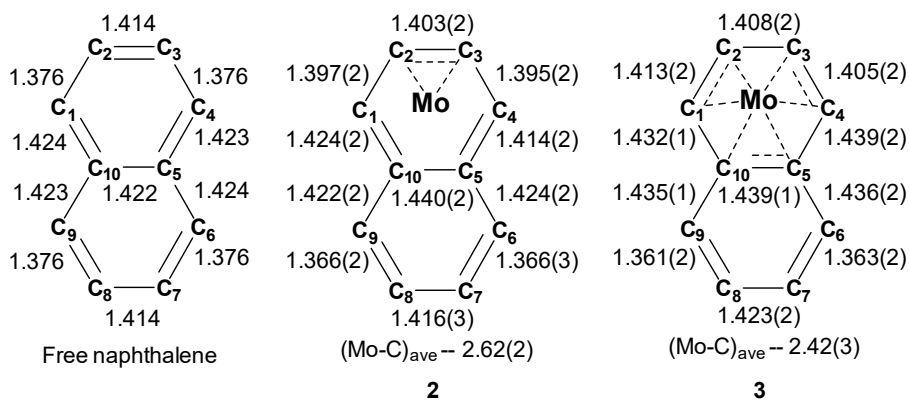


Figure 3.4. Naphthalene and naphthalenediyl linker bond metrics of complexes **2** and **3**.

Four-electron reduction of **3** with 4.2 equiv. KC_8 provided an asymmetric species spectroscopically analogous to previously dianionic phenylene-linked complex, suggesting dissociation of one of the *trans*-spanning phosphines.³⁰ Infrared (IR) spectroscopy showed highly-activated C=O stretches 1678 and 1580 cm^{-1} . Expecting the naphthalenediyl linker to be more readily reduced than the phenylene-linked analog,³⁹ the use of milder reductants was investigated. Compared to the phenylene-linked complex which required the use of potassium naphthalenide (-3.05 V vs Fc) to access, it was found that **3** could be reduced to the dianionic state with potassium anthracenide (-2.47 V vs. Fc), a shift of almost +0.6 V less reducing.⁴⁰

Quenching the dianionic species with chlorotrimethylsilane (Me_3SiCl) affords asymmetric species **4**. The ^1H and $^{31}\text{P}\{^1\text{H}\}$ NMR spectroscopy of **4** is consistent with a complex possessing a free phosphine arm, and with a bound *bis*(siloxo)acetylene ligand formed from C–C coupling of the two carbonyl ligands. In contrast with the phenylene-linked system wherein C–O bond cleavage was observed prior to C–C bond formation, exclusive C–C coupling without C–O bond cleavage was observed.³⁰ The observed difference in selectivity upon quenching may be due to several reasons: 1) the less electron-rich (less reducing) nature of the dianionic naphthalenediyl-linked species vs. phenylene and/or 2) the availability of more accessible η^4 -arene bound transition states or intermediates in the naphthalenediyl-linked system. These differences may result in the C–O cleavage step to become inaccessible, leading to exclusive C–C bond formation observed.

Because **4** converts to a new symmetric complex **5** even at $-35\text{ }^\circ\text{C}$, over days, or at $90\text{ }^\circ\text{C}$, over about an hour, solid-state characterization of **4** was not obtained. Complex **5** displays a broad ^{31}P resonance at 76.7 ppm suggestive of a fluxional process and renders both acetylene carbons equivalent in the ^{13}C NMR. Solid-state characterization confirmed the identity of **5** to be a *bis*(siloxo)acetylene complex with molybdenum binding to both phosphines and

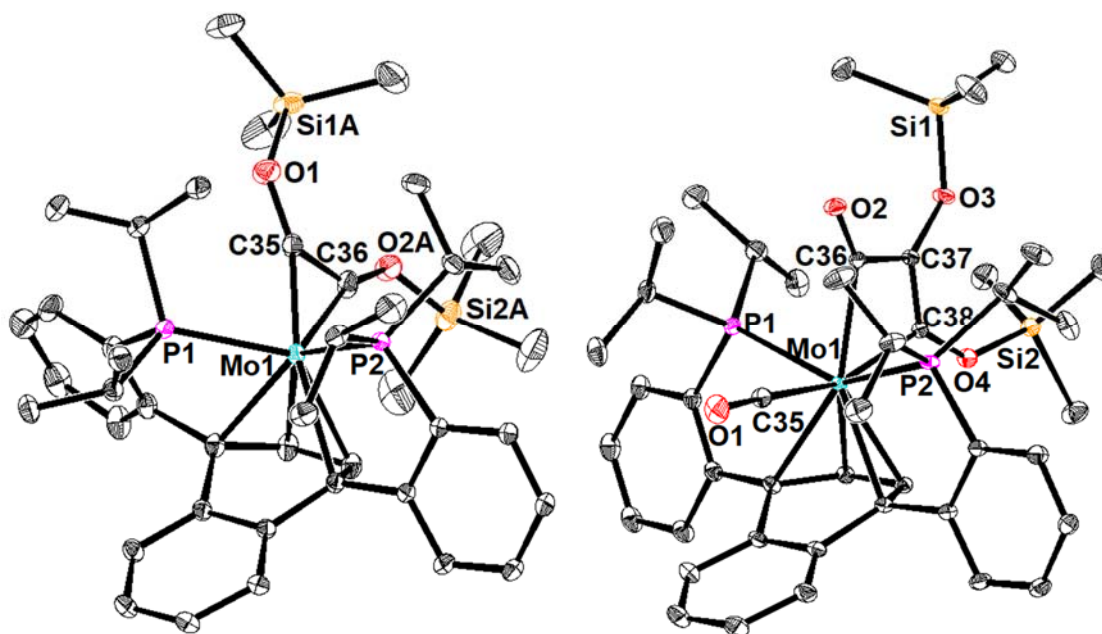


Figure 3.5. Solid-state structures of **5** and **6**. Thermal ellipsoids shown at 50% probability. Solvent molecules, counterions, and hydrogen atoms omitted for clarity.

interacting with the central arene in an η^4 -fashion (Figure 3.5). The phosphine arms appear to be twisted with the *bis*(siloxo)acetylene off leaning off to one side. The Mo center is also off-center with a significantly shorter Mo–C1 distance (2.2481(9)Å) compared to Mo–C4 (2.4341(9)Å). This asymmetry, if maintained in the solution state, would be consistent with the broadness of the NMR features. A significant deviation of the naphthalenediyl linker from planarity is observed (41° angle between the C1C2C3C4 and C1C4C5C10 planes), consistent with previously reported η^4 -bound naphthalene complexes.⁴¹⁻⁴² C1–C10 and C4–C5 distances are indicative of single bond character while aromaticity is maintained in the outer ring, with relatively similar C–C bond distances (Figure 3.6). The conversion of **4** to **5** is likely facilitated by the increased propensity for η^4 -arene binding in the naphthalenediyl vs. the phenylene linker, as the latter does not exhibit such a transformation nor have an η^4 -arene binding mode.

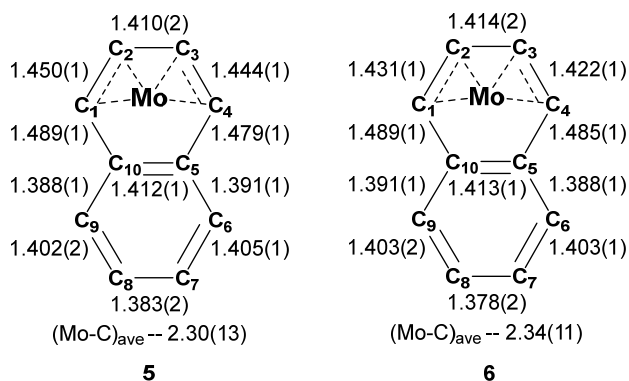
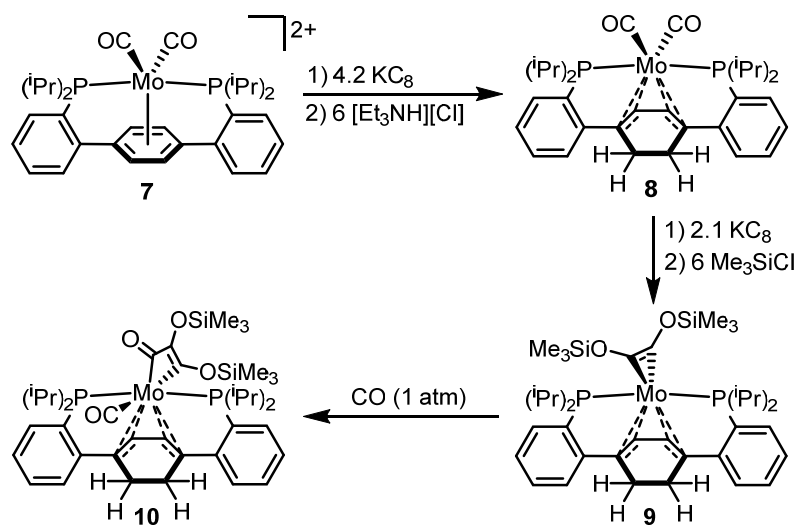


Figure 3.6. Naphthalenediyl linker bond metrics of complexes **5** and **6**.

In order to further investigate the origin of selectivity towards exclusive C–C coupling vs. C–O cleavage preceding C–C coupling, the synthesis of complexes supported by a 1,4-cyclohexadienediyl-linked diphosphine was targeted. Conveniently, the synthesis of neutral dicarbonyl complex **8** can be achieved by reduction of dication **7** followed with quenching with an acid (Scheme 3.2). $^{31}\text{P}\{^1\text{H}\}$ NMR revealed a singlet at 82.4 ppm while ^1H NMR spectrum showed coupling multiplets at 2.77 and 2.29 ppm that integrated to two protons each, consistent with the cyclohexadiene methylene protons and formal arene hydrogenation at adjacent carbons. When complex **8** was reduced by two electrons followed by quenching with Me_3SiCl , a *bis*(siloxy)acetylene complex **9** was afforded. Similar to **6**, a broad signal was

Scheme 3.2. Synthesis and reactivity of cyclohexadienediyl-diphosphine Mo complexes



observed in the $^{31}\text{P}\{^1\text{H}\}$ NMR spectrum. Since the electron richness of the reduced phenylene linker would be expected to lie between that of the naphthalenediyl and the cyclohexadienediyl linkers, it strongly suggests that the observed selectivity originates from the ability of the central ligand to support an η^4 -binding mode during quenching, which both the naphthalenediyl and the cyclohexadienediyl have in common.

Bis(siloxy)acetylene complex **5**, with the C_2 product still metal-bound, posed to be a good starting point for the generation of $\text{C}_{\geq 3}$ products through further CO catenation. Stirring a benzene solution of **5** under one atmosphere of CO at room temperature overnight resulted in a brown to red-brown color change. $^{31}\text{P}\{^1\text{H}\}$ NMR spectroscopy showed the formation of a new species **6** with a chemical shift at 56.1 ppm. In order to further probe the identity of this species, **5** was treated with ^{13}CO . Two enhanced resonances were observed in the ^{13}C NMR spectrum at 232.93 ppm and 225.15 ppm. Their triplet of doublets splitting pattern, alongside the observation of a doublet of doublets splitting pattern of the ^{31}P resonance, indicated the incorporation of two isotopically-enriched CO molecules into **6- ^{13}C** . Crystallization of **6** from slow evaporation of a saturated pentane solution provided single crystals suitable for XRD. The solid-state structure confirmed the incorporation of two CO molecules to yield metallacyclobutenone complex **6**. The molybdenum center displays η^4 -arene binding to the central arene, maintaining an 18-electron count, and corroborates the NMR spectroscopic data. The C37–C38 distance of 1.366(1)Å is consistent with a C–C double bond. The insertion of CO relieves steric strain near the metal center, previously caused by the Me_3Si group, resulting in a much more symmetric coordination environment. This, to the best of our knowledge, is the first example of further CO catenation of a CO-derived C_2 fragment to a C_3 product at a single metal site.

With the similar coordination environment at Mo of **5** and **9**, further CO catenation

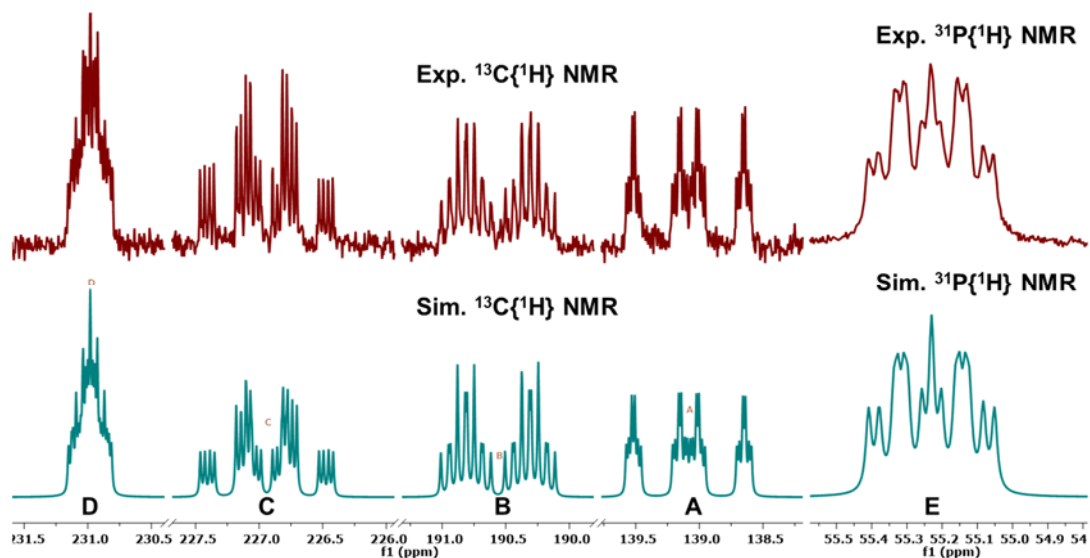


Figure 3.7. Experimental (top) and simulated (bottom) partial $^{13}\text{C}\{^1\text{H}\}$ (126 MHz, 25 °C, C_6D_6) and $^{31}\text{P}\{^1\text{H}\}$ (202 MHz, 25 °C, C_6D_6) NMR spectra of $11\text{-}^{13}\text{C}$.

with **9** was explored. Using ^{13}CO -derived *bis*(siloxy)acetylene complex $9\text{-}^{13}\text{C}$, treatment with ^{13}CO results in the formation of CO inserted complex $10\text{-}^{13}\text{C}$ showing rich coupling information in both the ^{13}C and $^{31}\text{P}\{^1\text{H}\}$ spectra (Figure 3.7), resulting from scalar coupling between the four $S = \frac{1}{2}$ ^{13}C atoms derived from CO and the two $S = \frac{1}{2}$ phosphine ligands.

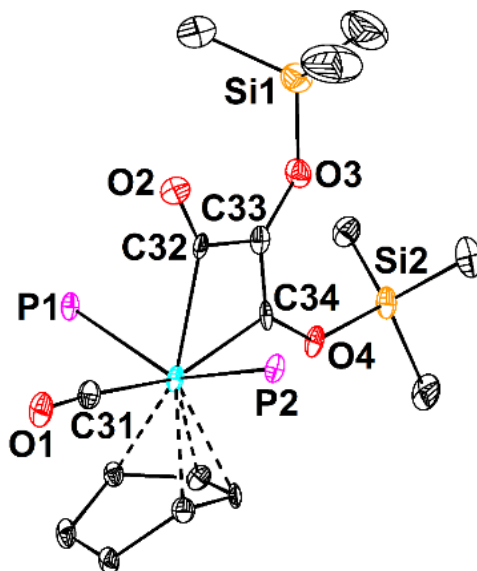


Figure 3.8. Truncated preliminary solid-state structure of **10**. Thermal ellipsoids are shown at the 50% probability level. Hydrogen atoms, phenylene linkers, and phosphine isopropyl groups are omitted for clarity.

The solubility of **10** prohibited growth of high-quality single crystals, but allowed for the collection of a preliminary structure via slow evaporation of a pentane solution at $-35\text{ }^{\circ}\text{C}$ (Figure 3.8). The signals A, B, C, D and E in Figure 3.7 correspond to C34, C33, C32, C31 and P1/2 in Figure 3.8, respectively, and corroborates the spectroscopic data, supporting the formation of the observed metallacyclobutenone.

CONCLUSION

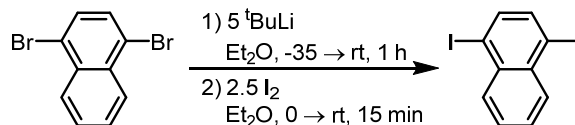
A series of naphthalenediyl-linked Mo complexes have been synthesized and characterized. Reduction of the dicarbonyl complex **3** followed by Me₃SiCl quenching resulted in reductive CO coupling to a *bis*(siloxy)acetylene complex **5**. This selectivity is proposed to be due to the ability of the central arene donor to support η^4 -binding modes that were not accessible on the phenylene-linked system. Exposure of **5** to one atmosphere of CO results in further CO catenation to give metallacyclobutenone complex **6** that features a C₃ fragment complete derived from CO and represents a functional-group rich building block. Efforts to liberate this organic motif are underway. Should these efforts prove successful, a synthetic cycle for the conversion of CO to reduced C₃ motifs will be targeted.

EXPERIMENTAL SECTION

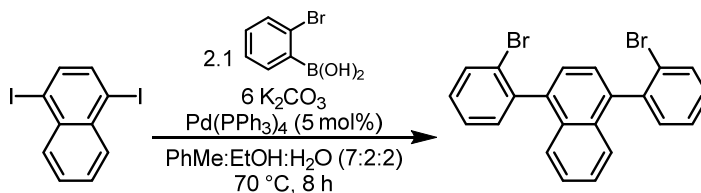
General Considerations

Unless otherwise specified, all operations involving air- or water-sensitive reagents were carried out in an MBraun drybox under a nitrogen atmosphere or using standard Schlenk and vacuum line techniques. Solvents for air- and moisture-sensitive reactions were dried by the method of Grubbs.⁴³ Deuterated solvents were purchased from Cambridge Isotope Laboratories. C₆D₆ was vacuum transferred from sodium benzophenone ketyl before use and CD₃CN was stirred over calcium hydride and vacuum distilled before use. All solvents, once dried and degassed, were stored under a nitrogen atmosphere over 4 Å molecular sieves. 1,4-dibromonaphthalene,⁴⁴ Mo(CO)₃(MeCN)₃,⁴⁵ and potassium graphite,⁴⁶ and **7**,³⁷ were prepared according to literature procedures. Potassium naphthalenide and potassium anthracenide solutions were prepared by stirring a THF solution of either naphthalene or anthracene in the presence of a potassium mirror for 30 minutes then filtered through a glass-fiber filter plug and used immediately. Pre-reduced Teflon-coated stir bars (prepared via stirring a Na[C₁₀H₈] solution overnight followed by rinsing three times with THF) were utilized in any stirred reaction in which KC₈, K[C₁₀H₈], K[C₁₄H₁₂] were employed as reagents. Naphthalene (sublimed under N₂), anthracene (sublimed under N₂), chlorotrimethylsilane (dried over CaH₂ and distilled prior to use), sodium metal (washed with hexanes), and potassium metal (washed with hexanes) were purified before use. All other reagents were used as received. ¹H, ¹³C{¹H}, ¹⁹F, and ³¹P{¹H} NMR spectra were recorded on Varian Mercury 300 MHz or Varian 400 MHz spectrometers at ambient temperatures unless otherwise denoted. ¹H and ¹³C{¹H} NMR spectra are reported referenced internally to residual solvent peaks reported relative to tetramethylsilane. ¹⁹F NMR chemical shifts are referenced to an external standard of C₆F₆ (-164.9 ppm). ³¹P{¹H} NMR chemical shifts are referenced to an external standard of H₃PO₄

(0.0 ppm). Fast atom bombardment-mass spectrometry (FAB-MS) analyses were performed with a JEOL JMS-600H high-resolution mass spectrometer.

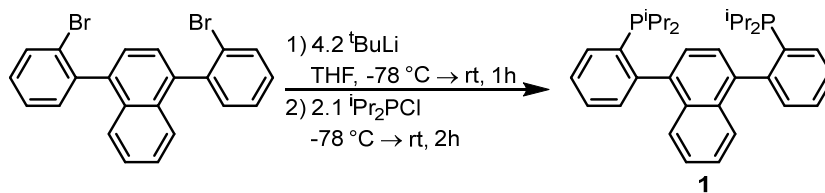


1,4-diiodonaphthalene. Adapted from a previously reported procedure.⁴⁷ To a solution of 1,4-dibromonaphthalene (10 g, 35.0 mmol) in diethyl ether (100 mL) cooled to -35°C was added, dropwise, a solution of *tert*-butyl lithium in pentane (92 mL, 1.9 M, 175 mmol). After complete addition, the reaction was allowed to warm to room temperature and stirred for 1 hour. The resulting suspension was cooled to 0°C and iodine (22.2 g, 87.5 mmol) was added slowly under a counter flow of nitrogen. After complete addition, the dark brown solution was allowed to warm to room temperature and stirred for an additional 15 minutes. The reaction was diluted with diethyl ether (100 mL) and washed thrice with a 25% $\text{Na}_2\text{S}_2\text{O}_3$ solution. The organic layer was dried over MgSO_4 , filtered, and concentrated in vacuo to yield the crude product. The crude solid was passed through a silica plug, eluting with CH_2Cl_2 , and the volatiles removed under vacuum once again. Recrystallization of the solid from boiling ethanol provided golden needles that were collected via filtration, washed with cold ethanol, and dried in vacuo (9.78 g, 73%). ^1H NMR characterization matches the reported literature values.



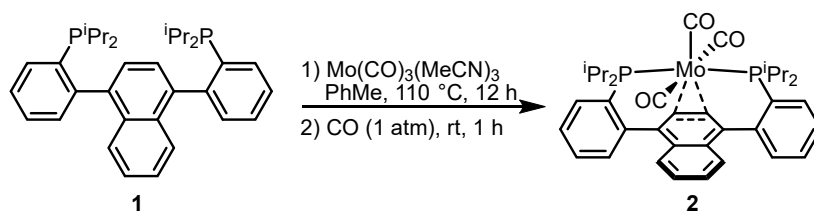
1,4-*bis*(2-bromophenyl)naphthalene. A Schlenk tube fitted with a screw-in Teflon stopper was charged with 1,4-diiodonaphthalene (9.0 g, 23.7 mmol), 2-bromophenylboronic acid

(10.0g, 50.0 mmol), and anhydrous potassium carbonate (19.6 g, 142 mmol) suspended in a mixture of toluene (350 mL), ethanol (100 mL), and water (100 mL). The suspension was degassed via three freeze-pump-thaw cycles, after which *tetrakis*(triphenylphosphine) palladium(0) (1.37 g, 1.19 mmol) was added under a counter flow of nitrogen. The flask was sealed and heated to 70 °C for 8 h with stirring. After cooling to room temperature, water (200 mL) was added and the organic layer separated. The aqueous layer was extracted with CH₂Cl₂ (2 × 200 mL). The organic extracts were combined and dried over MgSO₄, filtered, and concentrated in vacuo. The crude yellow oil was precipitated by trituration in MeOH (150 mL) overnight, collected via filtration, and dried in vacuo to yield the product as a pale yellow powder (10.0 g, 96 %). ¹H NMR (400 MHz, CDCl₃): δ 7.77 (d, ³J_{H,H} = 8.1 Hz, 2H, ArH), 7.55 (dd, ³J_{H,H} = 6.4 Hz, ⁴J_{H,H} = 3.4 Hz, 2H, ArH), 7.50 – 7.40 (m, 8H, ArH), 7.34 (ddd, ³J_{H,H} = 7.8, 6.6 Hz, ⁴J_{H,H} = 2.4 Hz, 2H); ¹³C {¹H} NMR (101 MHz, CDCl₃): δ 141.44 (aryl-C), 139.31 (aryl-C), 132.88 (aryl-C), 132.37 (aryl-C), 131.71 (aryl-C), 129.31 (aryl-C), 127.33 (aryl-C), 126.49 (aryl-C), 126.43 (aryl-C), 126.15 (aryl-C), 124.49 (aryl-C); HRMS (FAB+) m/z Calcd. for C₂₂H₁₄Br₂ [M]⁺ 437.9442, found 437.9426.



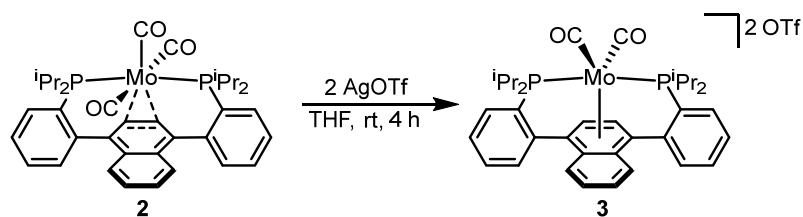
1,4-bis(2-(diisopropylphosphanyl)phenyl)naphthalene (1). To a stirred solution of 1,4-*bis*(2-bromophenyl)naphthalene (23.6 g, 53.9 mmol) in tetrahydrofuran (300 mL) cooled to -78 °C was added, dropwise, a pentane solution of tert-butyl lithium (119 mL, 1.9 M, 226 mmol). The reaction was allowed to warm to room temperature and stirred for 1 h. The reaction was cooled to -78 °C and chlorodiisopropylphosphine (17.8 mL, 113 mmol) was then added dropwise. The reaction was allowed to warm to room temperature and stirred for

an additional 2 h. The pale yellow solution was concentrated in vacuo and the subsequent workup was carried out in a nitrogen-purged wet box using degassed solvents. The residue was taken up in CH₂Cl₂ (200 mL) and water (200 mL). The organic layer was separated and the aqueous layer extracted with CH₂Cl₂ (2 × 200 mL). The combined extracts were concentrated under vacuum. The resultant sticky solid was triturated from methanol (100 mL), filtered, and dried in vacuo to yield the product as a pale yellow solid (22.5 g, 81.4 %). ¹H NMR (400 MHz, C₆D₆): δ 7.59 (dd, ³J_{H,H} = 6.5 Hz, ⁴J_{H,H} = 3.4 Hz, 2H, ArH), 7.47 (dt, ³J_{H,H} = 7.8 Hz, ⁴J_{H,H} = 1.6 Hz, 2H, ArH), 7.41 (s, 2H, ArH), 7.21 – 7.06 (m, 8H, ArH), 1.87 (heptd, ³J_{H,H} = 7.0 Hz, ²J_{P,H} 3.9 Hz, 2H, CH(CH₃)₂), 1.78 (hept, ³J_{H,H} = 6.9 Hz, 2H, CH(CH₃)₂), 0.98 (dd, ³J_{P,H} = 14.2, ³J_{H,H} 7.0 Hz, 6H, CH₃), 0.94 (dd, ³J_{P,H} = 10.2 Hz, ³J_{H,H} = 7.0 Hz, 6H, CH₃), 0.86 (dd, ³J_{P,H} = 12.3 Hz, ³J_{H,H} = 6.9 Hz, 6H, CH₃), 0.80 (dd, ³J_{P,H} = 14.5 Hz, ³J_{H,H} 6.9 Hz, 6H, CH₃); ¹³C{¹H} NMR (101 MHz, C₆D₆): δ 149.32 (d, J = 31.6 Hz, aryl-C), 140.52 (d, J = 6.6 Hz, aryl-C), 137.36 (d, J = 22.0 Hz, aryl-C), 133.38 (d, J = 1.9 Hz, aryl-C), 132.63 (d, J = 3.4 Hz, aryl-C), 131.87 (d, J = 5.7 Hz, aryl-C), 128.55 (d, J = 1.0 Hz, aryl-C), 127.73 (d, J = 0.9 Hz, aryl-C), 127.65 (d, J = 3.2 Hz, aryl-C), 125.35 (aryl-C), 26.09 (d, J = 16.5 Hz, PCH(CH₃)₂), 24.33 (d, J = 14.9 Hz, PCH(CH₃)₂), 20.98 (d, J = 18.9 Hz, CH₃), 20.45 (d, J = 13.8 Hz, CH₃), 20.38 (d, J = 21.9 Hz, CH₃), 19.76 (d, J = 8.5 Hz, CH₃); ³¹P{¹H} NMR (162 Hz, C₆D₆): δ -5.62(s); HRMS (FAB+) m/z Calcd. for C₃₄H₄₃P₂ [M+H]⁺ 513.2840, found 513.2828.

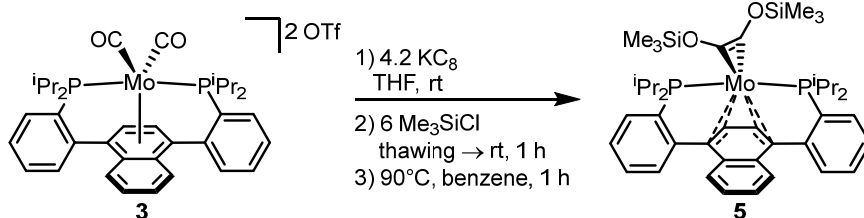


Synthesis of 2. To a Schlenk tube charged with a Teflon-coated stir bar was added 1,4-*bis*-(diisopropylphosphanyl)phenyl)naphthalene (200 mg, 0.39 mmol), Mo(CO)₃(MeCN)₃ (118 mg, 0.39 mmol), and toluene (10 mL). The tube was sealed and heated to 110 °C for 12 hours.

After cooling to room temperature, the resulting deep red solution was degassed and placed under 1 atm of CO. After stirring an additional 1 hour, the volatiles were removed in vacuo. The residue was washed with hexanes (10 mL), extracted with benzene, filtered over diatomaceous earth, and lyophilized to yield **2** as a dark purple-red solid (246 mg, 91 %). Crystals suitable for single crystal XRD were grown by slow diffusion of pentane into a saturated THF solution of **2**. ^1H NMR (400 MHz, C_6D_6): δ 7.98 (dd, $J = 6.6, 3.3$ Hz, 2H, ArH), 7.47 (dq, $J = 6.9, 2.0$ Hz, 2H, ArH), 7.40 (dq, $J = 7.6, 1.8$ Hz, 2H, ArH), 7.17 – 7.08 (m, 6H, ArH), 6.54 (app t, $J = 2.9$ Hz, 2H ArH), 2.56 (ddt, $J = 13.5, 10.3, 6.7$ Hz, 2H, $\text{CH}(\text{CH}_3)_2$), 2.22 – 2.06 (m, 2H, $\text{CH}(\text{CH}_3)_2$), 1.67 – 1.58 (m, 6H, $\text{CH}(\text{CH}_3)_2$), 1.28 (app q, $J = 7.1$ Hz, 6H, $\text{CH}(\text{CH}_3)_2$), 1.05 – 0.96 (m, 6H, $\text{CH}(\text{CH}_3)_2$), 0.73 (app q, $J = 6.9$ Hz, 6H, $\text{CH}(\text{CH}_3)_2$); $^{13}\text{C}\{^1\text{H}\}$ NMR (101 MHz, C_6D_6): δ 220.77 (t, $J_{\text{PC}} = 10.0$ Hz, Mo–CO), 215.62 (t, $J_{\text{PC}} = 8.6$ Hz, Mo–CO), 211.30 (t, $J_{\text{PC}} = 10.0$ Hz, Mo–CO), 147.35 (app t, $J = 7.4$ Hz, aryl-C), 135.17 (app t, $J = 4.0$ Hz), 133.69 (app t, $J = 9.3$ Hz, aryl-C), 131.56 (aryl-C), 131.40 (aryl-C), 131.09 (app t, $J = 2.2$ Hz, aryl-C), 128.38 (d, $J = 6.2$ Hz, aryl-C), 128.16 (d, $J = 5.7$ Hz, aryl-C), 127.94 (aryl-C), 126.45 (d, $J = 5.9$ Hz, aryl-C), 100.32 (central aryl-CH), 35.36 (t, $J = 9.2$ Hz, $\text{CH}(\text{CH}_3)_2$), 32.50 (t, $J = 8.9$ Hz, $\text{CH}(\text{CH}_3)_2$), 21.14 (app t, $J = 2.5$ Hz, $\text{CH}(\text{CH}_3)_2$), 19.91 (app t, $J = 4.2$ Hz, $\text{CH}(\text{CH}_3)_2$), 19.73 ($\text{CH}(\text{CH}_3)_2$), 19.69 (app t, $J = 2.0$ Hz, $\text{CH}(\text{CH}_3)_2$); $^{31}\text{P}\{^1\text{H}\}$ NMR (162 MHz, C_6D_6): δ 46.89 (s); Anal. calcd. for $\text{C}_{37}\text{H}_{42}\text{MoO}_3\text{P}_2$ (%): C, 64.16; H, 6.11. Found: C, 63.99; H, 6.02.

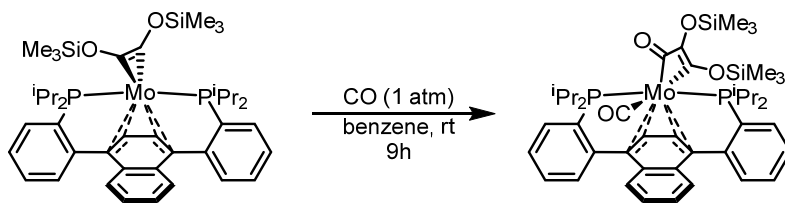


Synthesis of 3. To a stirred solution of **2** (4.00g, 5.77 mmol) in THF (50 mL), was added a solution of AgOTf (2.97 g, 11.5 mmol) in THF (30 mL). The reaction was allowed to stir at room temperature for 4 hours (extended stirring results in the formation of poly(THF)). The reaction was filtered over diatomaceous earth, the filtrate discarded, and the grey brown residue was extracted with MeCN (3 × 50 mL). The combined extracts were reduced in volume to about 20 mL and diethyl ether (150 mL) was added to induce precipitation. The product was collected via filtration and dried at 60 °C in vacuo to provide **3** as an orange microcrystalline solid (4.81 g, 86 %). Crystals suitable for single crystal XRD were grown by slow diffusion of diethyl ether into a saturated acetonitrile solution of **3**. ¹H NMR (400 MHz, CD₃CN): δ 8.03 – 7.90 (m, 6H, ArH), 7.88 (dd, J = 6.8, 3.2 Hz, 2H, ArH), 7.83 (dd, J = 7.8, 2.3 Hz, 2H, ArH), 7.37 – 7.26 (m, 4H, ArH), 3.33 – 3.18 (m, 4H, CH(CH₃)₂), 1.39 (dd, J = 16.0, 6.9 Hz, 6H, CH(CH₃)₂), 1.22 (dd, J = 13.1, 5.5 Hz, 6H, CH(CH₃)₂), 1.18 (dd, J = 11.1, 5.4 Hz, 6H, CH(CH₃)₂), 0.98 (dd, J = 18.7, 7.0 Hz, 6H, CH(CH₃)₂); ¹³C {¹H} NMR (101 MHz, CD₃CN): δ 223.17 (t, J_{FC} = 24.7 Hz, Mo–CO), 222.62 (t, J_{FC} = 22.9 Hz, Mo–CO), 140.14 (dd, J = 8.2, 5.9 Hz, aryl-C), 137.42 (aryl-C), 136.97 (app t, J = 3.7 Hz, aryl-C), 136.29 – 135.67 (m, aryl-C), 135.14 (app t, J = 1.3 Hz, aryl-C), 134.88 (aryl-C), 132.52 (app t, J = 3.4 Hz, aryl-C), 130.13 (d, J = 5.8 Hz, aryl-C), 128.33 (aryl-C), 122.12 (q, ¹J_{FC} = 321.0 Hz, CF₃), 114.52 (aryl-C), 103.27 (central aryl-CH), 30.03 – 29.40 (m, CH(CH₃)₂), 18.87 (CH(CH₃)₂), 18.50 (CH(CH₃)₂), 18.33 (app t, J = 2.0 Hz, CH(CH₃)₂), 18.23 (app t, J = 1.6 Hz, CH(CH₃)₂); ³¹P {¹H} NMR (162 MHz, CD₃CN): δ 72.50 (s); ¹⁹F NMR (372 MHz, CD₃CN): δ -79.25 (s); Anal. calcd. for C₃₈H₄₂F₆MoO₈P₂S₂ (%): C, 47.41; H, 4.40. Found: C, 47.56; H, 4.48.



Synthesis of 5. To a stirred suspension of **3** (1.00 g, 1.03 mmol) in THF (50 mL), was added KC8 (590 mg, 4.36 mmol) and allowed to stir at room temperature for 10 minutes, during which a deep red color developed. The reaction was then frozen in the cold well in the glovebox cooled with liquid nitrogen. The flask was removed from the cold well and trimethylsilyl chloride (0.8 mL, 6.23 mmol) was then added while thawing. The reaction was then allowed to warm to room temperature and stirred an additional hour, after which the volatiles were removed in vacuo. The residue was extracted with pentane and filtered over diatomaceous earth. The filtrate was concentrated under vacuum and the residue taken up in benzene (20 mL) and transferred to a Schlenk tube fitted with a screw-in Teflon stopcock. The flask was then sealed and warmed to 90 °C for 1 h. The reaction was cooled to room temperature and lyophilized to provide a dark brown powder. Recrystallization from slow evaporation of a saturated pentane solution at –35 °C yielded dark brown crystalline blocks (507 mg, 60%). Crystals suitable for single crystal XRD were grown similarly. ¹H NMR (300 MHz, C₆D₆): δ 7.39 (br dq, *J* = 7.4, 1.3 Hz, 2H, Ar*H*), 7.13 (br d, *J* = 6.2 Hz, 2H, Ar*H*), 7.00 (tt, *J* = 7.7, 1.2 Hz, 2H, Ar*H*), 6.91 (tt, *J* = 7.4, 1.3 Hz, 2H, Ar*H*), 6.66 (dd, *J* = 5.3, 3.2 Hz, 2H, Ar*H*), 6.52 (dd, *J* = 5.4, 3.2 Hz, 2H), 5.69 (s, 2H, central Ar*H*), 2.71 (dp, *J* = 18.2, 6.6 Hz, 2H, CH(CH₃)₂), 2.17 (hept, *J* = 7.1, 6.6 Hz, 2H, CH(CH₃)₂), 1.39 (dt, *J* = 12.1, 5.4 Hz, 12H, CH(CH₃)₂), 1.19 (dd, *J* = 12.5, 7.1 Hz, 6H, CH(CH₃)₂), 0.92 (dd, *J* = 12.2, 7.1 Hz, 6H, CH(CH₃)₂), 0.13 (s, 18H, Si(CH₃)₃); ¹³C {¹H} NMR (75 MHz, C₆D₆): δ 212.17 (br s, COSiMe₃), 150.58 (d, *J* = 21.7 Hz, aryl-C), 146.19 (d, *J* = 3.7 Hz, aryl-C), 144.80 (br d, *J* = 36.7 Hz, aryl-

C), 129.10 (d, $J = 1.6$ Hz, aryl-C), 128.27 (aryl-C), 127.90 (aryl-C), 125.62 (d, $J = 5.1$ Hz, aryl-C), 121.86 (aryl-C), 120.52 (br s, aryl-C), 86.95 (br s, central aryl-C), 83.12 (br s, central aryl-C), 29.47 (br s, $\text{CH}(\text{CH}_3)_2$), 28.07 (d, $J = 15.5$ Hz, $\text{CH}(\text{CH}_3)_2$), 22.47 (d, $J = 10.1$ Hz, $\text{CH}(\text{CH}_3)_2$), 22.48 (d, $J = 8.5$ Hz, $\text{CH}(\text{CH}_3)_2$), 19.89 ($\text{CH}(\text{CH}_3)_2$), 18.91 ($\text{CH}(\text{CH}_3)_2$), 0.89 ($\text{Si}(\text{CH}_3)_3$); $^{31}\text{P}\{^1\text{H}\}$ NMR (121 MHz, C_6D_6): δ 76.73 (s); Anal. calcd. for $\text{C}_{42}\text{H}_{60}\text{MoO}_2\text{P}_2\text{Si}_2$ (%): C, 62.20; H, 7.46. Found: C, 62.34; H, 7.65.



Synthesis of 6. A solution of **5** (100 mg, 0.123 mmol) in benzene (2 mL) was placed under 1 atm of CO and stirred for 9 h. The volatiles were then removed *in vacuo* to yield **6** as a red brown powder (106 mg, 99 %). Crystals suitable for single crystal XRD were grown by slow evaporation of a saturated pentane solution at -35 °C. ^1H NMR (300 MHz, C_6D_6): δ 7.54 (dq, $J = 7.7, 1.4$ Hz, 2H, ArH), 7.16 – 7.12 (m, 2H, ArH), 7.04 (t, $J = 7.1$ Hz, 2H, ArH), 6.98 (t, $J = 7.1$ Hz, 2H, ArH), 6.78 (dd, $J = 5.5, 3.3$ Hz, 2H), 6.38 (dd, $J = 5.5, 3.2$ Hz, 2H, ArH), 5.57 (t, $^3J_{\text{PH}} = 1.5$ Hz, 2H, central ArH), 2.68 (hept, $J = 7.0$ Hz, 2H, $\text{CH}(\text{CH}_3)_2$), 2.55 – 2.41 (m, 2H, $\text{CH}(\text{CH}_3)_2$), 1.84 – 1.74 (m, 6H, $\text{CH}(\text{CH}_3)_2$), 1.23 – 1.15 (m, 6H, $\text{CH}(\text{CH}_3)_2$), 1.15 – 1.07 (m, 6H, $\text{CH}(\text{CH}_3)_2$), 0.81 – 0.72 (m, 6H, $\text{CH}(\text{CH}_3)_2$), 0.36 (s, 9H $\text{Si}(\text{CH}_3)_3$), 0.18 (s, 9H, $\text{Si}(\text{CH}_3)_3$); $^{13}\text{C}\{^1\text{H}\}$ NMR (75 MHz, C_6D_6): δ 232.99 ($\text{C}\equiv\text{O}$), 225.19 ($\text{C}=\text{O}$), 187.13 (COSiMe_3), 148.10 (app t, $J = 12.0$ Hz, aryl-C), 142.99 (aryl-C), 140.07 (app t, $J = 4.6$ Hz, aryl-C), 138.99 (app t, $J = 13.9$ Hz, COSiMe_3), 131.10 (aryl-C), 129.86 (app t, $J = 4.9$ Hz, aryl-C), 128.81 (aryl-C), 128.59 (aryl-C), 127.03 (app t, $J = 1.6$ Hz, aryl-C), 123.26 (aryl-C), 120.64 (aryl-C), 92.90 (central aryl-C), 83.02 (central aryl-C), 31.17 (t, $J = 10.8$ Hz, $\text{CH}(\text{CH}_3)_2$), 20.75 ($\text{CH}(\text{CH}_3)_2$), 20.40 t, $J = 2.7$ Hz, ($\text{CH}(\text{CH}_3)_2$), 19.38 ($\text{CH}(\text{CH}_3)_2$), 18.87 (t, $J = 2.9$ Hz, $\text{CH}(\text{CH}_3)_2$), 2.33

(Si(CH₃)₃), 1.94 (Si(CH₃)₃); ³¹P{¹H} NMR (121 MHz, C₆D₆): δ 56.10 (s); Anal. calcd. for C₄₄H₆₀MoO₄P₂Si₂ (%): C, 60.95; H, 6.98. Found: C, 60.61; H, 6.97.

CRYSTALLOGRAPHIC INFORMATION

CCDC deposition numbers 1909081, 1909082, 1909083 and 1909084 contain the supplementary crystallographic data for this paper.⁴⁸ These data can be obtained free of charge from The Cambridge Crystallographic Data Centre via www.ccdc.cam.ac.uk/data_request/cif.

Refinement Details

In each case, crystals were mounted on a glass fiber or MiTeGen loop using Paratone oil, then placed on the diffractometer under a nitrogen stream. Low temperature (100 K) X-ray data were obtained on a Bruker D8 VENTURE Kappa Duo PHOTON 100 CMOS based diffractometer (Mo I μ S HB micro-focus sealed X-ray tube, $K\alpha = 0.71073 \text{ \AA}$ OR Cu I μ S HB micro-focused X-ray tube, $K\alpha = 1.54178$). All diffractometer manipulations, including data collection, integration, and scaling were carried out using the Bruker APEXII software.⁴⁹ Absorption corrections were applied using SADABS.⁵⁰ Space groups were determined on the basis of systematic absences and intensity statistics and the structures were solved in the Olex 2 software interface⁵¹ by intrinsic phasing using XT (incorporated into SHELXTL)⁵² and refined by full-matrix least squares on F2. All non-hydrogen atoms were refined using anisotropic displacement parameters, except in some cases with heavily distorted solvent. Hydrogen atoms were placed in the idealized positions and refined using a riding model. The structure was refined (weighed least-squares refinement on F2) to convergence. Graphical representations of structures with 50% probability thermal ellipsoids were generated using Diamond 3 visualization software.⁵³

Table 3.1. Crystal data and structure refinement for **2**, **3**, **5**, and **6**

	2	3	5	6
CCDC Number ⁴⁸	1909081	1909082	1909083	1909084
Empirical formula	C ₃₇ H ₄₂ MoO ₃ P ₂	C ₄₀ H ₄₅ F ₆ MoNO ₈ P ₂ S ₂	C ₄₂ H ₆₀ MoO ₂ P ₂ Si ₂	C ₄₄ H ₆₀ MoO ₄ P ₂ Si ₂
Formula weight	692.58	1003.77	810.96	866.98
Temperature/K	100.0	100	100.15	100.15
Crystal system	monoclinic	monoclinic	triclinic	monoclinic
Space group	P2 ₁ /c	P2 ₁ /n	P-1	P2 ₁ /n
a/Å	28.7301(7)	11.1859(5)	9.4793(7)	10.2194(3)
b/Å	12.2177(3)	20.4880(9)	11.1917(8)	22.9968(6)
c/Å	19.9479(5)	18.9117(8)	21.4257(15)	19.0948(5)
α/°	90	90	85.339(4)	90
β/°	108.7030(10)	95.489(2)	89.506(4)	104.4620(10)
γ/°	90	90	67.848(3)	90
Volume/Å ³	6632.3(3)	4314.2(3)	2097.7(3)	4345.3(2)
Z	8	4	2	4
ρ _{calc} /cm ³	1.387	1.545	1.284	1.325
μ/mm ⁻¹	0.527	0.553	0.479	0.471
Crystal size/mm ³	0.2 × 0.2 × 0.1	0.3 × 0.2 × 0.2	0.45 × 0.384 × 0.12	0.23 × 0.18 × 0.16
Radiation	MoKα (λ = 0.71073)	MoKα (λ = 0.71073)	MoKα (λ = 0.71073)	MoKα (λ = 0.71073)
2θ range/°	4.48 to 61.056	4.164 to 75.49	3.944 to 95.846	5.432 to 90.668
GOF	1.032	1.035	1.305	1.036
R ₁ , ^a wR ₂ ^b [I > 2σ(I)]	0.0294, 0.0641	0.0341, 0.0803	0.0443, 0.1063	0.0353, 0.0693

$$^a R_1 = \sum ||F_o| - |F_c|| / \sum |F_o|. \quad ^b wR_2 = [\sum [w(F_o^2 - F_c^2)^2] / \sum [w(F_o^2)^2]^{1/2}$$

REFERENCES

- (1) Appel, A. M.; Bercaw, J. E.; Bocarsly, A. B.; Dobbek, H.; DuBois, D. L.; Dupuis, M.; Ferry, J. G.; Fujita, E.; Hille, R.; Kenis, P. J. A.; Kerfeld, C. A.; Morris, R. H.; Peden, C. H. F.; Portis, A. R.; Ragsdale, S. W.; Rauchfuss, T. B.; Reek, J. N. H.; Seefeldt, L. C.; Thauer, R. K.; Waldrop, G. L., *Chem. Rev.* **2013**, *113*, 6621-6658.
- (2) Wayland, B.; Fu, X., *Science* **2006**, *311*, 790.
- (3) Kerr, R. A., *Science* **2005**, *310*, 1106.
- (4) West, N. M.; Miller, A. J. M.; Labinger, J. A.; Bercaw, J. E., *Coordination Chemistry Reviews* **2011**, *255*, 881-898.
- (5) Rofer-DePoorter, C. K., *Chemical Reviews* **1981**, *81*, 447-474.
- (6) Protasiewicz, J. D.; Lippard, S. J., *J. Am. Chem. Soc.* **1991**, *113*, 6564-6570.
- (7) Bianconi, P. A.; Vrtis, R. N.; Rao, C. P.; Williams, I. D.; Engeler, M. P.; Lippard, S. J., *Organometallics* **1987**, *6*, 1968-1977.
- (8) Carnahan, E. M.; Protasiewicz, J. D.; Lippard, S. J., *Acc. Chem. Res.* **1993**, *26*, 90-97.
- (9) Vrtis, R. N.; Rao, C. P.; Bott, S. G.; Lippard, S. J., *J. Am. Chem. Soc.* **1988**, *110*, 7564-7566.
- (10) Bianconi, P. A.; Williams, I. D.; Engeler, M. P.; Lippard, S. J., *J. Am. Chem. Soc.* **1986**, *108*, 311-313.
- (11) Suess, D. L. M.; Peters, J. C., *J. Am. Chem. Soc.* **2013**, *135*, 12580-12583.
- (12) Schulz, H., *Applied Catalysis A: General* **1999**, *186*, 3-12.
- (13) Maitlis, P. M.; Zanotti, V., *Chem. Commun.* **2009**, 1619-1634.
- (14) Li, C. W.; Ciston, J.; Kanan, M. W., *Nature* **2014**, *508*, 504-507.
- (15) Hu, Y. L.; Lee, C. C.; Ribbe, M. W., *Science* **2011**, *333*, 753-755.
- (16) Lee, C. C.; Hu, Y. L.; Ribbe, M. W., *Science* **2010**, *329*, 642-642.
- (17) Summerscales, O. T.; Cloke, F. G. N.; Hitchcock, P. B.; Green, J. C.; Hazari, N., *Science* **2006**, *311*, 829.
- (18) Summerscales, O. T.; Cloke, F. G. N.; Hitchcock, P. B.; Green, J. C.; Hazari, N., *J. Am. Chem. Soc.* **2006**, *128*, 9602-9603.
- (19) Frey, A. S.; Cloke, F. G. N.; Hitchcock, P. B.; Day, I. J.; Green, J. C.; Aitken, G., *J. Am. Chem. Soc.* **2008**, *130*, 13816-13817.
- (20) Arnold, P. L.; Turner, Z. R.; Bellabarba, R. M.; Tooze, R. P., *Chem. Sci.* **2011**, *2*, 77-79.
- (21) Mansell, S. M.; Kaltsoyannis, N.; Arnold, P. L., *J. Am. Chem. Soc.* **2011**, *133*, 9036-9051.

- (22) Tsoureas, N.; Summerscales, O. T.; Cloke, F. G. N.; Roe, S. M., *Organometallics* **2013**, *32*, 1353-1362.
- (23) Evans, W. J.; Lee, D. S.; Ziller, J. W.; Kaltsoyannis, N., *J. Am. Chem. Soc.* **2006**, *128*, 14176-14184.
- (24) Evans, W. J.; Grate, J. W.; Hughes, L. A.; Zhang, H.; Atwood, J. L., *J. Am. Chem. Soc.* **1985**, *107*, 3728-3730.
- (25) Wang, B.; Luo, G.; Nishiura, M.; Luo, Y.; Hou, Z., *J. Am. Chem. Soc.* **2017**, *139*, 16967-16973.
- (26) Watanabe, T.; Ishida, Y.; Matsuo, T.; Kawaguchi, H., *J. Am. Chem. Soc.* **2009**, *131*, 3474-3475.
- (27) Bennett, M. J.; Graham, W. A. G.; Smith, R. A.; Stewart, R. P., *J. Am. Chem. Soc.* **1973**, *95*, 1684-1686.
- (28) Kong, R. Y.; Crimmin, M. R., *J. Am. Chem. Soc.* **2018**, *140*, 13614-13617.
- (29) Buss, J. A.; Agapie, T., *J. Am. Chem. Soc.* **2016**, *138*, 16466-16477.
- (30) Buss, J. A.; Agapie, T., *Nature* **2016**, *529*, 72-75.
- (31) Kündig, E.; Perret, C.; Spichiger, S.; Bernardinelli, G., *J. Organomet. Chem.* **1985**, *286*, 183-200.
- (32) Thi, N. P. D.; Spichiger, S.; Paglia, P.; Bernardinelli, G.; Kündig, E. P.; Timms, P. L., *Helv. Chim. Acta* **1992**, *75*, 2593-2607.
- (33) Jang, M.; Ellis, J. E., *Angew. Chem. Int. Ed.* **1994**, *33*, 1973-1975.
- (34) Kündig, E. P.; Timms, P. L., *J. Chem. Soc., Chem. Commun.* **1977**, 912-913.
- (35) Kündig, E. P.; Timms, P. L., *J. Chem. Soc., Dalton Trans.* **1980**, 991-995.
- (36) Zhu, G.; Janak, K. E.; Figueroa, J. S.; Parkin, G., *J. Am. Chem. Soc.* **2006**, *128*, 5452-5461.
- (37) Buss, J. A.; Edouard, G. A.; Cheng, C.; Shi, J.; Agapie, T., *J. Am. Chem. Soc.* **2014**, *136*, 11272-11275.
- (38) Ponomarev, V.; Filipenko, O.; Atovmyan, L., *Kristallografiya (Russ.) (Crystallogr. Rep.)* **1976**, *21*, 392-394.
- (39) Mortensen, J.; Heinze, J., *Angew. Chem. Int. Ed.* **1984**, *23*, 84-85.
- (40) Connelly, N. G.; Geiger, W. E., *Chem. Rev.* **1996**, *96*, 877-910.
- (41) Bennett, M. A.; Lu, Z.; Wang, X.; Bown, M.; Hockless, D. C. R., *J. Am. Chem. Soc.* **1998**, *120*, 10409-10415.
- (42) Hull, J. W.; Gladfelter, W. L., *Organometallics* **1984**, *3*, 605-613.

- (43) Pangborn, A. B.; Giardello, M. A.; Grubbs, R. H.; Rosen, R. K.; Timmers, F. J., *Organometallics* **1996**, *15*, 1518-1520.
- (44) Guo, W.; Faggi, E.; Sebastián, R. M.; Vallribera, A.; Pleixats, R.; Shafir, A., *J. Org. Chem.* **2013**, *78*, 8169-8175.
- (45) Tate, D. P.; Knipple, W. R.; Augl, J. M., *Inorg. Chem.* **1962**, *1*, 433-434.
- (46) Weitz, I. S.; Rabinovitz, M., *J. Chem. Soc., Perkin Trans. 1* **1993**, 117-120.
- (47) Kajanus, J.; van Berlekom, S. B.; Albinsson, B.; Mårtensson, J., *Synthesis* **1999**, *1999*, 1155-1162.
- (48) Crystallographic data have been deposited at the CCDC, 12 Union Road, Cambridge CB2 1EZ, UK and copies can be obtained on request, free of charge, by quoting the publication citation and the respective deposition numbers.
- (49) APEX2, Version 2 User Manual, M86-E01078, Bruker Analytical X-ray Systems, Madison, WI, June 2006.
- (50) Sheldrick, G. M., "*SADABS (version 2008/1): Program for Absorption Correction for Data from Area Detector Frames*". University of Göttingen: 2008.
- (51) Dolomanov, O. V.; Bourhis, L. J.; Gildea, R. J.; Howard, J. A. K.; Puschmann, H., *J. Appl. Crystallogr.* **2009**, *42*, 339-341.
- (52) Sheldrick, G., *Acta Crystallographica Section A* **2008**, *64*, 112-122.
- (53) Brandenburg, K. (1999). DIAMOND. Crystal Impact GbR, Bonn, Germany.

CHAPTER 4

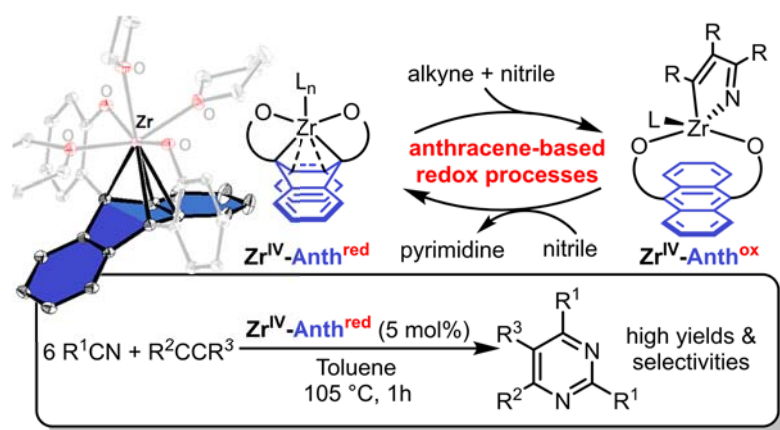
Oxidative Coupling with Zr(IV) Supported by a Non-Innocent Anthracene-Based Ligand: Application to the Catalytic Cocompounding of Alkynes and Nitriles to N-heteroaromatics

This work was published in part as:

J. Am. Chem. Soc. **2018**, *140*, 11906.

ABSTRACT

We report the synthesis and reactivity of Zr complexes supported by a 9,10-anthracenediyl-linked *bis*(phenoxide) ligand, **L**. $\text{Zr}^{\text{IV}}\text{LBn}_2$ (**1**) undergoes facile photolytic reduction with concomitant formation of bibenzyl and $\text{Zr}^{\text{IV}}\text{L}(\text{THF})_3$ (**2**), which displays a two-electron reduced anthracene moiety. Leveraging ligand-stored reducing equivalents, **2** promotes the oxidative coupling of internal and terminal alkynes to isolable zirconacyclopentadiene complexes, demonstrating the reversible utilization of anthracene as a redox reservoir. With diphenylacetylene under CO, cyclopentadienone is formed stoichiometrically. **2** is competent for the catalytic formation of pyrimidines from alkynes and nitriles. Mechanistic studies suggest that selectivity for pyrimidine originates from the preferred formation of an azazirconacyclopentadiene intermediate, which reacts preferentially with nitriles over alkynes. Formation of zirconacyclopentadiene can be biased with the use of tethered diynes, which upon coupling with nitriles affords fused-ring pyridines.



INTRODUCTION

The use of redox-active ligands has expanded the reaction toolkit for chemists, mediating challenging multi-electron chemical transformations not usually observed in their absence.¹⁻³ On early metals such as Zr, for which redox-neutral processes like olefin polymerization are prevalent, redox-active ligands can facilitate new reactivity.⁴⁻⁸ Typically, transformations involving redox non-innocent ligands result in formal changes of the ligand redox state without substantial changes in ligand coordination mode. Ligands that may change the coordination environment around the metal are expected to result in more facile reactivity if adapted to the electronic and steric demands of the metal center.

Our group and others have demonstrated the utility of labile and redox non-innocent pendant arene ligands in the development of new chemical reactivity, including CO cleavage and coupling, metal phosphide formation and coupling, metal nitride CO coupling, cross-coupling chemistry, and CO₂ activation.⁹⁻¹⁸ In most of these systems, the arene ligands are based on substituted benzene, requiring very negative potentials for formal reduction. Due to a smaller loss of aromaticity in its π -system,¹⁹ anthracene displays a more accessible reduction potential,²⁰ allowing for the formation of a dianionic state that coordinates metal ions at the bridgehead positions,²¹⁻²⁶ though such transition metal complexes are very rare.²⁷⁻²⁹ We envisioned that the anthracene motif will promote novel reactivity by functioning as a reductively non-innocent ligand at milder potentials than benzene, facilitating redox chemistry at the pendant arene. Additionally, the formation of new bonds to the metal filling coordination sites opened during reactions such as reductive elimination is expected to facilitate reaction turnover and catalysis (Figure 4.1).

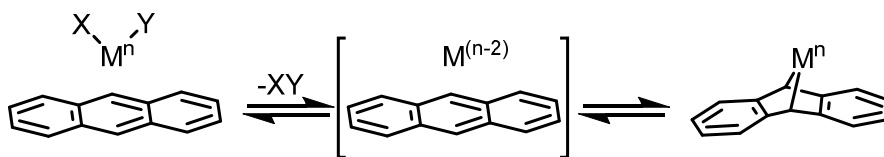
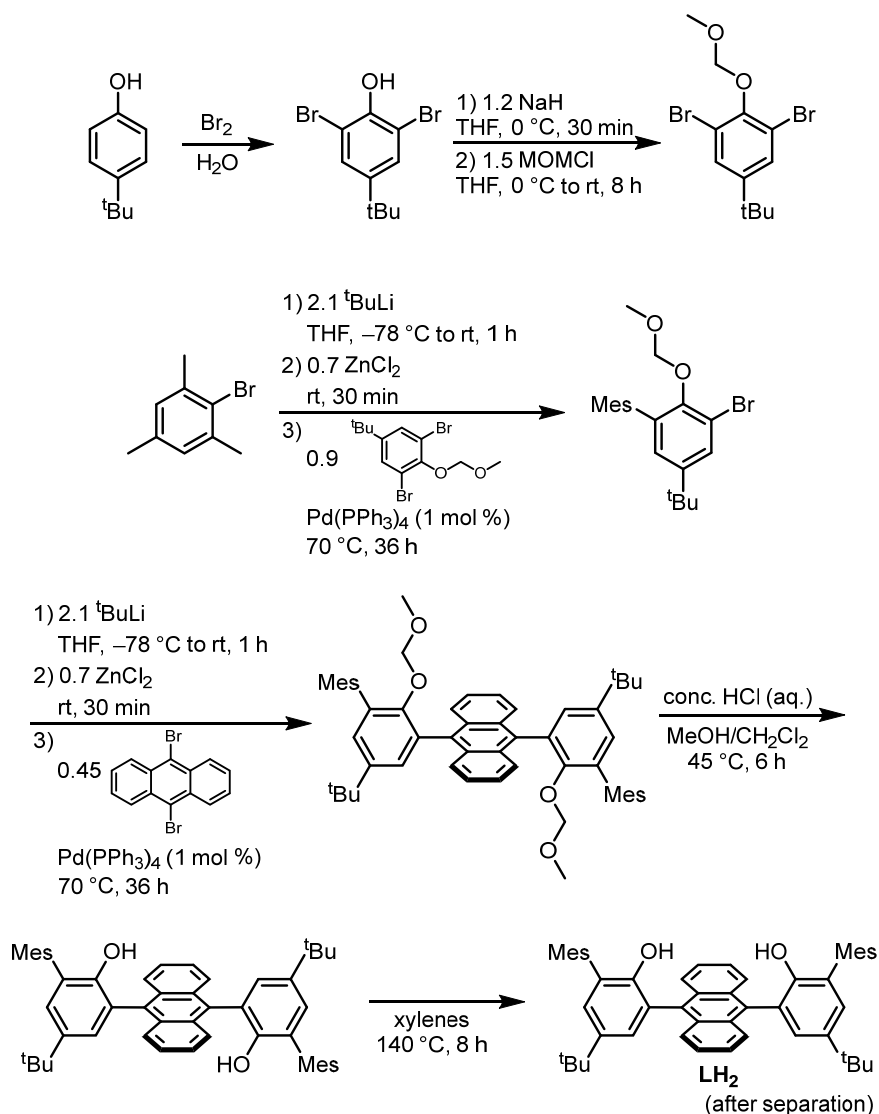


Figure 4.1. Non-innocent anthracene moiety facilitating reductive elimination.

RESULTS AND DISCUSSION

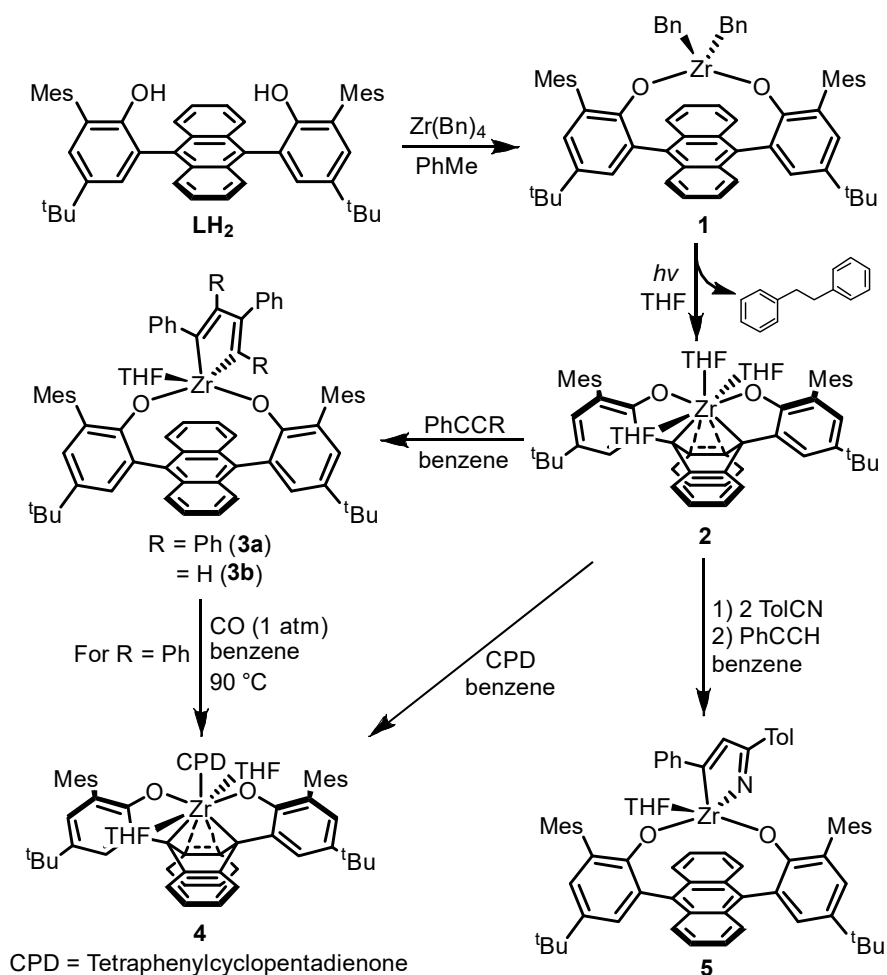
Syn-9,10-anthracenediyl-linked *bis*(phenol) (**LH₂**) was synthesized from commercially available starting materials in six steps (Scheme 4.1). The presence of the anthracenediyl linker results in hindered rotation of the phenols. The second Negishi coupling results in the exclusive formation of the anti-isomer. Upon acid-catalyzed deprotection, isolation of the desired syn-isomer is achieved by thermal isomerization followed by separation via column chromatography. Metalation by protonolysis of tetrabenzyl zirconium (ZrBn₄) with **LH₂**

Scheme 4.1. Synthesis *bis*(phenol) proligand **LH₂**



provides *bis*(benzyl) complex **1** (Scheme 4.2). Single-crystal X-ray diffraction (XRD) studies revealed long distances between Zr and the anthracene group which correlate with the C-C distances in the arene to suggest no significant interaction of the metal with the anthracene π -system (Figure 4.2). The ligand forms a distorted tetrahedral geometry around Zr1, with an additional weak interaction from C61 (2.520(2)Å) from one of the benzyl ligands.

Scheme 4.2. Synthesis and reactivity of *bis*(phenoxide) zirconium complexes with pendant anthracene



Toward promoting reductive elimination from **1**, photolysis was investigated.³⁰ After 18 h irradiation, ^1H NMR spectroscopy shows the loss of the benzylic signal in **1**, and the formation of bibenzyl and a new species, **2** (Scheme 4.2). The solid-state structure of **2** (Figure

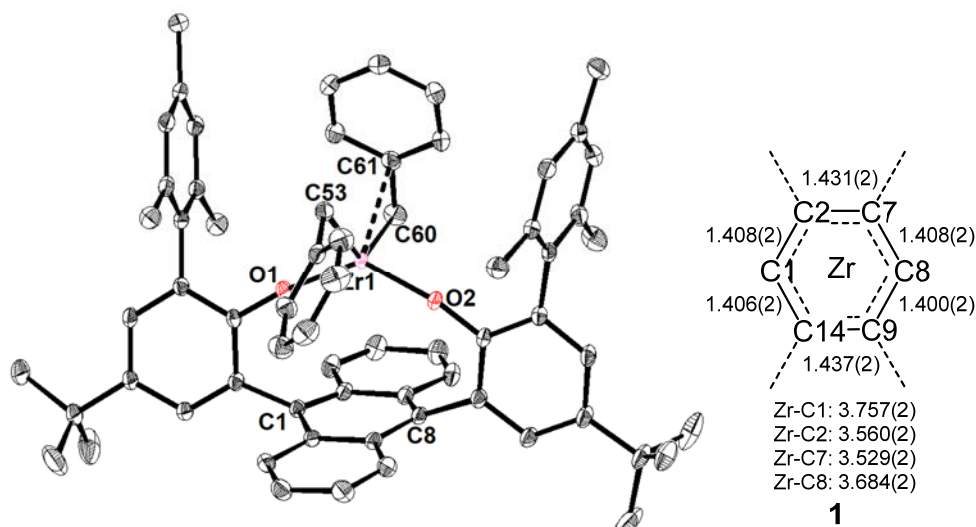


Figure 4.2. Solid-state structure and central ring bond metrics of **1**. Bond distances in Å. Thermal ellipsoids shown at 50% probability. Solvent molecules and hydrogen atoms omitted for clarity.

4.3) shows coordination to Zr of the two phenoxide donors, three THF molecules and the anthracene linker. The anthracene motif binds in an η^4 fashion, displaying short contacts to C1, C2, C7, and C8, with Zr-C distances in the range of 2.432(1)–2.525(1) Å indicative of strong interactions. These are slightly longer than the Zr-benzyl distances in **1** (2.257(2)–2.272(2) Å). Significant lengthening of the C1–C2, C1–14, C7–C8, and C8–C9 bonds suggests disruption of aromaticity in the central arene. Overall, the structural parameters observed are consistent with a two-electron reduced anthracene motif.²¹⁻²⁵ Although oxidatively or photolytically induced C–C reductive eliminations have been reported at Zr(IV),^{7, 30-34} such transformations are rare, and the reduced metal species can undergo undesired side reactivity such as C–H activation.³⁰

To determine whether a unimolecular pathway, via a concerted (Scheme 4.3, **a**) or homolytic cleavage/radical cage (**b**) mechanism, or an intermolecular free radical pathway (**c**) was in operation, a labeling crossover experiment was carried out. Photolysis of a mixture of

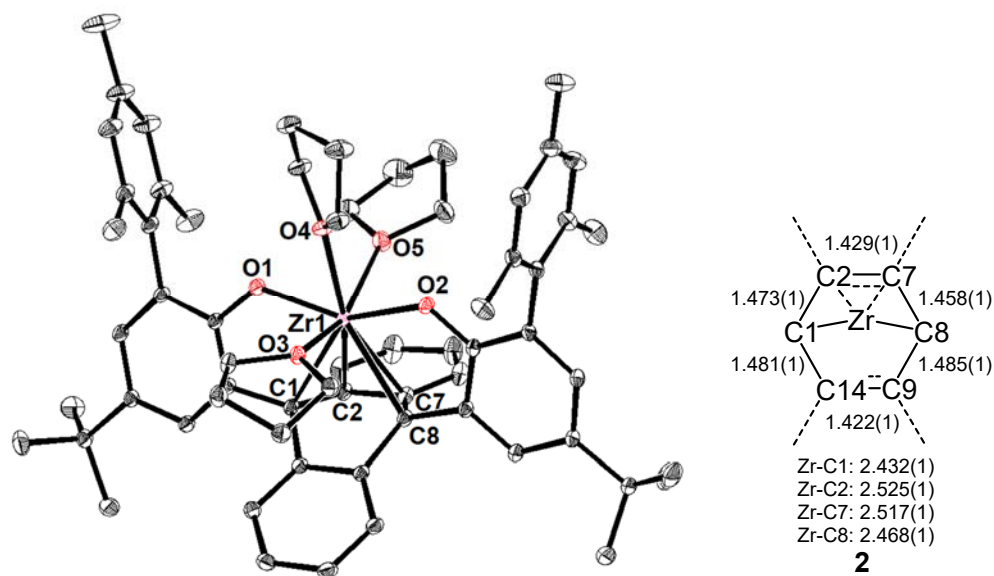
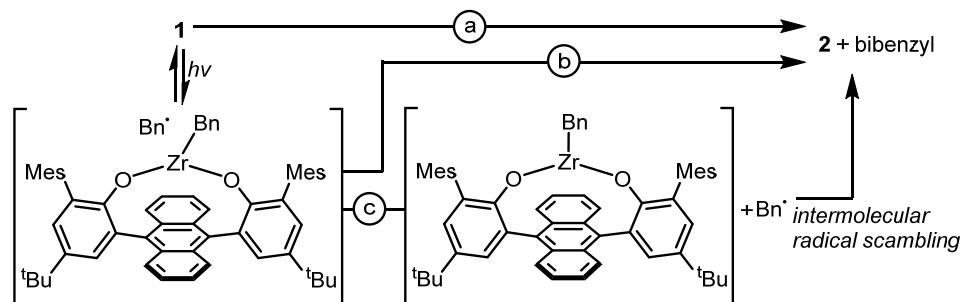


Figure 4.3. Solid-state structure and central ring bond metrics of **2**. Bond distances in Å. Thermal ellipsoids shown at 50% probability. Solvent molecules and hydrogen atoms omitted for clarity.

1 and $\text{LZr}(\text{CD}_2\text{C}_6\text{D}_5)$ (**1-d₁₄**) is expected to result in the formation of bibenzyl-d₀ and bibenzyl-d₁₄ for pathways **a** and **b**, while a 1:2:1 statistical mixture of bibenzyl-d₀, bibenzyl-d₇, and bibenzyl-d₁₄ would result from pathway **c**, assuming benzyl group exchange does not occur under photolytic conditions prior to the formation of **2**. The mixture obtained from the photolysis of a 1:1 ratio of **1** and **1-d₁₄**, obtained from the metalation of **LH₂** with $\text{Zr}(\text{CD}_2\text{C}_6\text{D}_5)_4$, was analyzed via gas chromatography-mass spectroscopy (GC-MS). An authentic sample of bibenzyl-d₀ has a retention time of 9.74 min and a parent fragment peak

Scheme 4.3. Potential pathways for formation for photolysis of **1**



at $m/z=182.1$, while that of bibenzyl- d_{14} , obtained from the photolysis of **1**- d_{14} , has a retention time of 9.69 min and a major fragment peak at $m/z=196.3$. The GC-MS analysis showed that besides bibenzyl- d_0 and - d_{14} isotopomers, a new species with an intermediate retention time of 9.71 min and a major fragment peak at $m/z=189.1$ corresponding to bibenzyl- d_7 was observed (Figure 4.4), consistent with pathway **c** being in operation, though this does not rule out the potential of pre-reduction scrambling of the benzyl ligands.³⁰

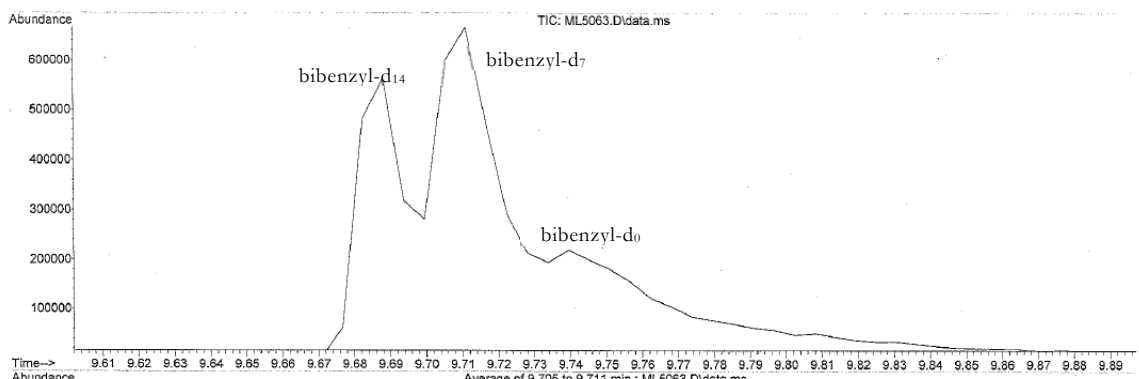


Figure 4.4. GC-MS trace of bibenzyl products observed from reductive elimination of a 1:1 mixture of **1** and **1**- d_{14} .

Complex **2**, although formally displaying a Zr(IV) center, stores two reducing equivalents in the anthracene motif. The possibility of **2** performing anthracene-based redox chemistry was investigated towards the oxidative cyclometalation of alkynes, a reaction with precedent for Zr(II).³⁵⁻³⁸ Heating a solution of **2** with diphenylacetylene (two equiv.) at 90 °C led to a red-to-yellow color change and formation of a 1:2 Zr:alkyne species (**3a**) by ¹H NMR spectroscopy. The solid-state structure of **3a** shows the formation of a zirconacyclopentadiene by the oxidative coupling of two alkynes with two reducing equivalents originating from the ligand (Figure 4.5). Within the zirconacyclopentadiene ring, localized double bonds at C58–C59 (1.357(2) Å) and C60–C61 (1.354(3) Å) are observed.

With examples of both reductive and oxidative C–C bond formation involving redox at the pendant anthracene, substrates with potential for regeneration of a masked Zr(II)

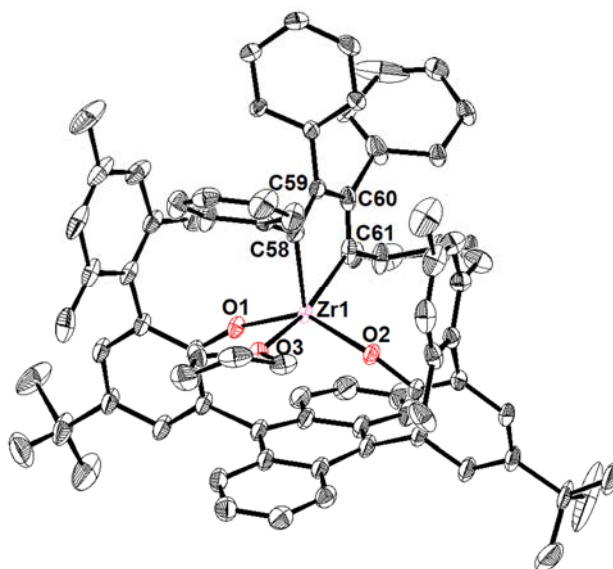


Figure 4.5. Solid-state structure of **3a**. Thermal ellipsoids shown at 50% probability. Solvent molecules and hydrogen atoms omitted for clarity.

complex were probed. Extended heating of **3a** in the presence of excess diphenylacetylene did not effect further reactivity, likely due to steric constraints. Treatment of *in situ*-generated **3a** with CO at 90 °C results in the formation of a new major species assigned as **4**, a 1:1 adduct between zirconium and a tetraphenylcyclopentadienone (CPD) molecule (Scheme 4.2). Independent synthesis by mixing one equiv. CPD with **2** resulting in a matching ¹H NMR spectrum support this assignment. The synthesis of cyclopentadienones via [2+2+1] coupling of two alkynes and CO has been reported but is limited to mid-to-late transition metal complexes.³⁹⁻⁴² CO insertion into zirconacyclopentadiene has not been reported, to our knowledge, though related systems involving CO-alkyne chemistry are known for Zr.⁴³⁻⁴⁶ Conceptually related, the catalytic aza-Pauson-Khand reaction involving Ti-imido complexes and alkynes to afford pyrroles, with diazenes acting as a nitrene source has been reported.⁴⁷ Although turnover was not achieved for CPD formation, this reaction demonstrates that the coupling of three substrates is possible, with an overall process that requires both oxidation

and reduction of the anthracene moiety.

To examine if a sterically more open zirconacyclopentadiene promotes further reactivity, terminal alkyne phenylacetylene was tested as a substrate. Addition of two equiv. phenylacetylene to **2** in benzene at room temperature led to a rapid red-to-yellow color change. Based on ^1H NMR spectroscopy, the new species (**3b**) was assigned as a zirconacyclopentadiene complex structurally analogous to **3a** (Scheme 4.2). Coupling of terminal alkynes by zirconium is rare,⁴⁸⁻⁵¹ primarily attributed to incompatibility of the acidic acetylenic proton with low-valent Zr(II) species and/or precursors.⁵²

Heating **3b** in benzene to 90 °C in the presence of excess phenylacetylene did not result in further insertion. However, in the presence of CO, instead of formation diphenylcyclopentadienone complex analogous to that **4**, triphenylbenzene products were instead observed by GC-MS. Probing other unsaturated substrates, heating of **3b** in the presence of one equiv. of *p*-tolunitrile (TolCN) and two equiv. of phenylacetylene led to the almost complete consumption of TolCN after one hour, with complex **3b** still present (^1H NMR spectroscopy). GC-MS analysis showed the formation of a mixture of homo- and heterotrimerized products, suggesting that **2** may be a competent precatalyst for the cotrimerization of alkynes with nitriles.

To further investigate this reactivity, benzonitrile and phenylacetylene were chosen as model substrates. A mixture of alkyne was heated at 90 °C with excess nitrile (7.5 equiv.), to disfavor potential alkyne trimerization,⁵³ in the presence of 5 mol% of **2**. After two hours, highly selective formation of 2,4,6-triphenylpyrimidine (**6a**) was observed, in 53% yield (Table 4.1, entry 1). GC-MS and NMR analysis showed no detectable formation of triphenylbenzene or triphenyltriazine, and minimal triphenylpyridine (<2%).

Pyrimidines feature in a wide variety of active pharmaceuticals and natural products,

Table 4.1. Cycloaddition of phenyl acetylene with benzonitrile under various conditions

PhCCH (1 equiv.) + PhCN $\xrightarrow[\text{105 } ^\circ\text{C}]{\text{2, toluene}}$ **6a**, **6a'**, **6a''**

entry	[2]/mol %	nitrile (equiv.)	time/h	^a PhCCH consumed/ %	^b selectivity/ %		
					6a	6a'	6a''
1 ^c	5	7.5	2	53	98	2	nd
2	5	7.5	1	>99	59	1	40
3	5	7.5	0.5	>99	99	1	nd
4	5	6	1	>99	99	1	nd
5	5	3	5	98	97	3	nd
6	5	2	8	79	95	5	nd
7	5	0.2	8	7	55	45	nd
8	3	6	5	95	98	2	nd

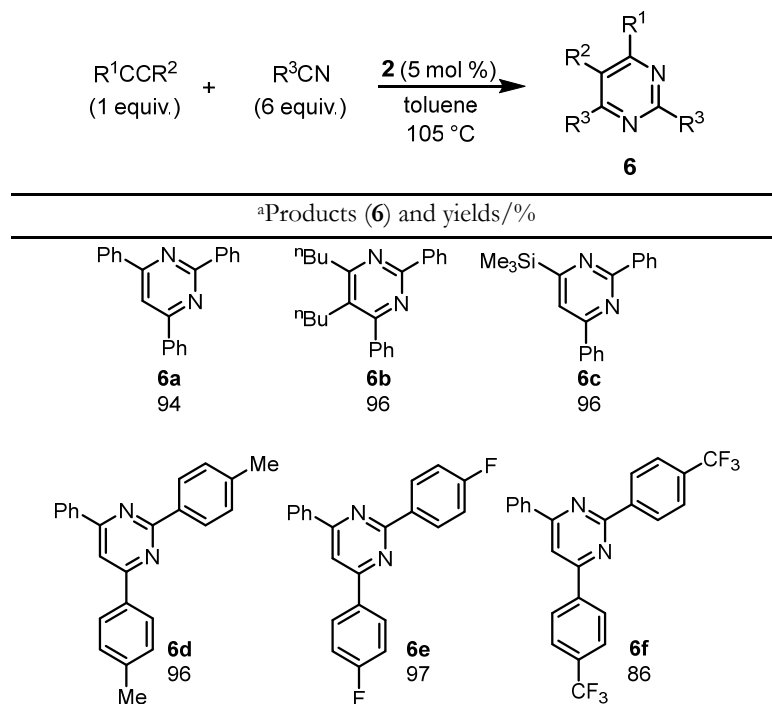
^abased on GC-MS analysis, averaged over 2 runs; ^bbased on ¹H NMR integration, averaged over 2 runs; ^cran at 90 °C in benzene; nd: not detected by GC-MS

and as ligands in coordination complexes.⁵⁴⁻⁵⁸ Syntheses of pyrimidines via the highly efficient and atom-economical [2+2+2] cycloaddition route⁵⁹⁻⁶¹ have been scarce.⁶²⁻⁷¹ This has been attributed to the difficulty in the incorporation of multiple nitrogen atoms via cycloaddition due to the more reactive nature of alkynes compared to nitriles,⁷² even when employing the nitrile as solvent.⁷³⁻⁷⁴ Of those, many are either stoichiometric or require high catalyst loadings ($\geq 20\%$),⁶⁵⁻⁶⁸ nitriles as solvents,⁶⁹⁻⁷⁰ or tethered alkyne-nitrile substrates.⁷¹ The observation of catalytic cycloaddition involving a nitrile is particularly notable for an early metal. Although there are several systems for pyridine synthesis based on Zr in combination with Ni⁷⁵ or Cu,⁷⁶ and Ti,⁷⁷⁻⁷⁹ these reactions are not catalytic, likely due to the strong binding of the nitrogen moiety to the highly Lewis acidic metal center. For the present catalyst, the propensity of the anthracene moiety to accept reducing equivalents is proposed to facilitate reductive cyclization, promoting turnover.

Optimization of the catalytic pyrimidine synthesis was carried out. Increasing the reaction temperature to 105 °C in toluene led to quantitative yields of **6a**, with longer reaction

times leading to triazine formation after alkyne substrate has been consumed (Table 4.1, entries 2 and 3). The nitrile excess can be reduced without appreciable loss in selectivity but results in slower conversions (entries 4 and 5). Even at the stoichiometric ratio of 2:1 PhCN:PhCCH, high selectivity for pyrimidine (94%) is retained, albeit with a lower yield of ~80% (entry 6). Notably, despite excess alkyne present (1:5 PhCN:PhCCH), the pyrimidine product is still favored over the pyridine product. Catalyst loading can be lowered to 3 mol% while providing similarly high yields and selectivities after five hours (entry 8). Control experiments ran with simple Zr complexes (ZrBn₄, ZrCl₄, and ZrBn₂Cl₂) reduced by Mg(THF)₃(anthracenide), or with KC₈ or photolytically in the presence of anthracene, did not result in catalysis.

Table 4.2. Substrate scope of cycloaddition of alkynes with nitriles to pyrimidines



Using the optimized conditions (Table 4.1, entry 4), the scope of pyrimidine synthesis was explored (Table 4.2). Internal dialkyl alkyne 5-decyne provides **6b** quantitatively, while diphenylacetylene is not competent. Terminal alkyl alkynes (see Table 4.4) did not produce any cotrimerized products detectable by GC-MS, with the exception of trimethylsilylacetylene,

which quantitatively afforded **6c**. A variety of nitriles were also found to be competent for catalysis (Table 4.2, **6d**, **6e**, and **6f**) though aryl nitriles with O or N-containing substituents and alkyl nitriles (see Table 4.4) did not lead to cyclotrimerized products. Addition of an equimolar amount of acetonitrile to PhCN under optimized conditions completely shuts down the generation of **6a**, suggesting that it acts as a strong inhibitor, likely through competitive binding to the metal.

To gain insight into the mechanistic basis of product selectivity, the synthesis of azazirconacycle **5**, a potential catalytic intermediate, was targeted (Scheme 4.2). Addition of two equiv. TolCN followed by one equiv. PhCCH to **2** results in the formation of azazirconacycle **5**. A stable species was formed upon addition of two equiv. nitrile to **2**, with the displacement of THF. The identity of this species could either be a *bis*(nitrile) adduct or a diazazirconacyclopentadiene complex, but was not further characterized. XRD studies took

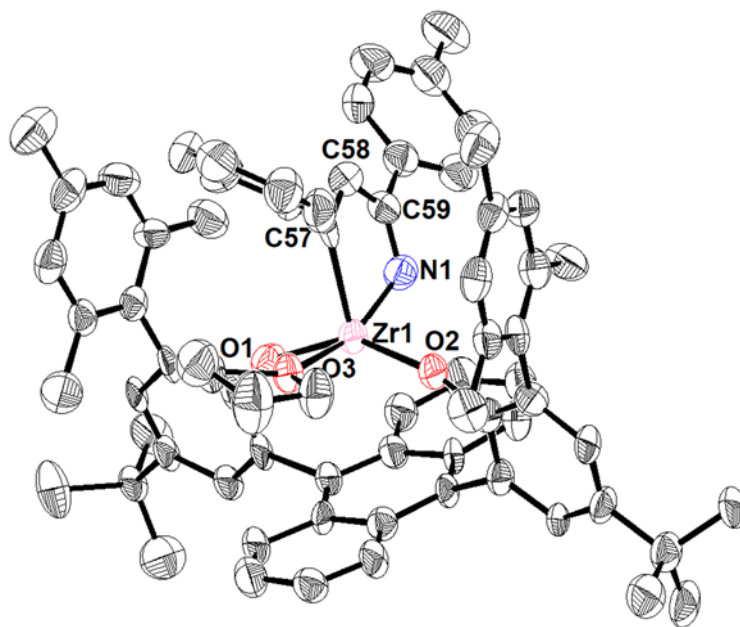
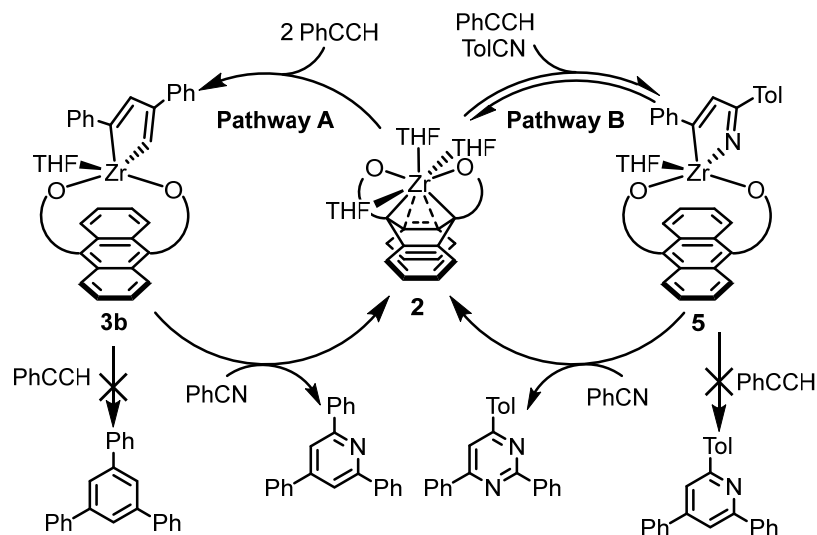


Figure 4.6. Solid-state structure of **5**. Thermal ellipsoids shown at 50% probability. Solvent molecules and hydrogen atoms omitted for clarity. Relevant bond distances (Å): Zr1–O1 1.984(7), Zr1–O2 1.981(7), Zr1–C57 2.27(1), Zr1–N1 2.043(9), C57–C58 1.34(1), C58–C59 1.46(2), C59–N1 1.27(1)

advantage of the distinct aryl groups in **5** to unambiguously assign N-coordination to Zr and 2,4-diaryl substitution (Figure 4.6). Although an initial reversible formation of a nitrile-nitrile coupled complex of the type previously reported for group IV metals⁸⁰⁻⁸² could not be ruled out, in the presence of both nitrile and alkyne, complex **5** is the major Zr-containing product. Stoichiometric reactions carried out from the isolated (aza)zirconacycles, **3b** and **5**, provide insight into catalytically relevant pathways (Scheme 4.4). The reaction of **3b** or **5** at 90 °C with PhCN results in pyridine or pyrimidine formation by ¹H NMR spectroscopy (Figure 4.7), respectively, while neither complex reacts in the presence of additional PhCCH (*vide supra* and Figure 4.7). The GC-MS analysis of the reaction of **5** with PhCN showed predominantly the formation of pyrimidine with mixed aryl substituents, with the minor formation of 2,4,6-triphenylpyrimidine and 6-phenyl-2,4-di(tolyl)pyrimidine, indicating that the coupling of alkyne and nitrile is reversible, but is slow relative to pyrimidine formation. Based on the selectivity in catalysis, pathway B is strongly favored over pathway A, leading to the high selectivities observed. The preference for the formation of **5** rather than **3b** from a mixture of nitrile and alkyne is likely due to the precoordination of nitrile. The small amount of

Scheme 4.4. Stoichiometric reactions involving catalytically relevant species



pyridine byproduct results from the formation of **3b** as a minor component through Pathway A.

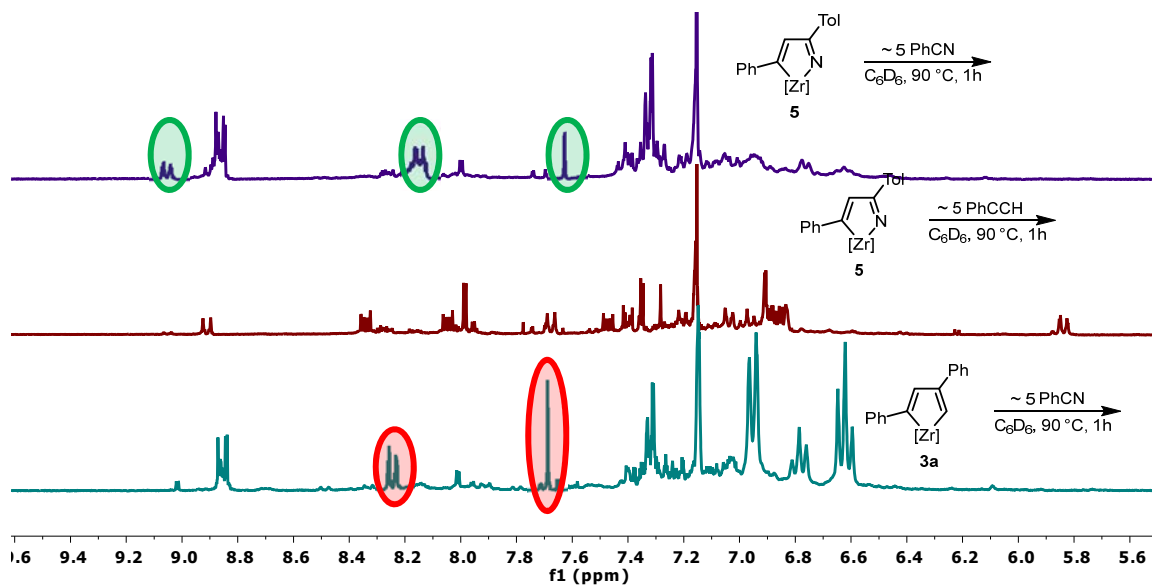


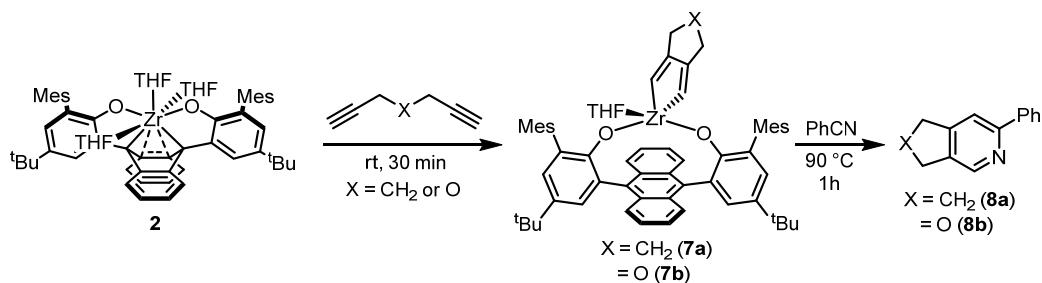
Figure 4.7. NMR spectra of stoichiometric reactions of **3a** and **5** with phenylacetylene or benzonitrile. Pyrimidine product circled in green, pyridine product circled in red.

Towards expanding the scope of products beyond pyrimidines, the reactivity of tethered diynes was explored. We postulated that the use of tethered diynes as substrates will favor the formation of a zirconacyclopentadiene invoked in pathway A (Scheme 4.4) as a route towards fused ring pyridines. The [2+2+2] cycloaddition of two alkyne motifs with a nitrile to yield pyridines represents a powerful method towards the efficient and atom-economical synthesis of functionally-rich pyridine motifs.^{61, 79, 83-86} Despite that, the catalytic synthesis of pyridines via [2+2+2] cycloaddition reactions have focused primarily on late-transition metals. The use of early metals such as zirconium and titanium have been limited to stoichiometric examples that either rely on a second metal (Ni/Cu) that functions as a surrogate for the organic fragment,⁷⁵⁻⁷⁶ or the incorporation of a leaving group in the organic framework,⁷⁷⁻⁷⁹ in order to overcome the strong binding affinity of the nitrogen moiety to the highly Lewis acidic Zr/Ti center. To the best of our knowledge, there are no Zr-based systems capable of catalytic

synthesis of pyridines from alkynes and nitriles.

The reaction of **2** with 1,6-heptadiyne resulted in the formation of a new species within 30 min at room temperature that was assigned to zirconacyclopentadiene complex **7a** (Scheme 4.5). Further reaction of **7a** with benzonitrile led to the formation of expected fused ring pyridine **8a** as confirmed by both ^1H NMR spectroscopy and GC-MS analysis. O-containing propargyl ether was also tested and similarly resulted in the initial formation of zirconacyclopentadiene complex **7b** and upon further reaction with benzonitrile afforded the expected pyridine product (**8b**).

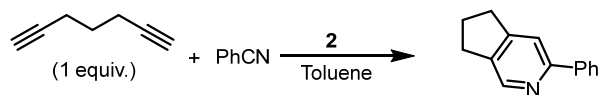
Scheme 4.5. Stoichiometric reactions with tethered diynes and benzonitrile



Catalytic synthesis of pyridines from these tethered diynes was explored. Propargyl ether as a substrate was found to not be competent for the catalytic synthesis of O-containing fused ring pyridine **8b**, likely due to catalyst poisoning by substrate or product (functioning similarly to a THF ligand). In contrast, the reaction of 1,6-heptadiyne with one equivalent of benzonitrile with 5 mol% **2** led to modest yields of **8a** either after several days at room temperature or several hours at 105 °C (Table 4.3, entries 1 and 2). It was found that beyond the first few hours at 105 °C, catalytic activity ceases, with longer reactions times not resulting in any improvement in yields (entry 3). Increasing the equivalents of nitrile was found to improve the yields. Raising the number of nitrile equivalents from 1 to 5 then to 10 was found to improve yields to ~75%. With 10 equiv. nitrile, a further increase in catalyst loading did not appear to have a significant effect on pyridine yields (Entry 7). The significant rates of

reactions when an excess of nitrile is increased suggests that the rate-limiting step was final nitrile insertion into **7a** via pathway A (*vide supra*). Notably, even in the presence of a significant excess of nitrile, exclusive synthesis of pyridine with no formation of pyrimidine and triazine products are detected in these catalytic runs.

Table 4.3. Cycloaddition of 1,6-heptadiyne with benzonitrile under various conditions



entry	2 /mol %	nitrile (equiv.)	temperature/ °C	time/h	^a yield/ %
1	5	1	rt	96	56
2	5	1	105	4	41
3	5	1	105	12	38
4	5	5	105	4	55
5	5	5	60 ^b	24	49
6	5	10	60 ^b	24	74
7	10	10	60 ^b	24	75
8	5	10	105	4	74

^abased on ¹H NMR integration with 1,3,5-trimethoxybenzene standard, ^brun in benzene

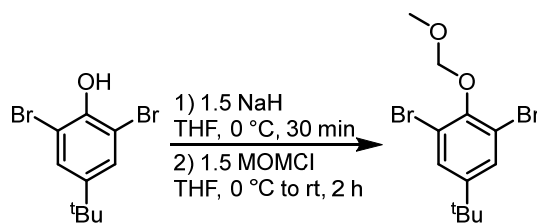
CONCLUSION

We have synthesized and characterized a series of zirconium complexes supported by a *bis*(phenoxide) ligand displaying a 9,10-anthracenediyl motif. The ligand exhibits both redox non-innocence and hemilability, facilitating two-electron chemistry at a Zr(IV) center such as the photolytic reductive elimination of bibenzyl, oxidative coupling of unsaturated organic substrates such as alkynes and nitriles and their subsequent reductive elimination to CPD or N-containing heterocycles. We have demonstrated an efficient Zr-catalyzed three-component [2+2+2] cycloaddition of alkynes and aryl nitriles to selectively afford tri- and tetra-substituted pyrimidines. The catalyst displays excellent selectivity even without the use of excess nitrile. When tethered diynes were used as substrates, coupling with aryl nitriles selectively afforded fused-ring pyridine products. With 1,6-heptadiyne, catalytic synthesis of 3-phenyl-6,7-dihydro-5H-cyclopenta[*c*]pyridine could be realized. The ability of this Zr catalyst to turnover, in contrast to other early metal systems, is proposed to stem from the ability of the anthracene motif to promote redox chemistry and product dissociation. Given the established efficient stoichiometric oxidative coupling chemistry characteristic of Zr,^{36, 87-88} the development of new types of catalysis based on it is of interest for a variety of applications.

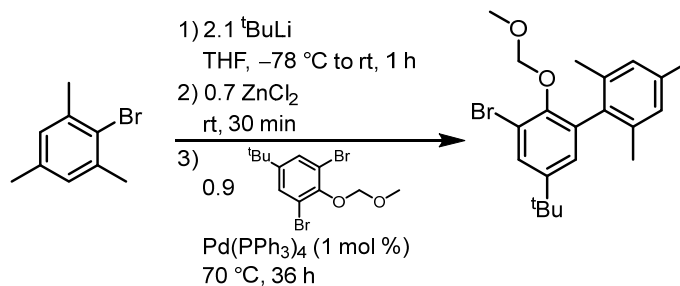
EXPERIMENTAL SECTION

General Considerations

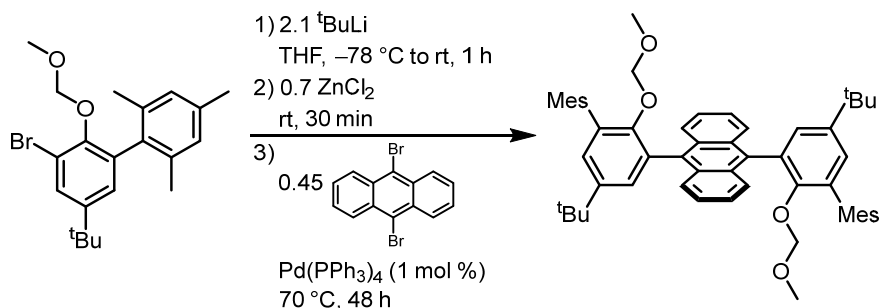
Unless otherwise specified, all operations involving air- or water-sensitive reagents were carried out in an MBraun drybox under a nitrogen atmosphere or using standard Schlenk and vacuum line techniques. Solvents for air- and moisture-sensitive reactions were dried by the method of Grubbs.⁸⁹ Deuterated solvents were purchased from Cambridge Isotope Laboratories and C₆D₆ vacuum transferred from sodium benzophenone ketyl before use. All solvents, once dried and degassed, were stored under a nitrogen atmosphere over 4 Å molecular sieves. Sodium hydride dispersion in oil was washed with multiple times with hexanes and dried in vacuo before used. 4-*tert*-butyl-2,6-dibromophenol,⁹⁰ chloromethyl methyl ether solution,⁹¹ tetrabenzylzirconium,⁹² and Mg(THF)₃(C₁₄H₁₀)⁹³ were prepared according to literature procedures. Alkynes and nitriles used were either sublimed under reduced pressure or distilled from calcium hydride before use. All other reagents were used as received. ¹H, ¹³C{¹H}, and ¹⁹F NMR spectra were recorded on Varian Mercury 300 MHz or Varian 400 MHz spectrometers at ambient temperatures unless otherwise denoted. ¹H and ¹³C{¹H} NMR spectra are reported referenced internally to residual solvent peaks reported relative to tetramethylsilane. ¹⁹F NMR chemical shifts are referenced to an external standard of C₆F₆ (-164.9 ppm). Fast atom bombardment-mass spectrometry (FAB-MS) analyses were performed with a JEOL JMS-600H high-resolution mass spectrometer. Gas chromatography-mass spectrometry (GC-MS) were performed with on an Agilent 6890A instrument using an HP-5MS column (30 m length, 0.25 mm diameter, 0.50 μm film) and an Agilent 5973N mass-selective EI detector. Photolyses were conducted using an Oriel Instruments arc lamp housing and an Osram 75 W Xe arc lamp set to a current of 5.4 A.



1,3-dibromo-5-(*tert*-butyl)-2-(methoxymethoxy)benzene. To a solution of 2,6-dibromo-4-(*tert*-butyl)phenol (100 g, 325 mmol) in THF (500 mL) at 0 °C was added portion-wise NaH (11.7 g, 487 mmol) slowly (caution: effervescence). After stirring for an additional 30 min, a toluene solution of chloromethyl methyl ether (232 mL, 487 mmol, 2.1 M) was added slowly at 0 °C. After complete addition, the reaction was allowed to warm up to room temperature and stirred an additional 2 h. The reaction was quenched by the slow addition of water (50 mL) and was then concentrated to *ca.* 200 mL under vacuum. The remaining suspension was partitioned between water (300 mL) and CH₂Cl₂ (200 mL). The organic layer was separated and the aqueous layer extracted with CH₂Cl₂ (2 × 200 mL). The combined organic extracts were then dried over MgSO₄, filtered, and concentrated in vacuo to provide a pale yellow oil (106.8 g, 98.4%). The product was further dried by stirring over calcium hydride and filtering before using in the next step. ¹H NMR (400 MHz, CDCl₃): δ 7.50 (s, 2H, ArH), 5.15 (s, 2H, CH₂), 3.72 (s, 3H, OCH₃), 1.28 (s, 9H, C(CH₃)₃); ¹³C{¹H} NMR (101 MHz, CDCl₃): δ 150.28 (aryl-C), 149.13 (aryl-C), 130.20 (aryl-C), 118.02 (aryl-C), 99.66 (CH₂), 58.58 (OCH₃), 34.72 (C(CH₃)₃), 31.26 (C(CH₃)₃); HRMS (FAB+) *m/z* Calcd. for C₁₂H₁₆Br₂O₂ [(M + H) – H₂]⁺ 350.9418, found 350.9406.



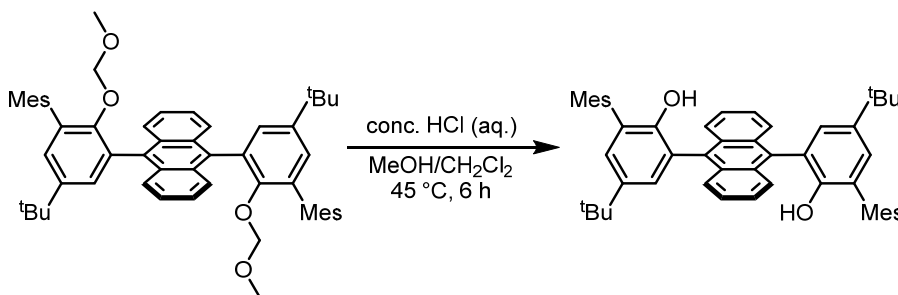
3-bromo-5-(*tert*-butyl)-2-(methoxymethoxy)-2',4',6'-trimethyl-1,1'-biphenyl. A Schlenk flask fitted with a screw-in Teflon stopper was charged with a solution of 2-bromomesitylene (24.1 mL, 157 mmol) in THF (500 mL) and cooled to -78 °C. A pentane solution of *tert*-butyllithium (174 mL, 1.9 M, 331 mmol) was added dropwise via cannula. The reaction was allowed to warm to room temperature and stirred for 1 h forming an orange solution. The reaction was then brought into an N₂-purged glovebox and ZnCl₂ (15.1 g, 110 mmol) was added slowly to the reaction resulting in the loss of the orange coloration. The mixture was allowed to stir at room temperature for 30 min. 1,3-dibromo-5-(*tert*-butyl)-2-(methoxymethoxy)benzene (50.0 g, 142 mmol) and Pd(PPh₃)₄ (1.82 g, 1.57 mmol) was added, the flask sealed and warmed to 70 °C for 36 h. After cooling to room temperature, water (50 mL) was added to quench the reaction, and the mixture concentrated in vacuo to about 100 mL. The resulting suspension was taken up in CH₂Cl₂ (200 mL) and filtered through a silica gel plug, eluting further with CH₂Cl₂. The filtrate was then washed with water (2 × 200 mL), dried over MgSO₄, filtered, and concentrated in vacuo to afford the crude product as a pale yellow oil. The crude mixture can be purified via Kugelrohr distillation, providing the desired product as a viscous colorless oil that crystallizes on standing (41.2 g, 74.1%). ¹H NMR (400 MHz, CDCl₃): δ 7.56 (d, ⁴J_{H,H} = 2.2 Hz, 1H, ArH), 7.06 (d, ⁴J_{H,H} = 2.2 Hz, 1H, ArH) 6.94 (s, 2H, ArH) 4.70 (s, 2H, CH₂), 2.99 (s, 3H, OCH₃), 2.32 (s, 3H, ArCH₃), 2.05 (s, 6H, ArCH₃) 1.30 (s, 9H, C(CH₃)₃); ¹³C{¹H} NMR (101 MHz, CDCl₃): δ 149.23 (aryl-C), 148.72 (aryl-C), 137.18 (aryl-C), 136.83 (aryl-C), 135.43 (aryl-C; coincidental overlap), 129.34 (aryl-C), 128.31 (aryl-C), 128.14 (aryl-C), 117.64 (aryl-C), 98.67 (CH₂), 56.88 (OCH₃), 34.64 (C(CH₃)₃), 31.44 (C(CH₃)₃), 21.18 (ArCH₃), 20.72 (ArCH₃); HRMS (FAB+) m/z Calcd. for C₂₁H₂₇BrO₂ [(M + H) – H₂]⁺ 391.1096, found 391.1099.



***Anti*-9,10-bis(5-(*tert*-butyl)-2-(methoxymethoxy)-2',4',6'-trimethyl-[1,1'-biphenyl]-3-**

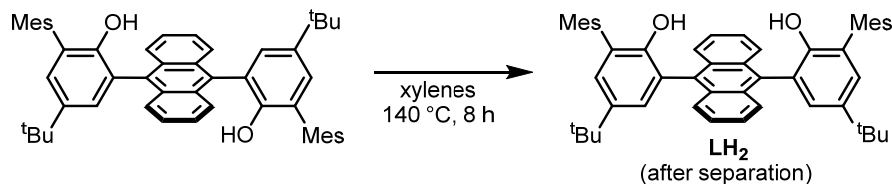
yl)anthracene. A Schlenk flask fitted with a screw-in Teflon stopper was charged with a solution of 3-bromo-5-(*tert*-butyl)-2-(methoxymethoxy)-2',4',6'-trimethyl-1,1'-biphenyl (20.0 g, 50.1 mmol) in THF (200 mL) and cooled to $-78\text{ }^{\circ}\text{C}$. A pentane solution of *tert*-butyllithium (56.5 mL, 1.9 M, 107 mmol) was added dropwise via cannula. The reaction was allowed to warm to room temperature and stirred for 1 h forming a dark orange solution. The reaction was then brought into an N_2 -purged and ZnCl_2 (4.89 g, 35.9 mmol) was added slowly to the reaction resulting in the formation of a cloudy pale yellow mixture. The reaction was allowed to stir at room temperature for 30 min after which 9,10-dibromoanthracene (7.73 g, 23.0 mmol) and $\text{Pd}(\text{PPh}_3)_4$ (591 mg, 0.51 mmol) were added. The flask was sealed and warmed to $70\text{ }^{\circ}\text{C}$ for 48 h. After cooling to room temperature, water (20 mL) was added to quench the reaction, and the mixture concentrated in vacuo to about 50 mL. The resulting suspension was taken up in CH_2Cl_2 (200 mL) and filtered through a silica gel plug, eluting further with CH_2Cl_2 . The filtrate was then washed with water ($2 \times 200\text{ mL}$), dried over MgSO_4 , filtered, and concentrated in vacuo to afford the crude product as a sticky yellow solid which was triturated in MeOH (250 mL) with aid of sonication, filtered and dried in vacuo to provide the product as a pale yellow powder (16.2 g, 88.2%). ^1H NMR (400 MHz, CDCl_3): δ 7.77 (app dd, $J_{\text{H,H}} = 6.8, 3.3\text{ Hz}$, 4H, anth-*H*), 7.38 (app dd, $J_{\text{H,H}} = 6.8, 3.3\text{ Hz}$, 4H, anth-*H*), 7.33 (d, $^4J_{\text{H,H}} = 2.5\text{ Hz}$, 2H, Ar*H*), 7.27 (d, $^4J_{\text{H,H}} = 2.5\text{ Hz}$, 2H, Ar*H*), 6.97 (s, 4H, Ar*H*), 4.06 (s, 4H, CH_2), 2.33 (s,

6H, ArCH₃), 2.27 (s, 12H, ArCH₃), 2.10 (s, 6H, OCH₃), 1.35 (s, 18H, C(CH₃)₃); ¹³C{¹H} NMR (101 MHz, CDCl₃): δ 151.09 (aryl-C), 147.11 (aryl-C), 136.94 (aryl-C), 136.78 (aryl-C), 136.27 (aryl-C), 134.72 (aryl-C), 134.29 (aryl-C), 132.29 (aryl-C), 130.34 (aryl-C), 129.11 (aryl-C), 128.64 (aryl-C), 128.15 (aryl-C), 127.18 (aryl-C), 125.25 (aryl-C), 97.98 (CH₂), 55.42 (OCH₃), 34.70 (C(CH₃)₃), 31.72 (C(CH₃)₃), 21.21 (ArCH₃), 21.04 (ArCH₃); HRMS (FAB+) m/z Calcd. for C₅₆H₆₂O₄ [M]⁺ 798.4648, found 798.4674.



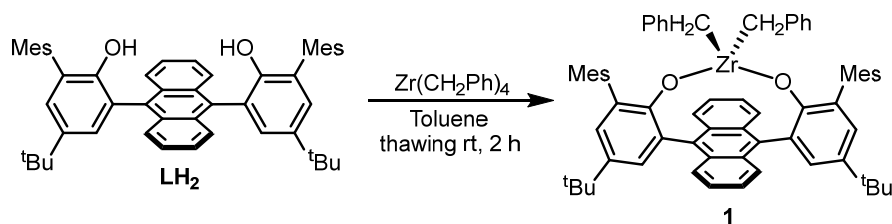
***Anti*-3,3''-(anthracene-9,10-diyl)bis(5-(*tert*-butyl)-2',4',6'-trimethyl-[1,1'-biphenyl]-2-ol).** A Schlenk flask fitted with a screw-in Teflon stopper was charged with *anti*-9,10-bis(5-(*tert*-butyl)-2-(methoxymethoxy)-2',4',6'-trimethyl-[1,1'-biphenyl]-3-yl)anthracene (15.0 g, 18.8 mmol), MeOH (100 mL) and CH₂Cl₂ (200 mL). Concentrated aqueous HCl (20 mL) was added, the flask sealed and heated to 45 °C, monitoring the progress of the reaction via ¹H NMR spectroscopy. After complete deprotection at about 6 h, the reaction was cooled and concentrated in vacuo. The suspension was taken up in CH₂Cl₂ (250 mL) and washed with H₂O (2 × 200 mL) and then saturated aqueous NaHCO₃ (100 mL). The organic fraction was dried over MgSO₄, filtered, and concentrated under reduced pressure to provide the product as a pale yellow solid (13.2 g, 98.9%). ¹H NMR (400 MHz, CDCl₃): δ 7.80 (app dd, *J*_{H,H} = 6.8, 3.3 Hz, 4H, anth-*H*), 7.41 (app dd, *J*_{H,H} = 6.8, 3.0 Hz, 4H, anth-*H*), 7.34 (d, ⁴*J*_{H,H} = 2.5 Hz, 2H, Ar*H*), 7.27 (d, ⁴*J*_{H,H} = 2.5 Hz, 2H, Ar*H*), 7.03 (s, 4H, Ar*H*), 4.47 (s, 2H, OH), 2.35 (s, 6H, ArCH₃), 2.22 (s, 12H, ArCH₃), 1.35 (s, 18H, C(CH₃)₃); ¹³C{¹H} NMR (101 MHz, CDCl₃): δ

148.56 (aryl-C), 143.58 (aryl-C), 137.67 (aryl-C), 137.50 (aryl-C), 133.68 (aryl-C), 133.28 (aryl-C), 130.73 (aryl-C), 128.76 (aryl-C), 128.68 (aryl-C), 127.64 (aryl-C), 126.94 (aryl-C), 126.54 (aryl-C), 125.72 (aryl-C), 124.03 (aryl-C), 34.55 (C(CH₃)₃), 31.86 (C(CH₃)₃), 21.28 (ArCH₃), 20.67 (ArCH₃); HRMS (FAB+) m/z Calcd. for C₅₂H₅₄O₂ [M]⁺ 710.4124, found 710.4142.

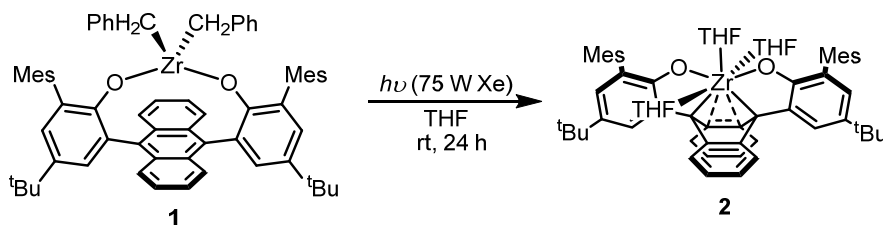


***Syn*-3,3''-(anthracene-9,10-diyl)bis(5-(*tert*-butyl)-2',4',6'-trimethyl-[1,1'-biphenyl]-2-**

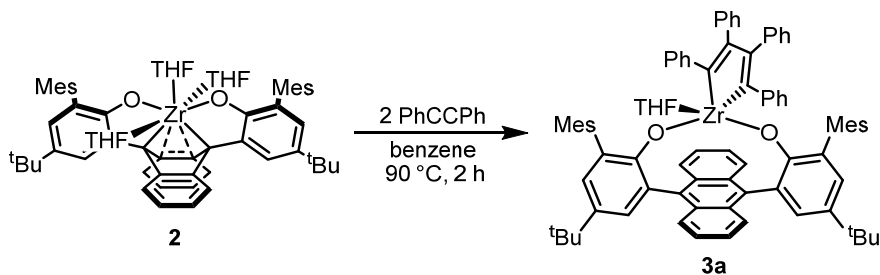
ol) (LH₂). A suspension of the *anti* atropisomer (13.0 g) in degassed xylenes (80 mL) was heated to reflux under N₂ for 6 h, after which the yellow solution was cooled to room temperature and the volatiles removed in vacuo. The isomeric mixture was separated by silica gel column chromatography, eluting first with 1:4 CH₂Cl₂:hexanes to separate the *anti*-isomer, and then 1:3:16 EtOAc:CH₂Cl₂:hexanes to obtain the desired *syn*-isomer LH₂ as a white to pale yellow solid after drying in vacuo (6.08 g 46.8%). The *anti*-isomer obtained (6.31 g, 48.5%) can be further isomerized and separated again by silica gel column chromatography to provide more desired *syn*-isomer. ¹H NMR (400 MHz, CDCl₃): δ 7.81 (app dd, *J*_{H,H} = 6.8, 3.2 Hz, 4H, anth-*H*), 7.43 (dd, *J*_{H,H} = 6.8, 3.2 Hz, 4H, anth-*H*), 7.31 (d, ⁴*J*_{H,H} = 2.5 Hz, 2H, Ar*H*), 7.28 (d, ⁴*J*_{H,H} = 2.5 Hz, 2H, Ar*H*), 7.01 (s, 4H, Ar*H*), 4.50 (s, 2H, OH), 2.34 (s, 6H, ArCH₃), 2.21 (s, 12H, ArCH₃), 1.35 (s, 18H, C(CH₃)₃); ¹³C{¹H} NMR (101 MHz, CDCl₃): δ 148.59 (aryl-C), 143.50 (aryl-C), 137.62 (aryl-C), 137.42 (aryl-C), 133.77 (aryl-C), 133.35 (aryl-C), 130.75 (aryl-C), 128.65 (aryl-C), 128.62 (aryl-C), 127.74 (aryl-C), 126.93 (aryl-C), 126.60 (aryl-C), 125.79 (aryl-C), 123.92 (aryl-C), 34.53 (C(CH₃)₃), 31.85 (C(CH₃)₃), 21.27 (ArCH₃), 20.69 (ArCH₃); HRMS (FAB+) m/z Calcd. for C₅₂H₅₄O₂ [M]⁺ 710.4124, found 710.4089.



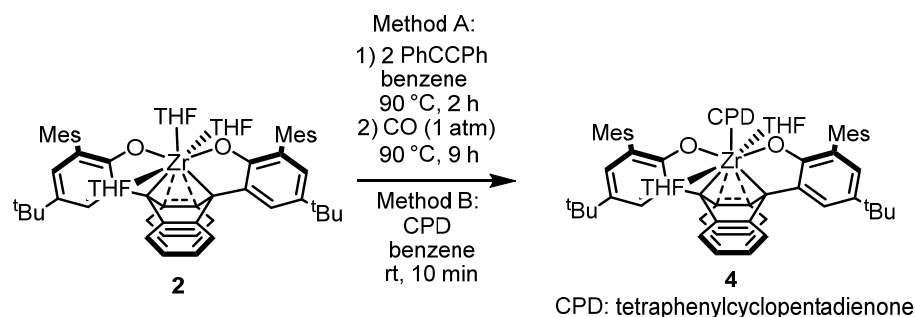
Synthesis of 1. All manipulations for this reaction until the workup was carried out in the glovebox in the absence of light to the extent possible. To a thawing solution of tetrabenzylzirconium (320.5 mg, 0.703 mmol) in toluene (20 mL) was added a thawing solution of LH_2 (500 mg, 0.703 mmol) in toluene (10 mL) with stirring. The reaction was allowed to warm up to room temperature and stirred an additional 2 h, forming a yellow solution. The solution was filtered through a pad of diatomaceous earth and volatiles were removed in vacuo to afford **1** as a yellow solid (681 mg 98.6%). X-Ray quality single crystals were grown by slow diffusion of pentane into a saturated toluene solution at $-35\text{ }^\circ\text{C}$. ^1H NMR (400 MHz, C_6D_6): δ 8.06 (app dd, $J_{\text{H,H}} = 6.7, 3.2$ Hz, 4H, anth-*H*), 7.95 (d, $^4J_{\text{H,H}} = 2.6$ Hz, 2H, Ar*H*), 7.20 (d, $^4J_{\text{H,H}} = 2.5$ Hz, 2H, Ar*H*), 7.12 (app dd, $J = 6.7, 3.2$ Hz, 4H, anth-*H*), 6.80 (s, 4H, Mes*H*), 6.78 – 6.66 (m, 6H, Ar*H*), 5.86 (d, $J = 7.2$ Hz, 4H, Ar*H*), 2.21 (s, 6H, Ar*CH*₃), 2.09 (s, 12H, Ar*CH*₃), 1.38 (s, 18H, C(*CH*₃)₃), 0.87 (s, 4H, Ph*CH*₂); $^{13}\text{C}\{^1\text{H}\}$ NMR (101 MHz, C_6D_6): δ 157.10 (aryl-C), 143.83 (aryl-C), 139.69 (aryl-C), 137.13 (aryl-C), 136.68 (aryl-C), 136.35 (aryl-C), 134.58 (aryl-C), 131.62 (aryl-C), 131.47 (aryl-C), 130.75 (aryl-C), 130.44 (aryl-C), 128.44 (aryl-C), 127.82 (aryl-C), 127.75 (aryl-C), 126.75 (aryl-C), 126.37 (aryl-C), 124.69 (aryl-C), 123.85 (aryl-C), 59.46 (Ph*CH*₂), 34.55 (C(*CH*₃)₃), 31.93 (C(*CH*₃)₃), 21.36 (Ar*CH*₃), 21.19 (Ar*CH*₃); Anal. Calcd. $\text{C}_{66}\text{H}_{66}\text{O}_2\text{Zr}$ (%): C, 80.69; H, 6.77. Found: C, 80.84; H, 6.62.



Synthesis of 2. A solution of **1** (1.00 g, 1.02 mmol) in THF (80 mL) was irradiated with light from a Xe arc lamp (75 W) with stirring. After 24 h, the volatiles were removed in vacuo, and the residue triturated with hexanes twice. Pentane (10 mL) was added and cooled to $-35\text{ }^{\circ}\text{C}$ overnight to allow precipitation. The suspension was filtered and the residue washed with cold pentane (5 mL), and then room temperature pentane ($2 \times 3\text{ mL}$). The residue was extracted with diethyl ether and dried in vacuo to provide **2** as a deep red solid (587 mg 56.9%). X-ray quality single crystals were grown by cooling a saturated pentane to $-35\text{ }^{\circ}\text{C}$. $^1\text{H NMR}$ (400 MHz, C_6D_6): δ 7.88 (d, $^4J_{\text{H,H}} = 2.5\text{ Hz}$, 2H, ArH), 7.34 (app dd, $J_{\text{H,H}} = 5.7, 3.3\text{ Hz}$, 4H, anth-H), 7.15 (d, $^4J_{\text{H,H}} = 2.5\text{ Hz}$, 2H, ArH), 6.90 (app dd, $J_{\text{H,H}} = 5.7, 3.2\text{ Hz}$, 4H, anth-H), 6.82 (s, 4H, MesH), 3.61 – 3.54 (m, 8H, THF-OCH₂), 3.18 – 3.11 (m, 4H, THF), 2.20 (s, 6H, ArCH₃), 2.16 (s, 12H, ArCH₃), 1.42 (s, 18H, C(CH₃)₃), 1.08 (m, 12H, THF-CH₂); $^{13}\text{C}\{^1\text{H}\}$ NMR (101 MHz, C_6D_6): δ 161.54 (aryl-C), 140.71 (aryl-C), 140.40 (aryl-C), 139.39 (aryl-C), 136.78 (aryl-C), 135.71 (aryl-C), 135.11 (aryl-C), 127.50 (aryl-C), 126.42 (aryl-C), 128.30 (aryl-C), 124.22 (2C, aryl-C), 123.12 (aryl-C), 94.78 (Zr-C), 73.82 (THF-OCH₂), 69.55 (THF-OCH₂), 34.44 (C(CH₃)₃), 32.38 (C(CH₃)₃), 25.39 (THF-CH₂), 24.80 (THF-CH₂), 21.45 (ArCH₃), 21.16 (ArCH₃). Anal. Calcd. $\text{C}_{64}\text{H}_{73}\text{O}_5\text{Zr}$ (%): C, 75.85; H, 7.26. Found: C, 75.48; H, 6.97.

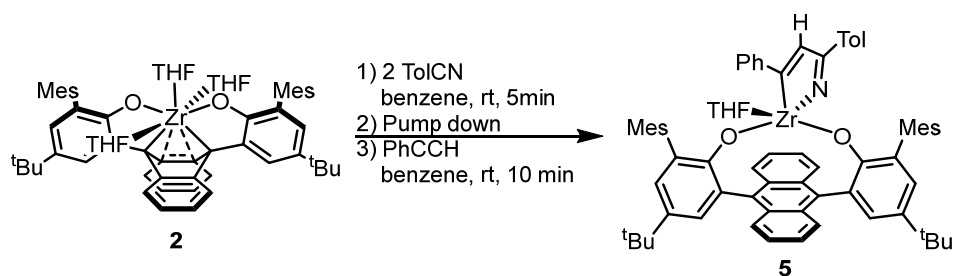


Synthesis of 3b. Phenylacetylene (22 μ L, 0.20 mmol) was added to a stirred solution of 2 (100 mg, 0.099 mmol) in benzene (5 mL) at room temperature resulting in red-brown to a yellow-brown color change. After 10 min, the volatiles were removed in vacuo and the residue extracted with pentane and filtered over diatomaceous earth. Drying under reduced pressure provided **3b** as an orange powder (77.6 mg, 73.3%). X-ray quality single crystals were grown by slow diffusion of pentane into a saturated benzene solution at room temperature. ^1H NMR (400 MHz, C_6D_6): δ 8.28 (app dd, $J_{\text{H,H}} = 6.8, 3.3$ Hz, 2H, anth-*H*), 7.96 (d, $^4J_{\text{H,H}} = 2.5$ Hz, 2H, Ar*H*), 7.41 (d, $J = 7.7$ Hz, 2H, Ar*H*), 7.36 (d, $^4J_{\text{H,H}} = 2.6$ Hz, 2H, Ar*H*), 7.28 – 7.19 (m, 5H, Ar*H*), 7.09 (t, $J = 7.7$ Hz, 1H, Ar*H*), 7.04 (d, $^4J_{\text{H,H}} = 4.3$ Hz, 1H, Zr*CH*), 6.96 (t, $J = 7.4$ Hz, 2H), 6.91 (s, 2H, Mes*H*), 6.90 (s, 2H, Mes*H*), 6.88 – 6.81 (m, 3H), 6.22 (d, $^4J_{\text{H,H}} = 4.5$ Hz, 1H, ZrC(Ph)*CH*), 5.87 (d, $^3J_{\text{H,H}} = 7.3$ Hz, 2H, Ar*H*), 2.52 (app t, br, $^3J_{\text{H,H}} = 5.7$ Hz, 4H, THF-O*CH*₂), 2.39 (s, 6H, Ar*CH*₃), 2.24 (s, 6H, Ar*CH*₃), 2.10 (s, 6H, Ar*CH*₃), 1.44 (s, 18H, C(*CH*₃)₃), 0.51 (app t, br, $^3J_{\text{H,H}} = 5.7$ Hz, 4H, THF-*CH*₂); $^{13}\text{C}\{^1\text{H}\}$ NMR (101 MHz, C_6D_6): δ 199.14 (ZrC), 188.17 (ZrC), 156.93 (aryl-C), 155.93 (ZrC(Ph)), 150.75 (aryl-C), 146.99 (Zr*CH*), 143.97 (aryl-C), 142.80 (aryl-C), 139.24 (aryl-C), 136.58 (aryl-C), 136.45 (aryl-C), 135.32 (aryl-C), 135.04 (aryl-C), 131.91 (aryl-C), 131.26 (aryl-C), 131.18 (aryl-C), 130.08 (aryl-C), 129.04 (aryl-C), 128.59 (aryl-C), 128.06 (aryl-C), 127.56 (aryl-C), 127.51 (aryl-C), 127.49 (aryl-C), 126.93 (aryl-C), 126.63 (aryl-C), 126.46 (aryl-C), 125.96 (aryl-C), 125.70 (aryl-C), 125.45 (aryl-C), 124.47 (aryl-C), 123.24 (aryl-C), 70.52 (THF-O*CH*₂), 34.61 (C(*CH*₃)₃), 32.06 (C(*CH*₃)₃), 24.43 (THF-O*CH*₂*CH*₂), 21.31 (Ar*CH*₃), 21.28 (Ar*CH*₃), 21.07 (Ar*CH*₃); Anal. Calcd. $\text{C}_{72}\text{H}_{71}\text{O}_3\text{Zr}$ (%): C, 80.40; H, 6.65. Found: C, 80.67; H, 6.74.



Synthesis of 4. Method A: A J. Young NMR tube charged with a solution of **2** (20.0 mg, 0.197 mmol) and diphenylacetylene (7.0 mg, 0.039 mmol) in C_6D_6 (0.6 mL) was heated to 90 °C. After 2 h, the atmosphere in the tube was degassed and replaced with CO (1 atm) and the tube was heated for an additional 9 h after which 1H NMR spectroscopy showed that the major product matched that of **4** synthesized via method B. Method B: To a solution of **2** (100 mg, 0.099 mmol) in benzene (5 mL) was added tetraphenylcyclopentadienone (37.9 mg, 0.099 mmol) at room temperature resulting in a red to yellow-brown color change. After 10 min, the volatiles were removed in vacuo and the solid residue washed with pentane and dried under reduced pressure to provide **4** as a dark brown powder (92.6 mg, 68.0%). 1H NMR (400 MHz, C_6D_6): δ 7.93 – 7.89 (m, 6H, overlapping anth-*H* and Ar*H*), 7.56 (dd, $J_{H,H} = 8.2, 1.3$ Hz, 4H, Ar*H*), 7.33 (d, $^4J_{H,H} = 2.6$ Hz, 2H, Ar*H*), 7.20 (dd, $J_{H,H} = 8.0, 1.3$ Hz, 4H, Ar*H*), 7.08 (s, 4H, Ar*H*), 7.04 (t, $^3J_{H,H} = 7.6$ Hz, 4H, Ar*H*), 6.92 – 6.83 (m, 6H, Ar*H*), 6.83 (dd, $J_{H,H} = 6.7, 3.3$ Hz, 4H, Ar*H*), 6.65 (t, $^3J_{H,H} = 7.3$ Hz, 2H, Ar*H*), 2.83 (t, $^3J_{H,H} = 6.6$ Hz, 8H, THF- OCH_2), 2.36 (s, 6H, Ar*CH*₃), 2.22 (s, 12H, Ar*CH*₃), 1.36 (s, 18H, C(CH_3)₃), 0.61 (d, $^3J_{H,H} = 6.1$ Hz, 8H, THF- CH_2); $^{13}C\{^1H\}$ NMR (101 MHz, C_6D_6): δ 156.95 (C=O), 144.31 (aryl-C), 143.70 (aryl-C), 142.48 (aryl-C), 137.87 (aryl-C), 136.14 (aryl-C), 134.57 (aryl-C), 133.49 (aryl-C), 132.87 (aryl-C), 131.88 (aryl-C), 131.35 (aryl-C), 131.28 (aryl-C), 130.22 (aryl-C), 129.99 (aryl-C), 129.05 (aryl-C), 128.59 (aryl-C), 127.19 (aryl-C), 126.66 (aryl-C), 125.69 (aryl-C), 125.23 (aryl-C), 124.92 (aryl-C), 122.89 (aryl-C), 120.83 (aryl-C), 118.86 (PhC), 110.21 (PhC), 73.46 (THF-

OCH₂), 34.56 (C(CH₃)₃), 31.81 (C(CH₃)₃), 22.90 (THF-OCH₂CH₂), 21.59 (ArCH₃), 21.46 (ArCH₃); Anal. Calcd. C₈₉H₈₆O₅Zr (%): C, 80.56; H, 6.53. Found: C, 80.32; H, 6.28.

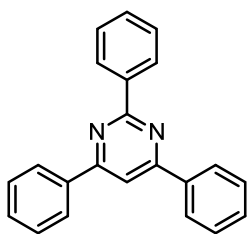


Synthesis of 5. *p*-Tolunitrile (23.2 mg, 0.198 mmol) was added to a solution of 2 (100 mg, 0.099 mmol) in benzene (5 mL) at room temperature resulting in the immediate formation of a deep purple solution. After 5 min, the volatiles were removed in vacuo. The resulting solid was taken up in benzene (5 mL) and phenylacetylene (10.8 μ L, 0.099 mmol) was added forming a red-orange solution. After stirring an additional 10 min, the reaction was concentrated under vacuum and the residue washed with cold pentane and dried to provide 5 as a red brown solid (76.8 mg, 71.4%). X-ray quality single crystals were grown by slow diffusion of pentane into a saturated benzene solution at room temperature. ¹H NMR (400 MHz, C₆D₆): δ 8.34 (app dd, $J_{H,H} = 6.8, 3.2$ Hz, 2H, anth-*H*), 8.05 (app dd, $J_{H,H} = 6.7, 3.3$ Hz, 2H), 7.99 (d, $^4J_{H,H} = 2.5$ Hz, 2H, Ar*H*), 7.67 (d, $^2J_{H,H} = 8.1$ Hz, 2H, Tol-*H*), 7.47 (app dd, $J_{H,H} = 6.8, 3.3$ Hz, 2H), 7.35 (d, $J = 2.5$ Hz, 2H, Ar*H*), 7.28 (s, 1H, alkenyl-*H*), 7.04 (d, $^2J_{H,H} = 8.0$ Hz, 2H, Tol-*H*), 6.97 (t, $^2J_{H,H} = 7.6$ Hz, 2H, Ar*H*), 6.91 (s, 2H, Mes*H*), 6.87 (m, 3H, anth-*H* and Ar*H*), 6.83 (s, 2H, Mes*H*), 5.84 (dd, $J_{HH} = 8.1, 1.4$ Hz, 2H, Ar*H*), 2.63 – 2.55 (m, 4H, THF-CH₂), 2.24 (s, 6H, ArCH₃), 2.23 (s, 6H, ArCH₃), 2.16 (s, 3H, ArCH₃), 2.11 (s, 6H, ArCH₃), 1.44 (s, 18H, C(CH₃)₃), 0.57 – 0.47 (m, 4H, THF-CH₂); ¹³C {¹H} NMR (101 MHz, CDCl₃): δ 210.36, 177.99, 156.96, 150.94, 147.50, 142.07, 140.20, 139.05, 136.75, 136.28, 135.59, 135.46, 135.06, 131.76, 130.85, 129.83, 129.62, 129.59, 128.97, 128.87, 128.43, 128.30, 127.95, 127.61, 127.54, 126.98, 126.77, 125.32, 124.78, 124.53, 70.92 (THF-OCH₂), 34.59 (C(CH₃)₃), 32.11

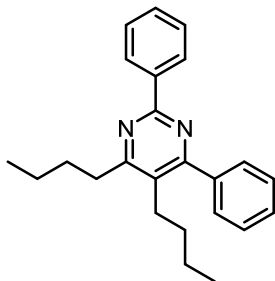
(C(CH₃)₃), 24.52 (THF-OCH₂CH₂), 21.48 (ArCH₃), 21.28 (ArCH₃), 21.25 (ArCH₃), 20.81 (ArCH₃); Anal. Calcd. C₇₂H₇₂NO₃Zr (%): C, 79.30; H, 6.65; N, 1.28. Found: C, 79.63; H, 6.41; N, 1.66.

General Setup for Screening of Conditions for Catalytic 1,3,5-Triphenylpyrimidine

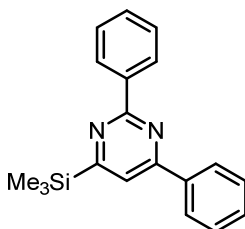
Synthesis. In the glovebox, stock solutions of nitrile, alkyne, 1-adamantane (internal standard), and **2** in the appropriate solvent were measured with syringes and added in that order to a vial equipped with a Teflon-coated stir bar, additional solvent was added to ensure total volume of the reaction was 3 mL. The vial was capped with a PTFE-lined septum cap, taken out of the box, and placed into a preheated heating block at the appropriate temperature. After the reaction time, the reaction was cooled to room temperature and quenched by exposure to air with stirring. A small volume was taken, filtered through a pad of silica gel, and eluted with CH₂Cl₂ for GC-MS analysis. Parallel runs were also set up in the absence of 1-adamantane to obtain isolated yields.



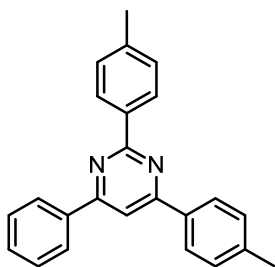
2,4,6-Triphenylpyrimidine (6a).⁶⁹ Synthesized using the general setup using phenylacetylene (10.8 μ L, 0.0987 mmol), benzonitrile (61.0 μ L, 0.592 mmol) and **2** (5.0 mg, 4.9 μ mol) in toluene (3 mL), and purified via silica gel column chromatography (5% EtOAc/hexanes). White solid. First run 28.8 mg (95%). Second run 28.5 mg (94%).



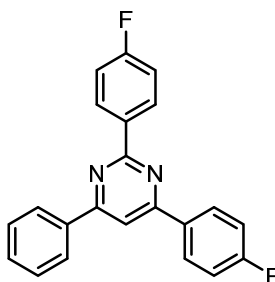
4,5-dibutyl-2,6-diphenylpyrimidine (6b).⁶⁹ Synthesized using the general setup using 5-decyne (17.8 μL , 0.0987 mmol), benzonitrile (61.0 μL , 0.592 mmol) and **2** (5.0 mg, 4.9 μmol) in toluene (3 mL), and purified via silica gel column chromatography (5% CH_2Cl_2 /hexanes). White solid. First run 32.8 mg (96%) Second Run 32.6 mg (96%).



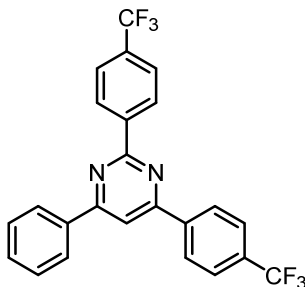
2,4-diphenyl-6-(trimethylsilyl)pyrimidine (6c). Synthesized using the general setup using trimethylsilylacetylene (14.1 μL , 0.0987 mmol), benzonitrile (61.0 μL , 0.592 mmol) and **2** (5.0 mg, 4.9 μmol) in toluene (3 mL), and purified via silica gel column chromatography (5% CH_2Cl_2 , 1% triethylamine in hexanes). White solid. First run 29.2 mg (97%) Second Run 28.9 mg (96%). ¹H NMR (400 MHz, CDCl_3): δ 8.80 (dd, $J = 8.1, 1.6$ Hz, 1H), 8.67 (dd, $J = 8.0, 1.8$ Hz, 2H), 8.24 (dd, $J = 7.8, 1.8$ Hz, 2H), 7.78 (s, 1H), 7.66 – 7.46 (m, 5H), 0.43 (s, 9H); ¹³C {¹H} NMR (101 MHz, CDCl_3): δ 178.35, 171.78, 163.32, 161.71, 138.68, 137.89, 136.39, 132.63, 130.67, 130.46, 129.10, 128.98, 128.77, 128.51, 128.49, 127.36, 119.46, -2.02; HRMS (FAB+) m/z Calcd. for $\text{C}_{19}\text{H}_{21}\text{SiN}_2$ $[\text{M}+\text{H}]^+$ 305.1474, found 305.1465.



6-phenyl-2,4-di(*p*-tolyl)pyrimidine (6d).⁹⁴ Synthesized using the general setup using phenylacetylene (10.8 μ L, 0.0987 mmol), *p*-tolunitrile (69.4 mg, 0.592 mmol) and 2 (5.0 mg, 4.9 μ mol) in toluene (3 mL), and purified via silica gel column chromatography (5% EtOAc/hexanes). White solid. First run 31.9 mg (96%) Second Run 31.7 mg (95%).



2,4-di(4-fluorophenyl)-6-phenylpyrimidine (6e). Synthesized using the general setup using phenylacetylene (10.8 μ L, 0.0987 mmol), 4-fluorobenzonitrile (71.7 mg, 0.592 mmol) and 2 (5.0 mg, 4.9 μ mol) in toluene (3 mL), and purified via silica gel column chromatography (5% EtOAc/hexanes). White solid. First run 33.0 mg (97%) Second Run 32.9 mg (97%). ¹H NMR (400 MHz, CDCl₃): δ 8.75 – 8.67 (m, 2H), 8.31 – 8.23 (m, 4H), 7.94 (s, 1H), 7.59 – 7.54 (m, 3H), 7.28 – 7.18 (m, 4H); ¹³C{¹H} NMR (101 MHz, CDCl₃): δ 165.00, 164.95 (d, ¹J_{CF} = 235.7 Hz), 164.86 (d, ¹J_{CF} = 229.9 Hz), 163.63 163.50, 137.42, 134.30 (d, ⁴J_{CF} = 3.0 Hz), 133.65 (d, ⁴J_{CF} = 3.1 Hz), 131.07, 130.68 (d, ³J_{CF} = 8.7 Hz), 129.41 (d, ³J_{CF} = 8.7 Hz), 129.09, 127.38, 116.11 (d, ²J_{CF} = 21.8 Hz), 115.52 (d, ²J_{CF} = 21.6 Hz), 109.90; ¹⁹F NMR (376 MHz, CDCl₃): δ 109.80 (m), 110.55 (m); HRMS (FAB+) *m/z* Calcd. for C₂₂H₁₅F₂N₂ [M+H]⁺ 345.1203, found 345.1206.



6-phenyl-2,4-bis[4-(trifluoromethyl)phenyl]pyrimidine (6f). Synthesized using the general setup using phenylacetylene (10.8 μL , 0.0987 mmol), 4-(trifluoromethyl)benzotrile (101.3 mg, 0.592 mmol) and **2** (5.0 mg, 4.9 μmol) in toluene (3 mL), and purified via silica gel column chromatography (3% EtOAc/hexanes). White solid. First run 37.4 mg (85%) Second Run 38.1 mg (87%). ^1H NMR (400 MHz, CDCl_3): δ 8.79 (d, $^3J_{\text{HH}} = 8.4$ Hz, 2H), 8.36 (d, $^3J_{\text{HH}} = 8.2$ Hz, 2H), 8.29 – 8.24 (m, 2H), 8.04 (s, 1H), 7.82 (d, $^3J_{\text{HH}} = 8.3$ Hz, 2H), 7.78 (d, $^3J_{\text{HH}} = 8.3$ Hz, 2H), 7.60 – 7.56 (m, 3H); $^{13}\text{C}\{^1\text{H}\}$ NMR (101 MHz, CDCl_3): δ 165.56, 163.60, 163.53, 141.17 (q, $^4J_{\text{CF}} = 1.1$ Hz), 140.65 (q, $^4J_{\text{CF}} = 1.2$ Hz) 136.92, 136.92, 132.79 (q, $^2J_{\text{CF}} = 32.6$ Hz), 132.55 (q, $^2J_{\text{CF}} = 32.3$ Hz), 131.46, 129.22, 128.88, 127.76, 127.44, 126.07 (q, $^3J_{\text{CF}} = 3.7$ Hz), 125.57 (q, $^3J_{\text{CF}} = 3.7$ Hz), 122.97, 122.72, 111.31; ^{19}F NMR (376 MHz, CDCl_3): δ 62.66 (s), 62.77 (s).

Catalytic controls

Photoreduction of ZrBn_4 in the presence of anthracene. A quartz Schlenk tube was charged with a Teflon-coated stir bar, ZrBn_4 (50.0 mg, 0.110 mmol), anthracene (19.6 mg, 0.110 mmol) and tetrahydrofuran (1 mL). The flask was sealed and irradiated with light from a Xe arc lamp (75 W) with stirring at room temperature for 12 h, forming a deep red-brown suspension. The volatiles were removed in vacuo. 5 mg of the crude solid was then tested under the general catalytic conditions in place of **2**.

Photoreduction of ZrBn_2Cl_2 in the presence of anthracene. A thawing THF solution (0.5 mL) of ZrBn_4 (25.0 mg, 0.055 mmol) was added to a thawing THF suspension (0.5 mL) of ZrCl_4 (12.8 mg, 0.055 mmol) with stirring. After warming the mixture to room temperature the suspension was transferred to a quartz Schlenk tube and anthracene (19.6 mg, 0.110 mmol) added. The flask was sealed and irradiated with light from a Xe arc lamp (75 W) with stirring at room temperature for 12 h forming a deep red-brown solution. The volatiles were removed in vacuo. 5 mg of the crude solid was then tested under the general catalytic conditions in place of **2**.

Reduction of ZrCl_4 by $\text{Mg}(\text{THF})_3(\text{C}_{14}\text{H}_{10})$. $\text{Mg}(\text{THF})_3(\text{C}_{14}\text{H}_{10})$ (35.7 mg, 0.0859 mmol) was added to a thawing suspension of ZrCl_4 (20.0 mg, 0.0859 mmol) and was allowed to warm to room temperature turning from orange to yellow then brown-green. After 10 min at room temperature, the volatiles were removed under reduced pressure and the residue extracted with benzene. Concentration of the filtrate provided an off-white solid. 5 mg of the crude solid was then tested under the general catalytic conditions in place of **2**.

In-situ reduction of ZrCl_4 by $\text{Mg}(\text{THF})_3(\text{C}_{14}\text{H}_{10})$. Following the general setup for catalysis, using ZrCl_4 in place of **2**, $\text{Mg}(\text{THF})_3(\text{C}_{14}\text{H}_{10})$ (2.3 mg) was added as the last step before sealing and heating the mixture.

In-situ reduction of ZrCl_4 by KC_8 in the presence of anthracene. Following the general setup for catalysis, using ZrCl_4 in place of **2**, anthracene (0.9 mg) and then KC_8 (0.7 mg) was added as the last step before sealing and heating the mixture.

Stoichiometric reactions from preformed (aza)zirconacyclopentadienes **3b and **5**.** To a solution of **3b** or **5** (20.0 mg) in C_6D_6 (0.5 mL) in a J. Young tube was added either phenylacetylene or benzonitrile (5 equiv.). The tube was sealed and heated in an oil bath at 90 °C for 1 h.

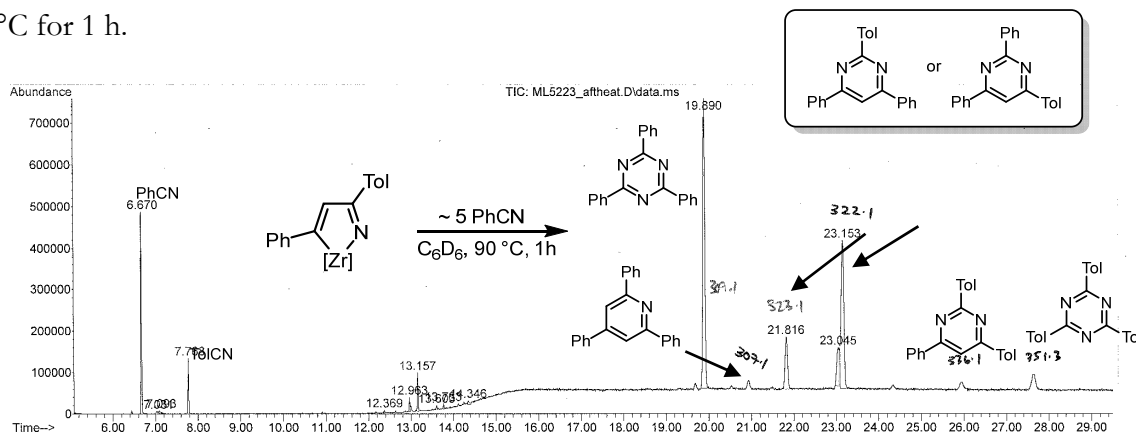


Figure 4.8. GC-MS chromatogram from the reaction of **5** with benzonitrile (5 equiv.) after 1 h heating at 90 °C.

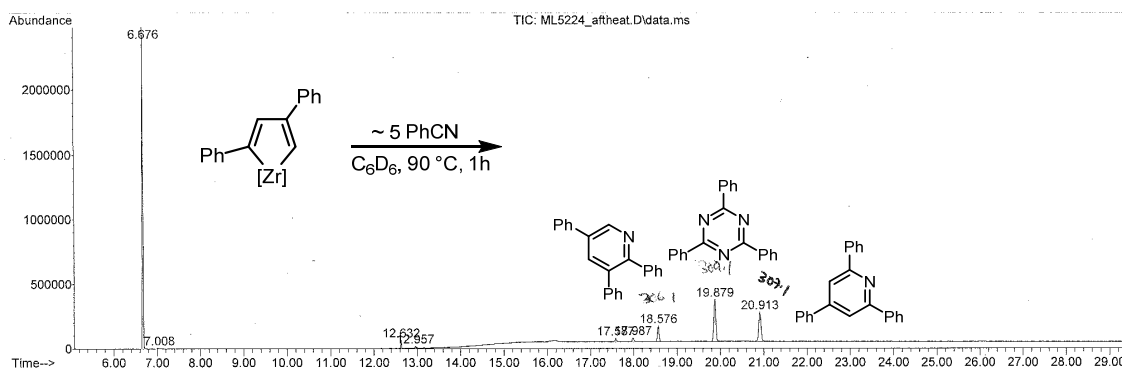
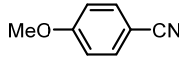
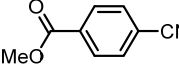
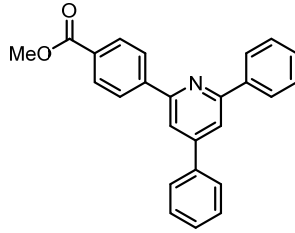
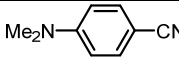
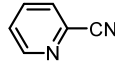
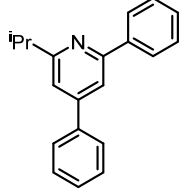
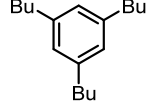
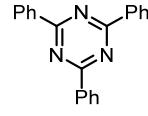


Figure 4.9. GC-MS chromatogram from the reaction of **3b** with benzonitrile (5 equiv.) after 1 h heating at 90 °C

Table 4.4. Additional substrates screened under optimized catalytic conditions^a

Entry	Alkyne	Nitrile	Products ^b (Yields ^c)
1	Ph—≡		nd
2	Ph—≡		 ($<5\%$)
3	Ph—≡		nd
4	Ph—≡		nd
5	Ph—≡	Me—≡N	nd
6	Ph—≡	ⁱ Pr—≡N	 ($<5\%$)
7	Ph—≡	^t Bu—≡N	nd
8	Ph—≡	Me ₃ Si—≡N	nd
9	Bu—≡	Ph—≡N	 ($<5\%$)
10	Oct—≡	Ph—≡N	nd
11	Ph—≡—Ph	Ph—≡N	nd
12	Me ₃ Si—≡—SiMe ₃	Ph—≡N	 (37%)

^aoptimized conditions: 6:1 nitrile:alkyne, 5 mol% **3a**, toluene (3 mL), 105 °C, 1h; ^bnd: not detected by GC-MS; ^cyields approximated from GC-MS based on PhCCH or PhCN consumption.

General Setup for Catalytic Pyridine Synthesis. In the glovebox, stock solutions of nitrile, diyne, and **2** in the appropriate solvent were measured with syringes and added in that order to a Schlenk tube equipped with a screw-down Teflon pin and a Teflon-coated stir bar, additional solvent was added to ensure the total volume of the reaction was 3 mL. The tube was sealed, taken out of the box, and placed into a preheated oil bath at the appropriate temperature. After the reaction time, the tube was cooled to room temperature and quenched by exposure to air with stirring. The entire reaction was concentrated in vacuo and 1,3,5-trimethoxybenzene was added as an NMR standard. The mixture was taken up in a small volume of CDCl₃ ensuring homogeneity and ¹H NMR recorded.

CRYSTALLOGRAPHIC INFORMATION

CCDC deposition numbers 1853068, 1853069, 1853070 and 1869798 contain the supplementary crystallographic data for this paper.⁹⁵ These data can be obtained free of charge from The Cambridge Crystallographic Data Centre via www.ccdc.cam.ac.uk/data_request/cif.

Refinement Details

In each case, crystals were mounted on a glass fiber or MiTeGen loop using Paratone oil, then placed on the diffractometer under a nitrogen stream. Low temperature (100 K) X-ray data were obtained on a Bruker D8 VENTURE Kappa Duo PHOTON 100 CMOS based diffractometer (Mo I μ S HB micro-focus sealed X-ray tube, $K\alpha = 0.71073 \text{ \AA}$ OR Cu I μ S HB micro-focused X-ray tube, $K\alpha = 1.54178$). All diffractometer manipulations, including data collection, integration, and scaling were carried out using the Bruker APEXII software.⁹⁶ Absorption corrections were applied using SADABS.⁹⁷ Space groups were determined on the basis of systematic absences and intensity statistics and the structures were solved in the Olex 2 software interface⁹⁸ by intrinsic phasing using XT (incorporated into SHELXTL)⁹⁹ and refined by full-matrix least squares on F2. All non-hydrogen atoms were refined using anisotropic displacement parameters, except in some cases with heavily distorted solvent. Hydrogen atoms were placed in the idealized positions and refined using a riding model. The structure was refined (weighted least-squares refinement on F2) to convergence. Graphical representations of structures with 50% probability thermal ellipsoids were generated using Diamond 3 visualization software.¹⁰⁰

Table 4.5. Crystal data and structure refinement for **1**, **2**, **3a**, and **5**

	1	2	3a	5
CCDC Number ⁹⁵	1853068	1853069	1853070	1869798
Empirical formula	C ₇₁ H ₇₈ O ₂ Zr	C _{72.44} H _{93.75} O _{6.57} Zr	C _{92.42} H _{96.5} O ₃ Zr	C ₇₇ H ₈₅ NO ₃ Zr
Formula weight	1054.55	1160.69	1346.44	1163.67
Temperature/K	100.15	100	100.0	100.02
Crystal system	triclinic	triclinic	triclinic	monoclinic
Space group	P-1	P-1	P-1	P2 ₁ /c
a/Å	11.101(4)	12.4092(6)	12.350(2)	13.2545(11)
b/Å	12.844(4)	12.7750(8)	12.845(2)	25.037(2)
c/Å	21.787(7)	20.5948(17)	27.404(4)	19.9334(16)
α/°	101.462(14)	93.281(3)	78.961(7)	90
β/°	99.260(9)	103.293(4)	80.374(5)	107.996(3)
γ/°	93.809(11)	99.373(3)	63.052(12)	90
Volume/Å ³	2989.4(17)	3119.7(4)	3787.6(11)	6291.2(9)
Z	2	2	2	4
ρ _{calc} /cm ³	1.172	1.236	1.181	1.229
μ/mm ⁻¹	0.227	0.229	0.195	1.803
Crystal size/mm ³	0.4 × 0.2 × 0.1	0.22 × 0.16 × 0.11	0.25 × 0.25 × 0.09	0.09 × 0.05 × 0.03
Radiation	MoKα (λ = 0.71073)	MoKα (λ = 0.71073)	MoKα (λ = 0.71073)	CuKα (λ = 1.54178)
2θ range/°	4.698 to 61.314	4.398 to 73.656	4.58 to 69.918	5.848 to 105.636
GOF	1.057	1.038	1.147	1.065
R ₁ , ^a wR ₂ ^b [I > 2σ(I)]	0.0396, 0.0990	0.0423, 0.0902	0.0661, 0.1721	0.0979, 0.2382

$${}^a R_1 = \sum ||F_o| - |F_c|| / \sum |F_o|. \quad {}^b wR_2 = [\sum [w(F_o^2 - F_c^2)^2] / \sum [w(F_o^2)^2]]^{1/2}$$

REFERENCES

- (1) Chirik, P. J.; Wieghardt, K., *Science* **2010**, *327*, 794-795.
- (2) Luca, O. R.; Crabtree, R. H., *Chem. Soc. Rev.* **2013**, *42*, 1440-1459.
- (3) Lyaskovskyy, V.; de Bruin, B., *ACS Catal.* **2012**, *2*, 270-279.
- (4) Blackmore, K. J.; Lal, N.; Ziller, J. W.; Heyduk, A. F., *J. Am. Chem. Soc.* **2008**, *130*, 2728-2729.
- (5) Blackmore, K. J.; Ziller, J. W.; Heyduk, A. F., *Inorg. Chem.* **2005**, *44*, 5559-5561.
- (6) Nguyen, A. I.; Zarkesh, R. A.; Lacy, D. C.; Thorson, M. K.; Heyduk, A. F., *Chem. Sci.* **2011**, *2*, 166-169.
- (7) Haneline, M. R.; Heyduk, A. F., *J. Am. Chem. Soc.* **2006**, *128*, 8410-8411.
- (8) Heins, S. P.; Wolczanski, P. T.; Cundari, T. R.; MacMillan, S. N., *Chem. Sci.* **2017**, *8*, 3410-3418.
- (9) Buss, J. A.; Agapie, T., *J. Am. Chem. Soc.* **2016**, *138*, 16466-16477.
- (10) Buss, J. A.; Agapie, T., *Nature* **2016**, *529*, 72-75.
- (11) Horak, K. T.; Velian, A.; Day, M. W.; Agapie, T., *Chem. Commun.* **2014**, *50*, 4427-4429.
- (12) Henthorn, J. T.; Lin, S.; Agapie, T., *J. Am. Chem. Soc.* **2015**, *137*, 1458-1464.
- (13) Velian, A.; Lin, S.; Miller, A. J. M.; Day, M. W.; Agapie, T., *J. Am. Chem. Soc.* **2010**, *132*, 6296-6297.
- (14) Kurogi, T.; Ishida, Y.; Kawaguchi, H., *Chem. Commun.* **2013**, *49*, 11755-11757.
- (15) Buss, J. V., David; Agapie, Theodor, *J. Am. Chem. Soc.* **2018**, Submitted.
- (16) Buss, J. A.; VanderVelde, D. G.; Agapie, T., *J. Am. Chem. Soc.* **2018**, *140*, 10121-10125.
- (17) Plundrich, G. T.; Wadepohl, H.; Clot, E.; Gade, L. H., *Chem. Eur. J.* **2016**, *22*, 9283-9292.
- (18) Jilek, R. E.; Jang, M.; Smolensky, E. D.; Britton, J. D.; Ellis, J. E., *Angew. Chem. Int. Ed.* **2008**, *47*, 8692-8695.
- (19) Schleyer, P. v. R.; Manoharan, M.; Jiao, H.; Stahl, F., *Org. Lett.* **2001**, *3*, 3643-3646.
- (20) Connelly, N. G.; Geiger, W. E., *Chem. Rev.* **1996**, *96*, 877-910.
- (21) Roitershtein, D. M.; Rybakova, L. F.; Petrov, E. S.; Ellern, A. M.; Antipin, M. Y.; Struchkov, Y. T., *J. Organomet. Chem.* **1993**, *460*, 39-45.
- (22) Bogdanovic, B., *Acc. Chem. Res.* **1988**, *21*, 261-267.
- (23) Fedushkin, I. L.; Bochkarev, M. N.; Dechert, S.; Schumann, H., *Chem. Eur. J.* **2001**, *7*, 3558-3563.

- (24) Lehmkuhl, H.; Mehler, K.; Shakoor, A.; Krüger, C.; Tsay, Y.-H.; Benn, R.; Ruffinowska, A.; Schroth, G., *Chem. Ber.* **1985**, *118*, 4248-4258.
- (25) Lehmkuhl, H.; Shakoor, A.; Mehler, K.; Krüger, C.; Angermund, K.; Tsay, Y.-H., *Chem. Ber.* **1985**, *118*, 4239-4247.
- (26) Bogdanović, B.; Janke, N.; Krüger, C.; Mynott, R.; Schlichte, K.; Westeppe, U., *Angew. Chem. Int. Ed.* **1985**, *24*, 960-961.
- (27) Fryzuk Michael, D.; Jafarpour, L.; Kerton Francesca, M.; Love Jason, B.; Rettig Steven, J., *Angew. Chem. Int. Ed.* **2000**, *39*, 767-770.
- (28) Huang, W.; Khan, S. I.; Diaconescu, P. L., *J. Am. Chem. Soc.* **2011**, *133*, 10410-10413.
- (29) Huang, W.; Abukhalil, P. M.; Khan, S. I.; Diaconescu, P. L., *Chem. Commun.* **2014**, *50*, 5221-5223.
- (30) Covert, K. J.; Mayol, A.-R.; Wolczanski, P. T., *Inorg. Chim. Acta* **1997**, *263*, 263-278.
- (31) Erker, G., *J. Organomet. Chem.* **1977**, *134*, 189-202.
- (32) Burk, M. J.; Tumas, W.; Ward, M. D.; Wheeler, D. R., *J. Am. Chem. Soc.* **1990**, *112*, 6133-6135.
- (33) Ishikawa, T.; Ogawa, A.; Hirao, T., *J. Organomet. Chem.* **1999**, *575*, 76-79.
- (34) Margulieux, G. W.; Semproni, S. P.; Chirik, P. J., *Angew. Chem. Int. Ed.* **2014**, *53*, 9189-9192.
- (35) Negishi, E.-i.; Cederbaum, F. E.; Takahashi, T., *Tetrahedron Lett.* **1986**, *27*, 2829-2832.
- (36) Nitschke, J. R.; Zürcher, S.; Tilley, T. D., *J. Am. Chem. Soc.* **2000**, *122*, 10345-10352.
- (37) Nugent, W. A.; Thorn, D. L.; Harlow, R. L., *J. Am. Chem. Soc.* **1987**, *109*, 2788-2796.
- (38) Wielstra, Y.; Gambarotta, S.; Meetsma, A.; De Boer, J. L.; Chiang, M. Y., *Organometallics* **1989**, *8*, 2696-2702.
- (39) Schaefer, C.; Werz, D. B.; Staeb, T. H.; Gleiter, R.; Rominger, F., *Organometallics* **2005**, *24*, 2106-2113.
- (40) Schore, N. E., *Chem. Rev.* **1988**, *88*, 1081-1119.
- (41) Gleiter, R.; Werz, D. B., *Organometallics* **2005**, *24*, 4316-4329.
- (42) Shibata, T.; Yamashita, K.; Ishida, H.; Takagi, K., *Org. Lett.* **2001**, *3*, 1217-1219.
- (43) Sikora, D. J.; Rausch, M. D., *J. Organomet. Chem.* **1984**, *276*, 21-37.
- (44) Guram, A. S.; Guo, Z.; Jordan, R. F., *J. Am. Chem. Soc.* **1993**, *115*, 4902-4903.
- (45) Takahashi, T.; Huo, S.; Hara, R.; Noguchi, Y.; Nakajima, K.; Sun, W.-H., *J. Am. Chem. Soc.* **1999**, *121*, 1094-1095.

- (46) Li, H.; Liu, L.; Zhao, F.; Wang, C.; Wang, C.; Song, Q.; Zhang, W.-X.; Xi, Z., *J. Org. Chem.* **2012**, *77*, 4793-4800.
- (47) Gilbert, Z. W.; Hue, R. J.; Tonks, I. A., *Nature Chemistry* **2015**, *8*, 63.
- (48) Denhez, C.; Médégan, S.; Hélicon, F.; Namy, J.-L.; Vasse, J.-L.; Szymoniak, J., *Org. Lett.* **2006**, *8*, 2945-2947.
- (49) Zirngast, M.; Marschner, C.; Baumgartner, J., *Organometallics* **2008**, *27*, 2570-2583.
- (50) Shenyong, R.; Takashi, S.; David, N.; Hiroyuki, S.; Kiyohiko, N.; Ken-ichiro, K.; Zhiying, S.; Tamotsu, T., *Chem. Lett.* **2011**, *40*, 1443-1444.
- (51) Bousrez, G.; Jaroschik, F.; Martinez, A.; Harakat, D.; Nicolas, E.; Le Goff, X. F.; Szymoniak, J., *Dalton Trans.* **2013**, *42*, 10997-11004.
- (52) Ma, W.; Yu, C.; Chen, T.; Xu, L.; Zhang, W.-X.; Xi, Z., *Chem. Soc. Rev.* **2017**, *46*, 1160-1192.
- (53) Although 1,3,5-triphenylbenzene was not produced when **3a** was reacted with excess phenylacetylene, in the presence of certain additives (nitriles, CO), its formation was observed.
- (54) Gómez-de la Torre, F.; de la Hoz, A.; Jalón, F. A.; Manzano, B. R.; Rodríguez, A. M.; Elguero, J.; Martínez-Ripoll, M., *Inorg. Chem.* **2000**, *39*, 1152-1162.
- (55) Kua, J.; Xu, X.; Periana, R. A.; Goddard, W. A., *Organometallics* **2002**, *21*, 511-525.
- (56) Warsink, S.; Chang, I. H.; Weigand, J. J.; Hauwert, P.; Chen, J.-T.; Elsevier, C. J., *Organometallics* **2010**, *29*, 4555-4561.
- (57) Walker, S. R.; Carter, E. J.; Huff, B. C.; Morris, J. C., *Chem. Rev.* **2009**, *109*, 3080-3098.
- (58) Undheim, K.; Benneche, T., 6.02 - Pyrimidines and their Benzo Derivatives A2 - Katritzky, Alan R. In *Comprehensive Heterocyclic Chemistry II*, Rees, C. W.; Scriven, E. F. V., Eds. Pergamon: Oxford, 1996; pp 93-231.
- (59) Perreault, S.; Rovis, T., *Chem. Soc. Rev.* **2009**, *38*, 3149-3159.
- (60) Gulevich, A. V.; Dudnik, A. S.; Chernyak, N.; Gevorgyan, V., *Chem. Rev.* **2013**, *113*, 3084-3213.
- (61) Chopade, P. R.; Louie, J., *Adv. Synth. Catal.* **2006**, *348*, 2307-2327.
- (62) Hill, M. D.; Movassaghi, M., *Chem. Eur. J.* **2008**, *14*, 6836-6844.
- (63) Mahfoudh, M.; Abderrahim, R.; Leclerc, E.; Campagne, J.-M., *Eur. J. Org. Chem.* **2017**, *2017*, 2856-2865.
- (64) Karad Somnath, N.; Liu, R. S., *Angew. Chem. Int. Ed.* **2014**, *53*, 9072-9076.

- (65) You, X.; Yu, S.; Liu, Y., *Organometallics* **2013**, *32*, 5273-5276.
- (66) Chen, P.; Song, C.-x.; Wang, W.-s.; Yu, X.-l.; Tang, Y., *RSC Adv.* **2016**, *6*, 80055-80058.
- (67) Burlakov, V. V.; Becker, L.; Bogdanov, V. S.; Andreev, M. V.; Arndt, P.; Spannenberg, A.; Baumann, W.; Rosenthal, U., *Eur. J. Inorg. Chem.* **2014**, *2014*, 5304-5310.
- (68) Fujii, M.; Obora, Y., *Org. Lett.* **2017**, *19*, 5569-5572.
- (69) Satoh, Y.; Yasuda, K.; Obora, Y., *Organometallics* **2012**, *31*, 5235-5238.
- (70) Xie, L.-G.; Niyomchon, S.; Mota, A. J.; González, L.; Maulide, N., *Nat. Commun.* **2016**, *7*, 10914.
- (71) Lane, T. K.; Nguyen, M. H.; D'Souza, B. R.; Spahn, N. A.; Louie, J., *Chem. Commun.* **2013**, *49*, 7735-7737.
- (72) Liu, Y.; Yan, X.; Yang, N.; Xi, C., *Catal. Commun.* **2011**, *12*, 489-492.
- (73) Hilt, G.; Vogler, T.; Hess, W.; Galbiati, F., *Chem. Commun.* **2005**, 1474-1475.
- (74) Hsieh, J.-C.; Cheng, C.-H., *Chem. Commun.* **2008**, 2992-2994.
- (75) Takahashi, T.; Tsai, F.-Y.; Kotora, M., *J. Am. Chem. Soc.* **2000**, *122*, 4994-4995.
- (76) Takahashi, T.; Tsai, F.-Y.; Li, Y.; Wang, H.; Kondo, Y.; Yamanaka, M.; Nakajima, K.; Kotora, M., *J. Am. Chem. Soc.* **2002**, *124*, 5059-5067.
- (77) Hill, J. E.; Balaich, G.; Fanwick, P. E.; Rothwell, I. P., *Organometallics* **1993**, *12*, 2911-2924.
- (78) Tanaka, R.; Yuza, A.; Watai, Y.; Suzuki, D.; Takayama, Y.; Sato, F.; Urabe, H., *J. Am. Chem. Soc.* **2005**, *127*, 7774-7780.
- (79) Varela, J. A.; Saá, C., *Chem. Rev.* **2003**, *103*, 3787-3802.
- (80) Becker, L.; Arndt, P.; Jiao, H.; Spannenberg, A.; Rosenthal, U., *Angew. Chem. Int. Ed.* **2013**, *52*, 11396-11400.
- (81) Becker, L.; Strehler, F.; Korb, M.; Arndt, P.; Spannenberg, A.; Baumann, W.; Lang, H.; Rosenthal, U., *Chem. Eur. J.* **2014**, *20*, 3061-3068.
- (82) Kiel, G. R.; Samkian, A. E.; Nicolay, A.; Witzke, R. J.; Tilley, T. D., *J. Am. Chem. Soc.* **2018**, *140*, 2450-2454.
- (83) Weding, N.; Hapke, M., *Chem. Soc. Rev.* **2011**, *40*, 4525-4538.
- (84) Richard, V.; Ipouck, M.; Mérel, D. S.; Gaillard, S.; Whitby, R. J.; Witulski, B.; Renaud, J.-L., *Chem. Commun.* **2014**, *50*, 593-595.
- (85) You, X.; Xie, X.; Wang, G.; Xiong, M.; Sun, R.; Chen, H.; Liu, Y., *Chemistry - A European Journal* **2016**, *22*, 16765-16769.

- (86) González-Bello, C.; Castedo, L., *Modern Heterocyclic Chemistry* **2011**, 1431-1525.
- (87) Kiel, G. R.; Patel, S. C.; Smith, P. W.; Levine, D. S.; Tilley, T. D., *J. Am. Chem. Soc.* **2017**, *139*, 18456-18459.
- (88) Kiel Gavin, R.; Ziegler Micah, S.; Tilley, T. D., *Angew. Chem. Int. Ed.* **2017**, *56*, 4839-4844.
- (89) Pangborn, A. B.; Giardello, M. A.; Grubbs, R. H.; Rosen, R. K.; Timmers, F. J., *Organometallics* **1996**, *15*, 1518-1520.
- (90) Baldwin, D.; Gates, P. S., Process for preparing pyrogallol. Google Patents: 1979.
- (91) Berliner, M. A.; Belecki, K., *J. Org. Chem.* **2005**, *70*, 9618-9621.
- (92) Sampson, J.; Choi, G.; Akhtar, M. N.; Jaseer, E. A.; Theravalappil, R.; Al-Muallem, H. A.; Agapie, T., *Organometallics* **2017**, *36*, 1915-1928.
- (93) Freeman, P. K.; Hutchinson, L. L., *J. Org. Chem.* **1983**, *48*, 879-881.
- (94) Wu, P.; Cai, X. M.; Wang, Q. F.; Yan, C. G., *Synth. Commun.* **2007**, *37*, 223-229.
- (95) Crystallographic data have been deposited at the CCDC, 12 Union Road, Cambridge CB2 1EZ, UK and copies can be obtained on request, free of charge, by quoting the publication citation and the respective deposition numbers.
- (96) APEX2, Version 2 User Manual, M86-E01078, Bruker Analytical X-ray Systems, Madison, WI, June 2006.
- (97) Sheldrick, G. M., "*SADABS (version 2008/1): Program for Absorption Correction for Data from Area Detector Frames*". University of Göttingen: 2008.
- (98) Dolomanov, O. V.; Bourhis, L. J.; Gildea, R. J.; Howard, J. A. K.; Puschmann, H., *J. Appl. Crystallogr.* **2009**, *42*, 339-341.
- (99) Sheldrick, G., *Acta Crystallographica Section A* **2008**, *64*, 112-122.
- (100) Brandenburg, K. (1999). DIAMOND. Crystal Impact GbR, Bonn, Germany.

CHAPTER 5

Synthesis of N-doped Nanographenes through Zirconium Catalysis and Reductive Cyclization

ABSTRACT

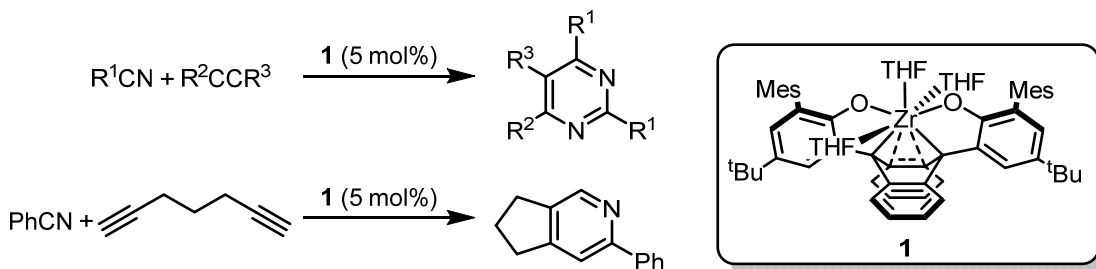
The synthesis and study of atomically-precise N-doped nanographenes for their use as electronic and optical materials are of much interest. However, methods towards their synthesis remain limited. Herein we report the Zr-catalyzed synthesis of a variety of pyridine-containing and pyrimidine-containing aromatic systems via coupling of alkynes and nitriles in good yields. This methodology offers an alternative route towards large asymmetric N-containing aromatic systems from simple alkyne and nitrile building blocks. These molecules can then be cyclized to N-doped nanographenes via an initial reductive cyclization step followed by oxidative dehydrogenation. This represents the first reported use of this methodology toward the synthesis of N-doped nanographenes. Additionally, full structural characterization of these N-doped nanographenes both in solution and in the solid state has also been carried out.

INTRODUCTION

The incorporation of nitrogen moieties into polycyclic aromatic hydrocarbons (PAHs) has attracted much interest, especially in their use as electronic or nonlinear optical materials.¹⁻³ Additionally, the ability to synthesize atomically-precise nanographenes (e.g. nanoribbons) provides scientists with avenues to tune their bandgaps, expanding their use in digital electronics.⁴⁻⁷ The presence of these nitrogen moieties also enable these frameworks to function as ligands to metal centers,⁸⁻⁹ some of which display oxygen-reduction reaction activity.¹⁰⁻¹¹ The controlled incorporation of nitrogen moieties into PAHs still remains a significant challenge.¹²⁻¹³ Current syntheses of these nitrogen-containing PAHs from a bottom-up approach often involve either a Diels-Alder [2+4] cycloaddition of alkynes with cyclopentadienones bearing N-heterocyclic substitutions,¹⁴ or [2+2+2] cyclotrimerization of N-heterocycle-substituted acetylenes.¹⁵ The use of [2+2+2] heterocyclization of alkynes with nitriles towards nitrogen-containing PAHs is far less explored even though it offers a more modular synthesis towards structurally complex asymmetric PAHs.¹⁶ The scarcity of its use is likely due to regio- and chemoselectivity issues when asymmetric substrates are employed, leading to complicated mixtures and/or poor yields.¹⁷⁻¹⁸

We have previously reported zirconium complex **1** to be competent in the [2+2+2] cyclotrimerization of alkynes and nitriles to yield tri- and tetra-substituted pyrimidines with exclusive regio- and chemoselectivities (Scheme 5.1).¹⁹ Additionally, we recently found that **1** was also a competent catalyst for the coupling of 1,6-heptadiyne with benzonitrile to yield a fused-ring pyridine product (see Chapter 4). The non-innocent nature of the anthracenediyl

Scheme 5.1. Catalytic synthesis of N-heteroaromatics by complex **1**



linker is proposed to be key in these transformations by acting both as an electron sink and a hemilabile donor, facilitating the turnover of intermediates that contain strong Zr–N bonds. We postulated that these methodologies can be extended towards the synthesis of N-containing PAHs through the judicious choice of polyaromatic alkyne and nitrile substrates. This would allow for the rapid and modular synthesis of large, complex N-containing PAHs from simple alkyne and nitrile building blocks.

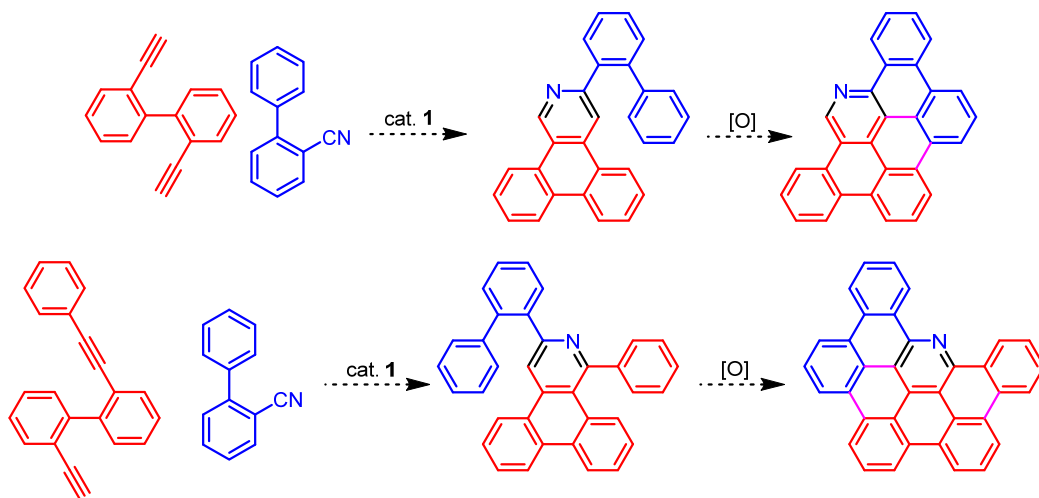
RESULTS AND DISCUSSION

1. Synthesis of Pyridine-containing PAHs

Leveraging the **1**-catalyzed pyridine synthesis we previously developed (see Chapter 4), the synthesis of polyaromatic compounds bearing a central pyridine motif was targeted. By using the basic motif of 2,2'-diethynylbiphenyl and 2-phenyl benzonitrile, the one-step catalytic synthesis of a complex pyridine-containing polyaromatic can be envisioned (Scheme 5.2). Upon, further oxidative cyclodehydrogenation, an N-doped nanographene may be prepared. Further expansion of the PAH will be targeted by the use of asymmetric variants of biphenyldiyne by substitution of an additional arene motif on one of the alkynes (Scheme 5.2). The use of biphenyldiynes to build up triphenylene-based polyaromatic molecules or natural products have been reported.²⁰⁻²¹ Additionally, dialkyl substituted biphenyldiyne motifs with internal alkynes have been used in the dicyclopentadienyl zirconium-mediated synthesis of expanded helicenes.²²

Initial studies and optimizations were carried out on 2,2'-bis(ethynyl)1,1'-biphenyl, **2a**,

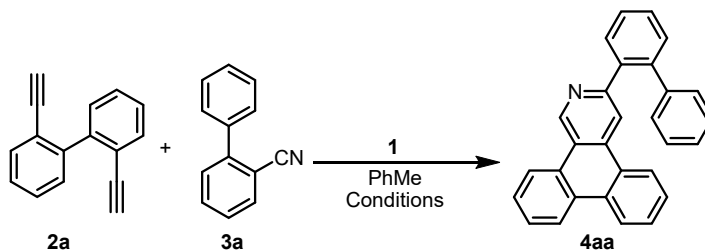
Scheme 5.2. Proposed synthesis of pyridine-containing nanographenes. Atoms originating from alkyne and nitrile are colored red and blue, respectively. Bonds formed on oxidative cyclodehydrogenation are colored pink.



and 2-phenyl benzonitrile, **3a**, as model substrates (Table 5.1). By varying the catalyst loading, it was found that an increase from 5 mol% to 10 mol% loading resulted in a significant increase in yields (entries 1 and 2), while a further increase to 15 mol% loading led to marginal improvements (entry 3). Reducing the nitrile excess to 5 equiv. relative to diyne led to a loss in yields (entry 4), while a further increase to 25 equiv. did not significantly improve yields (entry 5). As with the previously discussed pyridine synthesis, reaction times can be significantly shortened at elevated temperatures of 105 °C (entry 6). Using these optimized conditions, the reaction was scaled up 20-fold, with provided isolated yields of 74%. Additionally, prior to purification, the excess nitrile used in the catalysis can be recovered by sublimation or Kugelrohr distillation in a practically quantitative amount (>98%). While it was observed that no starting material was present after the reaction under the optimized conditions, attempts to identify side-products in these reactions have not yielded conclusive results

Expanding on the initial substrate scope and the potential size of the PAHs, the synthesis of asymmetric phenyl-substituted biphenyldiyne **2b** was targeted. We initially

Table 5.1. Optimization of **1**-catalyzed coupling of **2a** with **3a**

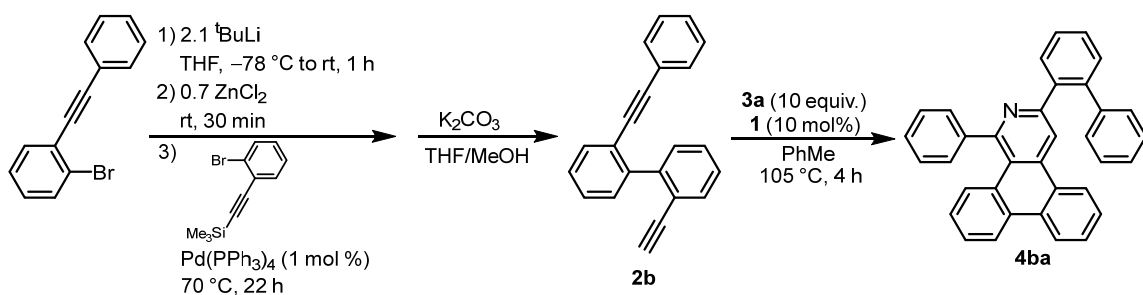


entry	^a 1 /mol %	nitrile (equiv.)	temperature/ °C	time/h	^b yield/ %
1	5	10	60	24	29
2	10	10	60	24	52
3	15	10	60	24	57
4	10	5	60	24	31
5	10	25	60	24	59
6	10	10	105	4	50

^aconditions: 4.9 μmol (**1**), 3 mL PhMe; ^bbased on ¹H NMR integration with 1,3,5-trimethoxybenzene standard

approached the synthesis of this compound via Sonogashira coupling of **2a** with iodobenzene. However, poor selectivity resulted in the formation of mixtures of starting, mono-coupled, and di-coupled diynes, which proved challenging to separate. Step-wise coupling of trimethylsilylacetylene followed by phenylacetylene (or in reverse) with 2-bromo-2'-iodobiphenyl led to a mixture of products including a significant amount of substituted phenanthrenes.²³ The successful synthesis of **2b** was realized via Negishi coupling of each half of the biphenyl motif followed by trimethylsilyl group deprotection (Scheme 5.3). Using similar conditions described before, **2b** can be catalytically coupled with **3a** to afford **4ba** in moderate yields (64%) (Scheme 5.3). The slight reduction in yield may be due to the sterically more challenging internal alkyne present in **2b**. In the previously reported pyrimidine synthesis, sterically comparable diphenylacetylene was not a competent substrate.¹⁹

Scheme 5.3. Synthesis of asymmetric biphenyldiyne **2b** and subsequent coupling with **3a**



Oxidative cyclodehydrogenation of **4aa** was initially probed with commonly employed Scholl reaction conditions.^{15, 24-26} Several reaction conditions tried, such as (i) $\text{FeCl}_3/\text{CH}_3\text{NO}_2/\text{CH}_2\text{Cl}_2$, (ii) $\text{AlCl}_3/\text{CuCl}_2/\text{CS}_2$, and (iii) $\text{CF}_3\text{SO}_3\text{H}/\text{DDQ}$ (2,3-Dichloro-5,6-dicyano-1,4-benzoquinone), did not result in significant reactivity with **4aa**. The Scholl reaction is suggested to take place via the generation of a proposed radical cation or arenium cation.²⁷⁻²⁸ The more electron-deficient nature of the pyridine motif and the absence of resonance-stabilizing groups may preclude the generation of such species. In contrast, it has been reported that pyridine and pyrimidine motifs can be reductively dimerized by the initial

generation of a radical anion in the presence of a reducing alkali metal, followed by subsequent oxidation to afford the neutral dimeric bipyridine or bipyrimidine species.²⁹⁻³¹ We postulated that this route may better activate the electron-deficient pyridine motif towards initial coupling with the neighboring arene moiety. If this route proves to be successful, it may offer an alternative strategy of cyclodehydrogenation of similar N-containing PAHs.

A variety of alkali metal-based reductants such as sodium, sodium-mercury amalgam, potassium and sodium-potassium alloy (NaK) were tested towards the reduction of **4aa**. Amongst those, it was found that only potassium or NaK was sufficiently reducing towards **4aa** resulting in an intense darkening minutes after addition of a THF solution of **4aa**. After stirring at room temperature for 48 hours, the deep purple-black suspension was quenched with isopropanol (iPrOH). Following oxidation via a variety of methods including bubbling air, bubbling O₂ and addition of DDQ, the presence of a copious amount of precipitate was observed. The precipitate was found to be insoluble in a variety of common NMR solvents, and what was observed in solution was only a trace amount of unreacted **4aa**. Recognizing that upon planarization, strong π - π stacking interactions between the cyclized molecules may result in poor solubility, we turned to target diynes **2c** and **2d** that contained solubilizing groups that would additionally mitigate these stacking effects, allowing the products to retain some solubility in organic solvents (Figure 5.1).³²

Tert-butyl substituted iodobromobenzene was synthesized via initial bromination of

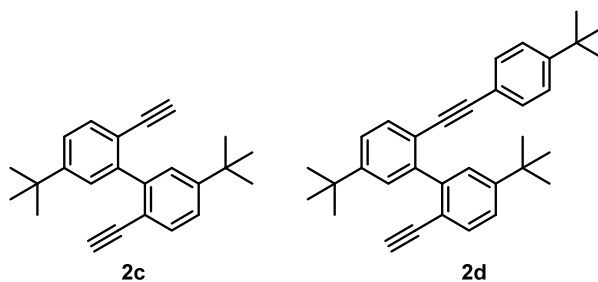
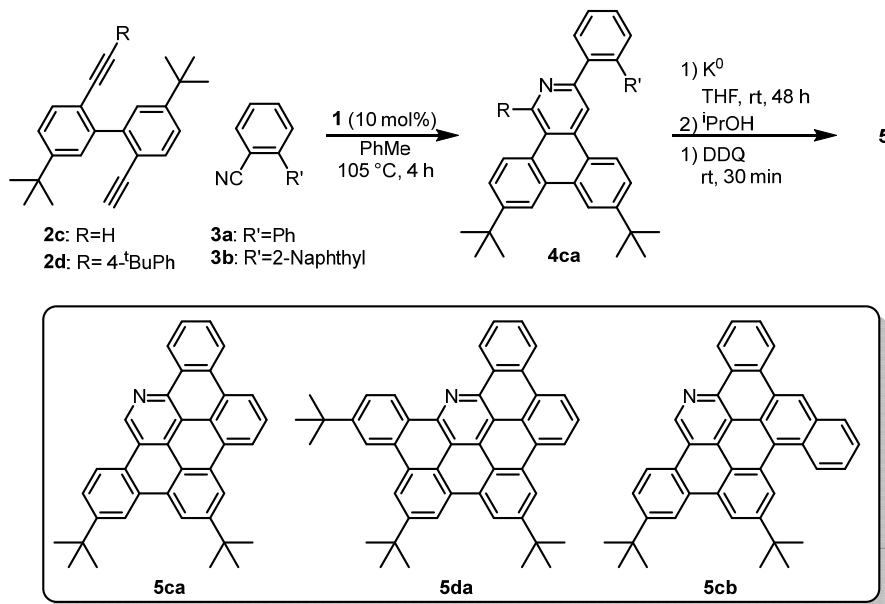


Figure 5.1. Biphenyldiynes **2c** and **2d** containing solubilizing groups.

4-*tert*-butylaniline followed by a Sandmeyer reaction to install the iodo group. Subsequently, symmetric diyne **2c** and asymmetric diyne **2d**, substituted with a 4-*tert*-butyl phenyl group, can

Scheme 5.4. Synthesis pyridine-containing N-doped nanographenes



be accessed via similar routes discussed previously.

Coupling of **2c** with **3a** under the optimized catalytic conditions provided pyridine **4ca** with similar yields (82%) (Scheme 5.4). Reduction of **4ca** with a K^0 mirror over 48 hours, followed by a protic quench with i PrOH and oxidation with DDQ provided a pale yellow solid after work up that was moderately soluble in $CDCl_3$. From the 1H NMR, the clean formation of a new species, **5ca**, was observed. Most of the resonances, both in the aromatic and aliphatic regions, are observed to shift downfield compared to **4ca** (Figure 5.2). The singlet that was could initially be assigned to the proton meta to the pyridine nitrogen is no longer present in **5ca**. Additionally, integrating the peaks observed in the aromatic region of **5ca**, 13 aromatic protons can be accounted for, consistent with the formation of two new aryl-aryl C–C bonds and loss of four protons compared to **4ca**.

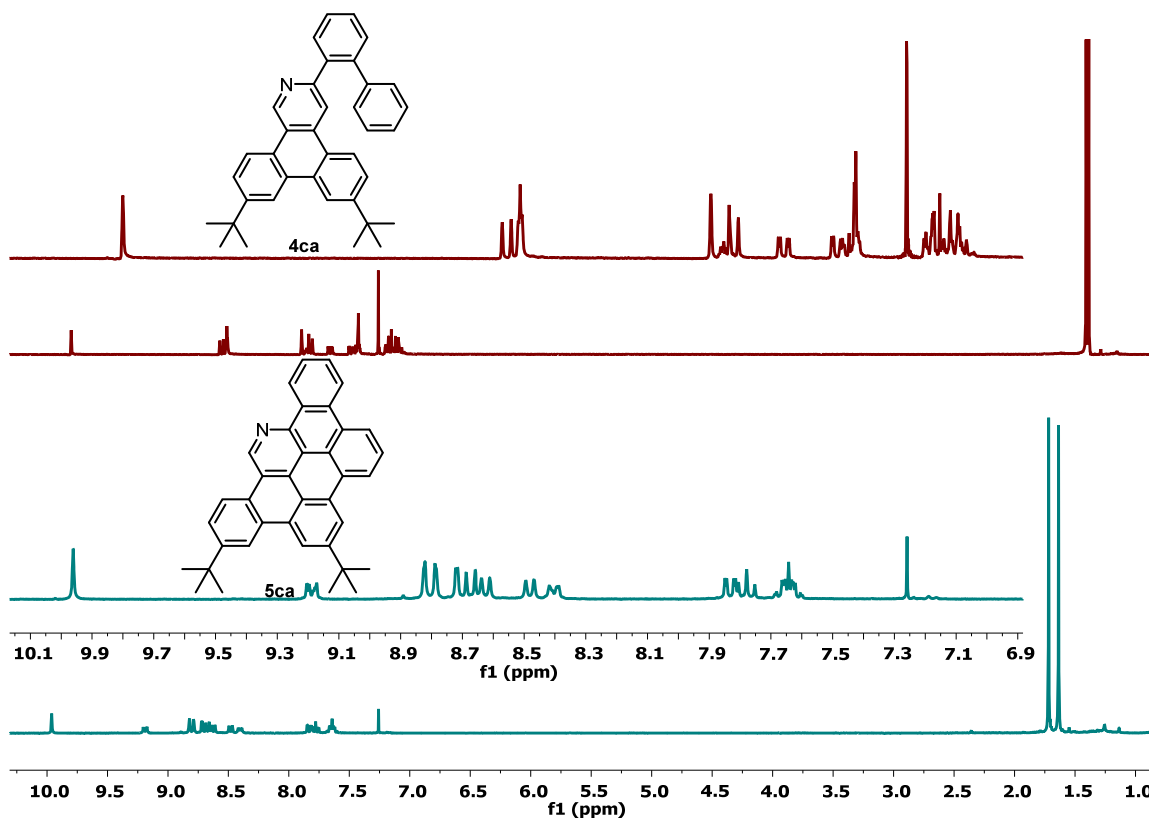


Figure 5.2. NMR spectra of **4ca** and **5ca**.

Recrystallization of **5ca** by slow evaporation of a saturated CHCl_3 solution provided crystals suitable for single crystal X-ray diffraction (XRD). The solid-state structure of **5ca** confirmed our initial assignment of **5ca** as planarized N-doped nanographene containing 30 π -electrons (Figure 5.3). From the side view, it is apparent that there is a slight curvature in the π -system, ranging from 8.0 - 10.3° between planes. Similar curvatures or twists have been observed in previously reported comparably-sized PAH systems³³⁻³⁵ When the unit cell is grown, π - π stacking is observed between molecules of **4ca** with the bulky *tert*-butyl groups on alternating ends of stacked units. The π - π stacking distance is approximately 3.33 \AA with the minimum interplane C-C distances at $3.463(3) \text{ \AA}$ which is in the range of that reported for graphite.³⁶ This method of reductive cyclodehydrogenation, to the best of our knowledge, is

the first example of its use towards the generation of N-doped nanographenes. It offers a powerful route, complementary to the more precedented oxidative cyclodehydrogenation,^{14,24,28} or solid surface routes,³⁷⁻³⁸ towards the challenging syntheses of these N-doped nanographenes.

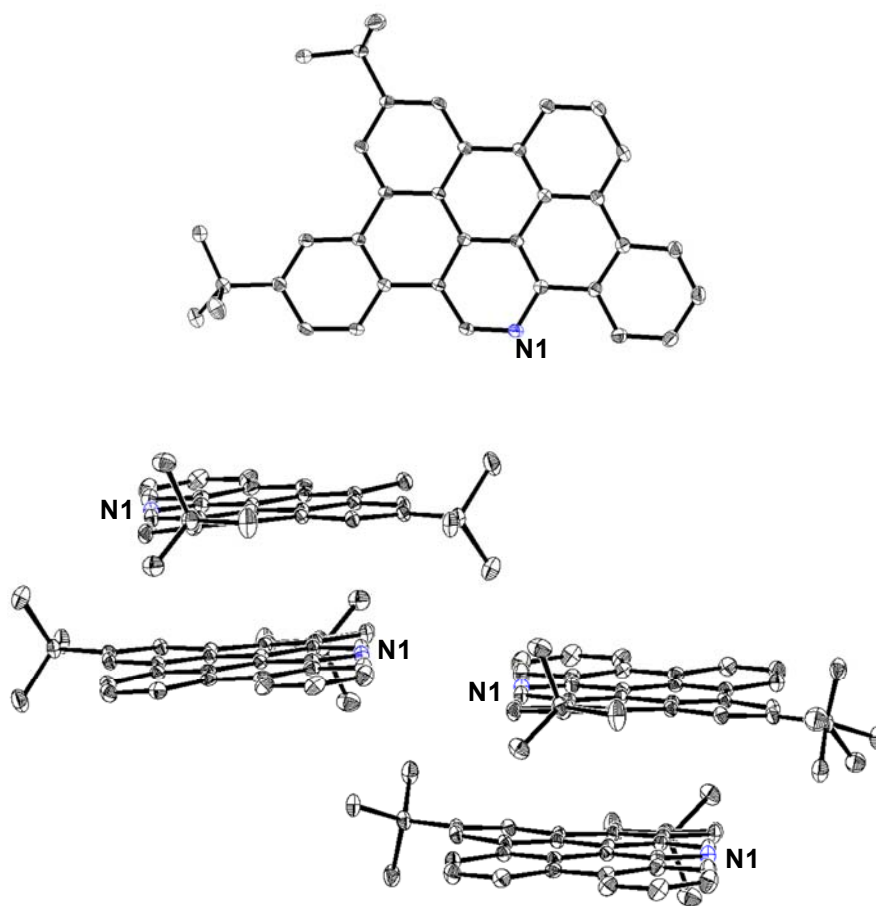


Figure 5.3. Solid-state structure of **5ca**. Top view of one of two molecules in asymmetric cell (top), side-on view showing stacking (bottom). Thermal ellipsoids shown at 50% probability. Nitrogen atoms shown in blue. Hydrogen atoms omitted for clarity.

Analogously, **4da**, with an additional phenyl substituent, can be accessed by **1**-catalyzed coupling of the asymmetric diyne **2d** with nitrile **3a** in moderate yields (56%) (Scheme 5.4). Reduction of **4da** with potassium for 48 hours followed by a protic quench with ^tPrOH and

oxidation with DDQ provided a new yellow species, **5da**, after workup. From the ^1H NMR, similar downfield shifts were observed compared to **4da** along with the loss of the singlet that was assigned to the proton on the pyridine ring. Solid-state studies on crystals grown from a saturated chloroform solution of **5da** confirmed the successful cyclodehydrogenation and planarization of **4da** to give an N-doped PAH containing 36 π -electrons (Figure 5.4). From the side-on view, very slight curvature is observed, and as with **5ca**, the bulky *tert*-butyl groups are oriented towards opposite ends between the stacked layers. The minimum C–C contact between layers is 3.507(5) Å with interlayer distances of about 3.39 Å, both slightly elongated

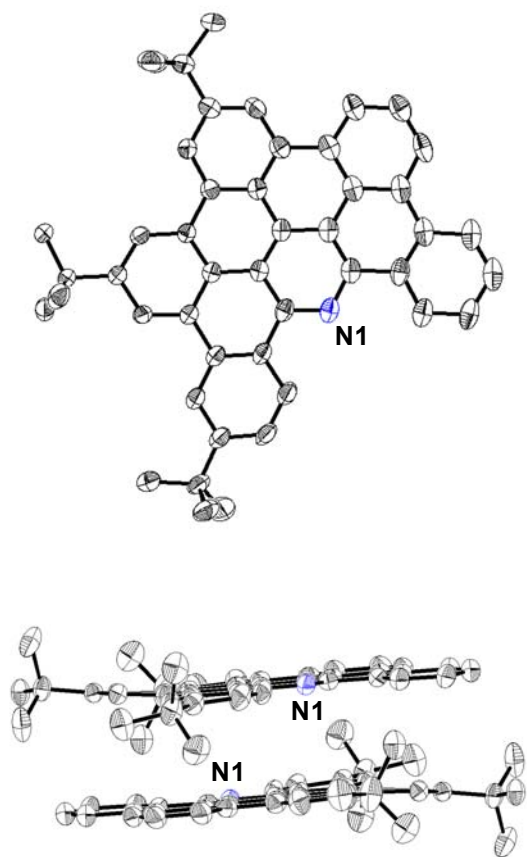


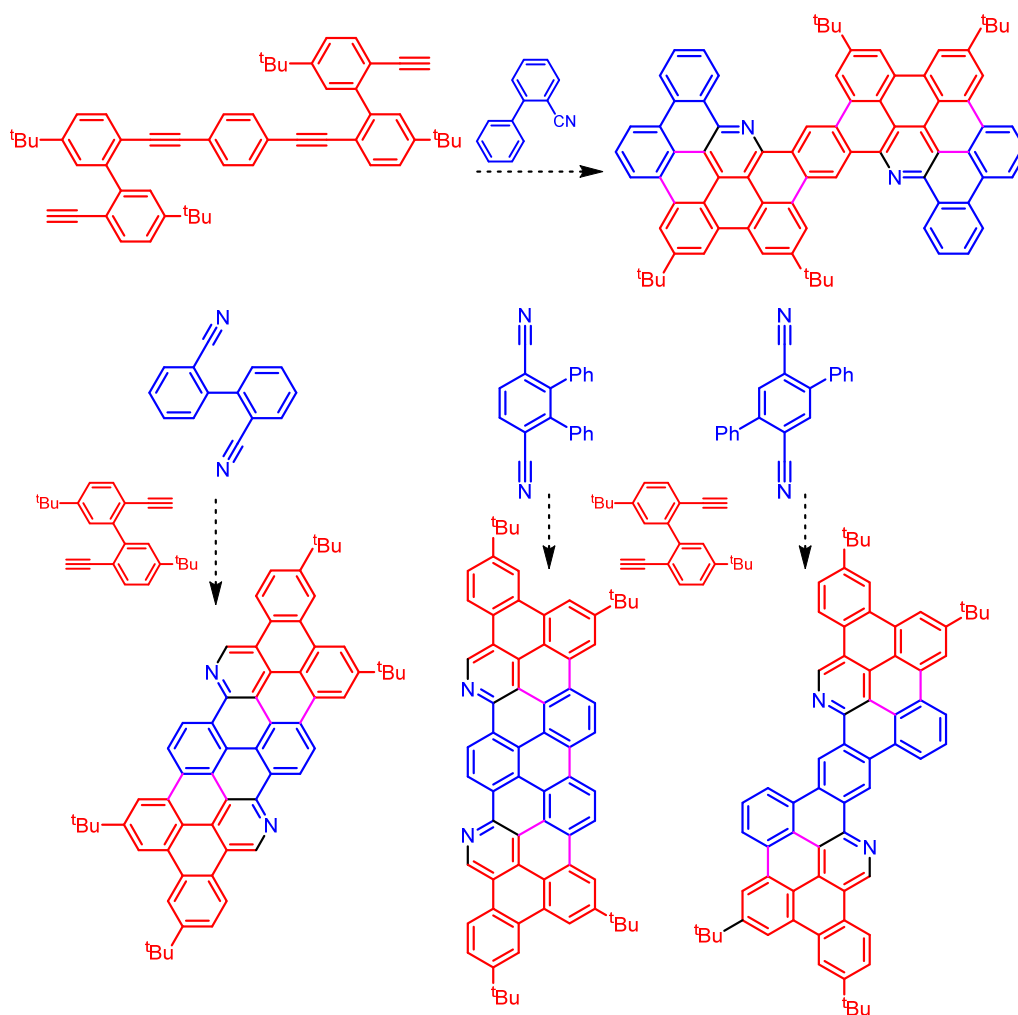
Figure 5.4. Solid-state structure of **5da**. Top view of one of two molecules in asymmetric cell (top), side-on view showing stacking (bottom). Thermal ellipsoids shown at 50% probability. Nitrogen atoms shown in blue. Hydrogen atoms omitted for clarity.

compared to **5ca**. In addition to **5ca** and **5da**, the evidence for the synthesis of naphthyl-substituted **4cb** and subsequent cyclodehydrogenation to **5cb** has also been obtained from ^1H NMR spectroscopy and recrystallization attempts are ongoing towards obtaining solid-state characterization for **5cb** (Scheme 5.4).

1.2 Dipyridine synthesis with dinitriles and tetraynes

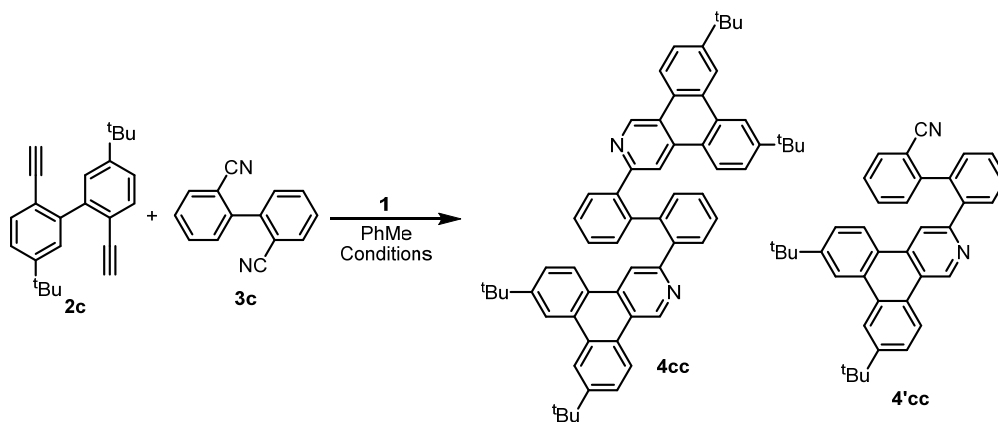
With the methodology suitable for the synthesis of a variety of pyridine containing nanographenes, the rapid expansion of the potential size of their π -systems was sought out

Scheme 5.5. Proposed synthesis of dipyridine-containing nanographenes. Atoms originating from alkyne and nitrile are colored red and blue, respectively. Bonds formed on oxidative cyclodehydrogenation are colored pink.



through the targeted synthesis of their “dimeric” variants. We envisioned that by employing dinitriles and tetraynes, larger, multi N-doped nanographenes may be accessed using this methodology (Scheme 5.5). Tetrayne **2e** can be obtained, following deprotection, through Negishi coupling of trimethylsilyl-protected 2-bromo-4-*tert*-butylphenylacetylene with phenylene-bridged diyne 1,4-bis((2-bromo-4-(*tert*-butyl)phenyl)ethynyl)benzene. The latter is readily synthesized by Sonogashira coupling between 2-bromo-4-*tert*-butyliodobenzene and 1,4-diethynylbenzene. Under the standard catalytic conditions with **3a**, ^1H NMR of the product is consistent with the formation of *bis*(pyridine) **4ea**. The presence of broad NMR feature suggests a potential fluxional process that arises from hindered bond rotation. Work in the reductive cyclization of **4ea** is currently ongoing.

Table 5.2. Optimization of catalytic conditions for **2c** with 2,2'-dicyanobiphenyl



entry	^a 1 /mol %	nitrile (equiv.)	temperature/ °C	time/h	^a ratio of 4cc : 4'cc : 2c
1	10	5	105	4	1 : 6.8 : 25
2	50	0.6	105	8	1 : nd : 0.1
3 ^c	10	0.6	105	8	1 : 0.6 : 2.3
4	10	0.6	140 ^d	8	1 : 0.8 : 5.1
5	40	0.6	105	8	1 : 0.04 : 0.1
6	30	0.6	105	8	1 : 0.1 : 0.2

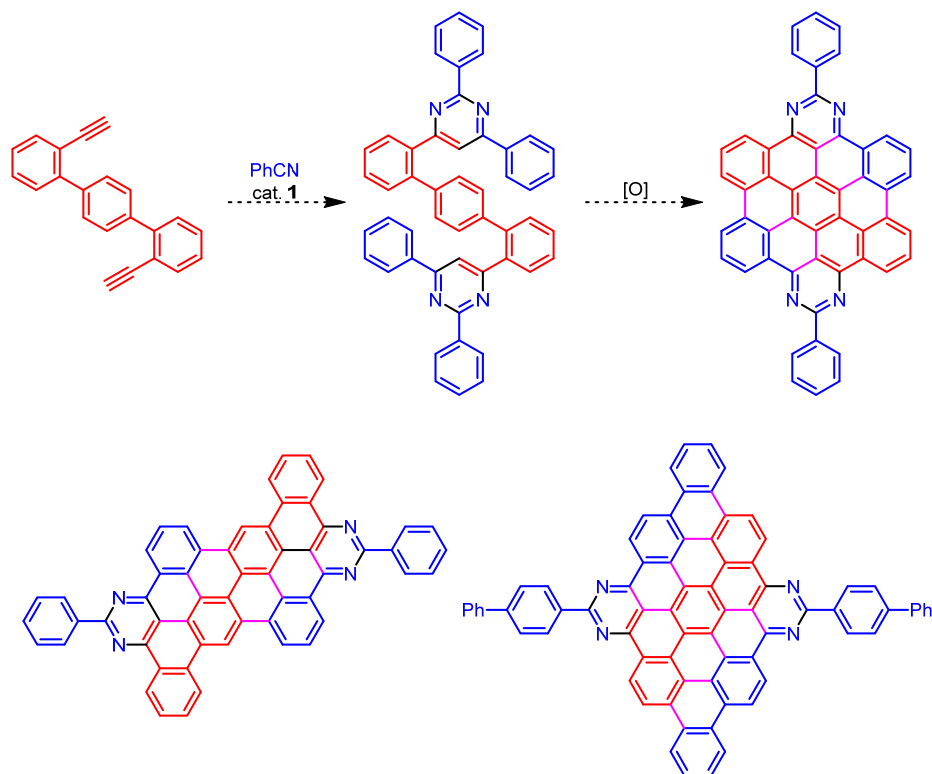
^aconditions: 4.9 μmol (**1**), 3 mL PhMe; ^bbased on ^1H NMR integration; ^cran at 30-fold concentration; ^dran in *m*-xylenes; nd: not detected.

The use of dinitriles as substrates will hypothetically allow for the generation of more expansive PAHs. However, unlike tetrayne substrates, dinitrile substrates pose a problem under the standard catalytic conditions, which requires a 10-fold excess of nitrile. The reaction of **2c** with 2,2'-biphenyldicarbonitrile (**3c**) under these conditions resulted in the predominant formation of the monopyridine product **4'cc** (Table 5.2, entry 1). Several conditions were explored in order to circumvent the need for excess nitrile. With 0.6 equiv. dinitrile (1.2 equiv. nitrile group per diyne), it was found that increasing the catalyst loading to 50 mol% led to exclusive formation of **4cc**, while either increasing the concentration of the reaction or running the reaction at higher temperatures led to moderately improved selectivity towards **4cc** over **4'cc** but displayed poor conversions. Reducing the catalyst loading to 40% and 30% showed marginal losses in selectivity, yielding approximately 4% and 10% of **4'cc**, respectively. Eventually, a 35% catalyst loading was chosen as our optimized conditions for catalytic dipyrindine synthesis from dinitriles. Notably, under all these conditions, there was no evidence for the intramolecular coupling of the dinitrile to yield a diazazirconacyclopentadiene intermediate and subsequently a pyrazine ring upon alkyne coupling. Such transformations have been reported in other “reduced” early metal complexes.¹⁶ Reductive cyclization of **4cc** is currently underway. Additionally, the syntheses of dicyanobenzenes **3d** and **3e** are also currently being targeted.

2. *Synthesis of Pyrimidine-containing PAHs*

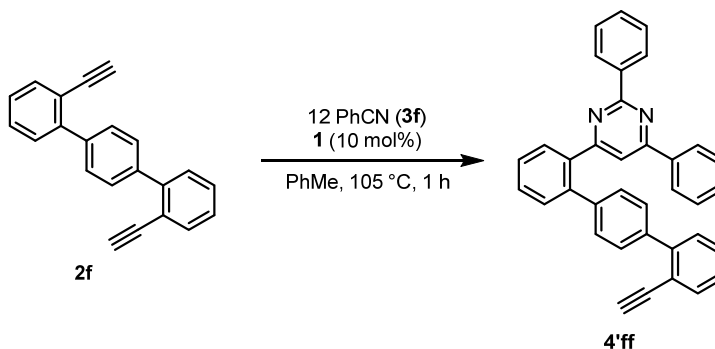
In addition to pyridine-containing PAHs, we wanted to leverage the powerful methodology previously developed for the synthesis of pyrimidines by the [2+2+2] cotrimerization of two nitriles with an alkyne to synthesize pyrimidine-containing PAHs.¹⁹ We envisioned that catalytic cotrimerization of terphenyldiyne **2f** with benzonitrile, **3f**, will generate dipyrindine PAH **4ff**, which upon oxidative cyclodehydrogenation will yield 4N-

Scheme 5.6. Proposed synthesis of dipyrimidine-containing nanographenes. Atoms originating from alkyne and nitrile are colored red and blue, respectively. Bonds formed on oxidative cyclodehydrogenation are colored pink.



doped nanographene **5ff** (Scheme 5.6). Larger variants may be accessed by extension of the substrates, for example using tetraphenyldiyne and 4-phenyl benzonitrile.

2f can be synthesized via Suzuki coupling of phenylene-1,4-diboronic acid with trimethylsilyl-protected 2-bromophenylacetylene followed by base-mediated deprotection. Using the optimized conditions for pyrimidine synthesis, the reaction of **2f** with a 12-fold excess of **3f** at 105 °C for one hour provided a new species along with some starting material. Longer reaction times did not significantly improve conversion. Further analysis of this species by ^1H NMR spectroscopy showed the presence of a resonance at 2.72 ppm, consistent with an alkynyl proton, but distinct from **2f**. Furthermore, integration of the aromatic region

Scheme 5.7. Formation of **4'ff** under standard catalytic conditions

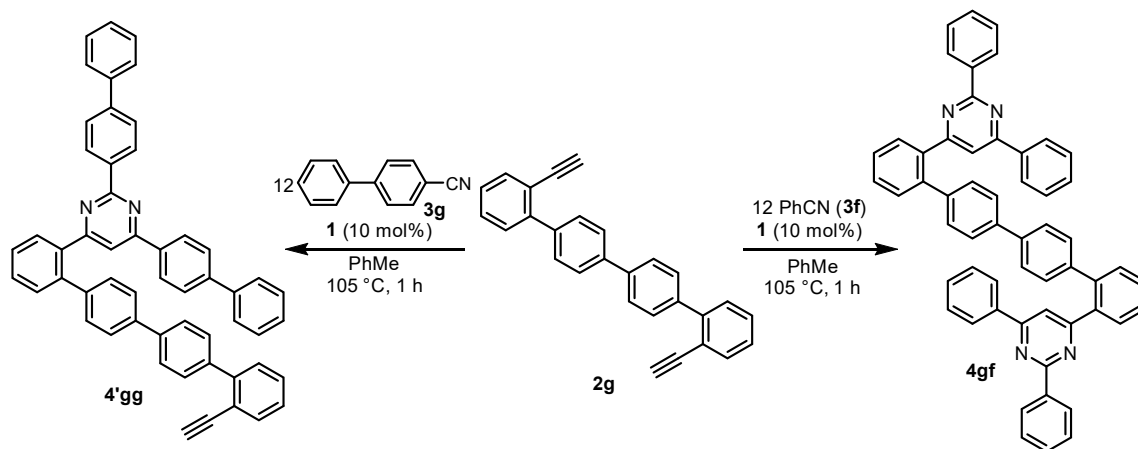
supported the presence of 22 aromatic protons. Both observations provide evidence for the assignment of this species as **4'ff**, a monopyrimidine formed from the cyclization of one of the alkyne arms of **2f** with two equivalents of **3f** (Scheme 5.7).

The lack of formation of the dipyrimidine product **4ff** could be due to a few reasons. **4'ff** may be sparingly soluble under the reaction conditions impeding the second cotrimerization. Alternatively, the dipyrimidine product **4ff** may be insoluble in the NMR solvent, preventing observation in the solution state. Another potential reason for the absence of **4ff** is due to steric reasons. Taking a closer look at the solid-state structure of previously reported azazirconacyclopentadiene (see chapter 4, Figure 4.6),¹⁹ a key intermediate for the synthesis of pyridines in this system, the phenyl ring that originated from the alkyne lies perpendicularly to zirconacyclopentadiene ring, likely to minimize steric repulsion with the adjacent alkenyl proton (on C58) and neighboring THF ligand. It is likely that upon the formation of **4'ff**, the second alkyne becomes sterically inaccessible to the zirconium center due to the steric pressure exerted by the newly formed proximal triarylpyrimidine motif.

We postulated that the use of tetraphenyl diyne **2g** should alleviate the steric issue by situating the bulky group further away from the catalytic site. **2g** was synthesized in an analogous fashion as **2f** starting from [1,1'-biphenyl]-4,4'-diyl diboronic acid. Gratifyingly, the reaction of **2g** and **3f** with 10 mol% **1** in toluene at 105 °C for four hours led to the clean

Scheme 5.8. Reaction of **2e** with **3f** or **3g** under standard catalytic conditions

formation of desired dipyrimidine product **4gf** in moderate yields (61%) (Scheme 5.8). This



observation, along with the generation of exclusively monopyrimidine product **4'gg** when 4-phenyl benzonitrile **3g** was used, supports the steric argument for the product distributions in these systems.

A variety of Scholl reaction conditions ($\text{FeCl}_3/\text{CH}_3\text{NO}_2/\text{CH}_2\text{Cl}_2$, $\text{AlCl}_3/\text{CuCl}_2/\text{CS}_2$, and $\text{CF}_3\text{SO}_3\text{H}/\text{DDQ}$) were tested to oxidatively cyclodehydrogenate **4gf**. However, intractable mixtures after workup were obtained. From the reaction with $\text{CF}_3\text{SO}_3\text{H}/\text{DDQ}$, a diprotonated **4gf** (based off of charge balance with triflates), co-crystallized with two DDQ molecules, was

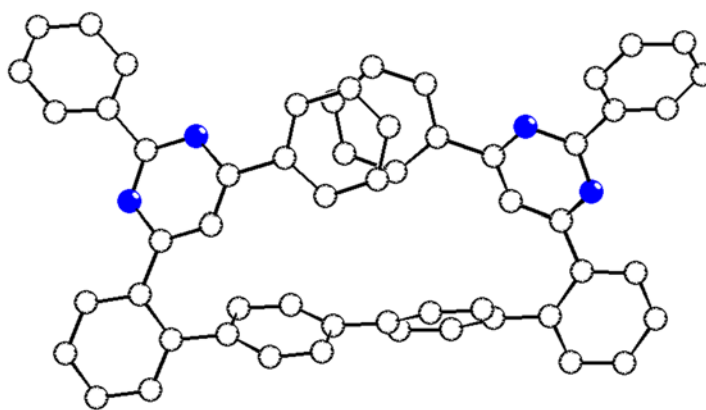


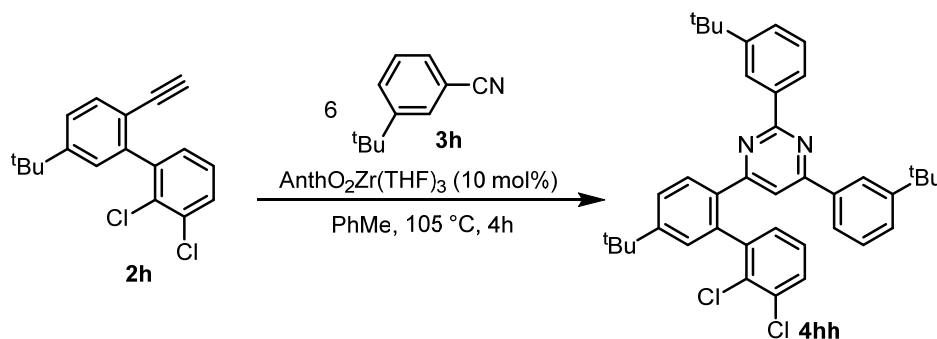
Figure 5.5. Preliminary solid-state structure of $[\mathbf{4gf-(H)_2}]^{2+}$. Nitrogen atoms shown in blue. Hydrogen atoms, counter anions, solvent, and cocrystallized DDQ omitted for clarity.

obtained, providing an approximate structure of **4gf** in the solid state (Figure 5.5).

In order to minimize the likelihood of forming sparingly soluble nanographene after cyclodehydrogenation, synthesis of 3-*tert*-butyl benzonitrile (**3h**) was targeted. With the bulkier nitrile, doubling the catalyst loading to 20% was necessary for complete conversion of starting materials, providing dipyrimidine, **4gh**, in yields of 60%. Unfortunately, under the same Scholl oxidative conditions, no reaction was observed. Likewise, under similar reductive cyclization conditions (K^0 or NaK followed by protic quench and reoxidation with DDQ) employed for pyridine polyaromatics in the previous section, no significant reactivity was observed with **4gh**.

The palladium-catalyzed intramolecular coupling of aryl chlorides with arenes has been reported for the synthesis of an azacorannulene and curved N-containing “Buckybowls”.³⁹⁻⁴⁰ In order to examine if such a method would be effective for our system, the use of a nitrile or an alkyne substrate with strategically-placed chlorides was targeted. Attempted catalytic cotrimerization of **2g** with 2,3-dichlorobenzonitrile **3i** did not lead to any pyrimidine formation under the standard conditions. This may be due to potential poisoning of the catalyst by the large excess, 120 equiv. vs. catalyst, of halogenated nitrile present. Instead, placement of chlorides on the alkyne coupling partner, used in a smaller excess, was targeted. Dichloro-substituted alkyne **2h** was synthesized and used in the catalytic coupling with **3h** to afford pyrimidine **4hh** in good yields (72%) (Scheme 5.9).

Scheme 5.9. Catalytic synthesis of **4hh**



Using the Pd-catalyzed cyclization conditions reported previously with **4hh**, however, resulted in an intractable mixture by ^1H NMR spectroscopy. It was hypothesized that subjecting **4hh** to reductive conditions in the presence of an alkali metal may allow for the reduction of the dichlorophenyl group that may then couple productively with the adjacent rings. Addition of **4hh** as a thawing THF solution to potassium and allowing to stir for 48 hours before quenching with $^i\text{PrOH}$ and oxidizing with DDQ provided a new major species **5hh** as a crude mixture. This species also formed as a minor product in the Pd reaction. Purification by silica gel chromatography allowed for the isolation of this species. From the ^1H NMR (Figure 5.6), a significant downfield shift of all the peaks with respect to **4hh** was observed. Similar shifts have been observed in the pyridine-containing nanographenes discussed previously. Additionally, if hydrodehalogenation had simply occurred, it would be expected that the NMR spectrum to have similar chemical shifts that of **4gh**, a rough approximation of a “dimer” of **4hh**. However, both species show significantly different resonances in both the aromatic and the aliphatic regions (Figure 5.6).

As the solid-state characterization of this species had initially eluded us, we turned to other techniques commonly employed for characterization of these nanographene products. From the ^1H NMR spectrum, integration of the aromatic region also revealed the presence of 13 aromatic protons. Additionally, using Distortionless Enhancement by Polarization

Scheme 5.10. Reductive cyclization of **4hh**

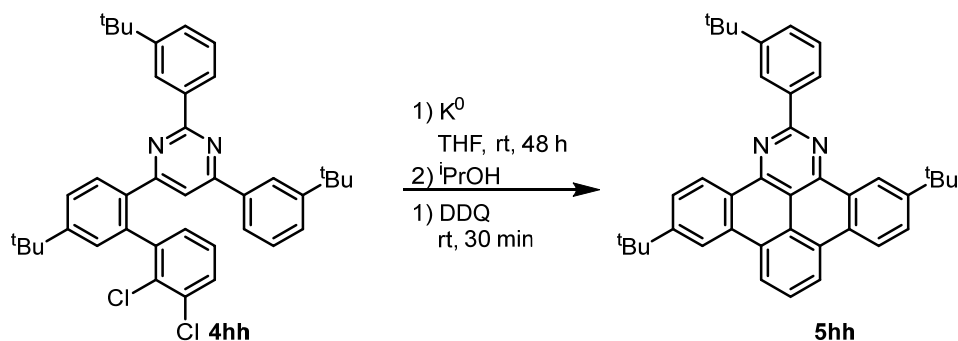
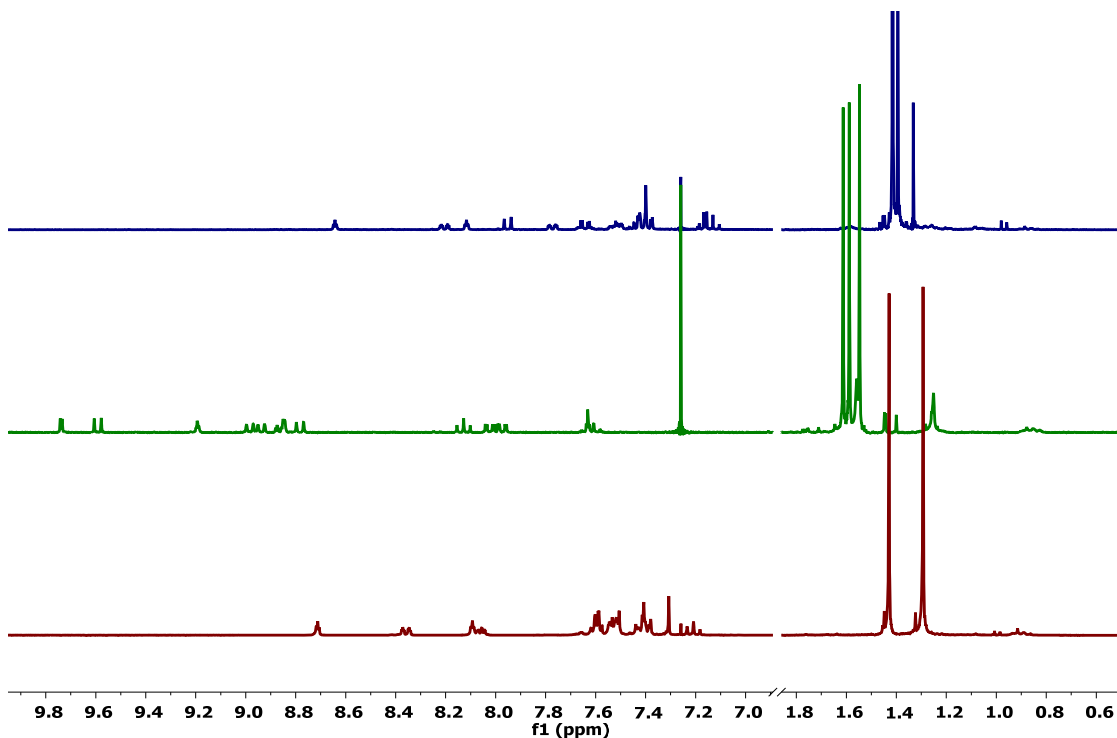


Figure 5.6. ^1H NMR spectra of **4hh** (blue), **5hh** (green), and **4gh** (red).



Transfer (DEPT) NMR pulse sequence which suppresses quaternary carbons, the presence of 13 aromatic C–H carbons is confirmed. With fast atom bombardment mass spectrometry, the presence of a species with a parent peak of m/z 549.3289 was also detected. All these observations are consistent with successful cyclization to provide the desired pyrimidine-containing nanographene **5hh** (Scheme 5.10). A preliminary solid-state structure was obtained (Figure 5.7), as due to the nature of the crystal growth, sufficiently large crystals could not be obtained to provide full structural characterization. The mechanism of this ring closing is unlikely to be the same as that observed with the pyridine-containing PAHs. Instead, the potential generation of a benzyne intermediate in the presence of the reducing potassium followed by intramolecular [2+4] cycloaddition may have taken place.⁴¹⁻⁴² Following oxidative dehydrogenation, **5hh** is afforded. With definitive evidence for the successful cyclization, ongoing efforts are currently underway to synthesize the halogenation variant of **2g** in order

to target the synthesis of *bis*(pyrimidine)-containing nanographenes.

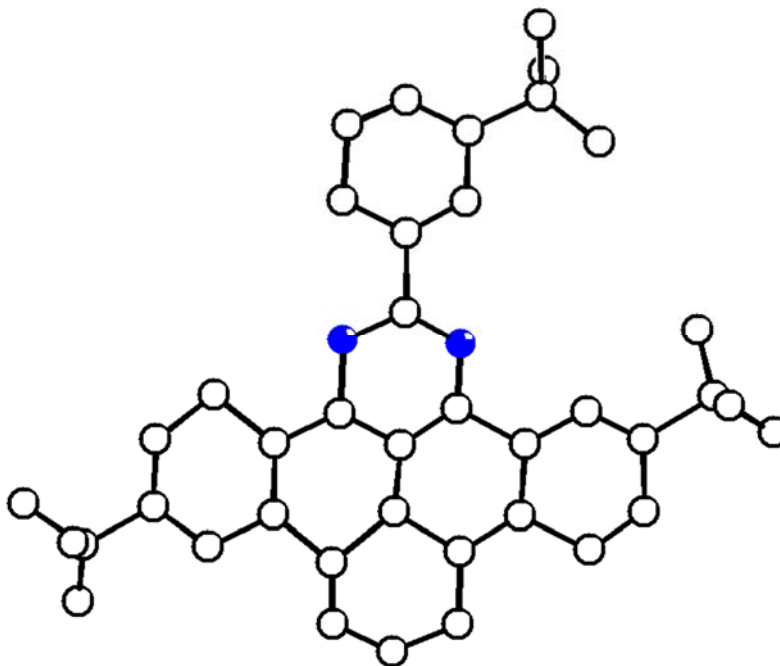


Figure 5.7. Preliminary solid-state structure of **5hh**. Nitrogen atoms shown in blue. Hydrogen atoms omitted for clarity.

CONCLUSION

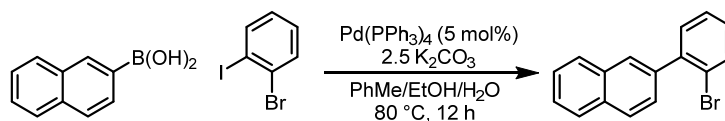
The catalytic synthesis of a variety of nitrogen-containing PAHs featuring pyridine or pyrimidine motifs using a zirconium complex supported by a non-innocent anthracenediyl motif has been demonstrated. This methodology allows for the rapid and divergent synthesis of a variety of PAHs by the coupling of either symmetric or asymmetric biphenyldiynes with a range of aryl nitriles. Additionally, further expanded PAHs can be afforded using dinitriles and tetraynes, effectively building “dimeric” variants of the initially synthesized PAHs. Additionally, we have developed a new methodology towards the dehydrocyclization of pyridine-containing PAHs to planar N-doped nanographenes under reductive conditions in the presence of K^0 . Following a protic quench and reoxidation by DDQ, N-doped nanographene products can be obtained in excellent yields. This new method offers an alternative, complementary route to the more common oxidative cyclodehydrogenation routes reported previously. For pyrimidine-containing PAHs that cannot be initially dehydrogenated via this route, the strategic installation of chloride groups at key ring-closing junctions allowed for successful cyclization under the same conditions. Ongoing work is currently focused on further expanding the scope of N-doped nanographenes that can be synthesized and studying their optical properties.

EXPERIMENTAL SECTION

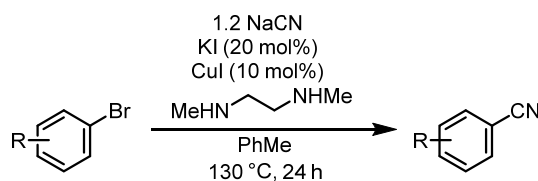
General Considerations

Unless otherwise specified, all operations involving air- or water-sensitive reagents were carried out in an MBraun drybox under a nitrogen atmosphere or using standard Schlenk and vacuum line techniques. Solvents for air- and moisture-sensitive reactions were dried by the method of Grubbs.⁴³ Deuterated solvents were purchased from Cambridge Isotope Laboratories and C₆D₆ vacuum transferred from sodium benzophenone ketyl before use. All solvents, once dried and degassed, were stored under a nitrogen atmosphere over 4 Å molecular sieves. 2-phenyl benzonitrile (**3a**),⁴⁴ 2,2'-bis(ethynyl)-1,1'-biphenyl (**2a**),⁴⁵ **1**,¹⁹ ((2-bromophenyl)ethynyl)trimethylsilane,⁴⁵ were prepared according to literature procedures. Pre-reduced Teflon-coated stir bars (prepared via stirring a Na[C₁₀H₈] solution overnight followed by rinsing three times with THF) were utilized in any stirred reaction in which K⁰ or NaK were employed as reagents. Alkynes and nitriles purchased were either sublimed under reduced pressure or distilled from calcium hydride before use as substrates for cotrimerization. Triethylamine was degassed and distilled from calcium hydride before use. All other reagents were used as received. ¹H, ¹³C{¹H}, and ¹⁹F NMR spectra were recorded on Varian Mercury 300 MHz or Varian 400 MHz spectrometers at ambient temperatures unless otherwise denoted. ¹H and ¹³C{¹H} NMR spectra are reported referenced internally to residual solvent peaks reported relative to tetramethylsilane. Fast atom bombardment-mass spectrometry (FAB-MS) analyses were performed with a JEOL JMS-600H high-resolution mass spectrometer.

Experimental



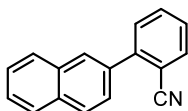
1-bromo-2-(2-naphthyl)benzene.⁴⁶ A Schlenk tube fitted with a screw-in Teflon stopper was charged with 2-bromoiodobenzene (3.0 mL g, 23.4 mmol), 2-naphthylboronic acid (4.02 g, 23.4 mmol) and anhydrous potassium carbonate (8.07 g, 58.4 mmol) suspended in a mixture of toluene (210 mL), ethanol (60 mL) and water (60 mL). The suspension was degassed via three freeze-pump-thaw cycles, after which *tetrakis*(triphenylphosphine) palladium(0) (1.35 g, 1.17 mmol) was added under a counter flow of nitrogen. The flask was sealed and heated to 70 °C for 8 h with stirring. After cooling to room temperature, water (100 mL) was added and the organic layer separated. The aqueous layer was extracted with CH₂Cl₂ (2 × 100 mL). The organic extracts were combined and dried over MgSO₄, filtered, and concentrated in vacuo. The crude yellow oil was purified via silica gel column chromatography (eluent: hexanes) yield the product as a white solid (6.03 g, 91 %). ¹H NMR (300 MHz, CDCl₃): δ 7.93 – 7.84 (m, 4H), 7.74 – 7.69 (m, 1H), 7.57 (dd, *J* = 8.5, 1.8 Hz, 1H), 7.55 – 7.48 (m, 2H), 7.45 – 7.36 (m, 2H), 7.28 – 7.21 (m, 1H).



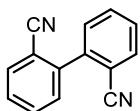
General procedure for the synthesis of aryl nitriles from aryl bromides.

Adapted from a previously reported procedure.⁴⁴ In a Schlenk flask fitted with a screw-in Teflon stopper was charged with NaCN (1.2 equiv.), KI (20 mol%) and CuI (10 mol%). The flask was then evacuated and refilled with nitrogen three times before dry, degassed toluene (to give a 1.3 M solution of aryl bromide) was added. *N,N*-dimethylethylenediamine (1 equiv.) followed by aryl bromide (1 equiv.) was then add. The flask was sealed and heated to 130 °C

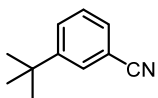
and stirred for 24 h. After the reaction was complete, it was allowed to cool to room temperature and 30% NH_4OH added. The mixture was then extracted with ethyl acetate, dried over MgSO_4 , filter and concentrated in vacuo to yield the desired nitrile after purification by silica gel column chromatography. Cyanide containing waste can be decontaminated using a solution of NaOCl in water (CLOROX bleach). See: Lunn, G.; Sansone, E. B. *Destruction of Hazardous Chemicals in the Laboratory*, 2nd ed., Wiley & Sons: New York, 1994; pp 133-138.



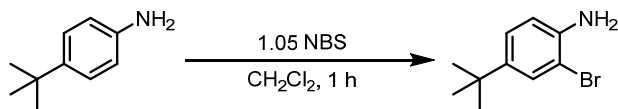
2-(naphthalen-2-yl)benzonitrile (3b).⁴⁷ Purified by silica gel column chromatography (eluent: hexanes \rightarrow 10% EtOAc in hexanes) then sublimed in vacuo. Colorless solid (1.01 g, 84%). ^1H NMR (300 MHz, CDCl_3): δ 8.05 (d, $J = 1.1$ Hz, 1H, *ArH*), 7.98 (d, $J = 8.5$ Hz, 1H, *ArH*), 7.96 – 7.87 (m, 2H, *ArH*), 7.81 (dtd, $J = 7.7, 1.2, 0.5$ Hz, 1H, *ArH*), 7.73 – 7.60 (m, 3H, *ArH*), 7.59 – 7.52 (m, 2H, *ArH*), 7.47 (dddd, $J = 7.8, 7.1, 1.6, 0.9$ Hz, 1H, *ArH*).



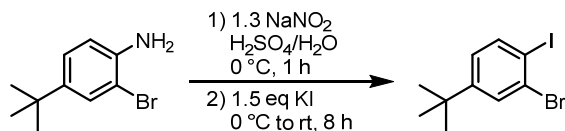
1,1'-biphenyl-2,2'-dicarbonitrile.⁴⁸ Recrystallized from hot EtOAc. Pale brown needles (0.96 g, 80%). ^1H NMR (300 MHz, CDCl_3): δ 7.86 – 7.82 (m, 2H), 7.73 (ddd, $J = 7.9, 7.4, 1.4$ Hz, 2H), 7.61 – 7.54 (m, 4H).



3-tert-butylbenzonitrile (3h).⁴⁹ Purified by silica gel column chromatography (3% EtOAc:hexanes). Colorless oil (6.43g, 86%). ^1H NMR (300 MHz, CDCl_3): δ 7.66 (ddd, $J = 2.1, 1.5, 0.7$ Hz, 1H, *ArH*), 7.62 (ddd, $J = 7.8, 2.0, 1.4$ Hz, 1H, *ArH*), 7.47 (dt, $J = 7.6, 1.5$ Hz, 1H, *ArH*), 7.39 (td, $J = 7.7, 0.7$ Hz, 1H, *ArH*), 1.32 (s, 9H, CH_3).

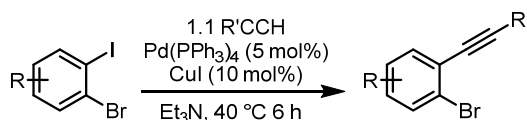


2-Bromo-4-*tert*-butylaniline. Modified from a previous procedure.⁵⁰ To a solution of 4-*tert*-butylaniline (20.0 g, 134 mmol) in CH₂Cl₂ (600 mL) was added *N*-bromosuccinimide (25.2 g, 142 mmol) in portions over 15 minutes. The reaction was allowed to stir at room temperature for 1 h and then the volatiles were removed in vacuo. The crude oily suspension was passed through a silica gel plug and eluted with hexanes. Concentration of the eluent provided 2-bromo-4-*tert*-butylaniline as a pale pink oil (27.7 g, 91%). ¹H NMR (300 MHz, CDCl₃): δ 7.41 (d, *J* = 2.2 Hz, 1H, ArH), 7.14 (dd, *J* = 8.3, 2.2 Hz, 1H, ArH), 6.73 (d, *J* = 8.3 Hz, 1H, ArH), 3.94 (br s, 2H, NH₂), 1.27 (s, 9H, CH₃).



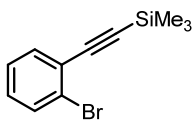
2-Bromo-4-*tert*-butyl iodobenzene. Modified from a previous procedure.⁵¹ 2-Bromo-4-*tert*-butylaniline (27.0 g, 118 mmol) was taken up in a mixture of H₂O (500 mL) and concentrated aqueous H₂SO₄ (60 mL) and cooled to 0 °C. A solution of sodium nitrite (10.6 g, 154 mmol) in H₂O (20 mL) was added dropwise to the reaction at 0 °C. After stirring for an hour at 0 °C, a solution of potassium iodide (29.5 g, 177 mmol) in H₂O was then added slowly at 0 °C (caution: effervescence). After complete addition, the reaction was allowed to warm to room temperature and stirred overnight. Saturated aqueous sodium metabisulfite was added till no addition decolorization was observed and stirred for 20 minutes. The reaction was then extracted with EtOAc (3 × 150 mL) and the combined extracted washed with H₂O (300 mL), dried over MgSO₄, filtered, and concentrated in vacuo to yield a dark brown oil. Purification via silica gel column chromatography (eluent: hexanes) to provide 2-bromo-4-*tert*-butyl iodobenzene as a colorless oil (31.1 g, 78%). ¹H NMR (300 MHz, CDCl₃): δ 7.75 (d, *J* =

8.3 Hz, 1H, *ArH*), 7.62 (d, $J = 2.3$ Hz, 1H, *ArH*), 7.02 (dd, $J = 8.4, 2.3$ Hz, 1H, *ArH*), 1.28 (s, 9H, CH₃).

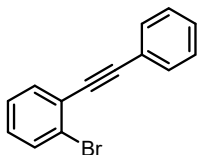


General conditions for Sonogashira coupling

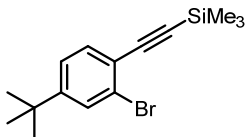
Modified from a previous procedure.⁵² To a Schlenk flask fitted with a screw-in Teflon stopper was added a solution of aryl iodide (1.0 equiv.) in 1:1 mixture of Et₃N and THF (0.8 M), *tetrakis*(triphenylphosphine) palladium(0) (5 mol%), and copper(I) iodide (10 mol%). Terminal alkyne (1.1 equiv.) was then introduced via syringe through a septum under N₂ or added as a solid under N₂ counter flow. The reaction was sealed and warmed to 40 °C for 6 to 12 h. After cooling to room temperature the reaction was filtered through a pad of silica gel and eluted with EtOAc. The eluent was concentrated in vacuo and the crude product purified via silica gel column chromatography.



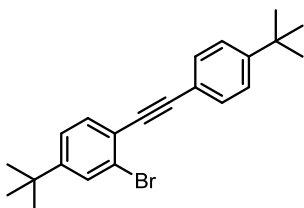
((2-bromophenyl)ethynyl)trimethylsilane.⁵³ Purified via silica gel column chromatography (eluent: hexanes) to provide 1-bromo-2-(phenylethynyl)benzene as a colorless oil (2.46 g, quant.). ¹H NMR (300 MHz, CDCl₃): 7.57 (dd, $J = 7.9, 1.3$ Hz, 1H, *ArH*), 7.49 (dd, $J = 7.6, 1.8$ Hz, 1H, *ArH*), 7.24 (td, $J = 7.6, 1.3$ Hz, 1H, *ArH*), 7.15 (td, $J = 7.6, 1.8$ Hz, 1H, *ArH*), 0.27 (s, 9H, CH₃).



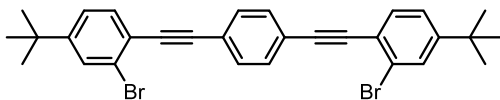
1-bromo-2-(phenylethynyl)benzene.⁵⁴ Purified via silica gel column chromatography (eluent: hexanes) to provide 1-bromo-2-(phenylethynyl)benzene as a colorless oil (2.38 g, 95%). ¹H NMR (300 MHz, CDCl₃): 7.64 – 7.54 (m, 4H, ArH), 7.40 – 7.34 (m, 3H, ArH), 7.30 (td, *J* = 7.6, 1.3 Hz, 1H, ArH), 7.18 (ddd, *J* = 8.0, 7.4, 1.8 Hz, 1H, ArH).



((2-Bromo-4-(*tert*-butyl)phenyl)ethynyl)trimethylsilane.⁵² Purified via silica gel column chromatography (eluent: hexanes) to provide ((2-Bromo-4-(*tert*-butyl)phenyl)ethynyl)trimethylsilane as a yellow oil (5.9 g, 81%). ¹H NMR (300 MHz, CDCl₃): δ 7.57 (d, *J* = 1.8 Hz, 1H, ArH), 7.41 (d, *J* = 8.2 Hz, 1H, ArH), 7.24 (dd, *J* = 8.2, 1.8 Hz, 1H, ArH), 1.29 (s, 9H, C(CH₃)₃), 0.27 (s, 9H, Si(CH₃)₃).

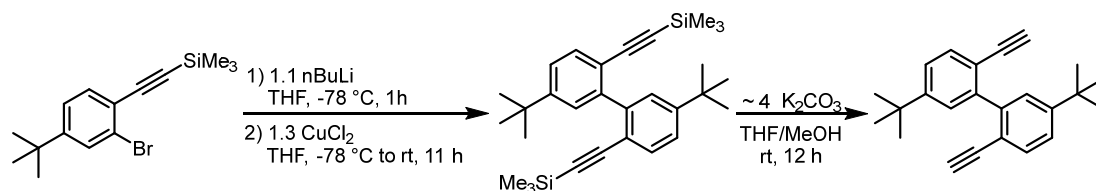


2-bromo-4-(*tert*-butyl)-1-((4-(*tert*-butyl)phenyl)ethynyl)benzene.⁵⁵ Purified via silica gel column chromatography (eluent: hexanes) to provide 2-bromo-4-(*tert*-butyl)-1-((4-(*tert*-butyl)phenyl)ethynyl)benzene as a white solid (6.9 g, 79%). ¹H NMR (300 MHz, CDCl₃): δ 7.62 (d, *J* = 1.9 Hz, 1H, ArH), 7.54 – 7.49 (m, 2H, ArH), 7.48 (d, *J* = 8.2 Hz, 1H, ArH), 7.41 – 7.36 (m, 2H, ArH), 7.30 (dd, *J* = 8.2, 1.9 Hz, 1H, ArH), 1.33 (s, 9H, C(CH₃)₃), 1.32 (s, 9H, C(CH₃)₃).

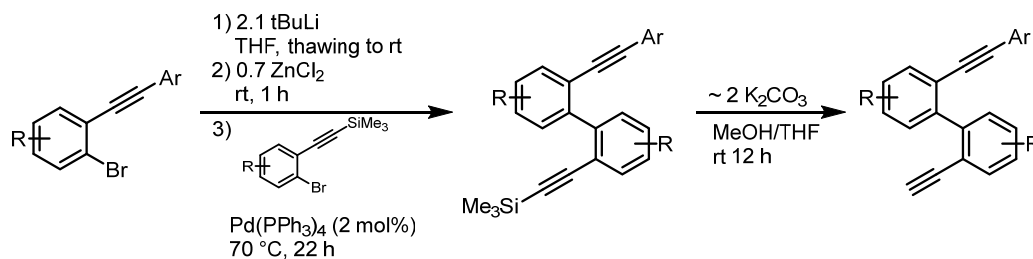


1,4-bis((2-bromo-4-(*tert*-butyl)phenyl)ethynyl)benzene. Purified via silica gel column chromatography (eluent: 2%EtOAc:hexanes). Yellow solid (4.5 g, 70%) ¹H NMR (300 MHz,

CDCl₃): δ 7.62 (d, J = 1.8 Hz, 2H, ArH), 7.55 (s, 4H, central ArH), 7.48 (d, J = 8.2 Hz, 2H, ArH), 7.31 (dd, J = 8.2, 1.9 Hz, 2H, ArH), 1.32 (s, 18H, CH₃).

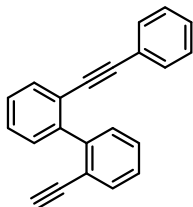


5,5'-di-tert-butyl-2,2'-diethynyl-1,1'-biphenyl (2c). Adapted from a previously reported procedure.⁴⁵ To a solution of ((2-Bromo-4-(*tert*-butyl)phenyl)ethynyl)trimethylsilane (5.5 g, 17.8 mmol) in THF (60 mL) at -78 °C was added dropwise ⁿBuLi (12.2 mL, 1.6 M in hexanes) and allowed to stir at -78 °C for an hour. Copper(II) chloride (3.1 g, 23.1 mmol) was then added under a counter flow of N₂. The mixture was allowed to warm to room temperature and stirred overnight. The reaction was quenched by the addition of H₂O (10 mL) and then reduced in volume in vacuo. 10% aqueous NH₄OH (50 mL) was added and then extracted with EtOAc (3 × 100 mL) The organic extracts were washed with H₂O (100 mL), dried over MgSO₄, filtered, and concentrated in vacuo. The crude residue was taken up in MeOH (60 mL) and THF (60 mL) and potassium carbonate (9.8 g, 70.9 mmol) was added and stirred overnight. The volatiles were removed and in vacuo the residue was partitioned between H₂O (100 mL) and EtOAc (100 mL). The aqueous phase was extracted with EtOAc (2 × 100 mL) and the combined extract dried over MgSO₄, filtered, and dried under reduced pressure. Purification by silica gel column chromatography (eluent: hexanes → 10% CH₂Cl₂:hexanes) provided 5,5'-di-*tert*-butyl-2,2'-diethynyl-1,1'-biphenyl as a white solid (1.82 g, 65.1 % over 2 steps). ¹H NMR (300 MHz, CDCl₃): δ 7.61 (d, J = 2.0 Hz, 2H, ArH), 7.57 (d, J = 8.2 Hz, 2H, ArH), 7.34 (dd, J = 8.2, 2.1 Hz, 2H, ArH), 2.93 (s, 2H, C≡CH), 1.34 (s, 18H, CH₃).

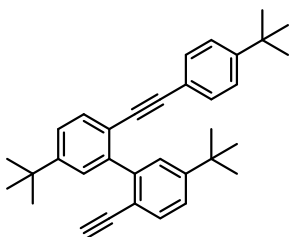


General procedures for Negishi coupling and deprotection towards asymmetric diynes

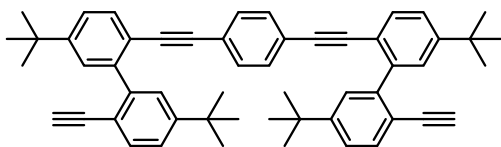
A Schlenk flask fitted with a screw-in Teflon stopper was charged with a solution of aryl bromide (1.0 equiv) in THF (0.4 M) and cooled to -78 °C. A 1.9M pentane solution of *tert*-butyllithium (2.1 equiv.) was added dropwise *via* cannula. The reaction was allowed to warm to room temperature and stirred for 1 h. The reaction was then brought into a N₂-purged glovebox and ZnCl₂ (0.7 equiv.) was added slowly in portions to the reaction. The mixture was allowed to stir at room temperature for 30 min. the second aryl bromide (0.95 equiv.) and Pd(PPh₃)₄ (2 mol%) was added, the flask sealed and warmed to 70 °C for 22 h. After cooling to room temperature, water was added to quench the reaction, and the reaction volume reduced in vacuo. The resulting suspension was taken up in CH₂Cl₂ and filtered through a silica gel plug, eluting further with CH₂Cl₂. The filtrate was then washed with water, dried over MgSO₄, filtered, and concentrated under reduced pressure. The crude mixture was taken up in MeOH and THF and to that suspension, potassium carbonate (2 equiv.) was added and then allowed to stir at room temperature for 12 h. The volatiles were then removed under reduced pressure and the residue was partitioned between H₂O and EtOAc. The aqueous phase was extracted with EtOAc and the combined extract dried over MgSO₄, filtered, and concentrated in vacuo to yield the crude product that was purified by silica gel column chromatography.



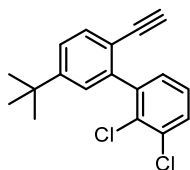
2-ethynyl-2'-(phenylethynyl)-1,1'-biphenyl (2b). Purified by silica gel column chromatography (eluent: 2% EtOAc:hexanes). Viscous yellow oil (3.78 g, 80% over 2 steps). ^1H NMR (300 MHz, CDCl_3): δ 7.70 – 7.60 (m, 2H, ArH), 7.54 – 7.32 (m, 6H, ArH), 7.31 – 7.20 (m, 5H, ArH), 2.97 (s, 1H, $\text{C}\equiv\text{CH}$).



5,5'-di-tert-butyl-2-((4-(tert-butyl)phenyl)ethynyl)-2'-ethynyl-1,1'-biphenyl (2d). Purified by silica gel column chromatography (eluent: 2% EtOAc:hexanes). Light brown solid (6.65 g, 84% over 2 steps). ^1H NMR (300 MHz, CDCl_3): δ 7.61 – 7.58 (m, 3H, ArH), 7.57 (s, 1H, ArH), 7.37 (ddd, $J = 8.2, 2.0, 1.4$ Hz, 2H, ArH), 7.31 – 7.10 (m, 4H, ArH), 2.92 (s, 1H, $\text{C}\equiv\text{CH}$), 1.36 (s, 9H, CH_3), 1.31 (s, 9H, CH_3), 1.28 (s, 9H, CH_3).



1,4-bis((5,5'-di-tert-butyl-2'-ethynyl-[1,1'-biphenyl]-2-yl)ethynyl)benzene (2e). Purified by silica gel column chromatography (eluent: 3%EtOAc:hexanes). Off white solid. ^1H NMR (300 MHz, CDCl_3): δ 7.61 (d, $J = 2.1$ Hz, 2H, ArH), 7.60 – 7.54 (m, 6H), 7.38 (t, $J = 2.0$ Hz, 2H, ArH), 7.35 (t, $J = 2.1$ Hz, 2H, ArH), 7.06 (s, 4H, central ArH), 2.92 (s, 2H, $\text{C}\equiv\text{CH}$), 1.35 (s, 18H, CH_3), 1.27 (s, 18H, CH_3).



5'-(tert-butyl)-2,3-dichloro-2'-ethynyl-1,1'-biphenyl (2h). Purified by silica gel column chromatography (eluent: hexanes). Pale yellow oil (8.0 g, 78% over 2 steps). ^1H NMR (300 MHz, CDCl_3): δ 7.57 (dd, $J = 8.2, 0.6$ Hz, 1H *ArH*), 7.50 (dd, $J = 7.0, 2.6$ Hz, 1H, *ArH*), 7.41 (dd, $J = 8.2, 2.1$ Hz, 1H, *ArH*), 7.32 – 7.30 (m, 1H, *ArH*), 7.29 (d, $J = 1.5$ Hz, 1H, *ArH*), 7.27 (d, $J = 6.1$ Hz, 1H, *ArH*), 2.93 (s, 1H, $\text{C}\equiv\text{CH}$), 1.35 (s, 9H, CH_3).

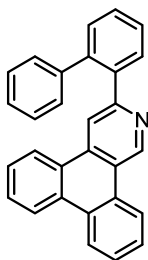
General screening procedure for the catalytic synthesis of pyridines PAHs from alkynes and nitriles

To a Schlenk flask charged with toluene (2 mL), diyne (49.3 μmol) nitrile (0.493 mmol) and a Teflon-coated stir bar was added a toluene solution of **1** (5 mg, 4.93 μmol), adjusting total volume of the reaction to 3 mL. The flask was then sealed and heated to the appropriate temperature for the desired reaction time. The reaction was allowed to cool to room temperature, and the volatiles removed in vacuo. 1,3,5-trimethoxybenzene was added at this stage if needed as an internal standard and an NMR taken to determine NMR yields.

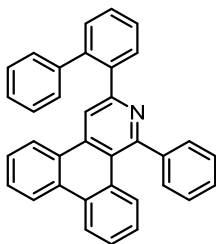
General procedure for the preparative scale catalytic synthesis of pyridines PAHs from alkynes and nitriles

The same procedure as with the screening with the exception of the use of between 50 to 100 mg **1**, with the diyne and nitrile substrates scaled accordingly and that half the scaled amount of solvent was used. After removal of the volatiles, the crude material was sublimed or Kugelrohr distilled to remove the bulk of the excess nitrile present. Further purification of

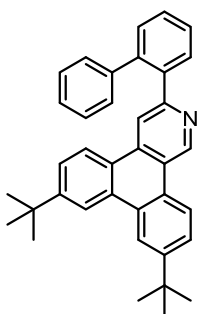
the crude residue was carried out via silica gel column chromatography to provide the desired product.



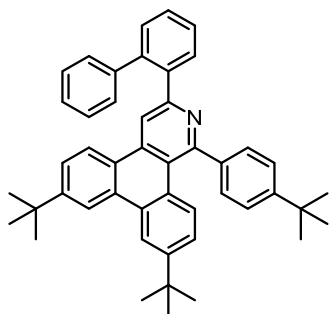
Synthesis of 4aa. Purified by silica gel column chromatography (5% EtOAc:hexanes). White solid (279 mg, 74%). $^1\text{H NMR}$ (300 MHz, CDCl_3): δ 9.97 (s, 1H, NCH), 8.78 – 8.71 (m, 1H, ArH), 8.67 – 8.58 (m, 2H, ArH), 8.04 (s, 1H, NCCH), 8.00 – 7.92 (m, 2H, ArH), 7.75 – 7.66 (m, 3H, ArH), 7.62 – 7.52 (m, 4H, ArH), 7.33 – 7.28 (m, 2H, ArH), 7.24 – 7.17 (m, 2H).



Synthesis of 4ba. Purified by silica gel column chromatography (5% EtOAc:hexanes). White solid (279 mg, 74%). $^1\text{H NMR}$ (300 MHz, CDCl_3): δ 8.58 (d, $J = 8.2$ Hz, 1H, ArH), 8.50 (d, $J = 8.2$ Hz, 1H, ArH), 8.15 (s, 1H, NCCH), 8.09 (d, $J = 8.4$ Hz, 1H, ArH), 8.07 – 8.02 (m, 1H, ArH), 7.76 (d, $J = 8.5$ Hz, 1H, ArH), 7.74 – 7.68 (m, 1H, ArH), 7.61 – 7.45 (m, 5H, ArH), 7.38 (d, $J = 1.0$ Hz, 5H, v), 7.32 (d, $J = 0.9$ Hz, 5H, ArH), 7.12 (ddt, $J = 8.3, 7.0, 1.2$ Hz, 1H, ArH).



Synthesis of 4ca. Purified by silica gel column chromatography (4% EtOAc:hexanes \rightarrow 8% EtOAc:hexanes). White solid (401 mg, 82%). ^1H NMR (300 MHz, CDCl_3): δ 9.91 (s, 1H, NCH), 8.66 (d, $J = 8.7$ Hz, 1H, ArH), 8.62 (t, $J = 2.0$ Hz, 2H), 8.00 (s, 1H, NCCH), 7.98 – 7.90 (m, 2H, ArH), 7.77 (dd, $J = 8.6, 1.9$ Hz, 1H, ArH), 7.59 (dd, $J = 8.6, 2.0$ Hz, 1H, ArH), 7.57 – 7.48 (m, 2H, ArH), 7.37 (d, $J = 0.6$ Hz, 2H, ArH), 7.32 – 7.16 (m, 4H, ArH), 1.51 (s, 9H, CH_3), 1.49 (s, 9H, CH_3).

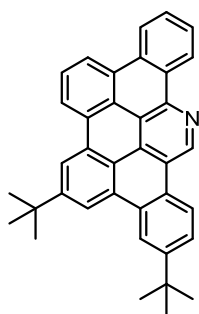


Synthesis of 4da. Purified by silica gel column chromatography (4% EtOAc:hexanes \rightarrow 8% EtOAc:hexanes). Pale brown solid (346 mg, 56%). ^1H NMR (300 MHz, CDCl_3): δ 8.58 (d, $J = 2.0$ Hz, 1H, ArH), 8.49 (d, $J = 2.1$ Hz, 1H, ArH), 8.09 (s, 1H, NCCH), 8.05 – 7.99 (m, 2H, ArH), 7.78 (d, $J = 8.9$ Hz, 1H, ArH), 7.63 (dd, $J = 8.6, 1.9$ Hz, 1H, ArH), 7.58 – 7.47 (m, 3H, ArH), 7.42 – 7.36 (m, 2H, ArH), 7.33 – 7.27 (m, 7H, ArH), 7.18 (dd, $J = 8.9, 2.0$ Hz, 1H, ArH), 1.51 (s, 9H, CH_3), 1.43 (s, 9H, CH_3), 1.37 (s, 9H, CH_3).

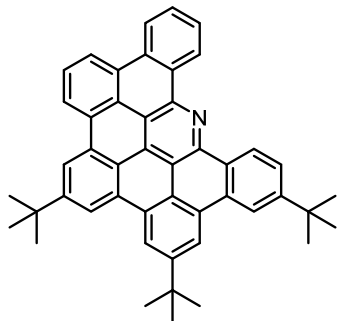
General procedure for oxidative dehydrogenation

To a 20 mL scintillation vial in a glove box was smeared some potassium metal (~ 30 mg) on its walls and then charged with a reduced Teflon-coated stir bar and THF (2 mL). To that, was added a solution of **4** (20 mg) in THF (~ 2 mL). The vial was then sealed and stirred at room temperature for two days, after which it was removed from the box. The reaction was decanted from excess potassium and then quenched by slow dropwise addition of isopropanol until the

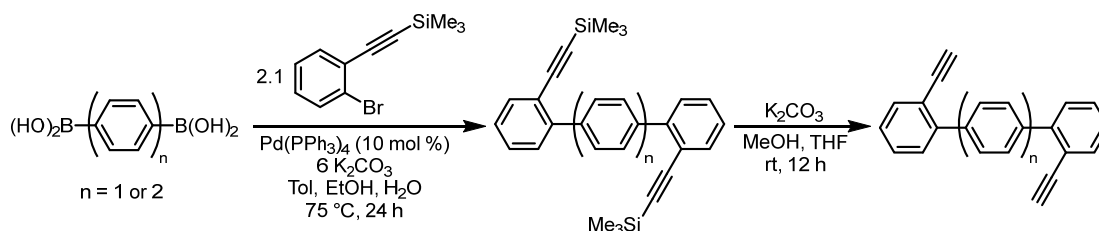
intense coloration faded to a light yellow-brown solution. To that, DDQ was added in small portions as a solid until a persistent deep red color is observed (~40 mg) and the reaction allowed to stir for 30 min. After the volatiles were removed in vacuo, the residue was taken up in chloroform and water (3 mL each). The chloroform layer was separated and the aqueous layer extracted with additional chloroform (2 × 2 mL). The combined organic extracts were washed with water (3 mL) until no significant color is observed in the washes. The extracts were then dried over MgSO₄, filtered, and dried under vacuum to yield **5**.



Synthesis of 5ca. Yellow solid (19.8 mg, quant.). Single crystals suitable for XRD were grown by slow evaporation of a chloroform solution of **5ca**. ¹H NMR (300 MHz, CDCl₃): δ 10.13 (s, 1H, NCH), 9.38 – 9.31 (m, 1H, ArH), 8.96 – 8.87 (m, 2H, ArH), 8.80 (d, *J* = 7.0 Hz, 1H, ArH), 8.81 – 8.73 (m, 2H, ArH), 8.67 (d, *J* = 7.9 Hz, 1H, ArH), 8.60 – 8.53 (m, 1H, ArH), 7.93 (t, *J* = 8.0 Hz, 1H, ArH), 7.87 (dd, *J* = 8.7, 1.8 Hz, 1H, ArH), 7.78 – 7.67 (m, 2H, ArH), 1.73 (s, 9H, CH₃), 1.63 (s, 9H, CH₃); ¹³C{¹H} NMR (101 MHz, CDCl₃): δ 151.20, 150.80, 143.92, 143.86, 142.06, 131.18, 131.08, 130.97, 130.78, 130.18, 130.03, 129.31, 128.66, 127.78, 127.17, 126.93, 126.57, 126.20, 125.37, 123.24, 122.94, 121.96, 121.75, 120.95, 120.75, 119.52, 119.08, 118.60, 116.34, 36.01 (C(CH₃)₃), 35.43 (C(CH₃)₃), 32.06 (C(CH₃)₃), 31.67 (C(CH₃)₃).



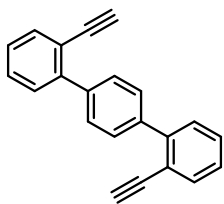
Synthesis of 5da. Recrystallized from vapor diffusion of hexanes into a saturated chloroform solution. Yellow solid (17.8 mg, 90%). ^1H NMR (300 MHz, CDCl_3): δ 9.81 – 9.75 (m, 2H, ArH), 9.07 (s, 1H, ArH), 9.07 – 8.99 (m, 3H, ArH), 8.86 (s, 1H, ArH), 8.84 (d, $J = 5.6$ Hz, 1H, ArH), 8.78 (d, $J = 8.1$ Hz, 1H, ArH), 8.68 (d, $J = 7.7$ Hz, 1H, ArH), 8.02 (dd, $J = 8.5, 1.9$ Hz, 1H, ArH), 7.96 (t, $J = 7.9$ Hz, 1H, ArH), 7.91 – 7.74 (m, 2H, ArH), 1.79 (s, 9H, CH_3), 1.78 (s, 9H, CH_3), 1.69 (s, 9H, CH_3).



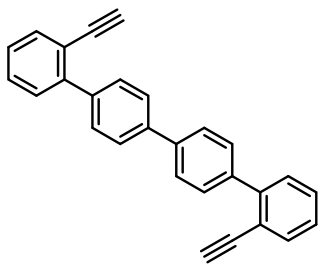
General synthesis of polyphenyl diynes.

A Schlenk tube fitted with a screw-in Teflon stopper was charged with 1,4-diiodonaphthalene (3.8 mmol, 1.0 equiv.), ((2-bromophenyl)ethynyl)trimethylsilane (2.1 equiv.) and anhydrous potassium carbonate (6 equiv.) suspended in a mixture of toluene (70 mL), ethanol (20 mL) and water (20 mL). The suspension was degassed via three freeze-pump-thaw cycles, after which *tetrakis*(triphenylphosphine) palladium(0) (10 mol%) was added under a counter flow of nitrogen. The flask was sealed and heated to 70 °C for 24 h with stirring. After cooling to room temperature, water (50 mL) was added and the organic layer separated. The aqueous layer was extracted with CH_2Cl_2 (2×50 mL). The organic extracts were combined and dried

over MgSO_4 , filtered, and concentrated in vacuo. The crude yellow oil was taken up in MeOH and THF and K_2CO_3 (~4 equiv.) was added and stirred at room temperature overnight. Water (50 mL) was added to quench the reaction and the volume was reduced in vacuo. The crude aqueous mixture was extracted with CH_2Cl_2 (3×50 mL), dried over MgSO_4 , filtered, and concentrated under reduced pressure affording the crude product which can be further purified via silica gel column chromatography.



2,2''-diethynyl-1,1':4',1''-terphenyl (2f). Purified by silica gel column chromatography (2% EtOAc:hexanes). Pale orange solid (681 mg, 65% over 2 steps). ^1H NMR (300 MHz, CDCl_3): 7.68 (s, 4H, central ArH), 7.66 – 7.62 (m, 2H, ArH), 7.49 – 7.40 (m, 4H, ArH), 7.35 – 7.29 (m, 2H, ArH), 3.09 (s, 2H, $\text{C}\equiv\text{CH}$).



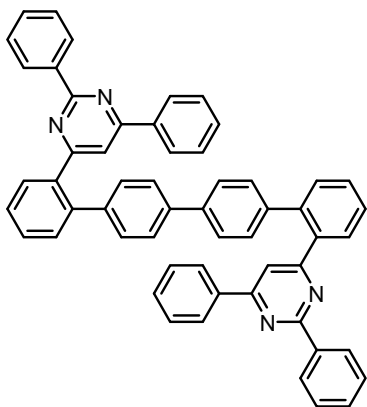
2,2'''-diethynyl-1,1':4',1'':4'',1'''-quaterphenyl (2g). Purified by silica gel column chromatography (3% EtOAc:hexanes) Yellow solid. (897 mg, 67% over 2 steps). ^1H NMR (300 MHz, CDCl_3): δ 7.78 – 7.62 (m, 10H, ArH), 7.47 – 7.43 (m, 4H, ArH), 7.39 – 7.29 (m, 2H, ArH), 3.10 (s, 2H, $\text{C}\equiv\text{CH}$).

General screening procedure for the catalytic synthesis of pyrimidines PAHs from alkynes and nitriles

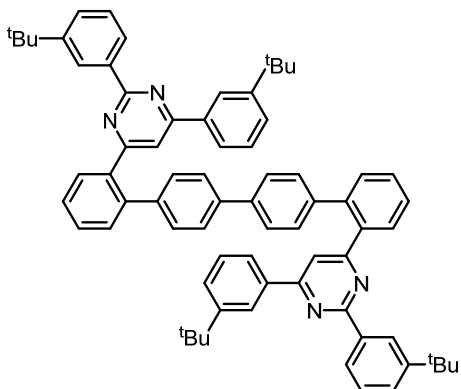
To a Schlenk flask charged with toluene (2 mL), diyne (49.3 μmol) nitrile (0.592 mmol) and a Teflon-coated stir bar was added a toluene solution of **1** (5 mg, 4.93 μmol), adjusting total volume of the reaction to 3 mL. The flask was then sealed and heated to the appropriate temperature for the desired reaction time. The reaction was allowed to cool to room temperature, and the volatiles removed in vacuo. 1,3,5-trimethoxybenzene was added at this stage if needed as an internal standard and an NMR taken to determine NMR yields.

General procedure for the preparative scale catalytic synthesis of pyrimidines PAHs from alkynes and nitriles

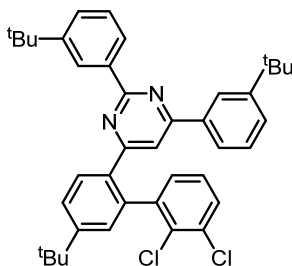
The same procedure as with the screening with the exception of the use of between 50 to 100 mg **1**, with the diyne and nitrile substrates, and solvent scaled accordingly. After removal of the volatiles, the crude material was sublimed or Kugelrohr distilled to remove the bulk of the excess nitrile present. Further purification of the crude residue was carried out via silica gel column chromatography to provide the desired product.



Synthesis of 4gg. Purified by silica gel column chromatography (3% EtOAc:hexanes). Pale yellow solid (232 mg, 61%). $^1\text{H NMR}$ (300 MHz, CDCl_3): δ 8.62 – 8.50 (m, 4H, *ArH*), 8.14 – 8.07 (m, 2H, *ArH*), 7.85 – 7.78 (m, 6H, *ArH*), 7.62 – 7.57 (m, 6H, *ArH*), 7.56 – 7.46 (m, 10H, *ArH*), 7.43 – 7.19 (m, 10H, *ArH*).

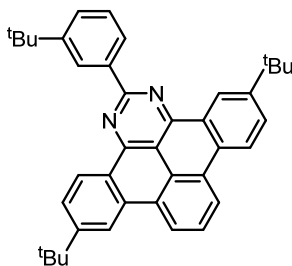


Synthesis of 4gh. Purified by silica gel column chromatography (3% EtOAc:hexanes). Pale yellow solid (296 mg, 60%). $^1\text{H NMR}$ (300 MHz, CDCl_3): δ 8.73 – 8.69 (m, 2H, *ArH*), 8.36 (ddd, $J = 7.6, 1.7, 1.2$ Hz, 2H, *ArH*), 8.09 (t, $J = 1.8$ Hz, 2H, *ArH*), 8.08 – 8.04 (m, 2H, *ArH*), 7.63 – 7.57 (m, 6H, *ArH*), 7.56 – 7.49 (m, 8H, *ArH*), 7.45 – 7.37 (m, 8H, *ArH*), 7.31 (s, 2H, *ArH*), 7.21 (t, $J = 7.7$ Hz, 2H, *ArH*), 1.43 (s, 18H, CH_3), 1.29 (s, 18H, CH_3).



Synthesis of 4hh. Purified by silica gel column chromatography (2% EtOAc:hexanes). Pale yellow solid (385 mg, 63%). $^1\text{H NMR}$ (300 MHz, CDCl_3): δ 8.64 (t, $J = 1.6$ Hz, 1H, *ArH*), 8.20 (ddd, $J = 7.6, 1.7, 1.2$ Hz, 1H, *ArH*), 8.12 (td, $J = 1.9, 0.5$ Hz, 1H, *ArH*), 7.95 (d, $J = 8.2$ Hz, 1H, *ArH*), 7.77 (ddd, $J = 7.6, 1.8, 1.2$ Hz, 1H, *ArH*), 7.69 – 7.60 (m, 2H, *ArH*), 7.55 – 7.49 (m,

2H, *ArH*), 7.45 – 7.37 (m, 4H, *ArH*), 7.16 (d, $J = 3.5$ Hz, 1H, *ArH*), 7.13 (t, $J = 7.6$ Hz, 1H), 1.42 (s, 9H, CH_3), 1.41 (s, 9H, CH_3), 1.39 (s, 9H, CH_3).



Synthesis of 5hh. Purified by silica gel column chromatography (2% EtOAc:hexanes). Pale yellow solid. 1H NMR (300 MHz, $CDCl_3$): δ 9.74 (d, $J = 2.2$ Hz, 1H), 9.59 (d, $J = 8.6$ Hz, 1H), 9.21 – 9.17 (m, 1H), 8.98 (d, $J = 8.0$ Hz, 1H), 8.94 (d, $J = 7.8$ Hz, 1H), 8.89 – 8.84 (m, 2H), 8.78 (d, $J = 8.7$ Hz, 1H), 8.13 (t, $J = 8.0$ Hz, 1H), 8.02 (dd, $J = 8.7, 2.3$ Hz, 1H), 7.97 (dd, $J = 8.5, 1.8$ Hz, 1H), 7.65 – 7.58 (m, 2H), 1.61 (s, 9H), 1.59 (s, 9H), 1.55 (s, 9H); HRMS (FAB+) m/z Calcd. for $C_{40}H_{41}N_2$ $[M + H]^+$ 549.3270, found 549.3289.

CRYSTALLOGRAPHIC INFORMATION

CCDC deposition numbers contain the supplementary crystallographic data for this paper.⁵⁶ These data can be obtained free of charge from The Cambridge Crystallographic Data Centre via www.ccdc.cam.ac.uk/data_request/cif.

Refinement Details

In each case, crystals were mounted on a glass fiber or MiTeGen loop using Paratone oil, then placed on the diffractometer under a nitrogen stream. Low temperature (100 K) X-ray data were obtained on a Bruker D8 VENTURE Kappa Duo PHOTON 100 CMOS based diffractometer (Mo I μ S HB micro-focus sealed X-ray tube, $K\alpha = 0.71073 \text{ \AA}$ OR Cu I μ S HB micro-focused X-ray tube, $K\alpha = 1.54178$). All diffractometer manipulations, including data collection, integration, and scaling were carried out using the Bruker APEXII software.⁵⁷ Absorption corrections were applied using SADABS.⁵⁸ Space groups were determined on the basis of systematic absences and intensity statistics and the structures were solved in the Olex 2 software interface⁵⁹ by intrinsic phasing using XT (incorporated into SHELXTL)⁶⁰ and refined by full-matrix least squares on F2. All non-hydrogen atoms were refined using anisotropic displacement parameters, except in some cases with heavily distorted solvent. Hydrogen atoms were placed in the idealized positions and refined using a riding model. The structure was refined (weighted least-squares refinement on F2) to convergence. Graphical representations of structures with 50% probability thermal ellipsoids were generated using Diamond 3 visualization software.⁶¹

Table 5.3. Crystal data and structure refinement for **5ca**, **5da**

	5ca	5da
CCDC Number ⁵⁶	-	-
Empirical formula	C ₃₇ H ₃₁ N	C ₄₇ H ₄₀ N
Formula weight	489.63	618.8
Temperature/ K	99.98	100
Crystal system	triclinic	triclinic
Space group	P-1	P-1
a/Å	10.601(14)	7.1911(11)
b/Å	12.732(11)	15.912(3)
c/Å	19.527(17)	16.170(2)
α/°	101.04(4)	65.690(8)
β/°	101.85(4)	77.356(10)
γ/°	93.10(5)	89.487(10)
Volume/Å ³	2520(5)	1638.4(5)
Z	4	2
ρ _{calc} /cm ³	1.291	1.254
μ/mm ⁻¹	0.074	0.54
Crystal size/mm ³	0.18 × 0.12 × 0.10	0.23 × 0.18 × 0.16
Radiation	MoKα (λ=0.71073)	CuKα (λ = 1.54178)
2θ range/°	3.538 to 69.024	10.366 to 144.47
GOF	1.051	1.075
R ₁ , ^a wR ₂ ^b [I>2 σ(I)]	0.0855, 0.1745	R ₁ = 0.0887, wR ₂ = 0.2711

^aR₁ = Σ||F₀| - |F_c||/Σ|F₀|. ^bwR₂ = [Σ[w(F₀²-F_c²)²]/Σ[w(F₀²)]^{1/2}

REFERENCES

- (1) Muhammad, S.; Chaudhry, A. R.; Irfan, A.; Al-Sehemi, A. G., *RSC Adv.* **2017**, *7*, 36632-36643.
- (2) Fan, M.; Feng, Z.-Q.; Zhu, C.; Chen, X.; Chen, C.; Yang, J.; Sun, D., *Journal of Materials Science* **2016**, *51*, 10323-10349.
- (3) Duan, J.; Chen, S.; Jaroniec, M.; Qiao, S. Z., *ACS Catal.* **2015**, *5*, 5207-5234.
- (4) Cai, J.; Pignedoli, C. A.; Talirz, L.; Ruffieux, P.; Söde, H.; Liang, L.; Meunier, V.; Berger, R.; Li, R.; Feng, X.; Müllen, K.; Fasel, R., *Nature Nanotechnology* **2014**, *9*, 896.
- (5) Chen, Y.-C.; de Oteyza, D. G.; Pedramrazi, Z.; Chen, C.; Fischer, F. R.; Crommie, M. F., *ACS Nano* **2013**, *7*, 6123-6128.
- (6) Son, Y.-W.; Cohen, M. L.; Louie, S. G., *Nature* **2006**, *444*, 347-349.
- (7) Sforzini, J.; Hapala, P.; Franke, M.; van Straaten, G.; Stöhr, A.; Link, S.; Soubatch, S.; Jelínek, P.; Lee, T. L.; Starke, U.; Švec, M.; Bocquet, F. C.; Tautz, F. S., *Phys. Rev. Lett.* **2016**, *116*, 126805.
- (8) Draper, S. M.; Gregg, D. J.; Schofield, E. R.; Browne, W. R.; Duati, M.; Vos, J. G.; Passaniti, P., *J. Am. Chem. Soc.* **2004**, *126*, 8694-8701.
- (9) Gregg, D. J.; Bothe, E.; Höfer, P.; Passaniti, P.; Draper, S. M., *Inorg. Chem.* **2005**, *44*, 5654-5660.
- (10) Zhang, C.; Sha, J.; Fei, H.; Liu, M.; Yazdi, S.; Zhang, J.; Zhong, Q.; Zou, X.; Zhao, N.; Yu, H.; Jiang, Z.; Ringe, E.; Yakobson, B. I.; Dong, J.; Chen, D.; Tour, J. M., *ACS Nano* **2017**, *11*, 6930-6941.
- (11) Wang, H.; Maiyalagan, T.; Wang, X., *ACS Catal.* **2012**, *2*, 781-794.
- (12) Stępień, M.; Gońka, E.; Żyła, M.; Sprutta, N., *Chem. Rev.* **2017**, *117*, 3479-3716.
- (13) Narita, A.; Wang, X.-Y.; Feng, X.; Müllen, K., *Chem. Soc. Rev.* **2015**, *44*, 6616-6643.
- (14) Draper, S. M.; Gregg, D. J.; Madathil, R., *J. Am. Chem. Soc.* **2002**, *124*, 3486-3487.
- (15) Wijesinghe, L. P.; Perera, S. D.; Larkin, E.; Ó Máille, G. M.; Conway-Kenny, R.; Lankage, B. S.; Wang, L.; Draper, S. M., *RSC Adv.* **2017**, *7*, 24163-24167.
- (16) Kiel, G. R.; Samkian, A. E.; Nicolay, A.; Witzke, R. J.; Tilley, T. D., *J. Am. Chem. Soc.* **2018**, *140*, 2450-2454.
- (17) Drev, M.; Grošelj, U.; Ledinek, B.; Perdih, F.; Svete, J.; Štefane, B.; Požgan, F., *Org. Lett.* **2018**, *20*, 5268-5273.
- (18) Suzuki, S.; Segawa, Y.; Itami, K.; Yamaguchi, J., *Nature Chemistry* **2015**, *7*, 227.

- (19) Low, C. H.; Rosenberg, J. N.; Lopez, M. A.; Agapie, T., *J. Am. Chem. Soc.* **2018**, *140*, 11906-11910.
- (20) Murayama, K.; Sawada, Y.; Noguchi, K.; Tanaka, K., *J. Org. Chem.* **2013**, *78*, 6202-6210.
- (21) McIver, A.; Young, D. D.; Deiters, A., *Chem. Commun.* **2008**, 4750-4752.
- (22) Kiel, G. R.; Patel, S. C.; Smith, P. W.; Levine, D. S.; Tilley, T. D., *J. Am. Chem. Soc.* **2017**, *139*, 18456-18459.
- (23) Jin, R.; Chen, Y.; Liu, W.; Xu, D.; Li, Y.; Ding, A.; Guo, H., *Chem. Commun.* **2016**, *52*, 9909-9912.
- (24) Grzybowski, M.; Skonieczny, K.; Butenschön, H.; Gryko, D. T., *Angew. Chem. Int. Ed.* **2013**, *52*, 9900-9930.
- (25) Graczyk, A.; Murphy, F. A.; Nolan, D.; Fernández-Moreira, V.; Lundin, N. J.; Fitchett, C. M.; Draper, S. M., *Dalton Trans.* **2012**, *41*, 7746-7754.
- (26) Narita, A., *Synthetic Methods for Conjugated Polymer and Carbon Materials* **2017**, 89.
- (27) Rempala, P.; Kroulík, J.; King, B. T., *J. Org. Chem.* **2006**, *71*, 5067-5081.
- (28) Rempala, P.; Kroulík, J.; King, B. T., *J. Am. Chem. Soc.* **2004**, *126*, 15002-15003.
- (29) Chaudhuri, J.; Kume, S.; Jagur-Grodzinski, J.; Szwarc, M., *J. Am. Chem. Soc.* **1968**, *90*, 6421-6425.
- (30) Polson, Matthew I. J.; Lotoski, John A.; Johansson, K. O.; Taylor, Nicholas J.; Hanan, Garry S.; Hasenknopf, B.; Thouvenot, R.; Loiseau, F.; Passalacqua, R.; Campagna, S., *Eur. J. Inorg. Chem.* **2002**, *2002*, 2549-2552.
- (31) Ioachim, E.; Medlycott, E. A.; Polson, M. I. J.; Hanan, G. S., *Eur. J. Org. Chem.* **2005**, *2005*, 3775-3780.
- (32) Watson, M. D.; Fechtenkötter, A.; Müllen, K., *Chem. Rev.* **2001**, *101*, 1267-1300.
- (33) Lungerich, D.; Hitzenberger, J. F.; Marcia, M.; Hampel, F.; Drewello, T.; Jux, N., *Angew. Chem. Int. Ed.* **2014**, *53*, 12231-12235.
- (34) Murphy, F. A.; Draper, S. M., *J. Org. Chem.* **2010**, *75*, 1862-1870.
- (35) Kratzer, A.; Englert, J. M.; Lungerich, D.; Heinemann, F. W.; Jux, N.; Hirsch, A., *Faraday Discuss.* **2014**, *173*, 297-310.
- (36) Pérez, E. M.; Martín, N., *Chem. Soc. Rev.* **2015**, *44*, 6425-6433.
- (37) Skidin, D.; Eisenhut, F.; Richter, M.; Nikipar, S.; Krüger, J.; Ryndyk, D. A.; Berger, R.; Cuniberti, G.; Feng, X.; Moresco, F., *Chem. Commun.* **2019**, *55*, 4731-4734.

- (38) Pinardi, A. L.; Martínez, J. I.; Jančařík, A.; Stará, I. G.; Starý, I.; López, M. F.; Méndez, J.; Martín-Gago, J. Á., *Chem. Commun.* **2014**, *50*, 1555-1557.
- (39) Tokimaru, Y.; Ito, S.; Nozaki, K., *Angew. Chem. Int. Ed.* **2018**, *57*, 9818-9822.
- (40) Ito, S.; Tokimaru, Y.; Nozaki, K., *Angew. Chem. Int. Ed.* **2015**, *54*, 7256-7260.
- (41) Gómez, B.; Guitián, E.; Castedo, L., *Synlett* **1992**, *1992*, 903-904.
- (42) Hayes, M. E.; Shinokubo, H.; Danheiser, R. L., *Org. Lett.* **2005**, *7*, 3917-3920.
- (43) Pangborn, A. B.; Giardello, M. A.; Grubbs, R. H.; Rosen, R. K.; Timmers, F. J., *Organometallics* **1996**, *15*, 1518-1520.
- (44) Zanon, J.; Klapars, A.; Buchwald, S. L., *J. Am. Chem. Soc.* **2003**, *125*, 2890-2891.
- (45) Matsuda, T.; Kato, K.; Goya, T.; Shimada, S.; Murakami, M., *Chem. Eur. J.* **2016**, *22*, 1941-1943.
- (46) Leifert, D.; Studer, A., *Org. Lett.* **2015**, *17*, 386-389.
- (47) Zhang, L.; Ang, G. Y.; Chiba, S., *Org. Lett.* **2010**, *12*, 3682-3685.
- (48) Cahiez, G.; Chaboche, C.; Mahuteau-Betzler, F.; Ahr, M., *Org. Lett.* **2005**, *7*, 1943-1946.
- (49) Yoshida, K.; Takeda, K.; Fueno, T., *J. Chem. Soc., Perkin Trans. 1* **1993**, 3095-3098.
- (50) Chou, C.-C.; Hu, F.-C.; Yeh, H.-H.; Wu, H.-P.; Chi, Y.; Clifford, J. N.; Palomares, E.; Liu, S.-H.; Chou, P.-T.; Lee, G.-H., *Angew. Chem. Int. Ed.* **2014**, *53*, 178-183.
- (51) Lee, S. H.; Jang, B.-B.; Kafafi, Z. H., *J. Am. Chem. Soc.* **2005**, *127*, 9071-9078.
- (52) Morisaki, Y.; Gon, M.; Sasamori, T.; Tokitoh, N.; Chujo, Y., *J. Am. Chem. Soc.* **2014**, *136*, 3350-3353.
- (53) Grubbs, R. H.; Kratz, D., *Chem. Ber.* **1993**, *126*, 149-157.
- (54) Schmidt-Radde, R. H.; Vollhardt, K. P. C., *J. Am. Chem. Soc.* **1992**, *114*, 9713-9715.
- (55) Shen, X.; Wu, Y.; Bai, L.; Zhao, H.; Ba, X., *J. Polym. Sci., Part A: Polym. Chem.* **2017**, *55*, 1285-1288.
- (56) Crystallographic data have been deposited at the CCDC, 12 Union Road, Cambridge CB2 1EZ, UK and copies can be obtained on request, free of charge, by quoting the publication citation and the respective deposition numbers.
- (57) APEX2, Version 2 User Manual, M86-E01078, Bruker Analytical X-ray Systems, Madison, WI, June 2006.
- (58) Sheldrick, G. M., "SADABS (version 2008/1): Program for Absorption Correction for Data from Area Detector Frames. University of Göttingen: 2008.

- (59) Dolomanov, O. V.; Bourhis, L. J.; Gildea, R. J.; Howard, J. A. K.; Puschmann, H., *J. Appl. Crystallogr.* **2009**, *42*, 339-341.
- (60) Sheldrick, G., *Acta Crystallographica Section A* **2008**, *64*, 112-122.
- (61) Brandenburg, K. (1999). DIAMOND. Crystal Impact GbR, Bonn, Germany.

Appendix A

Synthesis of Carbonyl-free Molybdenum Arylene Diphosphine Complexes: Observations of Nitrile Activation and Coupling

ABSTRACT

The synthesis and characterization of a series of naphthalenediyl-linked diphosphine molybdenum complexes are reported. Photolytic decarbonylation of previously discussed Mo(II) dicarbonyl complex provided a *tris*(acetonitrile) complex **3** displaying η^4 -arene interaction. Two-electron reduction of **3** provides the dinitrogen complex **4** along with acetonitrile complex **5** and enediiminato complex **6** formed from the four-electron coupling of two acetonitrile ligands. One electron reduction of **3** also yields diamagnetic diimido complex **7** which forms from the two-electron coupling of acetonitrile. With the bulkier nitrile, a similar coupling is not observed; instead, upon one-electron reduction solid-state structural determination showed the presence of mix nitrile complexes displaying bent and linear Mo-N-C angles, suggesting the presence of radical character on the nitrile carbon.

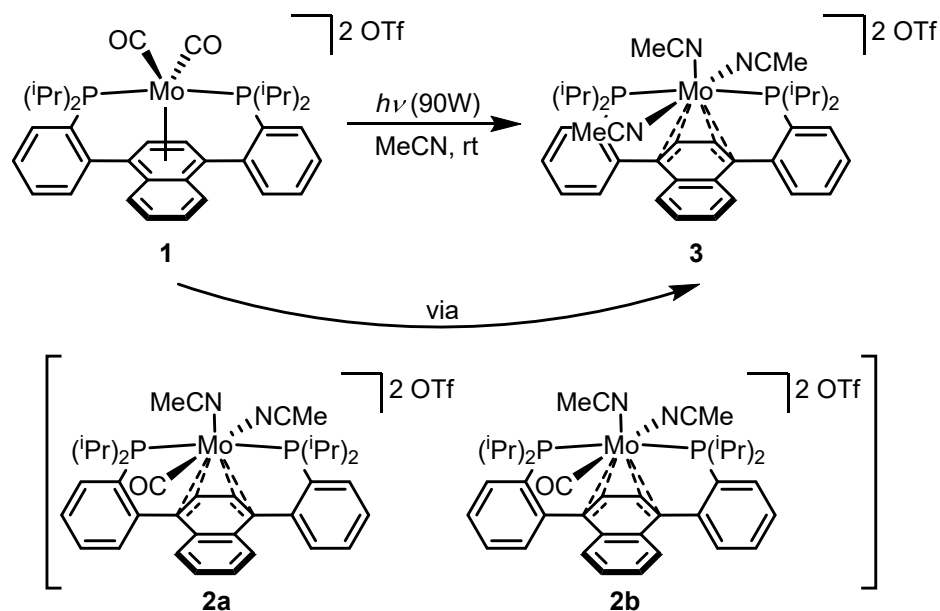
INTRODUCTION

The activation of small molecules such as CO and N₂ often involve the need for multi-electron transformation to break the C≡O and N≡N bonds.¹⁻⁶ Hence, the study of metal-mediated multi-electron bond-forming and bond-cleavage is crucial for the understanding and development of new catalysts. In Chapter 3, the study of naphthalene-linked teraryl diphosphine towards CO coupling was investigated. Two-electron reductive coupling of two CO molecules to a *bis*(siloxy)acetylene motif was demonstrated. In the phenylene-linked system, the four-electron reductive coupling of CO, involving both C≡O bond cleavage and C–C bond formation, was also achieved.⁵⁻⁶ The synthesis of carbonyl-free complexes is also of interest in the activation of other small molecules. The phenylene-linked molybdenum complex has been previously reported for the dehydrogenation of ammonia borane.⁷ Herein, we report the unusual reactivity of acetonitrile adducts of naphthalenediyl-linked diphosphine molybdenum complexes upon reduction, forming both two-electron coupled and four-electron coupled dimers.

RESULTS AND DISCUSSION

In order to investigate further reactivity on the Mo naphthalenediyl diphosphine system, a carbonyl-free complex was targeted. Using an analogous route as the previously reported phenylene-linked complex, photolytic decarbonylation was carried out with dicarbonyl *bis*(triflate) complex **1**. Photolysis of **1** in acetonitrile, degassing the liberated CO periodically, led to orange to brown color change over the course of 3 days. From the ^{31}P NMR, growth of two intermediate species at 61.7 and 58.5 ppm, with the former predominantly formed first, while the latter growing in over time along with the completely decarbonylated product (56.9 ppm).

Scheme A.1. Photolytic decarbonylation of **1**



Preliminary solid-state structural analysis of both the intermediates and the product provided confirmed on the identities monocarbonyls **2a** and **2b**, while full structural characterization was obtained for carbonyl-free *tris*(acetonitrile) complex **3** (Figure A.1). All three complexes display η^4 -binding to the central arene and are bound to three additional ancillary ligands (CO and/or acetonitrile), distinct from the phenylene

system where η^6 -binding is observed in both the monocarbonyl and *bis*(acetonitrile) complexes.⁷ These observations are consistent with those made in Chapter 3, where the naphthalene donor displayed a greater propensity to engage in η^4 interactions with the molybdenum center. In the structure of **3**, η^4 -binding significantly disrupts the central arene aromaticity, with elongation of C1–C10 and C4–C5 bond distances, while the outer ring of the naphthalene remains aromatic, with relatively uniform C–C bond distances.

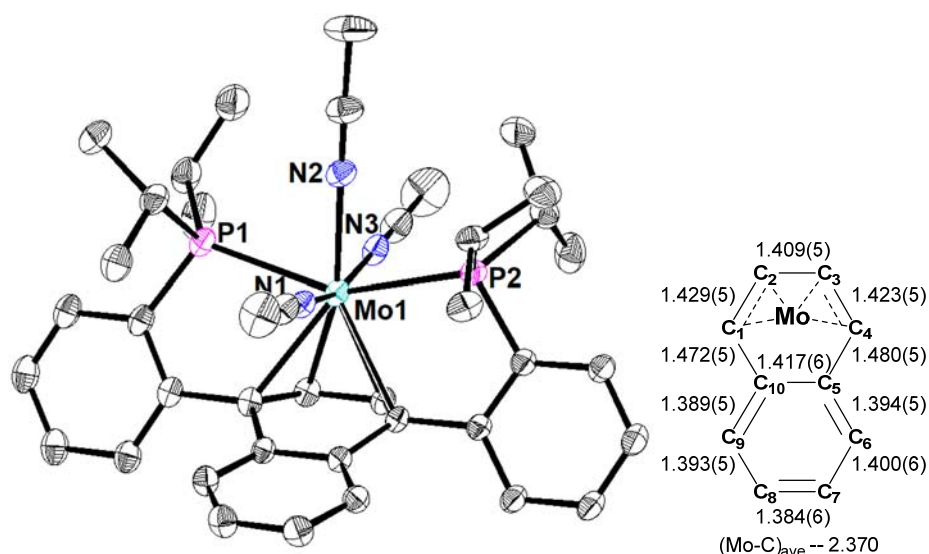


Figure A.1. Solid-state structure (left), and central arene bond metrics (right) for **3**. Only one of two asymmetric units shown. Thermal ellipsoids shown at 50% probability. Solvent molecules, counter anions, and hydrogen atoms omitted for clarity. Relevant bond lengths: Mo1–P1: 2.582(1), Mo1–P2: 2.588(1), Mo1–N1: 2.114(3), Mo1–N2: 2.160(4), Mo1–N3: 2.147(4).

Reduction of the complex **3** was carried out to target a Mo(0) dinitrogen complex that is observed with phenylene-linked variant.⁷ Complex **3** was stirred with magnesium turnings as a solution in acetonitrile and formed a green suspension over several hours. The ³¹P NMR spectrum of the solid after filtration showed three distinct phosphorous resonances at 84.9, 80.2, and 72.4 ppm, with the peak at 80.2 being in the smallest proportion. Repeated dissolution of the solid in benzene followed by removal of the

volatiles under vacuum resulted in the gradual conversion of the species at 84.9 ppm to that at 72.4 ppm, which is consistent with former being a complex bearing an acetonitrile ligand that converts, by repeated evacuations, to latter that bears fewer or no acetonitrile ligands. This equilibrium was supported by the reverse transformation observed upon addition of acetonitrile to a benzene solution of the mixture. Solid-state characterization confirmed the identity of the species at 72.4 ppm in the ^{31}P NMR to be dinitrogen complex **4** (Figure A.2). The molybdenum center takes on a three-legged piano-stool coordination and displays η^6 -binding to the central arene. The N–N IR stretching frequency of 1973 cm^{-1} is similar to previously reported phenylene diphosphine Mo dinitrogen complex (2020 cm^{-1}).⁷

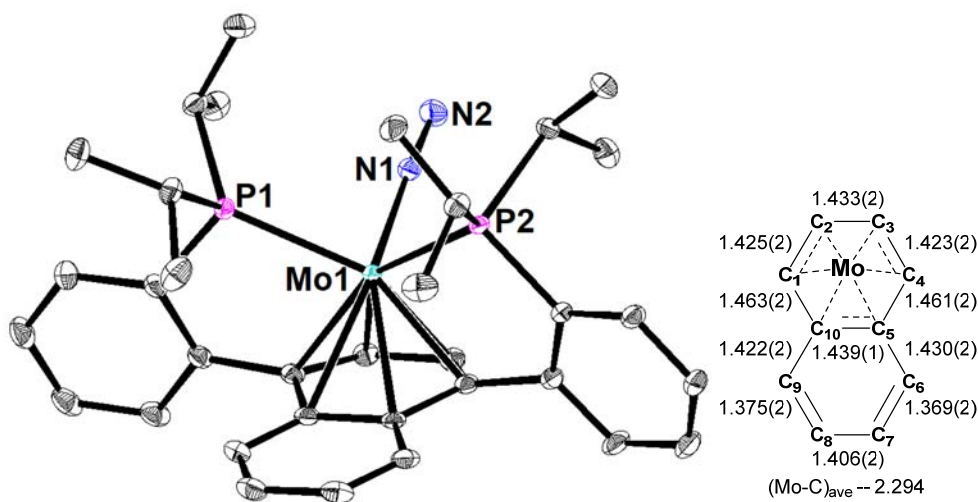


Figure A.2. Solid-state structure (left), and central arene bond metrics (right) for **4**. Only one of two asymmetric units shown. Thermal ellipsoids shown at 50% probability. Solvent molecules, counter anions, and hydrogen atoms omitted for clarity. Relevant bond lengths: Mo1–P1: 2.4739(5), Mo1–P2: 2.4833(5), Mo1–N1: 1.985(1), N1–N2: 1.129(1).

Likely owing to its lower solubility, single crystals of the minor species that displayed a ^{31}P NMR resonance at 80.2 ppm could be obtained. Solid-state characterization showed that this species was, in fact, a dimeric Mo(0/0) complex **6**

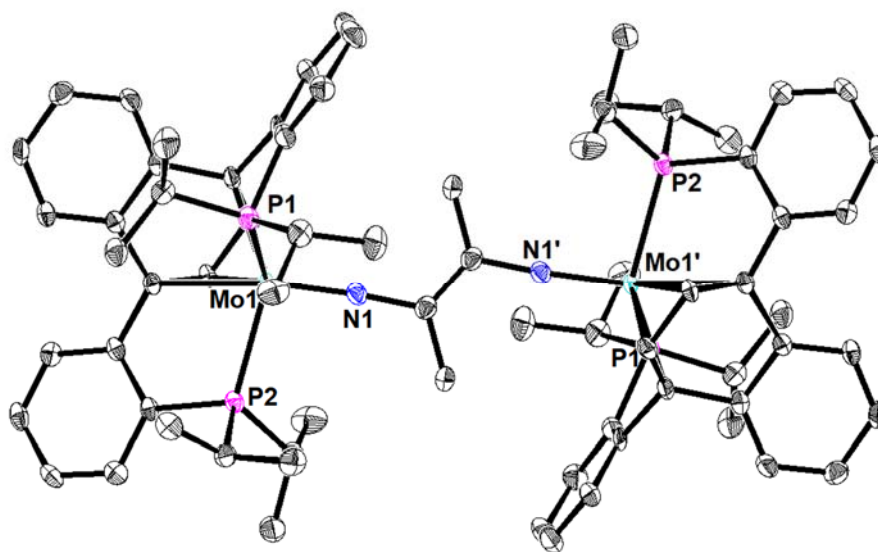
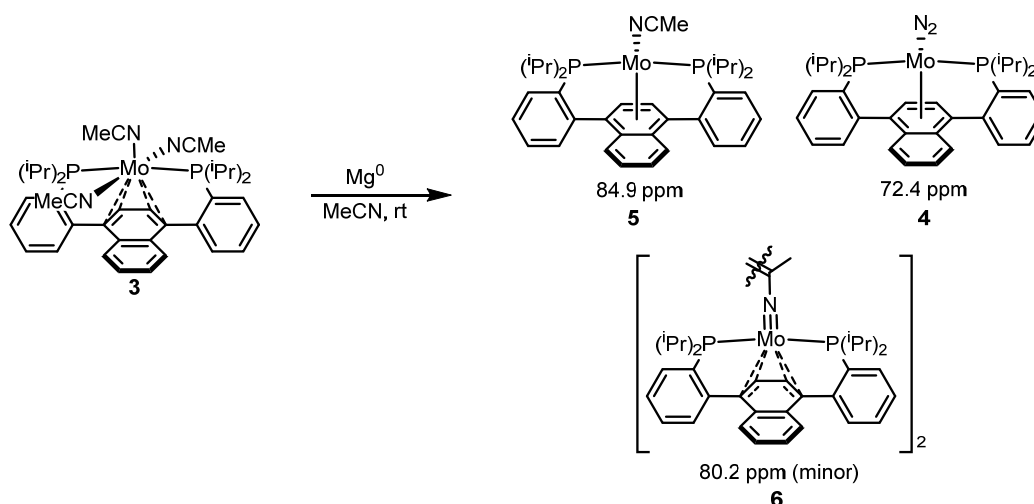


Figure A.3. Solid-state structure of **6**. Only one of four asymmetric units shown. Thermal ellipsoids shown at 50% probability. Solvent molecules, counter anions, and hydrogen atoms omitted for clarity.

bridged by two acetonitrile molecules that have coupled at the nitrile carbon (Figure A.3). The average C–C bond distance between the coupled acetonitrile is 1.36(1) Å, consistent with a C–C double bond, and the average bond C–N distance of 1.38(1) Å is consistent with a C–N single bond. These metrics are consistent with the four-electron coupling of

Scheme A.2. Reduction of **3**; ^{31}P NMR shifts of products indicated

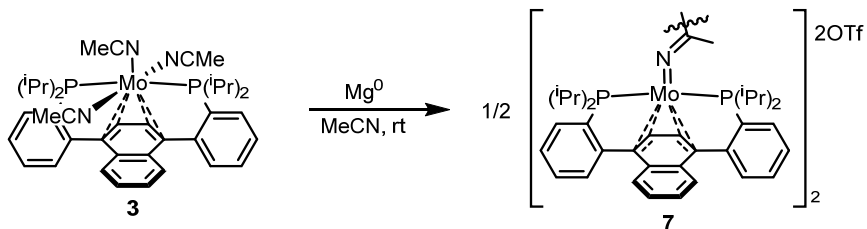


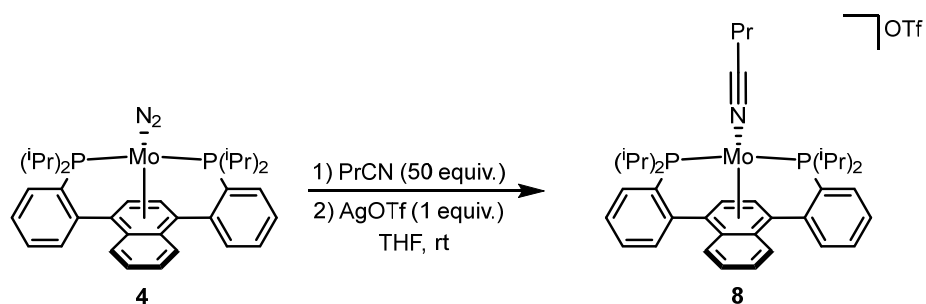
two acetonitrile ligands (Scheme A.2). This enediimido motif is relatively rare in the literature, with only five other structurally characterized examples on Ti, W, and Ta, and none on Mo.⁸⁻¹² The practically linear Mo-N-C angle ($\sim 177^\circ$) also suggests a dative donation of the N lone pair to Mo, formally forming a Mo-N triple bond (average 1.79(1) Å). The molybdenum center also shows η^4 -binding to the arene, retaining an 18-electron count. The nature of the naphthalene-based ligand to encourage η^4 -arene interactions may be key in the formation of **6** as the analogous species is not observed in the phenylene-linked system.

Attempts to circumvent the formation of this coupled species during the reduction process by substitution with a bulkier nitrile, *tert*-butyl cyanide (^tBuCN) by heating of a 1,4-dioxane solution of **3** with ^tBuCN led to no reactivity and by photolysis in the presence of ^tBuCN led to what appeared by ³¹P NMR spectroscopy as a mixture of Mo(nitrile)₃ complexes.

A Mo(I) acetonitrile complex was also targeted. It was found that 1.1 equiv. cobaltocene (CoCp₂) cleanly reduces **2** to a new diamagnetic species **7**. When KC₈ is used instead, species **7** is also observed along with a small amount of **6**. Additionally, **7** can also be accessed by either one-electron oxidation of comproportionation when Mo(0) complex **4** is mixed with Mo(II) complex **3**. The diamagnetic nature of **7** led us to assign its identity as a two-electron coupled diiminato complex with Mo(I) centers

Scheme A.3. One-electron reduction of **3**



Scheme A.4. Synthesis and reduction of PrCN adduct

antiferromagnetically coupled (Scheme A.3). Structural characterization of **8** has not been obtained to confirm this assignment. Attempting to rationally synthesize **6** by the stepwise reduction of **2** to **8** first, using CoCp_2 , and then an additional equiv. of KC_8 still led to the predominant formation of **4** and a small amount of **6**. To verify if **7** is indeed the bulk of the material present after the one-electron reduction, instead of a paramagnetic uncoupled Mo(I) species, the reaction with one equiv. CoCp_2 was run with PPh_3 as an internal standard. Based on the integration values, **7** indeed makes up the bulk of the material present. This observation suggests that the formation of **4** upon the next reduction result from the breaking up of the C–C bond between the dimido ligand to regenerate the acetonitrile adduct which is then reduced to **5** that then exchanges the acetonitrile ligand for dinitrogen to yield **4**.

To probe if similar reactivity can be extended to other nitriles, the synthesis and oxidation of butyronitrile (PrCN) adduct were carried out. The reaction of **5** with 50 equiv. PrCN led to a new species at 82.0 ppm, within the same region as the acetonitrile adduct. Subsequent oxidation of this new species with one equiv. AgOTf led to the formation of a paramagnetic species **8**. Structural characterization of **8** confirmed its assignment as a Mo(I) PrCN adduct (Figure A.4). Notably, the nitrile is disordered over two positions, one with a linear N–C–C angle ($175.8(3)^\circ$) at 77% occupancy and a minor

component that displays a bent N-C-C angle ($125.1(7)^\circ$) at 23% occupancy. The presence of the bent nitrile ligand likely indicates the presence of some amount of radical character on the carbon, which might explain the coupling that was observed in **6** and **7** that is first formed through the radical-radical coupling of the acetonitrile ligands. The bulkier propyl group may preclude the formation of the coupled species. A shorter Mo1–N1' bond ($1.959(8)$ Å) compared to Mo1–N1 ($2.072(2)$ Å) and a longer N1'–C bond ($1.26(1)$ Å) vs.

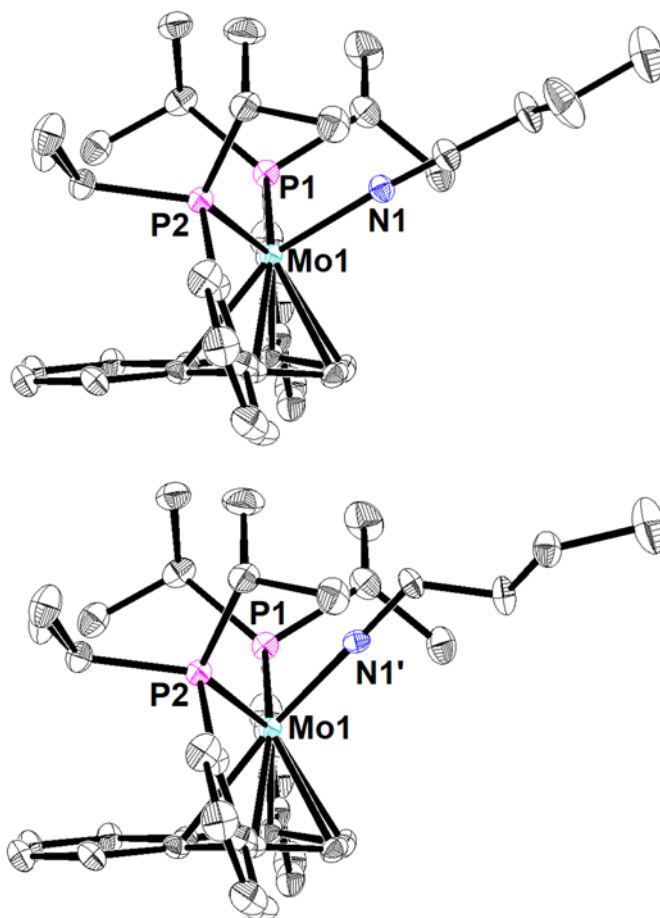


Figure A.4. Solid-state structure of **8** showing linear nitrile (top) and bent nitrile (bottom). Thermal ellipsoids shown at 50% probability. Solvent molecules, counter anions, and hydrogen atoms omitted for clarity.

N1–C bond ($1.156(3)$ Å) also support the assignment of partial radical character on the nitrile carbon.

CONCLUSION

A series of carbonyl-free naphthalenediyl-diphosphine molybdenum complexes have been synthesized and characterized. Consistent with the greater propensity of the naphthalene linker to bind metal center in an η^4 -fashion, a *tris*(acetonitrile) complex (**3**) was obtained upon photolysis of dicarbonyl complex **1**. Further reduction of this complex by Mg^0 provided an equilibrium mixture of Mo^0 dinitrogen adduct **4** and acetonitrile adduct **5**, which can be interconverted by removal or addition of MeCN. Addition a third minor product was observed and assigned to be a $\text{Mo}(0)$ dimer bridged by an enediimido ligand formed from the four-electron coupling of two acetonitrile ligands. When the $\text{Mo}(\text{I})$ acetonitrile complex was targeted a diamagnetic species assigned to be a dimer bridge by a diiminato ligand formed from the two-electron coupling of two acetonitrile molecules. When the analogous $\text{PrCN Mo}(\text{I})$ complex was synthesized, no coupling was observed, potentially due to the bulkier nitrile. From XRD, in one of the contributing components in a positional disorder, a minor (23%) structure showed the nitrile group bent at the nitrile carbon, suggesting some radical character on the carbon. This observation was also corroborated by the shortening of the Mo-N and elongation of the N-C bond distances. Detailed studies for the activation and coupling of nitriles is currently ongoing.

EXPERIMENTAL SECTION

General Considerations

Unless otherwise specified, all operations involving air- or water-sensitive reagents were carried out in an MBraun drybox under a nitrogen atmosphere or using standard Schlenk and vacuum line techniques. Solvents for air- and moisture-sensitive reactions were dried by the method of Grubbs.¹³ Deuterated solvents were purchased from Cambridge Isotope Laboratories and C₆D₆ vacuum transferred from sodium benzophenone ketyl before use. All solvents, once dried and degassed, were stored under a nitrogen atmosphere over 4 Å molecular sieves. All other reagents were used as received. ¹H, ¹³C{¹H}, and ¹⁹F NMR spectra were recorded on Varian Mercury 300 MHz or Varian 400 MHz spectrometers at ambient temperatures unless otherwise denoted. ¹H and ¹³C{¹H} NMR spectra are reported referenced internally to residual solvent peaks reported relative to tetramethylsilane. Photolyses were conducted using an Oriel Instruments arc lamp housing and an Osram 75 W Xe arc lamp set to a current of 5.4 A or a 450 W Xe/Hg lamp.

Synthesis of 3. A solution of **1** in acetonitrile is degassed by briefly placing under vacuum and is then photolyzed for 3 days, repeating the degassing process several times throughout the reaction time. The solution slowly turned from orange to brown over the time. Concentration of the reaction in vacuo provided **3** as a brown solid. ¹H NMR (400 MHz, CD₃CN): δ 7.69 – 7.61 (m, 2H), 7.60 – 7.49 (m, 6H), 6.61 – 6.55 (m, 2H), 6.51 – 6.43 (m, 4H), 3.28 (pd, *J* = 7.1, 2.5 Hz, 2H), 3.01 (tt, *J* = 14.0, 7.2 Hz, 2H), 1.29 – 1.21 (m, 6H), 1.18 – 1.11 (m, 6H), 1.08 – 1.00 (m, 6H), 0.86 – 0.78 (m, 6H); ¹³C NMR (101 MHz, CD₃CN): δ 137.45, 135.15, 134.88, 132.54, 130.13 (t, *J* = 5.3 Hz), 128.34, 116.00, 114.55, 103.24, 94.76, 29.72, 29.60, 18.86, 18.51, 18.32, 18.22; ³¹P{¹H} NMR (162 MHz,

CD₃CN): δ 56.93; ¹⁹F NMR (376 MHz, CD₃CN) δ -79.29.

Synthesis of 4. To a solution of **3** in acetonitrile was added magnesium turnings and stirred 2 h at room temperature. The green suspension formed was filtered over diatomaceous earth and washed with minimal acetonitrile. The solids were then extracted with benzene and lyophilized to a green solid. The solid was dissolved in benzene again and lyophilized twice more to provide **4** as a green solid.

REFERENCES

- (1) Holland, P. L., *Can. J. Chem.* **2005**, *83*, 296-301.
- (2) Speelman, A. L.; Holland, P. L., Sulfur-Supported Iron Complexes for Understanding N₂ Reduction. In *Nitrogen Fixation*, Nishibayashi, Y., Ed. Springer International Publishing: Cham, 2017; pp 197-213.
- (3) Schulz, H., *Applied Catalysis A: General* **1999**, *186*, 3-12.
- (4) Summerscales, O. T.; Cloke, F. G. N.; Hitchcock, P. B.; Green, J. C.; Hazari, N., *Science* **2006**, *311*, 829.
- (5) Buss, J. A.; Agapie, T., *J. Am. Chem. Soc.* **2016**, *138*, 16466-16477.
- (6) Buss, J. A.; Agapie, T., *Nature* **2016**, *529*, 72-75.
- (7) Buss, J. A.; Edouard, G. A.; Cheng, C.; Shi, J.; Agapie, T., *J. Am. Chem. Soc.* **2014**, *136*, 11272-11275.
- (8) Doxsee, K. M.; Garner, L. C.; Juliette, J. J. J.; Mouser, J. K. M.; Weakley, T. J. R.; Hope, H., *Tetrahedron* **1995**, *51*, 4321-4332.
- (9) Farrell, W. S.; Yonke, B. L.; Reeds, J. P.; Zavalij, P. Y.; Sita, L. R., *Organometallics* **2016**, *35*, 1132-1140.
- (10) Cotton, F. A.; Hall, W. T., *Inorg. Chem.* **1978**, *17*, 3525-3528.
- (11) Duchateau, R.; Williams, A. J.; Gambarotta, S.; Chiang, M. Y., *Inorg. Chem.* **1991**, *30*, 4863-4866.
- (12) Rahman, M. M.; Smith, M. D.; Amaya, J. A.; Makris, T. M.; Peryshkov, D. V., *Inorg. Chem.* **2017**, *56*, 11798-11803.
- (13) Pangborn, A. B.; Giardello, M. A.; Grubbs, R. H.; Rosen, R. K.; Timmers, F. J., *Organometallics* **1996**, *15*, 1518-1520.

Appendix B

Design and Synthesis of *Tris*(thiophenolate)benzene Iron Complexes As Potential Nitrogenase FeMoco Models

ABSTRACT

The synthesis of a novel *tris*(thiophenolate)benzene ligand is reported. Metalations with iron precursors generated dimeric “Fe₂L₂” structures with either a dianionic ligand, with a free thiol arm, or a trianionic ligand. In the latter case potassium counterions present were observed to be forming sandwich-type motifs between aryl groups on different ligand molecules. Sequestration of the ions with 18-crown-6 allowed for the synthesis of a monomeric iron *tris*(thiophenolate) complex.

GENERAL INTRODUCTION

Nitrogenases are enzymes found in certain strains of bacteria that converted dinitrogen (N_2) to ammonia (NH_3), a key step of nitrogen fixation.¹ Of these enzymes, the MoFe-nitrogenase is the most common and features an iron-molybdenum cofactor (FeMoco) active site, which is an iron and sulfur-rich cluster (Fe_7MoS_9).²⁻⁵ It is hypothesized by many that N_2 binds at one of the “belt” irons that feature a FeS_3C coordination environment which is followed by Fe–C bond elongation or dissociate.⁶⁻⁸ Other binding motifs, such as dissociation of one of the thiolates, have also been proposed.⁹⁻¹¹

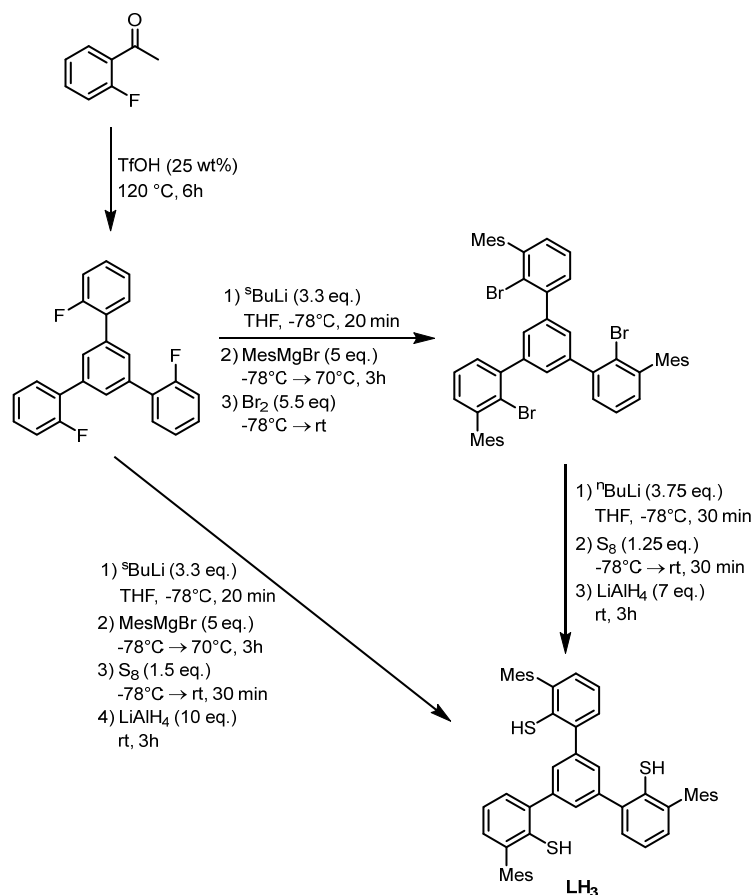
In order to better understand the potential iron coordination environment necessary for N_2 coordination, we postulated that a *tris*(thiophenolate) ligand bearing a central benzene donor might be a viable framework to model either binding modes. In Chapter 2, we’ve demonstrated that structural similar arene diphosphine iron complexes can bind in an η^6 -fashion to the central arene. Holland and coworkers have also reported the use of an arene *bis*(thiophenolate) to supported an N_2 -bound reduced iron center that displays significant interaction with the two of the carbons in the central arene. Herein we report the design and synthesis of a *tris*(thiophenolate) ligand bearing a central arene donor capable of binding irons in a variety of protic states and coordination environments.

RESULTS AND DISCUSSION

1. Ligand Synthesis

The synthesis of the target ligand was based on a related framework previously reported. In that synthesis an *ortho*-lithiation was carried out on a fluoroarene that generated a benzyne intermediate, which was then quenched with an aryl Grignard, installing both the an arene group and leaving the *ipso* position as a carbanion prime for further functionalization.⁹ 1,3,5-*tris*(2-fluorophenyl)benzene was synthesized in one-step from the dehydrative trimerization of 2-fluoroacetophenone in the presence of trifluoromethanesulfonic acid adapted from a previous report to the tribromide analogue (Scheme B.1).¹² From the trifluoride, *ortho*-lithiation of each phenylene arm at low

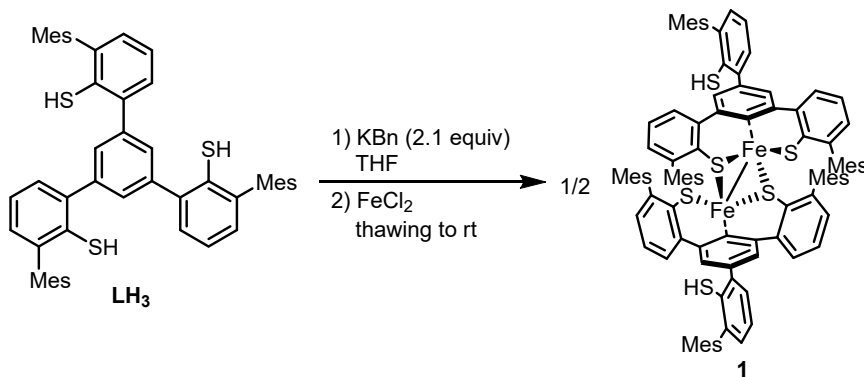
Scheme B.1. Synthesis of **LH₃**



temperature, followed by addition of mesityl magnesium bromide, provide presumably, the “tri-Grignard” species which can then be quenched with bromine to yield the trimesityl-substituted tribromide. Subsequently, a lithium-halogen exchange, quenching with elemental sulfur (S_8) followed by reduction with lithium aluminium hydride ($LiAlH_4$), the targeted *tris*(thiophenol) LH_3 can be obtained after a protic workup. The synthesis of LH_3 can also be streamlined, albeit with a small loss in overall yield, by quenching the “tri-Grignard” species with S_8 followed by reduction by $LiAlH_4$ followed by a protic quench to afford LH_3 directly.

Initial metalation studies targeted the use of various iron precursors ($FeCl_2$, $FeCl_3$ and $Fe[N(SiMe_3)_2]_2$) with varying stoichiometric. Using potassium benzyl as a base, a variety of ligand protic states were also explored for metalations. The two most promising metalations were obtained with 1:1 $LH_3:Fe[N(SiMe_3)_2]_2$, and 1:1 $LHK_2:FeCl_2$, both of which gave identical species **1** by 1H NMR, with the latter being a slightly cleaner reaction (Scheme B.2). Single crystals grown from the slow vapor diffusion of pentane into a saturated benzene solution of the reaction with $FeCl_2$ were suitable for X-ray diffraction (XRD). The solid-state structure revealed the formation of a *bis*(thiolate) iron complex with a free thiol arm, which is the expected based on the metalation stoichiometry (Figure

Scheme B.2. Metalation LH_3 to afford **1**



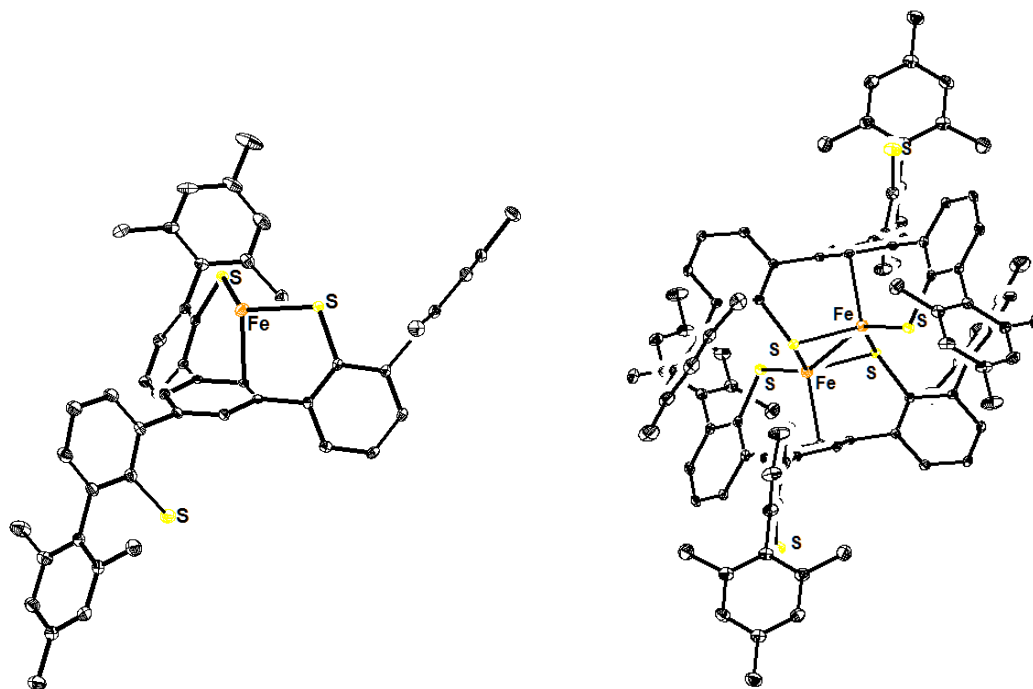


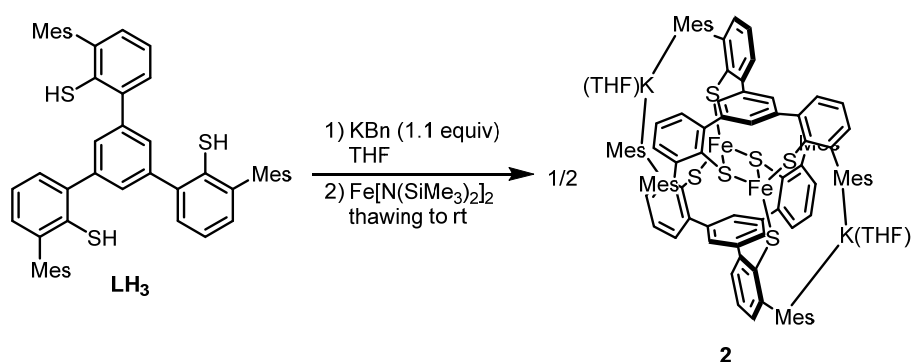
Figure B.1. Solid-state structure of **1**. Asymmetric unit (left) and grown structure (right). Thermal ellipsoids shown at 50% probability. Solvent molecules and hydrogen atoms omitted for clarity. Relevant bond lengths: Fe–Fe: 2.7601(8), Fe–S_{term}: 2.2533(7), Fe–S_{bridg}: 2.3341(7), Fe–S'_{bridg}: 2.3278(7), Fe–C1: 2.285(2).

B.1). In the asymmetric unit, a single iron center is observed to be binding to two thiolate donors on the same ligand and displaying a short Fe–C contact to one of the carbons at the central arene (2.285(2) Å), though still significantly longer than that found in FeMoCo (2.01 Å).³ When the asymmetric unit is grown, the full structure is that of a diiron complex. One of the two thiolates serves as a bridging ligand between the two iron centers. The Fe–Fe distance of 2.7601(8) Å is within the range of diiron complexes with a diamond core featuring bridging thiolates on separate ligands and is indicative of relatively weak interaction.

In order to try to access a C₃-symmetric monoiron complex wherein all three thiolate donors are bound, deprotonation of the third thiol arm in **1** was attempted but

has thus far been unsuccessful. Reduction with a variety of strong reductants (potassium graphite (KC_8) or potassium naphthalenide) has also led to the formation of intractable mixtures. Crystals grown from the reduction of **1** with 4.4 equiv potassium naphthalenide led to the formation of potassium clusters supported by the thiolate ligand (K_6L_2), with no iron present. Deprotonation with KBn and reduction with KC_8 also led to the formation of various other potassium thiolate clusters.

Scheme B.2. Metalation LH_3 to afford **2**



Addition of a thawing THF solution of monodeprotonated LH_2K to a thawing solution of $\text{Fe}[\text{N}(\text{SiMe}_3)_2]_2$ and allowing it to warm to room temperature resulted in the formation of species **2** as red-orange crystals (Scheme B.3). In C_6D_6 , the ^1H NMR of **2** did

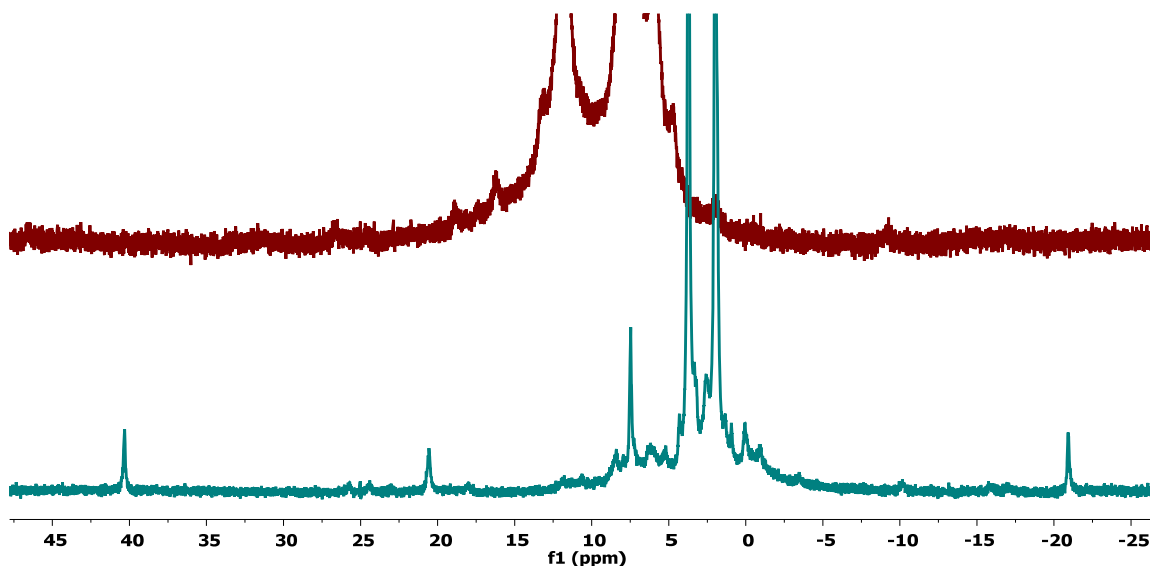


Figure B.2. ^1H NMR spectra of **2** in C_6D_6 (top) and CD_3CN (bottom).

not show any distinct paramagnetically shifted peaks. However, in CD_3CN , distinct paramagnetically shifted peaks were observed (Figure B.2). XRD studies of the crystals obtained the structure of complex **2** to be an iron dimer after growing the asymmetric unit (Figure B.3). All three thiols have been deprotonated and are iron bound. Each ligand has a thiolate arm bound to adjacent iron center while the third bridges between the two. A long Fe–Fe distance of 3.703(8) Å, suggesting no interaction. No significant interaction of the iron centers with the central arene is observed. Potassium ions are observed to be sandwiched between two mesityl groups on two different ligands, with weak interactions with the non-bridging thiolates.

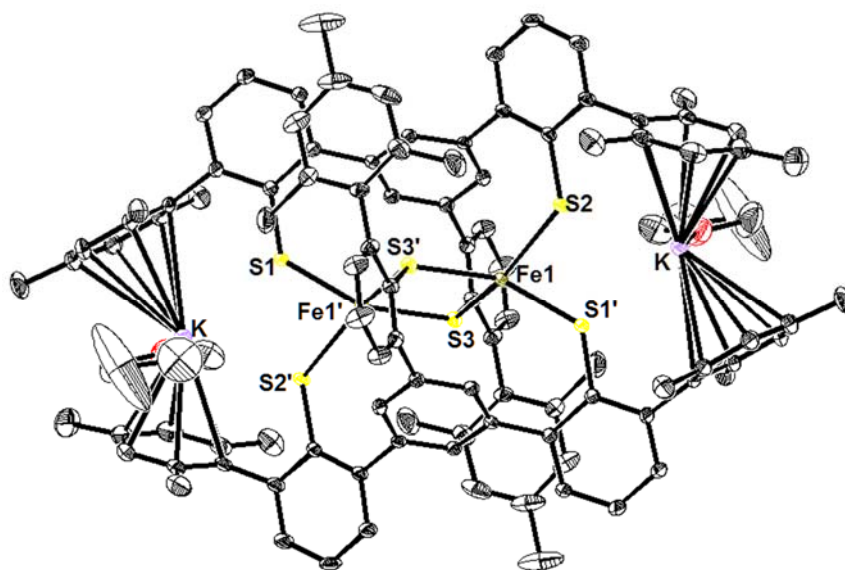


Figure B.3. Solid-state structure of **2** (grown). Thermal ellipsoids shown at 50% probability. Solvent molecules and hydrogen atoms omitted for clarity. Relevant bond lengths: Fe–Fe: 3.703(1), Fe1–S1': 2.405(1), Fe1–S2: 2.385(1), Fe1–S3: 2.428(1).

Probing the flexibility of the dimeric framework of **2**, protonation studies to target **1** was carried out but were unsuccessful, suggesting that upon protonation, the need for a large reorganization likely results in decomposition of the dimer. Postulating that the sandwiched potassium atoms may be holding the two ligand units together, we set out to

investigate if a monometallic complex can be obtained when the potassium atoms are abstracted from that binding pocket. Addition of two equiv. of 18-crown-6 to **2** resulted in the formation of a new species **3** by ^1H NMR showing sharp paramagnetically shifted peaks. Single crystal XRD studies revealed that indeed upon sequestration of the potassium ions by the crown ether, a monometallic species is obtained (Figure B.4). In this structure, no significant interaction of iron with the central arene carbons is observed, but it is in the pocket poised to interact with the arene moiety upon redox changes.

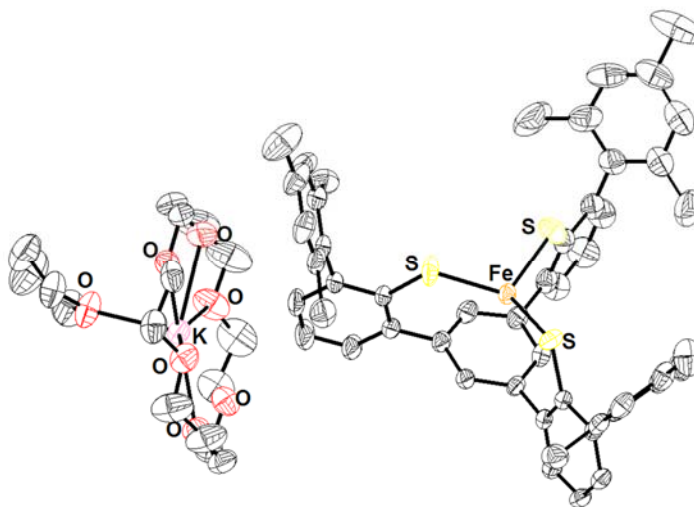


Figure B.4. Solid-state structure of **3**. Thermal ellipsoids shown at 50% probability. Solvent molecules and hydrogen atoms omitted for clarity. Relevant bond lengths: Fe–S: 2.3402(8); 2.3436(8); 2.357(1) Fe1–C_{avg}: 2.745.

In some of the decomposition products that we had obtained preliminary structural characterization on, we have observed that the complexes were able to accommodate a bridging atom between the iron centers. Therefore, the rational synthesis of dimeric iron complexes supported by this ligand framework bridged by a light atom/group (O, OH, S, SH) was explored. The reaction of **2** with either $[\text{Bu}_4\text{N}][\text{OH}]$ or KOH resulted in the formation of very similar new paramagnetic species with sharp peaks in the ^1H NMR spectra. Oxidation with iodosobenzene and reaction with water also lead

to the formation of new paramagnetic species. Unfortunately, solid-state characterization of these products has not been obtained.

Reduction reactions have been probed with **2** and **3** in targeting a formally iron(0) complex. Reductions under a variety of conditions, with or without the addition of 18-crown-6 to chelate additional potassium ions, have been attempted. However, these reactions often led to broad paramagnetic signals or NMR silent species. Solid-state characterization of these complexes has also, thus far, eluded us.

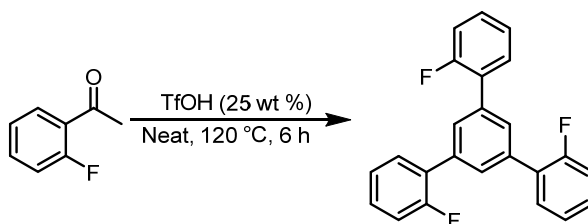
CONCLUSION

In summary, the synthesis and characterization of a series of iron complexes supported by novel benzene *tris*(thiophenol) proligand have been reported. Depending on the extent of deprotonation of the proligand and the precursor used, the synthesis of iron dimers featuring either a free thiophenol, as in complex **1**, or with three anionic thiophenolate donors, as in complex **2**. However, interconversion between **1** and **2** by deprotonation or protonation could not be realized, potentially due to the large organization of the ligand framework. Sequestration of the potassium ions in **2**, initially sandwiched between flanking mesityl groups, allowed for the isolation of monoiron complex **3**.

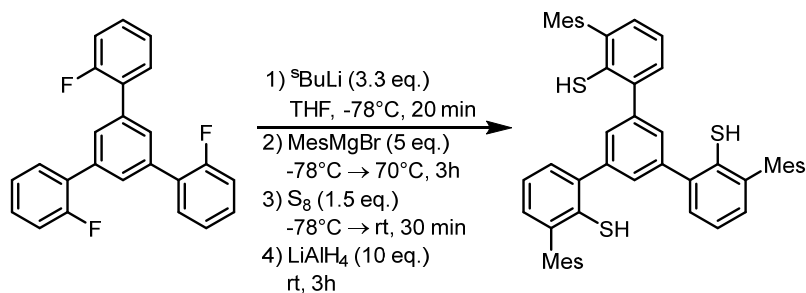
EXPERIMENTAL SECTION

General Considerations

Unless otherwise specified, all operations involving air- or water-sensitive reagents were carried out in an MBraun drybox under a nitrogen atmosphere or using standard Schlenk and vacuum line techniques. Solvents for air- and moisture-sensitive reactions were dried by the method of Grubbs.¹³ Deuterated solvents were purchased from Cambridge Isotope Laboratories and C₆D₆ vacuum transferred from sodium benzophenone ketyl before use. All solvents, once dried and degassed, were stored under a nitrogen atmosphere over 4 Å molecular sieves. Elemental sulfur was purchased from Strem Chemicals (99.999%). All other reagents were used as received. ¹H, ¹³C{¹H}, and ¹⁹F NMR spectra were recorded on Varian Mercury 300 MHz or Varian 400 MHz spectrometers at ambient temperatures unless otherwise denoted. ¹H and ¹³C{¹H} NMR spectra are reported referenced internally to residual solvent peaks reported relative to tetramethylsilane. Fast atom bombardment-mass spectrometry (FAB-MS) analyses were performed with a JEOL JMS-600H high-resolution mass spectrometer. Gas chromatography-mass spectrometry (GC-MS) were performed with on an Agilent 6890A instrument using an HP-5MS column (30 m length, 0.25 mm diameter, 0.50 μm film) and an Agilent 5973N mass-selective EI detector. Photolyses were conducted using an Oriel Instruments arc lamp housing and an Osram 75 W Xe arc lamp set to a current of 5.4 A.

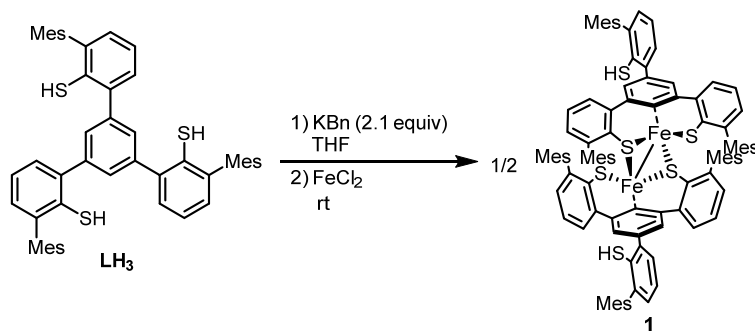


1,3,5-tris(2'-fluorophenyl)benzene. Modified from a previously reported procedure.¹² A neat mixture of 2-fluoroacetophenone (100 g, 0.724 mol) and trifluoromethanesulfonic acid (25g, 0.167 mol) was stirred at 120 °C for 6 h. Upon cooling to room temperature, a brown solid was formed. The solid was broken up with a mortar and pestle and washed with H₂O (3 × 200 mL), MeOH (5 × 100 mL) during which a free-flowing green-brown powder was observed to form on the frit during filtration. This powder was washed with minimal Et₂O (2 × 50 mL) and dried in vacuo to yield 1,3,5-tris(2'-fluorophenyl)benzene as a green-brown powder (52.3 g, 60.1 %). ¹H NMR (300 MHz, CDCl₃): δ 7.77 (app q, *J* = 1.1 Hz, 3H), 7.56 (td, *J* = 7.7, 1.9 Hz, 3H), 7.42 – 7.31 (m, 3H), 7.29 – 7.16 (m, 6H).

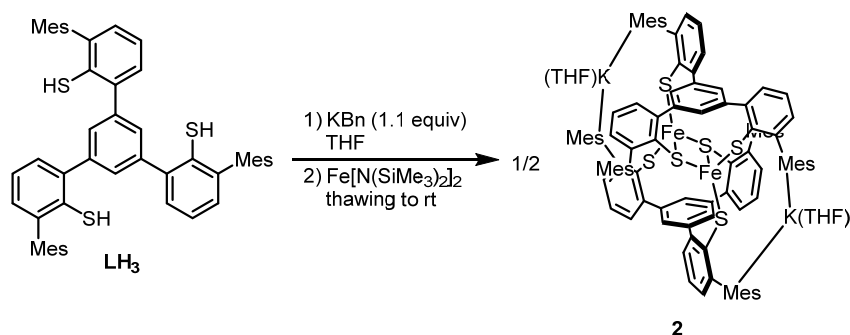


1,3,5-tris(3'-mesityl-2'-thiophenyl)benzene (LH₃). Mesitylmagnesium bromide was prepared by addition of 2-bromomesitylene (4.25 mL, 27.7 mmol) to a stirred THF suspension (30 mL) of magnesium turnings (1.35 g, 55.5 mmol), pre-activated by warming with 1,2-dibromoethane (~0.1 mL), in THF (30 mL) with gentle heating to initiate Grignard formation. The reaction was then warmed to reflux for 2 h yielding a pale brown solution. To a stirred solution of 1,3,5-tris(2'-fluorophenyl)benzene (2.00 g, 5.55 mmol) in THF (40 mL) at –78 °C

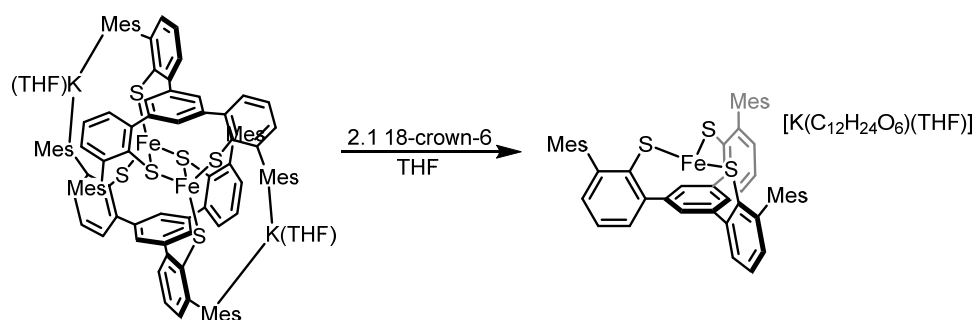
was added dropwise a cyclohexane solution of $^s\text{BuLi}$ (13.0 mL, 1.4 M, 19.6 mmol). The reaction was allowed to stir at $-78\text{ }^\circ\text{C}$ for 20 min. The mesitylmagnesium bromide solution prepared earlier was then added dropwise to the reaction at $-78\text{ }^\circ\text{C}$. After complete addition, the reaction was allowed to warm to room temperature and then heated to reflux for 3 h. The flask was then cool back to $-78\text{ }^\circ\text{C}$, and sulfur powder (2.13 g, 66.4 mmol) was added in one portion. The reaction was allowed to warm to room temperature and stirred for 30 min then cooled to $0\text{ }^\circ\text{C}$. LiAlH_4 (2.11 g, 55.5 mmol) was added slowly as a solid (caution: effervescence) and the reaction was warmed to room temperature and stirred an additional 3 h. The flask was cooled to $0\text{ }^\circ\text{C}$ again and concentrated aqueous HCl was added dropwise (caution: effervescence) until a grey precipitate was observed to form and settle and the pH was *ca.* 2. NaCl (*ca.* 25 g) and hexanes (50 mL) was added and stirred vigorously. The orange-brown supernatant was decanted and the residue extracted with CH_2Cl_2 ($2 \times 100\text{ mL}$). The supernatant and extracts were combined and dried over MgSO_4 , filtered, and concentrated *in vacuo* to yield a dark brown oil. Kugelrohr distillation to remove residual MesSH followed by purification by silica gel column chromatography (2% EtOAc :hexanes) provide **LH₃** as a white solid (0.96 g, 23%) $^1\text{H NMR}$ (300 MHz, CDCl_3): δ 7.59 (s, 3H, central *ArH*), 7.34 (dd, $J = 7.6$, 1.6 Hz, 3H, *ArH*), 7.22 (d, $J = 7.5$ Hz, 3H, *ArH*), 7.04 (dd, $J = 7.5$, 1.6 Hz, 3H, *ArH*), 6.98 (s, 6H, *MesH*), 3.39 (s, 3H, *SH*), 2.34 (s, 9H, *ArCH₃*), 2.03 (s, 18H, *ArCH₃*).



Synthesis of 1. To a solution of **LH₃** (30.0 mg) in THF (3 mL) was added KBn (10.3 mg) as a solid. The mixture was allowed to stir for 10 min before being added to a suspension of FeCl₂ (5.0 mg) in THF (2 mL) and stirred for 1 hour. The volatiles were removed in vacuo to yield **1** as a yellow solid.



Synthesis of 2. To a solution of **LH₃** (200 mg) in THF (10 mL) was added KBn (68.7 mg) as a solid. The mixture was allowed to stir for 10 min before being frozen in the cold well. This was then added thawing, to a thawing solution of Fe[N(SiMe₃)₂] in THF (10 mL). The reaction was allowed to warm to room temperature and stirred for 2 h forming an orange suspension. Pentane (50 mL) was added and the suspension filtered, washed with additional pentane, and dried in vacuo to yield **2** (180 mg).



Synthesis of 3. To a thawing solution of **2** in THF was added a THF solution of 18-crown-6 (2.1 equiv.). The reaction was allowed to warm to room temperature and stirred an additional 1 h. Removal of volatiles in vacuo provided **3** as an orange solid.

REFERENCES

- (1) Speelman, A. L.; Holland, P. L., Sulfur-Supported Iron Complexes for Understanding N₂ Reduction. In *Nitrogen Fixation*, Nishibayashi, Y., Ed. Springer International Publishing: Cham, 2017; pp 197-213.
- (2) Einsle, O.; Tezcan, F. A.; Andrade, S. L. A.; Schmid, B.; Yoshida, M.; Howard, J. B.; Rees, D. C., *Science* **2002**, *297*, 1696.
- (3) Spatzal, T.; Aksoyoglu, M.; Zhang, L.; Andrade, S. L. A.; Schleicher, E.; Weber, S.; Rees, D. C.; Einsle, O., *Science* **2011**, *334*, 940.
- (4) Lancaster, K. M.; Roemelt, M.; Ettenhuber, P.; Hu, Y.; Ribbe, M. W.; Neese, F.; Bergmann, U.; DeBeer, S., *Science* **2011**, *334*, 974.
- (5) Burgess, B. K.; Lowe, D. J., *Chem. Rev.* **1996**, *96*, 2983-3012.
- (6) Holland, P. L., *Can. J. Chem.* **2005**, *83*, 296-301.
- (7) Creutz, S. E.; Peters, J. C., *J. Am. Chem. Soc.* **2014**, *136*, 1105-1115.
- (8) Anderson, J. S.; Rittle, J.; Peters, J. C., *Nature* **2013**, *501*, 84.
- (9) Coric, I.; Mercado, B. Q.; Bill, E.; Vinyard, D. J.; Holland, P. L., *Nature* **2015**, *526*, 96-99.
- (10) Kästner, J.; Blöchl, P. E., *J. Am. Chem. Soc.* **2007**, *129*, 2998-3006.
- (11) Schimpl, J.; Petrilli, H. M.; Blöchl, P. E., *J. Am. Chem. Soc.* **2003**, *125*, 15772-15778.
- (12) Feng, X.; Wu, J.; Enkelmann, V.; Müllen, K., *Org. Lett.* **2006**, *8*, 1145-1148.
- (13) Pangborn, A. B.; Giardello, M. A.; Grubbs, R. H.; Rosen, R. K.; Timmers, F. J., *Organometallics* **1996**, *15*, 1518-1520.

Appendix C

**Metal Complexes Supported by 1,9-Anthracenediyl-Linked [O,O]-Pincers
Towards the Coupling of Unsaturated Organic Fragments with CO₂**

ABSTRACT

Reported herein is reactivity of coupling of alkynes with CO₂ on a zirconium complex supported by a non-innocent 9,10-anthracenediyl-linked *bis*(phenoxide). Depending on the bulk of the alkyne, either 5-membered or 7-membered zirconalactones can be synthesized. Additionally, we have demonstrated that this *bis*(phenoxide) ligand framework is also capable of supporting vanadium (III) complexes, on route to either targeting cationic complexes upon protonolysis or halide abstraction, or reduced to neutral V(II) complexes. The synthesis of a monoanionic variant of ligand featuring an ethereal donor one arm has also been accomplished and metalation studies on zirconium are also reported.

GENERAL INTRODUCTION

In Chapters 4 and 5, it was demonstrated that zirconium complex **1** supported by a 1,9-anthracenediyl-linked *bis*(phenoxide) ligand was capable in coupling a variety of unsaturated organic molecules such as nitriles with alkynes, and alkynes with carbon monoxide (CO). We hypothesized that this chemistry may be extended to coupling of other unsaturated heteroatom-containing small molecules, and with carbon dioxide (CO₂) or CO. Previous reports by the Kawaguchi group, have shown that structurally similar phenylene-linked *bis*(phenoxide) zirconium complexes are reactive towards CO₂ and CS₂,¹ although catalytic turnover of the products of these reactions was not reported. The use of CO₂ as a C₁ feedstock is attractive as it is abundant, renewable and nontoxic.²⁻³ However, due to its high thermodynamic and kinetic stability, the facile incorporation of CO₂ into organic molecules has remained a challenge.⁴⁻⁸ Strategies to overcome that stability include the use of high pressures, high temperatures, harsh conditions such as alkyllithiums and Grignard reagents, or a combination of the above. Although early transition metal complexes have been studied for CO₂ activation, the high metal oxophilicity renders most of these systems stoichiometric.⁹

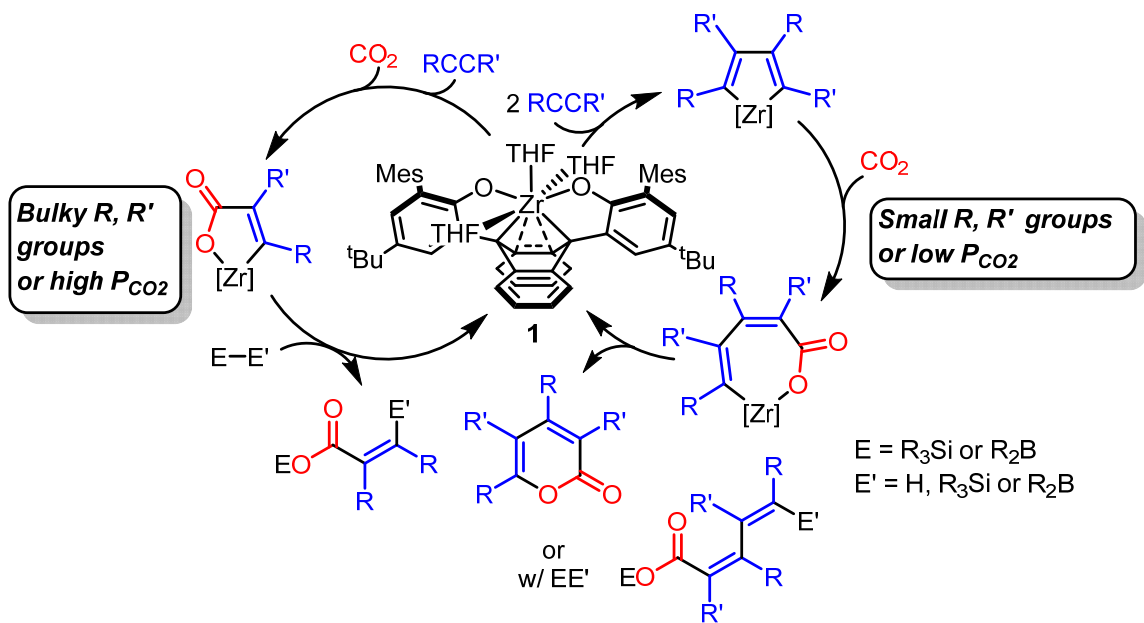
Based off of the chemistry that has been developed on the zirconium *bis*(phenoxide) system, the synthesis of vanadium complexes on the *bis*(phenoxide) ligand was of interest in order to access complexes of difference oxidation states and overall charge. This may allow for novel reactivity to be uncovered in terms of either making the complex more reactivity towards unsaturated substrates (in the case of a cationic complex) or facilitating reductive elimination of the metallocycle formed upon coupling (in the case of an anionic complex). In the same vein, ligand modifications to target a monoanionic variant are also of interest. With Group IV metals, cationic complexes can

be targeted. In the presence of the more electron-deficient metal center, enhanced reactivity towards less reactive unsaturated olefins may be viable towards oligomerization and/or polymerization, which has not been observed with the *bis*(phenoxide) complexes.

RESULTS AND DISCUSSION

The coupling of alkynes with CO₂ was investigated. Such a transformation can offer a rapid and atom-efficient route towards (Scheme C.1). Acrylates and their substituted variants are highly valued commodity chemicals for their wide use as monomers in the manufacture of plastics, coatings, adhesives, and paints.¹⁰ Current methods of synthesis typically involve either the esterification of the analogous acid,¹¹ which is derived from the two-stage oxidation of the olefin precursor, or carbalkoxylation of acetylene in the presence of CO and alcohol in the Reppe process.¹²⁻¹³ The carboxylation of alkynes, rather than olefins,¹⁴⁻¹⁷ provides the opportunity for further functionalization of the organic fragment, but remains relatively underexplored, with many prior reports employing protic sources for product release.¹⁸⁻²¹ Additionally, the use of CO₂ offers the benefit of a nontoxic alternative to functionalization by CO. Previous examples of early metal mediated coupling of CO₂ and alkynes to obtain substituted α,β -unsaturated carboxylic acids are not catalytic.^{9, 22} An alternative coupling pathway for

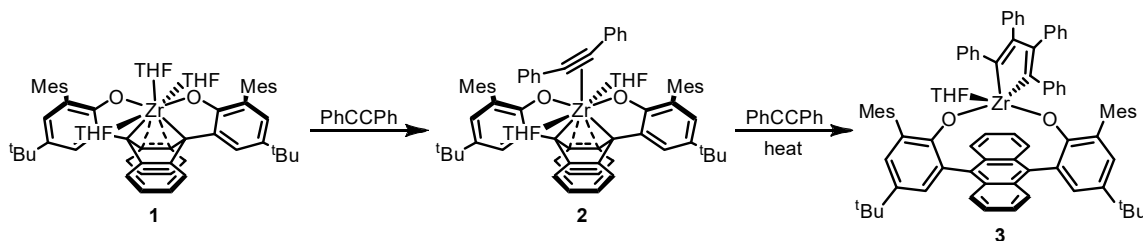
Scheme C.1. Proposed Zr-catalyzed coupling of alkynes with CO₂



alkynes and CO₂ results in the synthesis of 2-pyrones, a common motif in natural products,²³⁻²⁶ a versatile precursor in organic synthesis,²⁷⁻³¹ and a monomer for biodegradable polymer synthesis.³²⁻³³ Despite significant progress in the metal-catalyzed synthesis of 2-pyrones,³⁴⁻³⁶ the use of the atom-economical [2+2+2] cycloaddition route, with CO₂ and alkynes as feedstocks, has been less explored.³⁷⁻⁴⁰

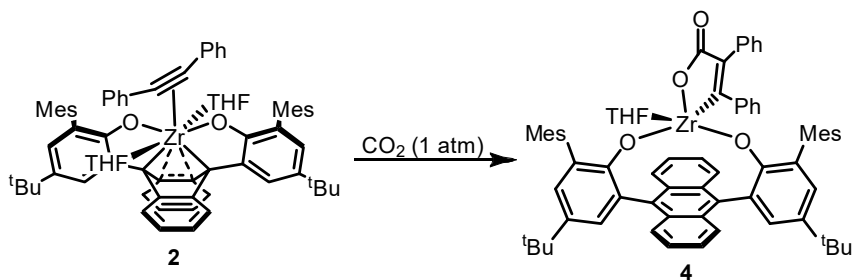
The reaction of **1** under one atmosphere of CO₂ in the absence of alkyne resulted in the formation of a complex mixture of products by ¹H NMR spectroscopy, further heating of that mixture mainly led to significant decomposition to an intractable mixture. Towards targeting the 5-membered metallalactone by the coupling of a single molecule of alkyne and CO₂, use of internal alkyne diphenylacetylene was selected. Based on previous observation, the reaction of **1** with the bulkier diphenylacetylene at room temperature leads to the initial formation of a 1:1 Zr:alkyne adduct **2**, with the tetraphenyl zirconacyclopentadiene complex **3** only forming on heating in the presence of additional alkyne (Scheme C.2).

Scheme C.2. Stepwise reaction of **1** with diphenylacetylene



Placing in-situ formed **2** under one atmosphere of CO₂ resulted in the formation of a new major species **4** by ¹H NMR spectroscopy (Scheme C.3). Three distinct 1:1:1 singlets were observed in the mesityl methyl region, suggesting the formation of a species lacking front-back symmetry. No zirconacyclopentadiene **3** was observed from the NMR. Group 4 metallalactones have been reported and are proposed to form through CO₂

Scheme C.3. Reactivity of **2** with CO₂



insertion into an η^2 -alkyne complex.^{9, 41-45} Recrystallization of **4** by vapor diffusion of pentane into a saturated benzene solution provided yellow crystals suitable for single crystal X-ray diffraction (XRD). The solid-state structure revealed the identity of complex **4** to be the targeted unsaturated zirconalactone formed from the coupling of diphenylacetylene with CO₂ (Figure C.1). The CO₂ motif is inserted *trans* to the THF ligand, potentially through the displacement of the other THF ligand present. The short C2A–C3A distance (1.356(2) Å) is consistent with a carbon-carbon double bond.

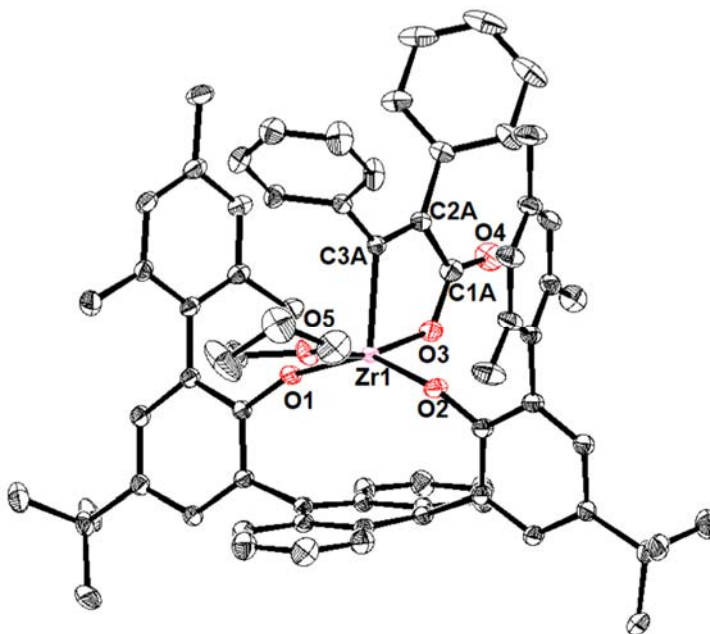
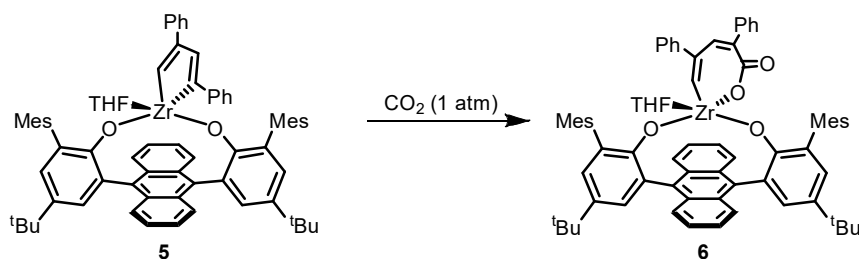


Figure C.1. Solid-state structure of **4**. Thermal ellipsoids shown at 50% probability. Solvent molecules and hydrogen atoms omitted for clarity; relevant bond distances (Å): O3 – C1A: 1.335 (3), C1A – C2A: 1.512 (3), C2A – C3A: 1.356 (2), C1A – O4: 1.207(3).

To allow for catalytic turnover, removal of the organic fragment from the metal center in a reductive fashion was targeted. Given the strength of Zr–O bonds (~ 180 kcal mol⁻¹),⁴⁶ this step will likely be the most challenging aspect of the proposed catalytic cycle. It is anticipated that a combination of strong O–E bond (E = Si or B, ~ 191 and 193 kcal mol⁻¹, respectively) and propensity for reductive elimination due to the presence of the pendant anthracene will drive the reaction toward the release of acrylate. A variety of silanes and disilanes (Et₃SiH, Ph₂SiH₂, PhSiH₃, Me₃SiSiMe₃) were initially tested. No reaction was observed with all these reagents after extended heating at 90 °C. Further increasing the reaction temperature to 140 °C in *m*-xylene resulted in decomposition to free ligand. No desired silicon-containing organic fragments were detected via GC-MS. Borane 9-borabicyclo(3.3.1)nonane (9-BBN) and diborane *bis*(catecholato)diboron (B₂cat₂) resulted in the formation of intractable mixtures, with no desired products detected by GC-MS.

The synthesis of a 7-membered metallalactone complex was also targeted as a route towards 2-pyrones and longer chain acrylates (Scheme C.1). Additionally, it was postulated that the formation of a 7-membered metallocycle may facilitate product release and due to its less favorable ring size compared to **4**. The reaction of tetraphenyl zirconacyclopentadiene complex **3** with CO₂ was tested. Unfortunately, heating a benzene solution of **3** at 90 °C in the presence of one atmosphere of CO₂ overnight did not lead to any appreciable change in the ¹H NMR spectrum. The use of harsher conditions, such as higher temperature or higher CO₂ pressures, however, have not been pursued. In contrast, the reaction of zirconacyclopentadiene complex **5**, afforded from the coupling of two equiv. of the less bulky phenylacetylene, with one atmosphere CO₂ at room temperature resulted in the formation of a new major species **6** based on ¹H NMR

Scheme C.4. Reactivity of **5** with CO₂



spectroscopy (Scheme C.4). Although attempts to characterize this species in the solid-state has thus far been unsuccessful, infrared (IR) spectroscopy showed the presence of an absorption at 1662 cm⁻¹, consistent with a C=O stretch of a carboxylate (Figure C.2).⁴³ This evidence, along with that from the ¹H NMR spectrum led to assign **6** as a

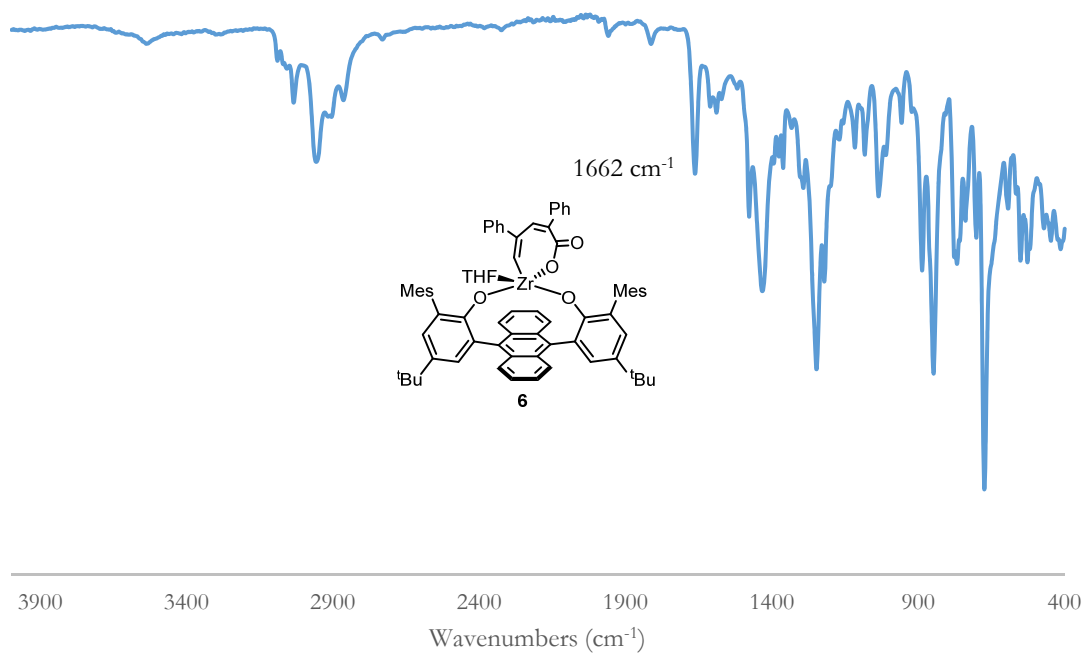


Figure C.2. IR spectra of **6**

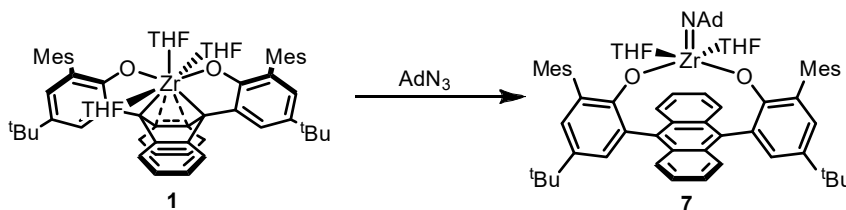
zirconolactone complex that we had set out to target.

Product release from complex **6** by reductive elimination to provide diphenyl substituted 2-pyrone was investigated. Heating of **6** to 90°C, unfortunately, led to the

formation of a complex mixture by ^1H NMR spectroscopy with some **6** still present after one hour. Gas chromatography-mass spectrometry (GC-MS) analysis of the mixture did not detect the presence of the desired 2-pyrone product. Instead, diphenylbutadiene was detected suggesting CO_2 deinsertion had occurred prior to or upon decomposition. Carrying out the reaction in the presence of an excess of both alkyne and CO_2 did not lead to the significant formation of any coupled species by GC-MS analysis. Photolysis of **6** led to the formation of broad intractable peaks by ^1H NMR with only phenylacetylene detected by GC-MS analysis. Silanes (Ph_2SiH_2 , PhSiH_3 , $\text{Me}_3\text{SiSiMe}_3$) and boranes (9-BBN, B_2cat_2) were investigated towards engendering product functionalization and release. In all cases, no significant reaction was observed at room temperature, but subsequent heating led to the formation of a complex mixture resembling that observed heating **6** by itself. By GC-MS, in the case with silanes or (di)boranes, some hydrosilylated or hydroborylated/diborylated products of phenylacetylene and its dimer were observed.

Targeting the synthesis of other heterocycles such as pyrroles,⁴⁷ the use of organic azides were explored. The reaction of **1** with 1 equiv. of 1-azidoadamantane (AdN_3) resulted in the evolution of a gas (most likely N_2) and the formation of a new species **7** that we assign to an imido complex (Scheme C.5). Addition of 2 equiv. of phenylacetylene to the formation of a new asymmetric species and does not significantly change after extended heating at $90\text{ }^\circ\text{C}$. However, by GC-MS, no pyrrole product was detected. Instead, predominantly phenylacetylene and adamantylamine were observed. The reaction

Scheme C.5. Reactivity of **1** with AdN_3



of AdN_3 with **5** only led to decomposition to an intractable mixture upon extended heating.

The synthesis of vanadium complexes supported by the anthracenediyl bisphenoxide complexes was also briefly explored (Scheme C.6). Metalation with $\text{VMes}_3(\text{THF})$ in toluene led to the formation of a green-brown species **8** displaying broad paramagnetically-shifted peaks in the ^1H NMR spectrum. Recrystallization of this species from slow diffusion of pentane into a saturated benzene solution provided crystals suitable for single crystal XRD. The solid-state structure showed **8** to be a vanadium

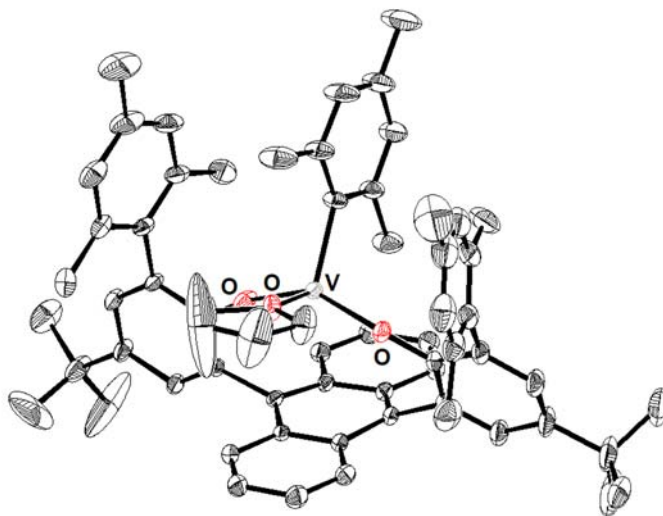
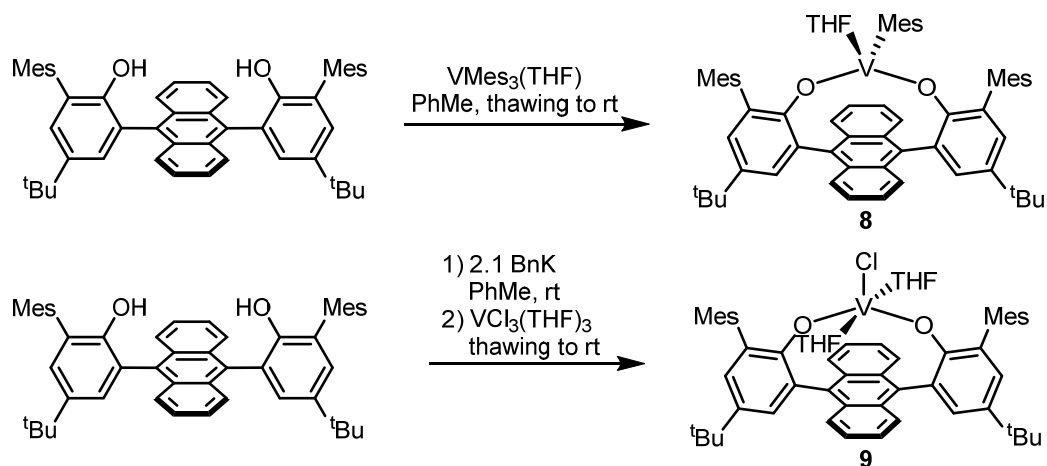


Figure C.3. Solid-state structure of **8**. Thermal ellipsoids shown at 50% probability. Solvent molecules and hydrogen atoms omitted for clarity

mesityl complex supported by the ligand and bound to an additional THF ligand (Figure C.3).

Metalation with $\text{VCl}_3(\text{THF})_3$ was pursued. Initial deprotonation of the *bis*(phenol) ligand with two equiv. potassium benzyl (KBn) in toluene to generate the *bis*(phenoxide) followed by addition to a suspension of $\text{VCl}_3(\text{THF})_3$ in THF provided a brown product **9** (Scheme C.6) that was mostly silent by ^1H NMR spectroscopy, displaying only one small

Scheme C.6. Synthesis of vanadium *bis*(phenoxide) complexes



paramagnetically-shifted peak at around 14 ppm. Single crystals suitable for XRD reveal the structure of **9** to be that shown in Figure C.4. Compared to **8**, an additional THF ligand is bound to the vanadium center, likely due to both the more sterically open and the more electron-poor metal center in **9**.

Protonolysis of **8** by Brookhart's acid or halide abstraction of **9** with silver *tetrakis*[3,5-*bis*(trifluoromethyl)phenyl]borate (AgBARF^{2+}) was attempted to target a cationic complex, but have eluded solid-state characterization. 1-electron reduction of **9**

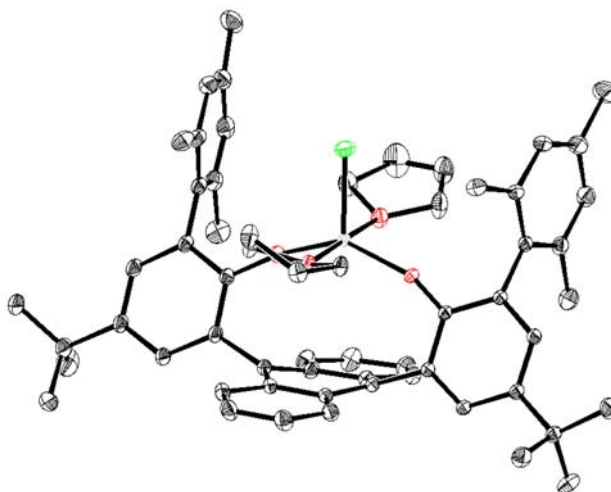
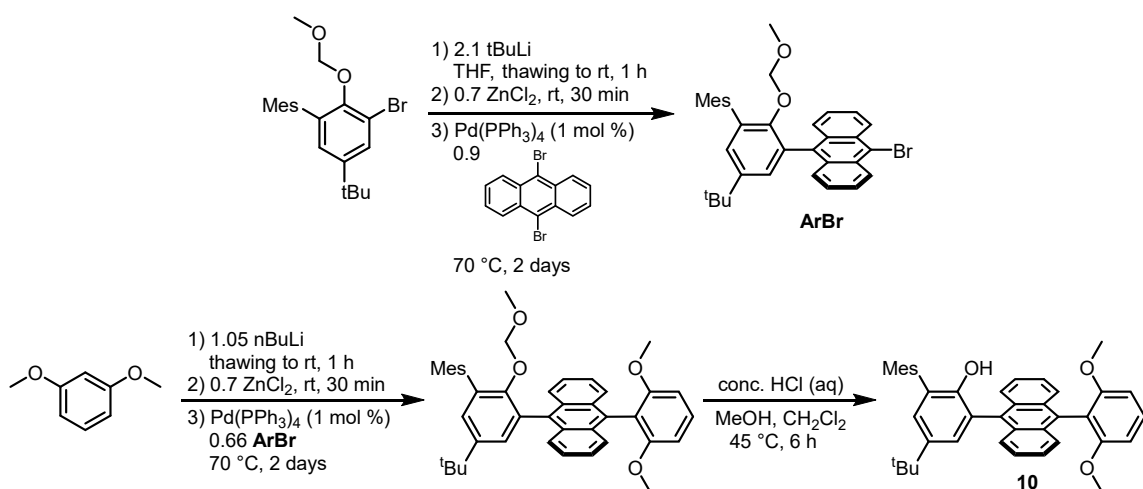


Figure C.4. Solid-state structure of **9**. Thermal ellipsoids shown at 50% probability. Solvent molecules and hydrogen atoms omitted for clarity

has also been attempted, and even though solid-state characterization to determine the structure of this reduced species has not been obtained, it has shown to be active in the coupling of phenylacetylene, with diphenylbutadiene and triphenylbenzene detected by GC-MS. **9**, on the other hand, did not display this reactivity with phenylacetylene.

The synthesis of an anthracenediyl-linked monoanionic ligand featuring a phenoxide donor and an ether donor was targeted (Scheme C.7). The choice to install a 2,6-dimethoxybenzene donor was to avoid the need for separation of syn and anti-

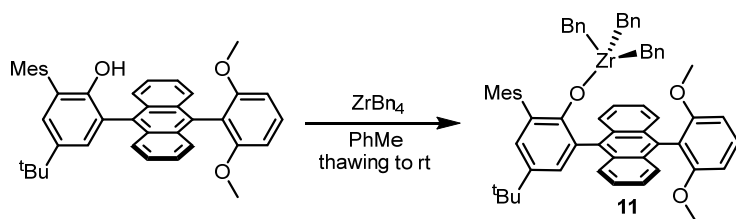
Scheme C.7. Synthesis of monoanionic monophenoxide ligand



isomers. Proligand **10** was synthesized in three steps from the common precursor used for the previously reported *bis*(phenol) proligand synthesis.

Metalation of proligand **10** was carried out by the addition of a thawing toluene solution of **10** to a thawing toluene solution of ZrBn_4 (Scheme C.8) then warmed to room temperature and stirred for an additional two hours. From the ^1H NMR spectrum, a new

Scheme C.8. Synthesis of **11**



species **11** was observed, with the loss of phenolic proton alongside the presence of a chemical resonance at 0.93 ppm that integrates to 6 protons, and is consistent with the chemical shift of the methylene protons on a zirconium-benzyl motif, suggesting that three benzyl groups are present in this new species. Solid-state characterization of **11** confirmed our initial assignment. Complex **11** has a phenoxide-bound zirconium center with three benzyl groups bound in a tetrahedral geometry (Figure C.5). No significant

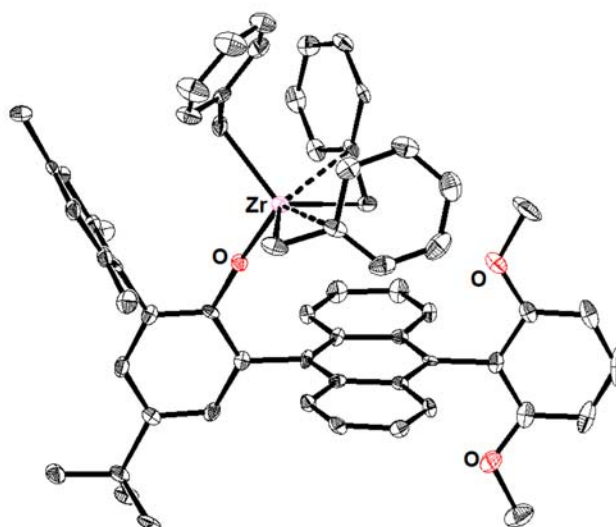


Figure C.5. Solid-state structure of **11**. Thermal ellipsoids shown at 50% probability. Solvent molecules and hydrogen atoms omitted for clarity

interaction with the ether groups was present. Further reactivity with **11** has not been explored at this point.

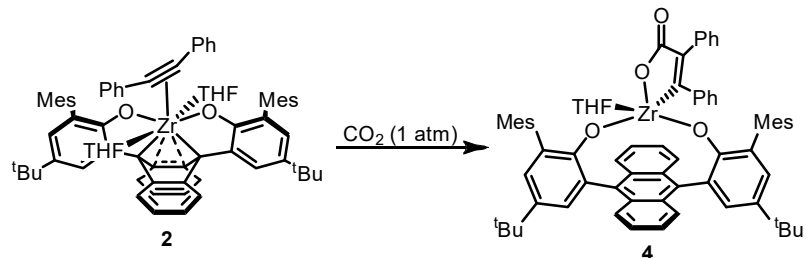
CONCLUSION

The coupling of alkynes with CO₂ is demonstrated on anthracenediyl-link *bis*(phenoxide) zirconium complexes to provide zirconalactone complexes. With bulkier diphenylacetylene, a 5-membered zirconalactone was formed, while with phenylacetylene, a 7-membered zirconalactone is afforded. Various silanes, disilane, borane, and diborane electrophiles have been tested with these lactones in order to engender organic product release but have thus far been unsuccessful. The synthesis of vanadium (III) complexes supported on this *bis*(phenoxide) ligand has also been achieved and characterized. Attempted protonolysis of mesityl complex **8** or halide abstraction of chloride **9** led to paramagnetic species which have eluded solid-state characterization. The synthesis of a monophenol proligand featuring an ether donor has also been synthesized. Metalation with ZrBn₄ provided a *tris*(benzyl) complex **11**.

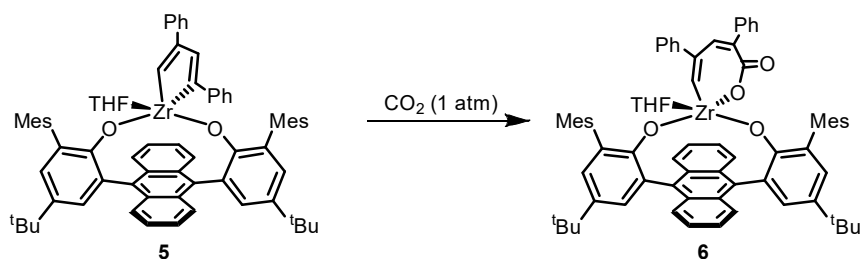
EXPERIMENTAL SECTION

General Considerations

Unless otherwise specified, all operations involving air- or water-sensitive reagents were carried out in an MBraun drybox under a nitrogen atmosphere or using standard Schlenk and vacuum line techniques. Solvents for air- and moisture-sensitive reactions were dried by the method of Grubbs.⁴⁸ Deuterated solvents were purchased from Cambridge Isotope Laboratories and C₆D₆ vacuum transferred from sodium benzophenone ketyl before use. All solvents, once dried and degassed, were stored under a nitrogen atmosphere over 4 Å molecular sieves. **1**,⁴⁹ **3**,⁴⁹ and **5**,⁴⁹ *syn*-3,3''-(anthracene-9,10-diyl)bis(5-(*tert*-butyl)-2',4',6'-trimethyl-[1,1'-biphenyl]-2-ol),⁴⁹ V(Mes)₃(THF),⁵⁰ 3-bromo-5-(*tert*-butyl)-2-(methoxymethoxy)-2',4',6'-trimethyl-1,1'-biphenyl,⁴⁹ tetrabenzylzirconium,⁵¹ were prepared according to literature procedures. Alkynes and nitriles used were either sublimed under reduced pressure or distilled from calcium hydride before use. All other reagents were used as received. ¹H, ¹³C{¹H}, and ¹⁹F NMR spectra were recorded on Varian Mercury 300 MHz or Varian 400 MHz spectrometers at ambient temperatures unless otherwise denoted. ¹H and ¹³C{¹H} NMR spectra are reported referenced internally to residual solvent peaks reported relative to tetramethylsilane. Fast atom bombardment-mass spectrometry (FAB-MS) analyses were performed with a JEOL JMS-600H high-resolution mass spectrometer. Gas chromatography-mass spectrometry (GC-MS) were performed with on an Agilent 6890A instrument using an HP-5MS column (30 m length, 0.25 mm diameter, 0.50 μm film) and an Agilent 5973N mass-selective EI detector. Photolyses were conducted using an Oriol Instruments arc lamp housing and an Osram 75 W Xe arc lamp set to a current of 5.4 A.

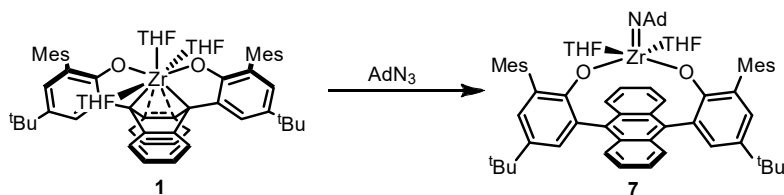


Synthesis of 4. A J-Young tube was charged with **1** (20 mg) and phenylacetylene (3.5 mg, 1 equiv.) and allowed to mix for overnight for form **2**. The tube was then degassed by 2 freeze-pump-thaw cycles and CO₂ (1 atm) was introduced and stirred for 2 hours at room temperature. Remove of volatiles yielded complex **6** as a yellow-orange solid. ¹H NMR (300 MHz, C₆D₆): δ 8.12 (dd, *J* = 6.7, 3.3 Hz, 2H), 8.06 (dd, *J* = 6.8, 3.3 Hz, 2H), 7.93 (d, *J* = 2.5 Hz, 2H), 7.55 – 7.50 (m, 1H), 7.44 – 7.37 (m, 4H), 7.29 – 6.56 (m, 10H), 5.44 (dd, *J* = 8.2, 1.4 Hz, 2H), 2.64 – 2.56 (m, 4H), 2.45 (s, 6H), 2.18 (s, 6H), 2.05 (s, 6H), 1.43 (s, 18H), 0.40 – 0.31 (m, 4H).

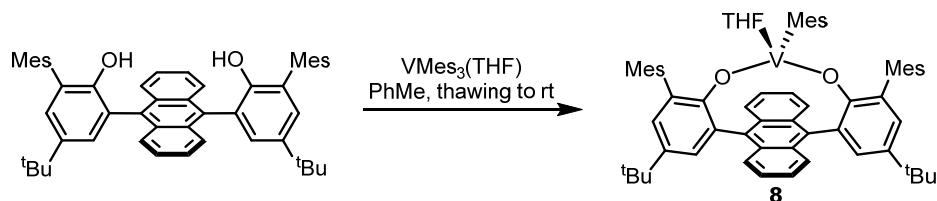


Synthesis of 6. A J-Young tube was charged with **1** (20 mg) and phenylacetylene (4.3 μL, 2 equiv.) and allowed to mix for 10 min. The tube was then degassed by 2 freeze-pump-thaw cycles and CO₂ (1 atm) was introduced and stirred for 1 hour at room temperature. Remove of volatiles yielded complex **6** as an orange solid. ¹H NMR (300 MHz, C₆D₆): δ 8.23 (dd, *J* = 6.8, 3.2 Hz, 2H), 8.11 (dd, *J* = 6.8, 3.3 Hz, 2H), 7.96 (d, *J* = 2.6 Hz, 2H), 7.80 (dd, *J* = 6.8, 3.2 Hz, 2H), 7.32 (d, *J* = 2.6 Hz, 2H), 7.25 – 7.20 (m, 2H), 7.02 – 6.97 (m, 3H), 6.95 – 6.72 (m, 10H), 6.43 (d, *J* = 0.8 Hz, 1H), 6.34 (d, *J* = 0.8 Hz, 1H), 5.63 –

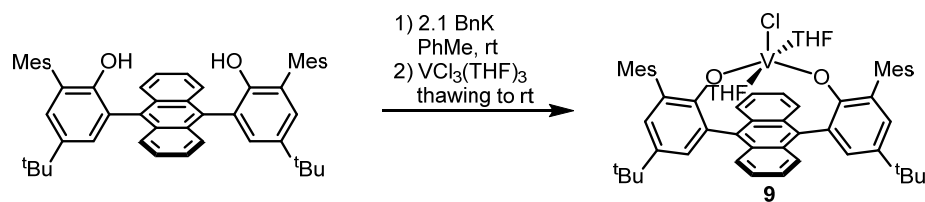
5.57 (m, 2H), 2.70 – 2.59 (m, 4H), 2.38 (s, 6H), 2.08 (s, 6H), 2.06 (s, 6H), 1.41 (s, 18H), 0.46 – 0.35 (m, 4H).



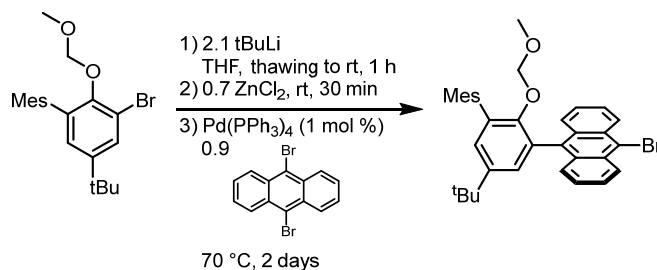
Synthesis of 7. To a solution of **1** (20 mg) in benzene (2 mL) was added 1-azidoadamantane (1 equiv.). The reaction was allowed to stir for 10 minutes and volatiles were removed in vacuo to yield **7** ^1H NMR (300 MHz, C_6D_6): δ 8.11 (dd, $J = 6.7, 3.2$ Hz, 4H), 7.93 (d, $J = 2.7$ Hz, 2H), 7.36 (d, $J = 2.7$ Hz, 2H), 7.14 – 6.92 (m, 8H), 3.26 – 3.18 (m, 8H), 2.24 (s, 6H), 2.24 (s, 12H) 1.60 – 1.52 (m, 3H), 1.45 (s, 18H), 1.43 – 1.31 (m, 6H), 1.11 – 1.06 (m, 8H), 0.92 (d, $J = 2.8$ Hz, 6H).



Synthesis of 8. A vial charged with a Teflon-coated stir bar and *syn*-3,3''-(anthracene-9,10-diyl)bis(5-(*tert*-butyl)-2',4',6'-trimethyl-[1,1'-biphenyl]-2-ol) (50.0 mg) in THF (1 mL) was frozen in the cold well in a glove box. Allowing to warm till thawing, a solution of $\text{V}(\text{Mes})_3(\text{THF})$ (33.7 mg, 1equiv.) in THF (5 mL) was added slowly. The reaction was allowed to warm to room temperature stirring for an additional 2 h turning into a green-brown color. After removal of the volatiles under vacuum, the residue was triturated with hexanes. The residue was extracted with benzene and dried in vacuo to yield **8**.

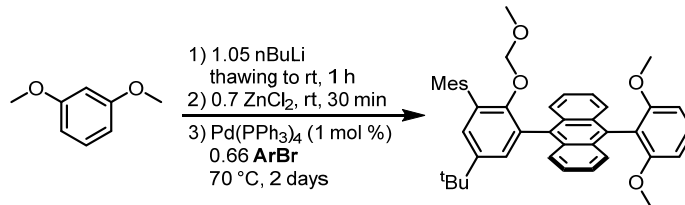


Synthesis of 9. To a vial charged with a Teflon-coated stir bar and *syn*-3,3''-(anthracene-9,10-diyl)bis(5-(*tert*-butyl)-2',4',6'-trimethyl-[1,1'-biphenyl]-2-ol) (50.0 mg) in toluene (2 mL) was added a suspension of KBn (19.2 mg, 2.1 equiv.) in toluene, resulting in the formation of a bright yellow solution that slowly turned dark brown. That solution was frozen and then added as a thawing solution to a thawing suspension of $VCl_3(THF)_3$ (26.1 mg, 1 equiv.) and allowed to warm to room temperature and stirred 2 h. After removal of the volatiles under vacuum, the residue was triturated with hexanes. The resulting solid was extracted with benzene and dried in vacuo to yield yellow-brown **9**.



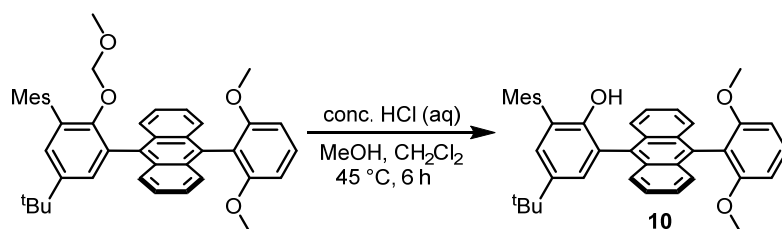
9-bromo-10-(5-(*tert*-butyl)-2-(methoxymethoxy)-2',4',6'-trimethyl-[1,1'-biphenyl]-3-yl)anthracene. A Schlenk flask fitted with a screw-in Teflon stopper was charged with a solution of 3-bromo-5-(*tert*-butyl)-2-(methoxymethoxy)-2',4',6'-trimethyl-1,1'-biphenyl (5.0 g) in THF (50 mL) and cooled to -78 °C. A pentane solution of *tert*-butyllithium (14.2 mL, 1.9 M) was added dropwise via cannula. The reaction was allowed to warm to room temperature and stirred for 1 h forming a dark orange solution. The reaction was then brought into an N_2 -purged and $ZnCl_2$ (1.22 g) was added slowly to the reaction, resulting in the formation of a cloudy pale yellow mixture. The reaction was allowed to

stir at room temperature for 30 min after which 9,10-dibromoanthracene (3.86 g) and Pd(PPh₃)₄ (148 mg) were added. The flask was sealed and warmed to 70 °C for 48 h. After cooling to room temperature, water (5 mL) was added to quench the reaction, and the mixture concentrated in vacuo to about 15 mL. The resulting suspension was taken up in CH₂Cl₂ (50 mL) and filtered through a silica gel plug, eluting further with CH₂Cl₂. The filtrate was then washed with water (2 × 50 mL), dried over MgSO₄, filtered, and concentrated in vacuo to afford the crude product as a sticky yellow solid which was triturated in MeOH (80 mL) with aid of sonication, filtered, and dried in vacuo to provide the product as a pale yellow powder (5.92 g). ¹H NMR (300 MHz, CDCl₃): δ 8.64 – 8.59 (m, 2H), 7.81 – 7.75 (m, 2H), 7.65 – 7.58 (m, 2H), 7.45 (ddd, *J* = 8.8, 6.5, 1.2 Hz, 2H), 7.35 (dd, *J* = 2.6, 0.6 Hz, 1H), 7.30 (dt, *J* = 2.6, 0.6 Hz, 1H), 6.98 (s, 2H), 4.00 (s, 2H), 2.33 (s, 3H), 2.26 (s, 6H), 1.97 (s, 3H), 1.35 (s, 9H).



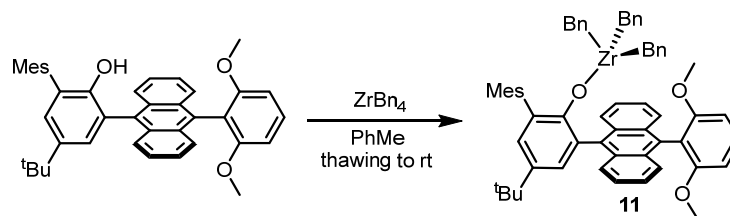
9-(5-(*tert*-butyl)-2-(methoxymethoxy)-2',4',6'-trimethyl-[1,1'-biphenyl]-3-yl)-10-(2,6-dimethoxyphenyl)anthracene. A Schlenk flask fitted with a screw-in Teflon stopper was charged with a solution of 1,3-dimethoxybenzene (0.70 mL) in THF (20 mL) and cooled to –78 °C. A hexanes solution of *n*-butyllithium (2.2 mL, 2.5 M) was added dropwise via syringe. The reaction was allowed to warm to room temperature and stirred for 1 h. The reaction was then brought into an N₂-purged and ZnCl₂ (511 mg) was added slowly to the reaction resulting in the formation of a cloudy pale yellow mixture. The reaction was allowed to stir at room temperature for 30 min after which 9-bromo-10-(5-(*tert*-butyl)-2-(methoxymethoxy)-2',4',6'-trimethyl-[1,1'-biphenyl]-3-yl)anthracene (2.0 g)

and Pd(PPh₃)₄ (45 mg) was added. The flask was sealed and warmed to 70 °C for 48 h. After cooling to room temperature, water (2 mL) was added to quench the reaction, and the mixture concentrated in vacuo to about 5 mL. The resulting suspension was taken up in CH₂Cl₂ (15 mL) and filtered through a silica gel plug, eluting further with CH₂Cl₂. The filtrate was then washed with water (2 × 15 mL), dried over MgSO₄, filtered, and concentrated in vacuo to afford the crude product which was purified via silica gel column chromatography as a pale yellow powder (1.8 g). ¹H NMR (300 MHz, CDCl₃): δ 7.78 (ddd, *J* = 8.7, 1.5, 0.8 Hz, 2H), 7.61 (ddd, *J* = 8.4, 1.6, 0.7 Hz, 2H), 7.49 – 7.46 (m, 1H), 7.41 – 7.27 (m, 5H), 6.96 (q, *J* = 0.7 Hz, 2H), 6.81 (ddd, *J* = 19.2, 8.4, 0.8 Hz, 2H), 4.04 (s, 2H), 3.64 (s, 3H), 3.44 (s, 3H), 2.32 (s, 3H), 2.26 (s, 6H), 1.82 (s, 3H), 1.37 (s, 9H).



Synthesis of 10. A Schlenk flask fitted with a screw-in Teflon stopper was charged with 9-(5-(*tert*-butyl)-2-(methoxymethoxy)-2',4',6'-trimethyl-[1,1'-biphenyl]-3-yl)-10-(2,6-dimethoxyphenyl)anthracene (1.8 g, 18.8 mmol), MeOH (50 mL) and CH₂Cl₂ (10 mL). Concentrated aqueous HCl (5 mL) was added, the flask sealed and heated to 45 °C, monitoring the progress of the reaction via ¹H NMR spectroscopy. After complete deprotection, about 6 h, the reaction was cooled and concentrated in vacuo. The suspension was taken up in CH₂Cl₂ (250 mL) and washed with H₂O (2 × 200 mL) and then saturated aqueous NaHCO₃ (100 mL). The organic fraction was dried over MgSO₄, filtered, and concentrated under reduced pressure to provide the product as a pale yellow solid (1.55 g, 93%). ¹H NMR (300 MHz, C₆D₆): δ 8.14 – 7.95 (m, 4H), 7.32 (t, *J* = 8.4 Hz,

1H), 7.28 (d, $J = 2.5$ Hz, 1H), 7.25 (d, $J = 2.5$ Hz, 1H), 7.25 – 7.08 (m, 5H). 6.82 (q, $J = 0.8$ Hz, 2H), 6.50 (dq, $J = 8.5, 0.9$ Hz, 2H), 4.31 (s, 1H), 3.00 (s, 3H), 2.96 (s, 3H), 2.23 (s, 6H), 2.12 (s, 3H), 1.16 (s, 9H).



Synthesis of 11. A vial charged with a Teflon-coated stir bar and **10** (50.0 mg) in toluene (1 mL) was frozen in the cold well in a glove box. Allowing to warm till thawing, it was added to a thawing solution of $ZrBn_4$ (33.7 mg, 1equiv.) in toluene (3 mL). The reaction was allowed to warm to room temperature stirring for an additional 2 h. After removal of the volatiles under vacuum, the residue was extracted with benzene and dried in vacuo to yield **11**. Recrystallized from toluene/pentane vapor diffusion in the freezer. 1H NMR (300 MHz, C_6D_6): δ 8.22 (d, $J = 8.7$ Hz, 2H), 7.93 (d, $J = 8.7$ Hz, 2H), 7.38 – 7.14 (m, 6H), 6.94 (s, 2H), 6.84 – 6.66 (m, 8H), 6.46 (d, $J = 8.4$ Hz, 2H), 5.80 (d, $J = 7.0$ Hz, 6H), 2.98 (s, 3H), 2.95 (s, 3H), 2.44 (s, 6H), 2.18 (s, 3H), 1.18 (s, 9H), 0.88 (s, 6H).

REFERENCES

- (1) Watanabe, T.; Ishida, Y.; Matsuo, T.; Kawaguchi, H., *Dalton Trans.* **2010**, *39*, 484-491.
- (2) Appel, A. M.; Bercaw, J. E.; Bocarsly, A. B.; Dobbek, H.; DuBois, D. L.; Dupuis, M.; Ferry, J. G.; Fujita, E.; Hille, R.; Kenis, P. J. A.; Kerfeld, C. A.; Morris, R. H.; Peden, C. H. F.; Portis, A. R.; Ragsdale, S. W.; Rauchfuss, T. B.; Reek, J. N. H.; Seefeldt, L. C.; Thauer, R. K.; Waldrop, G. L., *Chem. Rev.* **2013**, *113*, 6621-6658.
- (3) Aresta, M., *Carbon Dioxide as Chemical Feedstock*. John Wiley & Sons: 2010.
- (4) Yu, D.; Teong, S. P.; Zhang, Y., *Coord. Chem. Rev.* **2015**, *293*, 279-291.
- (5) Tsuji, Y.; Fujihara, T., *Chem. Commun.* **2012**, *48*, 9956-9964.
- (6) Liu, Q.; Wu, L.; Jackstell, R.; Beller, M., *Nat. Commun.* **2015**, *6*, 5933.
- (7) Pinaka, A.; Vougioukalakis, G. C., *Coord. Chem. Rev.* **2015**, *288*, 69-97.
- (8) Yeung, C. S.; Dong, V. M., *Top. Catal.* **2014**, *57*, 1342-1350.
- (9) Yamashita, K.; Chatani, N., *Synlett* **2005**, *2005*, 0919-0922.
- (10) Nagai, K., *Appl. Catal., A* **2001**, *221*, 367-377.
- (11) Ströhlein, G.; Assunção, Y.; Dube, N.; Bardow, A.; Mazzotti, M.; Morbidelli, M., *Chem. Eng. Sci.* **2006**, *61*, 5296-5306.
- (12) Bhattacharyya, S. K.; Bhattacharyya, D. P., *J. Appl. Chem.* **1966**, *16*, 202-205.
- (13) Bhattacharyya, S.; Sen, A., *J. Chem. Technol. Biotechnol.* **1963**, *13*, 498-505.
- (14) Huguet, N.; Jevtovikj, I.; Gordillo, A.; Lejkowski, M. L.; Lindner, R.; Bru, M.; Khalimon, A. Y.; Rominger, F.; Schunk, S. A.; Hofmann, P.; Limbach, M., *Chem. Eur. J.* **2014**, *20*, 16858-16862.
- (15) Lejkowski, M. L.; Lindner, R.; Kageyama, T.; Bódizs, G. É.; Plessow, P. N.; Müller, I. B.; Schäfer, A.; Rominger, F.; Hofmann, P.; Futter, C.; Schunk, S. A.; Limbach, M., *Chem. Eur. J.* **2012**, *18*, 14017-14025.
- (16) Wang, S.; Shao, P.; Chen, C.; Xi, C., *Org. Lett.* **2015**, *17*, 5112-5115.
- (17) Tang, C.-M.; Li, X.-L.; Wang, G.-Y., *Korean J. Chem. Eng.* **2012**, *29*, 1700-1707.
- (18) Saito, N.; Abdullah, I.; Hayashi, K.; Hamada, K.; Koyama, M.; Sato, Y., *Org. Biomol. Chem.* **2016**, *14*, 10080-10089.
- (19) Doi, R.; Abdullah, I.; Taniguchi, T.; Saito, N.; Sato, Y., *Chem. Commun.* **2017**, *53*, 7720-7723.
- (20) Wang, X.; Nakajima, M.; Martin, R., *J. Am. Chem. Soc.* **2015**, *137*, 8924-8927.

- (21) Fujihara, T.; Xu, T.; Semba, K.; Terao, J.; Tsuji, Y., *Angew. Chem. Int. Ed.* **2011**, *50*, 523-527.
- (22) Six, Y., *Eur. J. Org. Chem.* **2003**, *2003*, 1157-1171.
- (23) Goel, A.; Ram, V. J., *Tetrahedron* **2009**, *65*, 7865.
- (24) Turner, S. R.; Strohbach, J. W.; Tommasi, R. A.; Aristoff, P. A.; Johnson, P. D.; Skulnick, H. I.; Dolak, L. A.; Seest, E. P.; Tomich, P. K.; Bohanon, M. J.; Horng, M. M.; Lynn, J. C.; Chong, K. T.; Hinshaw, R. R.; Watenpaugh, K. D.; Janakiraman, M. N.; Thaisrivongs, S., *J. Med. Chem.* **1998**, *41*, 3467.
- (25) Zhang, J.; Jiang, Y.; Cao, Y.; Liu, J.; Zheng, D.; Chen, X.; Han, L.; Jiang, C.; Huang, X., *J. Nat. Prod.* **2013**, *76*, 2126-2130.
- (26) Shin, H. J.; Lee, H.-S.; Lee, J. S.; Shin, J.; Lee, M. A.; Lee, H.-S.; Lee, Y.-J.; Yun, J.; Kang, J. S., *Mar. Drugs* **2014**, *12*, 3283-3291.
- (27) Tam, N. T.; Jung, E.-J.; Cho, C.-G., *Org. Lett.* **2010**, *12*, 2012-2014.
- (28) Sagar, R.; Park, J.; Koh, M.; Park, S. B., *J. Org. Chem.* **2009**, *74*, 2171-2174.
- (29) Nicolaou, K. C.; Yang, Z.; Liu, J. J.; Ueno, H.; Nantermet, P. G.; Guy, R. K.; Claiborne, C. F.; Renaud, J.; Couladouros, E. A.; Paulvannan, K.; Sorensen, E. J., *Nature* **1994**, *367*, 630.
- (30) West, F. G.; Chase, C. E.; Arif, A. M., *J. Org. Chem.* **1993**, *58*, 3794-3795.
- (31) Posner, G. H.; Lee, J. K.; White, M. C.; Hutchings, R. H.; Dai, H.; Kachinski, J. L.; Dolan, P.; Kensler, T. W., *J. Org. Chem.* **1997**, *62*, 3299-3314.
- (32) Michinobu, T.; Hishida, M.; Sato, M.; Katayama, Y.; Masai, E.; Nakamura, M.; Otsuka, Y.; Ohara, S.; Shigehara, K., *Polym. J.* **2007**, *40*, 68.
- (33) Michinobu, T.; Bito, M.; Yamada, Y.; Tanimura, M.; Katayama, Y.; Masai, E.; Nakamura, M.; Otsuka, Y.; Ohara, S.; Shigehara, K., *Polym. J.* **2009**, *41*, 1111.
- (34) Lee, J. S., *Mar. Drugs* **2015**, *13*, 1581-1620.
- (35) Luo, T.; Dai, M.; Zheng, S.-L.; Schreiber, S. L., *Org. Lett.* **2011**, *13*, 2834-2836.
- (36) Manikandan, R.; Jeganmohan, M., *Org. Lett.* **2014**, *16*, 652-655.
- (37) Inoue, Y.; Itoh, Y.; Hashimoto, H., *Chem. Lett.* **1977**, *6*, 855-856.
- (38) Inoue, Y.; Itoh, Y.; Hashimoto, H., *Chem. Lett.* **1978**, *7*, 633-634.
- (39) Tsuda, T.; Morikawa, S.; Sumiya, R.; Saegusa, T., *J. Org. Chem.* **1988**, *53*, 3140-3145.
- (40) Louie, J.; Gibby, J. E.; Farnworth, M. V.; Tekavec, T. N., *J. Am. Chem. Soc.* **2002**, *124*, 15188-15189.

- (41) Pellny, P.-M.; Kirchbauer, F. G.; Burlakov, V. V.; Baumann, W.; Spannenberg, A.; Rosenthal, U., *J. Am. Chem. Soc.* **1999**, *121*, 8313-8323.
- (42) Thomas, D.; Peulecke, N.; Burlakov, V. V.; Baumann, W.; Spannenberg, A.; Kempe, R.; Rosenthal, U., *Eur. J. Inorg. Chem.* **1998**, *1998*, 1495-1502.
- (43) Pellny, P.-M.; Burlakov, V. V.; Baumann, W.; Spannenberg, A.; Rosenthal, U., *Z. Anorg. Allg. Chem.* **1999**, *625*, 910-918.
- (44) Burlakov, V. V.; Yanovsky, A. I.; Struchkov, Y. T.; Rosenthal, U.; Spannenberg, A.; Kempe, R.; Ellert, O. G.; Shur, V. B., *J. Organomet. Chem.* **1997**, *542*, 105-112.
- (45) Podiyanachari, S. K.; Bender, G.; Daniliuc, C. G.; Kehr, G.; Erker, G., *Organometallics* **2014**, *33*, 3481-3488.
- (46) Luo, Y.-R.
- (47) Gilbert, Z. W.; Hue, R. J.; Tonks, I. A., *Nature Chemistry* **2015**, *8*, 63.
- (48) Pangborn, A. B.; Giardello, M. A.; Grubbs, R. H.; Rosen, R. K.; Timmers, F. J., *Organometallics* **1996**, *15*, 1518-1520.
- (49) Low, C. H.; Rosenberg, J. N.; Lopez, M. A.; Agapie, T., *J. Am. Chem. Soc.* **2018**, *140*, 11906-11910.
- (50) Vivanco, M.; Ruiz, J.; Floriani, C.; Chiesi-Villa, A.; Rizzoli, C., *Organometallics* **1993**, *12*, 1794-1801.
- (51) Sampson, J.; Choi, G.; Akhtar, M. N.; Jaseer, E. A.; Theravalappil, R.; Al-Muallem, H. A.; Agapie, T., *Organometallics* **2017**, *36*, 1915-1928.

Appendix D

Nuclear Magnetic Resonance Spectra for Characterization of Isolated and in situ Generated Complexes

CHAPTER 2

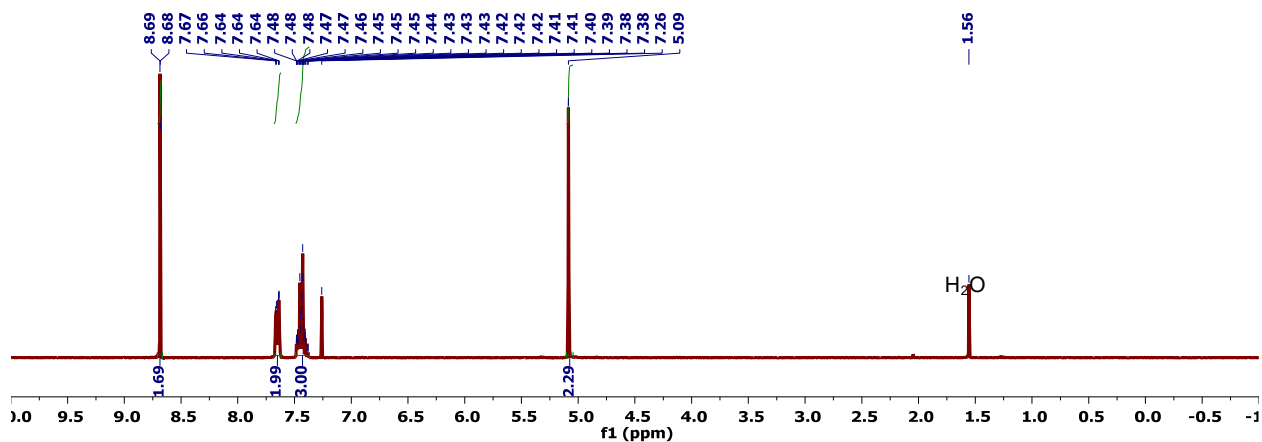


Figure D.1. ^1H NMR spectrum (300 MHz, CDCl_3) of 2-(benzyloxy)-1,3-diiodo-5-nitrobenzene.

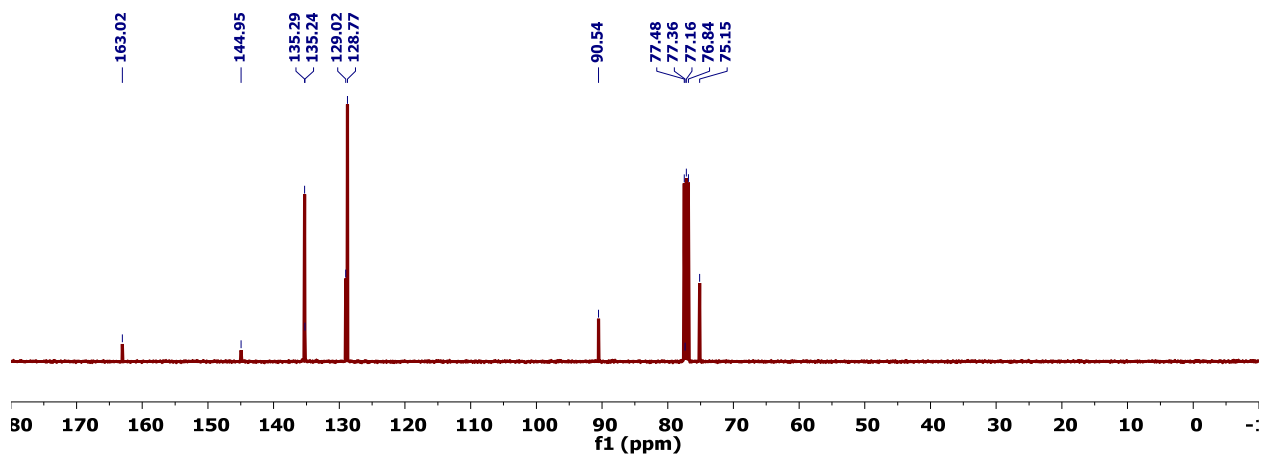


Figure D.2. $^{13}\text{C}\{^1\text{H}\}$ NMR spectrum (75 MHz, CDCl_3) of 2-(benzyloxy)-1,3-diiodo-5-nitrobenzene.

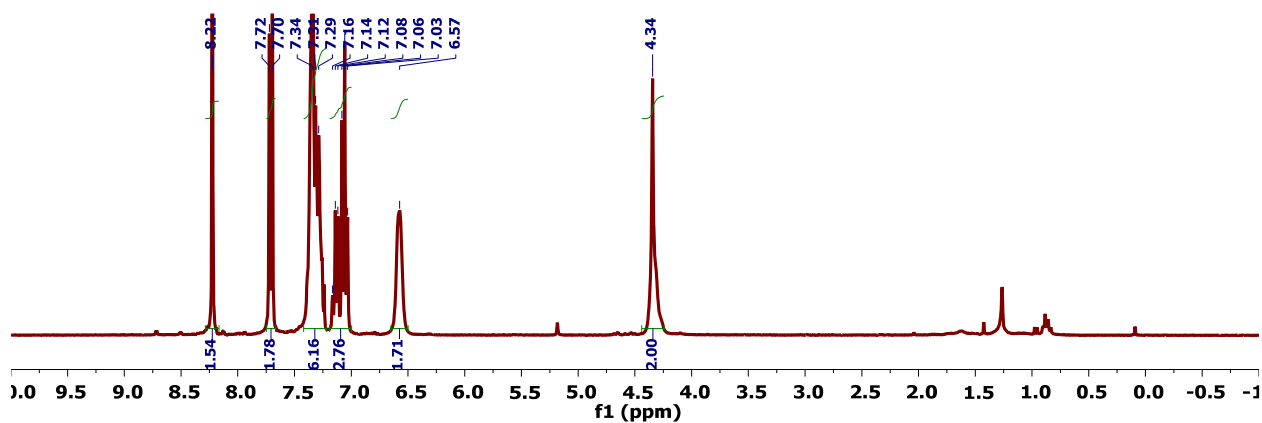


Figure D.3. ^1H NMR spectrum (300 MHz, CDCl_3) of 2-(benzyloxy)-1,3-bis(2'-bromophenyl)-5-nitrobenzene.

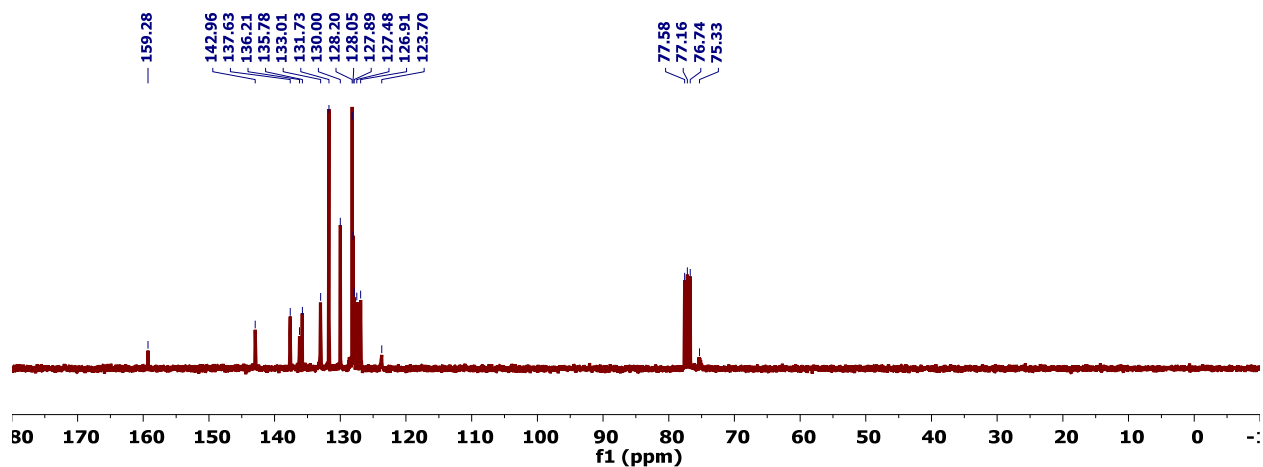


Figure D.4. $^{13}\text{C}\{^1\text{H}\}$ NMR spectrum (75 MHz, CDCl_3) of 2-(benzyloxy)-1,3-bis(2'-bromophenyl)-5-nitrobenzene.

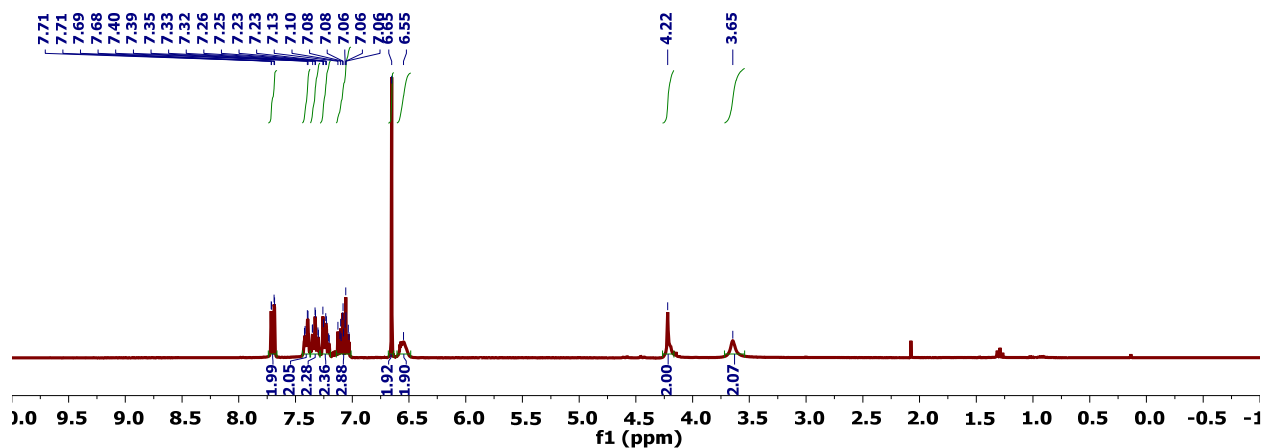


Figure D.5. ^1H NMR spectrum (300 MHz, CDCl_3) of 4-(benzyloxy)-3,5-bis(2'-bromophenyl)aniline.

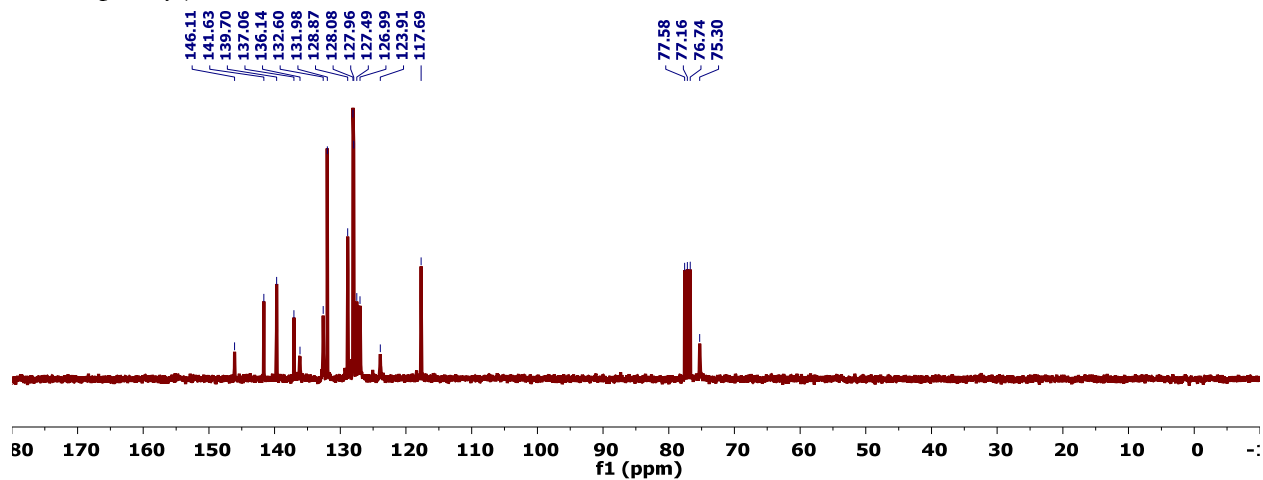


Figure D.6. $^{13}\text{C}\{^1\text{H}\}$ NMR spectrum (75 MHz, CDCl_3) of 4-(benzyloxy)-3,5-bis(2'-bromophenyl)aniline.

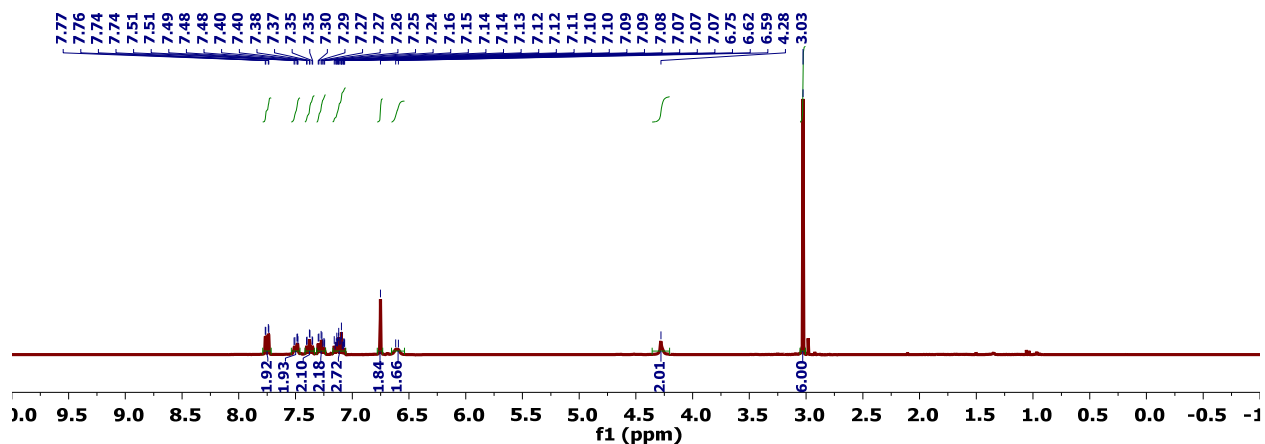


Figure D.7. ^1H NMR spectrum (300 MHz, CDCl_3) of 4-(benzyloxy)-3,5-bis(2'-bromophenyl)-*N,N*-dimethylaniline.

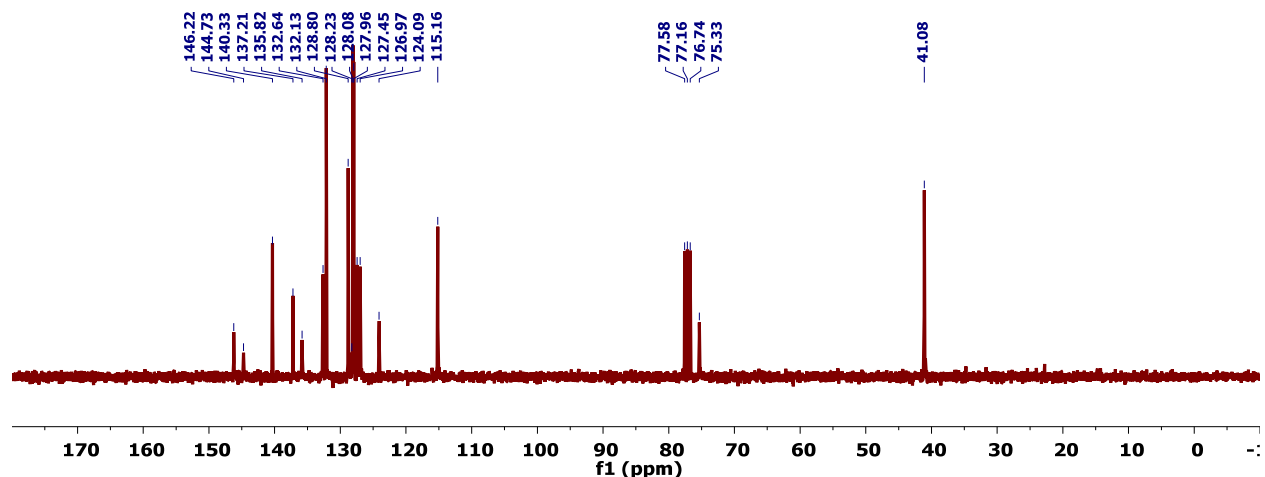


Figure D.8. $^{13}\text{C}\{^1\text{H}\}$ NMR spectrum (75 MHz, CDCl_3) of 4-(benzyloxy)-3,5-bis(2'-bromophenyl)-*N,N*-dimethylaniline.

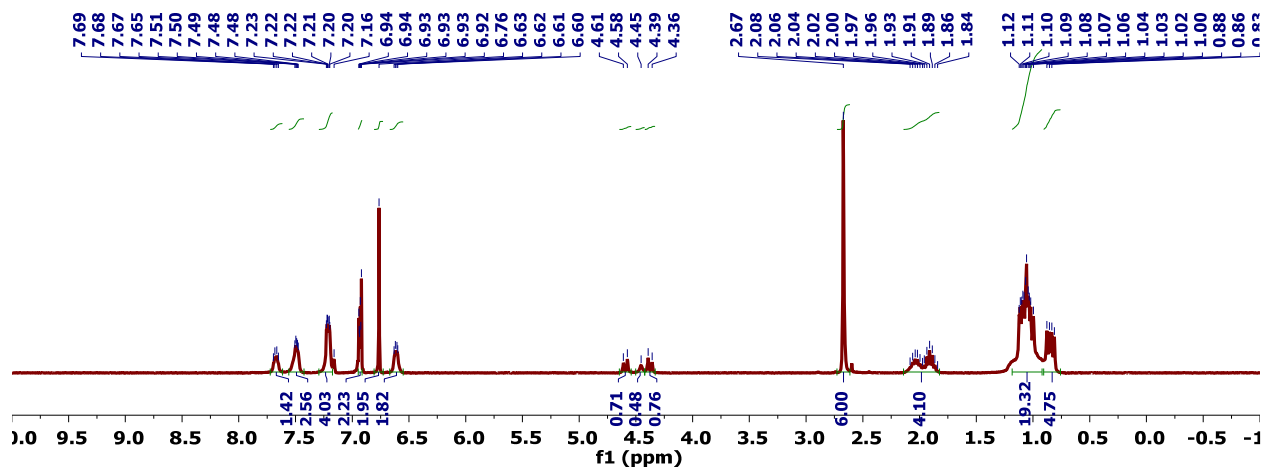


Figure D.9. ^1H NMR spectrum (300 MHz, C_6D_6) of 4-(benzyloxy)-3,5-bis(2'-diisopropylphosphinophenyl)-*N,N*-dimethylaniline.

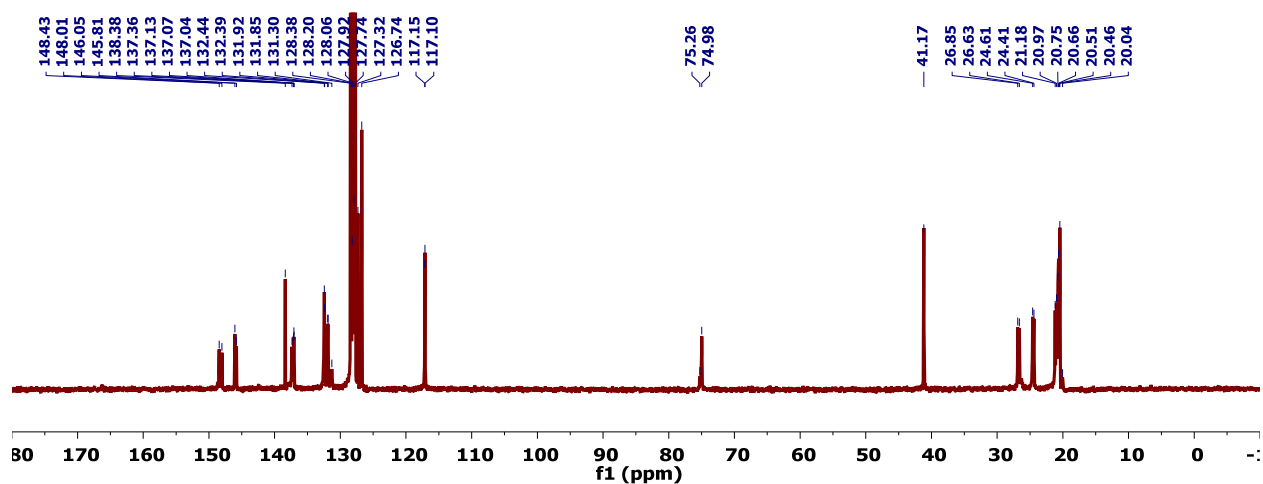


Figure D.10. $^{13}\text{C}\{^1\text{H}\}$ NMR spectrum (75 MHz, C_6D_6) of 4-(benzyloxy)-3,5-bis(2'-diisopropylphosphinophenyl)-*N,N*-dimethylaniline.

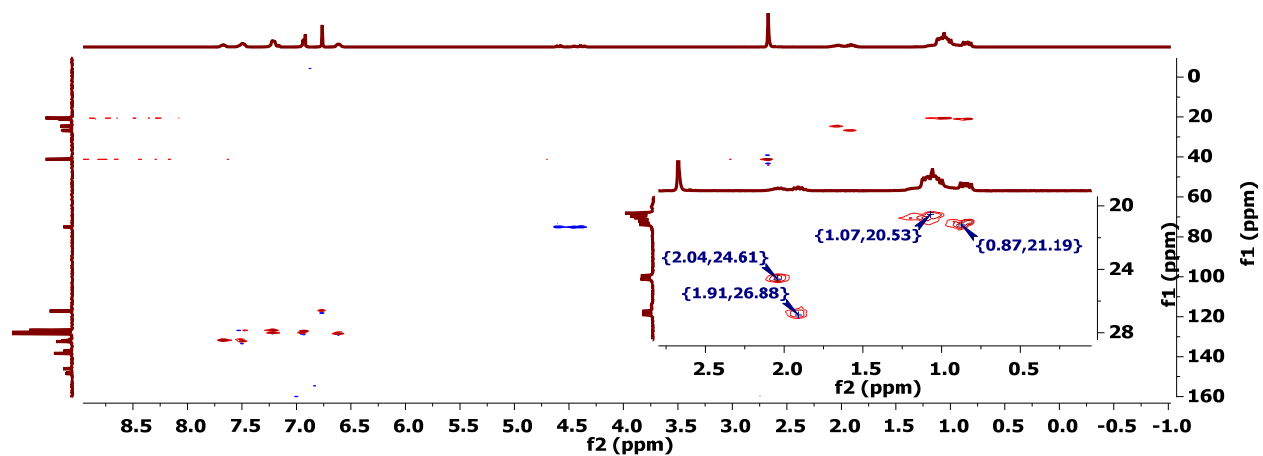


Figure D.11. HSQC NMR spectrum (C_6D_6) of 4-(benzyloxy)-3,5-bis(2'-diisopropylphosphinophenyl)-*N,N*-dimethylaniline.

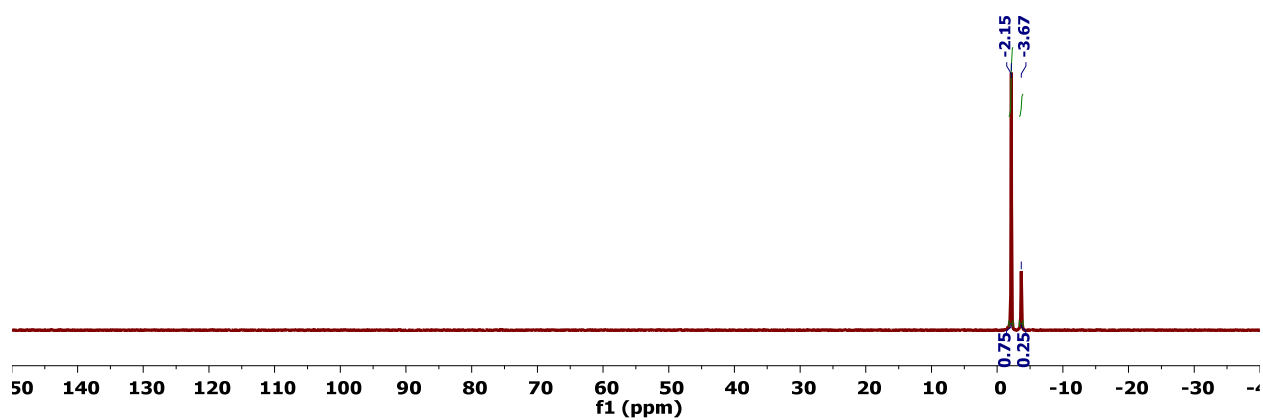


Figure D.12. $^{31}\text{P}\{^1\text{H}\}$ NMR spectrum (121 MHz, C_6D_6) of 4-(benzyloxy)-3,5-bis(2'-diisopropylphosphinophenyl)-*N,N*-dimethylaniline.

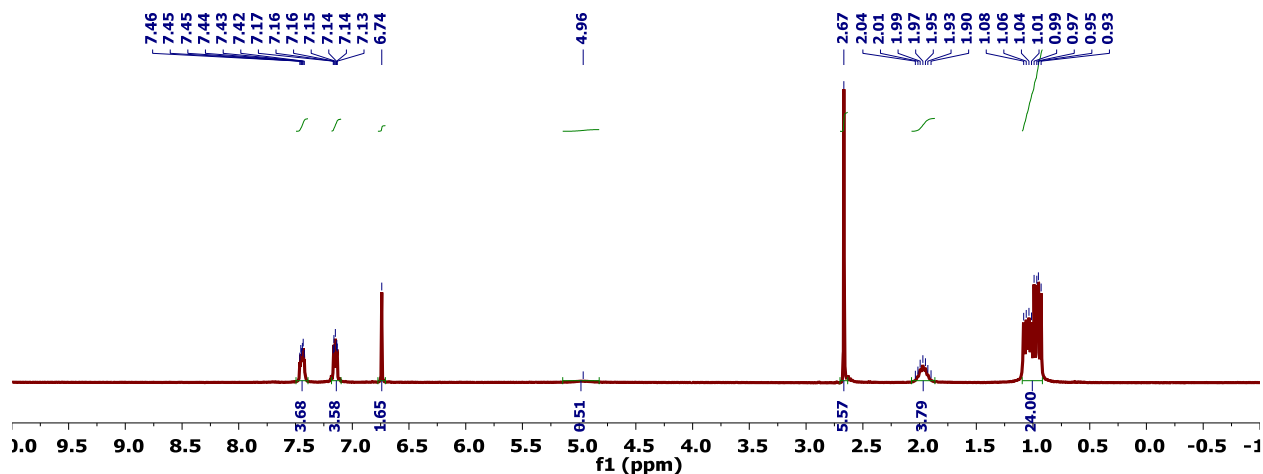


Figure D.13. ^1H NMR spectrum (300 MHz, C_6D_6 , 70 °C) of 2,6-bis(2'-diisopropylphosphinophenyl)-4-dimethylaminophenol (**1-H**).

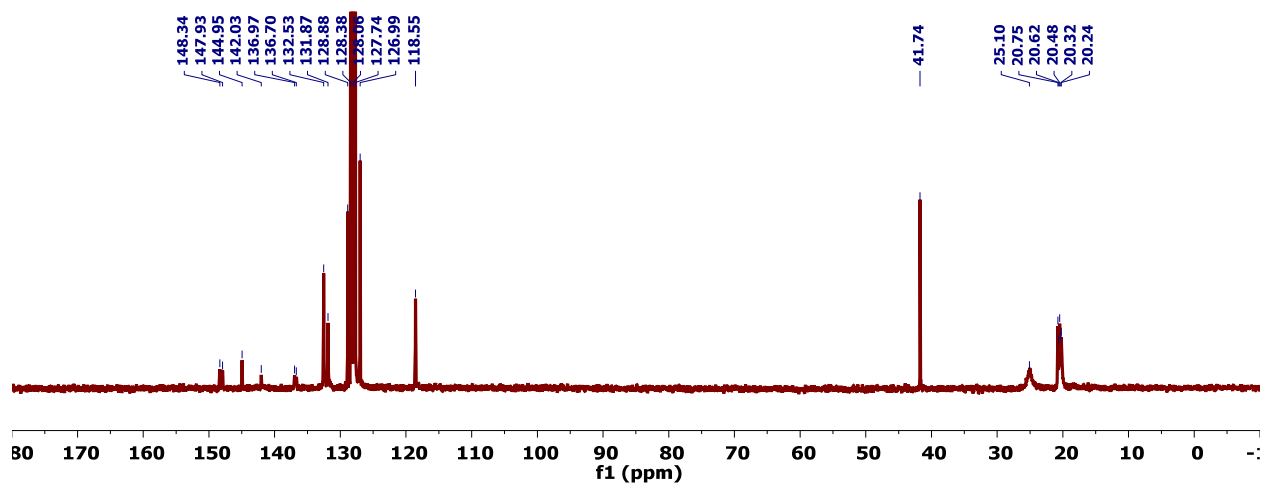


Figure D.14. $^{13}\text{C}\{^1\text{H}\}$ NMR spectrum (75 MHz, C_6D_6 , 70 °C) of 2,6-bis(2'-diisopropylphosphinophenyl)-4-dimethylaminophenol (**1-H**).

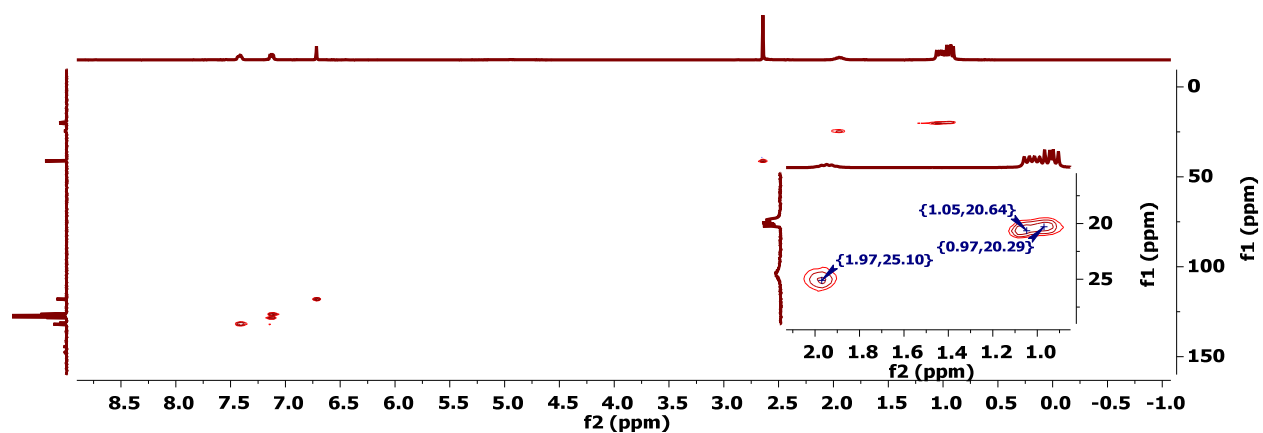


Figure D.15. HSQC NMR spectrum (C_6D_6) of 2,6-bis(2'-diisopropylphosphinophenyl)-4-dimethylaminophenol (**1-H**).

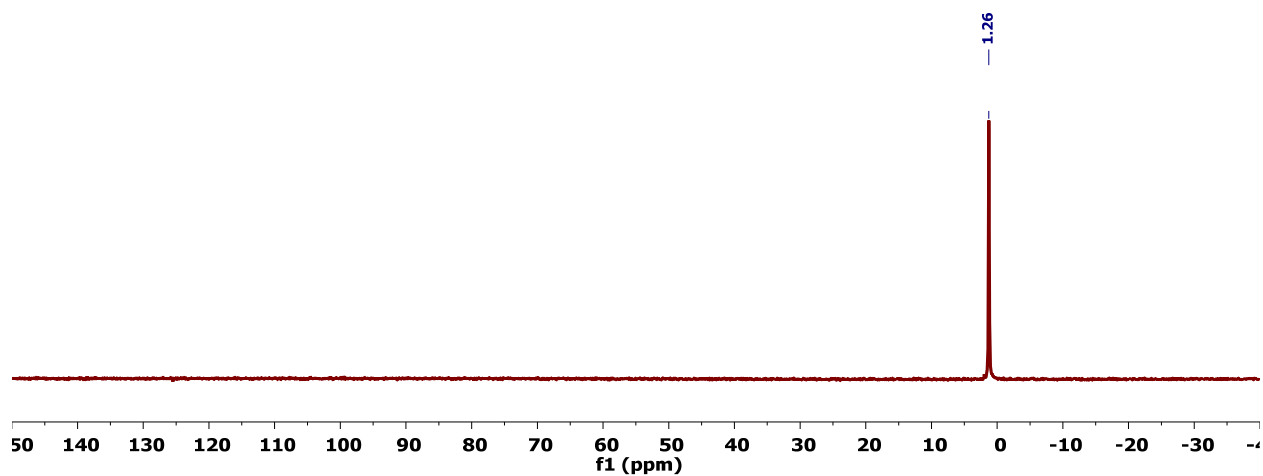


Figure D.16. $^{31}\text{P}\{^1\text{H}\}$ NMR spectrum (121 MHz, C_6D_6 , 70 °C) of 2,6-bis(2'-diisopropylphosphinophenyl)-4-dimethylaminophenol (1-H).

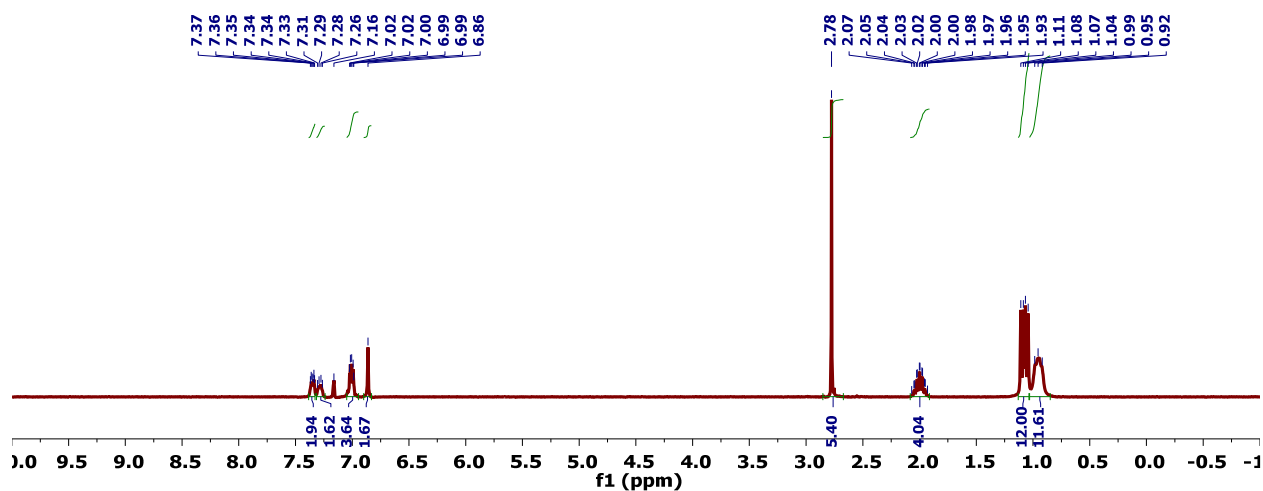


Figure D.17. ^1H NMR spectrum (300 MHz, C_6D_6 , 70 °C) of 1-K.

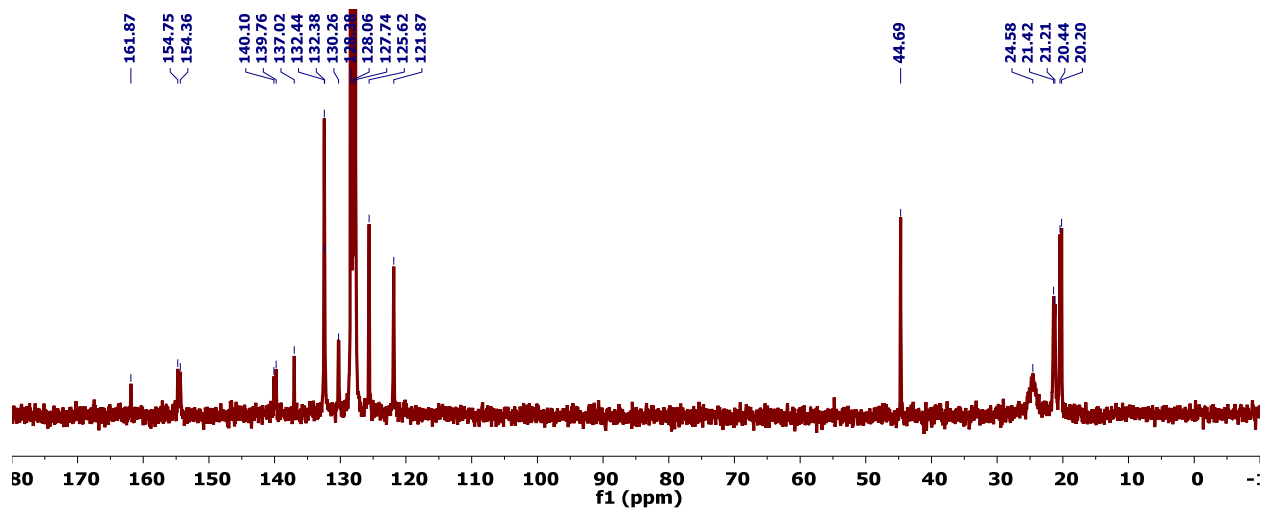


Figure D.18. $^{13}\text{C}\{^1\text{H}\}$ NMR spectrum (75 MHz, C_6D_6 , 70 °C) of 1-K.

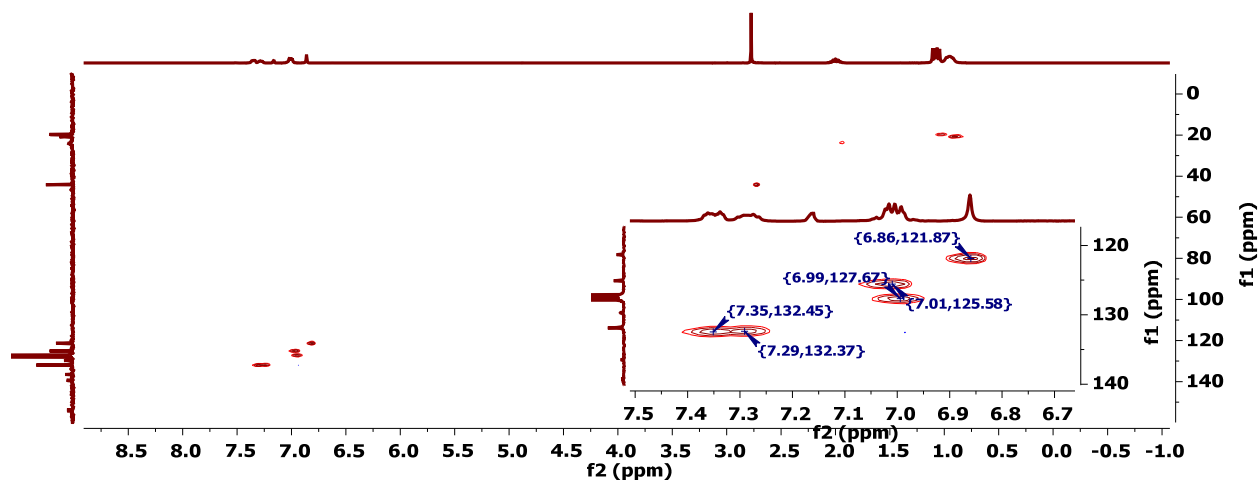


Figure D.19. HSQC NMR spectrum (C_6D_6) of 1-K.

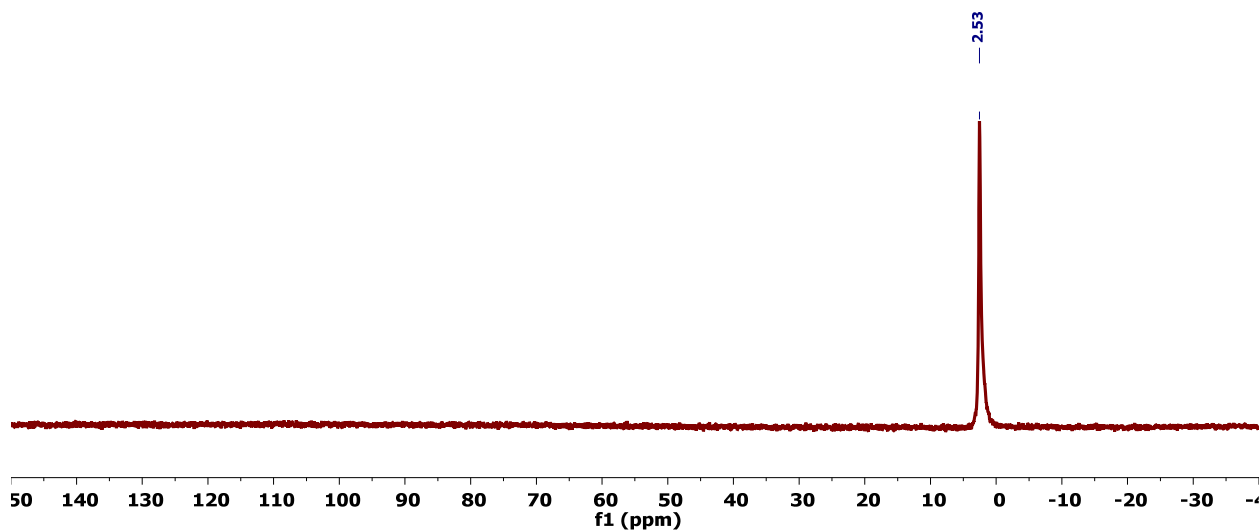


Figure D.20. $^{31}P\{^1H\}$ NMR spectrum (121 MHz, C_6D_6 , 70 °C) of 1-K.

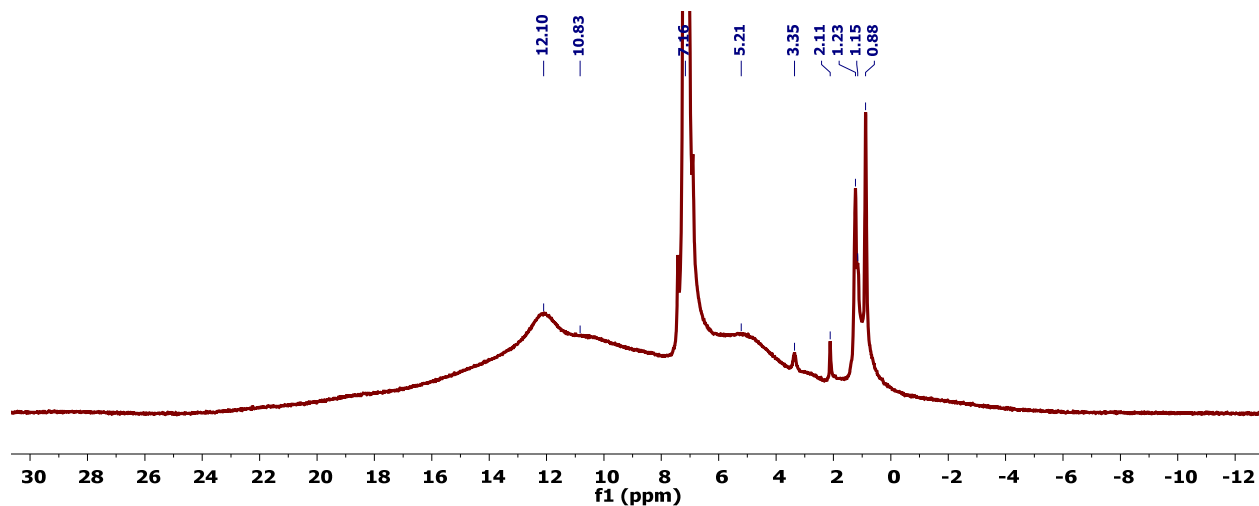


Figure D.21. 1H NMR spectrum (300 MHz, C_6D_6) of 2.

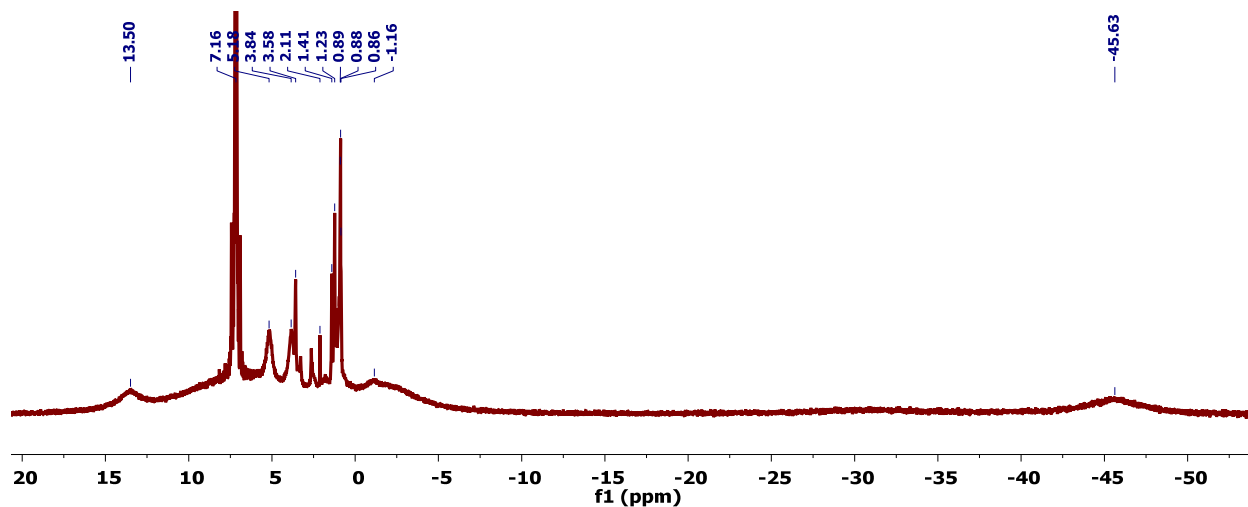


Figure D.22. ^1H NMR spectrum (300 MHz, C_6D_6) of 3 (trace hexanes and THF present).

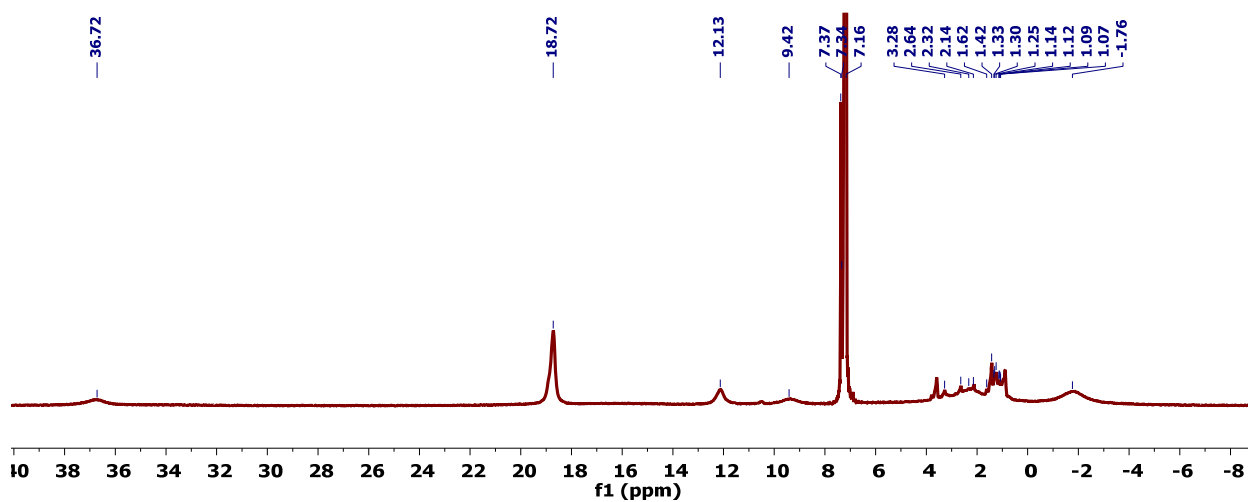


Figure D.23. ^1H NMR spectrum (300 MHz, C_6D_6) of 4 (trace hexanes and THF present).

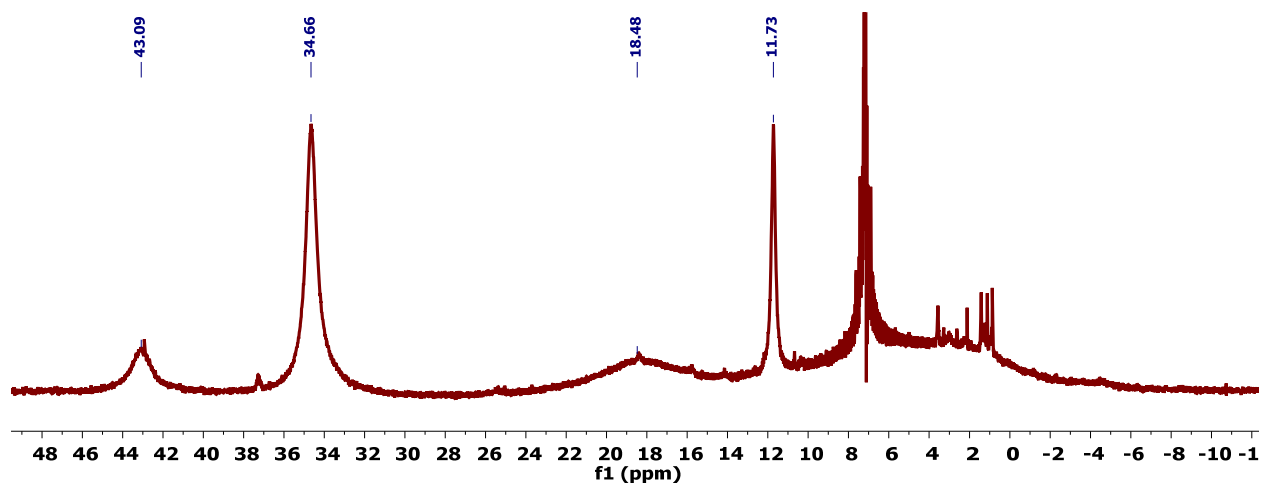


Figure D.24. ^1H NMR spectrum (300 MHz, C_6D_6) of 5 (trace THF and hexanes present).

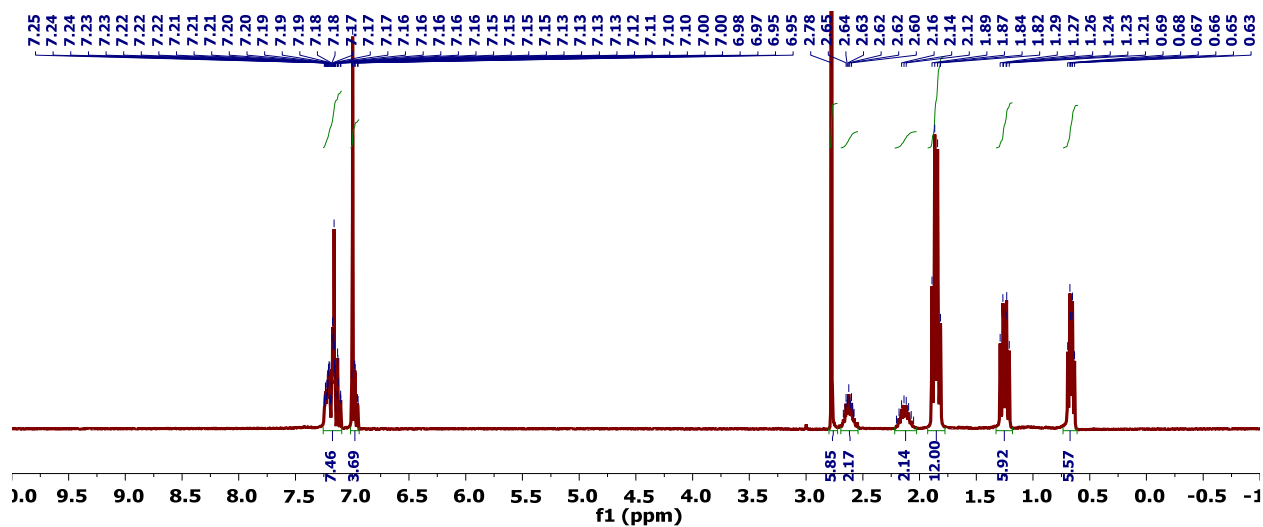


Figure D.25. ^1H NMR spectrum (300 MHz, C_6D_6) of 6.

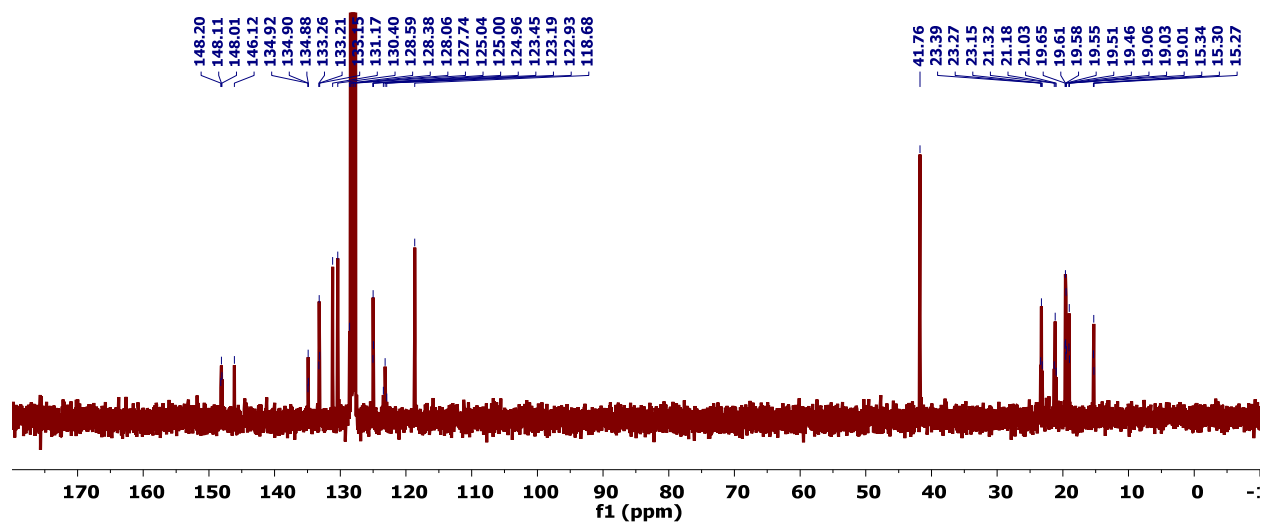


Figure D.26. $^{13}\text{C}\{^1\text{H}\}$ NMR spectrum (75 MHz, C_6D_6) of 6.

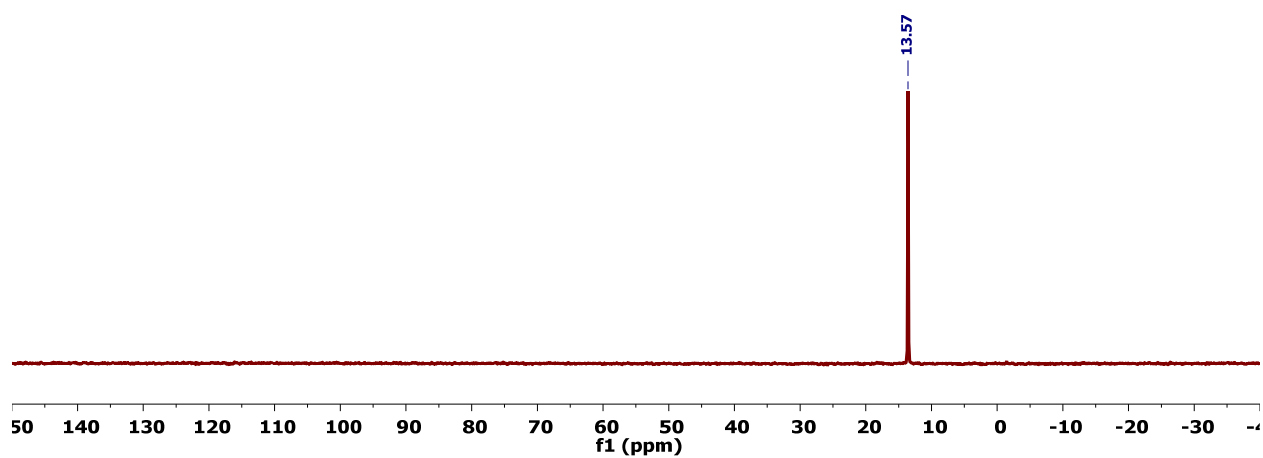


Figure D.27. $^{31}\text{P}\{^1\text{H}\}$ NMR spectrum (121 MHz, C_6D_6) of 6.

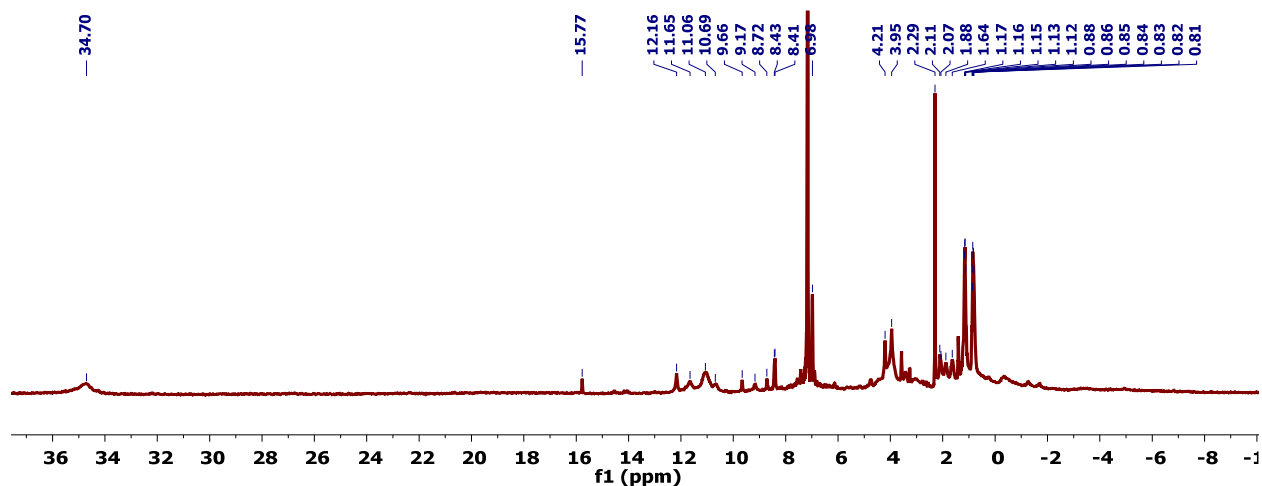


Figure D.28. ^1H NMR spectrum (300 MHz, C_6D_6) of 8.

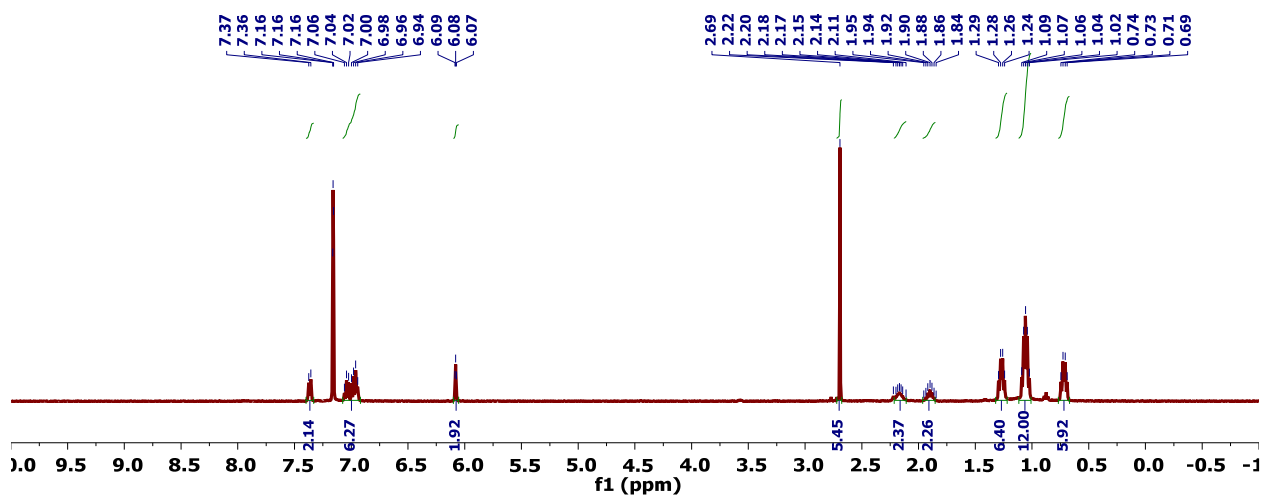


Figure D.29. ^1H NMR spectrum (400 MHz, C_6D_6) of 9.

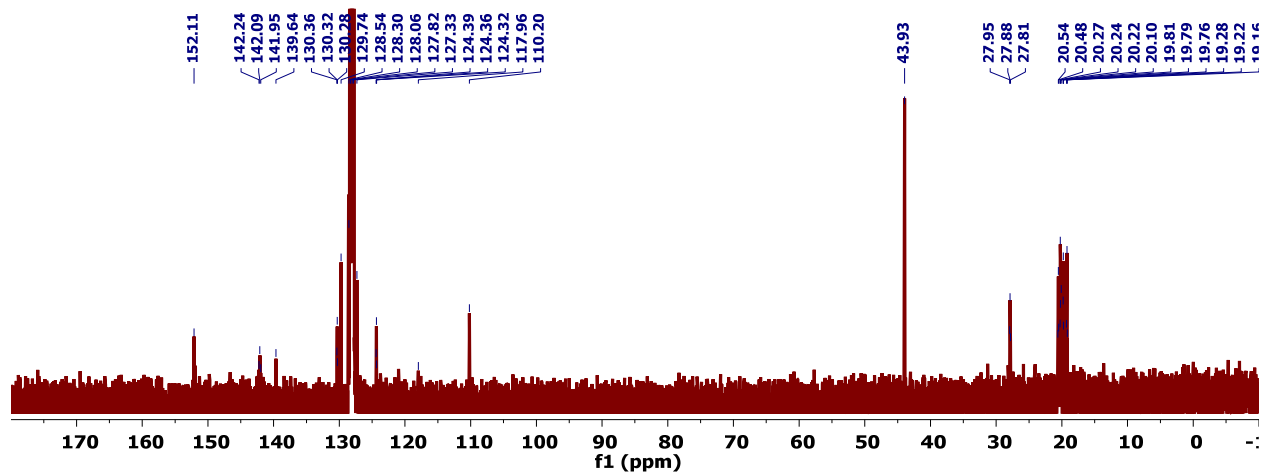


Figure D.30. $^{13}\text{C}\{^1\text{H}\}$ NMR spectrum (101 MHz, C_6D_6) of 9.

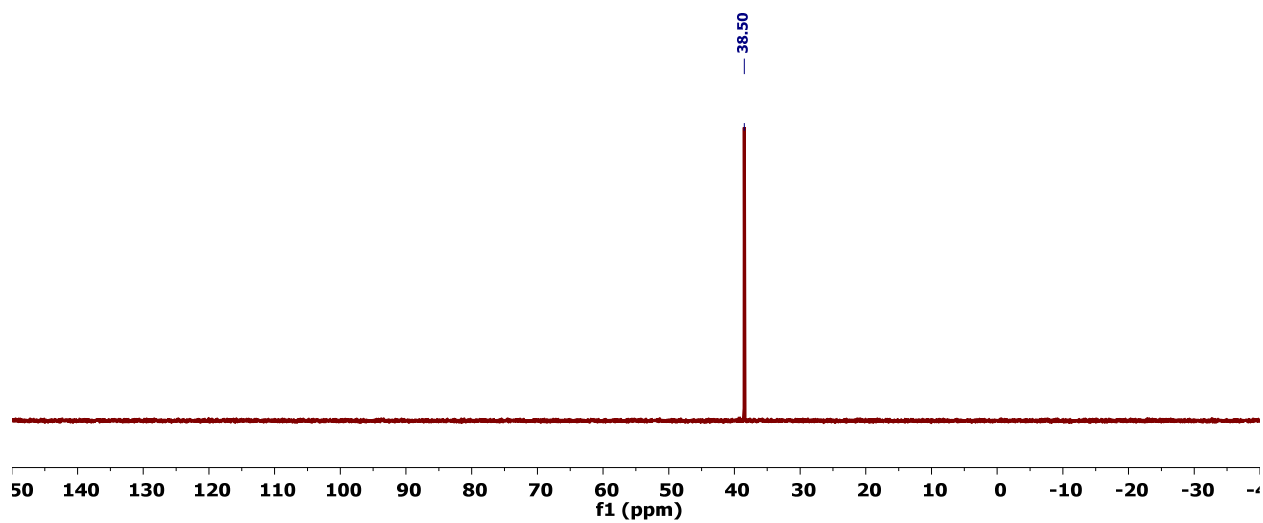


Figure D.31. $^{31}\text{P}\{^1\text{H}\}$ NMR spectrum (162 MHz, C_6D_6) of **9**.

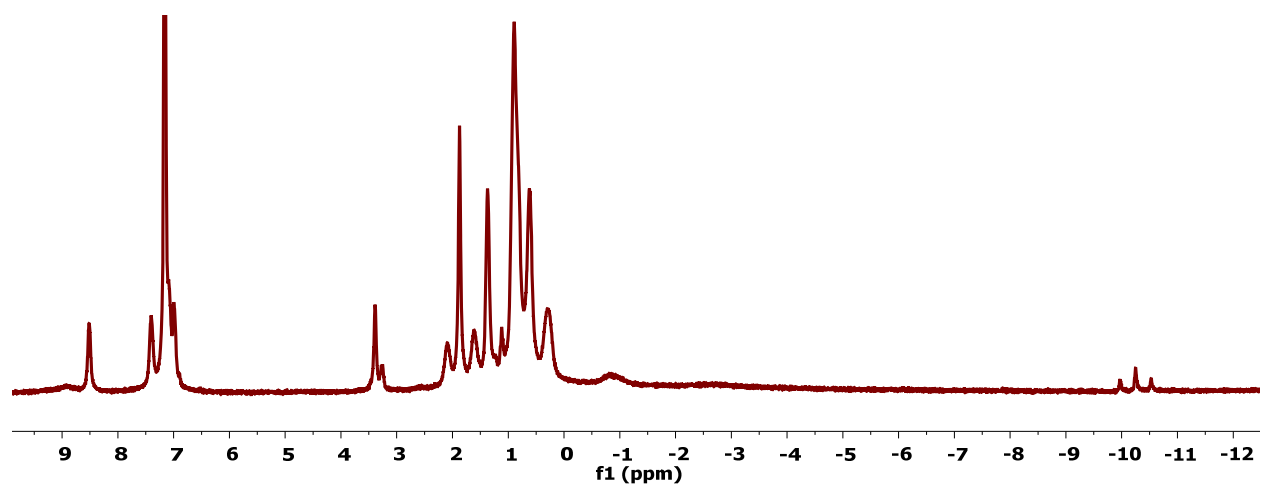


Figure D.32. ^1H NMR spectrum (300 MHz, C_6D_6) of **12**.

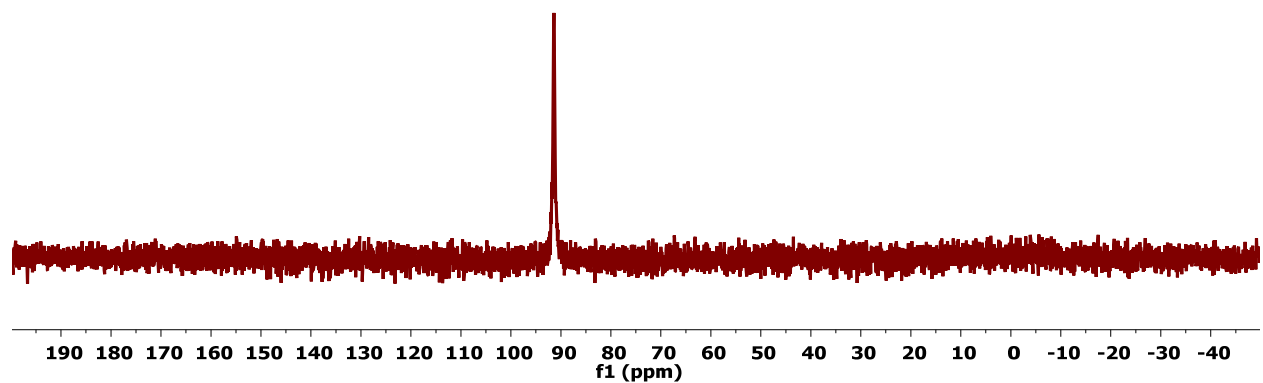


Figure D.33. $^{31}\text{P}\{^1\text{H}\}$ NMR spectrum (126 MHz, C_6D_6) of **12**.

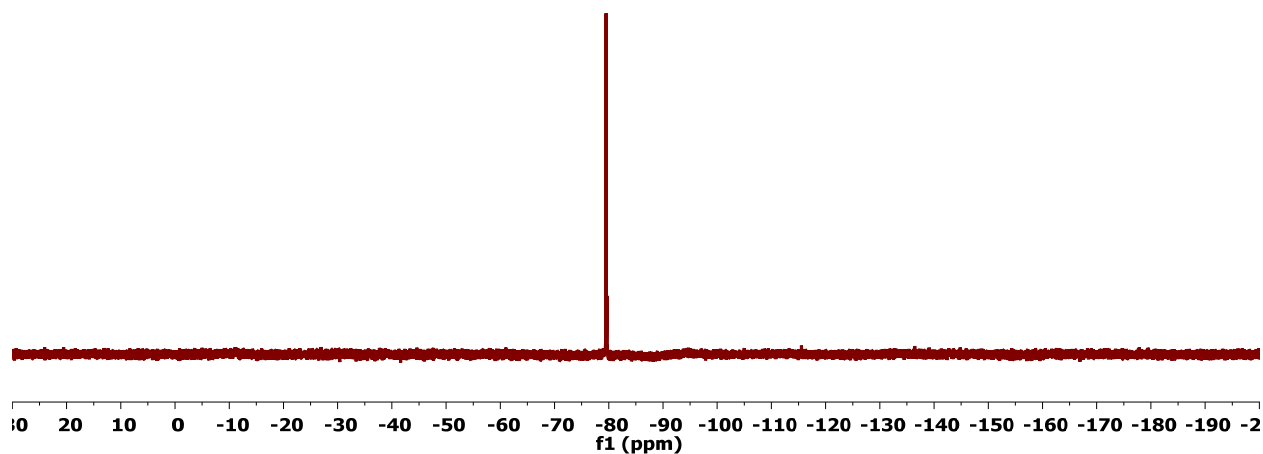


Figure D.34. ^{19}F NMR spectrum (296 MHz, C_6D_6) of 12.

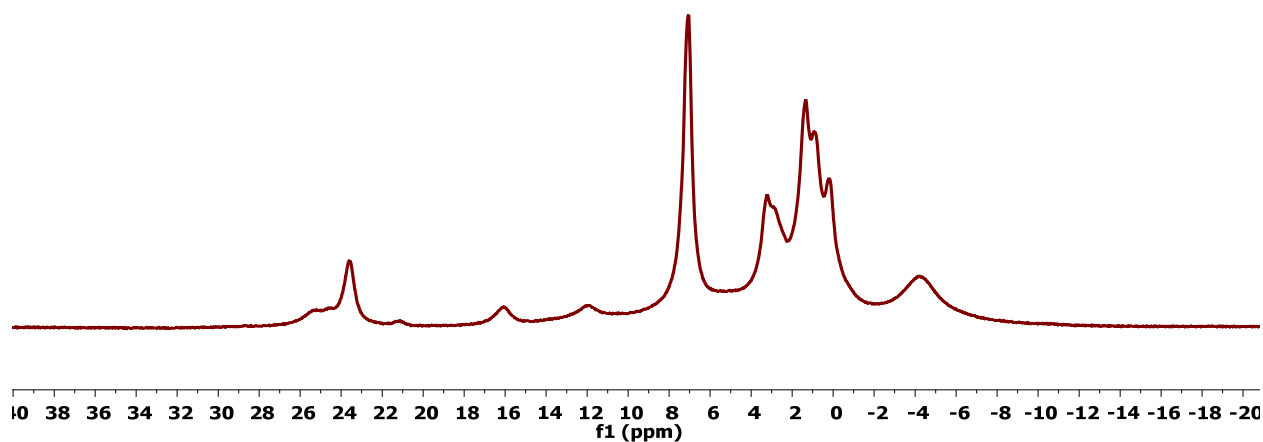


Figure D.35. ^1H NMR spectrum (300 MHz, C_6D_6) of 13.

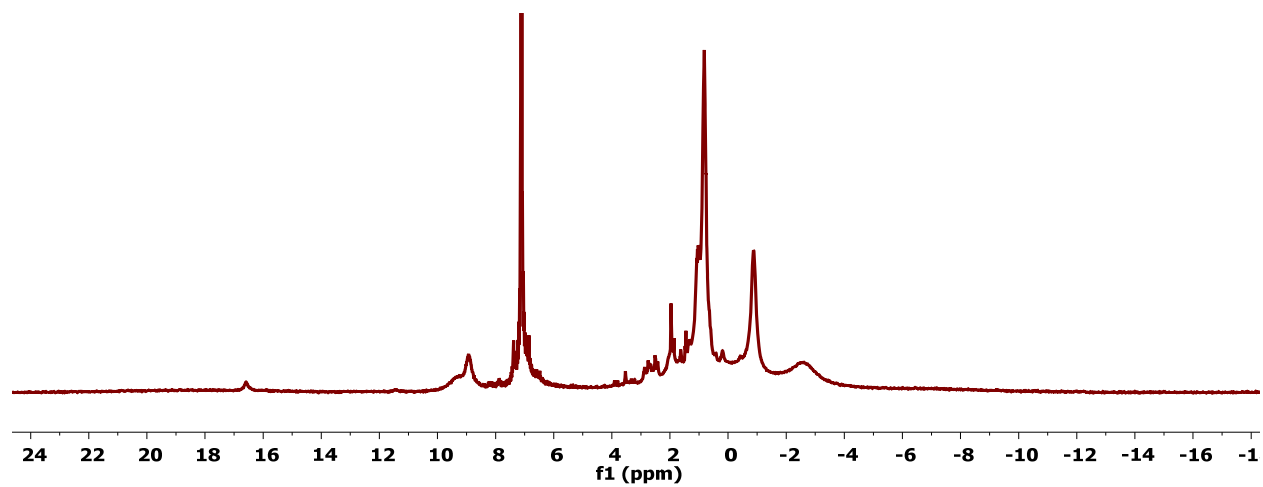


Figure D.36. ^1H NMR spectrum (300 MHz, C_6D_6) of 14.

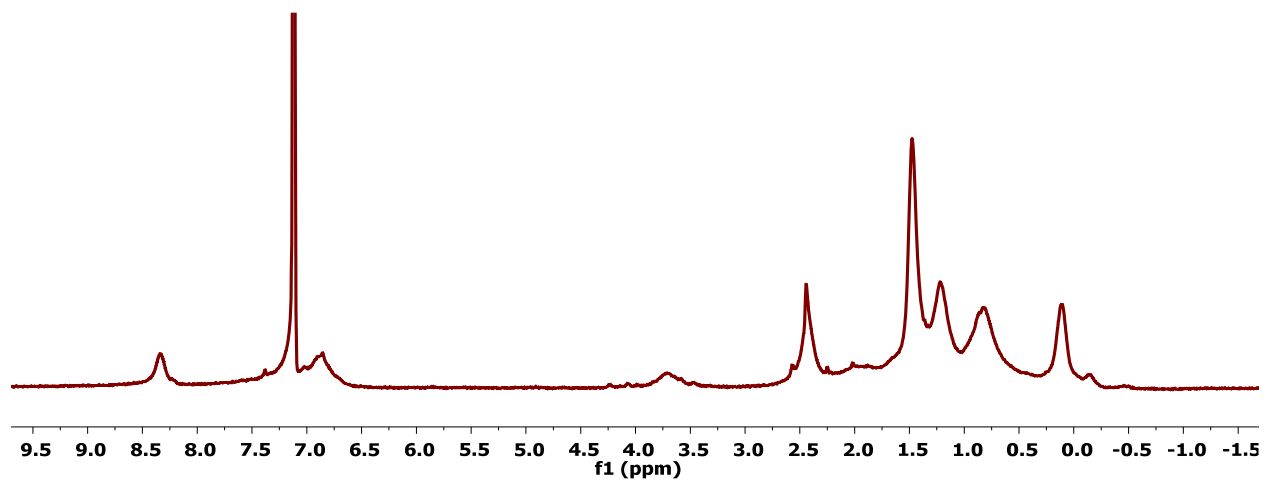


Figure D.37. ^1H NMR spectrum (300 MHz, C_6D_6) of 15.

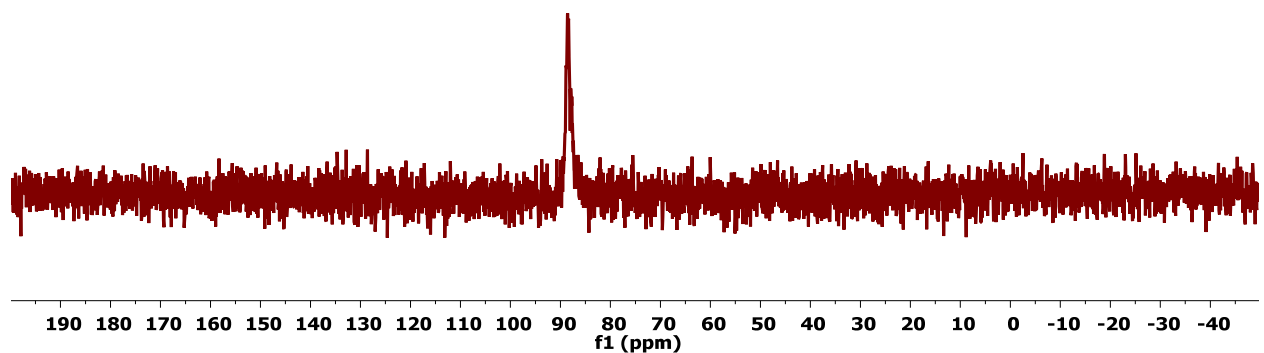


Figure D.38. $^{31}\text{P}\{^1\text{H}\}$ NMR spectrum (126 MHz, C_6D_6) of 15.

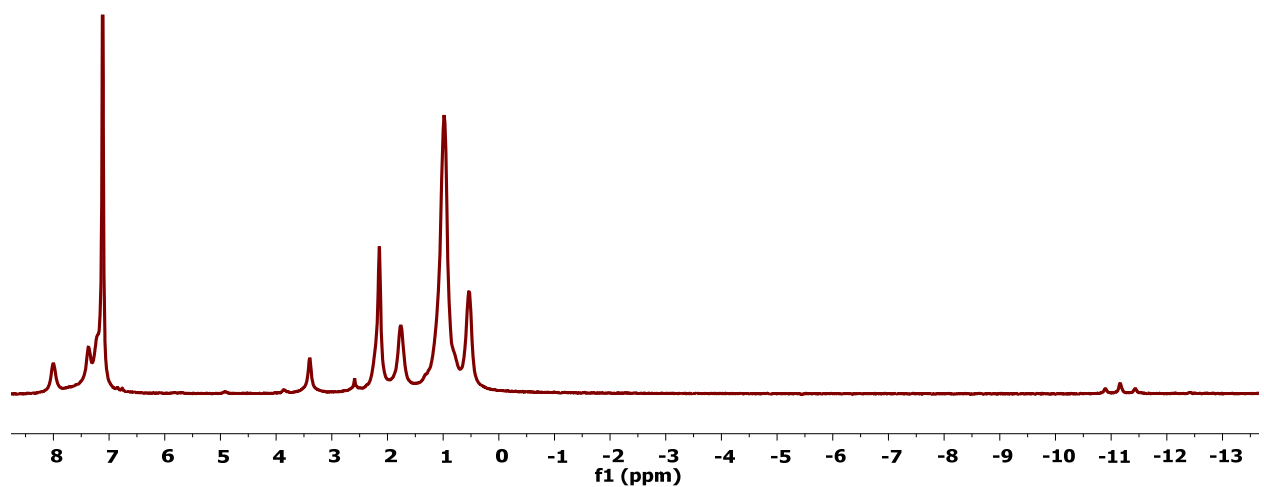


Figure D.39. ^1H NMR spectrum (300 MHz, C_6D_6) of 16.

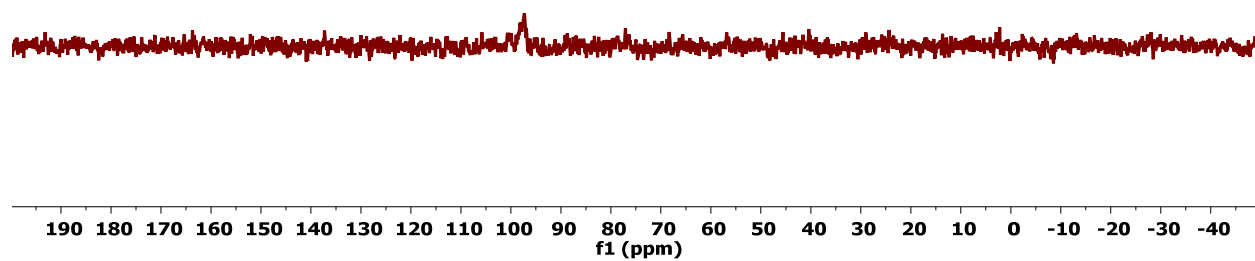


Figure D.40. $^{31}\text{P}\{^1\text{H}\}$ NMR spectrum (126 MHz, C_6D_6) of **16**.

CHAPTER 3

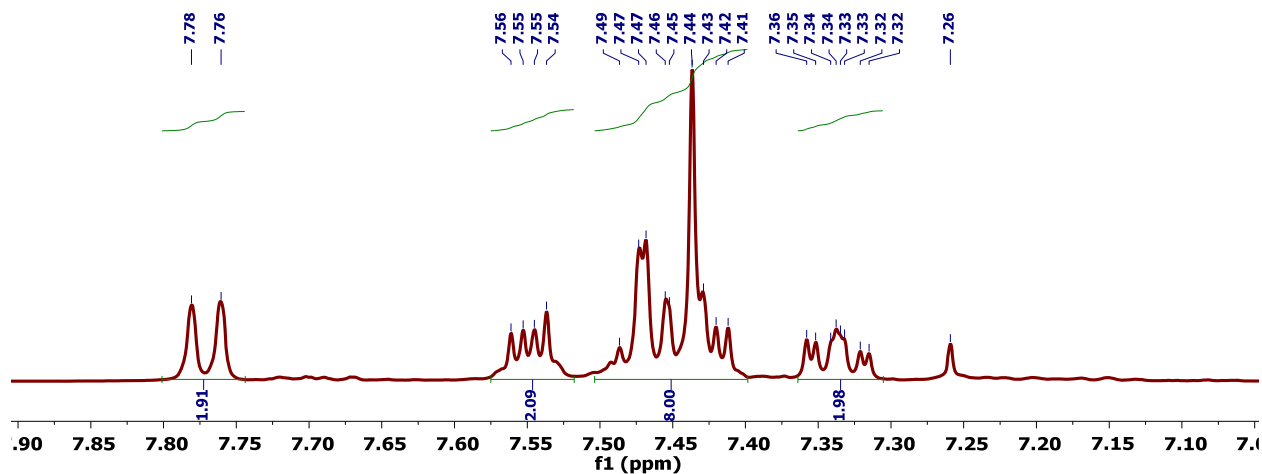


Figure D.41. ^1H NMR spectrum (400 MHz, CDCl_3) of 1,4-*bis*(2-bromophenyl)naphthalene.

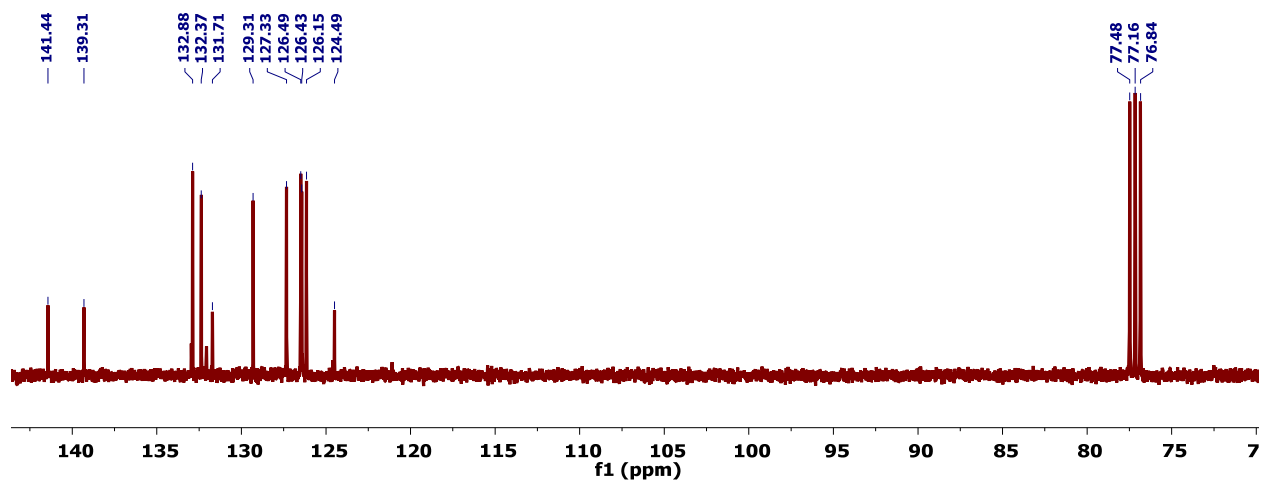


Figure D.42. $^{13}\text{C}\{^1\text{H}\}$ NMR spectrum (101 MHz, CDCl_3) of 1,4-*bis*(2-bromophenyl)naphthalene.

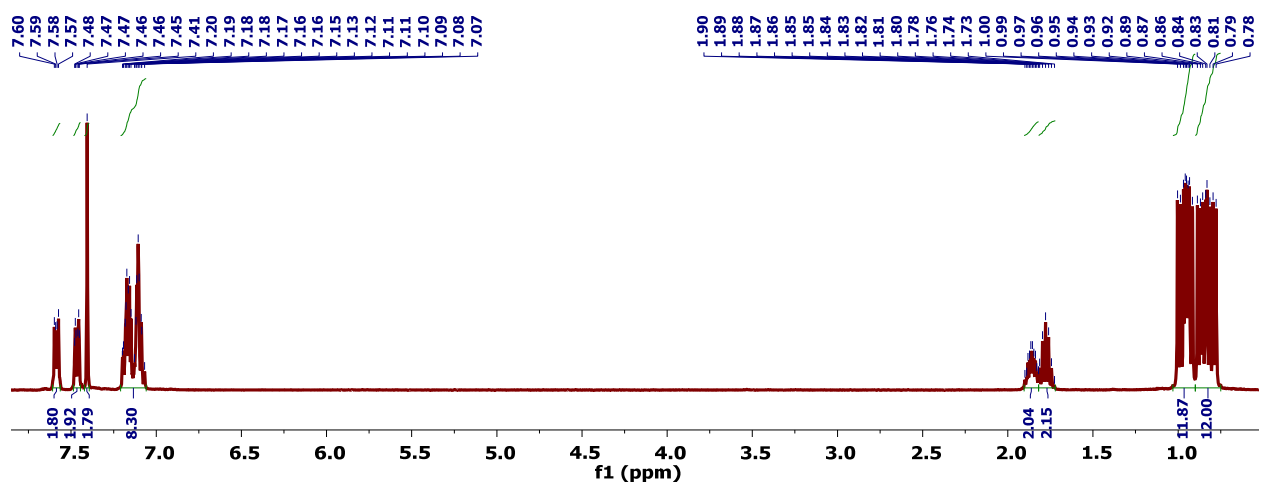


Figure D.43. ^1H NMR spectrum (400 MHz, C_6D_6) of 1.

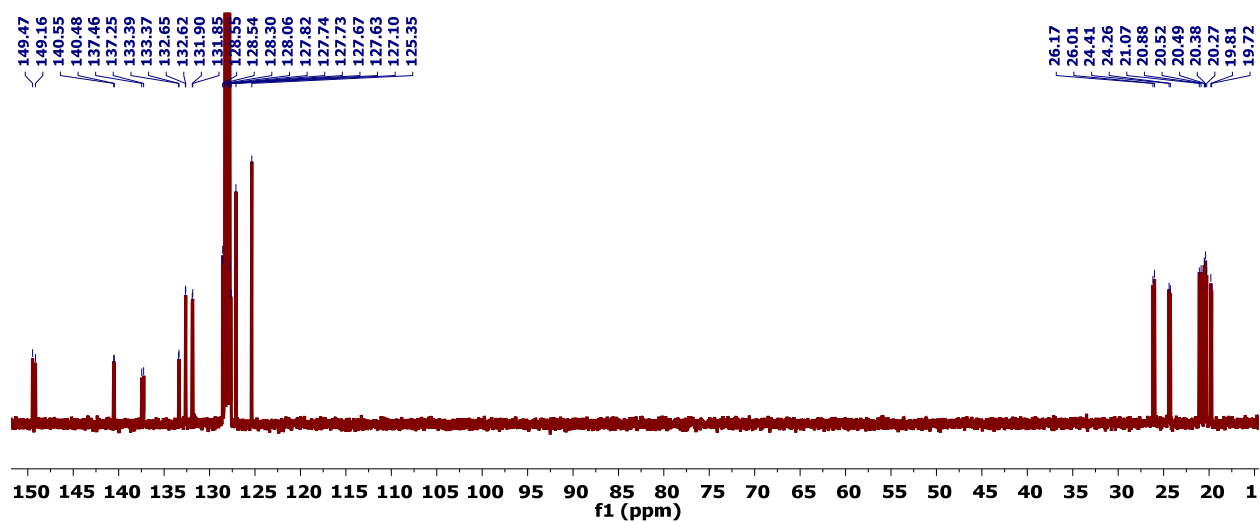


Figure D.44. ¹³C{¹H} NMR spectrum (101 MHz, C₆D₆) of 1.

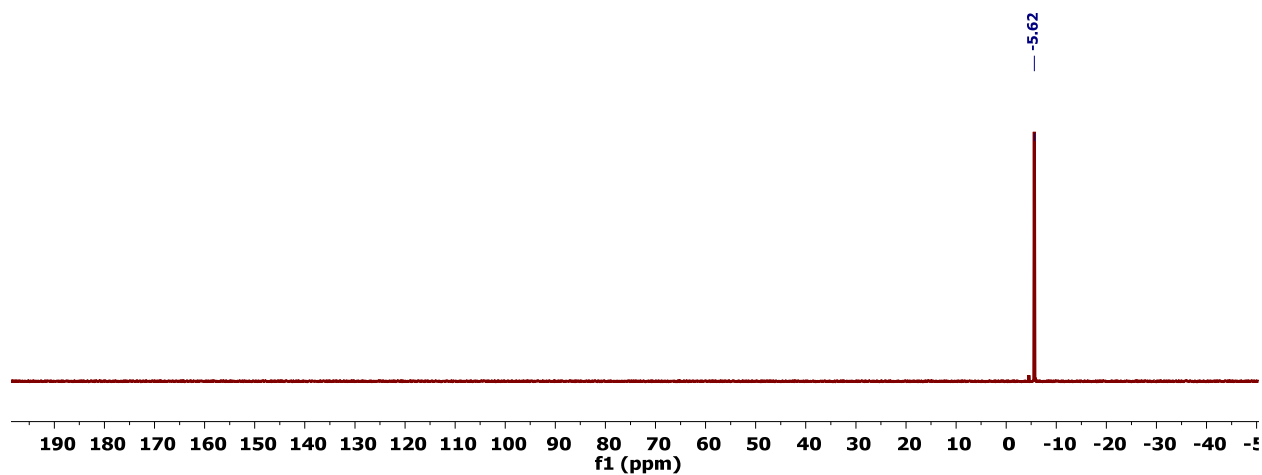


Figure D.45. ³¹P{¹H} NMR spectrum (162 MHz, C₆D₆) of 1.

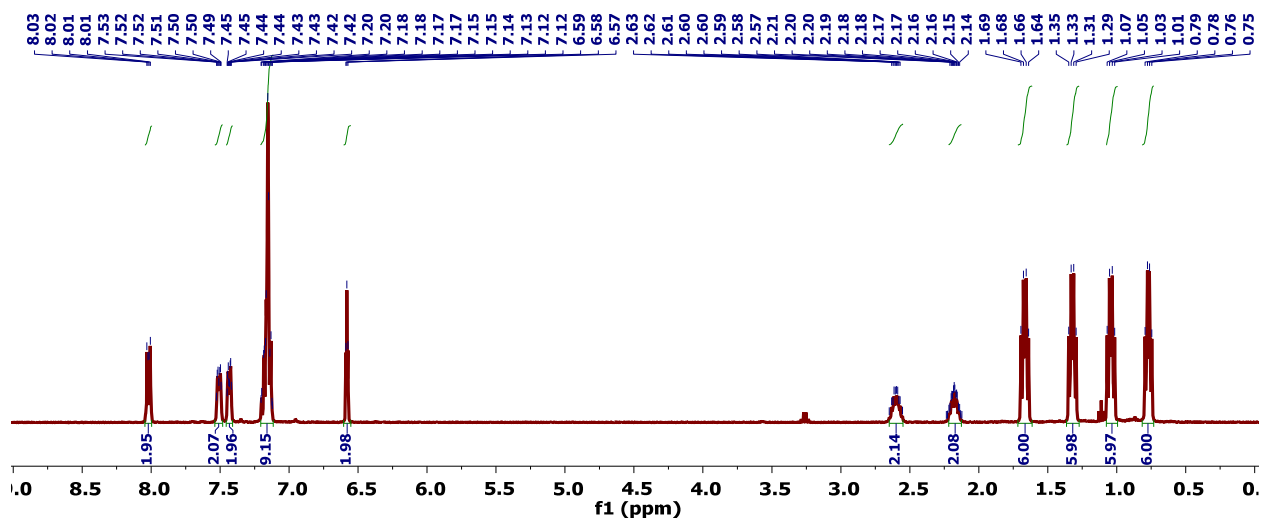


Figure D.46. ¹H NMR spectrum (400 MHz, CDCl₃) of 2.

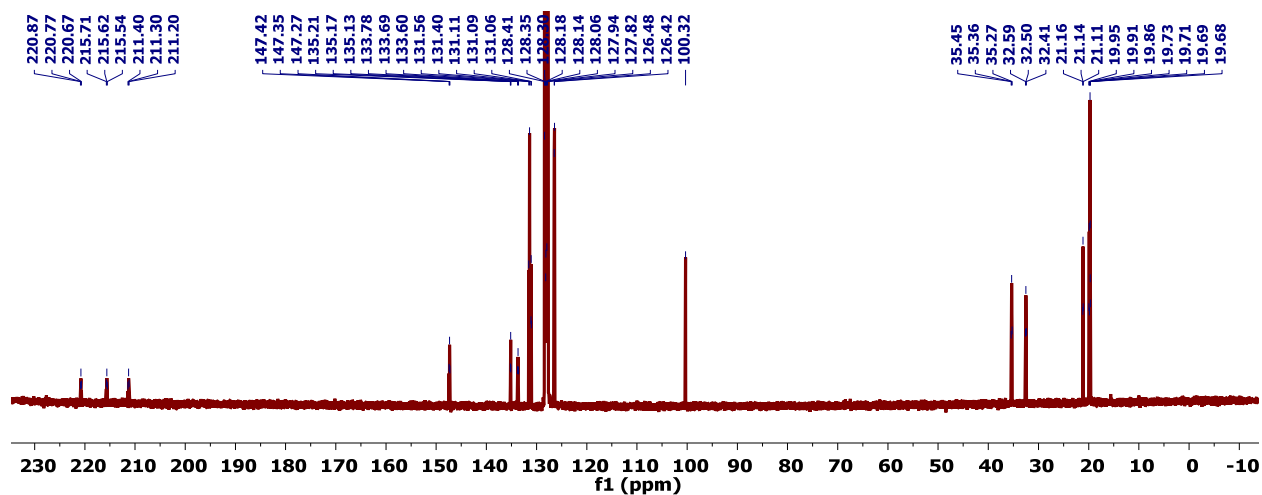


Figure D.47. $^{13}\text{C}\{^1\text{H}\}$ NMR spectrum (101MHz, CDCl_3) of **2**.

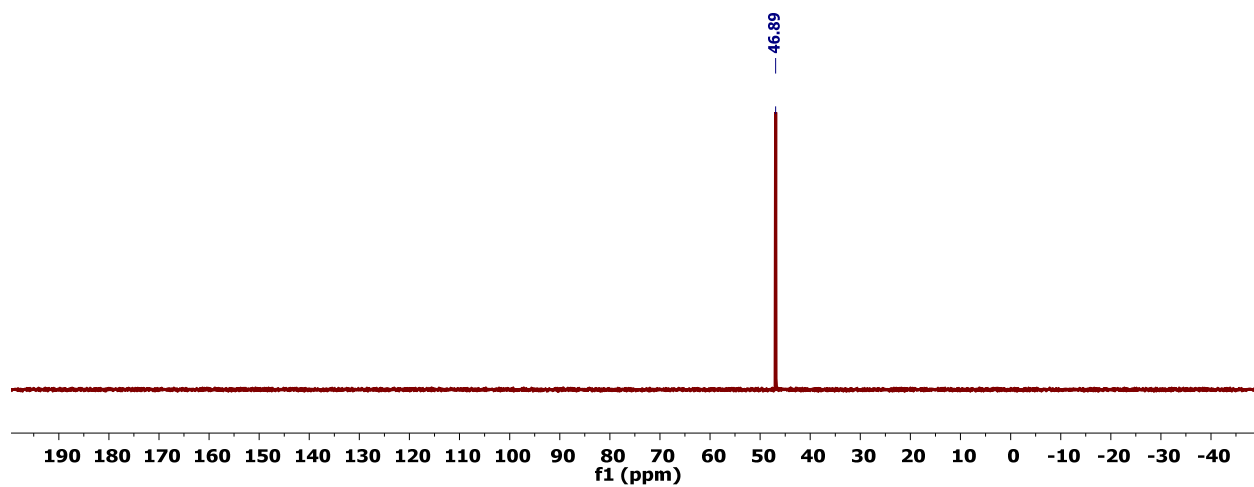


Figure D.48. $^{31}\text{P}\{^1\text{H}\}$ NMR spectrum (162 MHz, C_6D_6) of **2**.

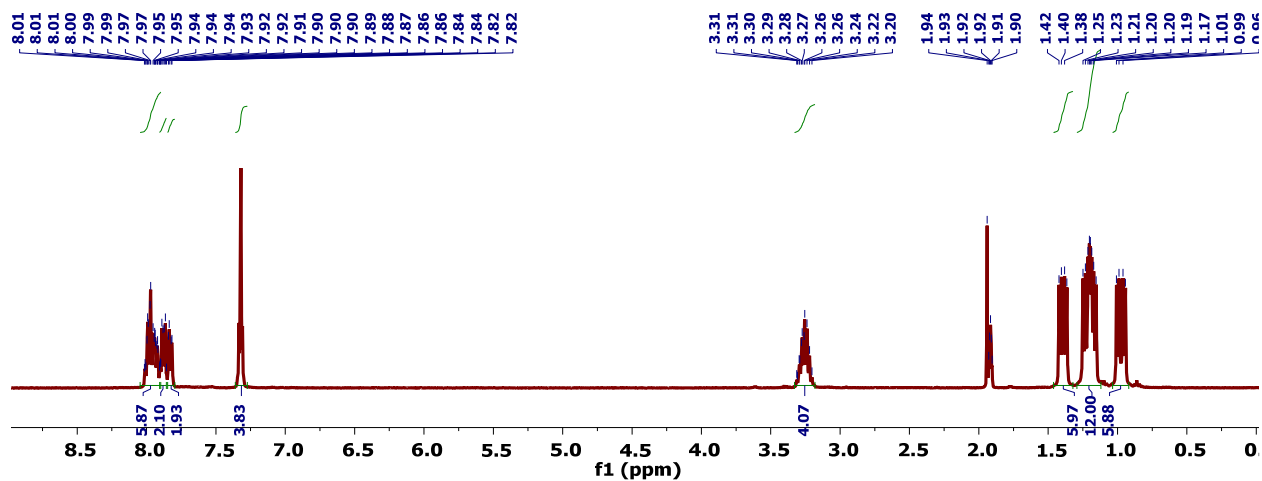


Figure D.49. ^1H NMR spectrum (400 MHz, CD_3CN) of **3**.

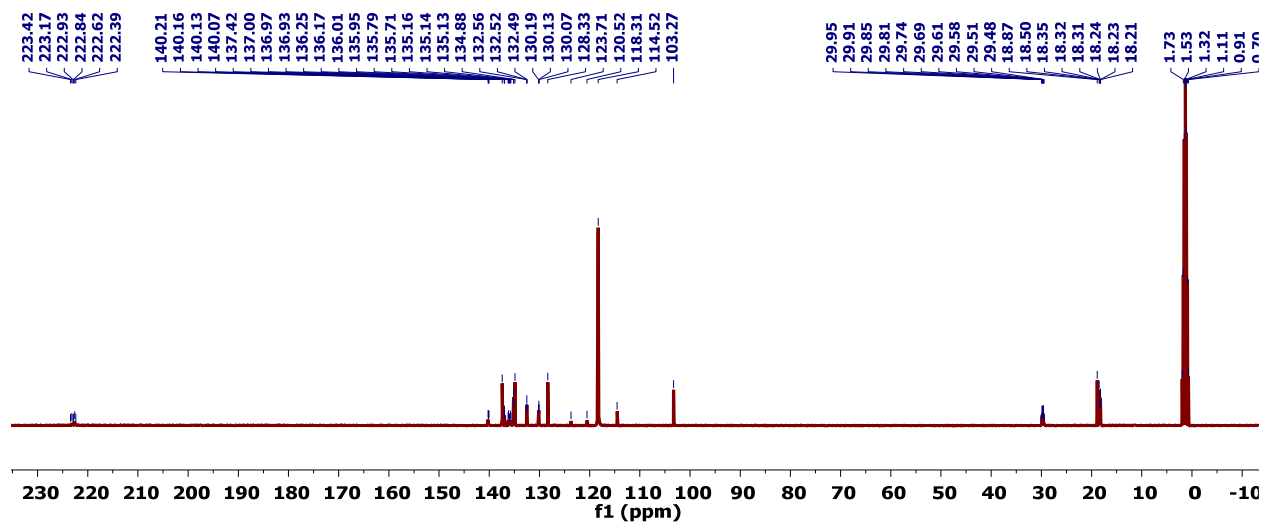


Figure D.50. $^{13}\text{C}\{^1\text{H}\}$ NMR spectrum (101 MHz, CD_3CN) of **3**.

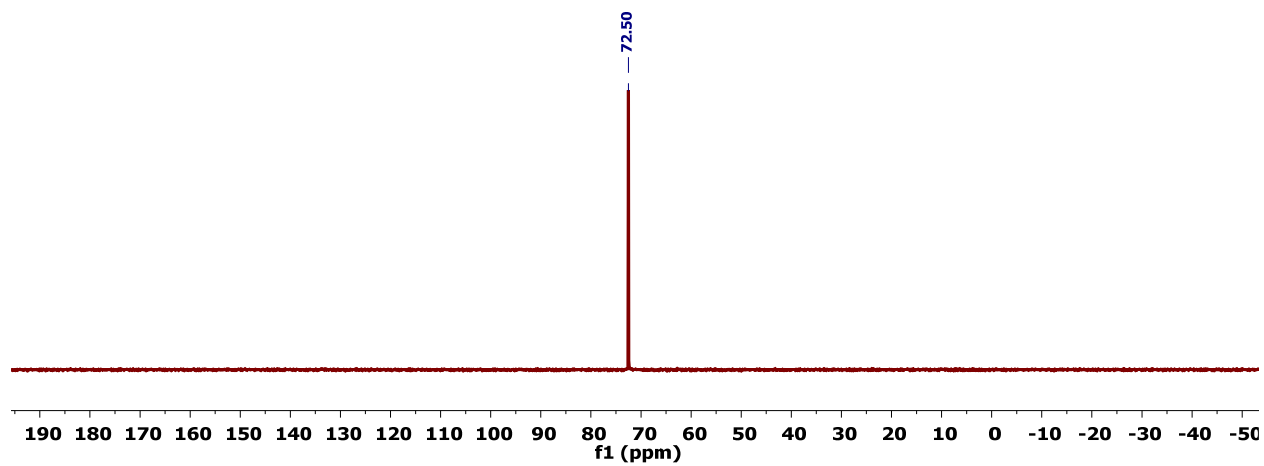


Figure D.51. $^{31}\text{P}\{^1\text{H}\}$ NMR spectrum (162 MHz, CD_3CN) of **3**.

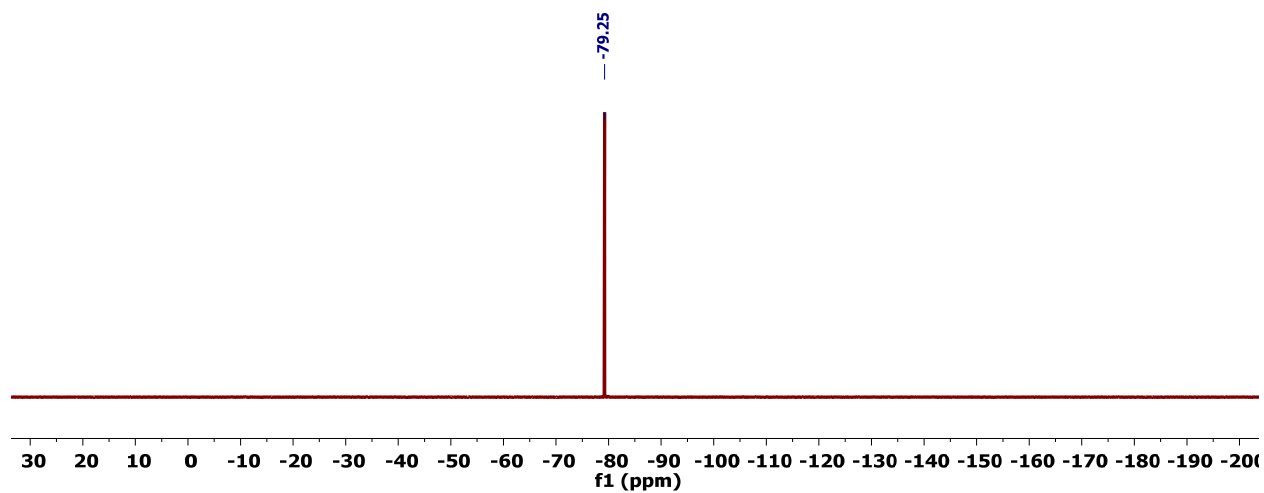


Figure D.52. ^{19}F NMR spectrum (376 MHz, CD_3CN) of **3**.

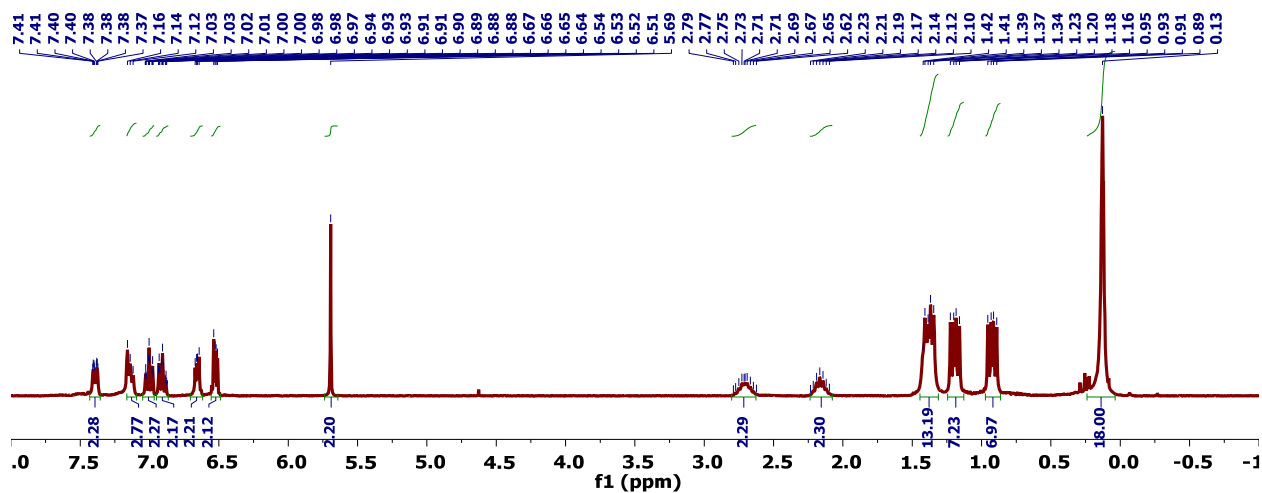


Figure D.53. ^1H NMR spectrum (300 MHz, C_6D_6) of 5.

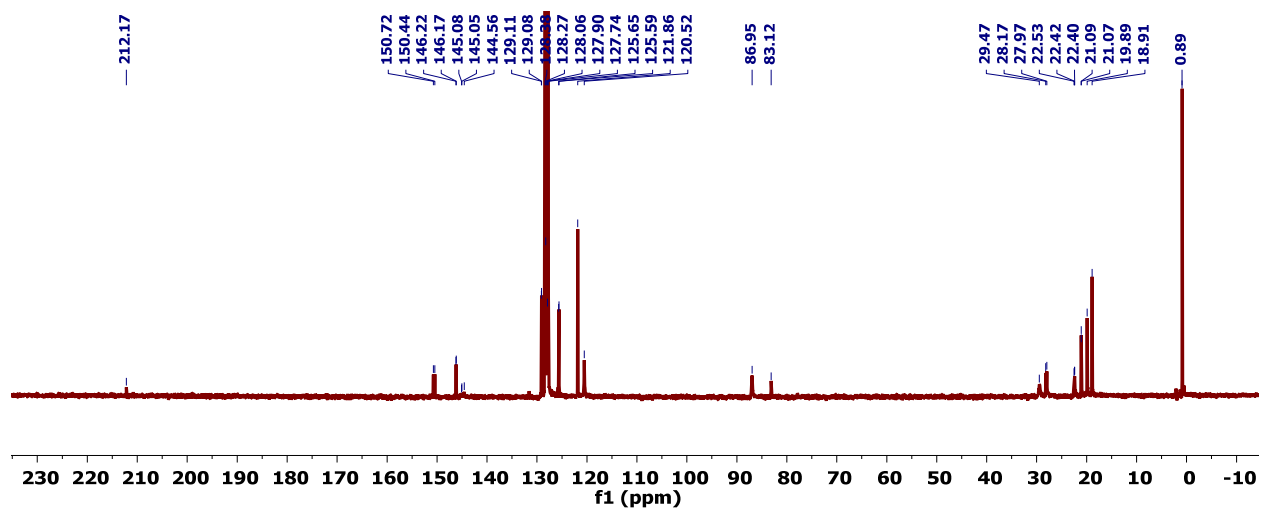


Figure D.54. $^{13}\text{C}\{^1\text{H}\}$ NMR spectrum (75 MHz, C_6D_6) of 5.

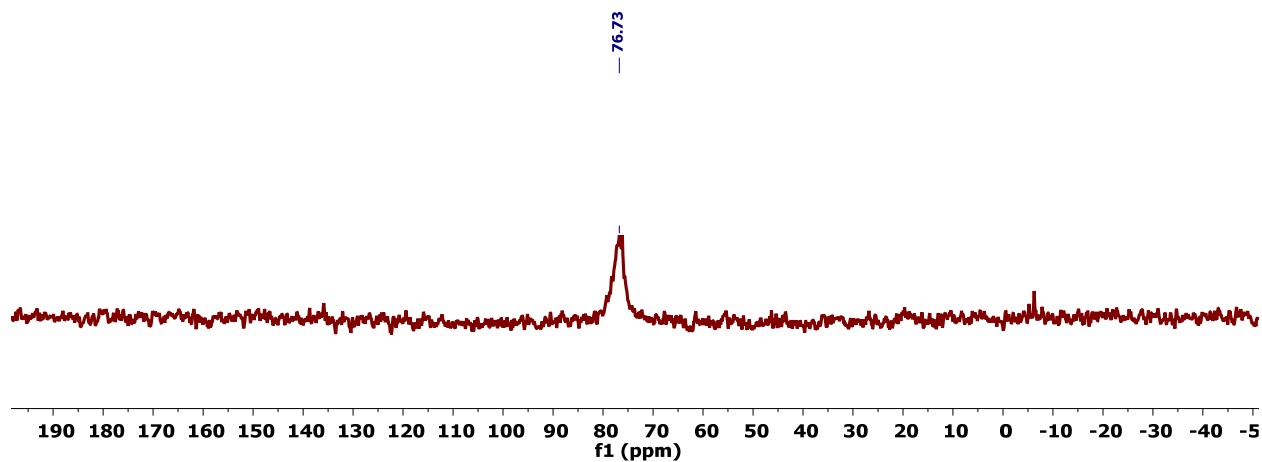


Figure D.55. $^{31}\text{P}\{^1\text{H}\}$ NMR spectrum (121 MHz, C_6D_6) of 5.

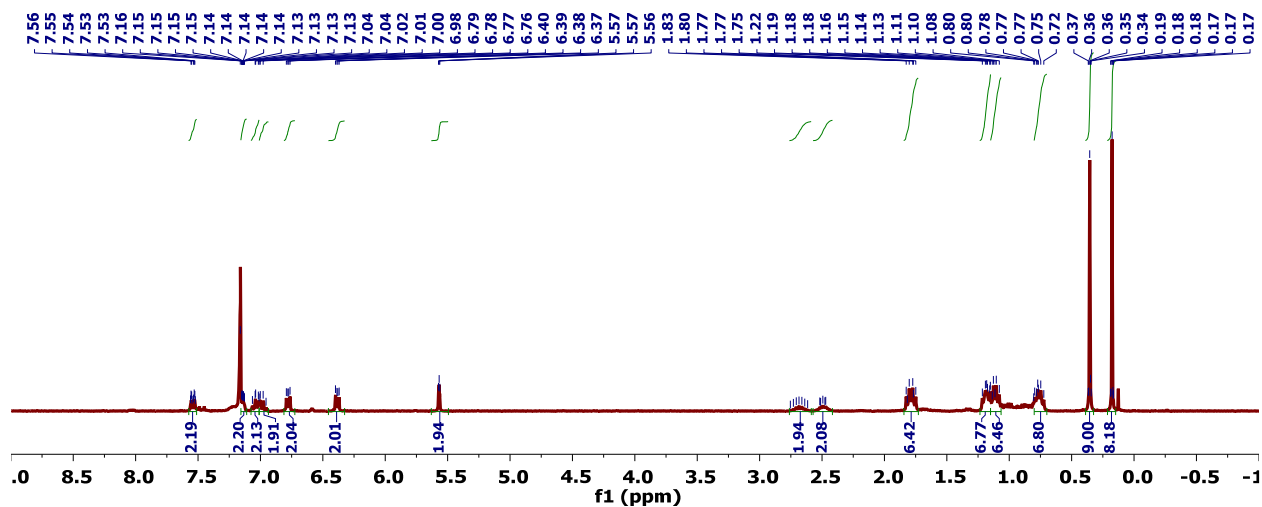


Figure D.56. ^1H NMR spectrum (300 MHz, C_6D_6) of 6.

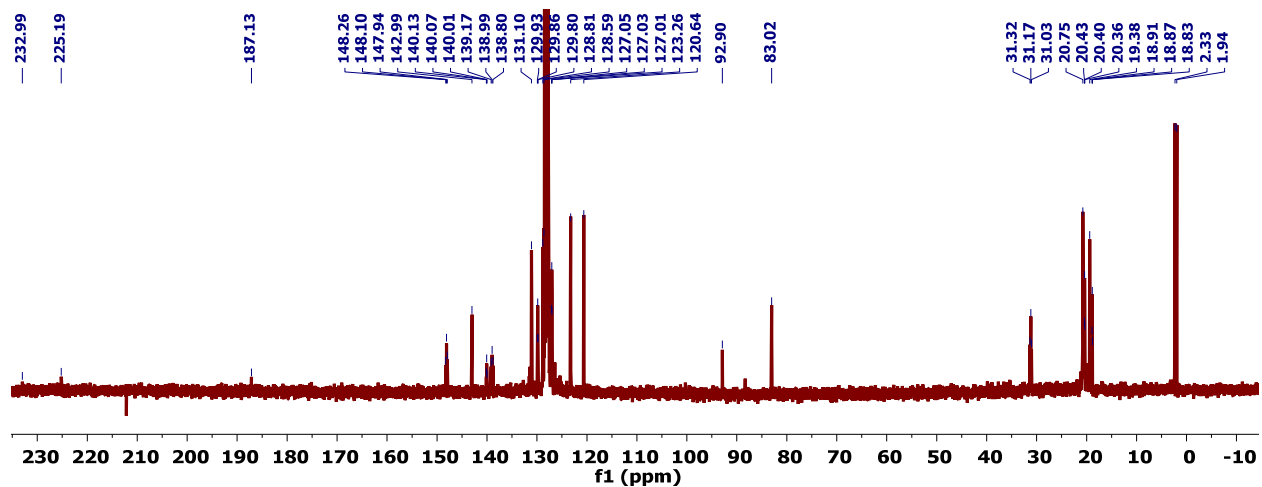


Figure D.57. $^{13}\text{C}\{^1\text{H}\}$ NMR spectrum (75 MHz, C_6D_6) of 6.

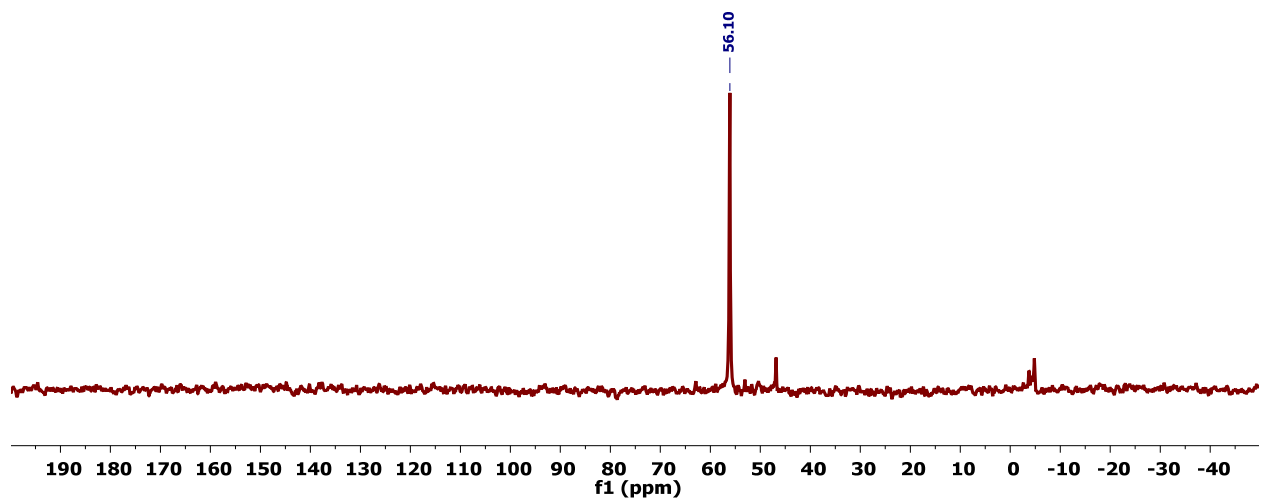


Figure D.58. $^{31}\text{P}\{^1\text{H}\}$ NMR spectrum (121 MHz, C_6D_6) of 6.

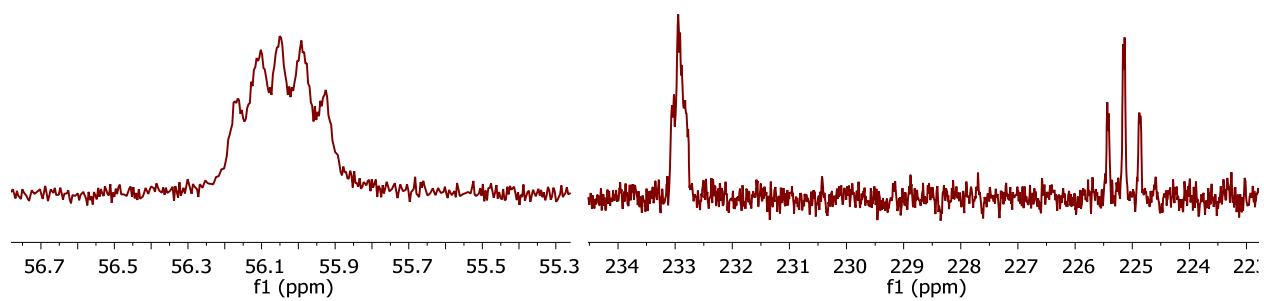


Figure D.59. $^{31}\text{P}\{^1\text{H}\}$ and $^{13}\text{C}\{^1\text{H}\}$ NMR spectra (121 MHz, C_6D_6) of **6- ^{13}C** .

CHAPTER 4

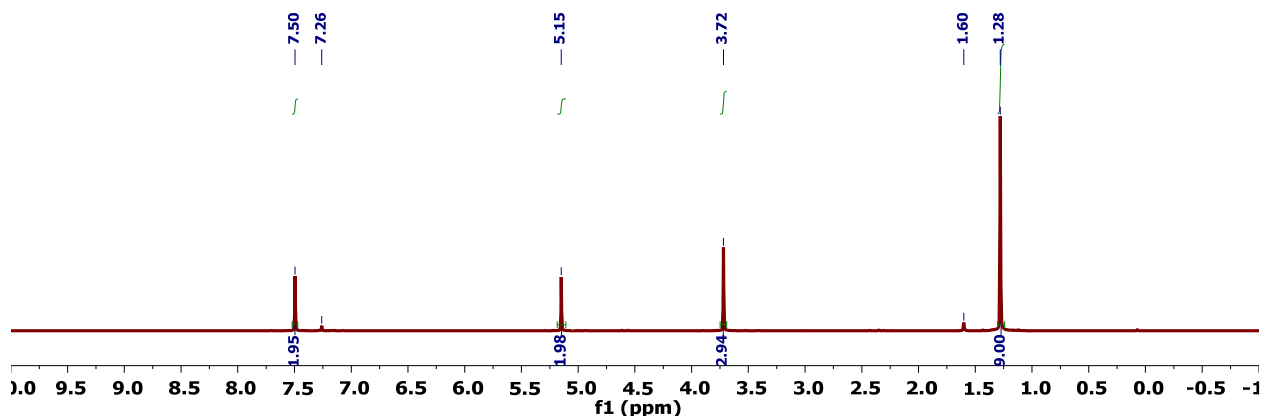


Figure D.60. ^1H NMR spectrum (400 MHz, CDCl_3) of 1,3-dibromo-5-(*tert*-butyl)-2-(methoxymethoxy)benzene.

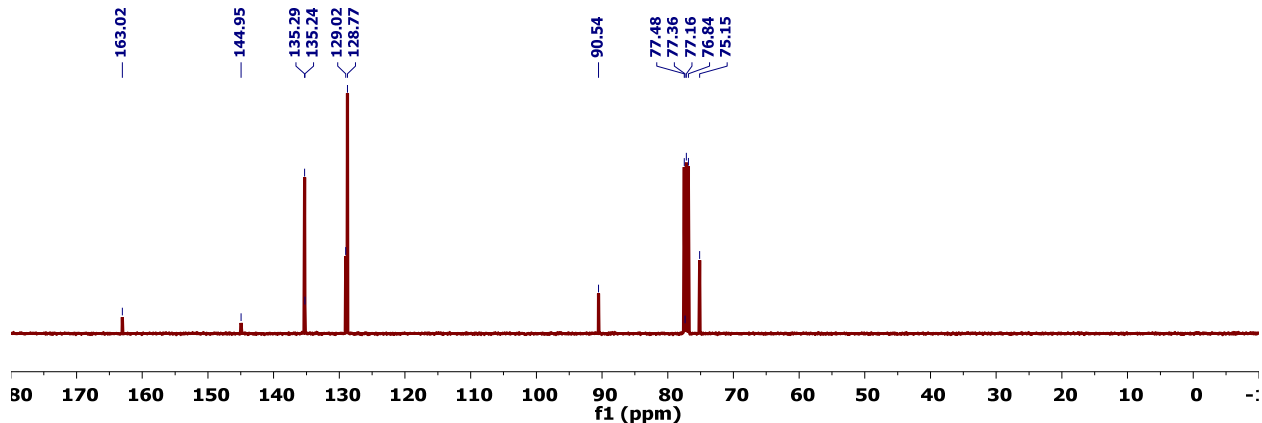


Figure D.61. $^{13}\text{C}\{^1\text{H}\}$ NMR spectrum (101 MHz, CDCl_3) of 1,3-dibromo-5-(*tert*-butyl)-2-(methoxymethoxy)benzene.

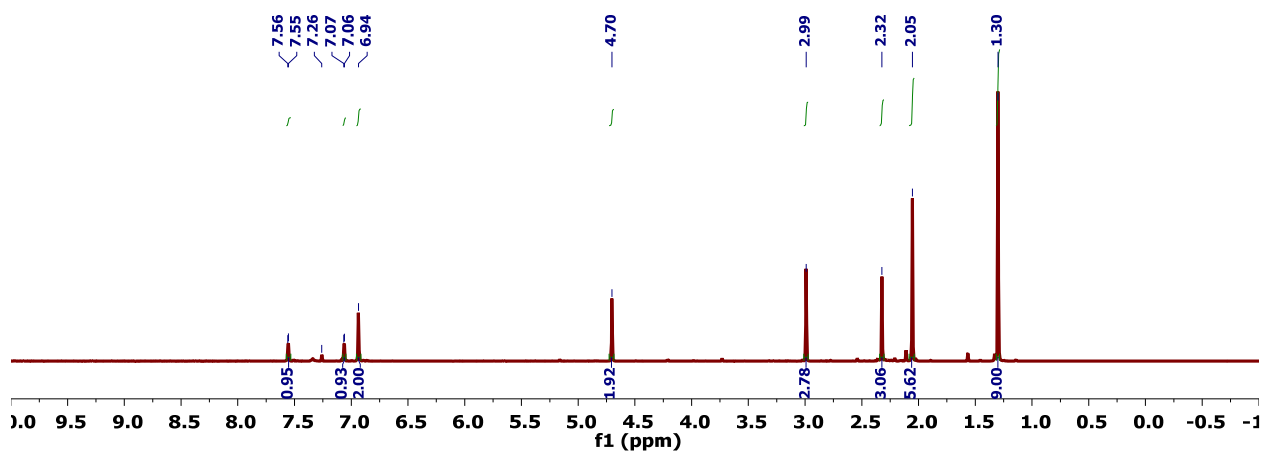


Figure D.62. ^1H NMR spectrum (400 MHz, CDCl_3) of 3-bromo-5-(*tert*-butyl)-2-(methoxymethoxy)-2',4',6'-trimethyl-1,1'-biphenyl.

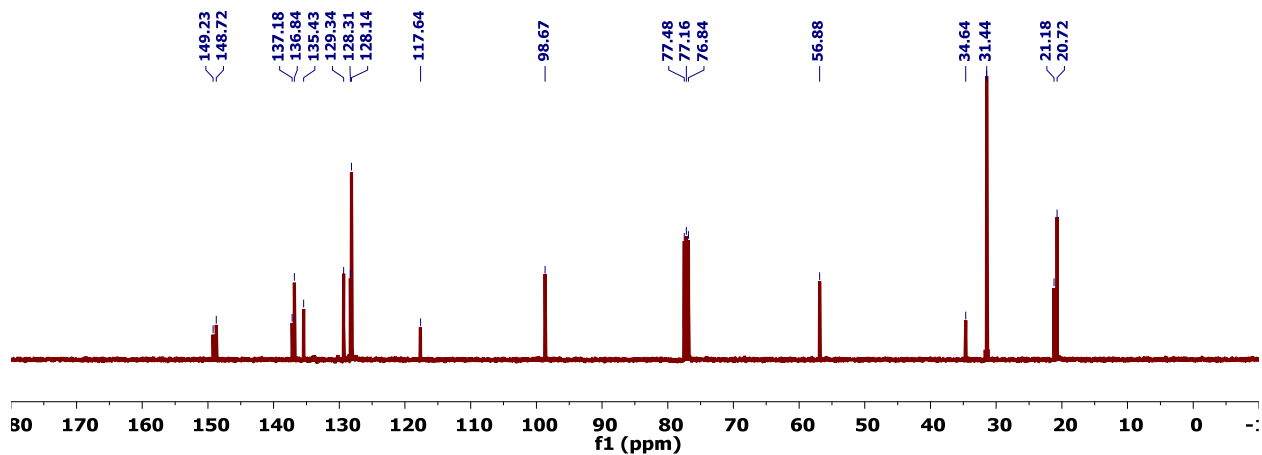


Figure D.63. $^{13}\text{C}\{^1\text{H}\}$ NMR spectrum (101MHz, CDCl_3) of 3-bromo-5-(*tert*-butyl)-2-(methoxymethoxy)-2',4',6'-trimethyl-1,1'-biphenyl.

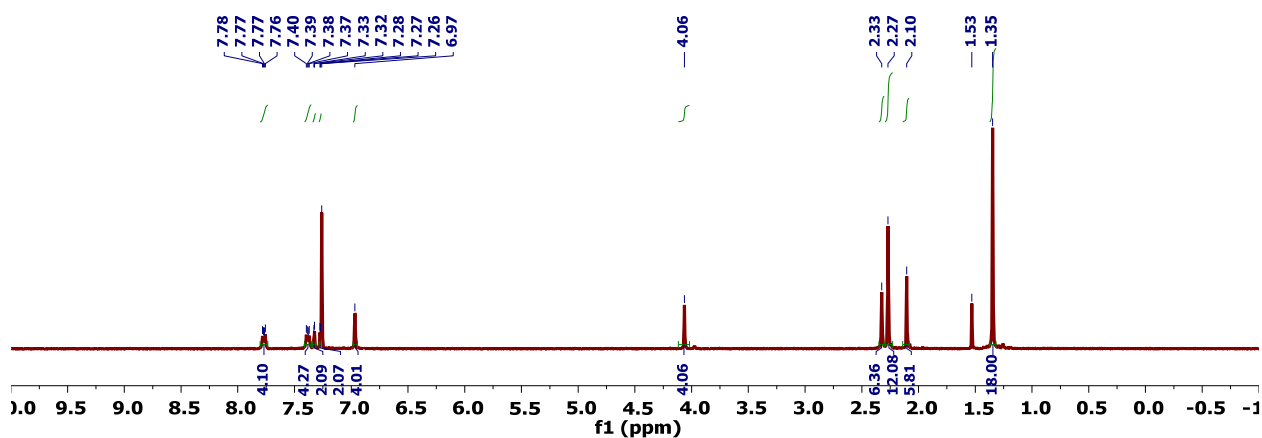


Figure D.64. ^1H NMR spectrum (400 MHz, CDCl_3) of *anti*-9,10-bis(5-(*tert*-butyl)-2-(methoxymethoxy)-2',4',6'-trimethyl-[1,1'-biphenyl]-3-yl)anthracene.

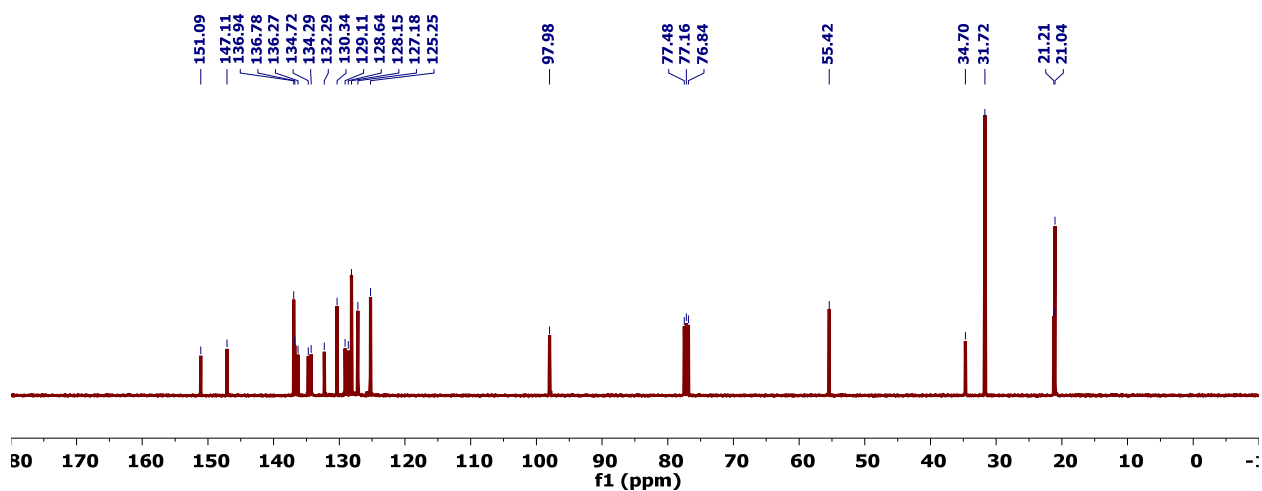


Figure D.65. $^{13}\text{C}\{^1\text{H}\}$ NMR spectrum (101MHz, CDCl_3) of *anti*-9,10-bis(5-(*tert*-butyl)-2-(methoxymethoxy)-2',4',6'-trimethyl-[1,1'-biphenyl]-3-yl)anthracene.

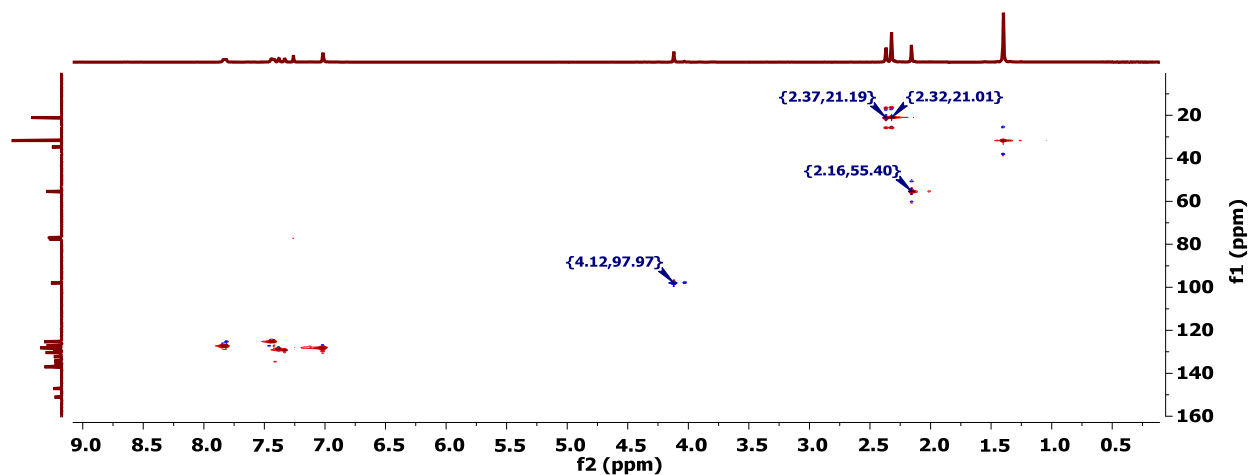


Figure D.66. HSQC NMR spectrum of *anti*-9,10-bis(5-(*tert*-butyl)-2-(methoxymethoxy)-2',4',6'-trimethyl-[1,1'-biphenyl]-3-yl)anthracene.

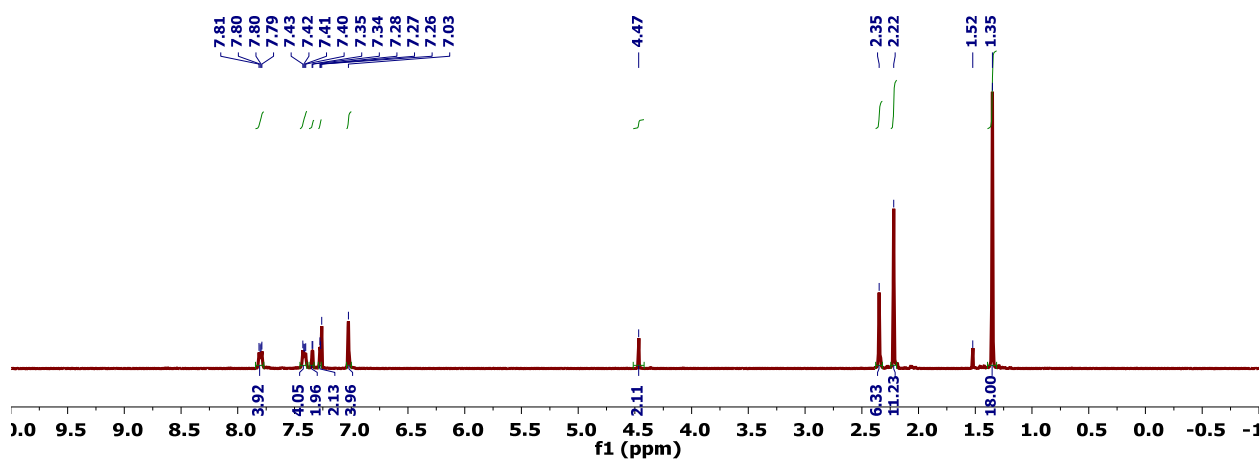


Figure D.67. ^1H NMR spectrum (400 MHz, CDCl_3) of *anti*-3,3''-(anthracene-9,10-diyl)bis(5-(*tert*-butyl)-2',4',6'-trimethyl-[1,1'-biphenyl]-2-ol).

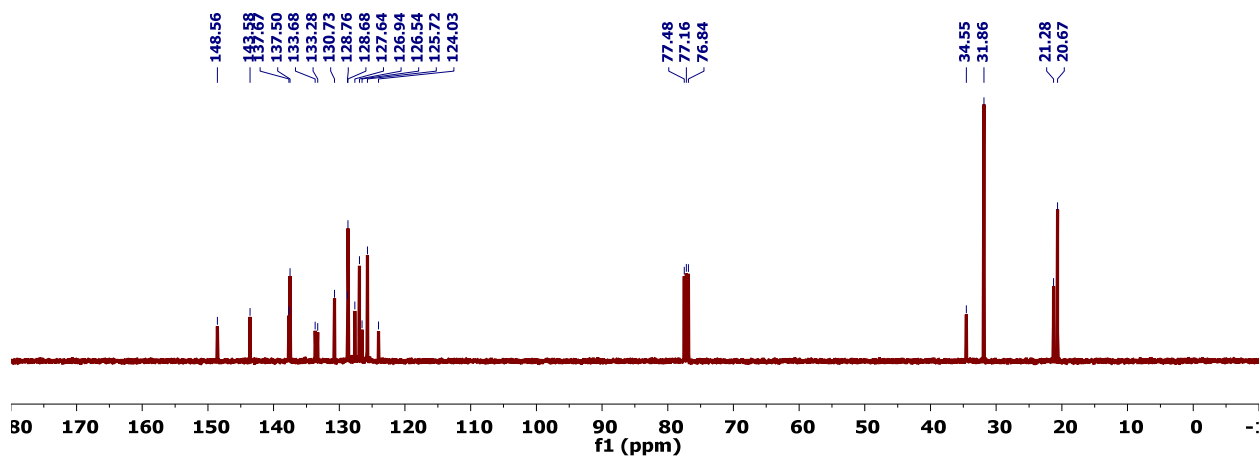


Figure D.68. $^{13}\text{C}\{^1\text{H}\}$ NMR spectrum (101 MHz, CDCl_3) of *anti*-3,3''-(anthracene-9,10-diyl)bis(5-(*tert*-butyl)-2',4',6'-trimethyl-[1,1'-biphenyl]-2-ol).

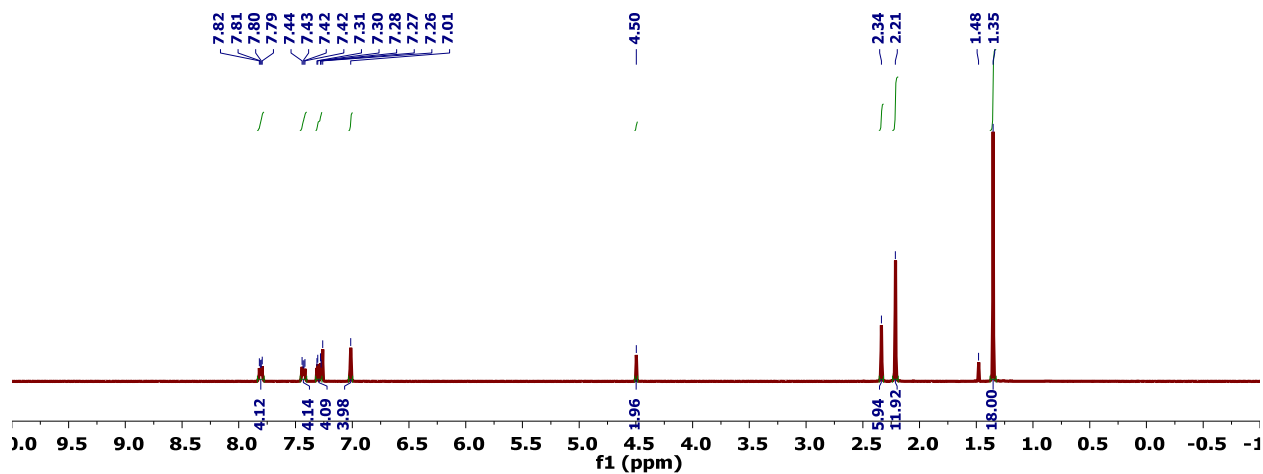


Figure D.69. ^1H NMR spectrum (400 MHz, CDCl_3) of *syn*-3,3''-(anthracene-9,10-diyl)bis(5-(*tert*-butyl)-2',4',6'-trimethyl-[1,1'-biphenyl]-2-ol) (**LH**₂).

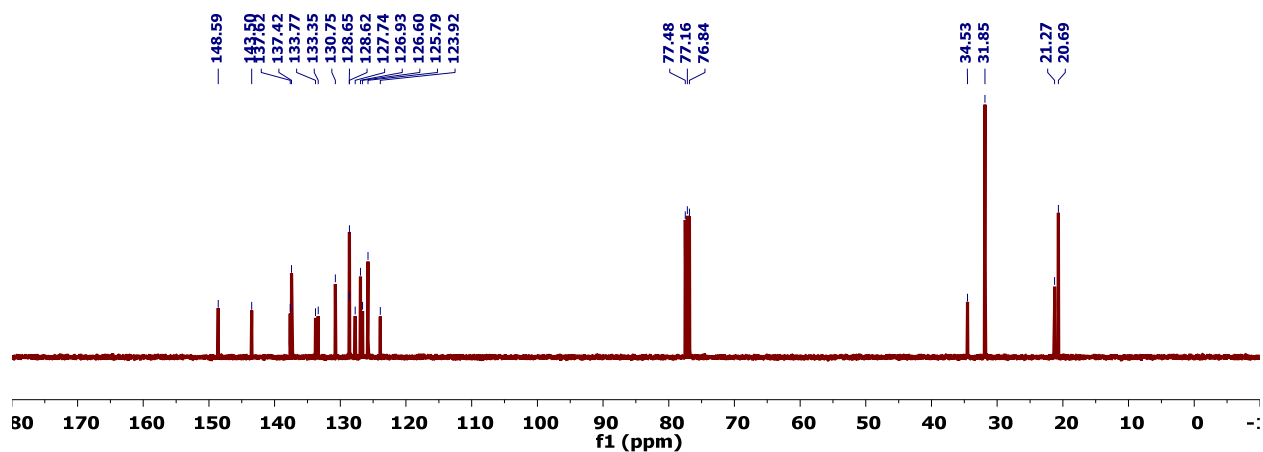


Figure D.70. $^{13}\text{C}\{^1\text{H}\}$ NMR spectrum (101 MHz, CDCl_3) of *syn*-3,3''-(anthracene-9,10-diyl)bis(5-(*tert*-butyl)-2',4',6'-trimethyl-[1,1'-biphenyl]-2-ol) (**LH**₂).

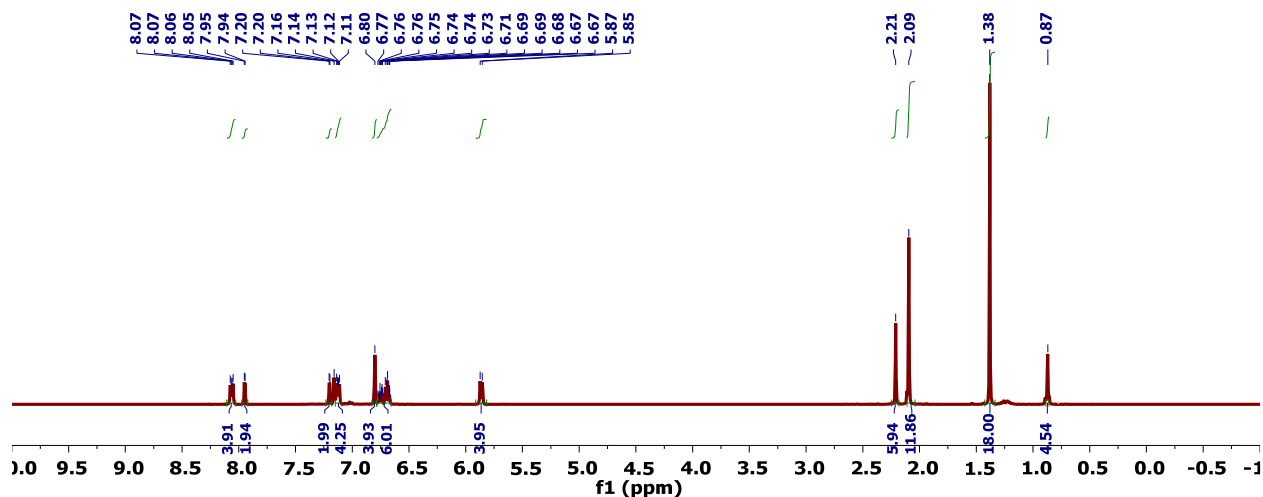


Figure D.71. ^1H NMR spectrum (400 MHz, C_6D_6) of **1**.

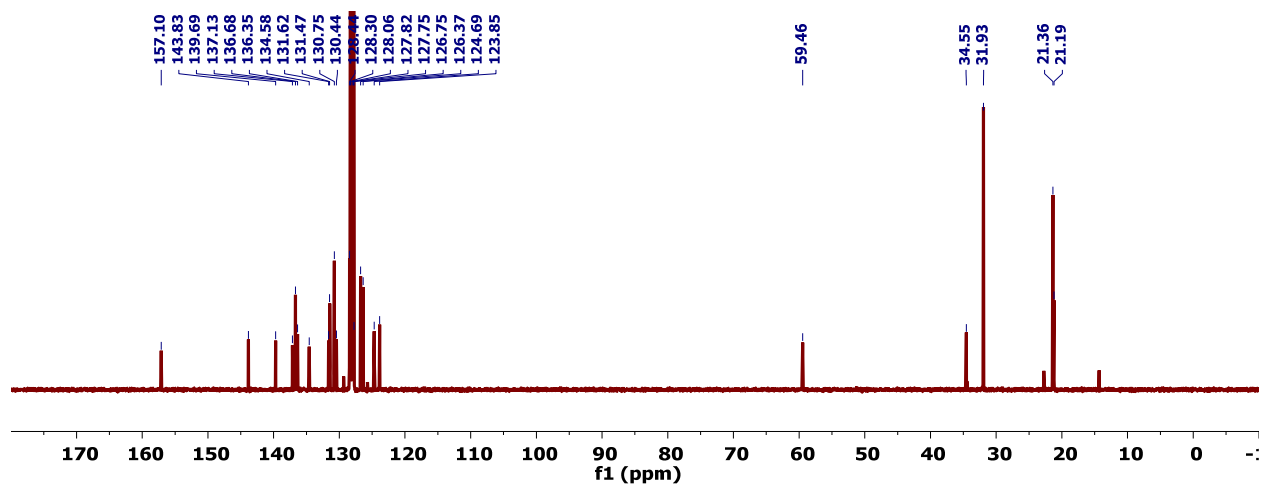


Figure D.72. $^{13}\text{C}\{^1\text{H}\}$ NMR spectrum (101MHz, C_6D_6) of 1.

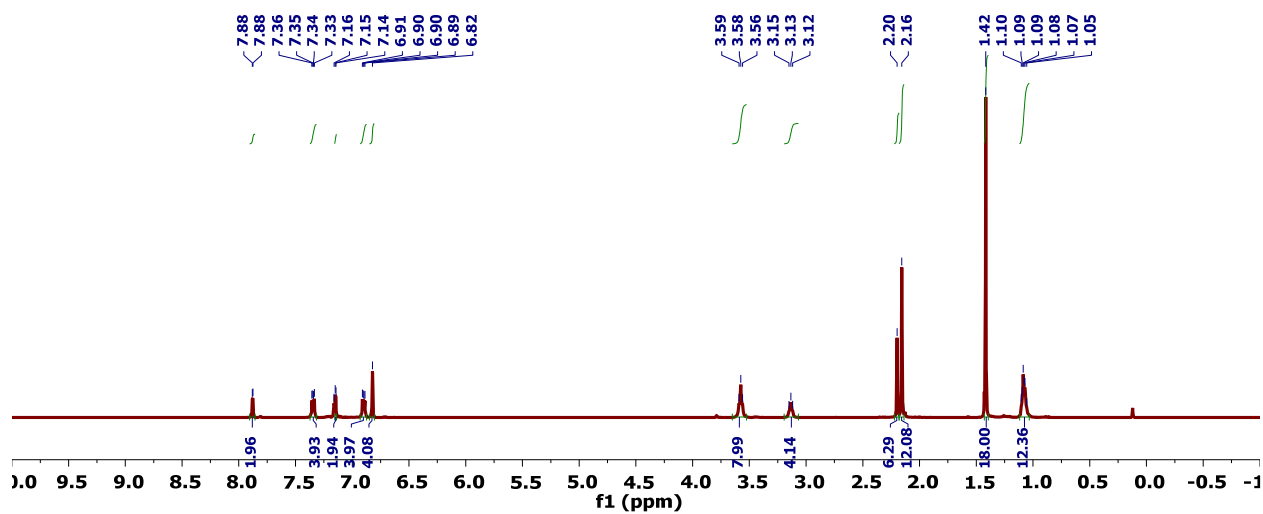


Figure D.73. ^1H NMR spectrum (400 MHz, C_6D_6) of 2.

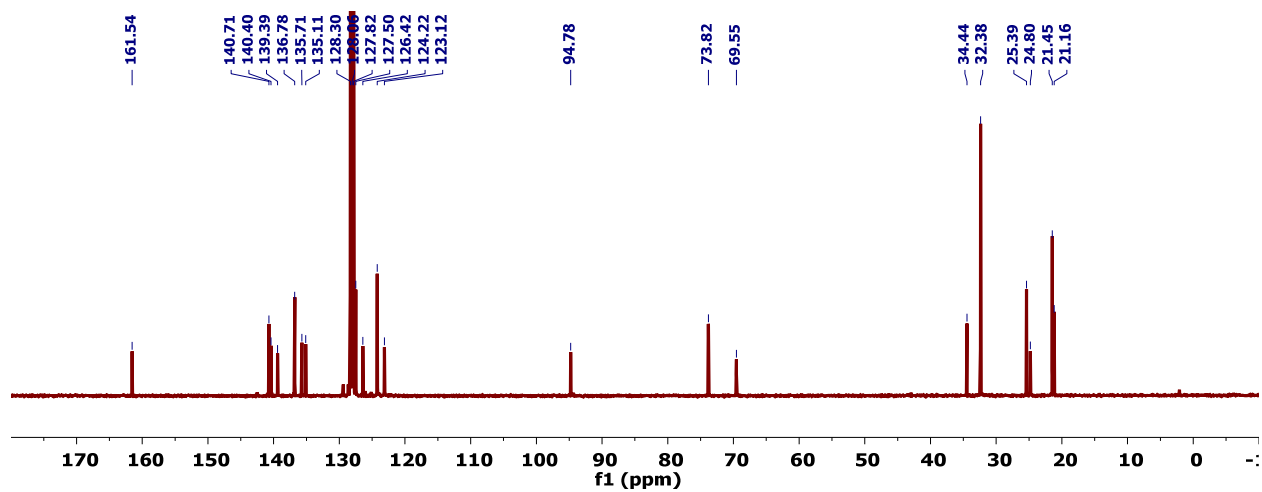


Figure D.74. $^{13}\text{C}\{^1\text{H}\}$ NMR spectrum (101MHz, C_6D_6) of 2.

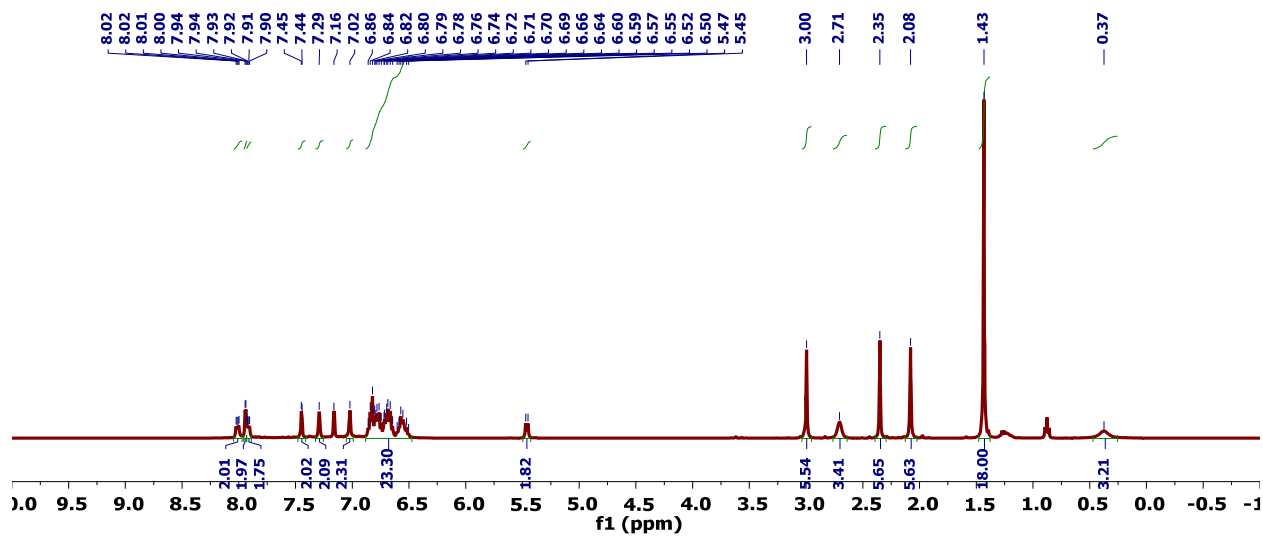


Figure D.75. ^1H NMR spectrum (400 MHz, C_6D_6) of 3a.

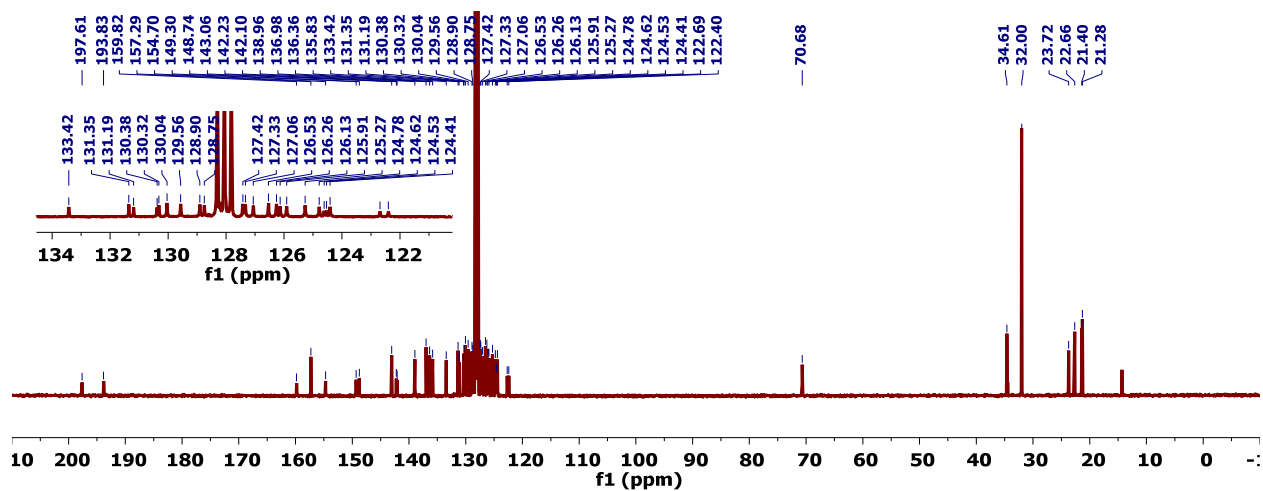


Figure D.76. $^{13}\text{C}\{^1\text{H}\}$ NMR spectrum (101 MHz, C_6D_6) of 3a.

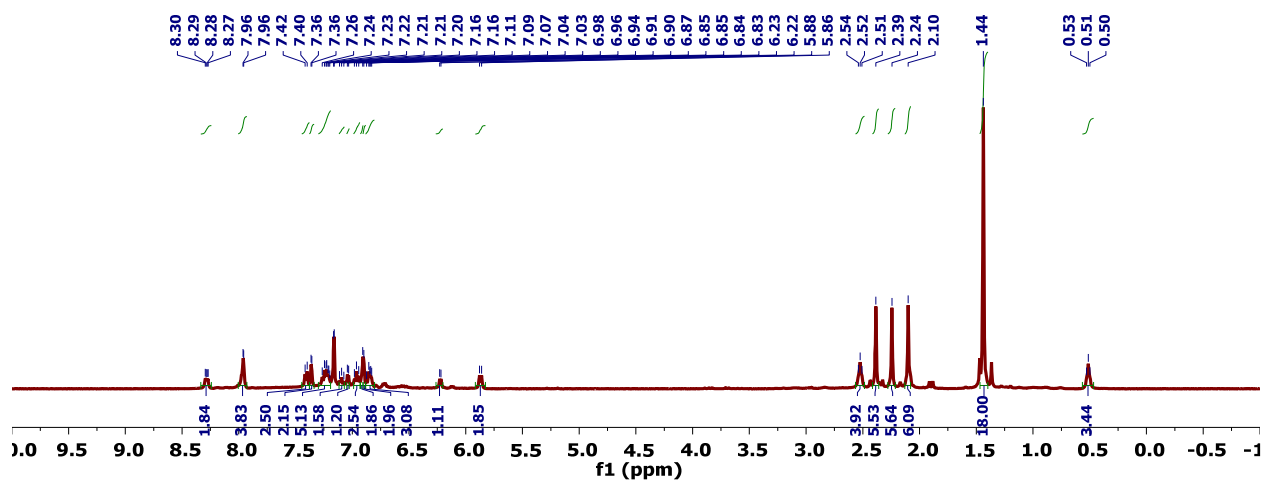


Figure D.77. ^1H NMR spectrum (400 MHz, C_6D_6) of 3b.

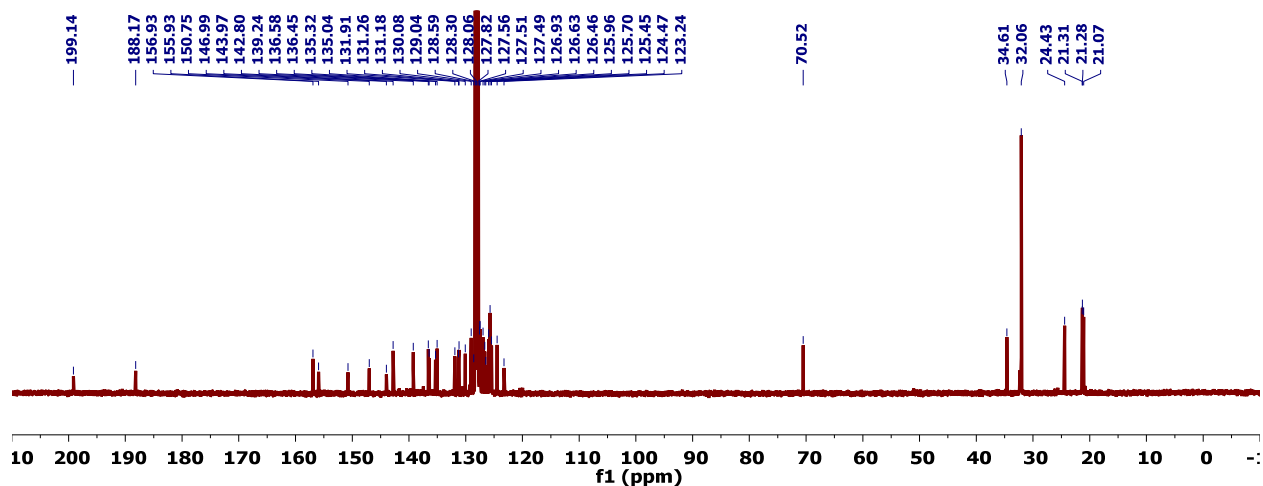


Figure D.78. $^{13}\text{C}\{^1\text{H}\}$ NMR spectrum (101MHz, C_6D_6) of 3b.

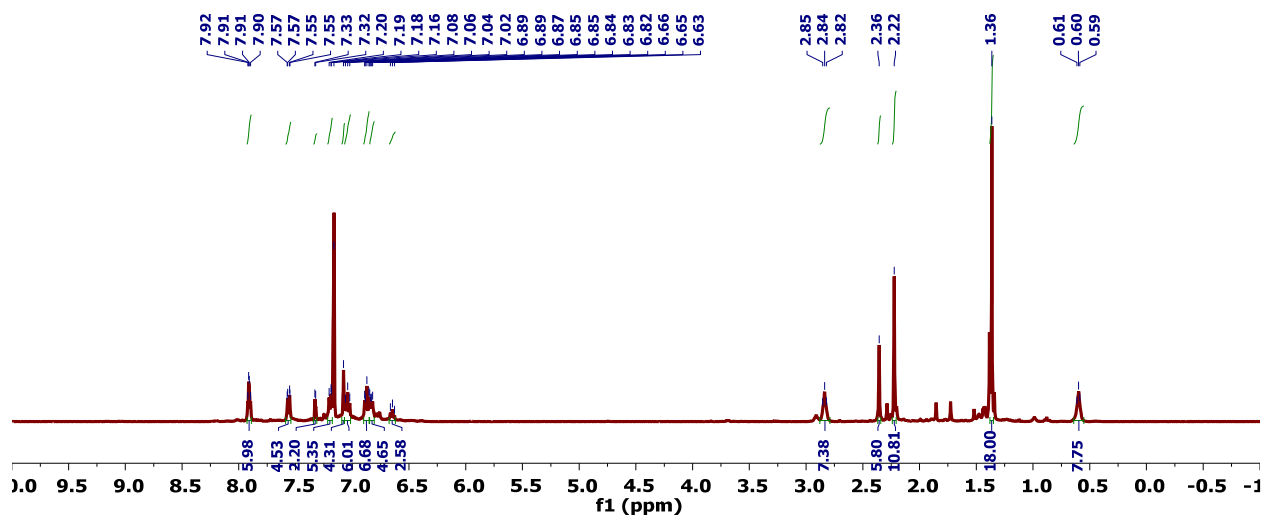


Figure D.79. ^1H NMR spectrum (400 MHz, C_6D_6) of 4.

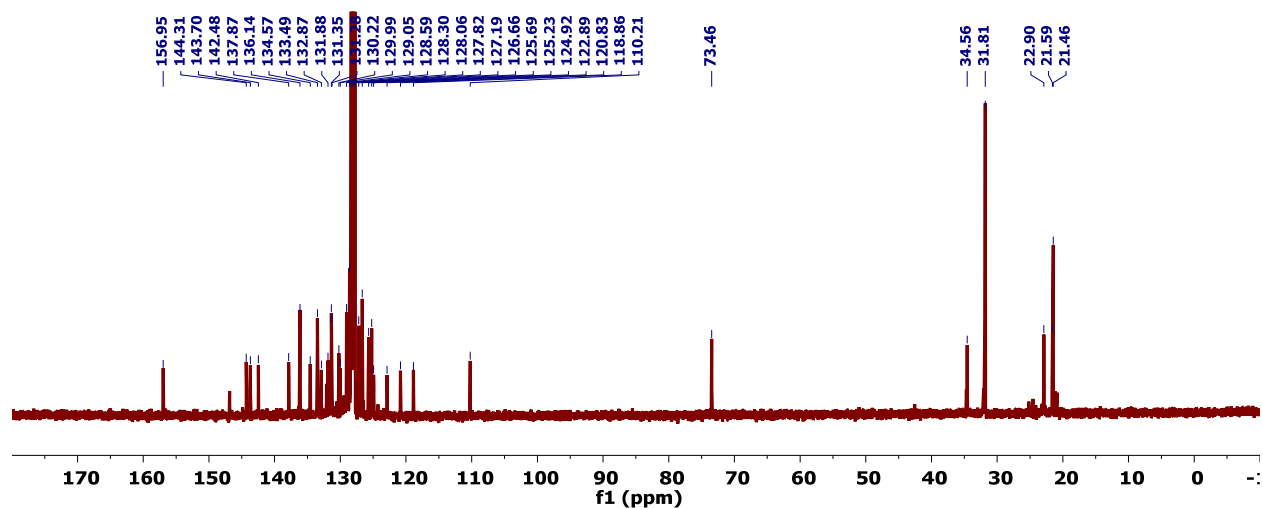


Figure D.80. $^{13}\text{C}\{^1\text{H}\}$ NMR spectrum (101MHz, C_6D_6) of 4.

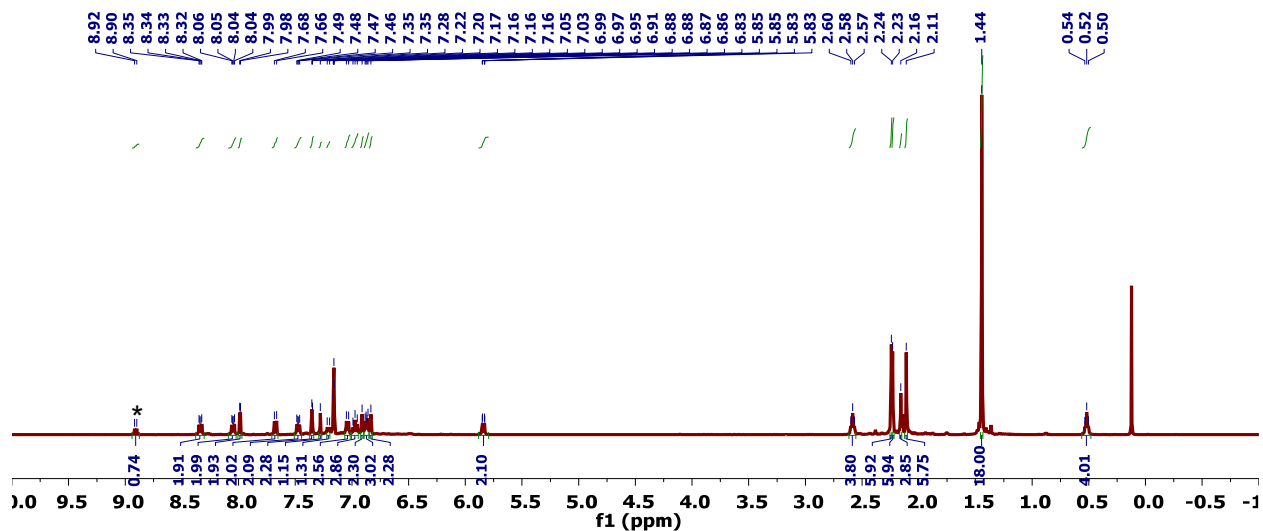


Figure D.81. ^1H NMR spectrum (400 MHz, C_6D_6) of **5**.

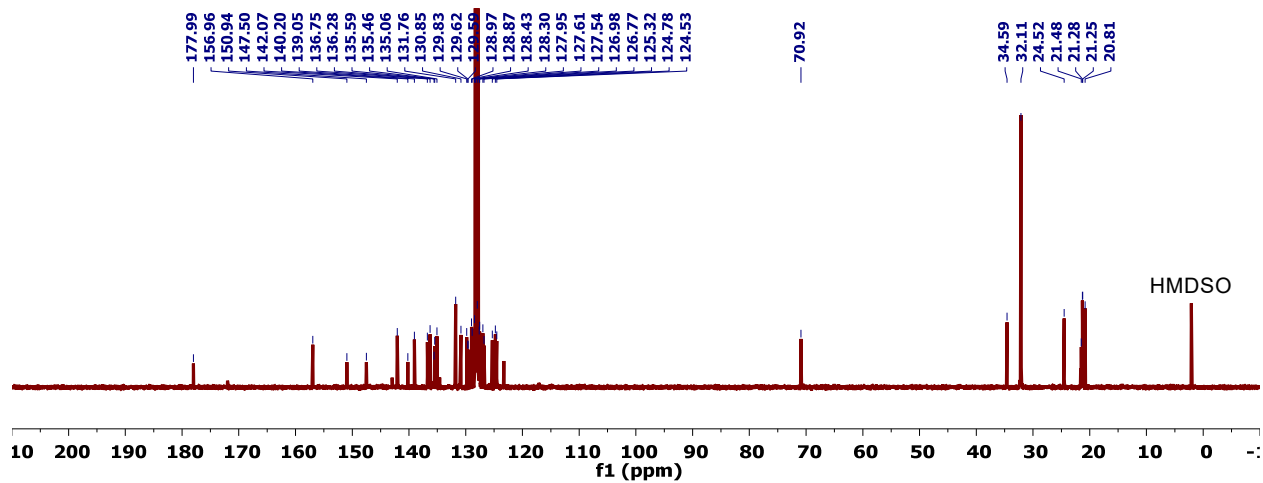


Figure D.82. $^{13}\text{C}\{^1\text{H}\}$ NMR spectrum (101MHz, C_6D_6) of **5**.

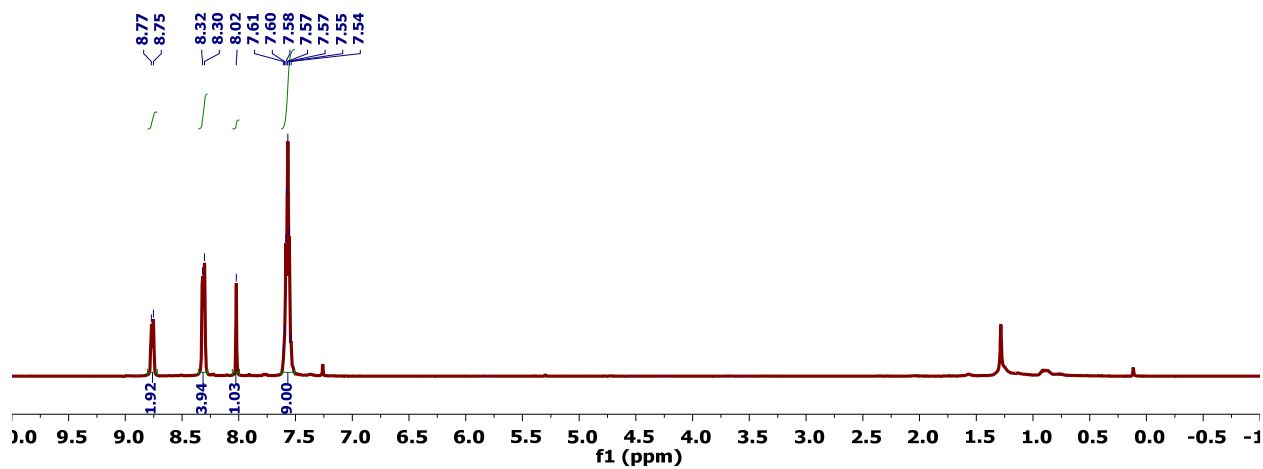


Figure D.83. ^1H NMR spectrum (400 MHz, CDCl_3) of **6a**.

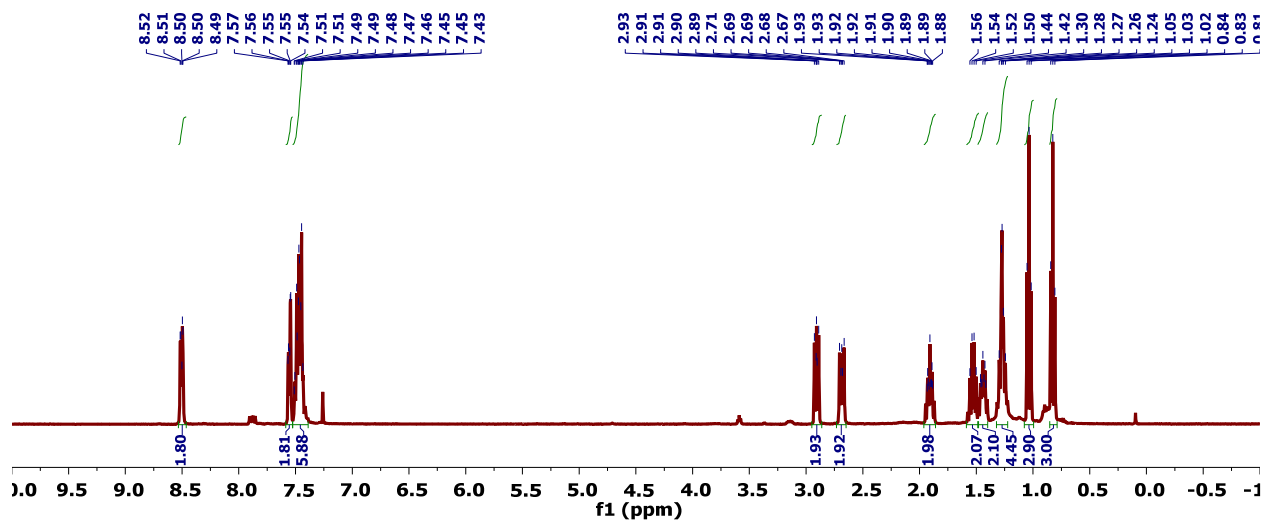


Figure D.84. ^1H NMR spectrum (400 MHz, CDCl_3) of **6b**.

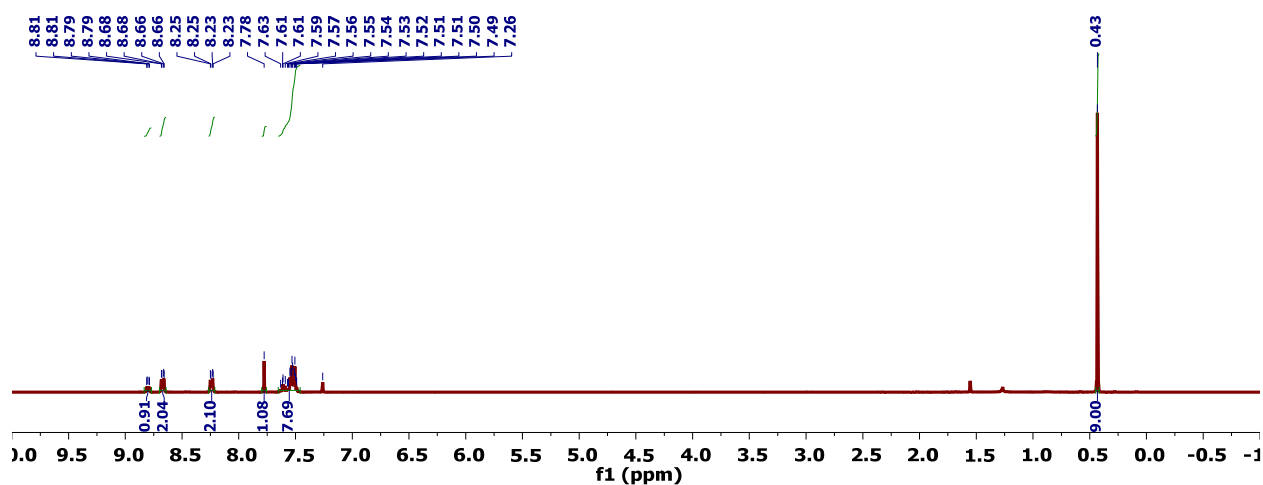


Figure D.85. ^1H NMR spectrum (400 MHz, CDCl_3) of **6c**.

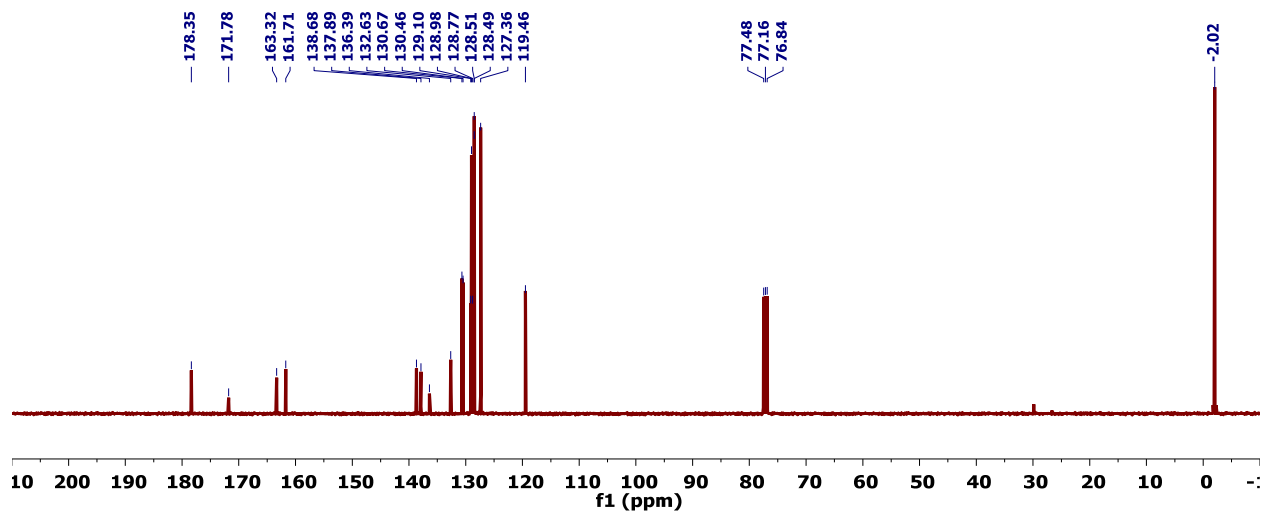


Figure D.86. $^{13}\text{C}\{^1\text{H}\}$ NMR spectrum (101 MHz, CDCl_3) of **6c**.

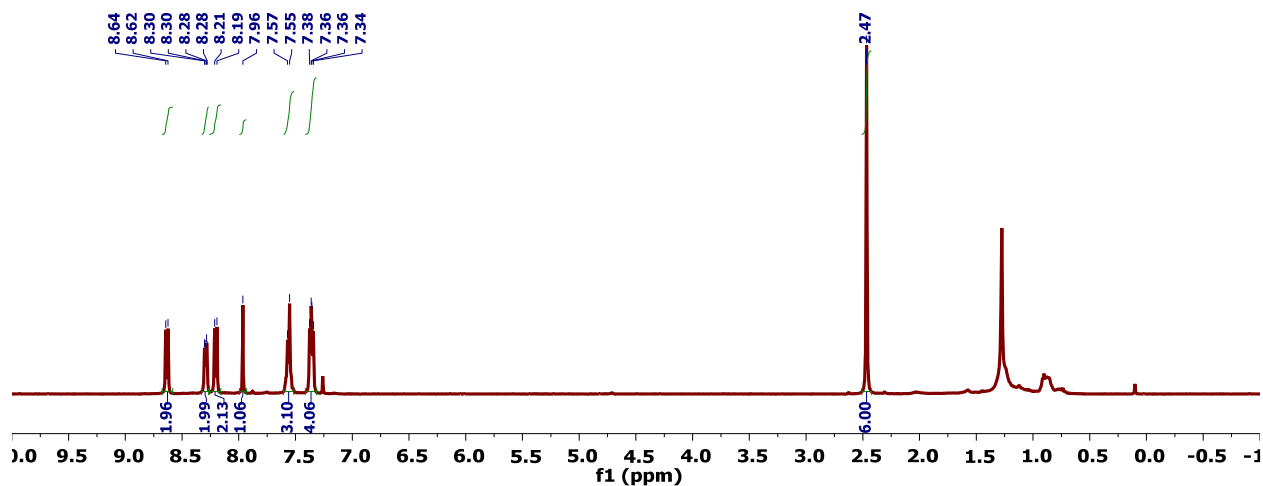


Figure D.87. ^1H NMR spectrum (400 MHz, CDCl_3) of **6d**.

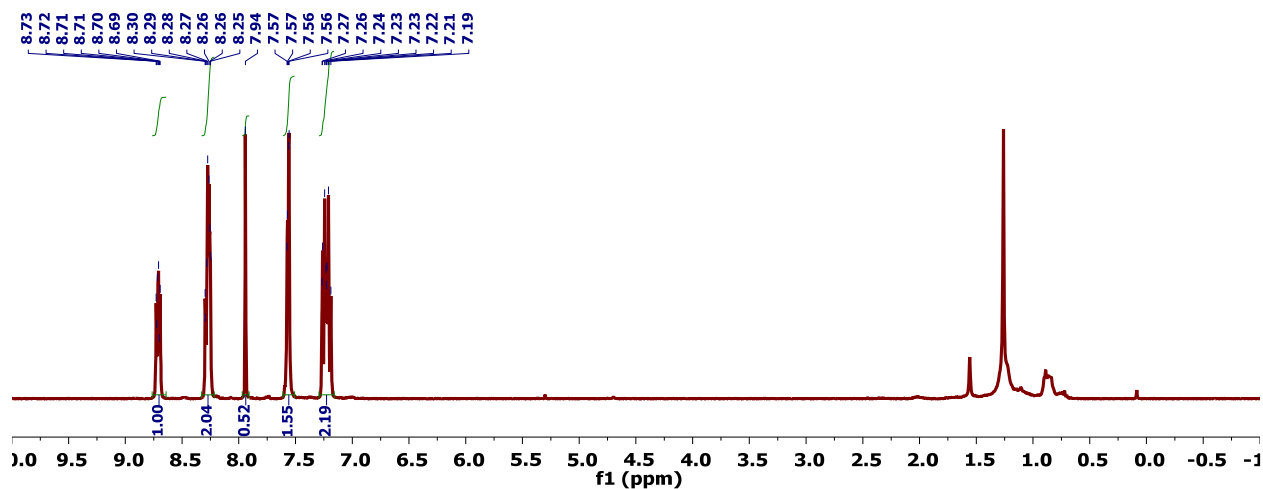


Figure D.88. ^1H NMR spectrum (400 MHz, CDCl_3) of **6e**.

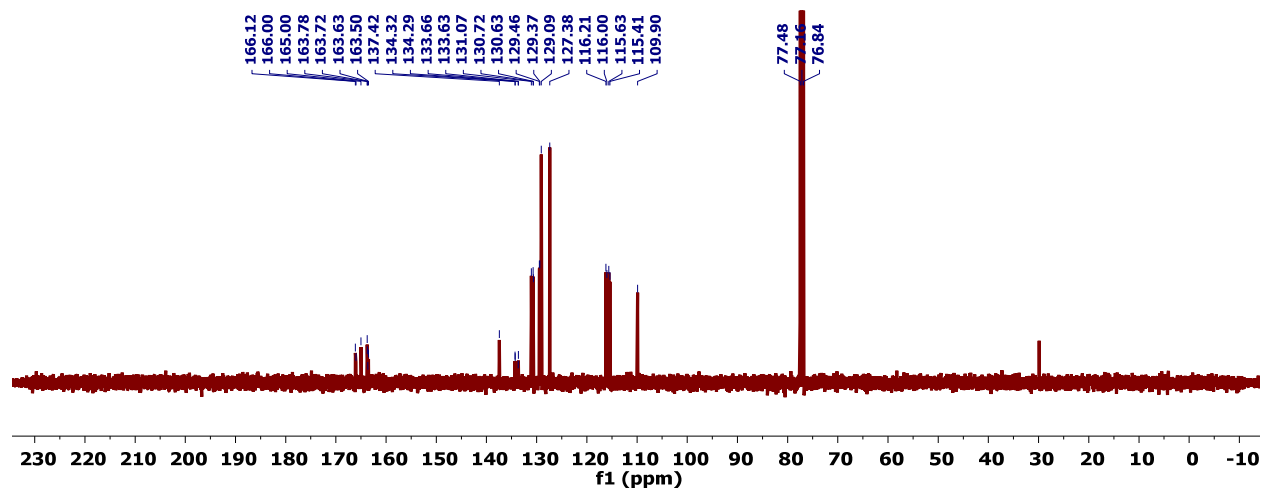


Figure D.89. $^{13}\text{C}\{^1\text{H}\}$ NMR spectrum (101 MHz, CDCl_3) of **6e**.

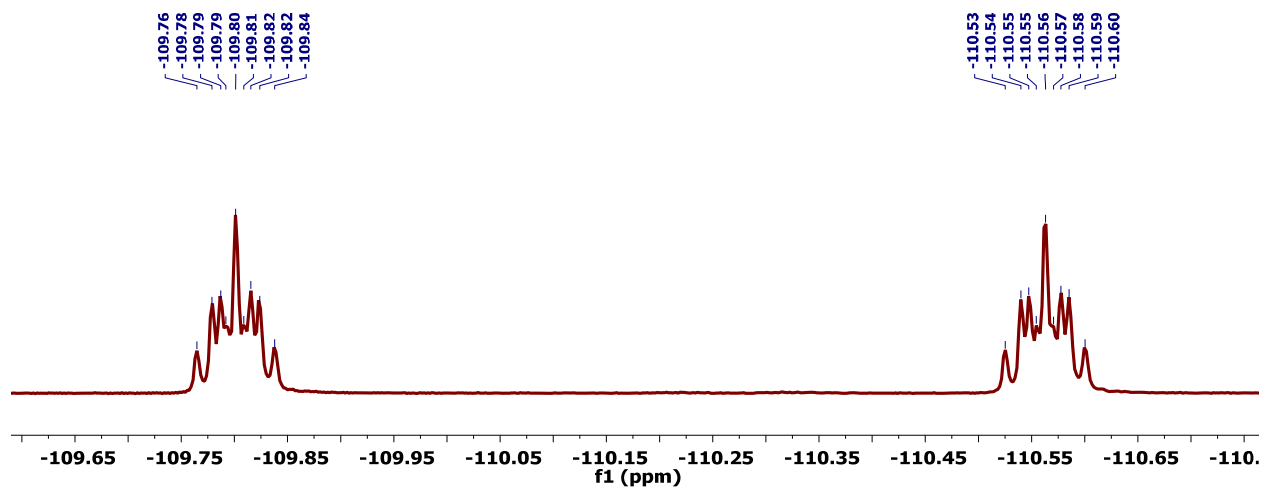


Figure D.90. ^{19}F NMR spectrum (376 MHz, CDCl_3) of **6e**.

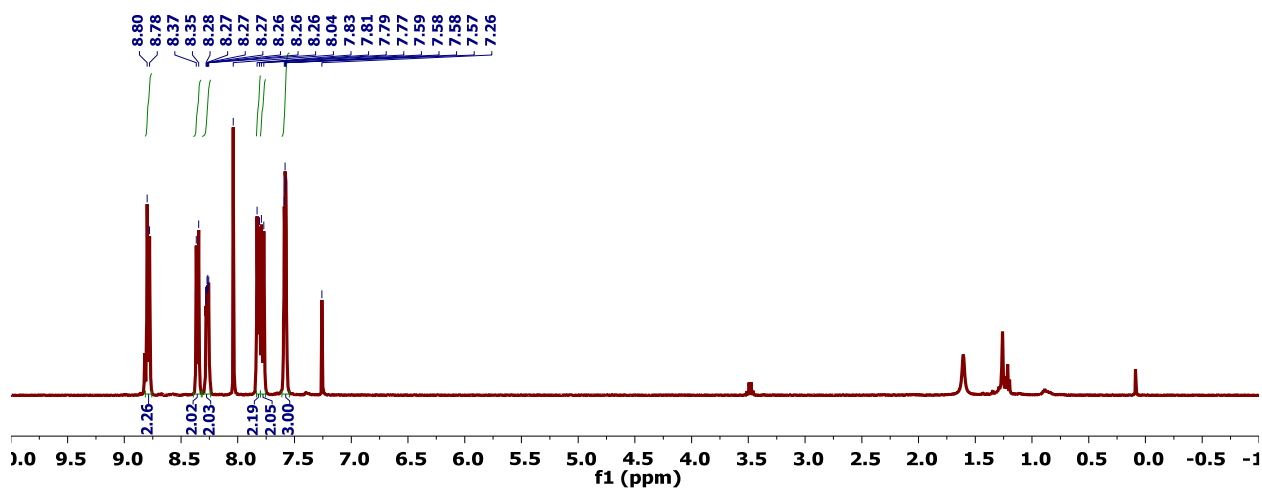


Figure D.91. ^1H NMR spectrum (400 MHz, CDCl_3) of **6f**.

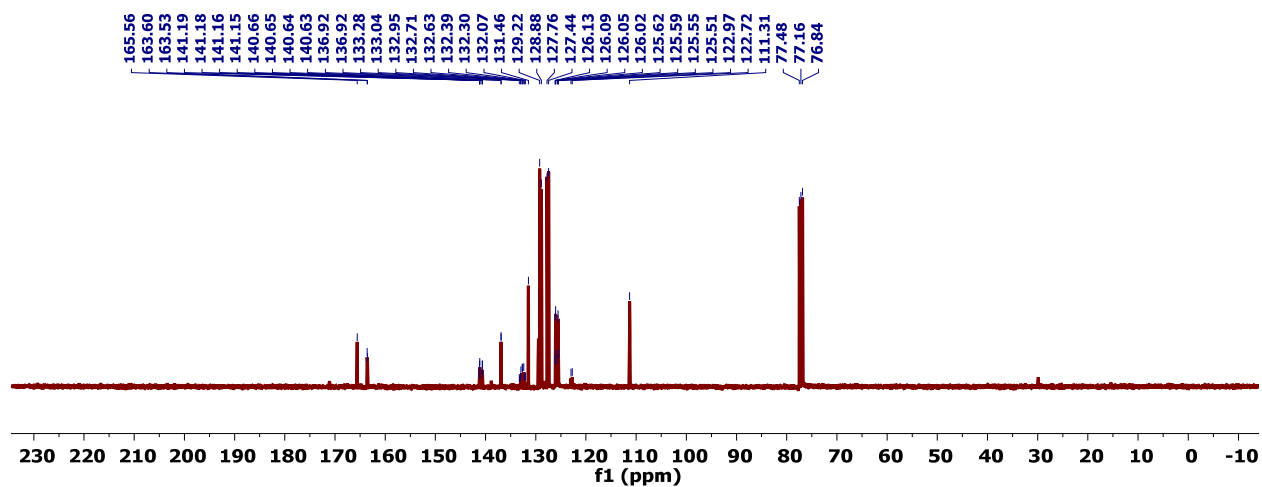


Figure D.92. $^{13}\text{C}\{^1\text{H}\}$ NMR spectrum (101 MHz, CDCl_3) of **6f**.

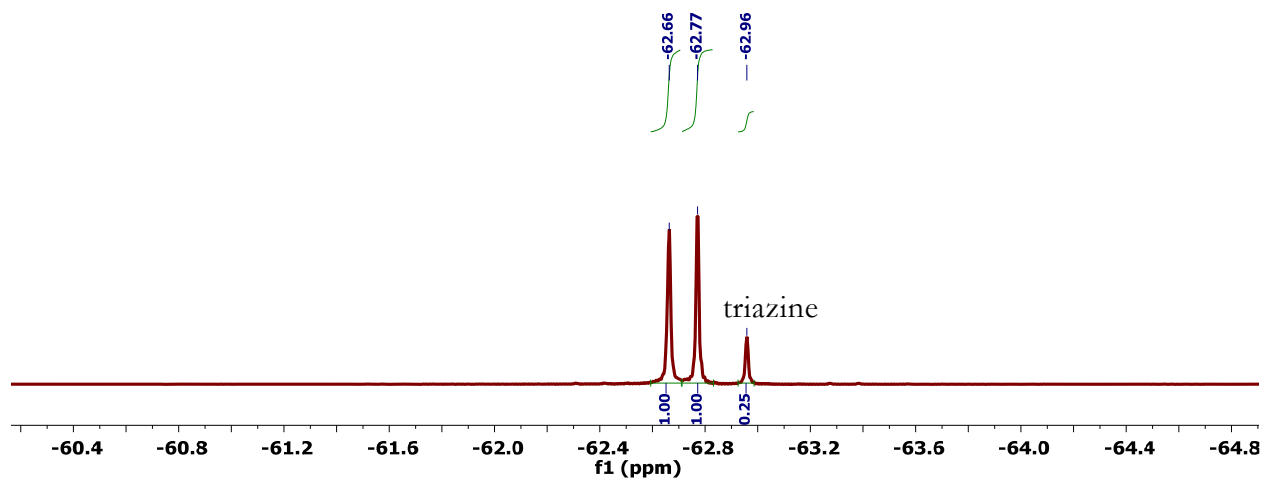


Figure D.93. ^{19}F NMR spectrum (376 MHz, CDCl_3) of **6f**.

CHAPTER 5

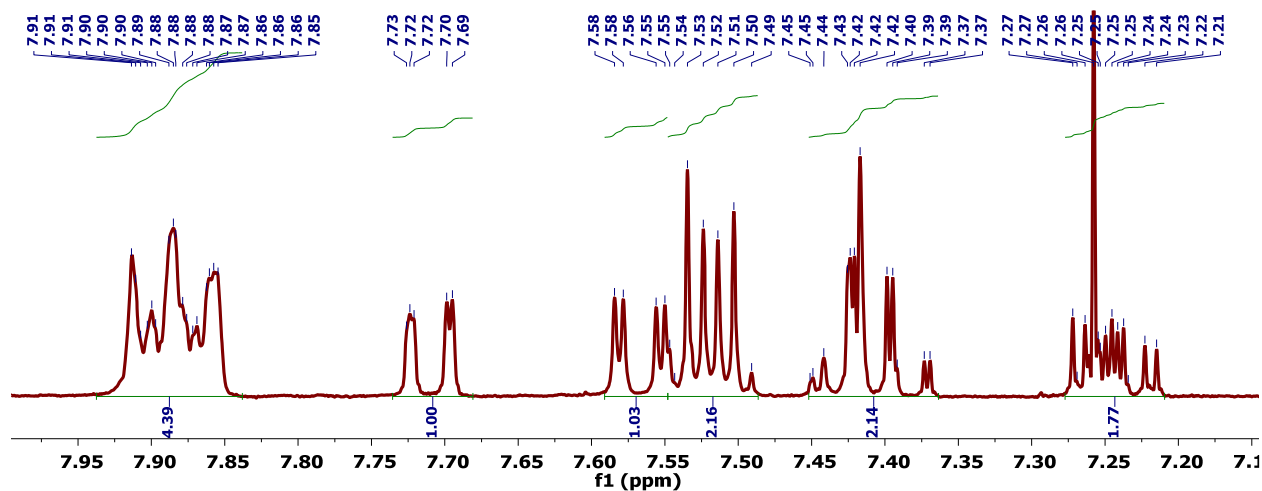


Figure D.94. ^1H NMR spectrum (300 MHz, CDCl_3) of 1-bromo-2-(2-naphthyl)benzene.

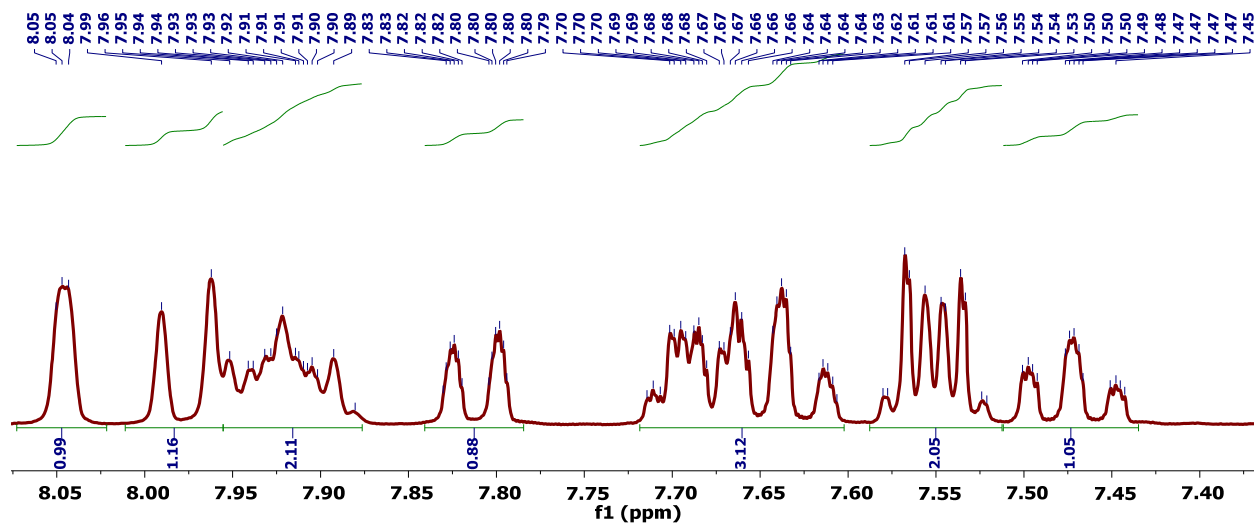


Figure D.95. ^1H NMR spectrum (300 MHz, CDCl_3) of 2-(naphthalen-2-yl)benzointrile (**3b**).

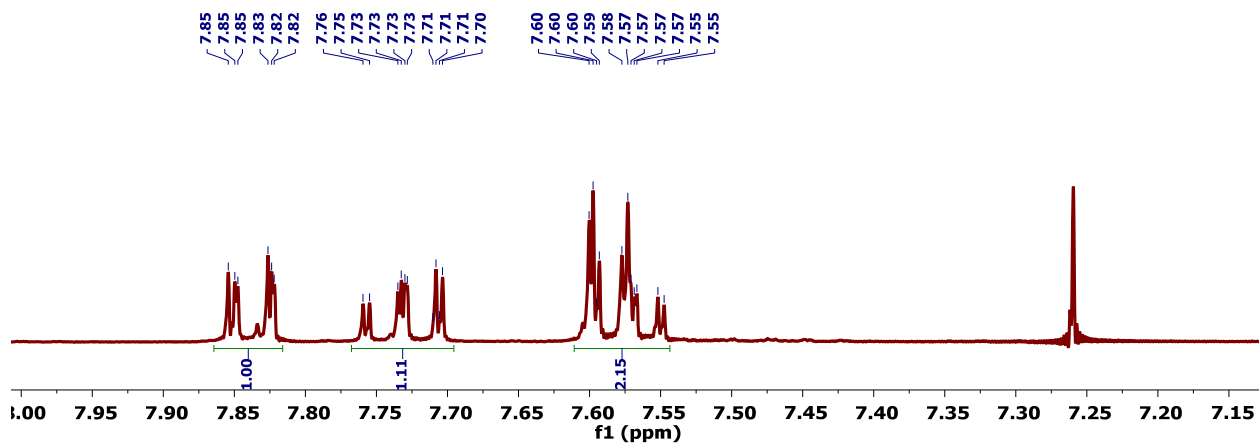


Figure D.96. ^1H NMR spectrum (300 MHz, CDCl_3) of 1,1'-biphenyl-2,2'-dicarbonitrile (**3c**).

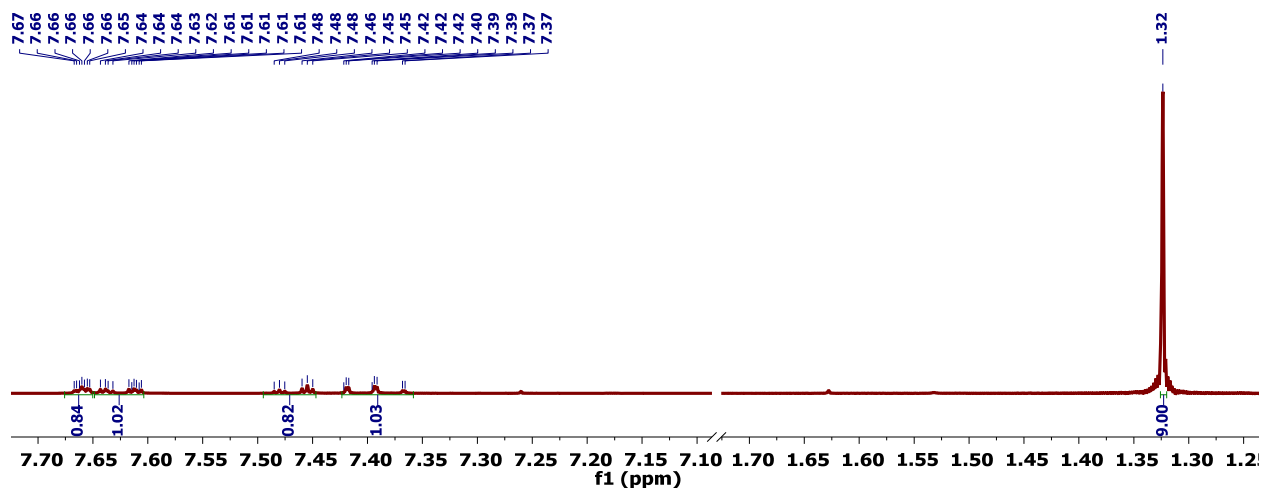


Figure D.97. ¹H NMR spectrum (300 MHz, CDCl₃) of 3-*tert*-butylbenzonitrile (**3h**).

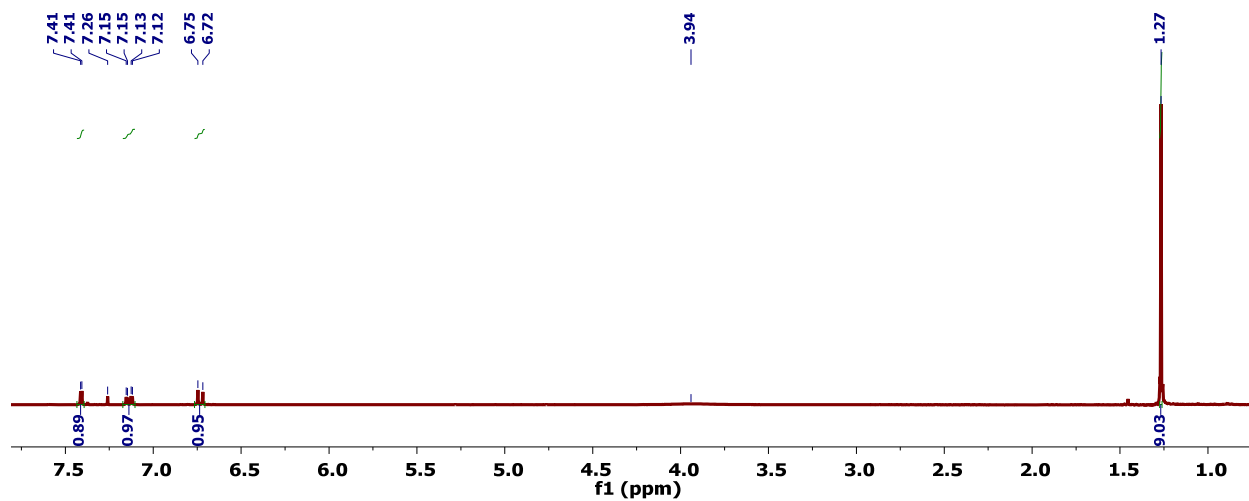


Figure D.98. ¹H NMR spectrum (300 MHz, CDCl₃) of 2-bromo-4-*tert*-butylaniline

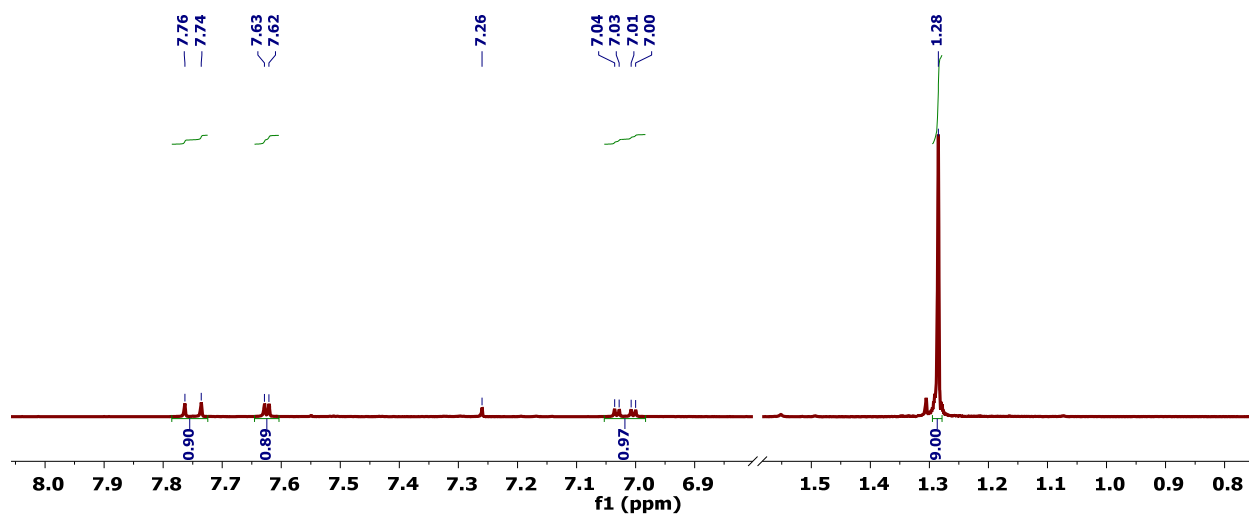


Figure D.99. ¹H NMR spectrum (300 MHz, CDCl₃) of 2-bromo-4-*tert*-butylidobenzene.

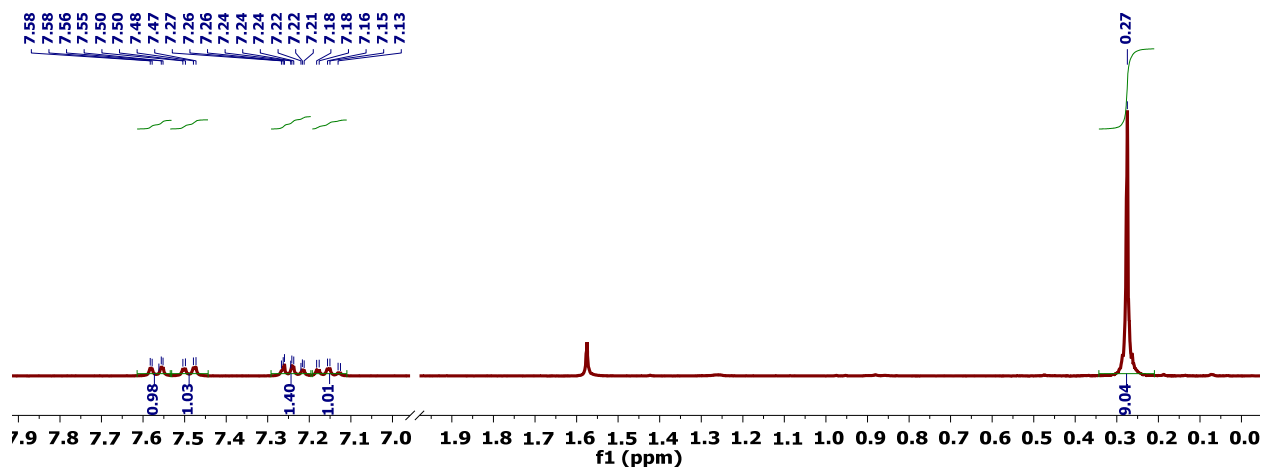


Figure D.100. ^1H NMR spectrum (300 MHz, CDCl_3) of ((2-bromophenyl)ethynyl)trimethylsilane.

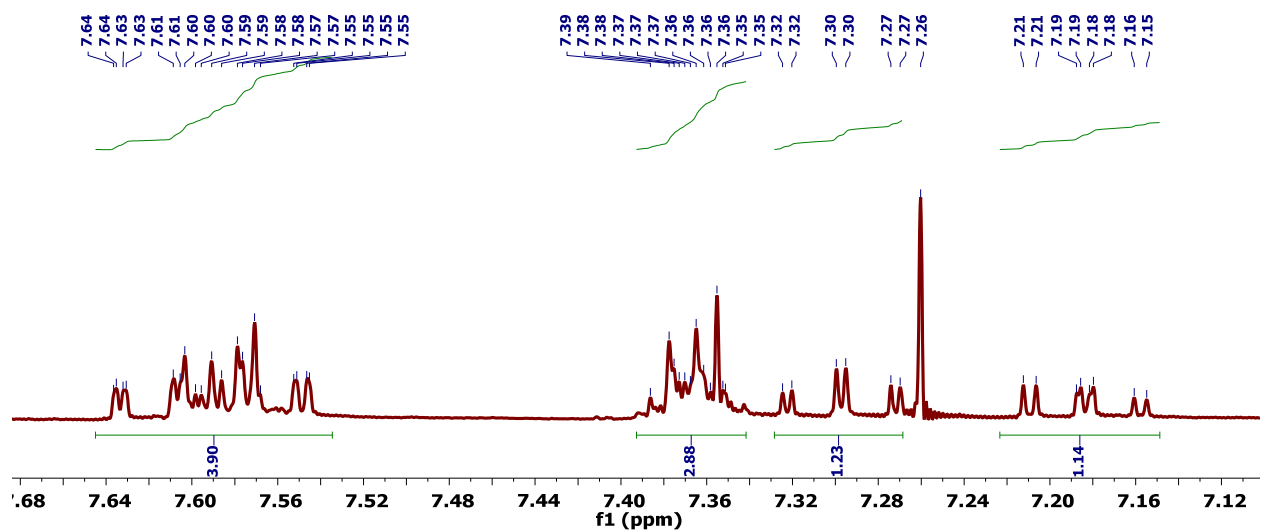


Figure D.101. ^1H NMR spectrum (300 MHz, CDCl_3) of 1-bromo-2-(phenylethynyl)benzene.

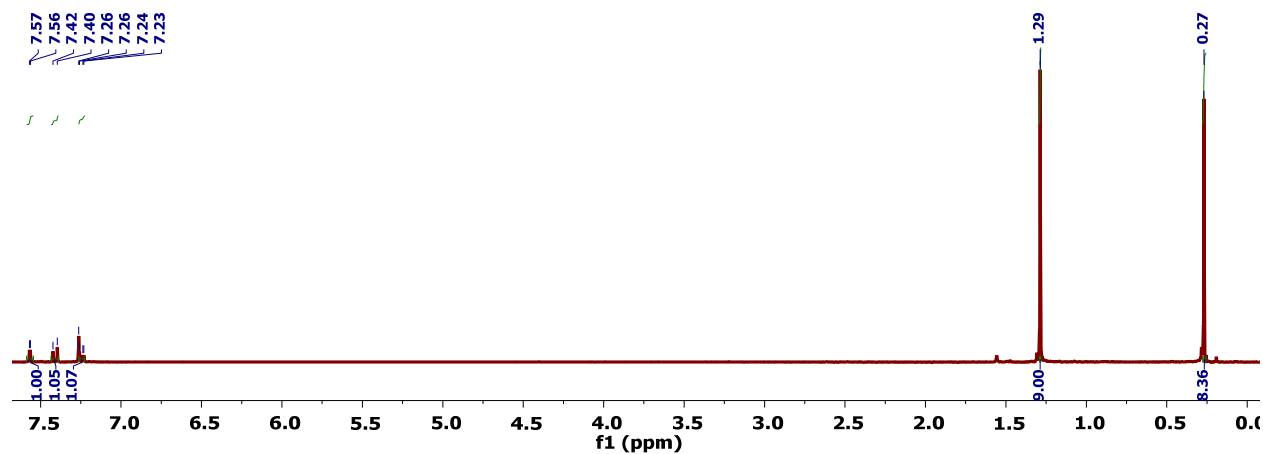


Figure D.102. ^1H NMR spectrum (300 MHz, CDCl_3) of ((2-Bromo-4-(*tert*-butyl)phenyl)ethynyl)trimethylsilane.

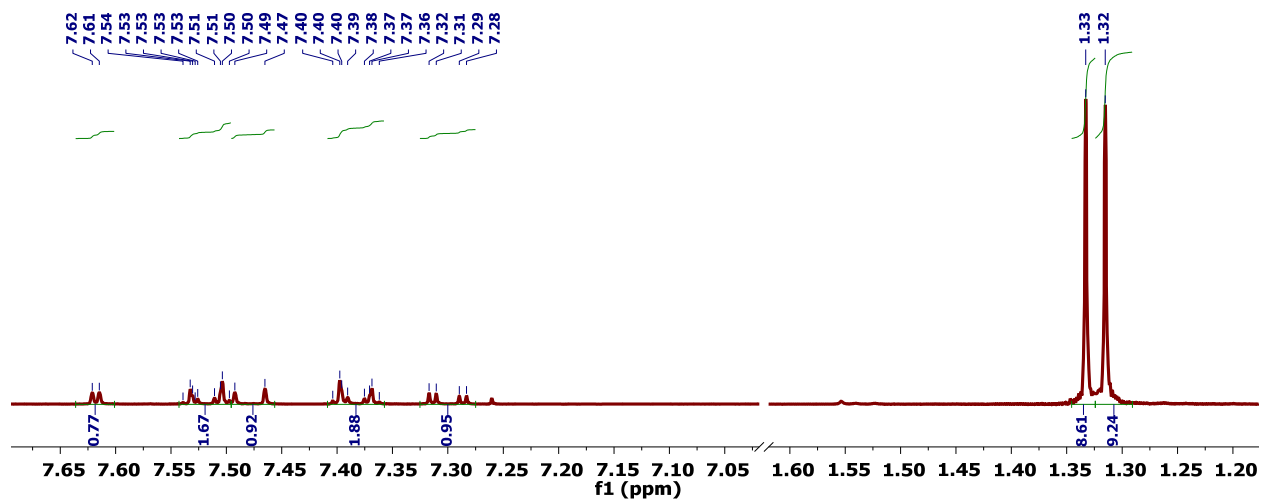


Figure D.103. ^1H NMR spectrum (300 MHz, CDCl_3) of 2-bromo-4-(tert-butyl)-1-((4-(tert-butyl)phenyl)ethynyl)benzene.

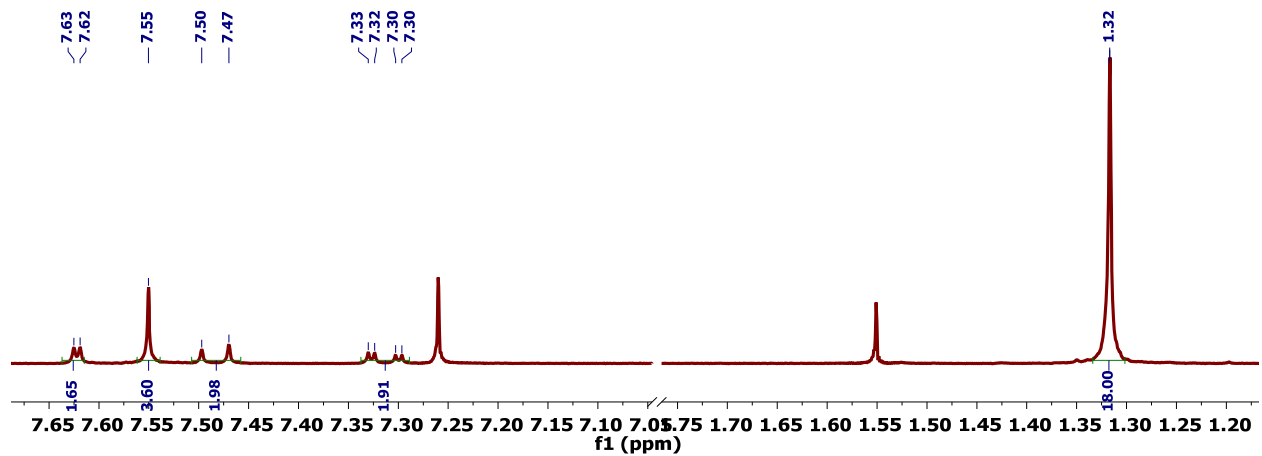


Figure D.104. ^1H NMR spectrum (300 MHz, CDCl_3) of 1,4-bis((2-bromo-4-(tert-butyl)phenyl)ethynyl)benzene.

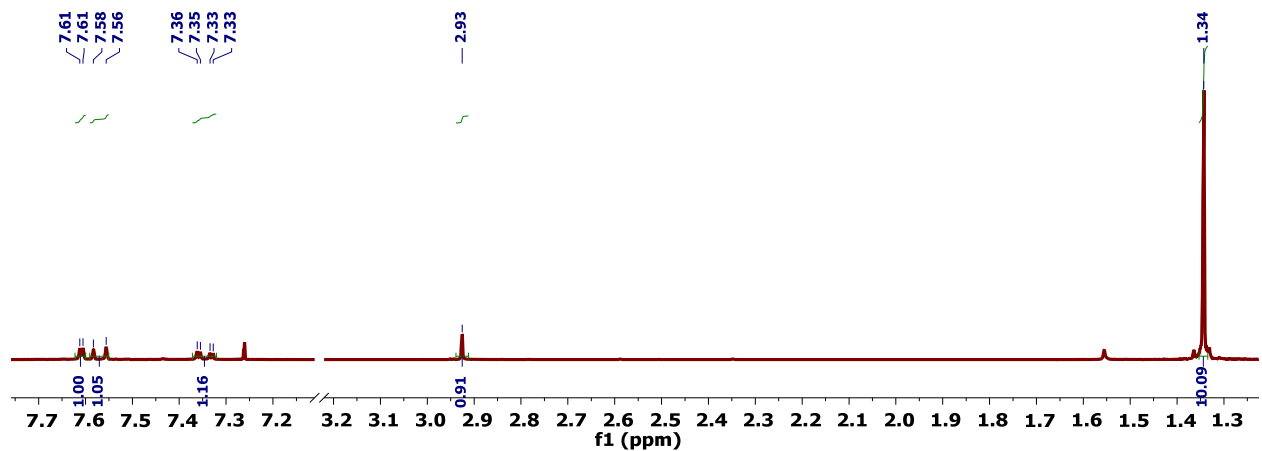


Figure D.105. ^1H NMR spectrum (300 MHz, CDCl_3) of 5,5'-di-tert-butyl-2,2'-diethynyl-1,1'-biphenyl (2c).

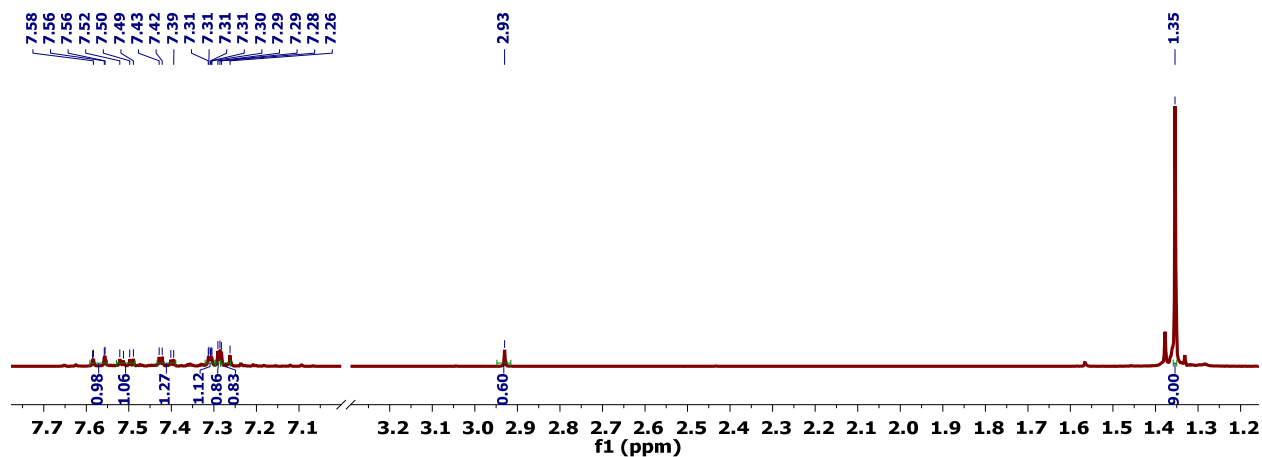


Figure D.109. ^1H NMR spectrum (300 MHz, CDCl_3) of 5'-(*tert*-butyl)-2,3-dichloro-2'-ethynyl-1,1'-biphenyl (**2h**).

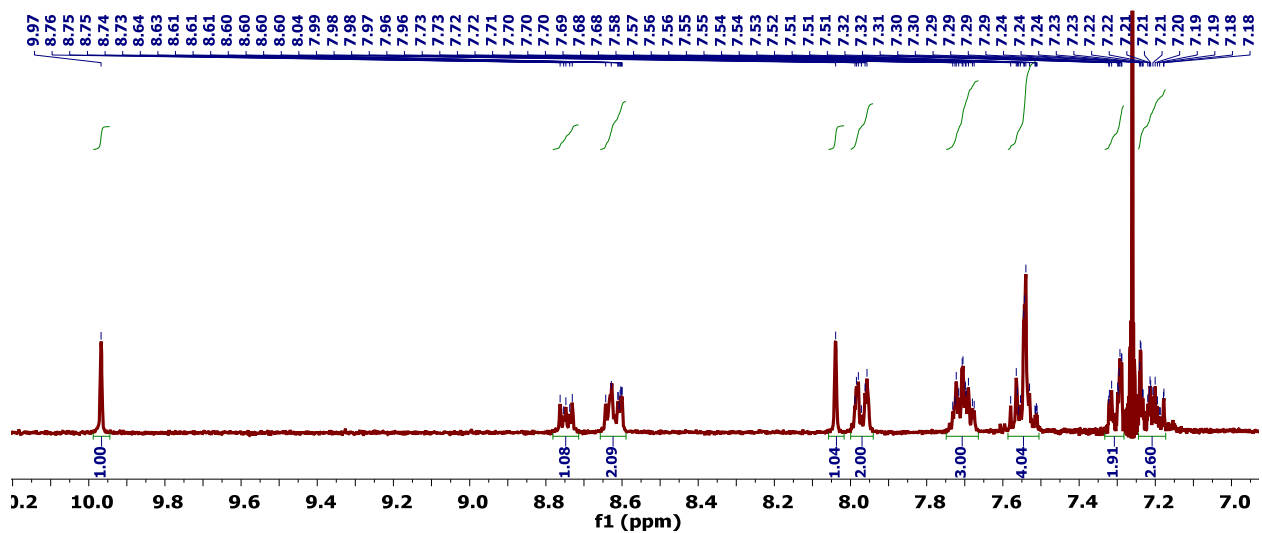


Figure D.110. ^1H NMR spectrum (300 MHz, CDCl_3) of **4aa**.

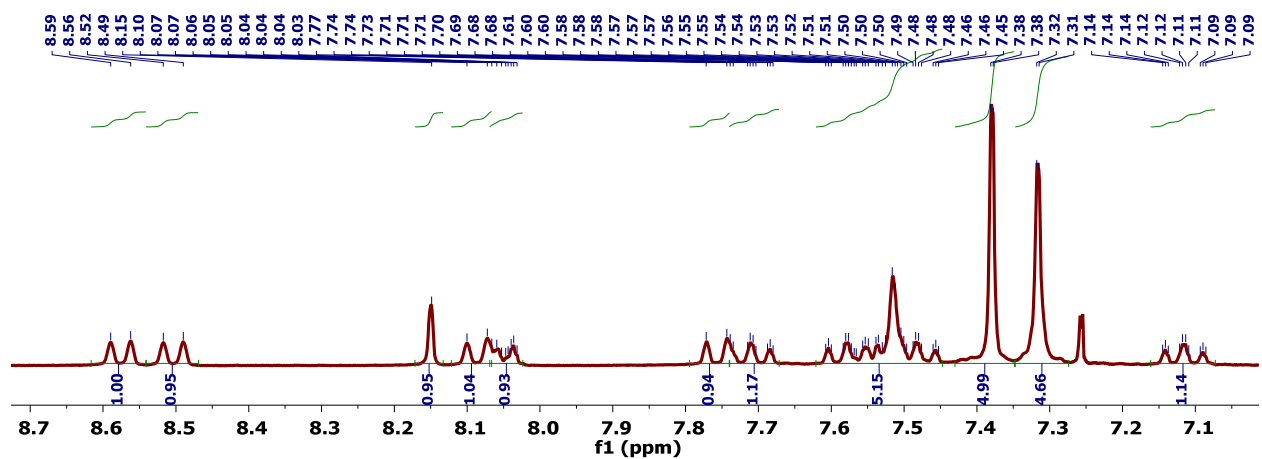


Figure D.111. ^1H NMR spectrum (300 MHz, CDCl_3) of **4ba**.

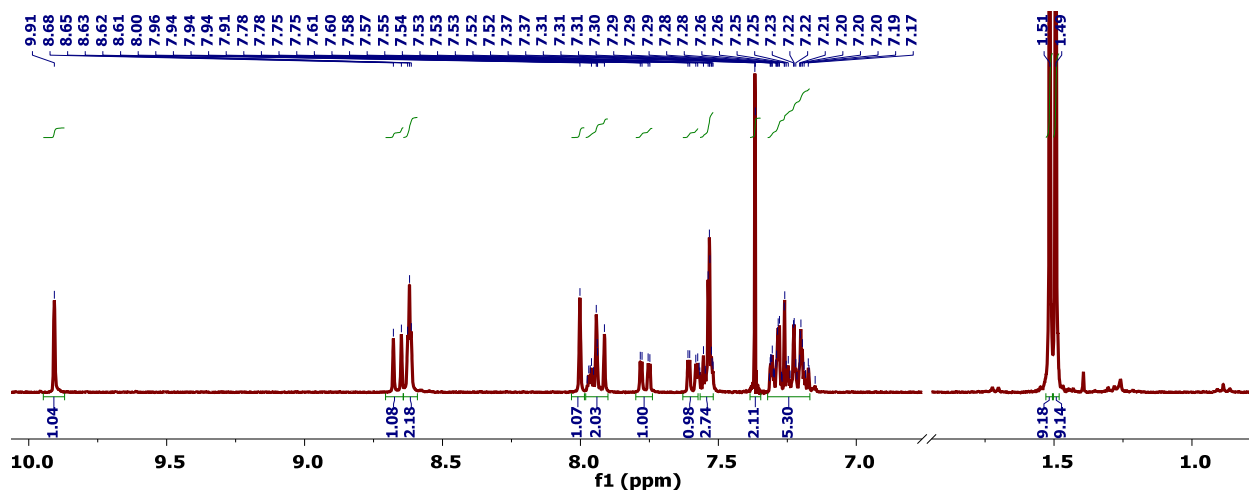


Figure D.112. ^1H NMR spectrum (300 MHz, CDCl_3) of 4ca.

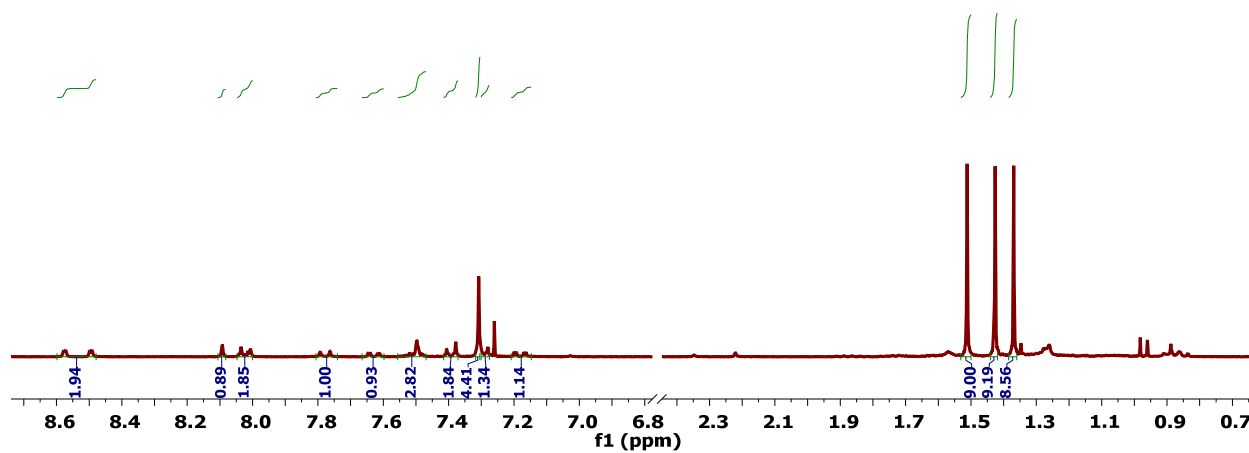


Figure D.113. ^1H NMR spectrum (300 MHz, CDCl_3) of 4da.

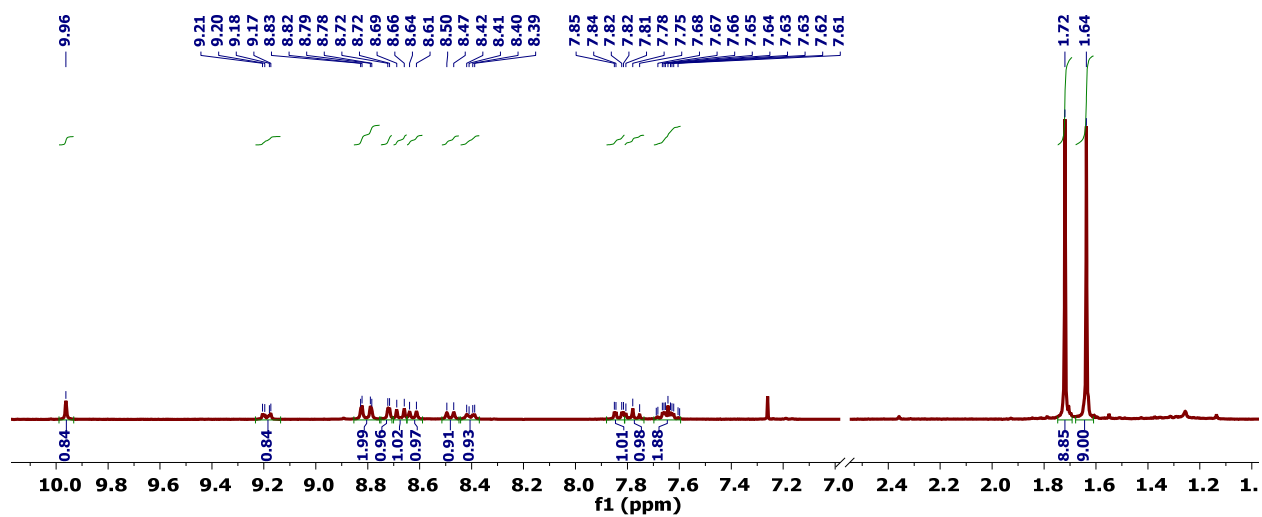


Figure D.114. ^1H NMR spectrum (300 MHz, CDCl_3) of 5ca.

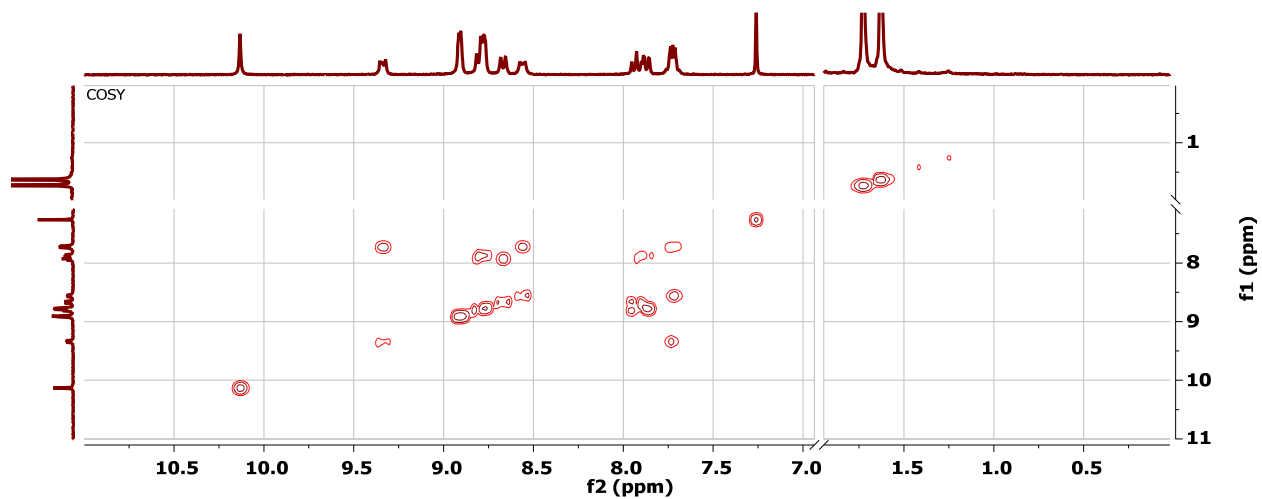


Figure D.115. COSY NMR spectrum (300 MHz, CDCl_3) of 5ca.

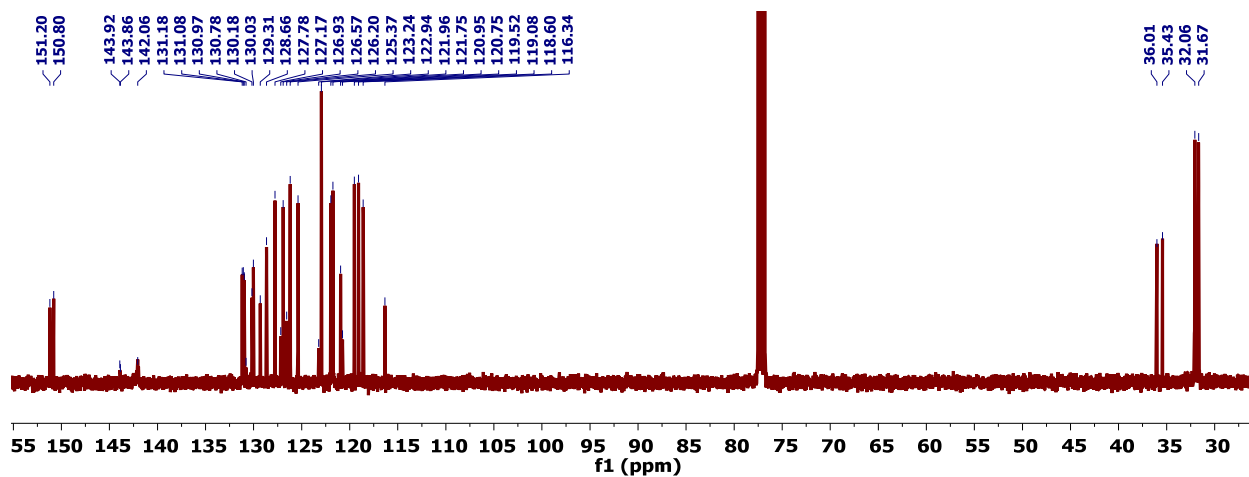


Figure D.116. $^{13}\text{C}\{^1\text{H}\}$ NMR spectrum (101 MHz, CDCl_3) of 5ca.

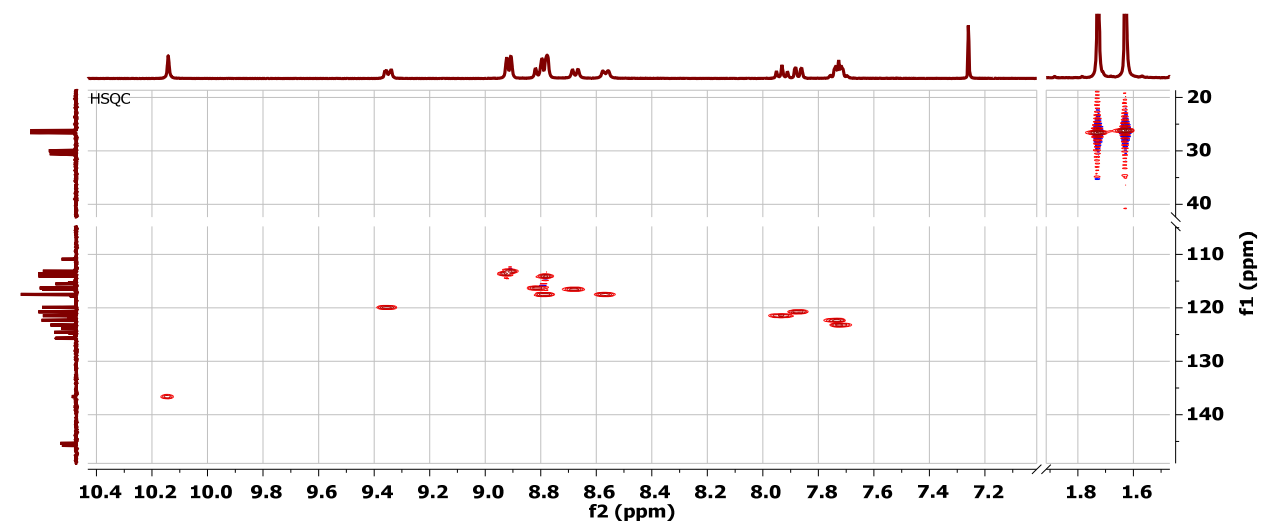


Figure D.117. HSQC NMR spectrum (CDCl_3) of 5ca.

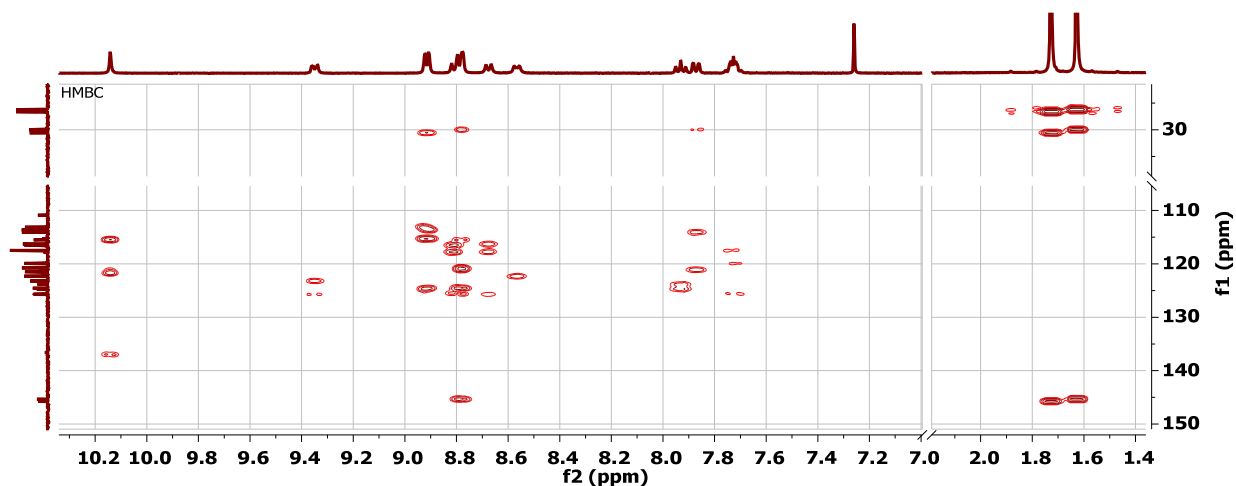


Figure D.118. HMBC spectrum (CDCl_3) of 5ca.

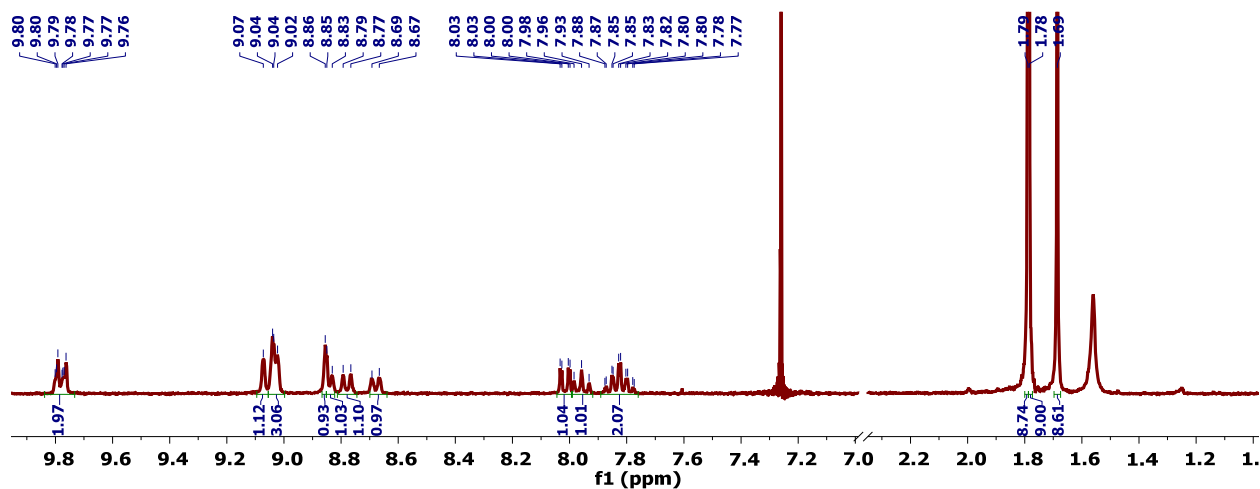


Figure D.119. ^1H NMR spectrum (300 MHz, CDCl_3) of 5da.

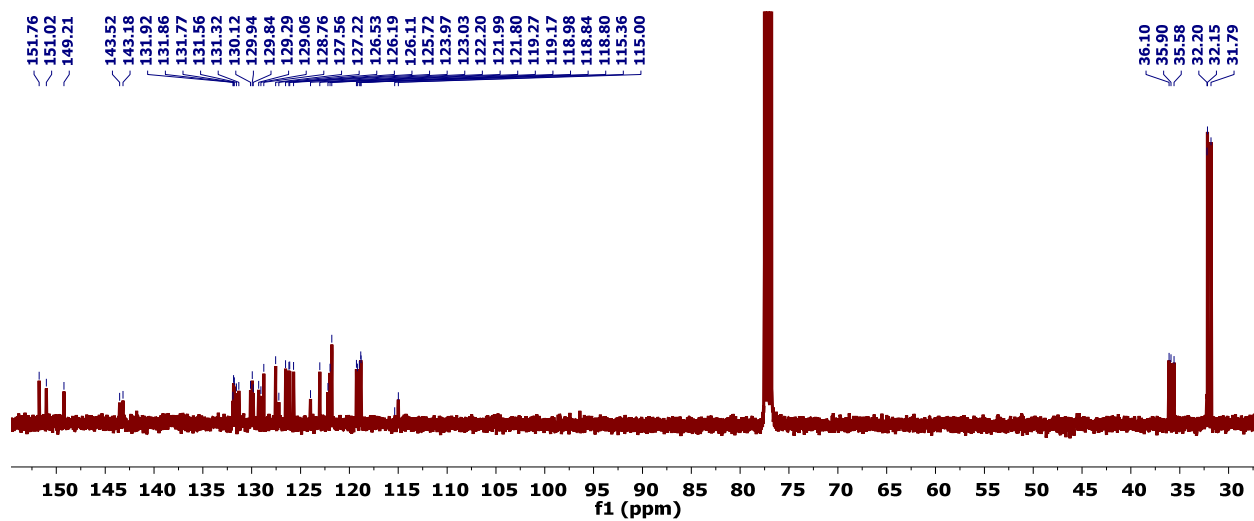


Figure D.120. $^{13}\text{C}\{^1\text{H}\}$ NMR spectrum (101 MHz, CDCl_3) of 5da.

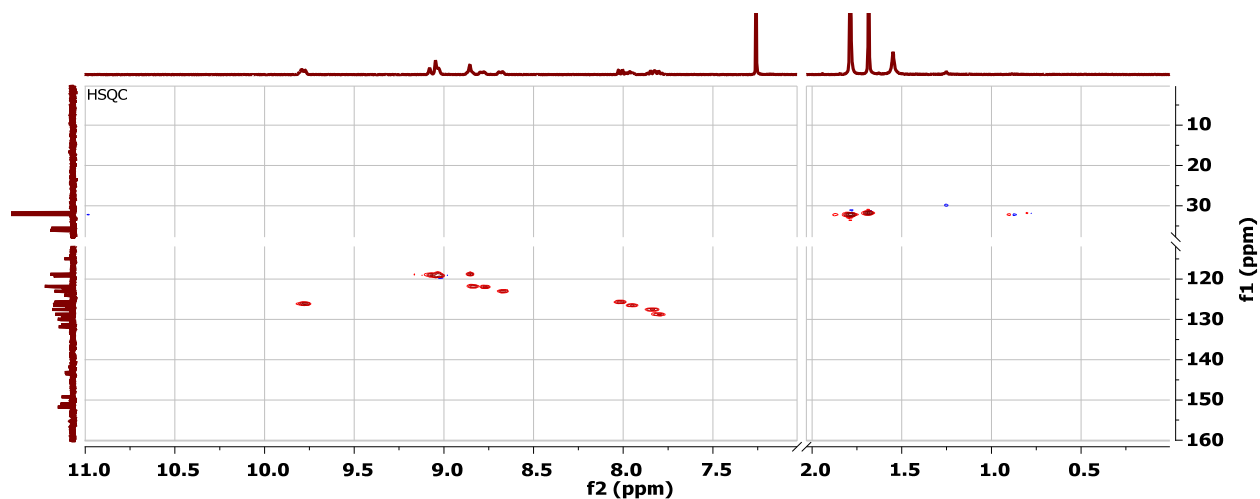


Figure D.121. HSQC spectrum (CDCl_3) of 5da.

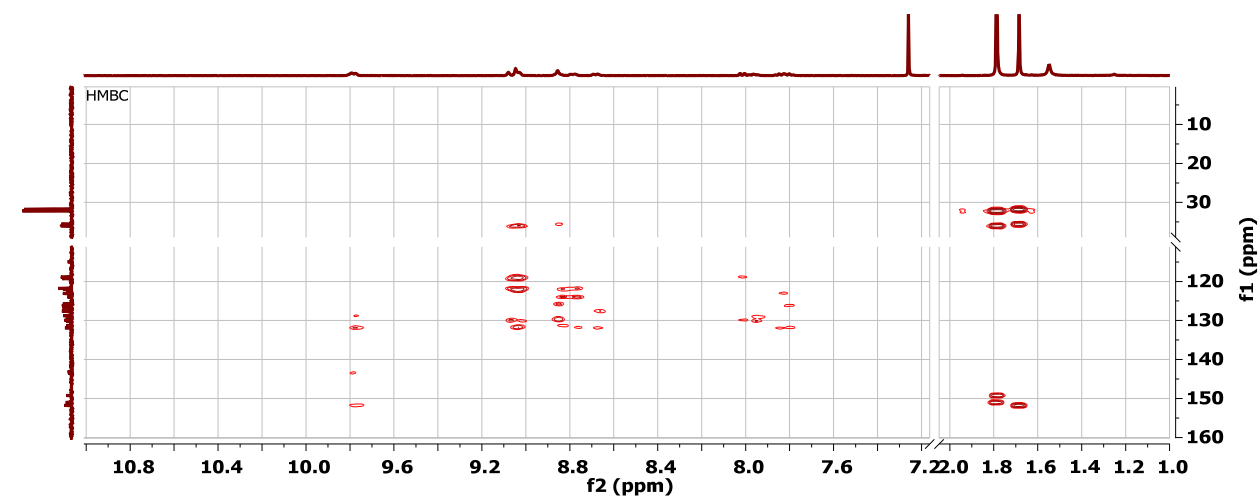


Figure D.122. HMBC spectrum (CDCl_3) of 5da.

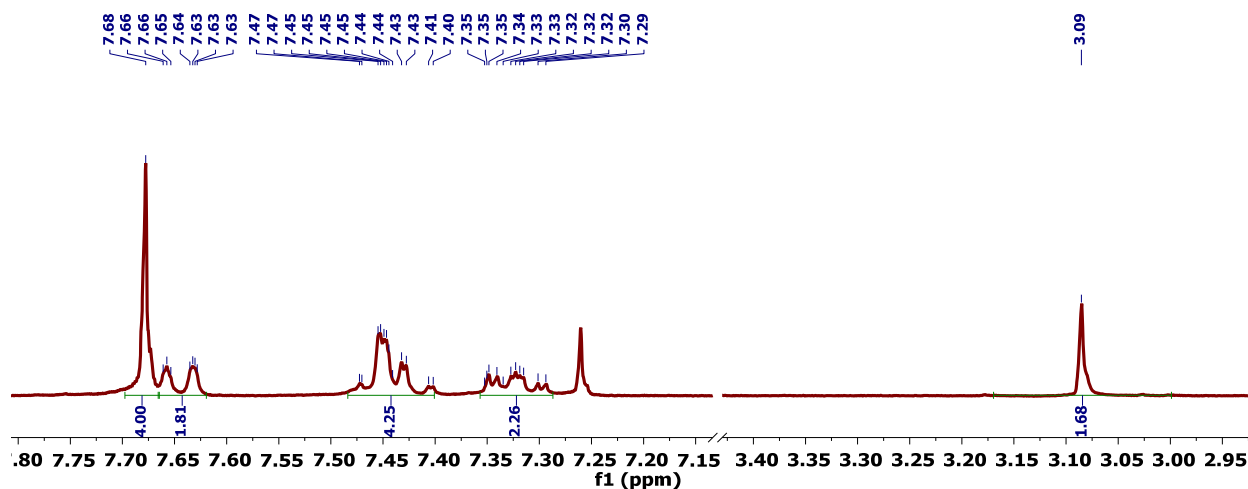


Figure D.123. ^1H NMR spectrum (300 MHz, CDCl_3) of 2,2''-diethynyl-1,1':4',1''-terphenyl (2d).

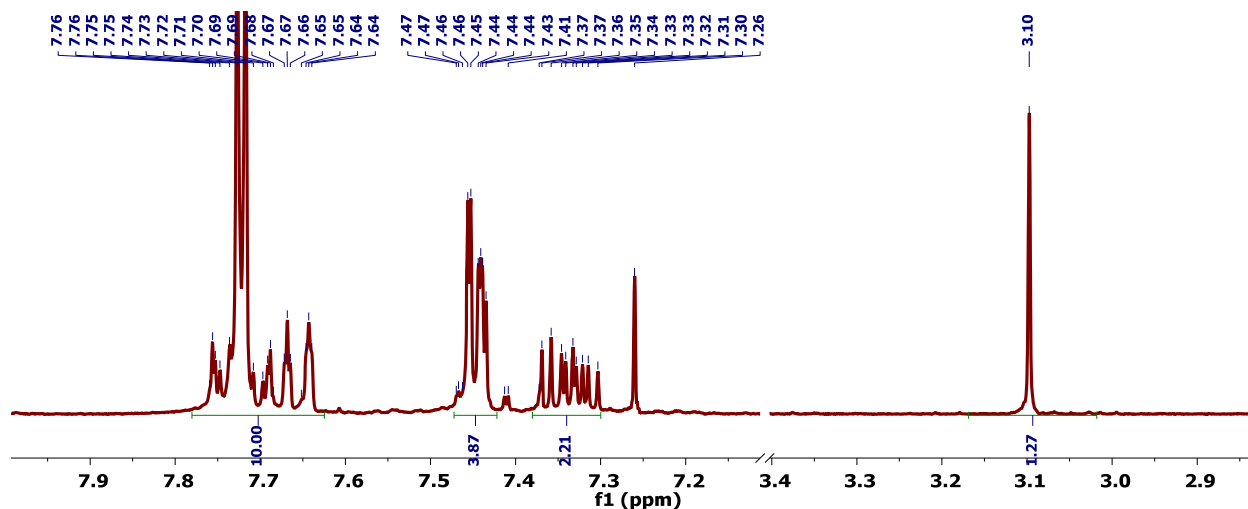


Figure D.124. ^1H NMR spectrum (300 MHz, CDCl_3) of 2,2''-diethynyl-1,1':4',1''-terphenyl (2e).

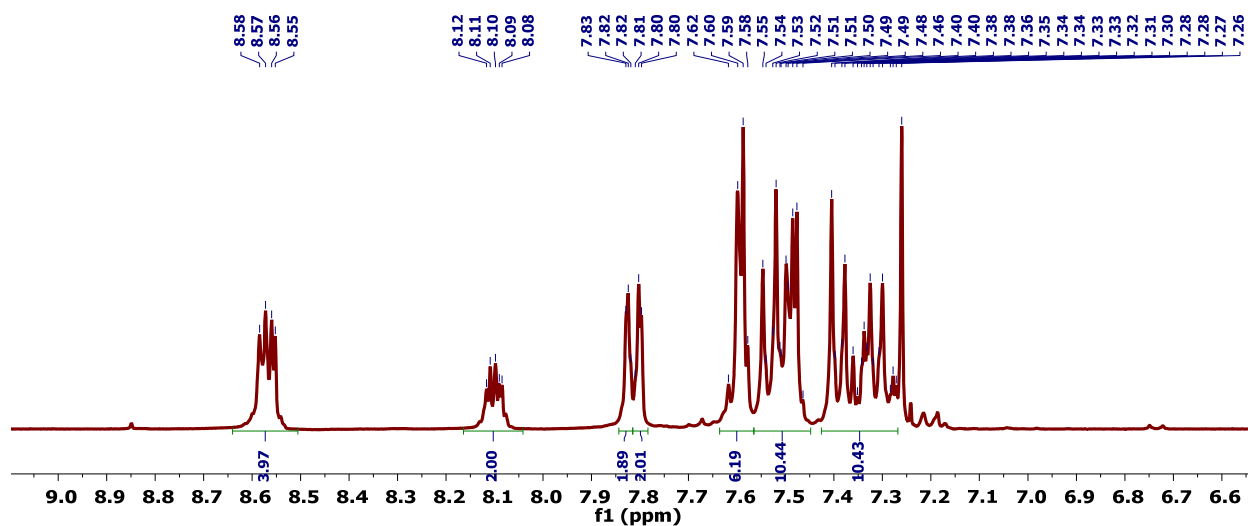


Figure D.125. ^1H NMR spectrum (300 MHz, CDCl_3) of 4gf.

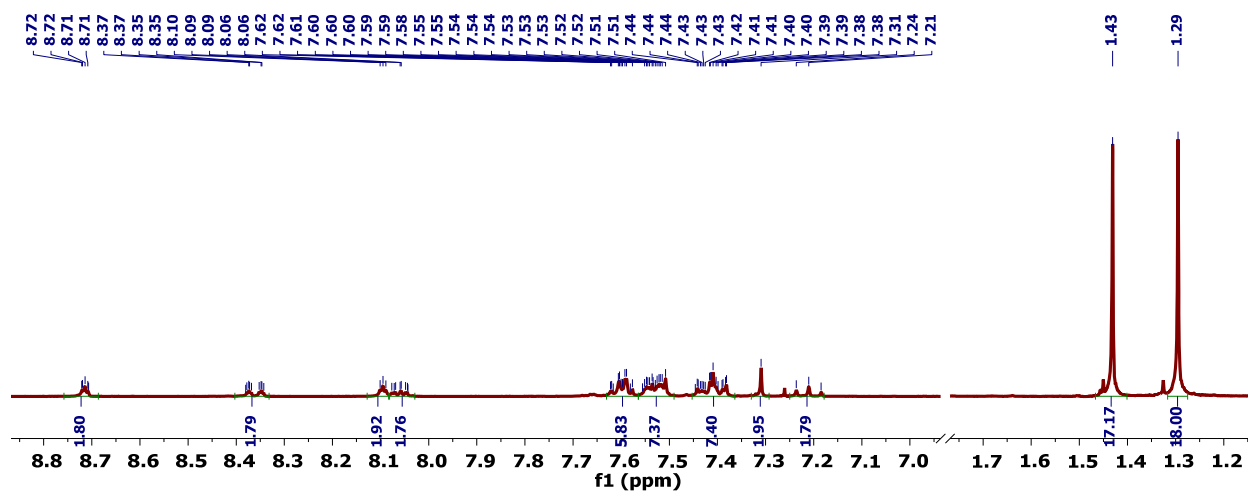
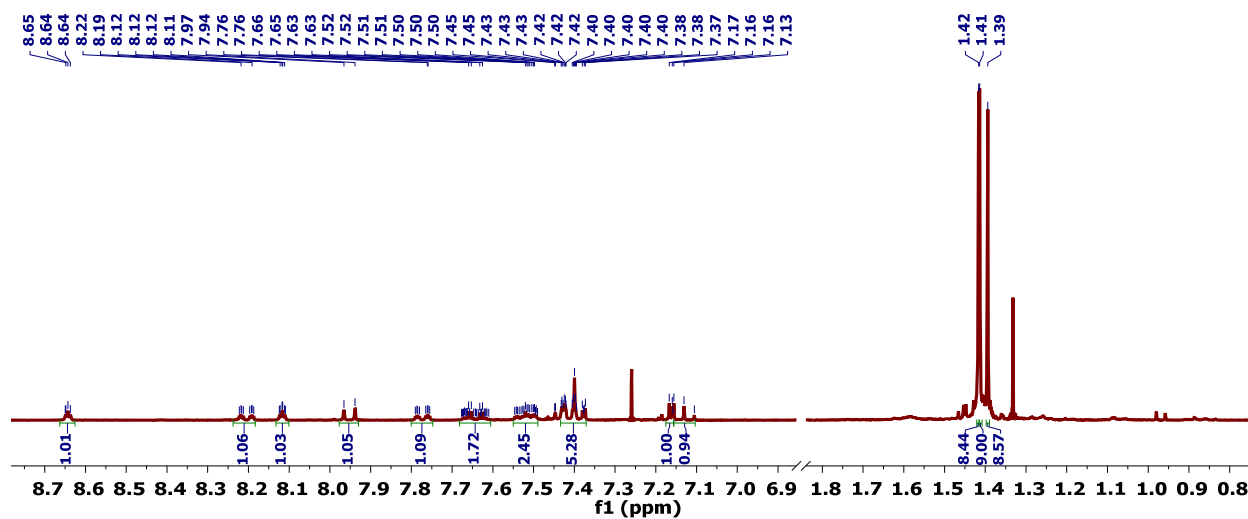
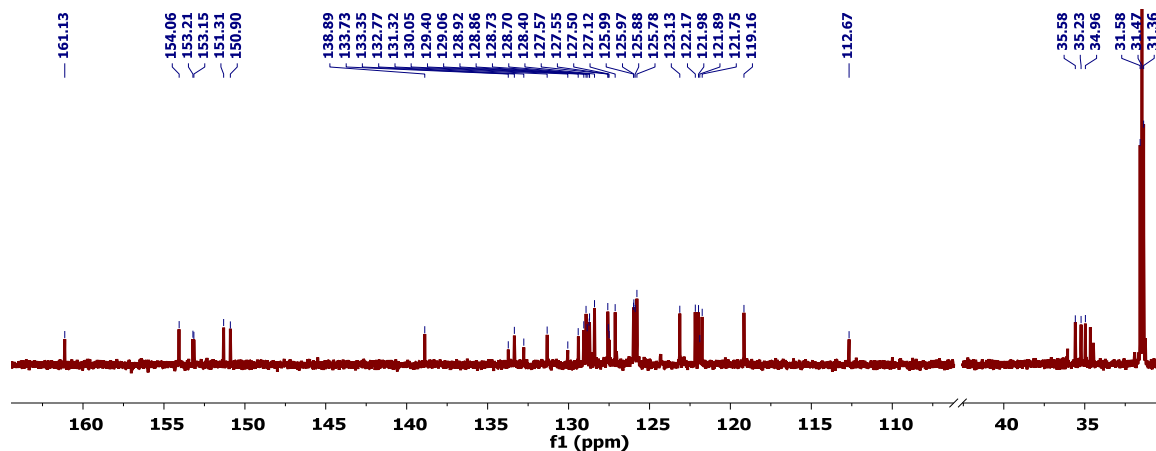
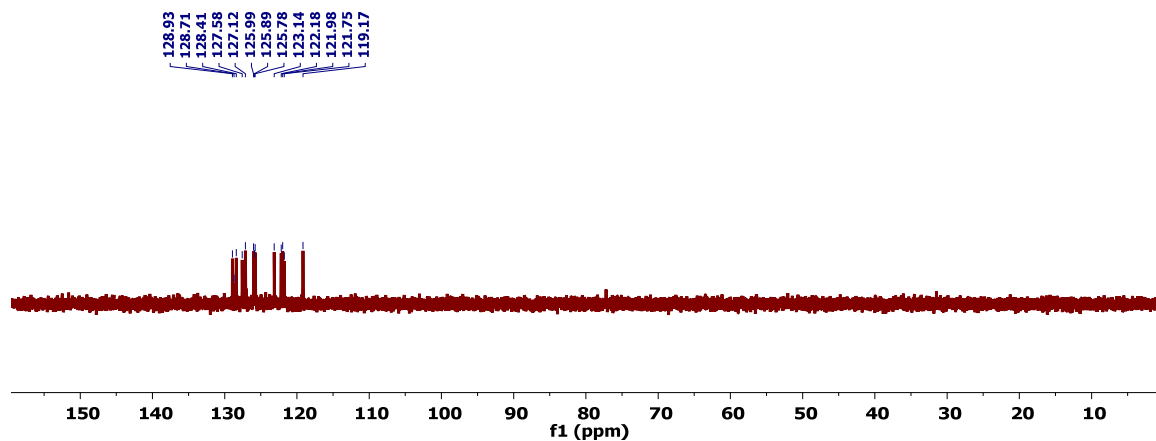


Figure D.126. ^1H NMR spectrum (300 MHz, CDCl_3) of 4gh.Figure D.127. ^{13}C NMR spectrum (300 MHz, CDCl_3) of 4hh.Figure D.128. $^{13}\text{C}\{^1\text{H}\}$ NMR spectrum (101 MHz, CDCl_3) of 4hh.Figure D.129. DEPT NMR spectrum (101 MHz, CDCl_3) of 4hh.

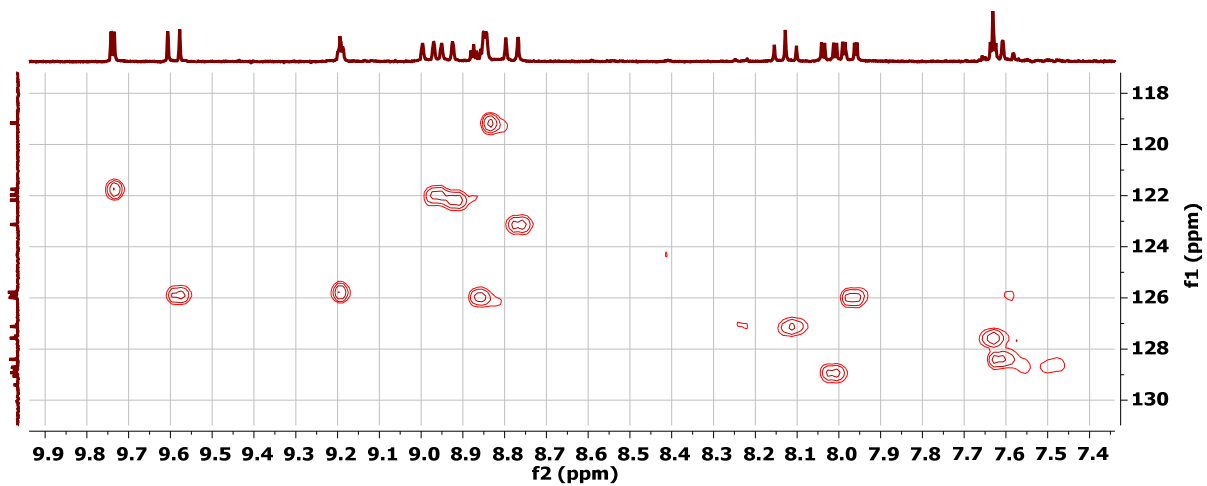


Figure D.130. HSQC NMR (CDCl_3) of 4hh.

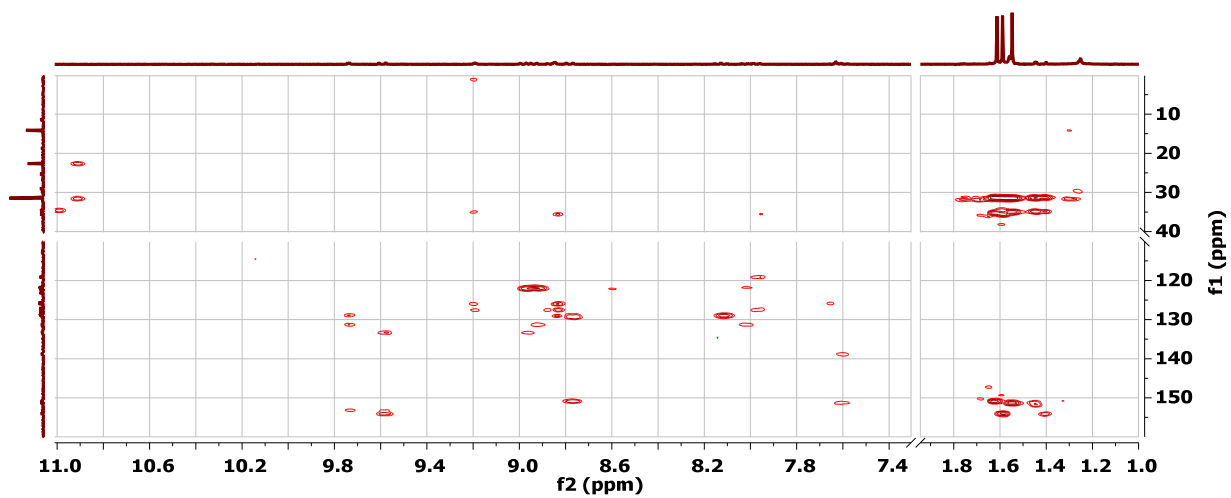
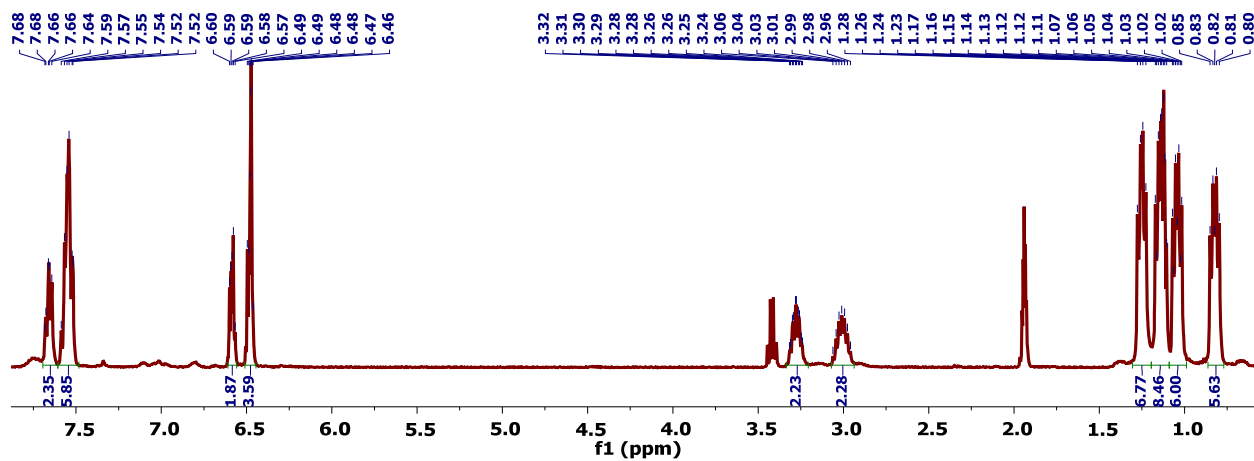
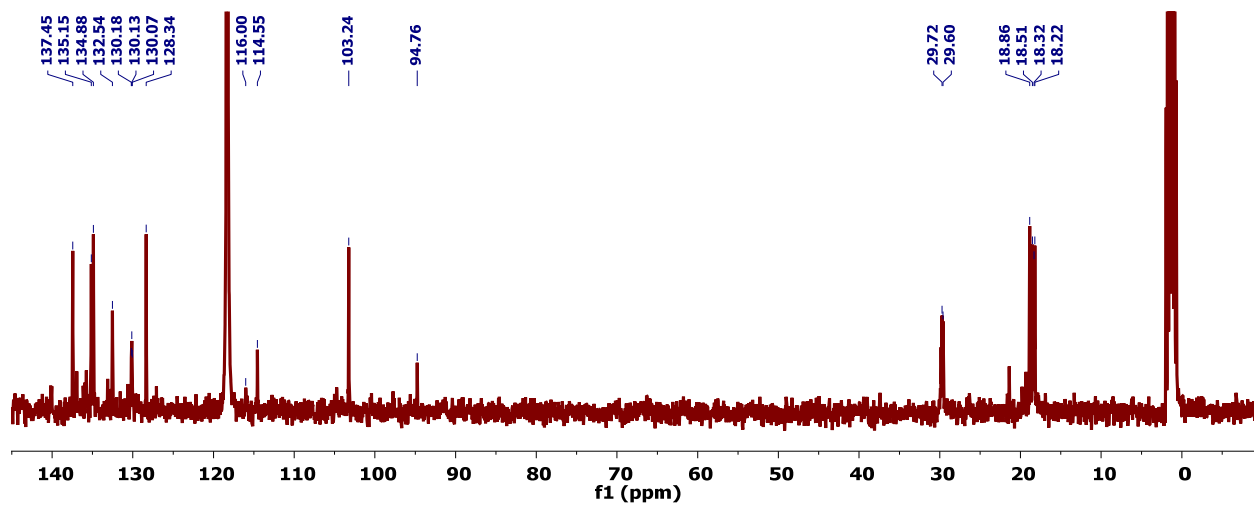
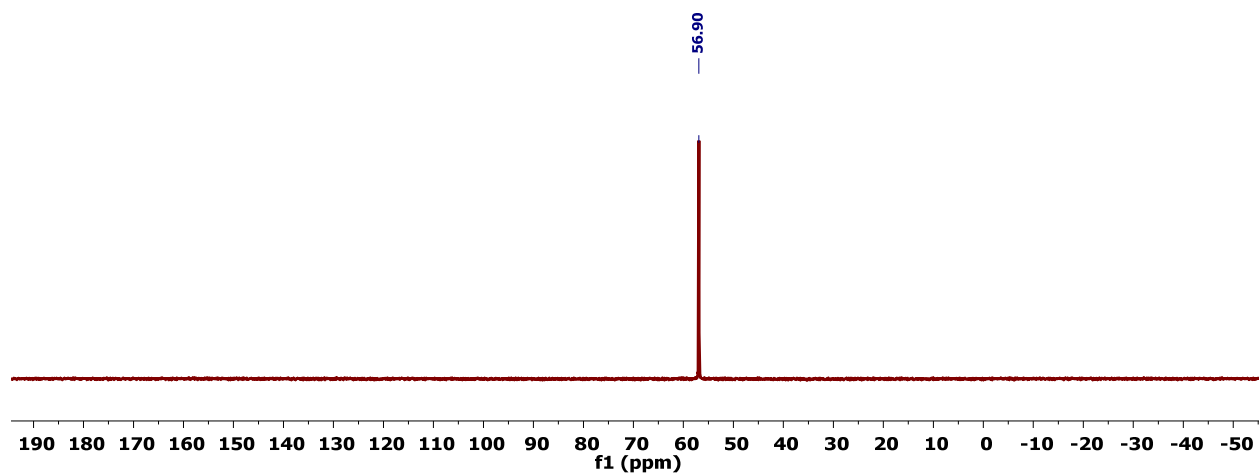


Figure D.131. HMBC NMR (CDCl_3) of 4hh.

APPENDIX A

Figure D.132. ¹H NMR spectrum (400 MHz, CDCl₃) of 2.Figure D.133. ¹³C{¹H} NMR spectrum (101 MHz, CDCl₃) of 2.Figure D.134. ³¹P{¹H} NMR spectrum (162 MHz, C₆D₆) of 2.

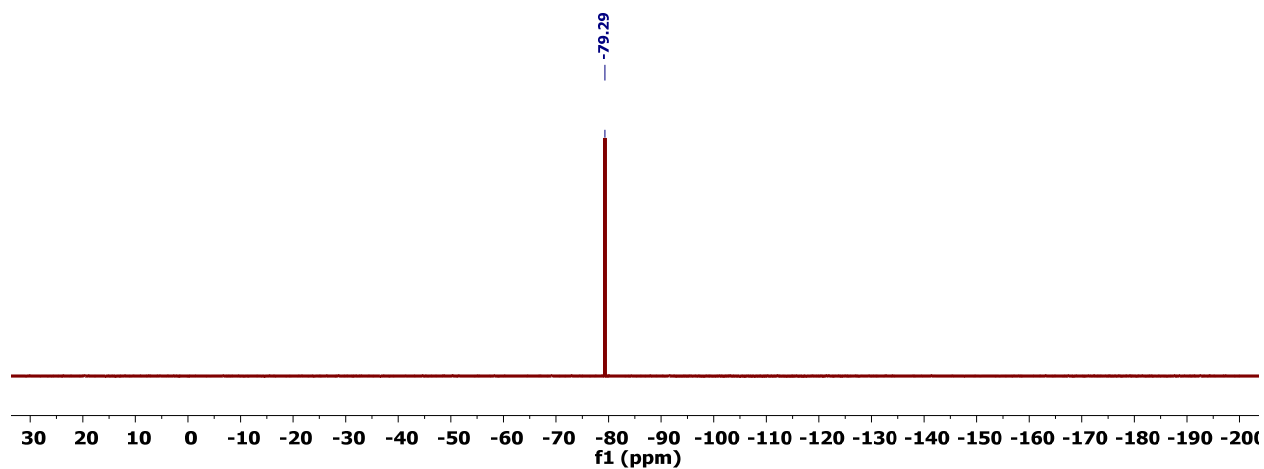


Figure D.135. ^{19}F NMR spectrum (376 MHz, CDCl_3) of **2**.

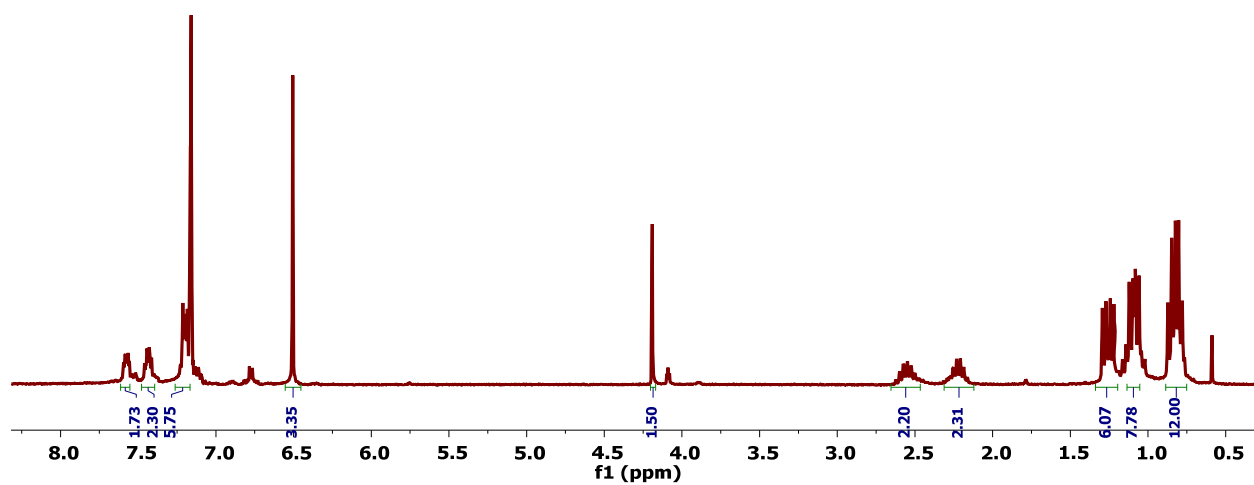


Figure D.136. ^1H NMR spectrum (300 MHz, CDCl_3) of **4**.

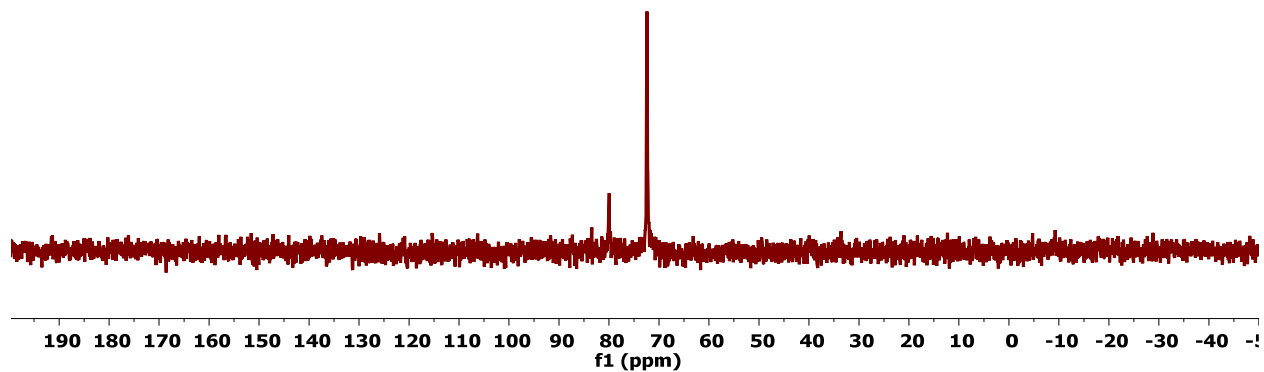


Figure D.137. $^{31}\text{P}\{^1\text{H}\}$ NMR spectrum (121 MHz, C_6D_6) of **4**.

APPENDIX B

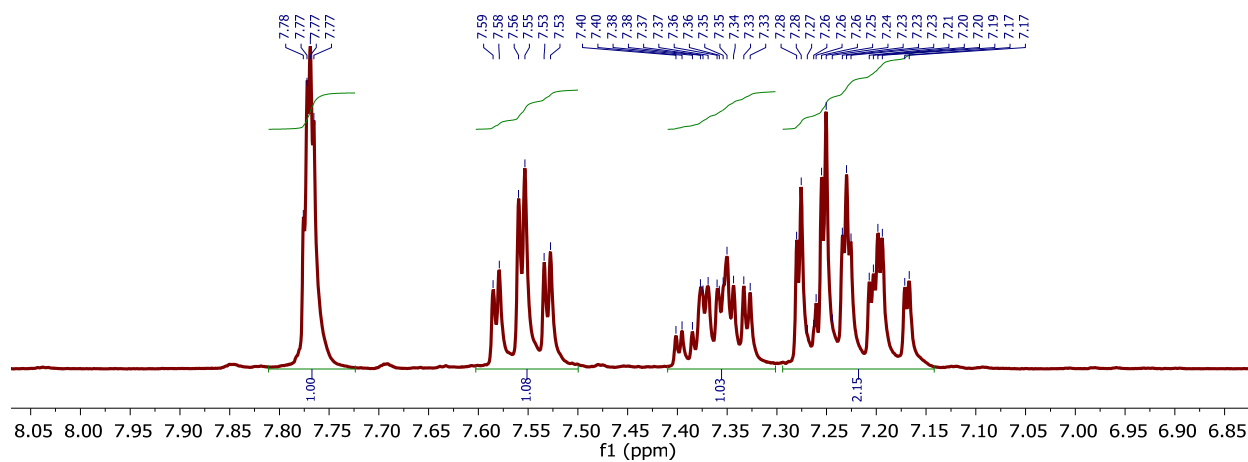


Figure D.138. ^1H NMR spectrum (300 MHz, CDCl_3) of 1,3,5-*tris*(2'-fluorophenyl)benzene.

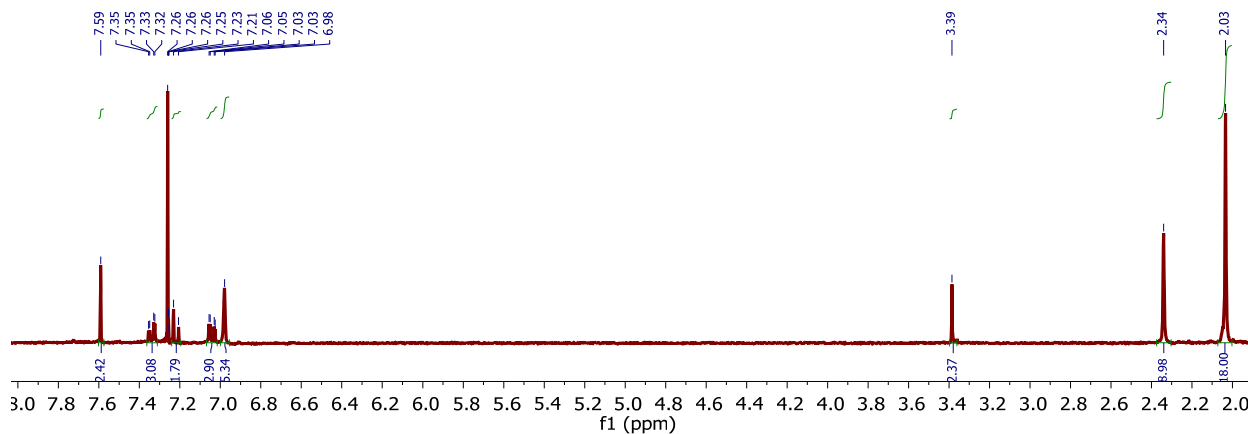


Figure D.139. ^1H NMR spectrum (300 MHz, CDCl_3) of LH_3 .

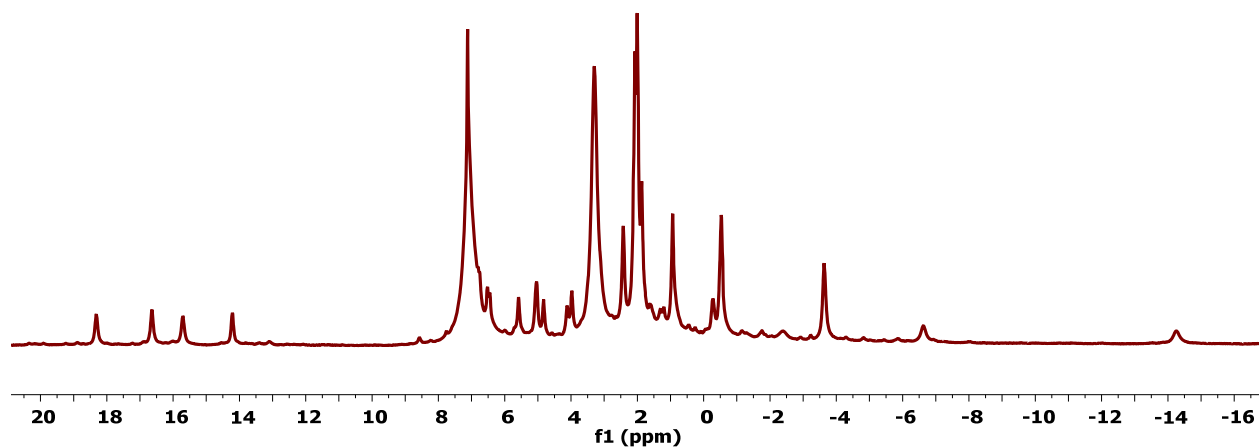


Figure D.140. ^1H NMR spectrum (300 MHz, C_6D_6) of 1.

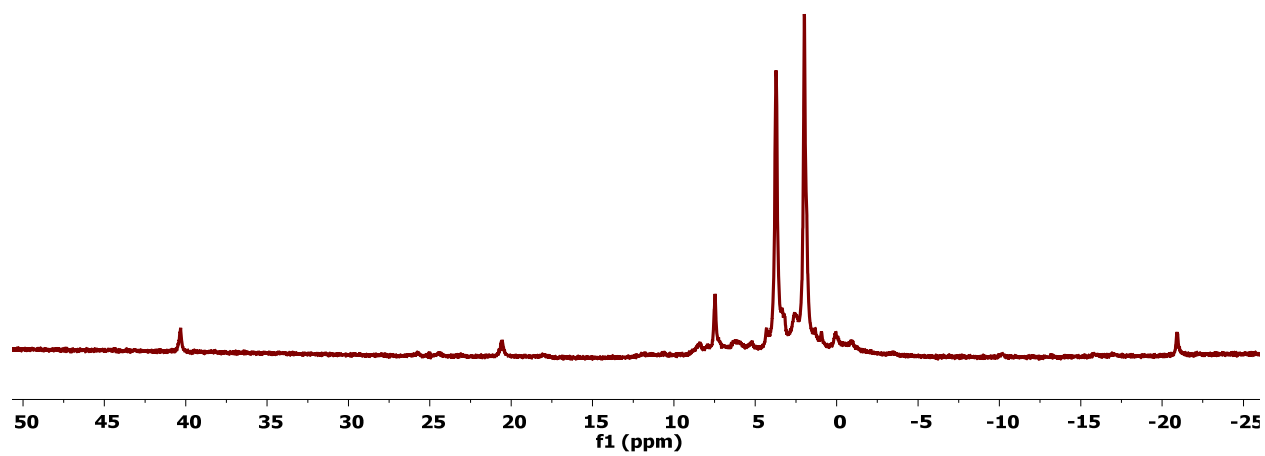


Figure D.141. ^1H NMR spectrum (300 MHz, CD_3CN) of 2.

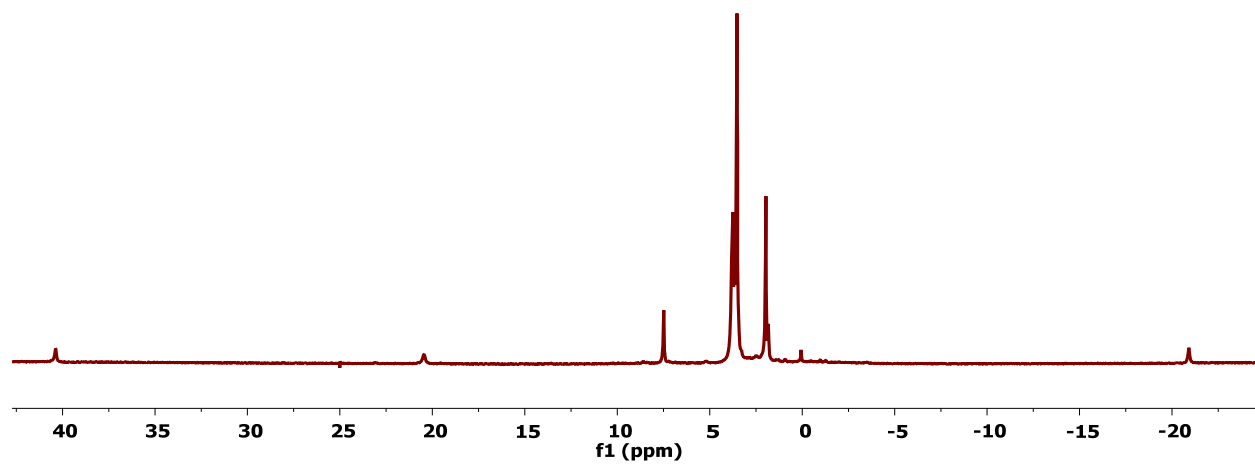
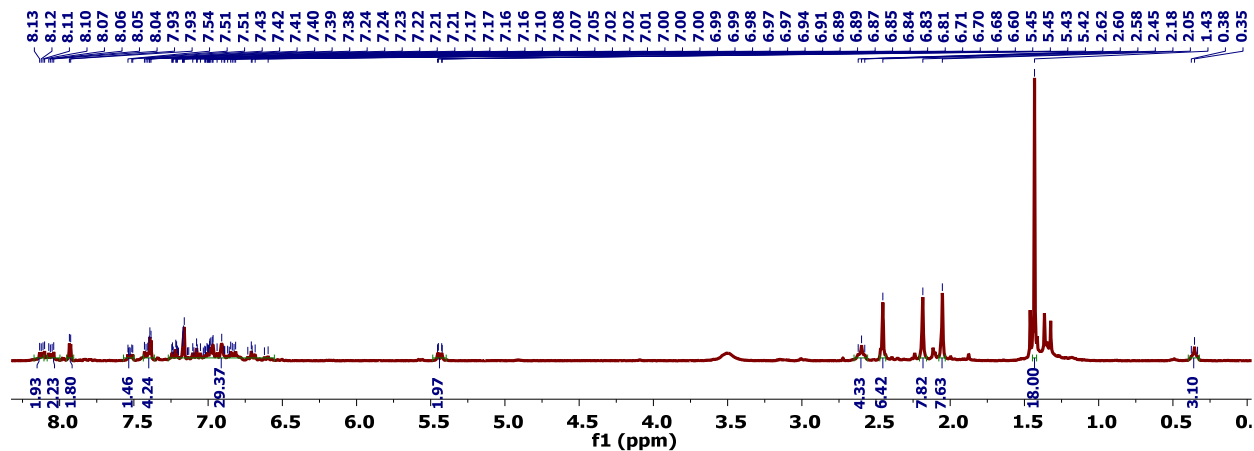
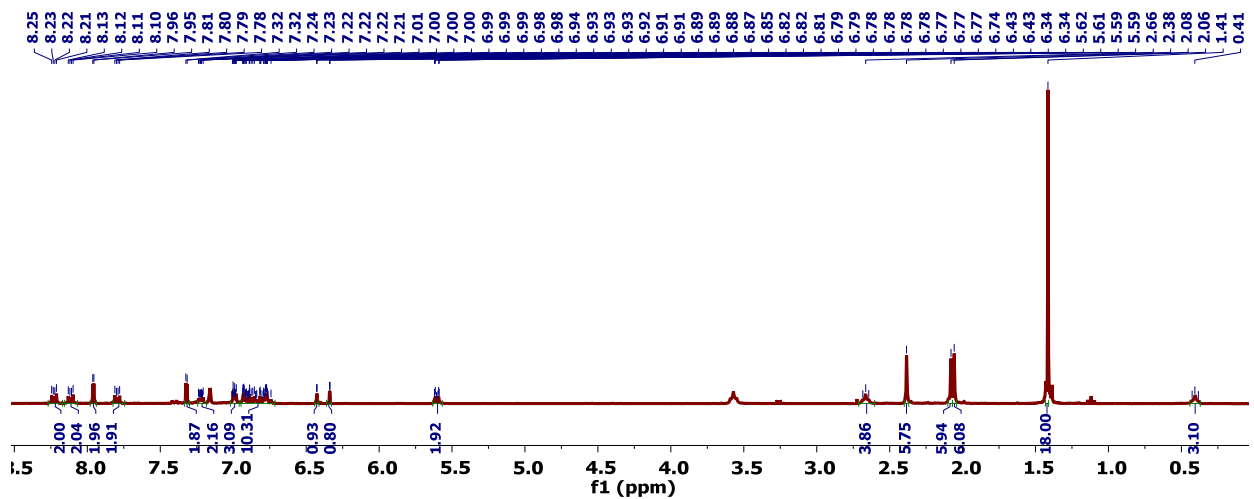
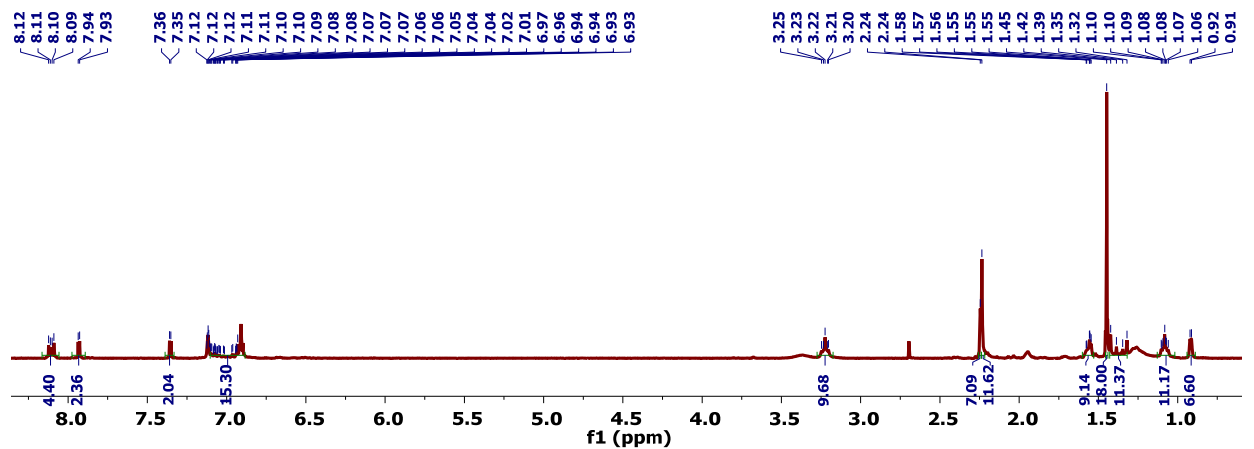


Figure D.142. ^1H NMR spectrum (300 MHz, CD_3CN) of 3.

APPENDIX C

Figure D.143. ^1H NMR spectrum (300 MHz, C_6D_6) of 4.Figure D.144. ^1H NMR spectrum (300 MHz, C_6D_6) of 6.Figure D.145. ^1H NMR spectrum (300 MHz, C_6D_6) of 7.

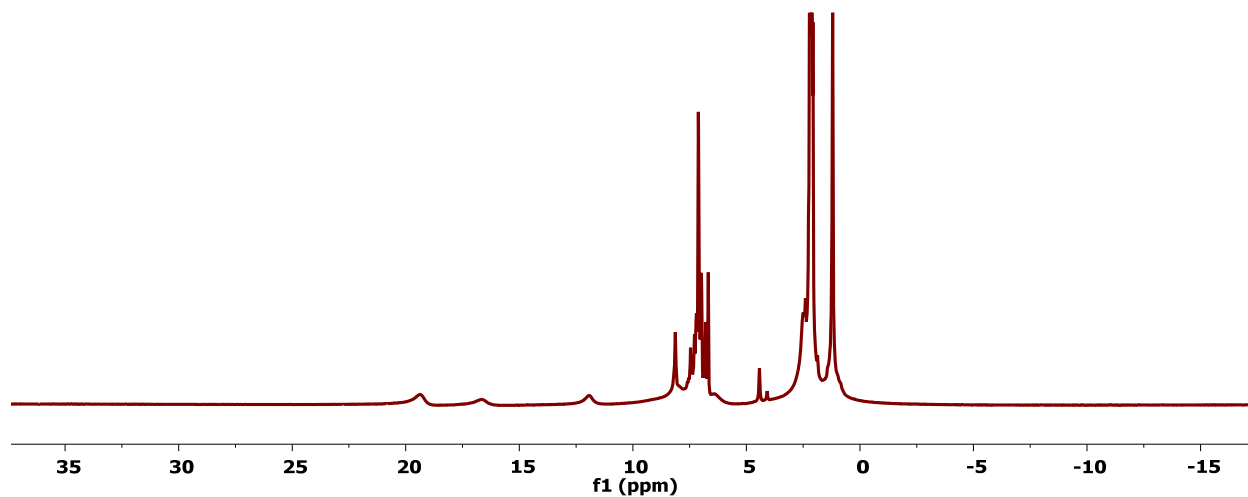


Figure D.146. ^1H NMR spectrum (300 MHz, C_6D_6) of 8.

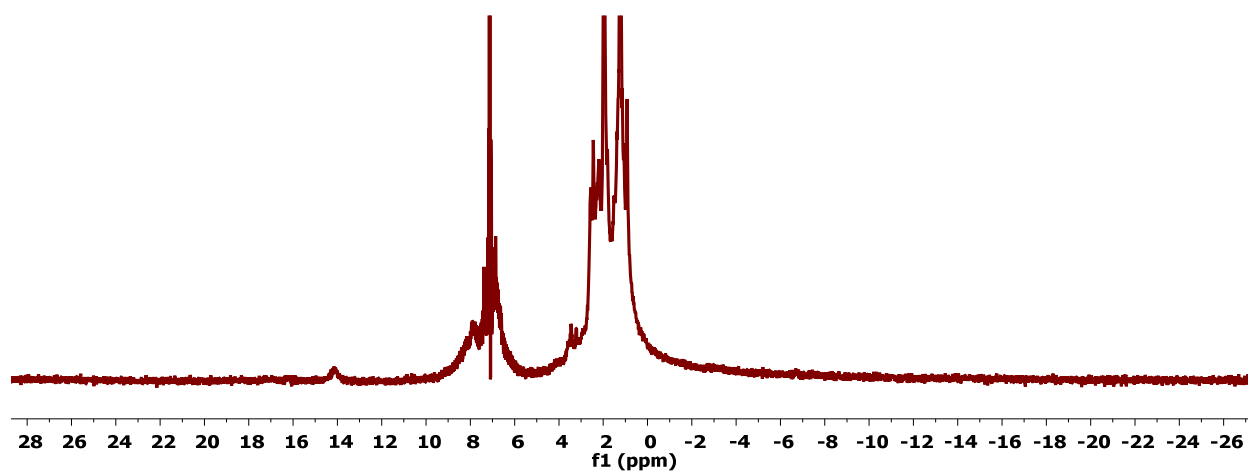


Figure D.147. ^1H NMR spectrum (300 MHz, C_6D_6) of 9.

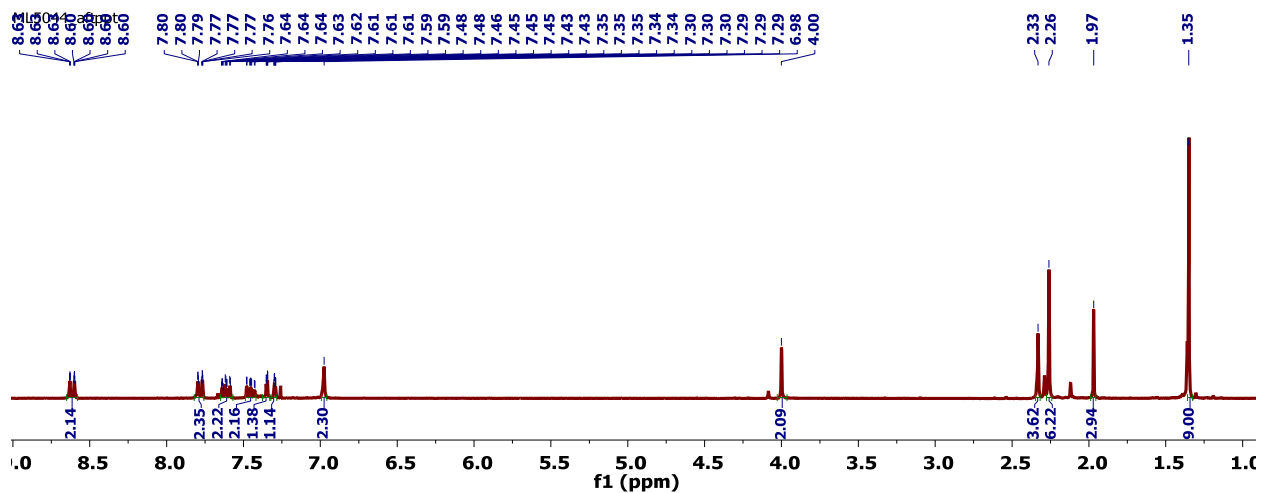


Figure D.148. ^1H NMR spectrum (300 MHz, CDCl_3) of 9-bromo-10-(5-(*tert*-butyl)-2-(methoxymethoxy)-2',4',6'-trimethyl-[1,1'-biphenyl]-3-yl)anthracene.

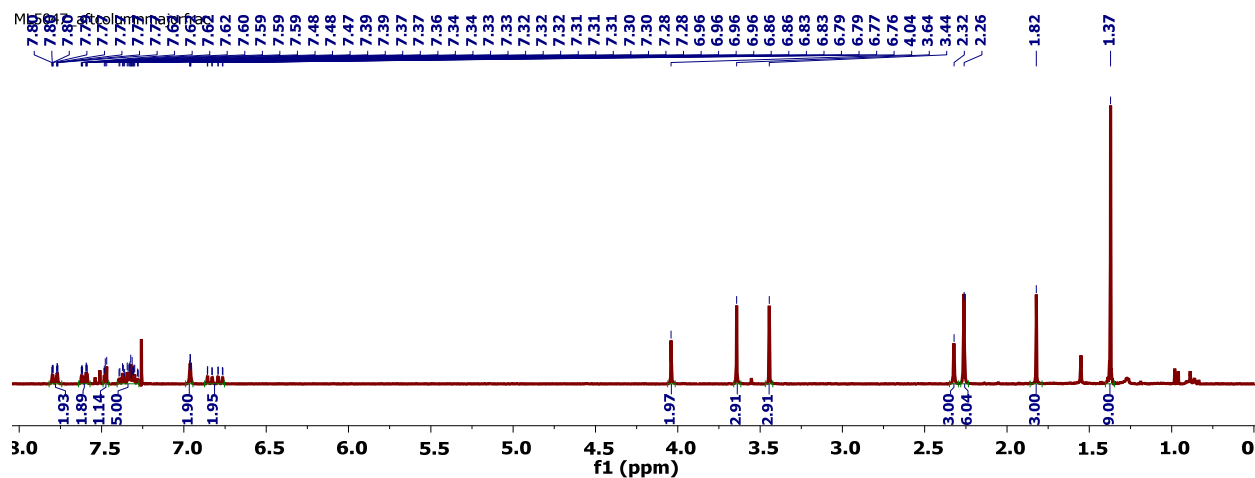


Figure D.149. ^1H NMR spectrum (300 MHz, CDCl_3) of 9-(5-(*tert*-butyl)-2-(methoxymethoxy)-2',4',6'-trimethyl-[1,1'-biphenyl]-3-yl)-10-(2,6-dimethoxyphenyl)anthracene.

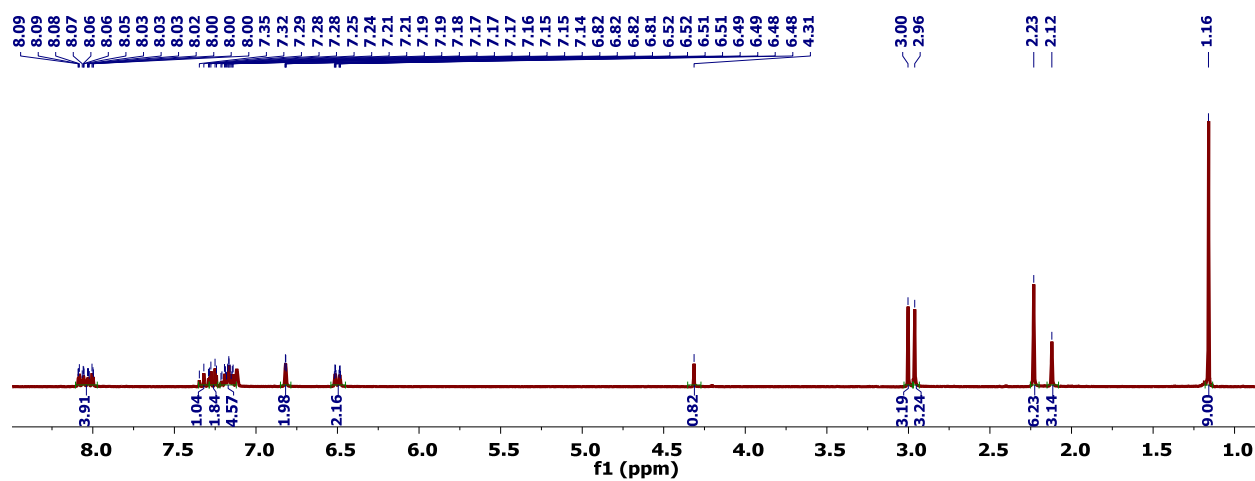


Figure D.150. ^1H NMR spectrum (300 MHz, CDCl_3) of 10.

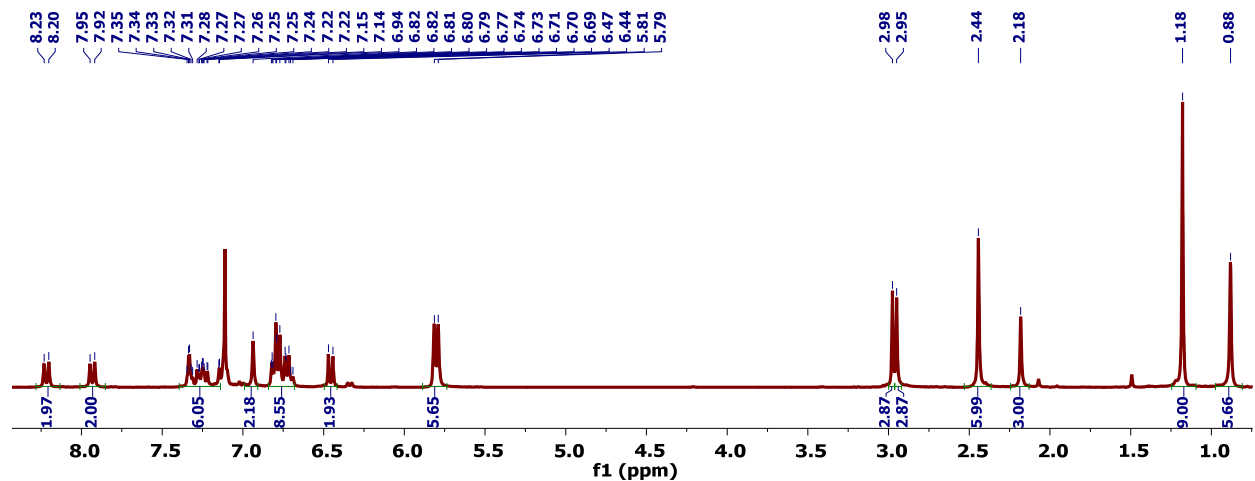


Figure D.151. ^1H NMR spectrum (300 MHz, C_6D_6) of 11.

ABOUT THE AUTHOR



Choon Heng Low, or Marcus, a name he chose to start using just prior to starting college in the UK (and one that stuck), was born in Singapore on July 6th, 1988 to Kay Hiang and Mei Moon Low. He and his elder brother Choon Meng Low were raised in Singapore. He attended Anderson Secondary School, finishing in 2004 and continued to National Junior College finishing in 2006. After completing his military service as a combat engineer in 2009, and having been awarded an A*STaR scholarship, he took the opportunity to leave the country and embark on his college education in London, UK at Imperial College London. During his time there, he worked in the labs of Prof. Andrew Ashley, getting his first taste of synthetic inorganic chemistry and also spent a summer in Tokyo, working for Prof. Shu Kobayashi at the University of Tokyo. Marcus graduated with a BSc in Chemistry in 2012 and started a one-year research assistantship back in Singapore at the Institute of Chemical Engineering and Sciences in the Polymer Engineering and Catalysis Department. He completed his Ph. D. studies, as an A*STaR scholar, in in the laboratories of Prof. Theodor Agapie at the California Institute of Technology in 2019. He plans to move back to Singapore to start work at one of the institutes under A*STaR. When not in the lab, Marcus is often found in the kitchen baking or cooking, out hunting for new and delicious food to savor, or playing some rather intense Euro-style board game.

“This is how you do it: you sit down at the keyboard and you put one word after the other until it’s done. It’s that easy, and that hard.”

– Neil Gaiman